INTERAGENCY SYMPOSIUM ON UNIVERSITY RESEARCH IN TRANSPORTATION NOISE (2ND), HELD AT NORTH CAROLINA STATE UNIVERSITY, RALEIGH, ON JUNE 5-7, 1974

BOOK OF PROCEEDINGS, VOLUME II

North Carolina State University

June 1974

DISCLAIMER NOTICE

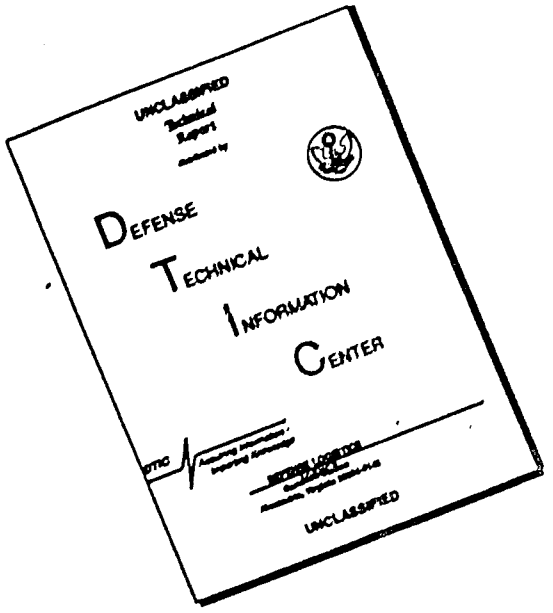

THIS DOCUMENT IS BEST QUALITY AVAILABLE. THE COPY FURNISHED TO DTIC CONTAINED A SIGNIFICANT NUMBER OF PAGES WHICH DO NOT REPRODUCE LEGIBLY.

BIBLIOGRAPHIC DATA SHEET	1. Report No. DOT-TST-74-29	2.	3. Recipient's Accession No.
4. Title and Subtitle Second Interagency Symposium on University Research in Transportation Noise, Vol. II			5. Report Date June 5-7, 1974 6.
7. Author(s)			8. Performing Organization Rept. No.
9. Performing Organization Name and Address North Carolina State University Raleigh, N.C			10. Project/Task/Work Unit No. 11. Contract/Grant No. DOT-OS-40040
12. Sponsoring Organization Name and Address Department of Transportation Office of Noise Abatement 2100 2nd St. S.W., rm. 522 Washington, D.C.			13. Type of Report & Period Covered Final 14.

15. Supplementary Notes

16. Abstracts

The intent of the Second Interagency Symposium on University Research in Transportation Noise was to continue to focus attention on university research in basic and applied noise problems related to transportation. The purpose of these proceedings is to record and discuss current research studies, and objectives of research programs.

Volume II of the Proceedings covers papers presented on Selected Problems II, Societal Problems, Combustion Noise, Duct Acoustics.

17. Key Words and Document Analysis. 17a. Descriptors

Transportation Noise

University Research Symposium

17b. Identifiers/Open-Ended Terms

17c. COSATI Field/Group

PRICES SUBJECT TO CHANGE

18. Availability Statement	19. Security Class (This Report)	21. No. of Pages
Unlimited	UNCLASSIFIED	403
	20. Security Class (This Page) UNCLASSIFIED	22. Price $11.00

SECOND INTERAGENCY SYMPOSIUM ON UNIVERSITY RESEARCH IN TRANSPORTATION NOISE

NORTH CAROLINA STATE UNIVERSITY
RALEIGH, NORTH CAROLINA

JUNE 5-7, 1974

PROCEEDINGS

VOLUME II

BOOK OF PROCEEDINGS

Volume II

SECOND INTERAGENCY SYMPOSIUM

ON UNIVERSITY RESEARCH IN TRANSPORTATION NOISE

North Carolina State University
Raleigh, North Carolina
June 5-7, 1974

Symposium Sponsor

U. S. Department of Transportation

Cooperating Agencies

National Aeronautics and Space Administration
National Science Foundation
Department of Defense:
Air Force Office of Scientific Research
Office of Naval Research
Army Research Office
Environmental Protection Agency

PREFACE

The contents of these Proceedings are papers contributed to the Symposium. Most of the papers are presented at the Symposium, while some are included only in the Proceedings. It is intended that these volumes will provide a broad current view of university research in basic and applied noise problems related to transportation that is being carried out under the support of the various Federal Agencies.

The contents of the volumes are arranged according to the subject topic as they appear in the program of presentations at the Symposium. For convenience, a complete author index is provided at the end in each of the volumes.

Our appreciation is extended to Ms. Anne Gregory for her patience and diligence in the preparation of these volumes.

Gordon Banerian

William F. Reiter

North Carolina State University
Raleigh, North Carolina
June, 1974

TABLE OF CONTENTS

BANQUET SPEAKER

Albert C. Trakowski

Deputy Assistant Administrator for Environmental Engineering

Environmental Protection Agency

401 M Street S.W.

Washington, D. C.

INVITED LECTURERS

Dr. M. Goldstein

"Recent Developments in Fan Noise Analysis"

Dr. J. E. Ffowcs-Williams

"Aircraft Noise and Prospects for Its Control"

Dr. R. John

"Surface Transportation Noise Abatement Programs in TSC"

Dr. A. Novick

"Nature's Sonar (Echo Location in Bats)"

Dr. H. E. von Gierke

"Noise Exposure Compatible with Public Health and Welfare"

Mr. H. Johnson

"The Price of Noise"

SELECTED PROBLEMS II

VIBRATION OF ELEVATED RAIL RAPID TRANSIT STRUCTURES

by

Marshall L. Silver and Thomas Venema

Department of Materials Engineering
University of Illinois at Chicago Circle
Chicago, Illinois 60680

The measurement of the dynamic response of existing elevated transportation structures is a meaningful first step in any research into the problems of noise abatement, vibration control, and vehicle ride comfort. By measuring the dynamic characteristics of the various structural components of the structure, it is possible to develop a basic understanding of the following factors that should be useful in the evaluation of existing structures and the design of new structures:

1. The form and magnitude of the loads generated by the transportation vehicle.

2. The natural frequencies of each structural component.

3. The magnitude of structural noise and vibration damping present in the structure.

4. Values of the annoying frequencies that need to be eliminated to reduce unpleasant noise and vibration levels.

5. Measurements of dynamic response that may be used to check the validity of analytical techniques that are used to design and analyze the behavior of elevated transportation structures.

With these goals in mind, an extensive field measurement program was carried out to evaluate the dynamic response of many types of steel elevated structures used on the rapid transit lines of the Chicago Transit Authority (CTA). The structures tested are of the same type as the transit structures in use in Boston, Philadelphia, and New York, and thus will directly aid transit operators in many cities concerned with performance, repair, and evaluation of existing structures.

Instrumentation and Mounting Techniques

The strain gage accelerometer instrumentation system schematically shown in Figure 1 was selected to meet low frequency response specifications (0 to 1000 hertz) required to evaluate structural analysis techniques. Calibration difficulties, inherent in piezoelectric and other instrumentation systems, were therefore minimized. For example, it was possible to use a 1g reversal test ($1g = 32.2\ ft/sec^2$) as a field and laboratory check at the beginning and end of each measurement series to insure that the recording system was properly calibrated (Dove and Adams, 1964).

The quality of the acceleration data obtained from vibrating structures is only as good as the techniques used to mount the accelerometers and the

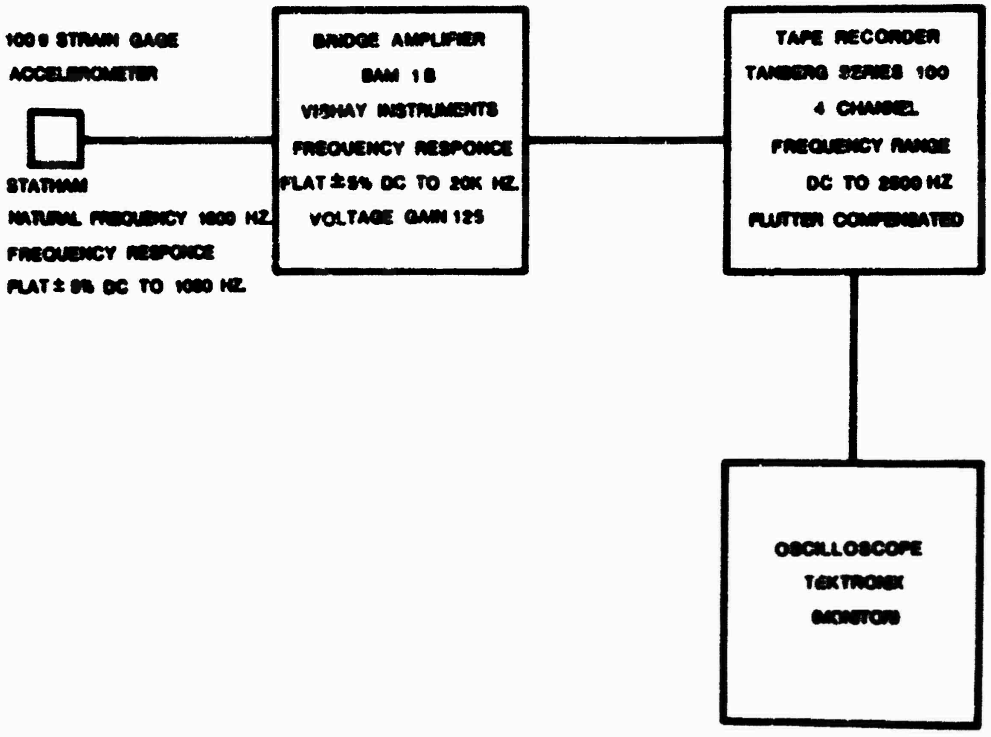

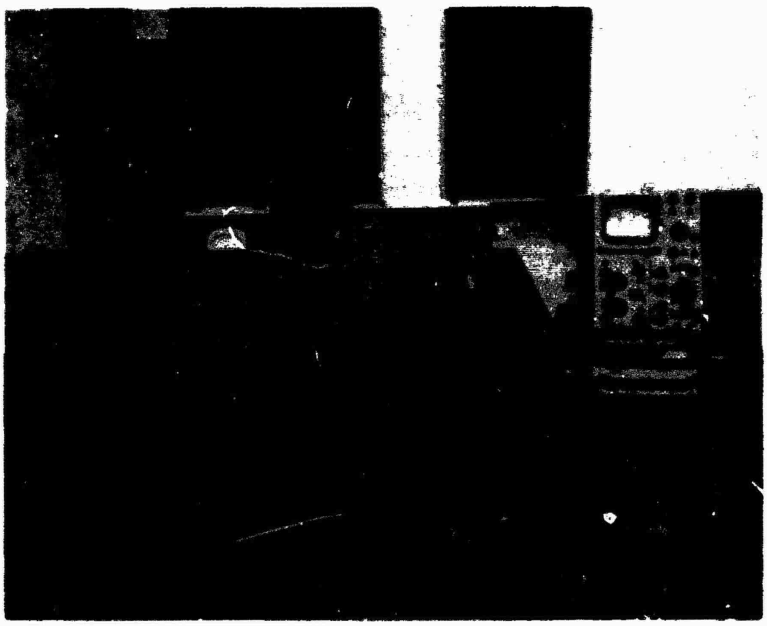

Fig. 1 The strain gage accelerometer instrumentation system.

methods used to clean and prepare ths surface of tested structural members. Therefore, an extensive series of laboratory and field tests were performed to evaluate alternative accelerometer mounting and surface preparation techniques.

Results of these tests showed that the use of triaxial and uniaxial transducer mounting blocks did not influence the measured response of the structure as long as these blocks were epoxied to the structure. On the other hand magnetic mounting techniques resulted in the measurement of abnormally high acceleration values. For this reason, epoxy mounting was used except where the surface condition of the structure did not make it possible to secure a satisfactory epoxy bond. In these cases, magnet mounting was used and the peak acceleration values were corrected using laboratory and field correlation data. A more detailed description of the test instrumentation, mounting techniques and evaluation tests are presented elsewhere (Venema and Silver, 1974).

Field Test Sites

Four different structures on three different transit lines were chosen for field testing:

Site 1 Douglas Park Service, located at the University of Illinois Medical Center

Site 2 Milwaukee Service, South of Francis Street

Site 3 Milwaukee Service, South of Logan Square

Site 4 Ravenswood Service, South of the Montrose Street Station

All of the structures are steel throughout, except for the Milwaukee Service at Logan Square, which has concrete columns and diaphram cross bracing. The map showing the location of these test sites is shown in Figure 2.

The steel elevated structures on the Milwaukee Service at Francis Street and on the Douglas Park Service were selected because they are similar to structures being modeled with computer finite element methods in another phase of the research (Traubenik, et al, 1974). These structures consist of a track deck carried by built-up plate girders supported by latticed columns. The elevated portion on the Milwaukee Service at Logan Square is a composite structure consisting of concrete cross beams supported by concrete columns carrying rolled longitudinal plate girders. This structure was chosen in order to evaluate the effect of concrete supports and columns on the transmission of vibrations through the structure. Structures on the Ravenswood Service consist of a track deck carried by built-up plate girders supported by non-latticed, built-up columns. Measurements on this structure were made and compared to measurements on the Douglas Park Service to evaluate the effect of column design on generated vibration levels.

Rapid Transit Vehicle Characteristics

Three types of rapid transit vehicles commonly called 6000, 2000, and 2200 series cars are used on the Chicago Transit Authority system. The characteristics of these vehicles are summarized in Table 1. The oldest

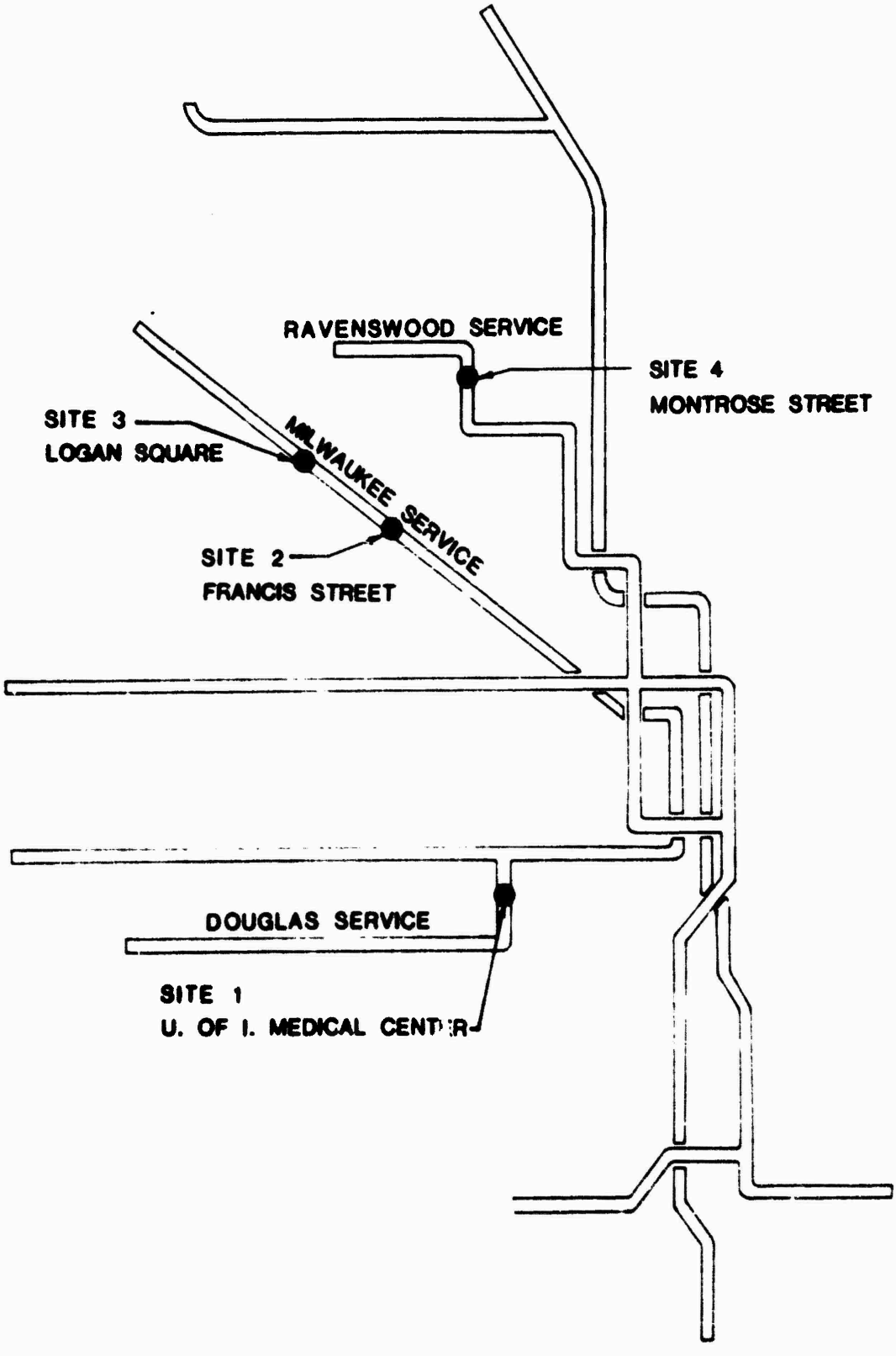

Fig. 2 Location of Field Sites for Measurements of the Vibration Properties of Steel Elevated Structures

vehicles, the 6000 series, were built in the 1950's, the 2000 series vehicles were built in 1964 and the 2200 series vehicles were built in 1969.

TABLE 1

SUMMARY OF RAPID TRANSIT VEHICLE CHARACTERISTICS
CHICAGO TRANSIT AUTHORITY

Series Type	Year Built	Weight	Construction and Appearance	Routes Served
6000	1950-1951 (initial production)	41,700 to 42,700 lb (18,950 to 19,400 kg)	Steel Construction non-sealed windows, green and white	Howard Englewood Jackson Douglas Ravenswood
6000	1957-1957	44,350 lb (20,150 kg)	Different trucks and wheels than the initial production	Milwaukee
2000	1964	47,000 lb (21,360 kg)	Steel construction sealed windows, air-conditioned, silver and black	Lake Street Dan Ryan
2200	1969-1970	45,000 lb (20,452 kg)	Stainless steel construction, cab signals, sealed windows, air-conditioned, unpainted	Lake Street Dan Ryan Douglas Congress Milwaukee

Field Measurement

The acceleration levels generated by transit vehicles on the four structures at the four different test sites were obtained by mounting a single accelerometer underneath the rail in the vertical direction and by moving three accelerometers attached to a triaxial mount to various locations on the structure. The rail measurement was used to monitor input train excitation and any measurements that indicated wheel flats or abnormal vehicle behavior were not used to evaluate structural response. For each train pass-by, a record was made of the car type and the number of cars. Vehicle speed was determined by timing the train as it passed between two predetermined points.

Accelerometers were placed at a minimum distance of ten feet from rail joints to minimize vibration generated by impact between the wheel of the vehicle and the rail joint. In addition, all measurements on the longitudinal plate girders were made at mid-span between columns to minimize column and

connection effects. Specific accelerometer placement locations are illustrated in Figure 3.

Measurement of Peak acceleration Values

In the laboratory, magnetic tape records of field accelerometer output was displayed on a storage oscilloscope using a static field calibration signal to determine the magnitude of the peak accelerations. Care was taken in the evaluation of any data where wheel-flats or any wheel-truck abnormalties would possibly cause an erratic reading. For example, in the field if a distinct thumping sound was heard or if the train passing over the test accelerometer emitted noise which was unlike the other transit train passbys, this was noted and the time history was inspected for any abnormal peaks which were not considered in the analysis.

Peak acceleration values for all of the field measurements were summarized using the coordinate system shown in Figure 3. Some of this data is combined for different train passbys on the basis of train type, number of cars, and train speed in Figures 4 and 5. These figures show that the highest accelerations were recorded on the rail with lower accelerations recorded on the structure. For example, accelerations on the longitudinal plate girder and diagonal cross bracing were lower than levels recorded on the rail by approximately 40%. For columns and footing bases, the maximum level was substantially lower than the level recorded on the rail or on the longitudinal plate girder.

The effect of train speed on peak acceleration levels can be obtained from a comparison of Figure 4 and Figure 5. For example, it may be seen in Figure 4 that a two car 2200 series train traveling at 45 mph generates a peak acceleration of 76 g in the rail and acceleration levels of 45, 25 and 34 g on the web of the longitudinal plate girder in the x, y, and z directions, respectively. In comparison, a two car 2200 series train traveling at 15 mph generates a peak acceleration level of 22 g in the rail and acceleration levels of 12, 4, and 6 g on the web of the longitudinal plate girder in the x, y, z directions respectively as shown in Figure 5. These figures clearly show that increasing the train speed from 15 to 45 mph under operating conditions can increase generated acceleration levels more than 3 times.

Analysis of Data in the Frequency Domain

A real time spectrum analysis can provide information on how the energy of a signal is distributed over the range of the frequencies of interest. Such information describes what frequencies predominate in the vibration signal and this information can be used to evaluate the effectiveness of both vibration and noise control techniques.

Real time analysis of the time history obtained from acceleration measurements on each structural element were performed with a Spectral Dynamic SD-330-20 analyzer. A peak-hold mode of the analysis was selected because of the form of the data which contained peak acceleration levels from wheel impacts. It was felt that rather than averaging these peaks, it would be more meaningful to find frequencies at which these peaks occurred and then compare their relative amplitude to the rest of the power spectrum. An analysis frequency range of 0 to 1000 hz, giving a bandwidth of 4 hz was used to match the frequency range of the field measurement equipment. The low frequency limit for meaningful analysis was set at 50 hz based on a consideration of the short sampling period for a moving transit train.

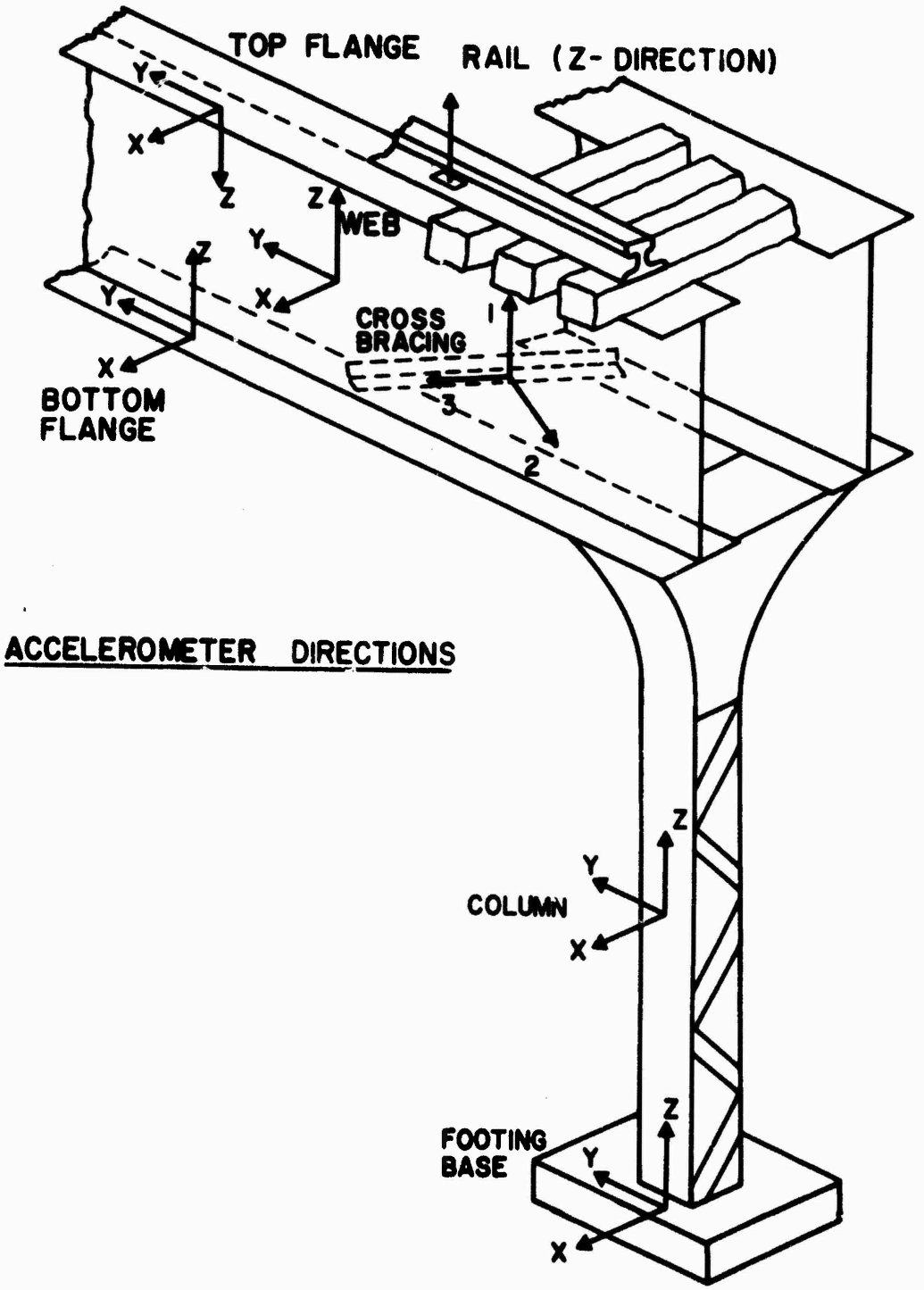

Fig. 3 A three dimensional view of the test structure illustrating names of structural members, accelerometer placement positions and accelerometer axis directions.

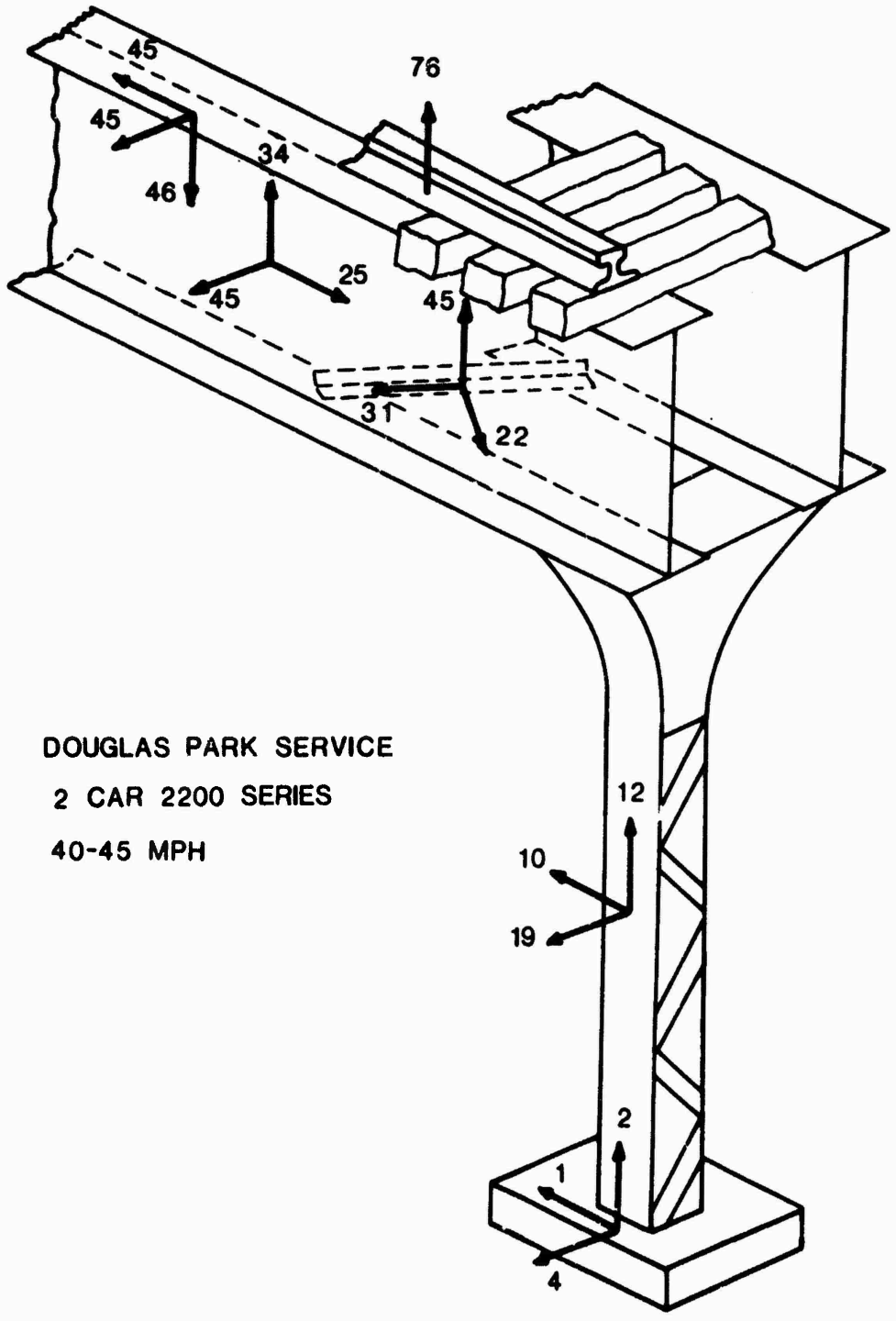

Fig. 4 Peak acceleration levels in g's for 2 car 2200 series trains travelling at 40-45 mph (Douglas Park Service).

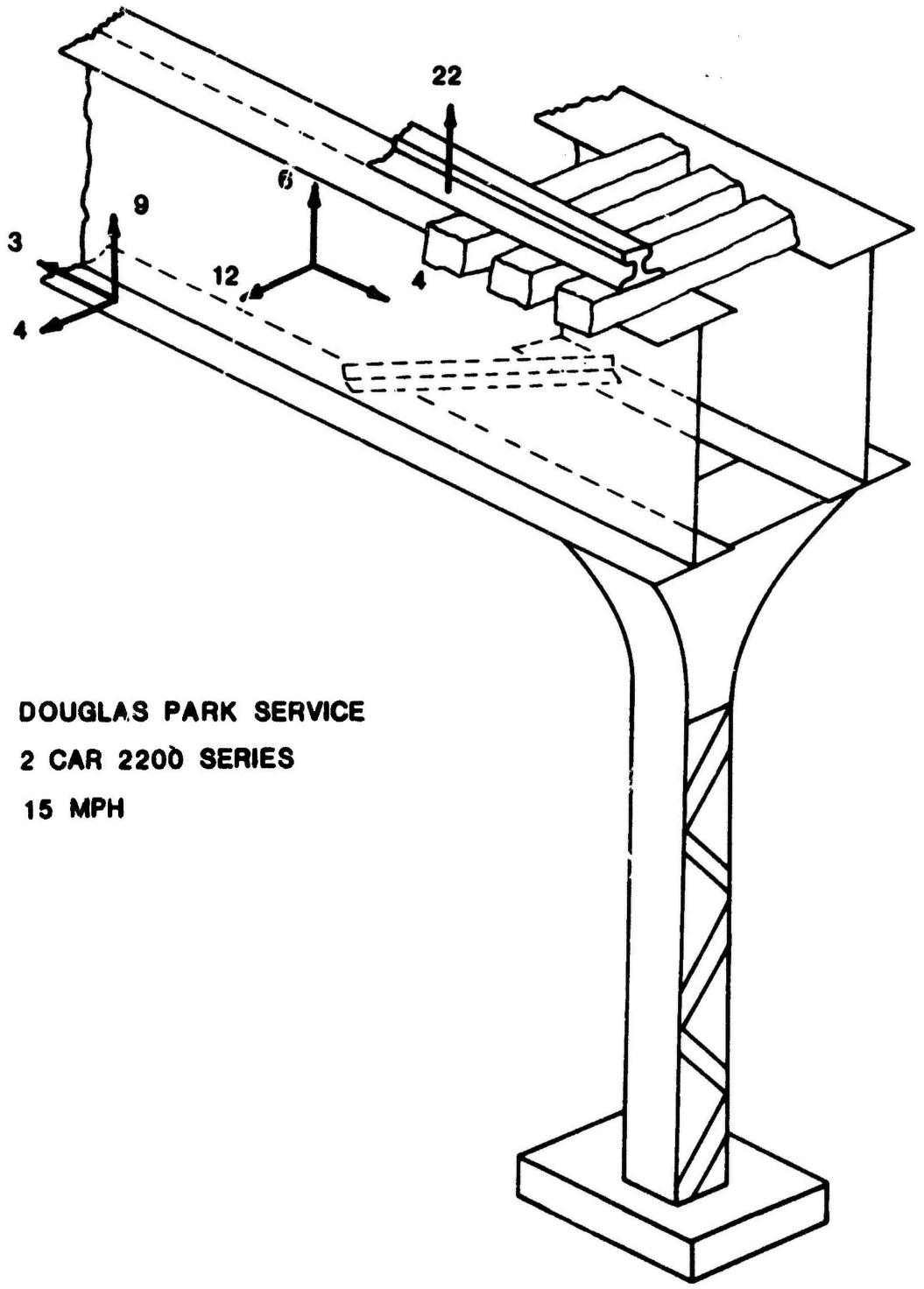

Fig. 5 Peak acceleration levels in g's for 2 car 2200 series trains travelling at 15 mph (Douglas Park Service).

Figure 6 presents four plots showing triaxial acceleration frequency distributions for each accelerometer placement position. For each plot, a three-dimensional view of the elevated structure shows the location and measurement direction for each accelerometer.

It may be seen from this figure that the rail accelerations contained spectral power peaks between 400 hz and 500 hz with an occasional peak around 700 hz. Similar peaks at the same frequencies may also be seen on the structural member. An analysis of these and other data (Vanema and Silver, 1974) showed a strong relationship between vehicle speed and structural shaking frequencies, with increasing speeds producing peaks at higher frequencies.

Summary and Conclusions

Knowledge of the relative magnitude and dominant frequencies of transit induced vibrations that are generated in the rail and in each structural component of elevated transportation structures may be used to determine what elements are most responsible for transmitted noise and vibration.

Measurements of the peak acceleration magnitudes and the frequency content of vibrations on steel elevated transit structure of the type common in Chicago, New York, Boston and Philadelphia have shown the following:

1. Measurement transducers must be bolted or epoxied to the structure to accurately measure peak acceleration values.

2. Peak acceleration values were measured in decreasing order of magnitude on the rail, on the top and bottom flanges, on the web, on cross bracing, on the column and at the footing base on steel elevated transit structures.

3. Peak acceleration values on the order of 70 g generated in the rail by the passage of rapid transit vehicles are little attenuated as they are transmitted to the structure where peak structural member accelerations were on the order of 45 g.

4. Peak acceleration magnitudes significantly increased for increasing train speeds.

5. Narrowband frequency analysis of the acceleration time histories from the rail and from structural members showed spectral poer peaks between 400 hz and 500 hz. There was a strong relationship between vehicle speed and the frequency of these peaks with higher speeds producing peaks at the highest frequencies.

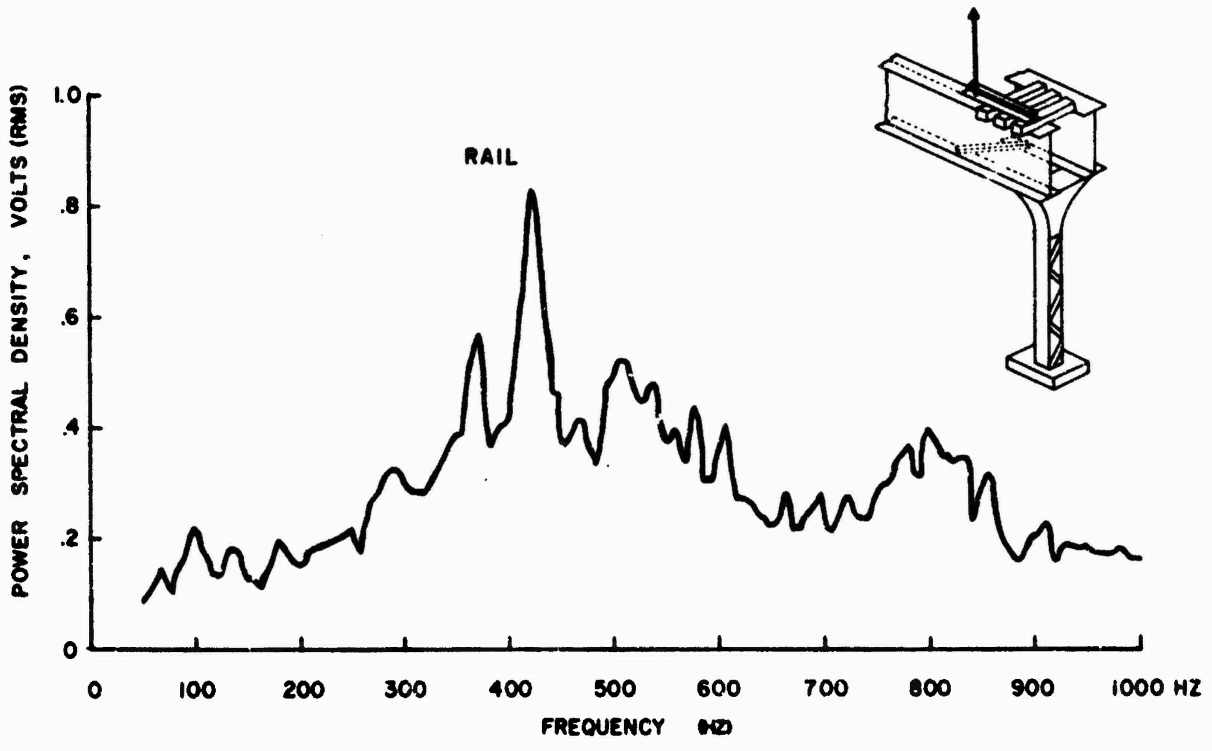

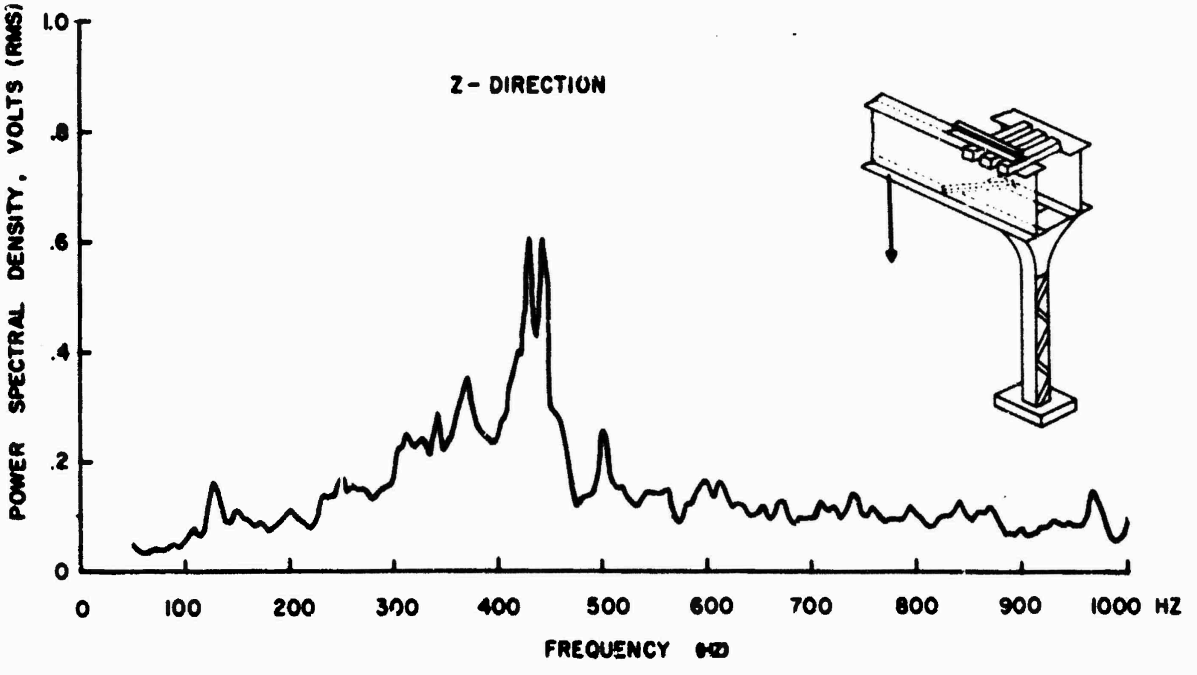

Fig. 6 Frequency analysis of the acceleration data for a 2 car, 2200 series train travelling at 35 m.p.h. (Bottom flange measurement, Douglas Park Service, steel structure).

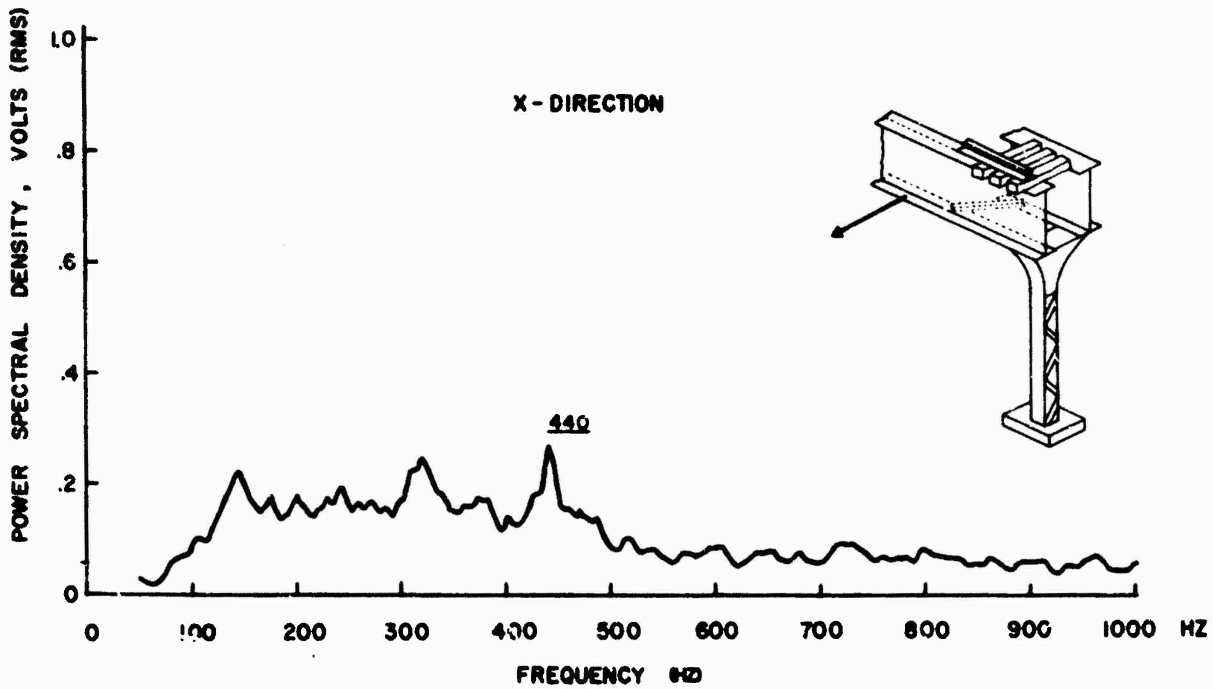

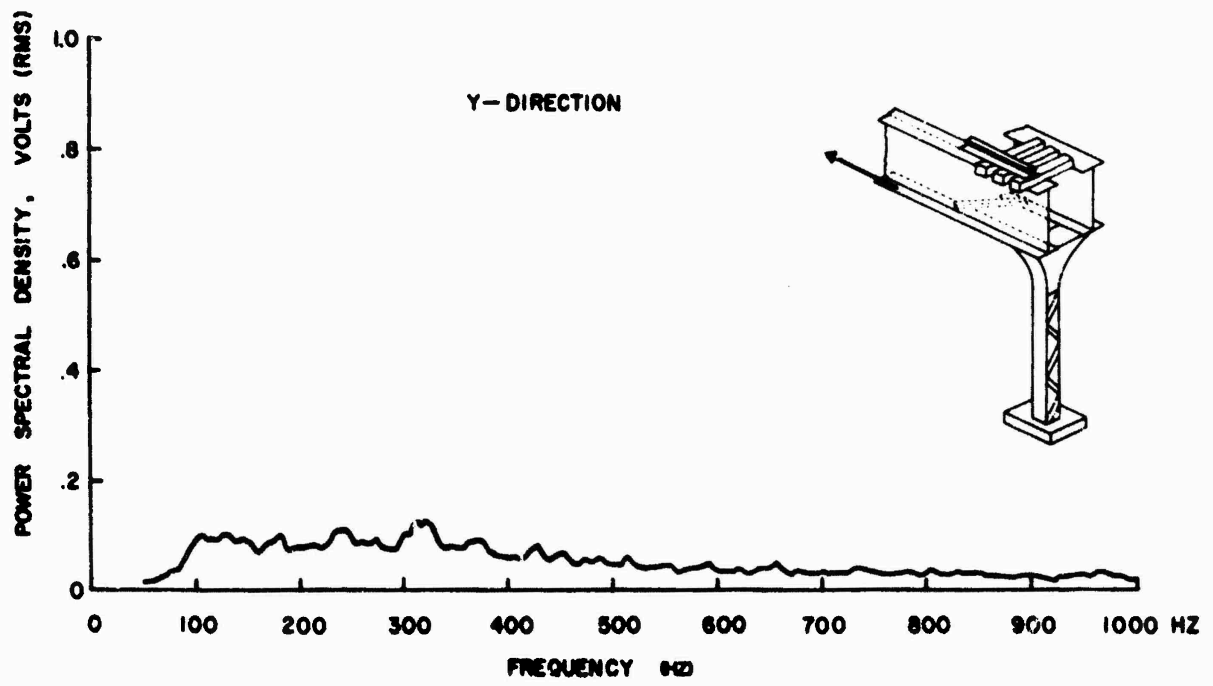

Fig. 6 (continued) Frequency analysis of the acceleration data for a 2 car, 2200 series train travelling at 35 m.p.h. (Bottom flange measurements, Douglas Park Service, steel structure).

Acknowledgments

The research reported in this paper was sponsored by the Office of the Secretary, U.S. Department of Transportation under the Program of University Research (Contract DOT-OS-30092) for the project entitled "An Integrated Engineering Planning Approach to the Preservation, Improvement and Replacement of Elevated Transportation Structures". The support and assistance of Dr. R. E. Goodson, R. K. McFarland and L. McKenzie of the Office of the Secretary is gratefully acknowledged. The assistance of the Chicago Transit Authority and the help of E. Olmstead, P. Swanson and W. Tushinski is also appreciated.

Recognition is also given to T. Park, M. Traubenik, R. Masek and D. Leavell of the University of Illinois at Chicago Circle for their assistance in the field.

Reference

1. Dove, R. C. and Adams, P. H. (1964), Experimental Stress Analysis and Motion Measurement, Charles E. Merrill Books, Columbus, Ohio.

2. Traubenik, M., Silver, M. L. and Belytschko, T. B. (1974), "Static Finite Element Analysis of Steel Elevated Transportation Structures", Report No. 74-3, Geotechnical Engineering Research Laboratory, Department of Materials Engineering, University of Illinois at Chicago Circle, Chicago, Illinois, May.

3. Venema, T. and Silver, M. L. (1974), "Field Measurements of the Vibration Properties of Steel Elevated Rapid Transit Structures, Report No. 74-2, Geotechnical Engineering Research Laboratory, Department of Materials Engineering, University of Illinois at Chicago Circle, Chicago, Illinois, May.

A NUMERICAL MODEL OF SOUND PROPAGATION IN URBAN AREAS

by

D. Graham Holmes and Richard H. Lyon

Mass. Institute of Technology, Dept. of Mech. Eng.
Cambridge, Massachusetts 02139

I. INTRODUCTION

1.1 The Purpose of the Model

This paper describes a computer-based method for predicting the noise levels resulting from the passage of transportation vehicles (cars, buses, trucks and railroad vehicles) through urban areas. Many computerized methods for predicting noise levels due to vehicular sources already exist [1], but none appear to be applicable to an "urban environment". Figure 1 gives an example of the sort of urban situation which can be handled by this model. A-A is a traffic artery; this main street and the side streets are walled by more or less continuous building facades. We wish, say, to know the sound levels on the street segment B-B, perhaps because block C contains a hospital. The sound propagates between A-A and B-B by a multiplicity of paths, each involving several reflections from the building facades. Present prediction models are not capable of handling propagation paths of such complexity.

Prediction of environmental noise levels requires information of two types: information on the distribution of sources in space, in time, and in sound power level; and information on the sound propagation between sources and receivers. The model described here provides information only of the second type: the locations and sound power levels of the sources are supplied by the user, and the model calculates the resulting sound pressure levels at designated receiver locations. For example, in Figure 2, the source S radiates uniformly in all directions and produces an open field SPL of 90 dBA at 50 ft. The numbers shown in the figure are the sound pressure levels due to the source S, as calculated by the model.

1.2 The Basic Assumptions

The model uses two basic assumptions:

i. Typical urban length scales are assumed to be many times greater than the wavelengths of sound contributing significantly to A-weighted sound levels. This assumption makes it possible to use ray acoustics, but prevents inclusion of any diffraction effects.

ii. The noise sources are broad band, with auto-correlation length scales much less than the urban length scales. Interference between sound paths can thus be assumed to be negligible, and the SPL at the receiver location can be

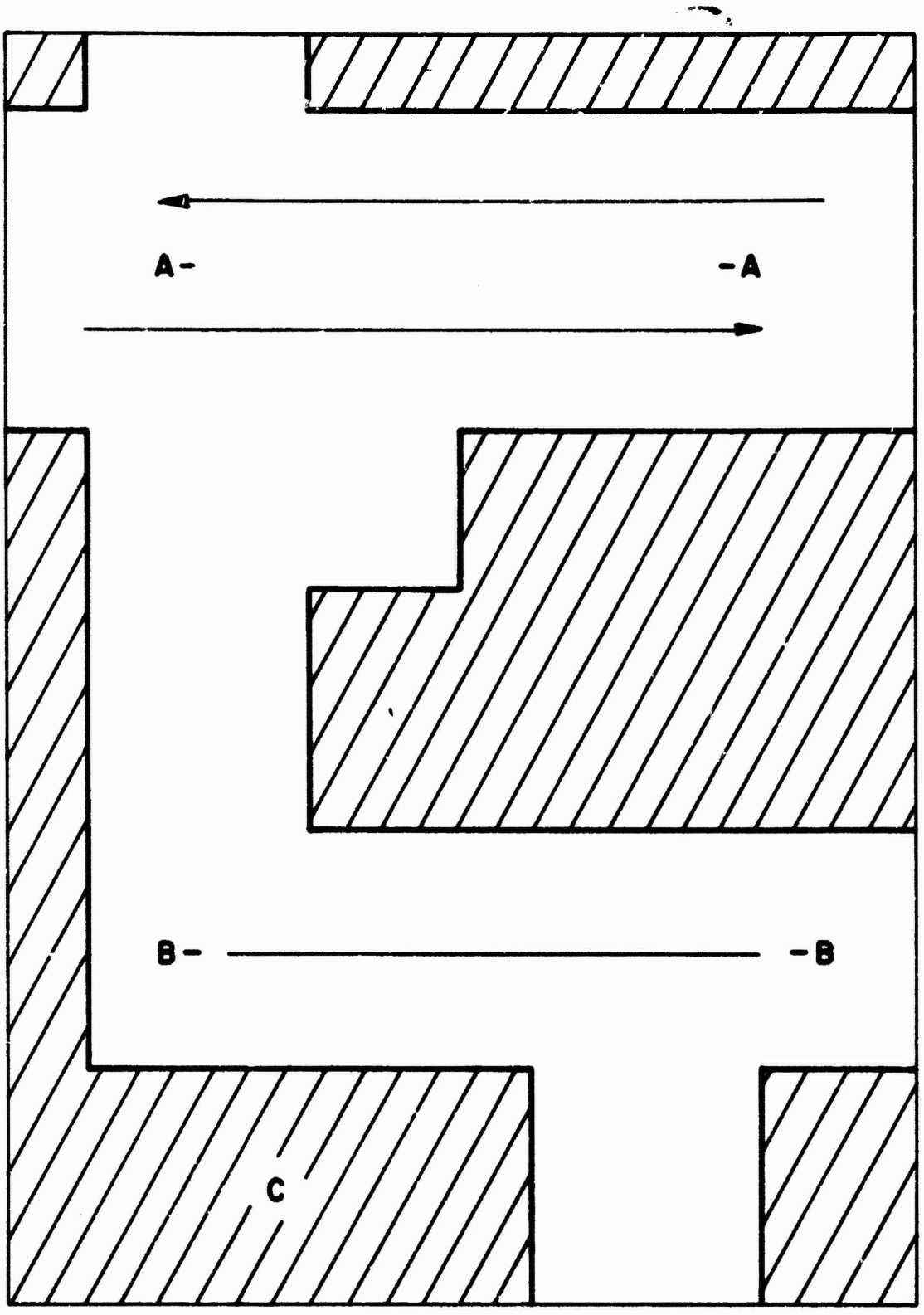

FIGURE 1: A Possible Street Plan

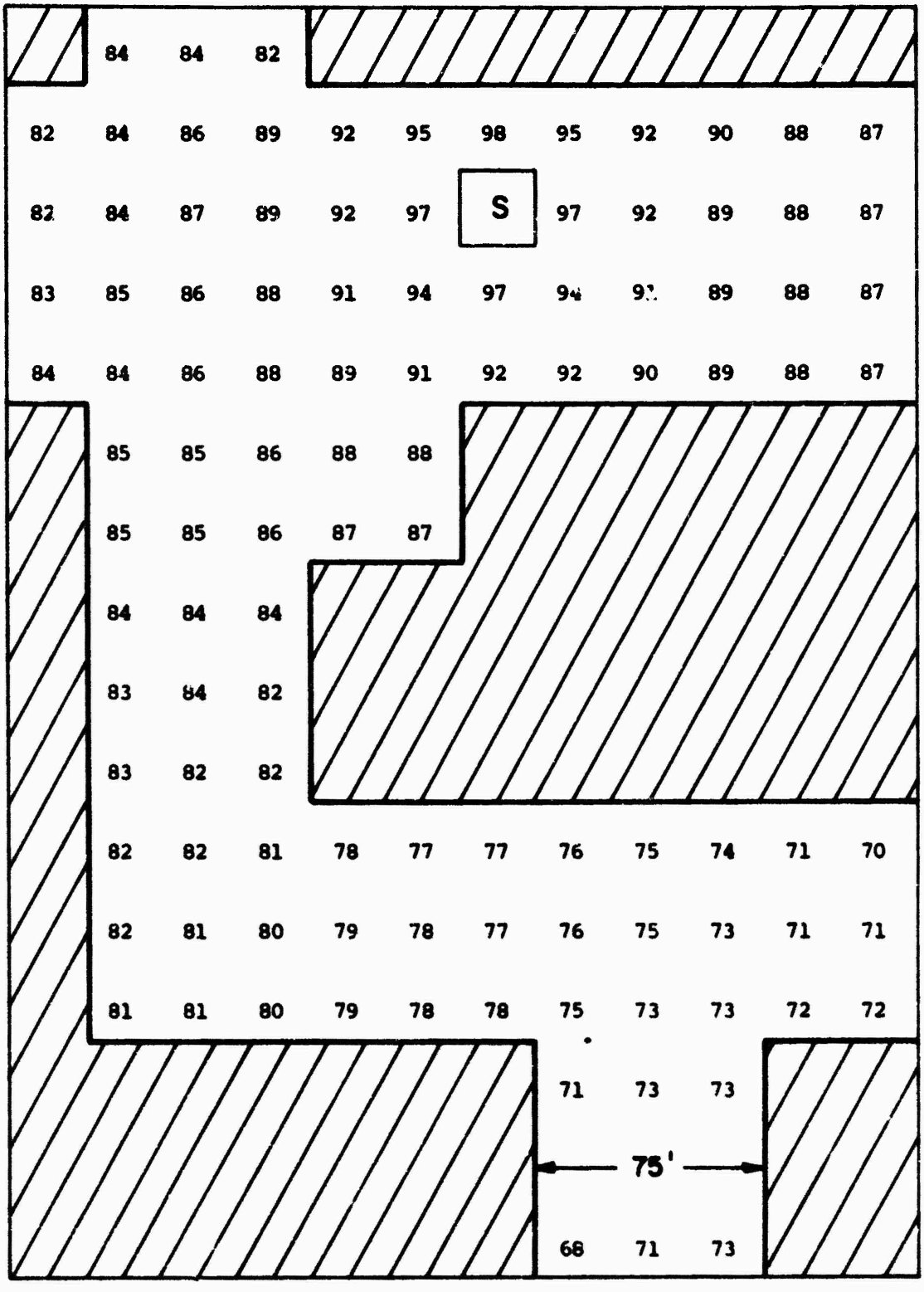

FIGURE 2: Calculated Sound Pressure Levels

obtained by adding the mean square pressures resulting from the separate sound paths. The only case in which path differences may not be large enough is that of ground reflections. Ground reflections are ignored in the current model, but some allowance for them could be made in future versions of the model.

These two assumptions would make it possible to use a conventional ray acoustics model, which operated by locating all the images of the source which were seen by the receiver, and summing the sound pressure levels at the receiver due to this multitude of image sources. This approach is not used in the model described here, since it is hard to conceive of a systematic image location procedure which would be applicable to complex situations such as that in Figure 1.

1.3 The Quantum Approach

The model operates as follows. Since the sound rays produced by the source have such short correlation length scales, the source can be thought of as producing discrete quanta of acoustic energy. These quanta are of fixed energy and are emitted at a constant rate, but in random directions. The quanta propagate through the area, repeatedly encountering building facades. This process is shown schematically in Figure 3. The SPL at the receiver location is obtained by observing the passage of quanta through a small rectangular "receiver cell". The SPL estimate obtained is thus the SPL averaged over the area of the receiver cell.

This model could be thought of either as a random search for images, or more usefully as a simulation model. The computer is, in effect, performing numerical experiments. Results are not achieved by a finite process, but by a random process which is terminated when a desired level of accuracy is attained. Methods of this sort are often described as "Monte Carlo" methods [2].

An important side effect of the simulation approach is that the model is completely flexible: within certain constraints of size and detail, the model can deal with any building configuration. This flexibility has been recognized in the programming of the model. The user is provided with a library of operator commands which he can use to specify the desired building configuration, the locations and sound power levels of the sources, the locations of the receivers, etc. The user can interact with the program, observing the results, modifying the parameters of the calculation, and exploring the effects of changing, for example, the location of the source, or the absorption coefficient of the building facades.

Section II of this paper describes some tests of the validity of the model. Section III describes the model in greater detail.

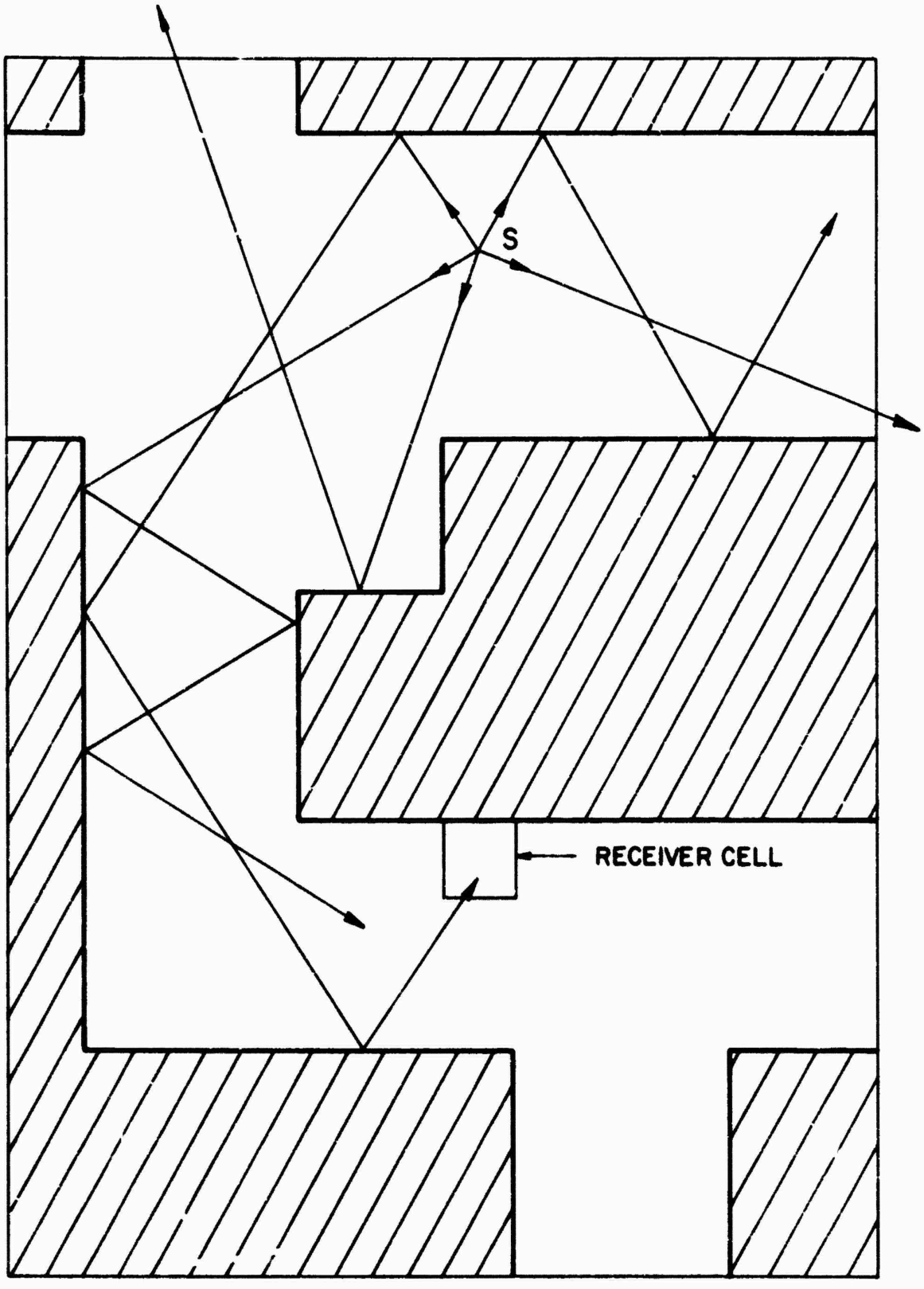

FIGURE 3: Propagation of Acoustic Quanta

II. TESTS OF THE VALIDITY OF THE MODEL

SPL estimates obtained using the model can be compared with

1. analytical results obtained using the same assumptions,
2. scale model tests, and
3. full scale experiments.

Comparisons with analytical results serve to check the correct operation of the model algorithm; comparisons with scale model and with full scale experiments serve to check the validity of the assumptions inherent in the model.

2.1 Comparison with Analytical Results

The sketch in Figure 4 shows a source located centrally in a long straight street. There is absorption but no scattering at the facades. Closed form expressions for the SPL at any point in the street can be obtained in two cases: complete absorption (α=1), corresponding to open-field propagation, and zero absorption (α=0). These SPL results have been compared to estimates obtained using the numerical model (Figure 5). The continuous lines are the analytical results, which, to conform to the numerical results, have been averaged over a square cell one street width wide. The circles are the SPL estimates obtained using the simulation model, with an error tolerance of 0.1 dB. The agreement is well within the error limit used.

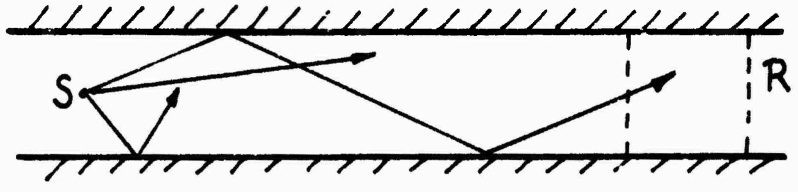

FIGURE 4: Source in a Straight Street

2.2 Comparison with Scale Model Experiments

Figure 6 shows a 1/32 scale model of a street intersection. The model street is 2' wide, corresponding to 64' full scale. The building facades are plywood with a pattern of vertical slats, as sketched in the figure

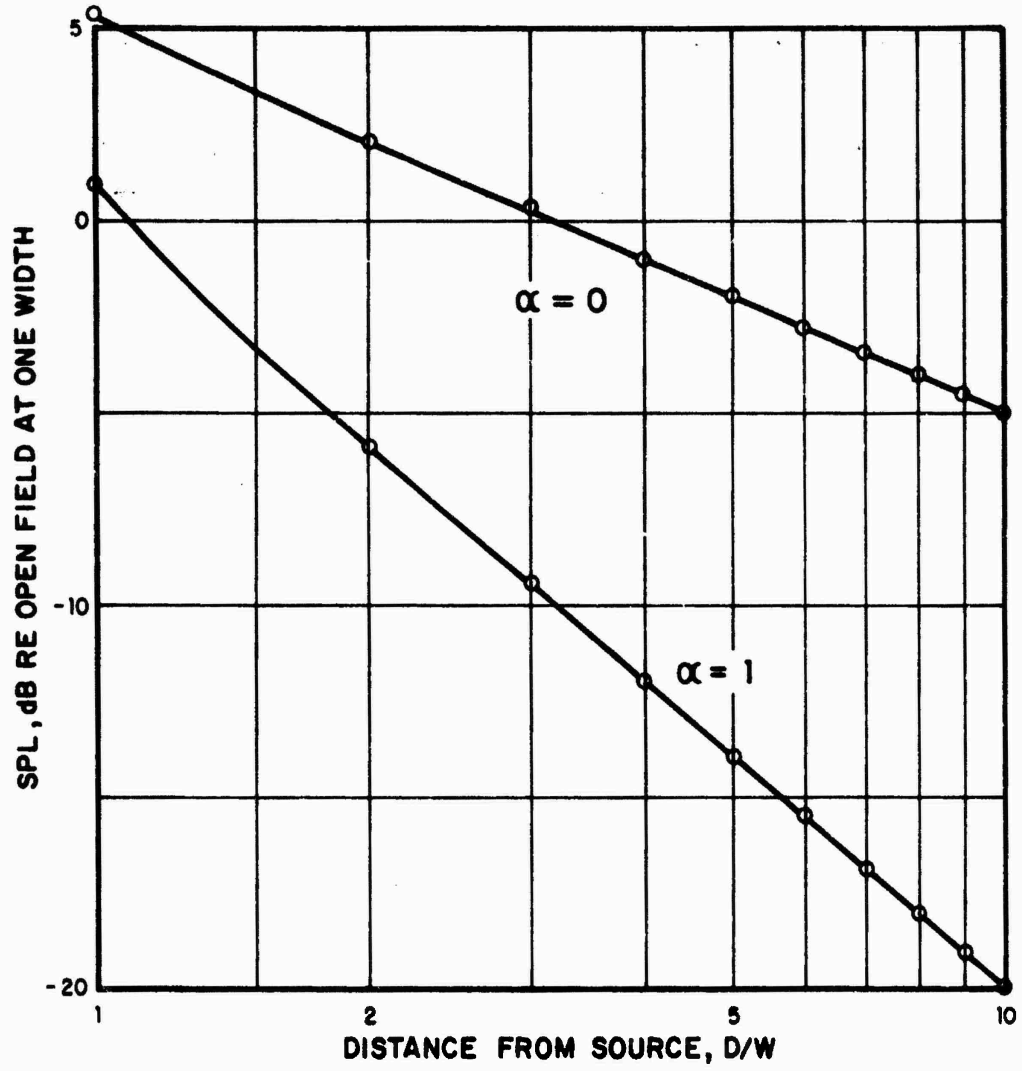

FIGURE 5: Comparison of Analytical and Simulation Results

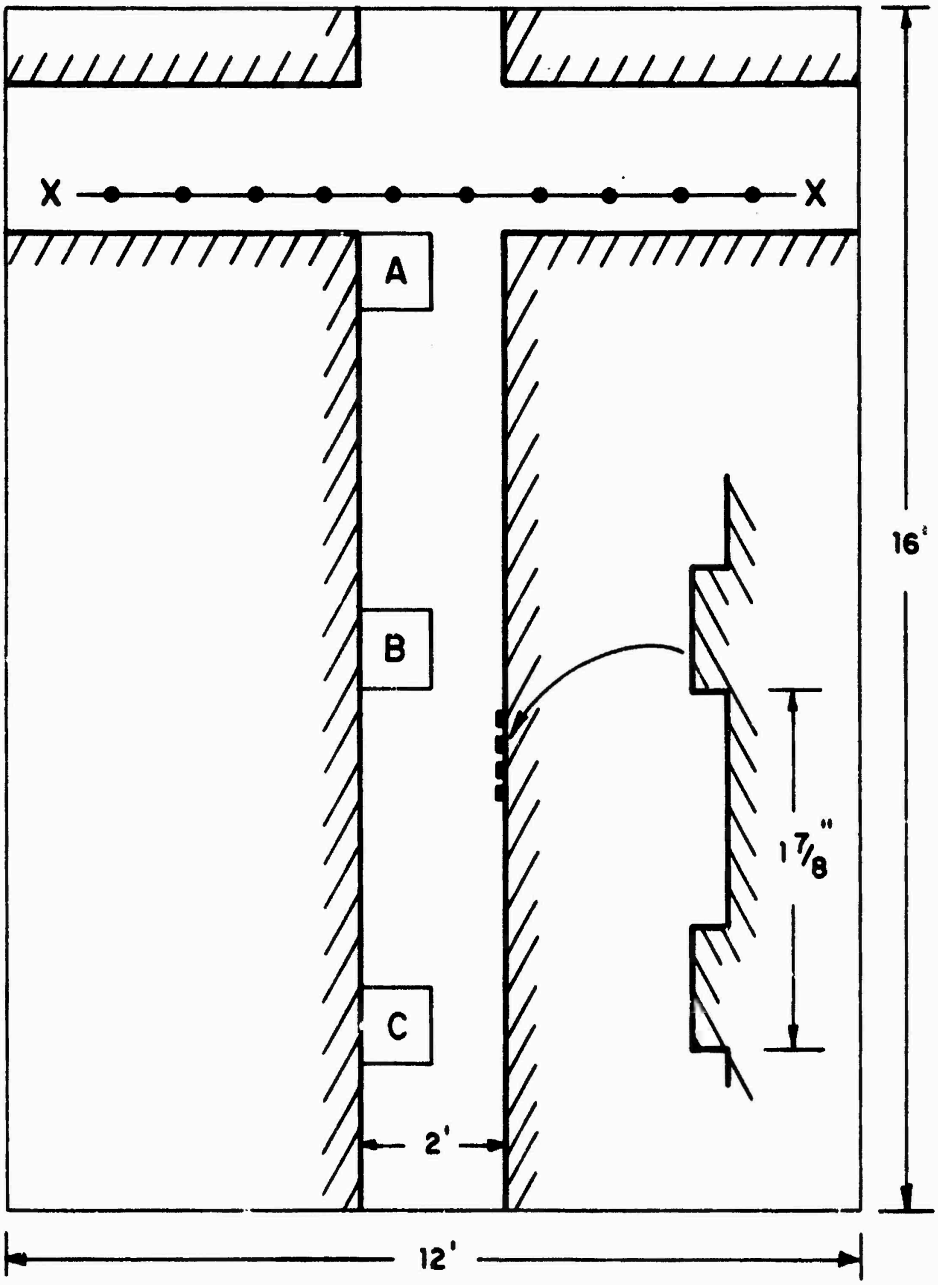

FIGURE 6: 1/32 Scale Model of a Street Intersection

to represent irregularities such as window bays. The street surface is linoleum tile on concrete. Measurements were made using an air jet source, in the 16 kHz octave band (500 Hz full scale). Microphone locations are shown as A, B and C in the figure. The ten source locations are shown as the circles on the line X-X. The SPL results are normalized to a source output of 90 dB in the 16 kHz band, at a distance of 1.56' (50' full scale), and are corrected for air absorption. Further details of the experimental technique can be found in Reference 3 .

For the numerical calculation the basic cell was a square, one half of a street width on a side. No attempt was made to measure absorption and scattering coefficients in the model; instead the calculations were repeated until values for the absorption and scattering coefficients were found which gave good agreement between the scale model and the calculation results. (The way in which the numerical model handles scattering is described in Section III). The two sets of SPL estimates are shown in Figure 7, with the absorption and scattering coefficients used in the calculations both set at 0.2. The agreement seems to be good enough to warrant further comparisons of this type.

As yet, no attempt has been made to compare SPL estimates produced by the numerical model with the results of full scale experiments.

III. THE MODEL ALGORITHM

3.1 Assumptions

In addition to the two basic assumptions described in Section I, a number of other simplifying assumptions have been made and are listed below. None are essential; each could be eliminated with more programming effort, if tests of the model indicated that the increased complexity was worthwhile.

i. It is assumed that building facades can be characterized by a single absorption coefficient, valid at all frequencies, and at all angles of incidence. The frequency independence can be justified since only single-number A-weighted results are sought. The angle independence is included for simplicity; angle-dependent absorption could be included if necessary.

ii. Building facades contain irregularities, such as window bays, with length scales of the same order as the significant acoustic wavelengths. Some scattering is thus to be expected. The model takes account of this scattering by specifying a "diffuse scattering" coefficient, exactly analogous to the absorption coefficient. It is simply assumed that a specified fraction of the acoustic energy incident on a building facade is scattered uniformly in all azimuthal directions. This is the simplest possible model of the scattering process; a more elaborate model could be substituted if necessary.

iii. Air absorption is assumed to be negligible; this assumption

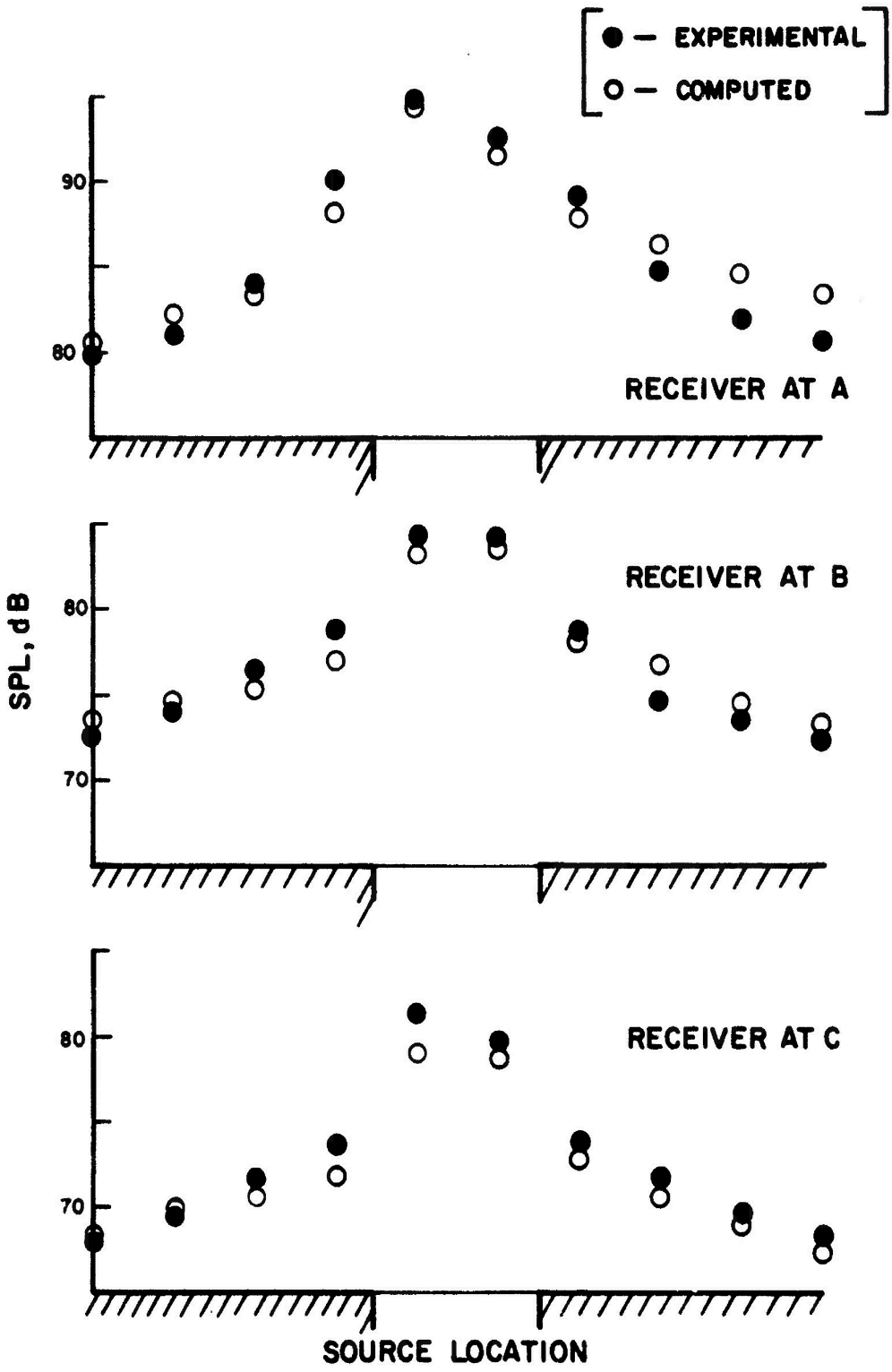

FIGURE 7: Comparison of Scale Model and Simulation Results

could easily be eliminated.

iv. Meteorological effects such as turbulence and wind shear are neglected.

v. The source is assumed to be omnidirectional.

3.2 The Structure of the Algorithm

For programming simplicity, the urban plan is adapted to a rectangular grid (see Figure 8). Building facades lie along grid lines, and each cell of the grid is either part of a street or of a building. All surfaces have the same absorption and scattering coefficients. It is also possible, in the interests of program efficiency, to define "sink" cells, which fully absorb all quanta entering them. The source is positioned at the center of one of the open cells. One or more of the remaining open cells are designated as receiver cells. All of this information, the size and shape of the basic cell, the location of built-on and sink cells, the absorption and scattering coefficients, the source and receiver locations, and information about the sound power level of the source is entered at a keyboard by the user.

The algorithm proceeds as follows:

i. A random number is generated to determine the direction in which the quantum is emitted.

ii. The location of the first cell boundary encountered by the quantum is determined. If this boundary lies within a street, the quantum continues (iii). If the boundary is an outer edge of the grid, the quantum is absorbed. If it is a building facade, another random number is generated to determine whether the quantum is reflected, absorbed or scattered: the probabilities of reflection, absorption and scattering are equal to the reflection, absorption and scattering coefficients. If it is scattered, a random number is generated to determine the direction of scattering.

iii. The location of the next cell boundary encountered by the quantum is determined. This process continues until the quantum is finally absorbed, whereupon another quantum is issued (i).

iv. Whenever a quantum passes through a receiver cell, its contribution to the cumulative energy density in that cell is determined (see 3.3 below).

v. Periodic tests are made to determine the stability of the estimates of the energy density in the receiver cells (see 3.4 below). When the desired convergence is achieved, computation stops and the results are printed. The calculation also terminates when a specified number of quanta (numbered usually in the tens of thousands) are issued

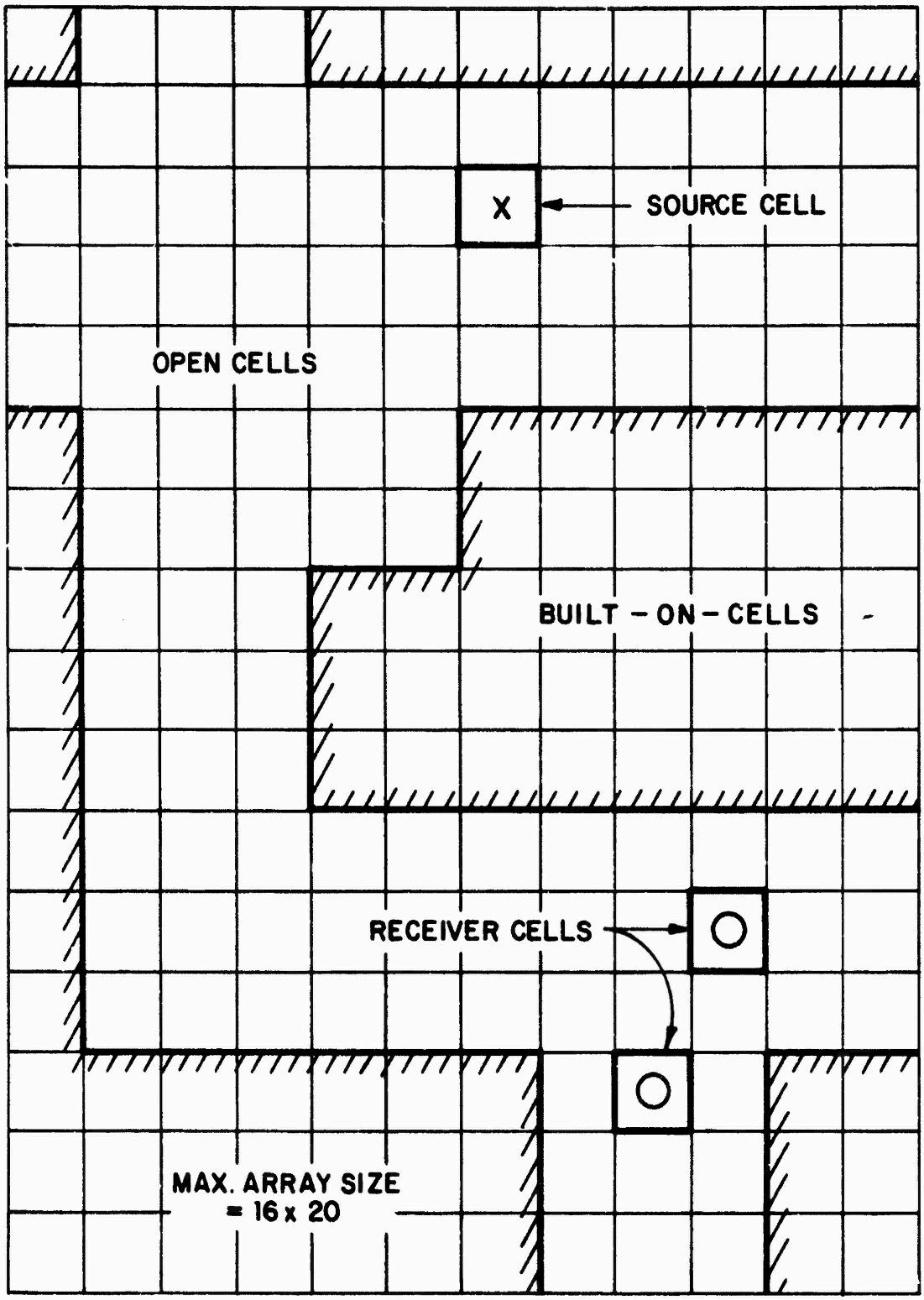

FIGURE 8: Cell Arrangement

without achieving the desired convergence.

3.3 Calculation of the Sound Pressure Levels

Suppose the acoustic source and the quantum source have the same power output P, and the same propagation velocity c. Let $P=\sigma E$, where E is the individual energy of the quanta, and σ is the rate at which quanta are emitted.

Consider first the simplest case of spherical spreading. At a distance R from the source, the acoustic energy density e is

$$e = P/(4\pi R^2 c) \tag{1}$$

The average number density of quanta is

$$n = \sigma/(4\pi R^2 c) \tag{2}$$

Thus the mean energy density associated with the quanta is

$$nE = \sigma E/(4\pi R^2 c) = P/(4\pi R^2 c) \tag{3}$$

- the same as the acoustic energy density, and independent of the actual quantum energy E.

In more complex situations such as explicit comparison is not possible, but the question remains as to how we relate the simulation results to the sound pressure levels.

Suppose that we observe the fate of a large number N of quanta emitted by the source; equivalently we are observing the radiation for a time $T=N/\sigma$. Suppose that the receiver cell of interest lies in the horizontal (x,y) plane, and has dimensions Δx, Δy, Δz. After travelling a distance R_j, one of the quanta enters this receiver cell. However, this quantum was emitted in a horizontal plane; an acoustic ray emitted at the same azimuthal angle would travel at some non-zero angle to the horizontal, and only enter the receiver cell with a probability which can be shown to be $(\Delta z/2R_j)$. Thus, we allow the quanta to decay, so that the energy they carry is proportional to $(\Delta z/2R_j)$.

In the time T let M quanta enter the receiver cell, and let each travel a distance ΔR_j before leaving. The average energy density in the cell in this time is thus:

$$e_1 = \frac{1}{\Delta x \Delta y \Delta z} \sum_{j=1}^{M} \frac{E\Delta z}{2R_j} \frac{\Delta R_j}{cT} \tag{4}$$

For the case of spherical spreading, the average energy density in a cell at distance R_o is

$$e_2 = \frac{P}{4\pi R_o^2 c} = \frac{NE}{4\pi R_o^2 c T} \tag{5}$$

The ratio of the two energy densities is:

$$\frac{e_1}{e_2} = \frac{2\pi R_o^2}{N\Delta x \Delta y} \sum_{j=1}^{M} \frac{\Delta R_j}{R_j} \tag{6}$$

- a result which does not depend on E, c, T or Δz. It is this normalized energy density which the simulation procedure calculates. (This is equivalent to measuring the sound power output of a truck as the SPL produced at a specified distance in an open field). Finally, we can make allowances for the fact that the cell dimensions may not be small compared to R_j. If the cell has sides a_x and a_y, and $R_j = A_j$ on entering the cell, B_j on leaving, then:

$$\frac{\bar{e}_1}{e_2} = \frac{2\pi R_o^2}{N a_x a_y} \sum_{j=1}^{M} \log_e \left(\frac{B_j}{A_j}\right) \tag{7}$$

-by averaging the energy density over the elementary cells of sides Δx, Δy.

3.4 Convergence

Each quantum radiated contributes an amount, e_j to the energy density in receiver cell. (In most cases, e_j will be zero). Successive values of e are uncorrelated random variables. We can estimate the mean energy density in the cell as being proportional to

$$e_m = e_t/N, \text{ where } e_t = \sum_{j=1}^{N} e_j$$

and N is the total number of quanta radiated. A sequence of numerical experiments in which N quanta are radiated will produce a sequence of estimates e_m. We only perform a single such experiment so that we cannot know the statistics of the estimate e_m. However, as we perform the experiment, we do accumulate information on the statistics of individual quantum contributions e_j, in particular the summed contribution e_t, and the sum of the squares of the contributions, say e_s. One can then show that an estimate of the variance v_e of e_m is:

$$v_e = e_m^2 \left[\frac{e_s}{e_t^2} - \frac{1}{N} \right]$$

This estimate of the variance is used to terminate the calculation. The user supplies a desired standard deviation for the estimate of the energy density in the receiver cell, normalized with respect to the mean energy density. The program periodically checks to see if the latest estimate of the variance meets the criterion. Computation is discontinued at any receiver cells which meet the variance requirement. Results are printed when all designated reeeiver cells have converged.

IV. PROGRAM OPERATION

The model is currently running on a 16 bit mini-computer. The computer cycle time is 1 μsec, and instruction execution times range up to 100 μsec for a floating point divide. The program and operating system occupy about 20 kilobytes of memory. Input/output is via a teletype.

The program is coded in Fortran, and should be usable on other machines with only minor modifications.

Execution times depend on the size and complexity of the urban plan, and on the accuracy desired. The effect of the size on the execution time is hard to quantify. A doubling of the desired accuracy quadruples the execution time, as one would expect. To illustrate the order of magnitude of execution times achieved, the results in Figure 2, with an error limit of 0.1 dB, were obtained in about 15 minutes; for the simpler configuration of Figure 4, execution times were one minute or less.

V. CONCLUSION

A working version of the numerical model is being used:

i. in development of the model itself -- possible extensions include provision for line sources, directional sources, ground reflections, etc.

ii. in basic studies of outdoor sound propagation, in support of scale model and field experiments, and

iii. in exploring the possibilities of using numerical models of this type in transportation planning in urban areas.

ACKNOWLEDGEMENT

This work was partially supported by DOT under contract DOT-TSC-93.

REFERENCES

1. Modig, Carl, "Directory of Computerized Noise Prediction Models", Informatics Inc. 1973.

2. Fishman, George S., Concepts and Methods in Discrete Event Digital Simulation, John Wiley, N. Y., 1973.

3. Donavan, Paul R., "Model Study of the Propagation of Sound from V/STOL Aircraft into Urban Environs", DOT Interim Report, Contract DOT-TSC-93, 1973.

SOUND PROPAGATION NEAR GROUND LEVEL IN THE VICINITY OF STREET INTERSECTIONS

by

Paul R. Donavan and Richard H. Lyon

Mass. Institute of Technology, Dept. of Mech. Eng.
Cambridge, Massachusetts 02139

Common vehicular noise sources once introduced into built-up urban areas produce sound fields considerably more complicated than those of the open area counterpart. These complexities can be characterized by a combination of simple divergence, local reverberation and building shielding. Previously, some of these effects have been experimentally quantified for several particular urban configurations [1,2]. However, only for the case of source and receiver both located in a single street has propagation been analyzed [3].

As a first step in an investigation of noise propagation in built-up urban areas, a study of noise propagation near street intersections is in progress. The particular situations considered are those of propagation down a street for a source located in a "four-way" or "tee" intersection, and propagation around a corner at both types of intersections. These cases have been investigated both with modeling studies and the conceptual tool of acoustical imaging. These results have been compared to existing published field data and found to be quite compatible.

The experimental portion of this investigation was conducted using a 1:32 scale model of an urban street intersection. The intersection, constructed from two-foot plywood boxes, could be readily modified to be either the four-way or tee intersections shown in Figure 1. For any given ratio of source street to receiver street width, a steady state noise source was successively moved to different positions in the source street while the sound level was measured in the receiver street. Levels for each source position were obtained in the receiver street at increments of 1 street width, up to 14 street widths away from the intersection. The relative source-receiver positions are indicated in Figure 1.

Since acoustic modeling requires the maintenance of the ratio of acoustic wavelength to geometric length, the modeling frequencies were 32 times full scale frequencies. For this study, the full scale frequencies dominate in typical "A-weighted", urban noise were of interest, hence measurements were made in 8, 16 and 31.5 kHz octave bands. Simulating typical urban environments, materials which are acoustically hard at these higher frequencies were selected for the model. The noise source used was a small air jet impinging on a circular plate which produced broad-band, high frequency noise and was omnidirectional in the horizontal plane. Sound levels were monitored with a 1/10 inch microphone.

With this experimental arrangement two sets of experiments were performed. The first was conducted with a smooth building wall model which although corresponds to some full size buildings is not generally common in urban areas. In the second set, the smooth walls were replaced by walls

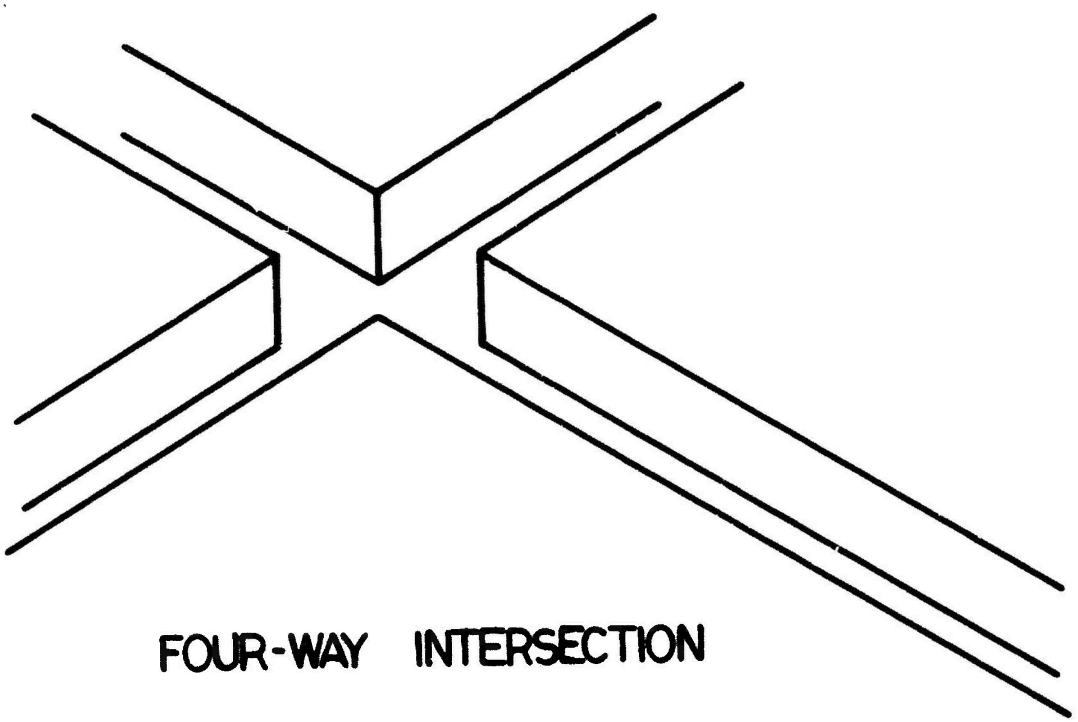

FOUR-WAY INTERSECTION

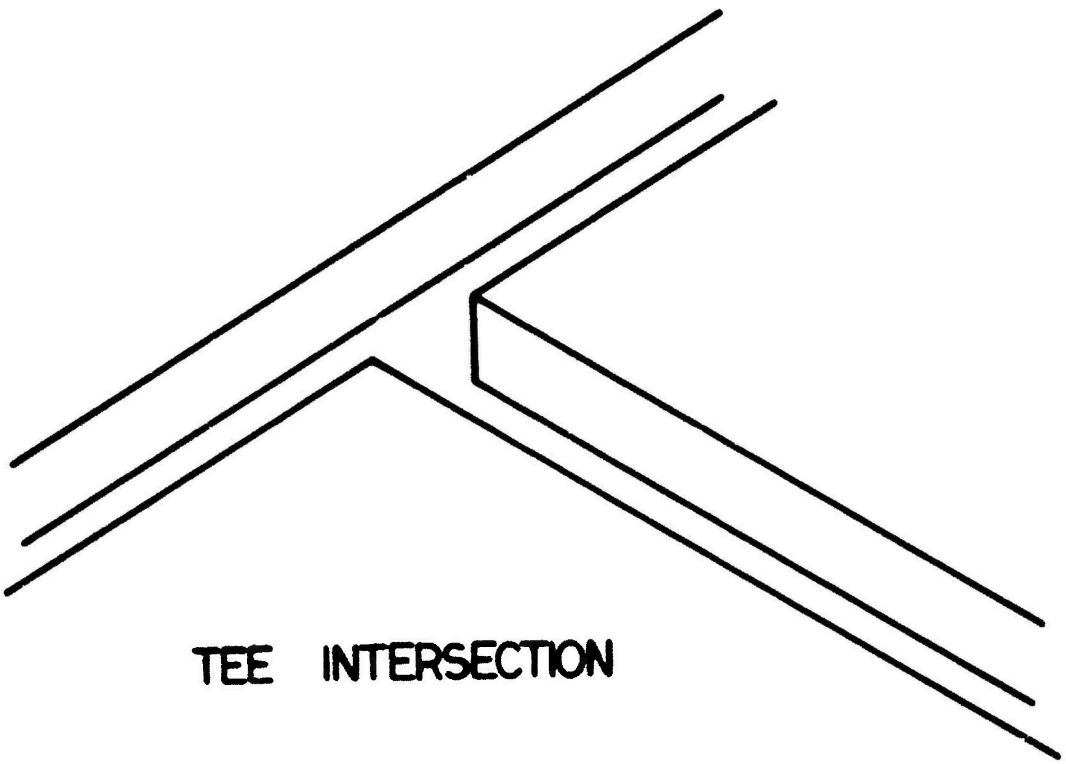

TEE INTERSECTION

FIGURE 1: INTERSECTION CONFIGURATIONS

with modeled building facades. The facade structure modeled was that of vertical protrusions, typically of 4 to 12 inches, between columns of windows. Application of this type of facade to the urban model resulted in the geometry shown in Figure 2. From this figure, it should be noted that the geometry of the protrusions is on the order of an acoustic wavelength for the three octave bands of concern. Thus the scattering properties of the walls and their effect on propagation are not readily predictable [4].

A useful technique for the evaluation of sound propagation in urban areas is the acoustic imaging of source and receiver. This technique is appropriate in those cases where the simplification of geometrical acoustics is appropriate, that is, when the acoustic wavelength is much smaller than typical geometric length [4]. This criterion is generally satisfied at most urban noise frequencies as street widths are on the order of 50 feet or more. Acoustic imaging is applied to urban propagation by representing each reflected path between source and receiver by a corresponding image source or image receiver as dictated by the street configuration.

As an illustration of the use of imaging, the case of sound propagation around a corner at an intersection as shown in Figure 3. In this example, a semi-infinite array of image sources is produced perpendicular to the source street starting at the wall furthest from the receiver street. This array accounts for all possible reflected paths by which sound could be introduced into the cross street. Since sound entering the receiver street can also be reflected before reaching the receiver, a semi-infinite array of image receivers is also necessary. This array runs perpendicular to the receiver street and extends away from the source street. The reflecting paths which contribute to the total sound pressure at a given receiver point are thus straight lines drawn between source (or image source) and receivers. These lines are, however, constrained to pass through the opening to the receiver street and for the source images, to pass through the reflecting wall on the source street. The total sound pressure level is thus found by summing all contributions incoherently [5]. A little more sophistication can be added to this technique by allowing for partial absorption of the incidence sound at each reflection. This leads to semi-infinite, exponentially decaying source and receiver image arrays.

A second example of imaging applied to urban propagation is afforded by considering a source located in a tee intersection as depicted in Figure 4. For this configuration, arrays of image receivers extend in both directions perpendicular to the receiver street while there is only one image source. The contributing reflecting paths in this case are determined solely by the criterion of passage through the receiver street opening.

For the purposes of analyzing urban propagation, the image methods described above are carried out by computer. In considering the results of such analysis, it must be kept in mind that the method is based on ray acoustics, hence diffraction effects which may occur at particular source-receiver geometries are not taken into account.

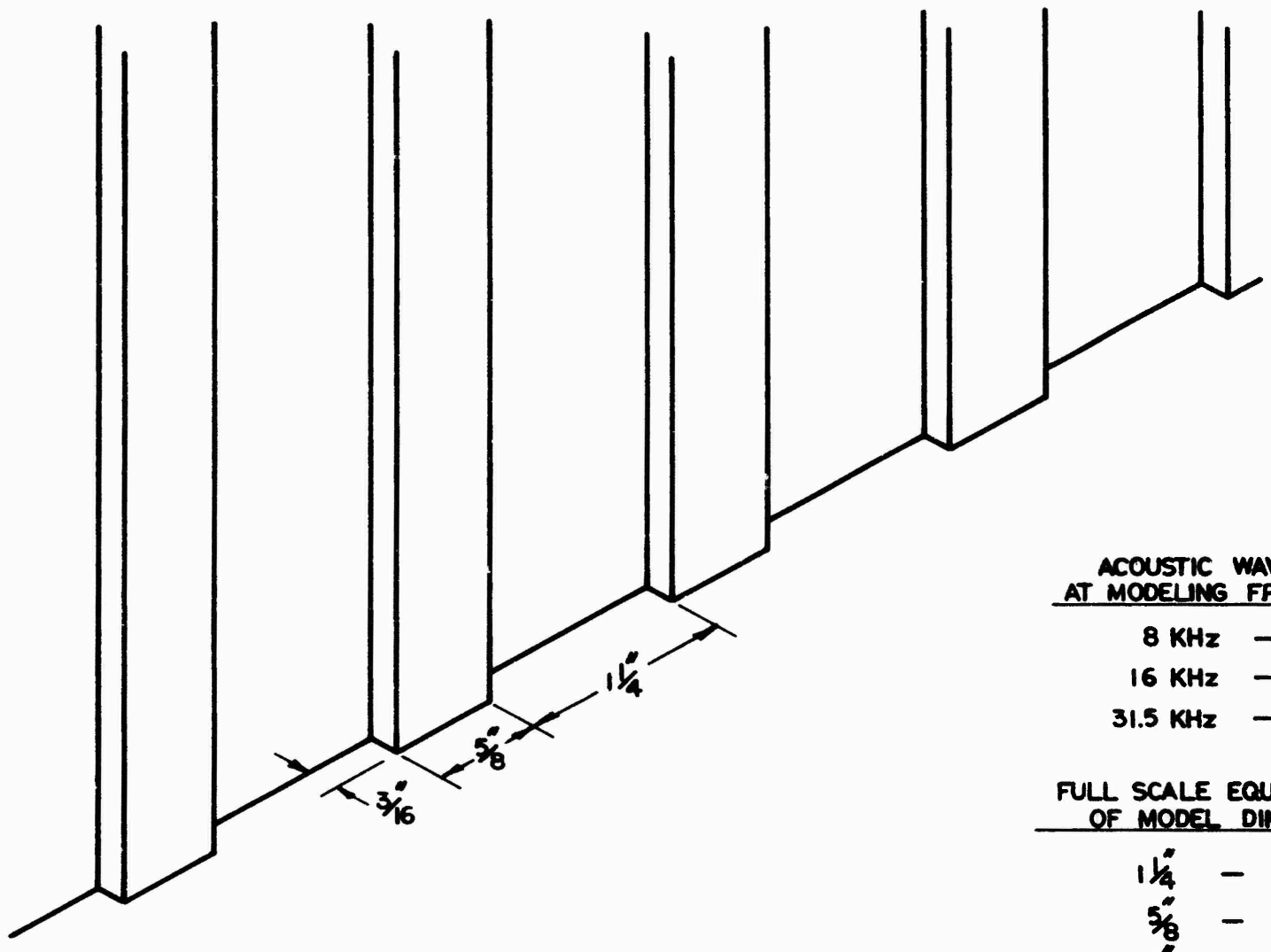

ACOUSTIC WAVELENGTH AT MODELING FREQUENCIES:

8 KHz — 1¾"
16 KHz — ⅞"
31.5 KHz — 7/16"

FULL SCALE EQUIVALENTS OF MODEL DIMENSIONS:

1¼" — 3'-4"
⅝" — 1'-8"
3/16" — 6"

FIGURE 2: BUILDING FACADE MODEL

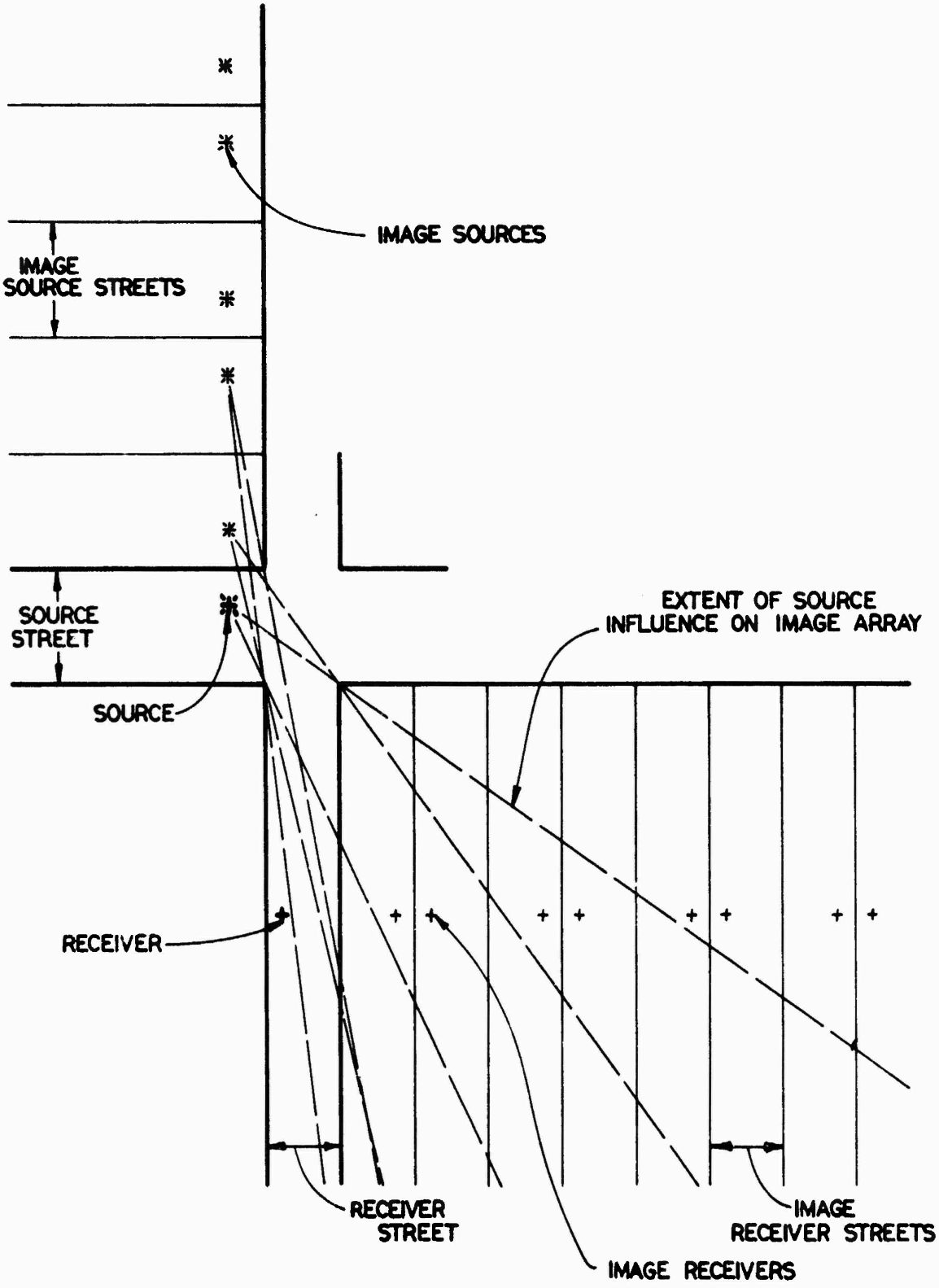

FIGURE 3: IMAGING AT A FOUR-WAY INTERSECTION

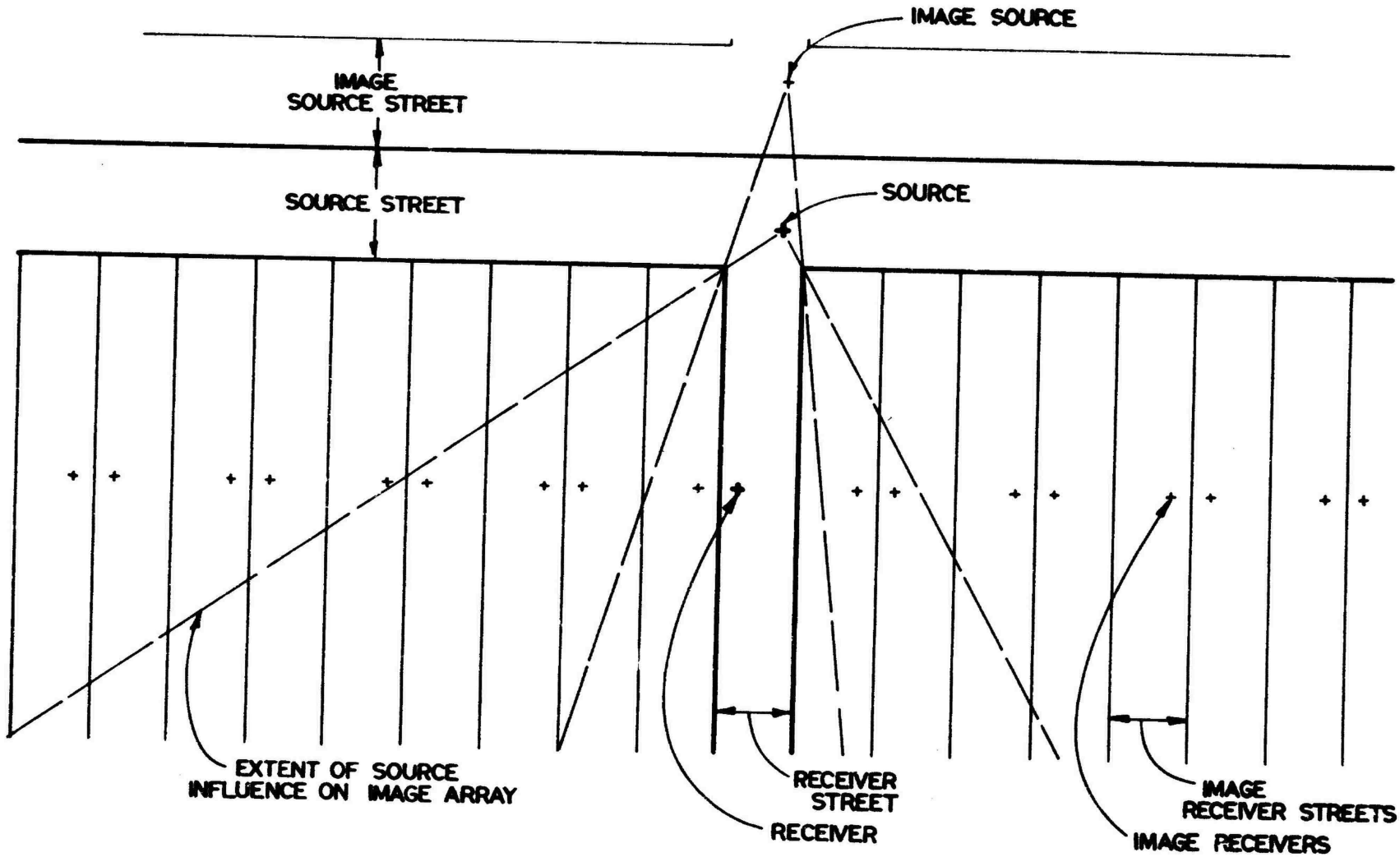

FIGURE 4: IMAGING AT A TEE INTERSECTION

A typical set of results for a source located in a smooth wall intersection is given in Figure 5. The levels in each frequency band as well as those generated by the computer have been normalized to a free field source level of 105 dB at 2 feet. Although there is appreciable scatter in the model results, there is indication that a straight line with slope of about -3.5 dB per doubling of distance (dd) from the source approximates the data. Decay rate is quite consistent with that found by Schlatter [3] for a street with finite wall absorption, and corresponds to the decay with distance expected for a line source [6]. It should be also noted that the computed levels agree fairly well with the measured and that there is no decipherable frequency dependence in the results. The tendency to -3.5 dB/dd indicated by this figure was found not to vary with source street width, source position in the intersection, or receiver position at a given receiver street cross-section. Further placing the source in a tee intersection merely raised sound levels uniformly 1 to 2 dB all along the street leaving the slope the same.

As would be expected, as the source moves out of the intersection and into the cross-street the situation changes markedly. Figures 6 and 7 present smooth wall results for source locations of 1/3 and 1 2/3 street widths into the source street. The sound levels shown were all taken near the receiver street center line as it is found that the sound levels become uniform on a receiver street cross-section within two street widths from the intersection. In both figures, there is a distinct frequency dependence which was absent for the source-in-intersection case. Using Pierce's finite barrier theory [7], this dependence can quantitatively be attributed to diffraction around the corner. The computed results for this situation follow the higher frequencies quite closely further indicating the presence of diffraction effects.

The results of Figure 6 and 7 were normalized as before and distance was again taken to be distance from the source. The approximate slope of -5.5 to -6.0 dB/dd for the higher frequencies indicated in Figure 7 was found to hold generally for source positions greater than 1/2 street width into the source street. With this result in mind, Figure 6 indicates that for source positions very near the intersection, decay down the receiver street has two regions: the first region is like that of the source in the intersection, -3.5 dB/dd, the second like that of Figure 7, -5.5 to -6.0 dB/dd. This result also agrees quite well with that obtained by Schlatter [4] for in-street propagation with finite wall absorption. Schlatter obtained a decay of -3.0 dB/dd to a point specified by the amount of wall absorption and then a transition to -6.0 dB/dd.

The addition of building facades to the modeled intersection significantly altered the distribution of sound down the receiver street. An an indication of this effect, the smooth-wall, around the corner propagation case presented in Figure 6 for a source 1/3 street width in the source street is shown again in Figure 8. The corresponding results from the facaded model are also presented. This figure has several interesting features worthy of note. The first of these is that the levels at distances of 4 or more street widths are much lower relative to the smooth-walled values, on the order of 5 dB or 8 and 31.5 KHz and 10 dB for 16 KHz. A second feature is a frequency dependence different from that

FIGURE 5: SOUND LEVELS DOWN STREET -- SOURCE IN INTERSECTION

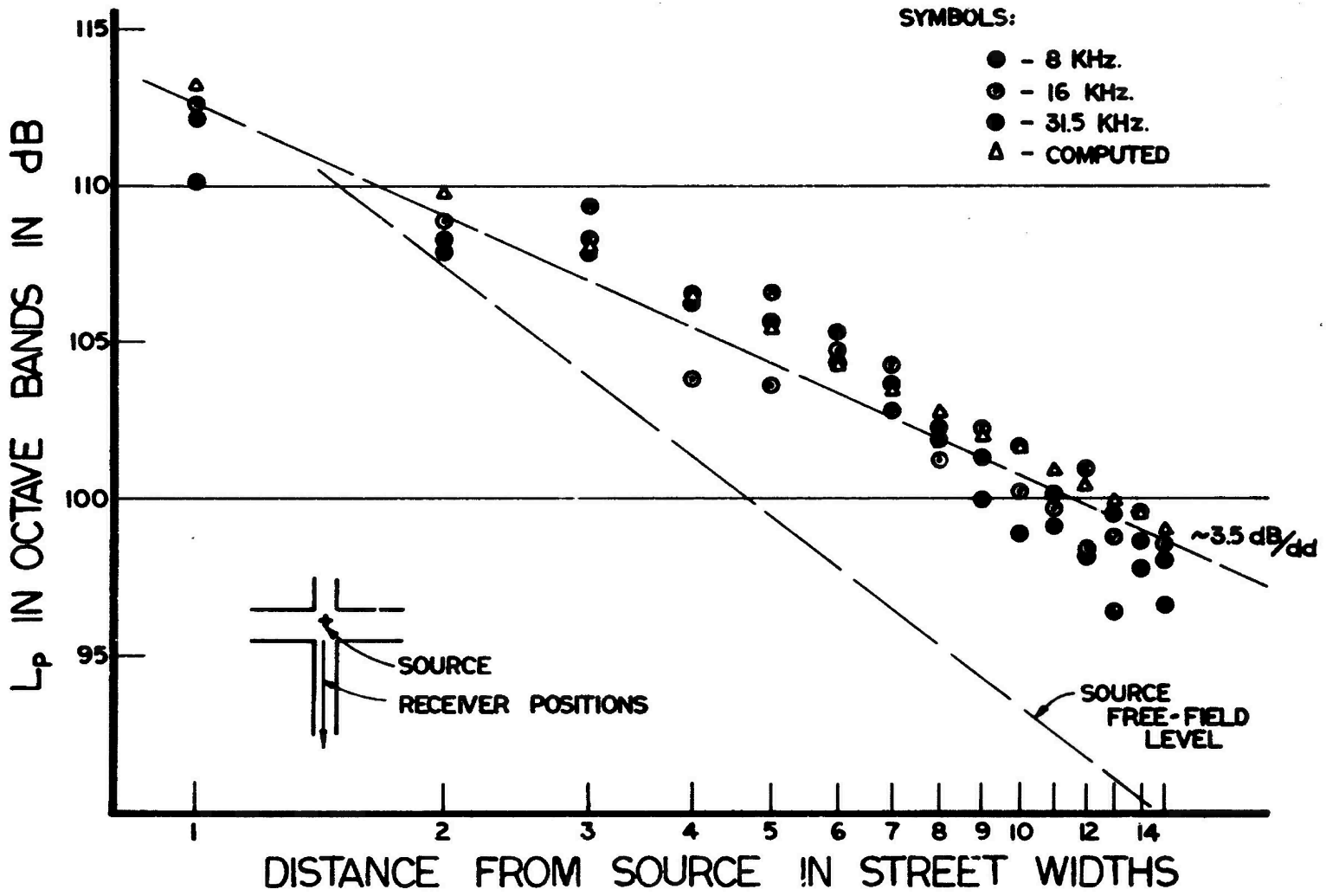

FIGURE 6: SOUND LEVELS DOWN STREET -- SOURCE OUT OF INTERSECTION

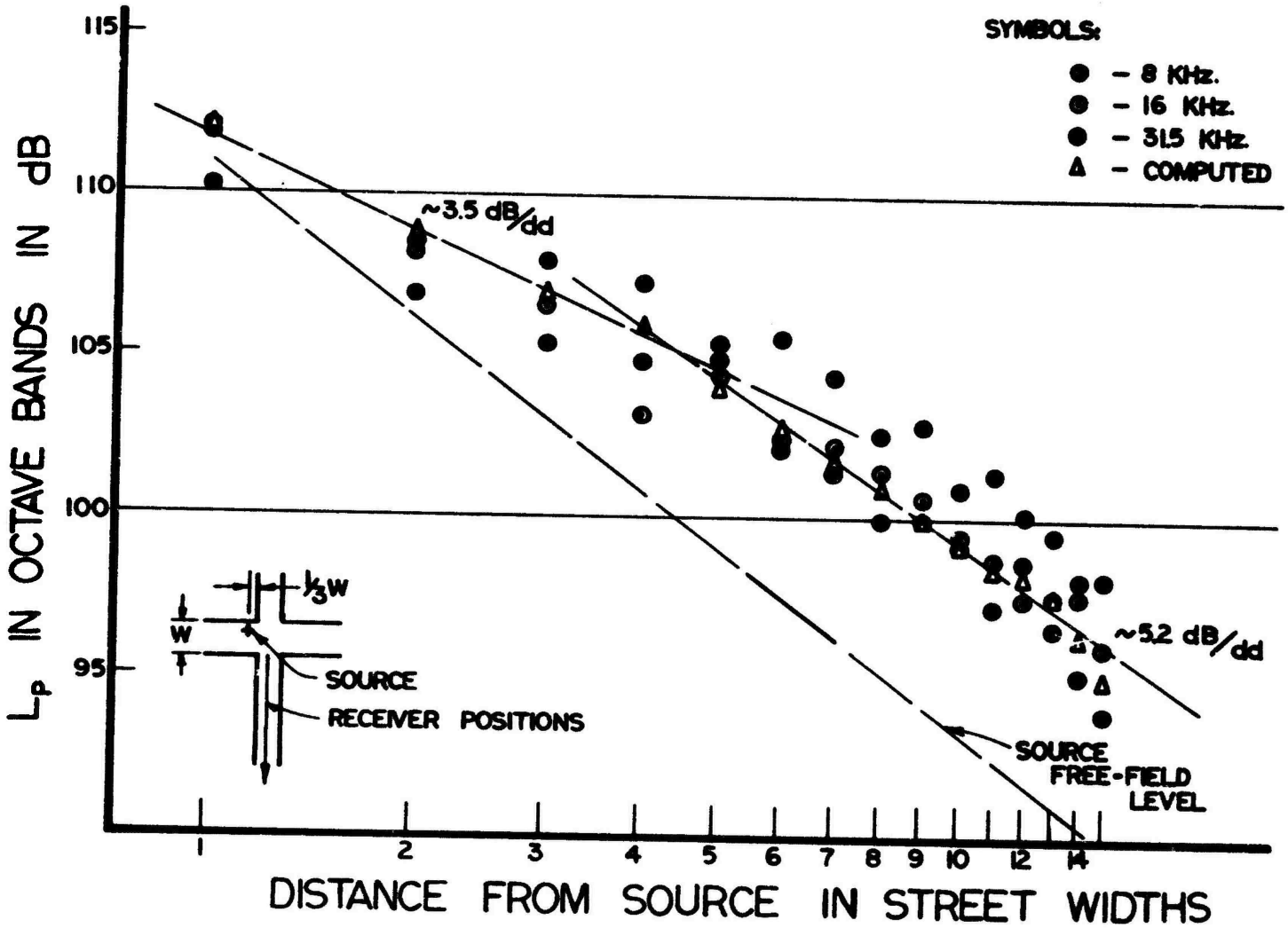

FIGURE 7: SOUND LEVELS DOWN STREET-- SOURCE OUT OF INTERSECTION

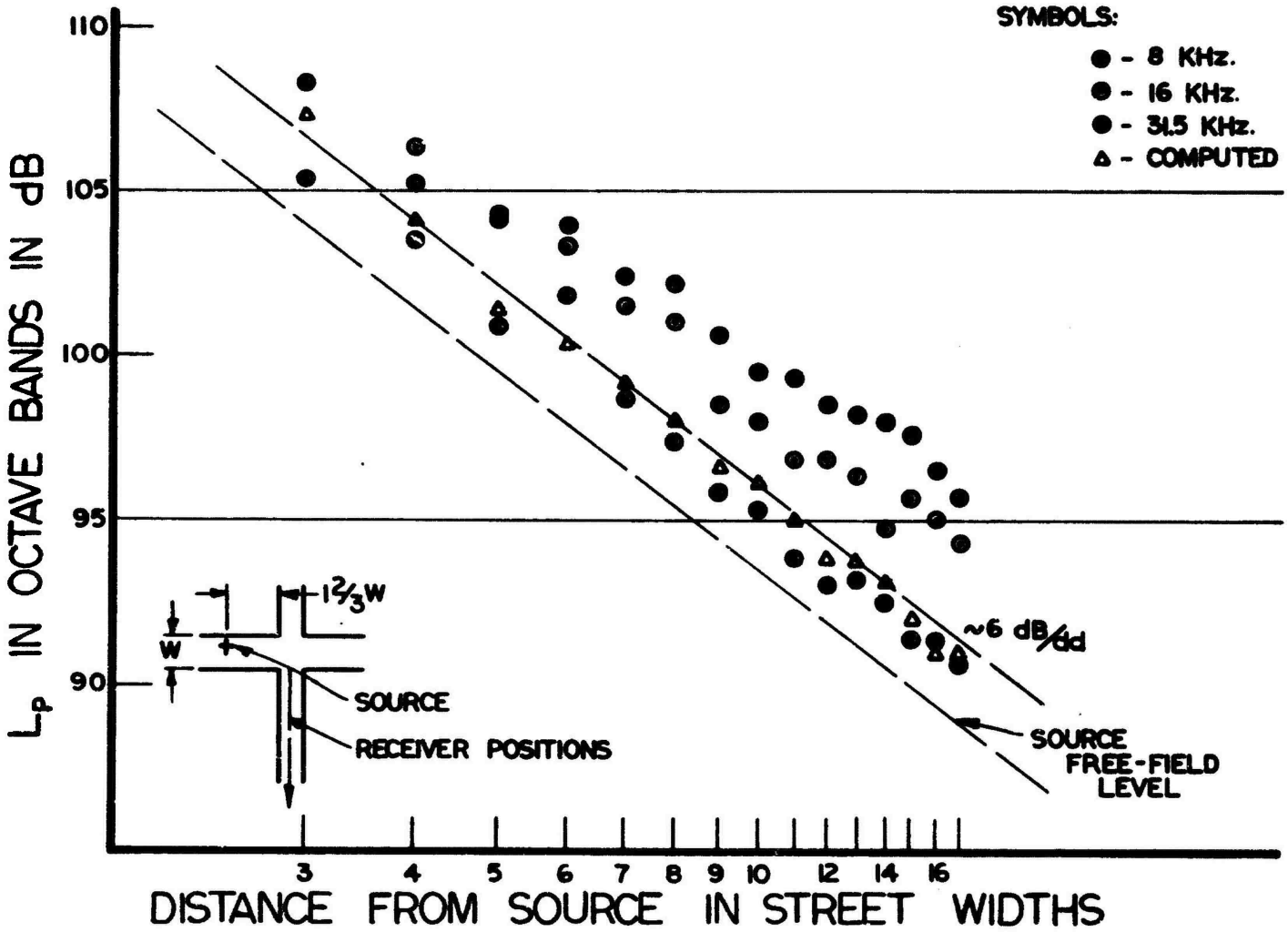

FIGURE 8: SOUND LEVELS DOWN STREET-- SMOOTH WALL & FACADED INTERSECTIONS

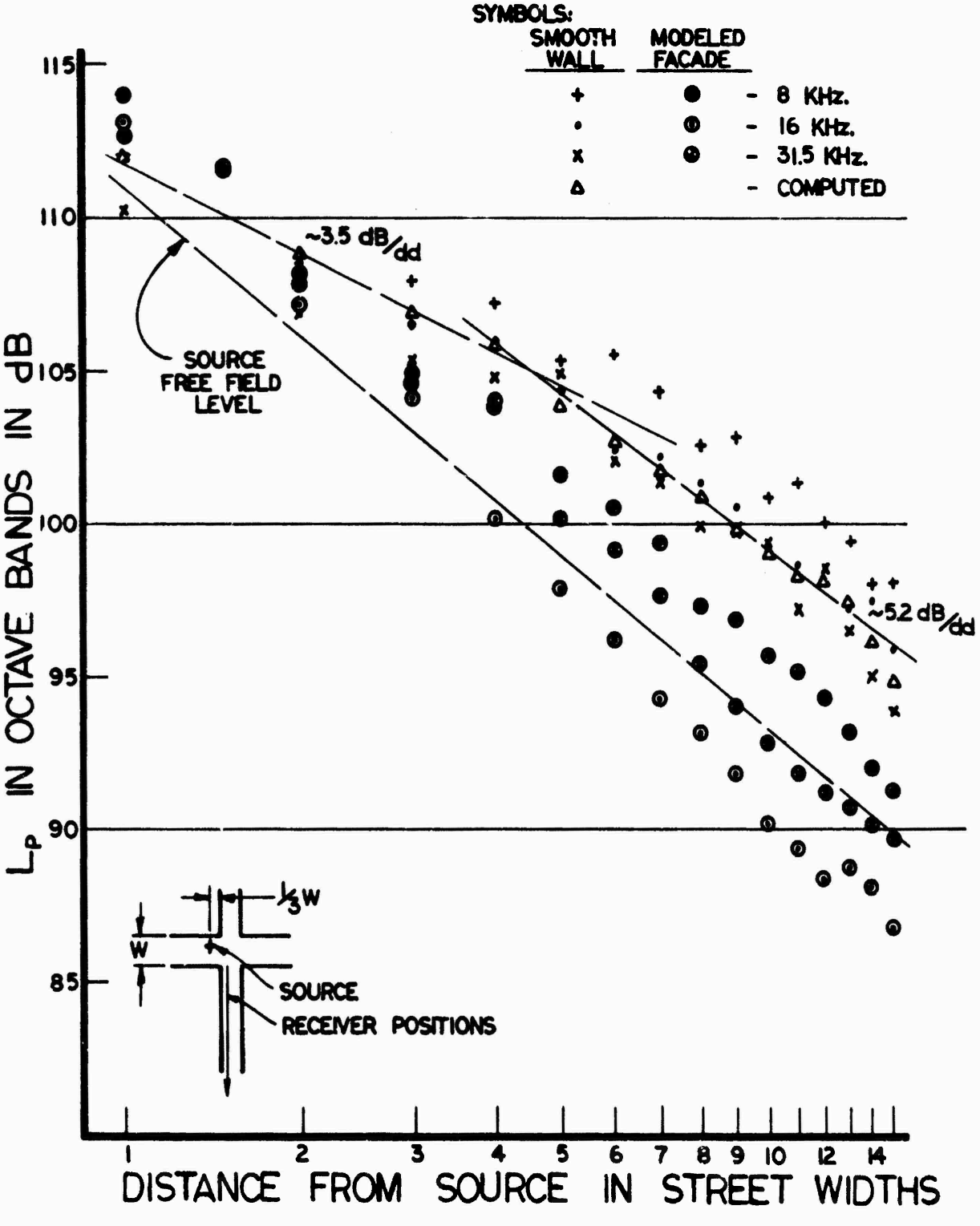

due to diffraction alone, particularly for the 16 KHz octave band. Another feature seen in this figure is the local amplification above that of the smooth-wall results for receiver positions within the first street width of the intersection. This result is indicative of back-scattering from those protrusions further down the receiver street. This effect can be considered as a retention of acoustic energy near the head of the street at the expense of energy further the down street due to scattering from the building surfaces.

Another method of presenting the facaded-wall results is to plot sound level versus distance from the entrance of the receiver street. Figure 9 presents results in this manner for the two cases of a source in the intersection and of a source 3/4 street width into the source street. The results for both of these cases exhibit initial decay with distance of -2.5 to -3.0 dB/dd and a transition to a decay of about -7.0 to -9.0 dB/dd. This behavior is identical with that found by Delany, Copeland and Payne [1], who conducted field measurements of sound level down a side street from an intersection with a main street containing freely-flowing traffic. In their investigation, sound levels down the side street were referenced to a microphone at the intersection. In plotting level versus distance from the reference microphone, their data indicates an initial scope of -3.0 dB/dd with a transition to -8.0 dB/dd.

The investigation of sound propagation in vicinity of street intersections is not yet completed. Field measurements testing the type of configurations discussed in this paper are planned with particular attention to be given to the nature of scattered reflection from building surfaces. Also, more extensive model testing and computer analysis is to be continued.

FIGURE 9: SOUND LEVELS DOWN STREET -- MODELED FACADE INTERSECTION

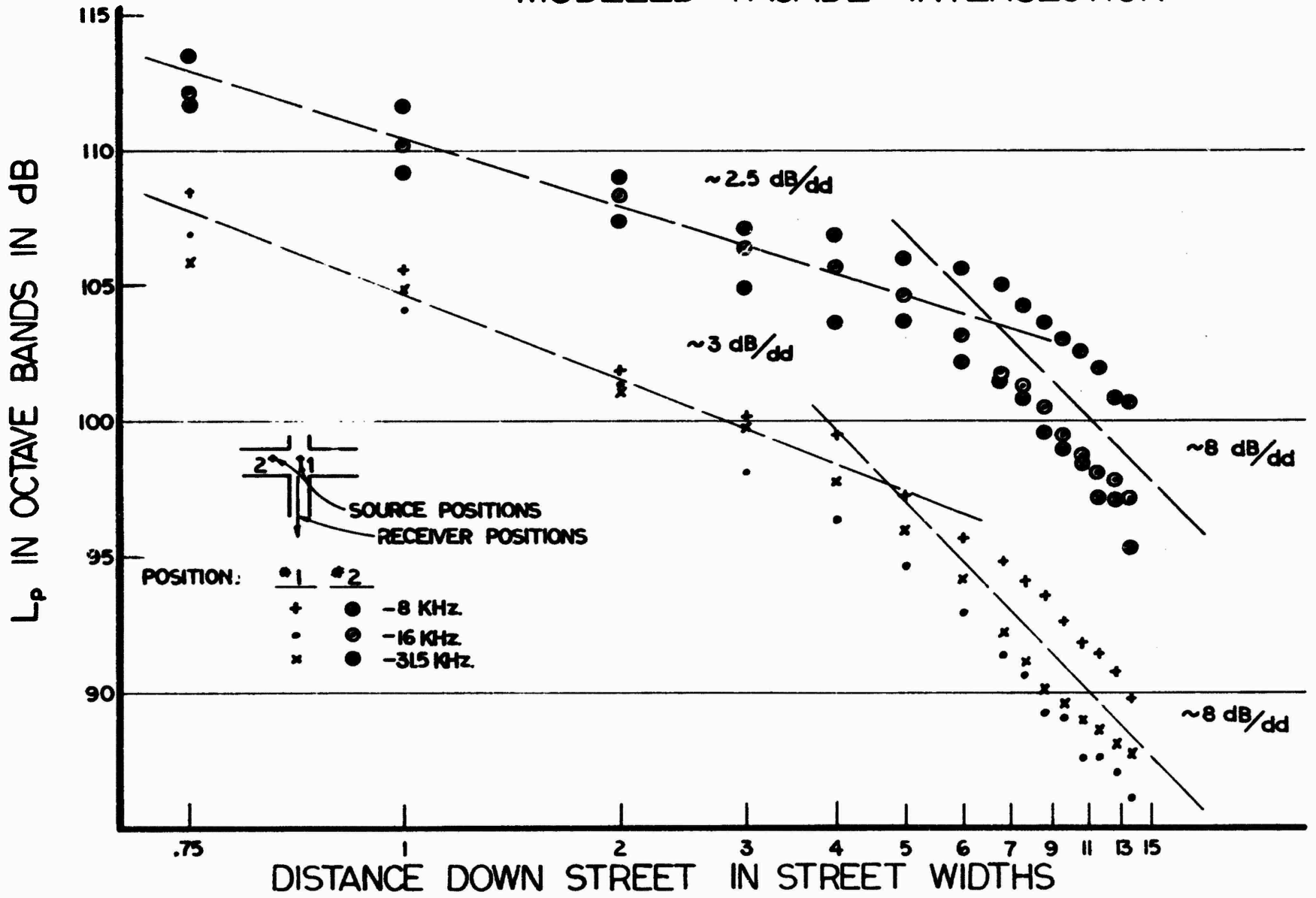

REFERENCES:

1. Delany, M.E.; Copeland, W.C., and Payne, R. C.; "Propagation of Traffic Noise in Typical Urban Situations", NPL Acoustics Report, No. Ac54, October, 1971.

2. Delany, M.E.; Rennie, A.J.; and Collins, K.M.; "Scale Model Investigations of Traffic Noise Propagation," NPL Acoustics Report, No. Ac58, September, 1972.

3. Schlatter, W.R., "Sound Power Measurement in a Semi-Confined Space" M.Sc. Thesis, Massachusetts Institute of Technology, Cambridge, Mass., July, 1971.

4. Morse, P.M. and Ingard, K.U., Theoretical Acoustics, McGraw-Hill Book Co., 1968, pp. 441-449, 576-577.

5. Beranek, L.L., Noise Reduction, McGraw-Hill Book Co., 1960, p.55-60.

6. Lyon, R.H., Lectures In Transportation Noise, Grozier Publishing, Inc., 1973, pp. 23-24.

7. Pierce, A.D., "Noise Diffraction: Suggested Estimation Procedures", Inter-Noise 72 Proceedings, October 4-6, 1972, pp. 110-115.

A MODEL STUDY OF THE PROPAGATION OF SOUND FROM V/STOL AIRCRAFT INTO URBAN ENVIRONS

by

Paul R. Donavan and Richard H. Lyon

Mass. Institute of Technology, Dept. of Mech. Eng.
Cambridge, Massachusetts 021

This paper is addressed to the problem of noise intrusion into urban areas from low altitude V/STOL aircraft operations. It is clear that for such propagation situations, simple geometric divergence is not a realistic approximation due to local amplification and shielding effects within the area. This assumption has indeed been borne out in earlier work concerned with this problem. [1, 2, 3] The current investigation has quantified these amplification and shielding effects and has developed three methods for sound level prediction. These methods include direct acoustic modeling, the use of an experimentally obtained average amplification factor, and the use of a derived theoretical propagation model. From the experimental results obtained in the development of these methods, and with basic psychoacoustic considerations, the perceived noise intrustion aspects of V/STOL operations have also been determined.

Originating in architectural acoustics, acoustic modeling has become increasingly popular in studying transportation noise propagation. Maintaining the constancy of the ratio of wavelength to geometric length, acoustic modeling can be applied to a wide variety of situations as long as air absorption effects are corrected for [2]. It is especially suited for use in urban propagation since typical urban structures are made of materials which are nearly perfectly reflecting and, hence, easily simulated at the higher modeling frequencies.

In order to form a link between field and model data, helicopter street flyover experiments performed by Kinney and Pierce [3] at Summer Street in downtown Boston were duplicated with a 1 to 64 scale model. A typical time history from this field study is presented in Figure 1, along with the time history of a similar open field flyover. A corresponding model time history is also included in this figure. The 1 to 64 scale model of the field experiment was constructed with plywood boxes placed on a linoleum floor in a room anechoic at modeling frequencies. The noise source used consisted of four impinging air jets shown in Figure 2. This source produced intense broad-band noise from 8 to 125 kilo-hertz and was found to be omnidirectional in the plane of the impinging jets. To simulate the field experiments, the source was passed over the model street with the use of a cart-I beam arrangement. The results in terms of maximum transmission gains relative to similar open field flyovers are presented here in Table 1 for both sets of experiments. The results of this comparative study indicated rather good agreement between field and model studies.

In order to obtain results for a more general urban situation, the 1 to 64 scale model was extended so that propagation into an area could be considered. The resulting model is shown in Figures 3 and 4.

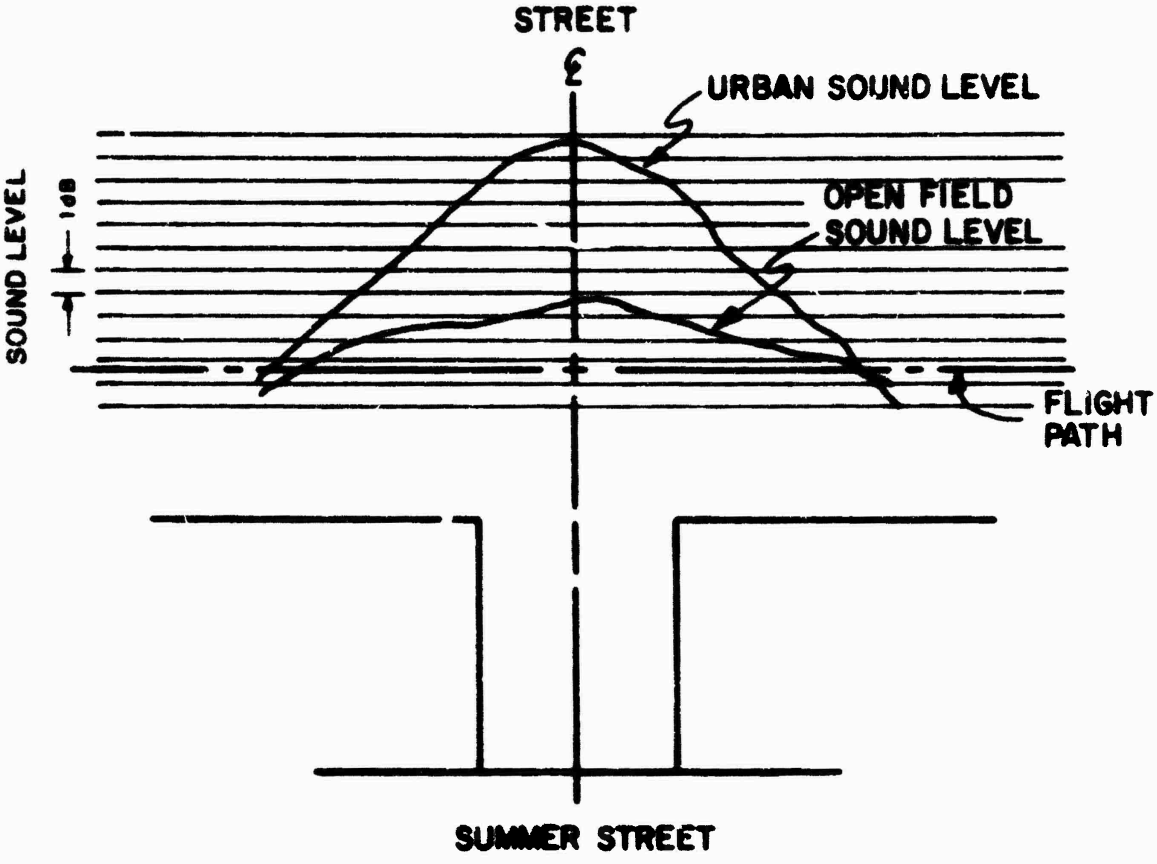

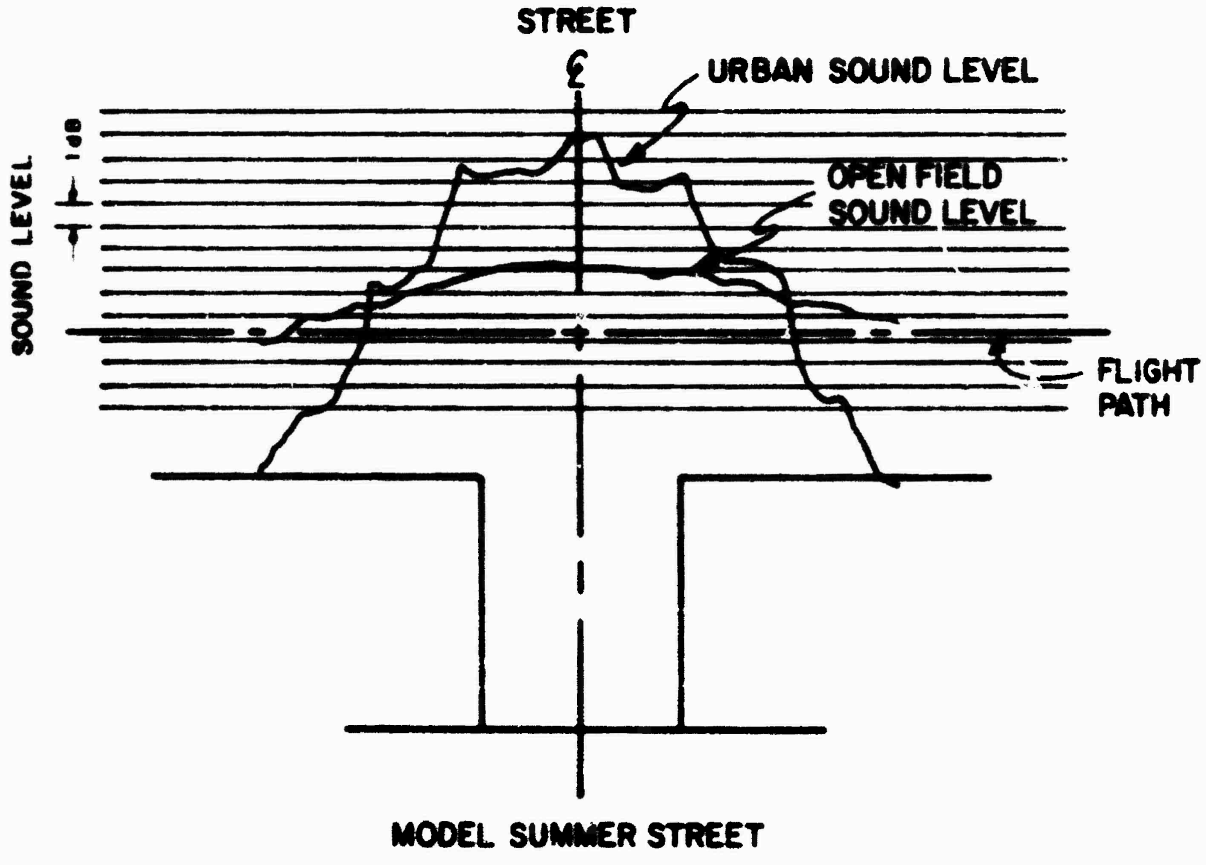

Fig. 1 Comparison of [illegible] & model data

FIGURE 2: AIR JET NOISE SOURCE

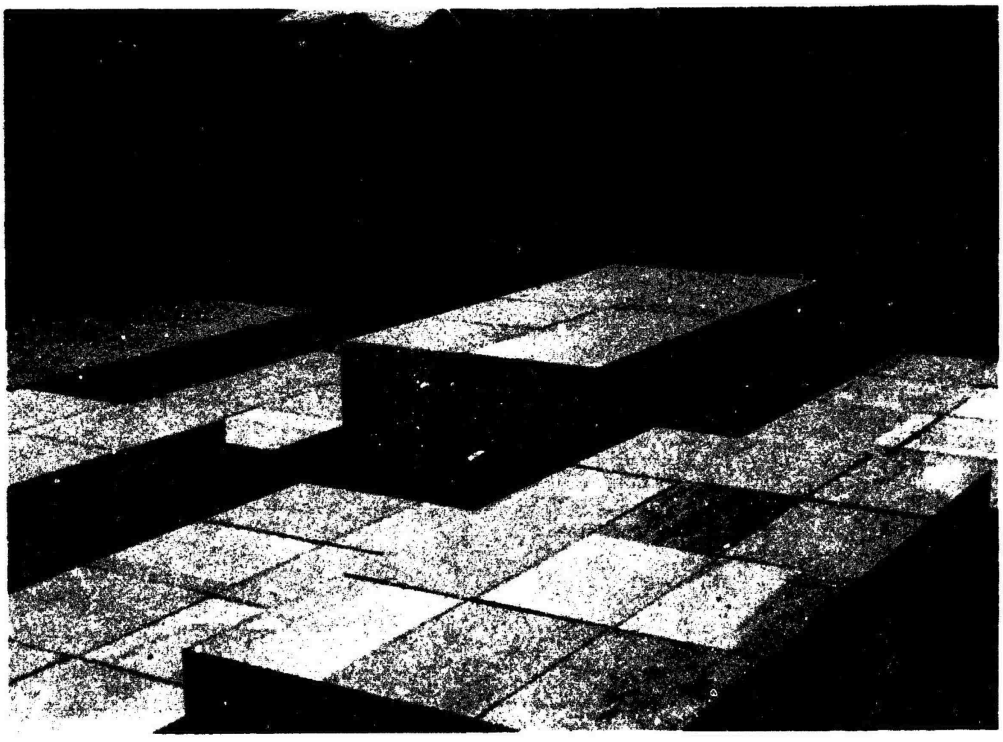

FIGURE 4: URBAN MODEL

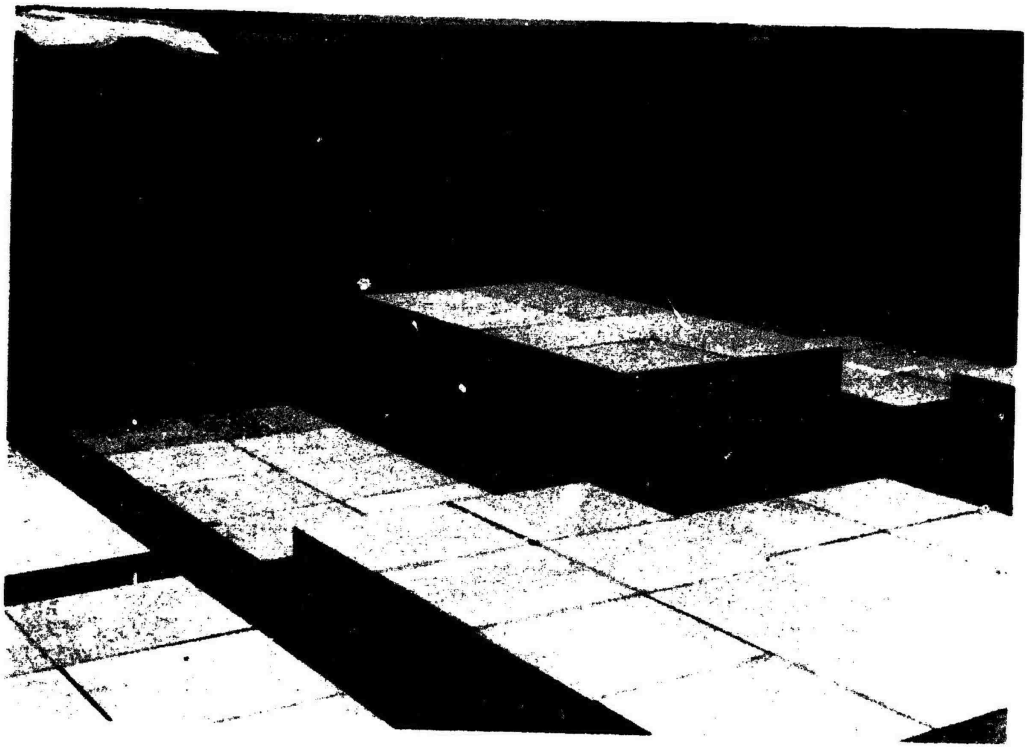

FIGURE 4: URBAN MODEL

Simulating a flyby of a V/STOL aircraft, the air jet source was moved past the model while the sound level time history was monitored at positions in the city. To eliminate source power level dependence, the data generated by the fly-bys was reduced to transmission gain time histories where transmission gain was defined simply as the difference between the measured urban levels and corresponding open field levels. By considering the maximum transmission gain at points through the model city, and averaging over these values for each street, the average sound enhancement in each street was obtained and is shown in Figure 5. The standard deviations corresponding to these averages are also included in this figure. The figure indicates a uniformity of maximum transmission gain in all three streets running perpendicular to the flight path. This observation leads to the general approximation that the transmission gain relative to an open field sound level is about 4 to 4 1/2 dB for flight path altitudes from 1 1/2 to 4 1/2 times the surrounding building height and for propagation up to about 2000 ft into the city for streets perpendicular to the flight path.

As it is clear that not all urban situations will fall neatly into the geometric range in which this average result is valid, and since it is not desirable to build models for each new situation, a theoretical propagation model was developed. The technique used in this development was that of acoustic imaging [4]. For a source and receiver located in a street, the multiple reflections from the building faces can be idealized as an array of image receivers, or equivalently sources set up perpendicular to the building surfaces. Thus, a receiver located in the street may look through the building walls and see a row of images of decreasing strength going out infinitely in each direction as shown in Figure 6. As the receiver moves out of the street, although the source image array remains, the receiver can now only see a portion of the array since the edges of building walls limit the view. Determining the sound level for receiver points outside the street is thus a matter of using geometry to find how many images are seen and then summing their source strengths incoherently [5].

This theoretical propagation model was used to predict transmission gain time histories for several of the model fly-bys. A comparison of these predicted and measured time histories are afforded in Figures 7 and 8. It is seen that the measured values closely follow the predicted and that the predicted values generally set the upper bound on transmission gain.

To assess perceived noise intrusion into an urban area from a V/STOL fly-by, it is not only necessary to know the sound level time history of the event as heard in the street, but also to have some quantitative idea of how this noise will be perceived. To obtain such an understanding, three representative A-weighted time histories were computed from the fly-by data for a predicted helicopter spectrum [6]. These time histories are shown in Figure 9 along with the corresponding receiver positions which produce them.

In considering these histories, there are four items which are known to be important in terms of the loudness perceived by an observer. These are: durational effects, onset duration effects, startle effects, and the presence of pure tone components [1]. Of these items, only the first two, event duration and onset duration were found to be of importance in normal V/STOL

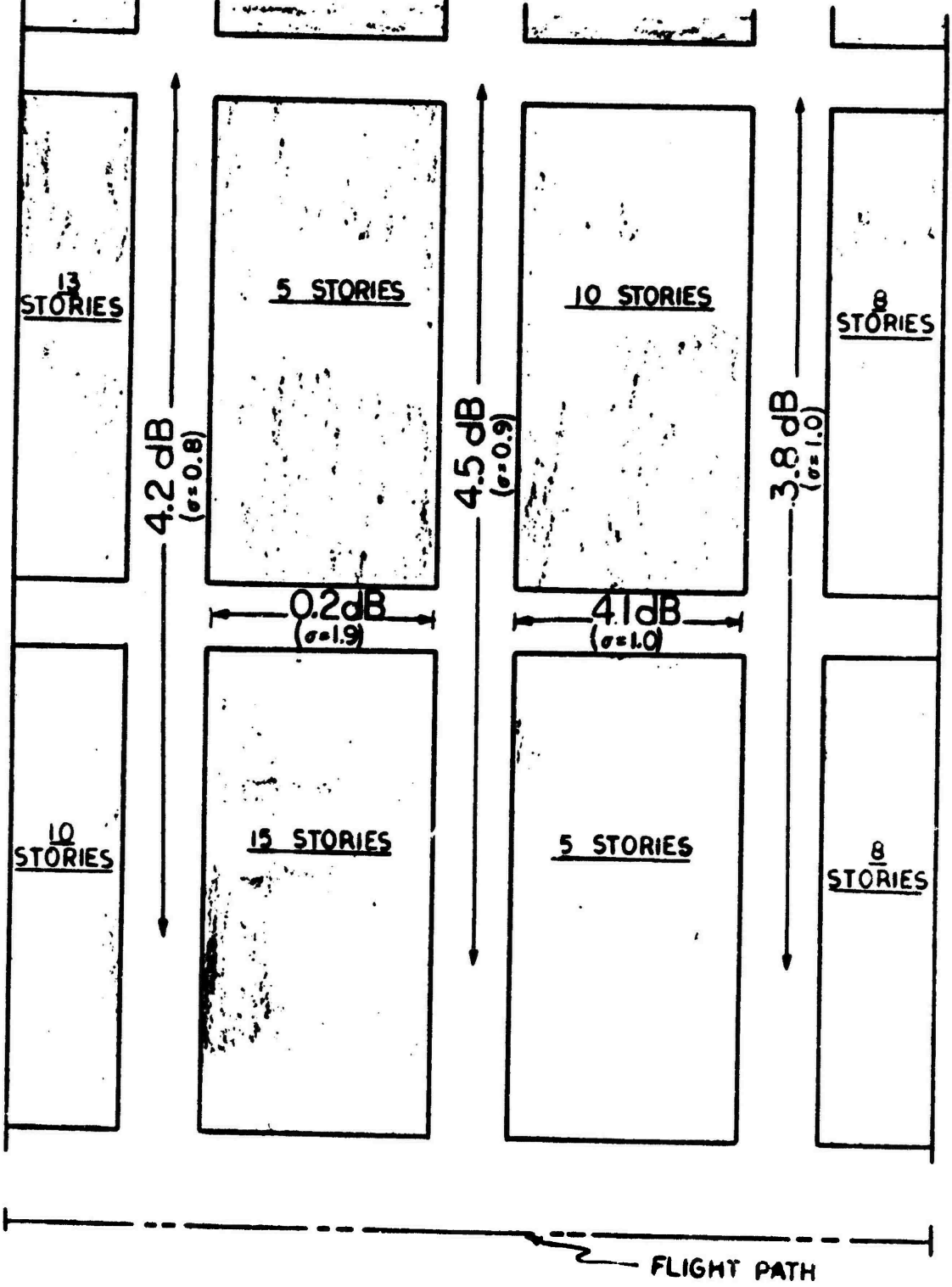

Fig. 5: Street averaged maximum Transmission Gain [TG]

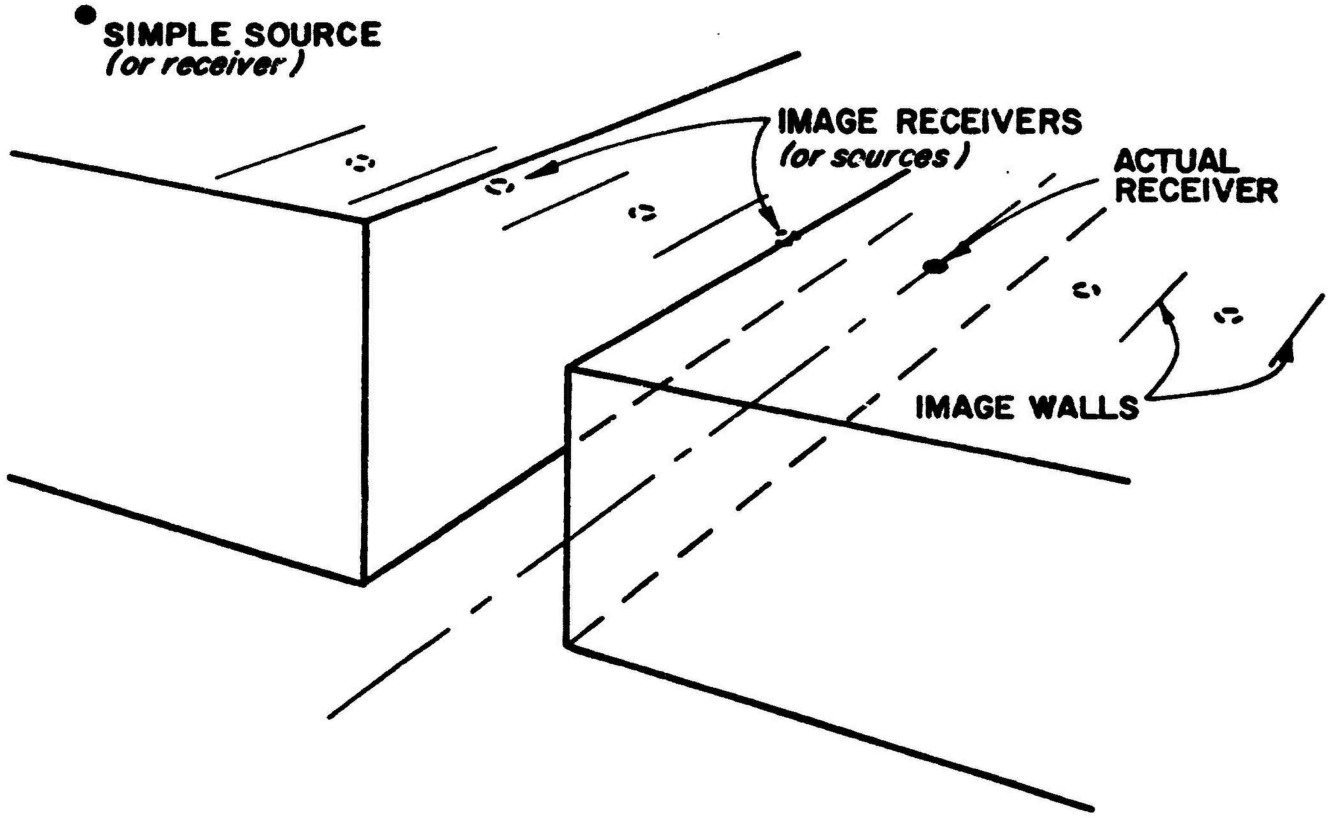

Fig. 6: Array of images

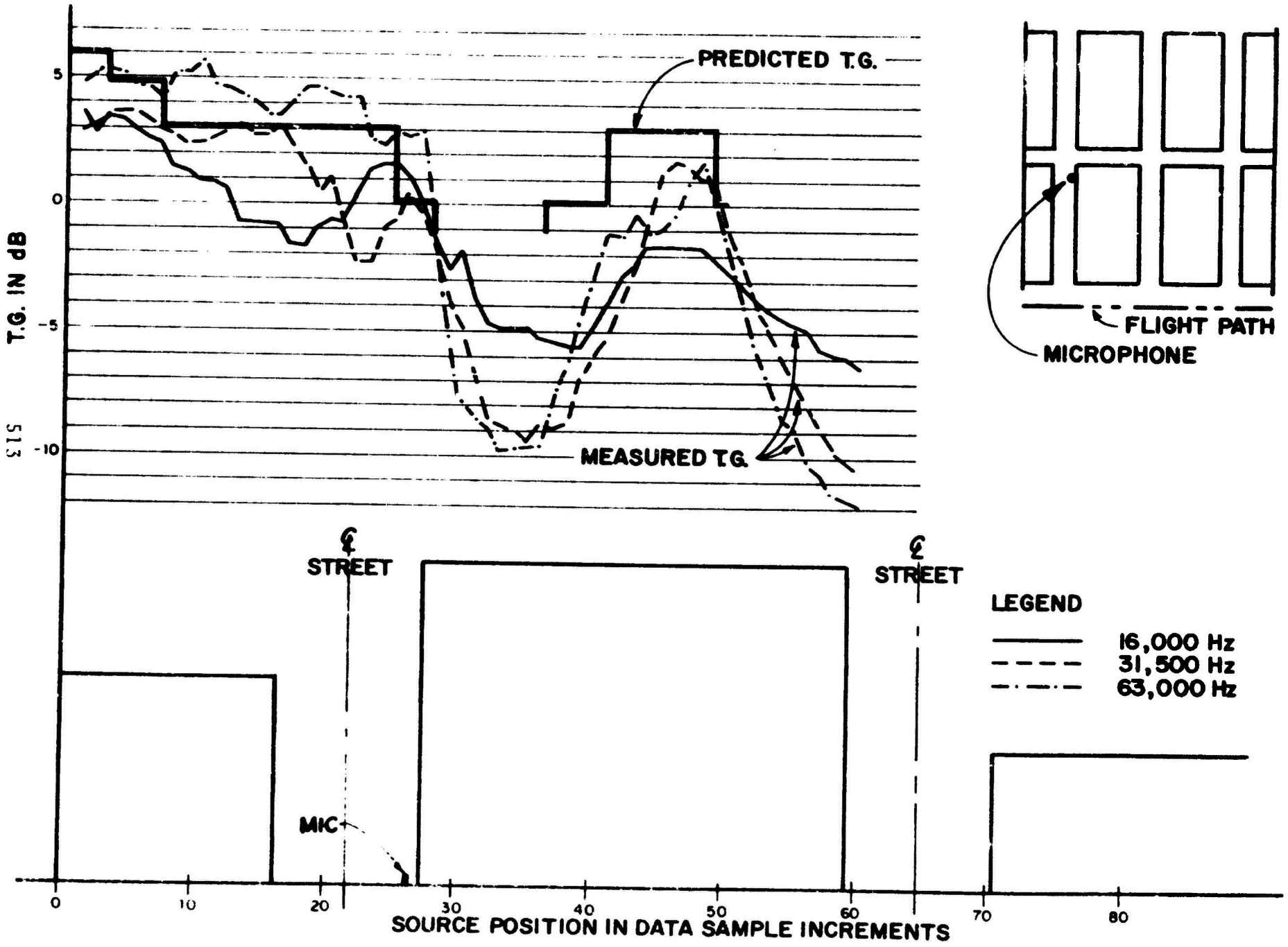
PREDICTED T.G.
MEASURED T.G.
T.G. IN dB
5
0
-5
-10
FLIGHT PATH
MICROPHONE
℄ STREET
℄ STREET
MIC
LEGEND
16,000 Hz
31,500 Hz
63,000 Hz
0
10
20
30
40
50
60
70
80
SOURCE POSITION IN DATA SAMPLE INCREMENTS

Fig. 8 : Measured & predicted TG's

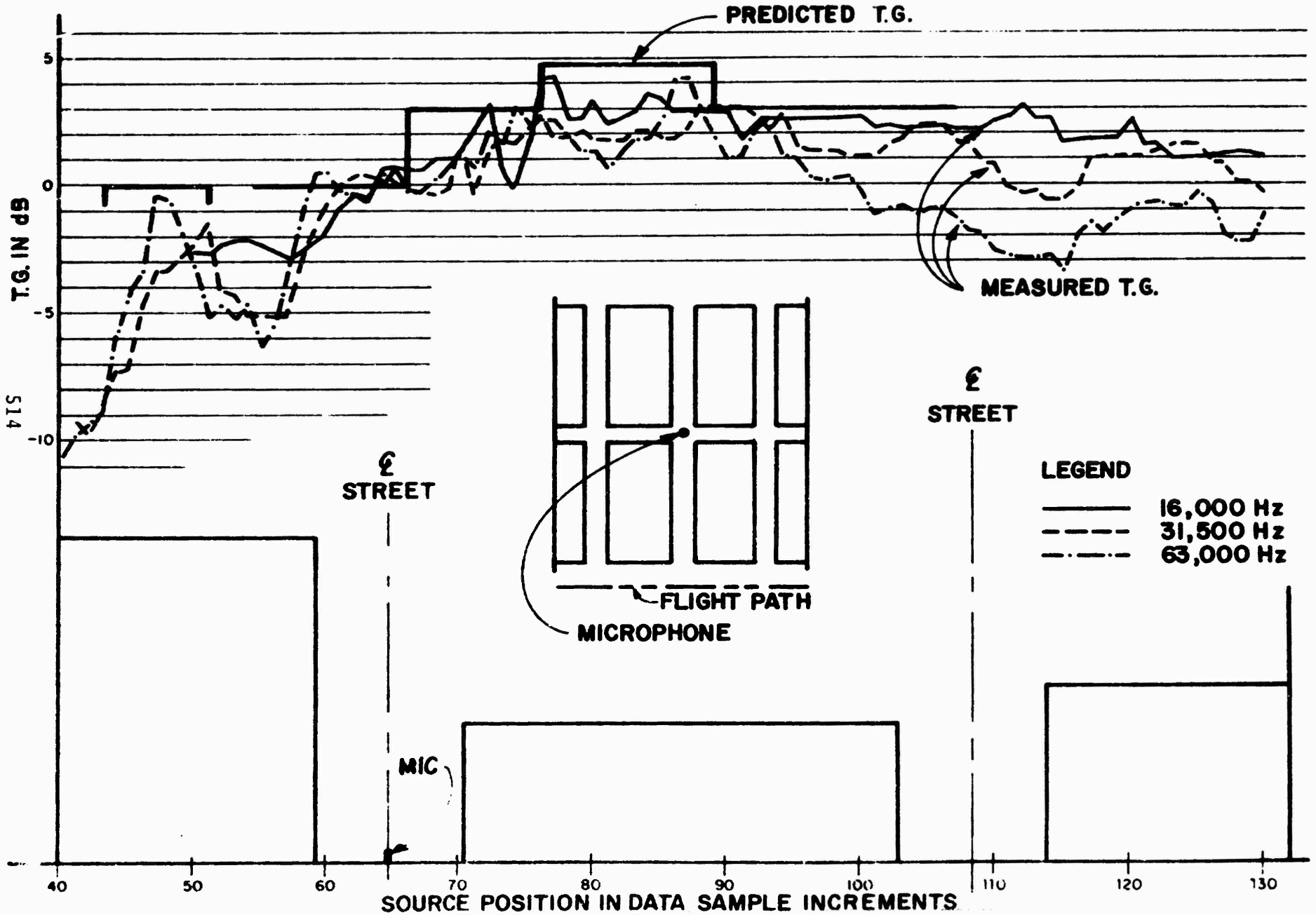

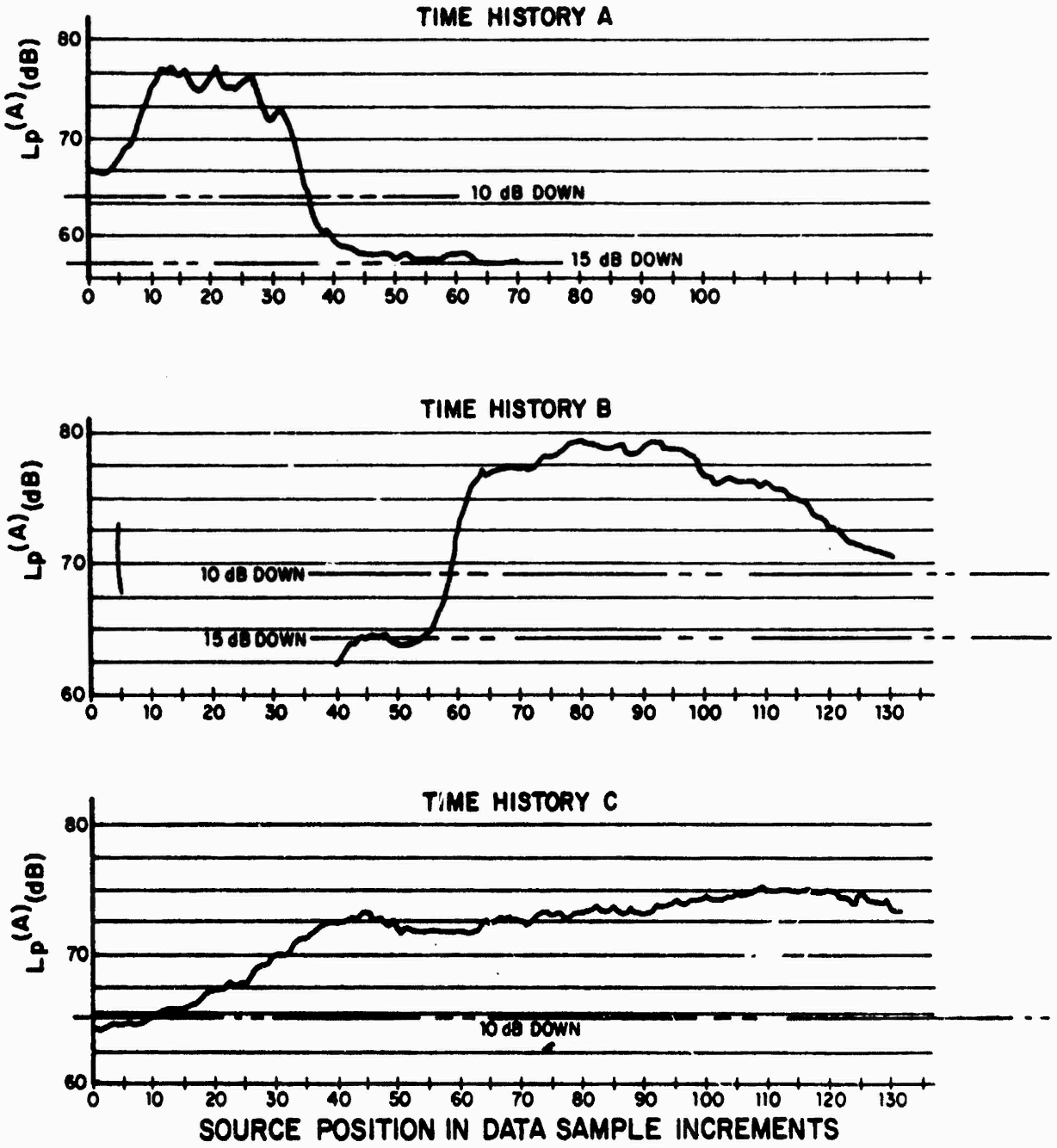

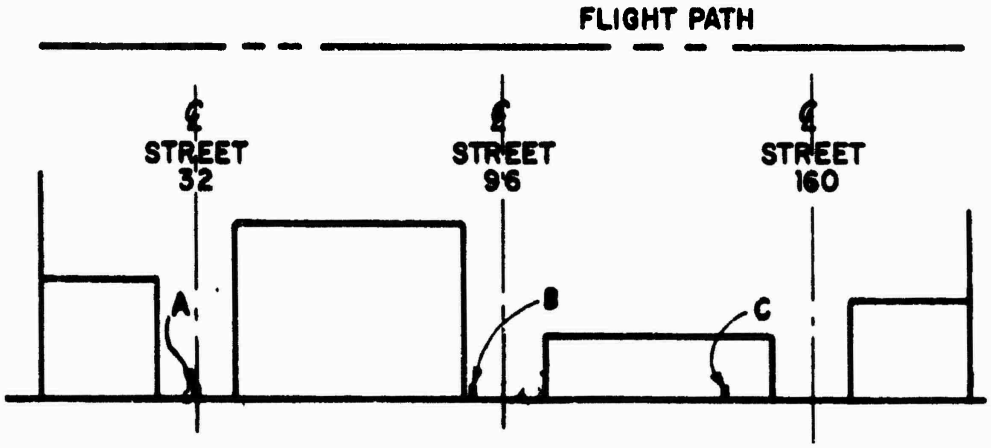

Fig. 9: A-Weighted time-histories

operations [7]. For a quantitative estimate of these effects, the applicable corrections to the maximum perceived noise level for the three time histories are shown in Table 2.

With these correction factors in mind and recalling Figure 5, there are two geometric configurations which should be avoided in order to minimize noise intrusion. The first of these (refer to Figure 5) is that of having a short building near the flight path with a taller building adjacent to it for streets parallel to the flight path. A configuration such as this is penalized in three ways: a high peak level, a large duration correction and an onset correction. A second configuration (refer to Figure 5) to be avoided is that of a tall building adjacent to a low building on streets perpendicular to the flight path. For this situation, the disadvantage is not in maximum transmission gain, but rather in increased event duration. The effect of this longer duration is not only in terms of a larger duration correction, but also in an onset correction depending on the direction of approach of the aircraft.

Just as there are situations to be avoided, there are also situations to be sought. One such configuration (refer to Figure 5) is that of a tall building nearest the flight path with a low building adjacent to it for streets parallel to the flight path. The barrier effect achieved by this configuration relative to the other parallel street configuration can be illustrated with the plots of A-weighted time history for two similar microphone positions in each of these two streets shown in Figure 10. Considering the 7 to 14 dB noise level reduction shown in this Figure (refer to Figure 10), an ideal urban geometry to minimize noise intrusion would be something like what is depicted in Figure 11.

In addition to appropriate flight path placement, two operational techniques can be used to minimize noise intrusion. The first of these is to increase flight path altitude so that more spherical divergence is provided between source and observer. Although the technique carries with it the perception penalty of increased duration, the lower level achieved will be more significant. Although the technique carries with it the perception penalty of increased duration, the lower level achieved will be more significant. The second technique is to have V/STOL aircraft operate at their maximum safe speed. This will reduce durational penalties for perceived loudness on the order of 4 1/2 dB/doubling of speed in cases where duration is of concern, assuming source sound power levels remain constant.

In addressing the problem of V/STOL noise intrusion into urban areas, three methods of sound level prediction were developed. The first method was that of direct acoustic modeling. The second was use of an average enhancement level which added 4 to 4 1/2 dB to the open field noise level for flight paths 1 1/2 to 4 1/2 times the surrounding building height. The third method of sound level prediction was that of using a discrete image propagation model. In addition to the development of these prediction methods, two approaches to minimizing noise intrusion were suggested. The first of these approaches was the selection of flight paths such that the surrounding buildings produce the least amount of perceived intrusion. The second was a purely aircraft operational approach which consisted of increasing flight path altitudes and increasing fly-over speeds within safe limits.

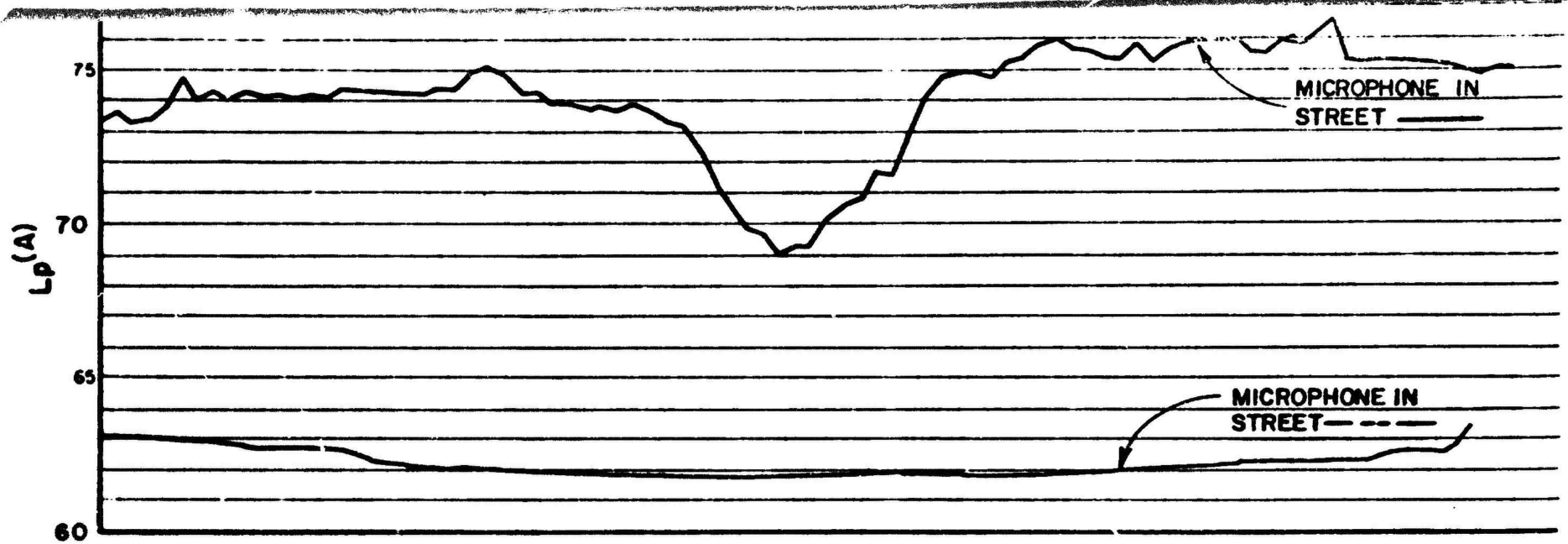

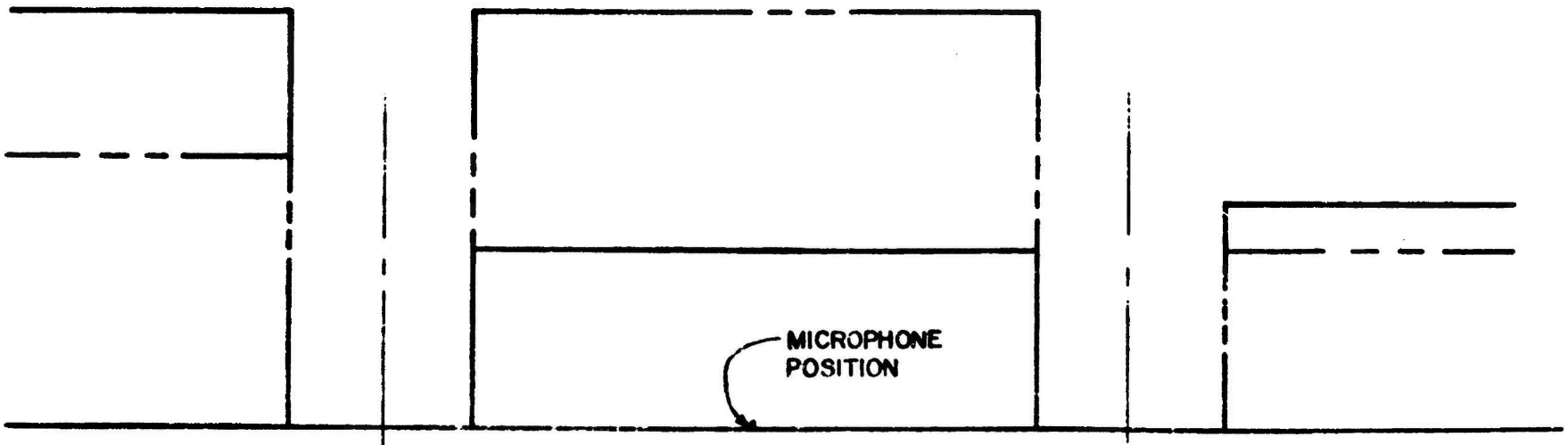

FIG. C: BUILDING BARRIER EFFECTS

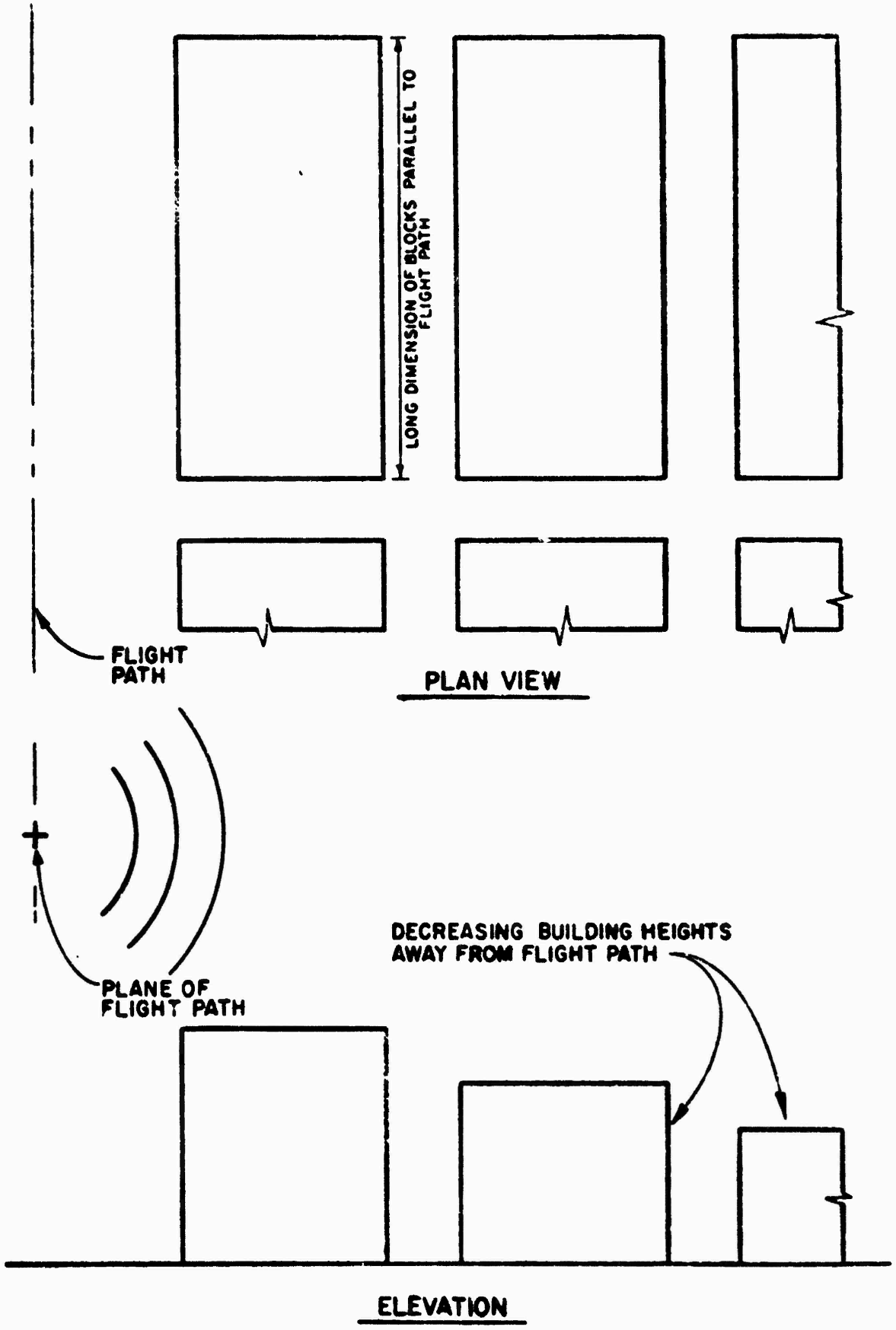

FIG. 11: OPTIMUM URBAN CONFIGURUATION

REFERENCES

1. Wiener, F. M., Malme, C. I., and Gogos, C. M. "Sound Propagation in Urban Areas", J. Acoustical Soc. of America, Vol. 37, No. 4, April, 1965, pp. 738-747.

2. Pande, L. "Model Study of Aircraft Noise Reverberation in a City Street", Interim Report DOT-TSC-93, Department of Mechanical Engineering, Massachusetts Institute of Technology, Cambridge, Mass., April, 1972.

3. Kinney, W.A. "Helicopter Noise Experiments in an Urban Environment", M.Sc. Thesis, Massachusetts Institute of Technology, Cambridge, Mass., January, 1973.

4. Morse, P. M., and Ingard, K. U. Theoretical Acoustics, McGraw-Hill Book Co., 1968, pp. 366-369.

5. Beranek, L. L., Noise Reduction, McGraw-Hill Book Co., 1960, pp. 55-60.

6. Marte, J. E. and Kurtz, D. W., "A Review of Aerodynamic Noise from Propellers, Rotors, and Lift Fans," Technical Report 32-1462, Jet Propulsion Laboratory, Pasadena, California, January, 1970.

7. Kryter, K.D., The Effects of Noise on Man, Academic Press, Inc., 1970, pp. 300-304.

APPLICATION OF THE COHERENCE FUNCTION IN TRUCK TIRE NOISE ANALYSIS

by

A. C. Eberhardt and W. F. Reiter
Center for Acoustical Studies
North Carolina State University
Raleigh, North Carolina 27607

INTRODUCTION

Motor vehicle noise is recognized as a significant contributor to the noise environment in most locations. Adjacent to interstate type highways the noise problem is intensified and is usually dominated by tire noise. Thus, it is understandable why trucks with as many as eighteen or more tires operating at high speeds and under heavy loads are major contributors to the vehicle noise problem. Studies such as conducted by the National Bureau of Standards at Wallops Island, Va. have characterized truck tire noise through variations in speed, load, wear, tread pattern and road surface (1,2,3). In many cases these parameters are related to others such as tread crown height, tread randomization, carcass construction and a number of road surface roughness parameters. Results of the studies cited show significant variation in the peak A-weighted sound pressure level as a function of speed, tread type and other parameters. Typical results of these studies are shown in Figure 1. These valuable results however provide little understanding of the nature of the tire road surface interaction and the details of the induced tire vibration field and the radiated tire noise.

TIRE SOUND AND VIBRATION DATA

A particular goal of this study is to assess the importance of tire surface vibration induced through the tire pavement interaction on the tire noise generated. To date, the experimental approach has enabled simultaneous monitoring of the sound field in the proximity of the contact patch and the tire surface acceleration signal of the sidewall or tread. The acceleration measurements are made via a miniature accelerometer and an FM-telemetry system mounted on the wheel. Acceleration signals are transmitted to a receiver in the truck cab where they are recorded along with the tire sound signal (4). Time histories of the acceleration signals show characteristics related to the location of the accelerometer on the tire. Data for accelerometer locations on the sidewall, shoulder, and in the tread area are shown in Figure 2. The length of each time history is 100 millisec or approximately 270 degrees of tire rotation. The tire histories in Figure 2 are for the same tire under the same load, speed and pavement conditions. It may be observed that the acceleration levels increase significantly from an average of 15 g's on the sidewall to approximately 50 g's in the tread area. Sidewall accelerations are less sensitive to the severe acceleration changes that result as the area adjacent to the accelerometer enters or exits road contact. Shoulder and in-tread accelerometer locations clearly show these abrupt acceleration changes.

Figure 3 shows the effect of speed on tire sidewall acceleration time history. As speed increases it is observed that both signal magnitude and average level increase. The time per single revolution varies in these photographs from 110 to 160 millisec.

A comparison of the time averaged sound and acceleration levels shows the general trends between these two signals as parameters are changed. For example, Figure 4 provides a comparison of sound and acceleration levels for a typical cross bar tire under two load conditions. In all of the tests performed the variations in average acceleration level are paralleled by nearly identical variations in sound level.

Frequency domain analysis of the acceleration and sound signals provide for visual comparison of spectral content. Figure 5 shows similarities between the sound and acceleration spectra of a typical cross bar tire at 50 mph. These spectra were obtained on a 500 line real time analyzer. Both signals were analyzed using a sample length of 250 millisec and 32 ensemble averages.

Time domain, average level and frequency analysis of the tire acceleration and sound signals leave many questions unanswered concerning the mechanics of tire noise generation. For example, frequency components occur in sound and acceleration spectra that do not appear to relate to each other. A number of factors influence this phenomena such as the measurement location of the accelerometer and microphone, and the fact that the acceleration is monitored at only one point on the tire circumference. This problem is magnified since certain regions of the tire contribute most of the energy to the tire sound and vibration field.

COHERENCE ANALYSIS

The coherence function provides a means for the resolution of some of these difficulties. The coherence function provides a measure of the degree to which an output (B) is caused by an input (A). Its magnitude is a fraction between zero and one and is defined by the ratio of the square of the magnitude of the cross-spectral density to the product of the input and output auto spectra at each component of frequency. The expression for the coherence function for two signals is

$$\gamma^2_{AB}(k) = \frac{S_{AB}(k)\, S_{AB}(k)^*}{S_{AA}(k)\, S_{BB}(k)}$$

at each frequency k (5). Figure 6 illustrates the processing steps required in the computation of the coherence function.

Application of the coherence function to the simultaneously recorded acceleration and sound signals provides a measure of the extent to which the sound is related to the acceleration at each frequency. The product of the sound spectrum and the coherence function (between sound and vibration) gives a spectrum showing only sound related to the acceleration at the monitoring point on the tire. Incoherent sound such as engine noise, aerodynamic noise or noise of other tires is eliminated from the spectrums. Figure 7 shows the sound spectrum, acceleration spectrum, coherence function, and the sound coherent with the acceleration of typical cross bar tire at 60 mph. This analysis provides additional confidence that similarities between sound and acceleration signals are statistically related.

Through digital processing the acceleration time history is broken into a number of segments Figure 8. Each segment is analyzed separately for frequency content and coherence with the sound field, the result is of some significance. Figure 9 depicts a single plot of the total sound along with six plots of vibration-coherent sound, each of the six represents a 60 degree segment of a single tire rotation. In the vicinity of road contact reasonable coherence exists at many points across the entire spectrum. These may be viewed as high frequency tread element response in addition to carcass resonances. As the distance from road contact increases the higher frequencies are quickly damped out and become remote to the microphone location while low resonance effects are carried through the complete revolution. Analysis in this manner points to the frequency components of the acceleration signal that are major sound field contributors.

SUMMARY

These preliminary results of coherence analysis in the diagnosis of tire noise mechanisms are encouraging. Future work will concentrate on diagnosis of the tread area versus sidewall area vibrations and their relative importance to the tire noise generated. The analyses planned include multiple coherence work to separate road exitation effects from tread exitation effects and their relative importance to the tire noise generated.

[ONA-DOT is acknowledged for support of this work.]

REFERENCES

1. Tetlow, D. 1971. Truck tire noise. Sound and Vibration 5(8):17-23.

2. National Bureau of Standards. 1970. Truck tire noise I - peak A-weighted sound levels due to truck tires. Report No. OST-ONA-71-9.

3. Truck tire noise. 1971. Society of Automotive Engineers, Inc. Report No. SP-373. New York.

4. Eberhardt, A.C., W. F. Reiter and L. J. Harper, "Experimental Investigation of In-Service Truck Tire Vibration", Proceedings of the Interagency Symposium on University Research in Transportation Noise, Stanford, California, March 1973.

5. Bendat, J. S. and A. G. Piersol, "Randon Data: Analysis and Measurement Procedures . Wiley-Interscience, New York, 1971.

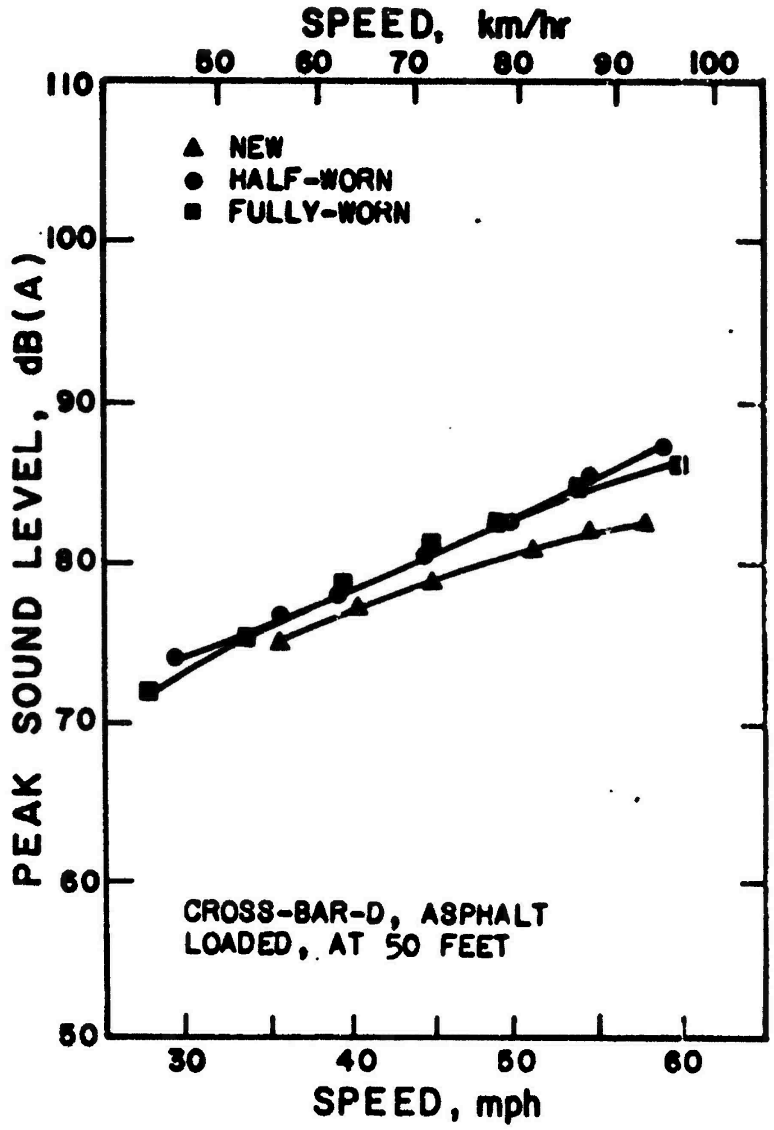

Figure 1. Results typical of parametric studies indicating variations in peak A-weighted sound pressure level as a function of speed and tread wear.

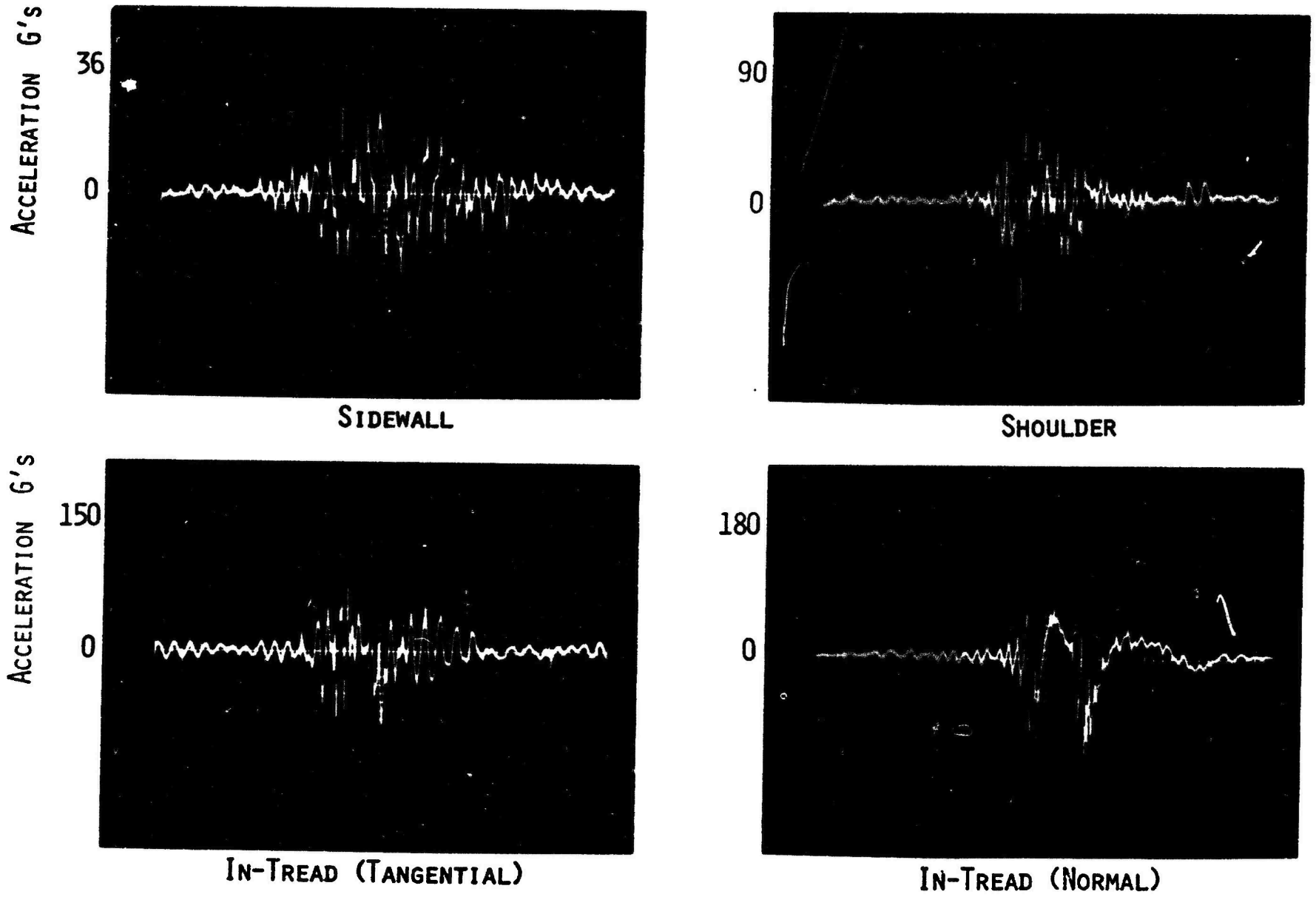

Figure 2. Acceleration time histories for the sidewall, shoulder, and in-tread area.

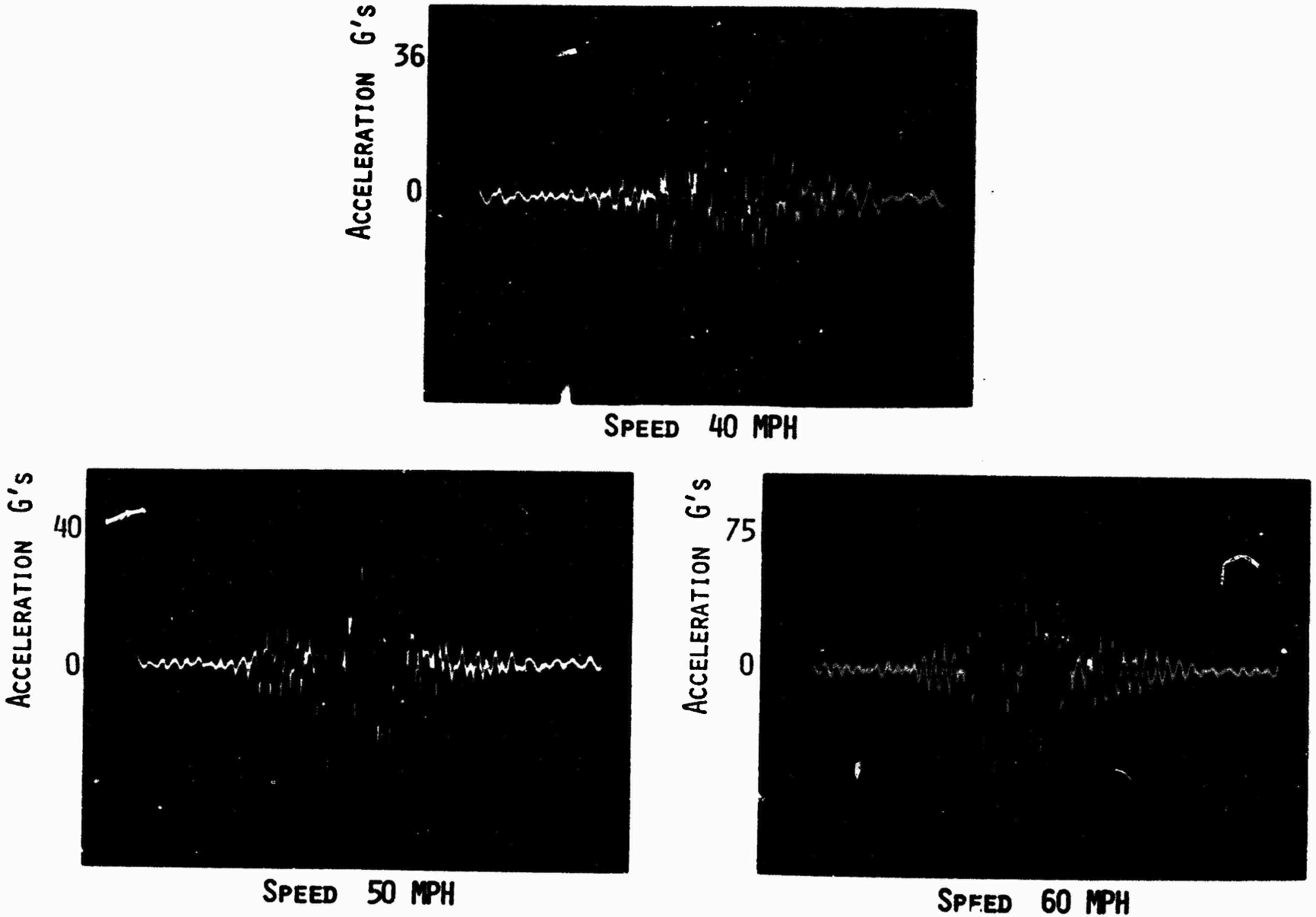

Figure 3. Effect of speed on the sidewall acceleration time history.

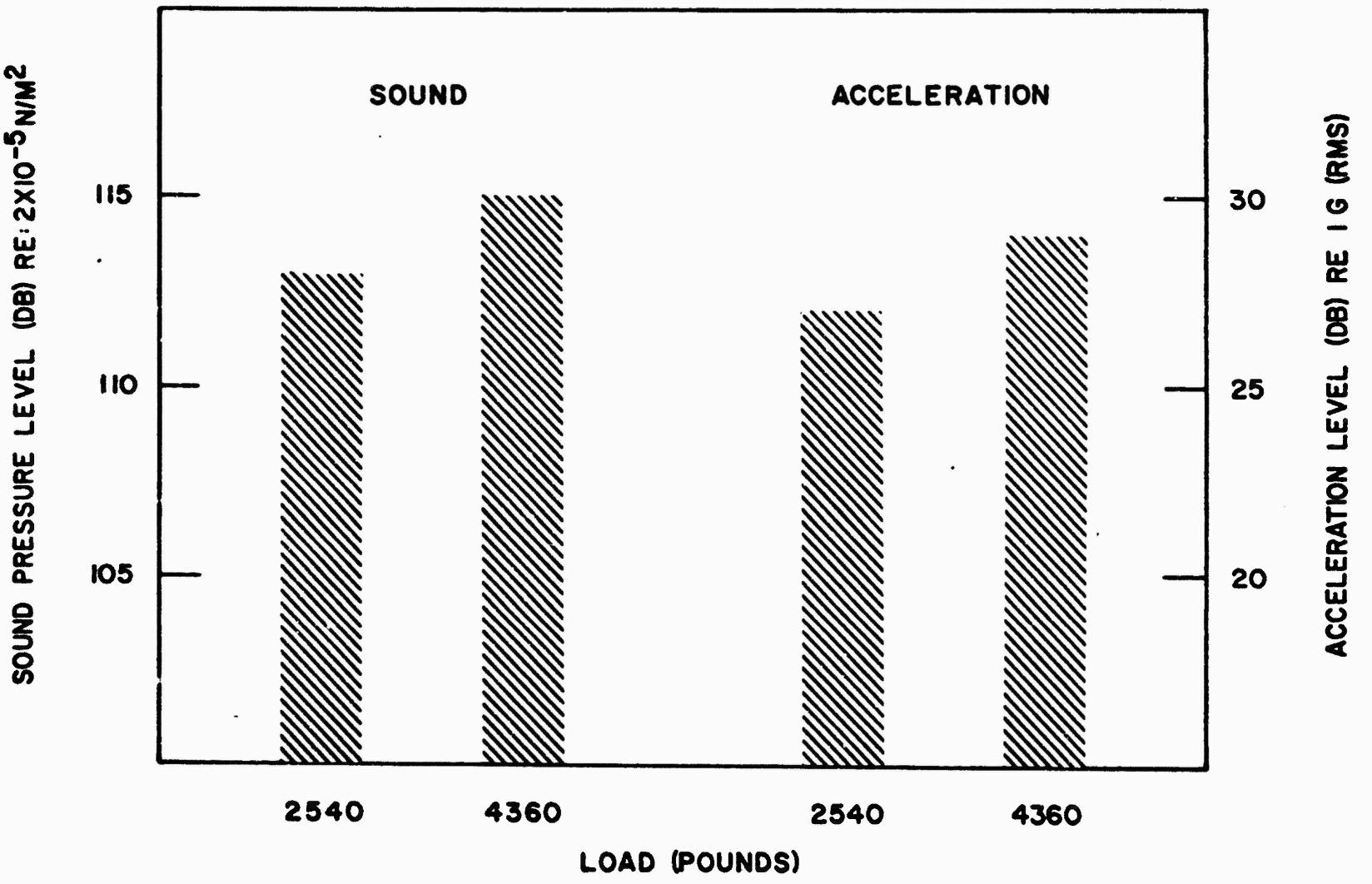

Figure 4. Effect of load on sidewall acceleration and sound levels for a typical cross bar tire at 50 mph.

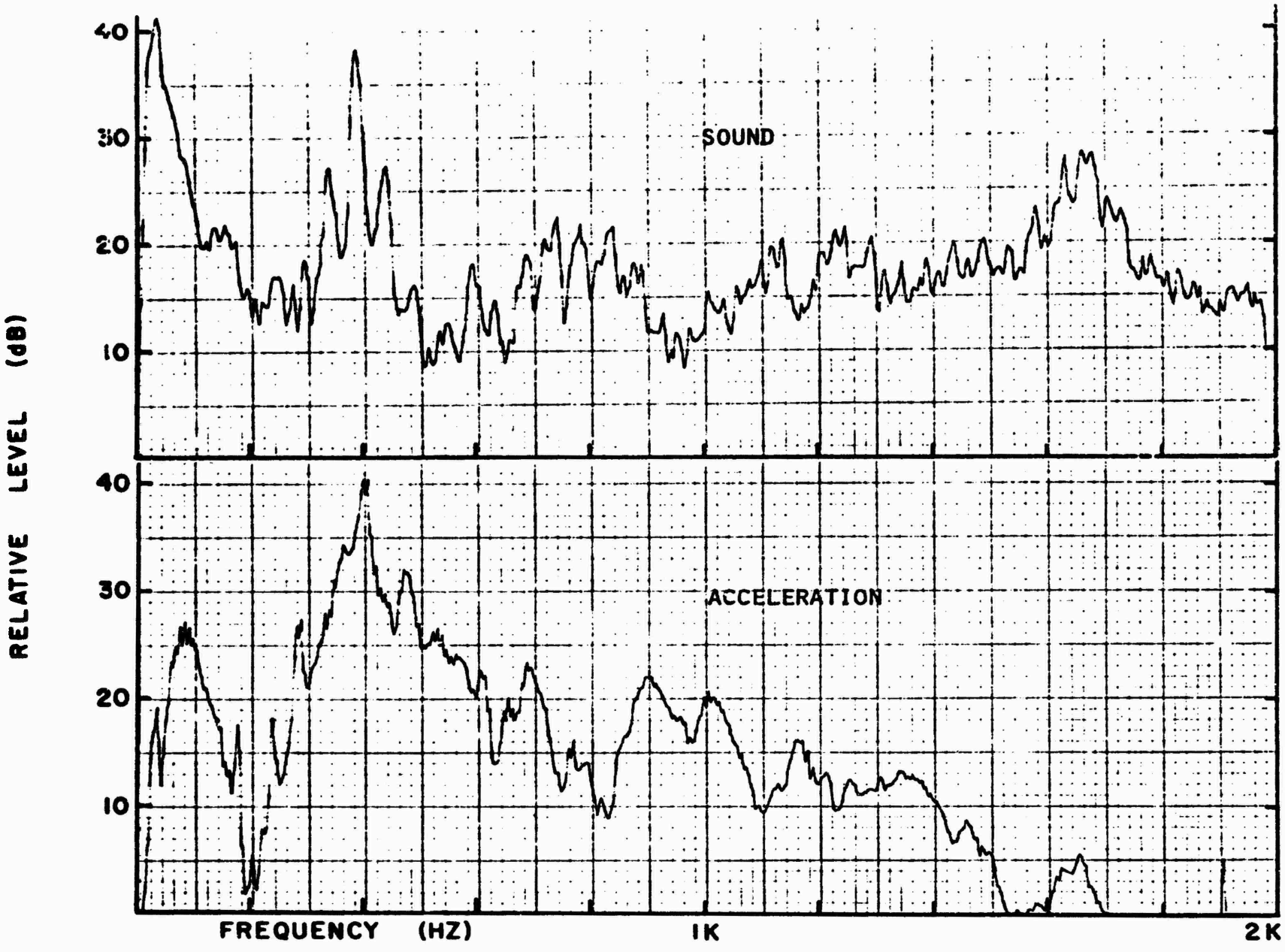

Figure 5. Sound and sidewall acceleration spectra for a typical cross bar tire at 50 mph.

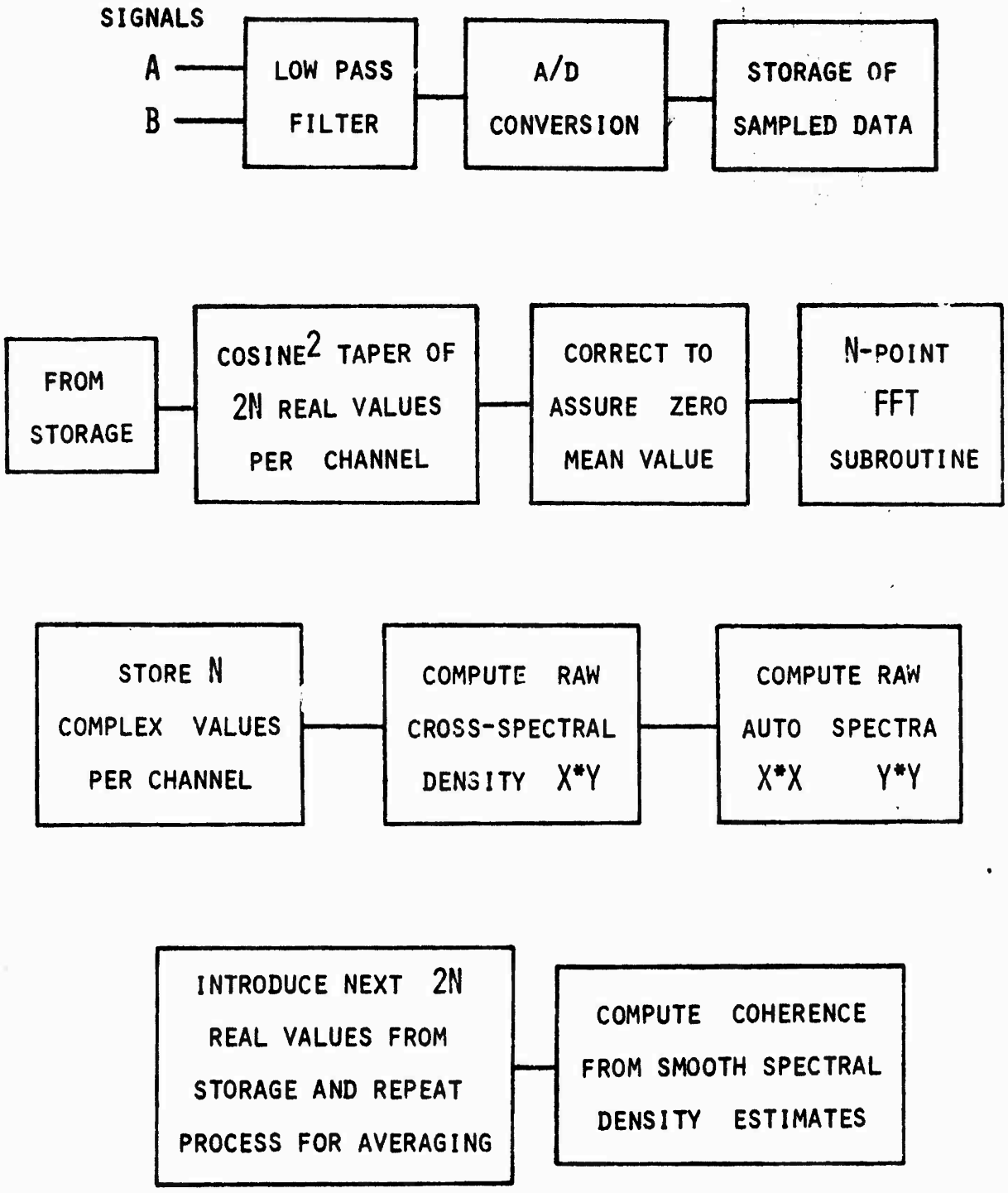

Figure 6. Processing steps required in computation of the coherence function.

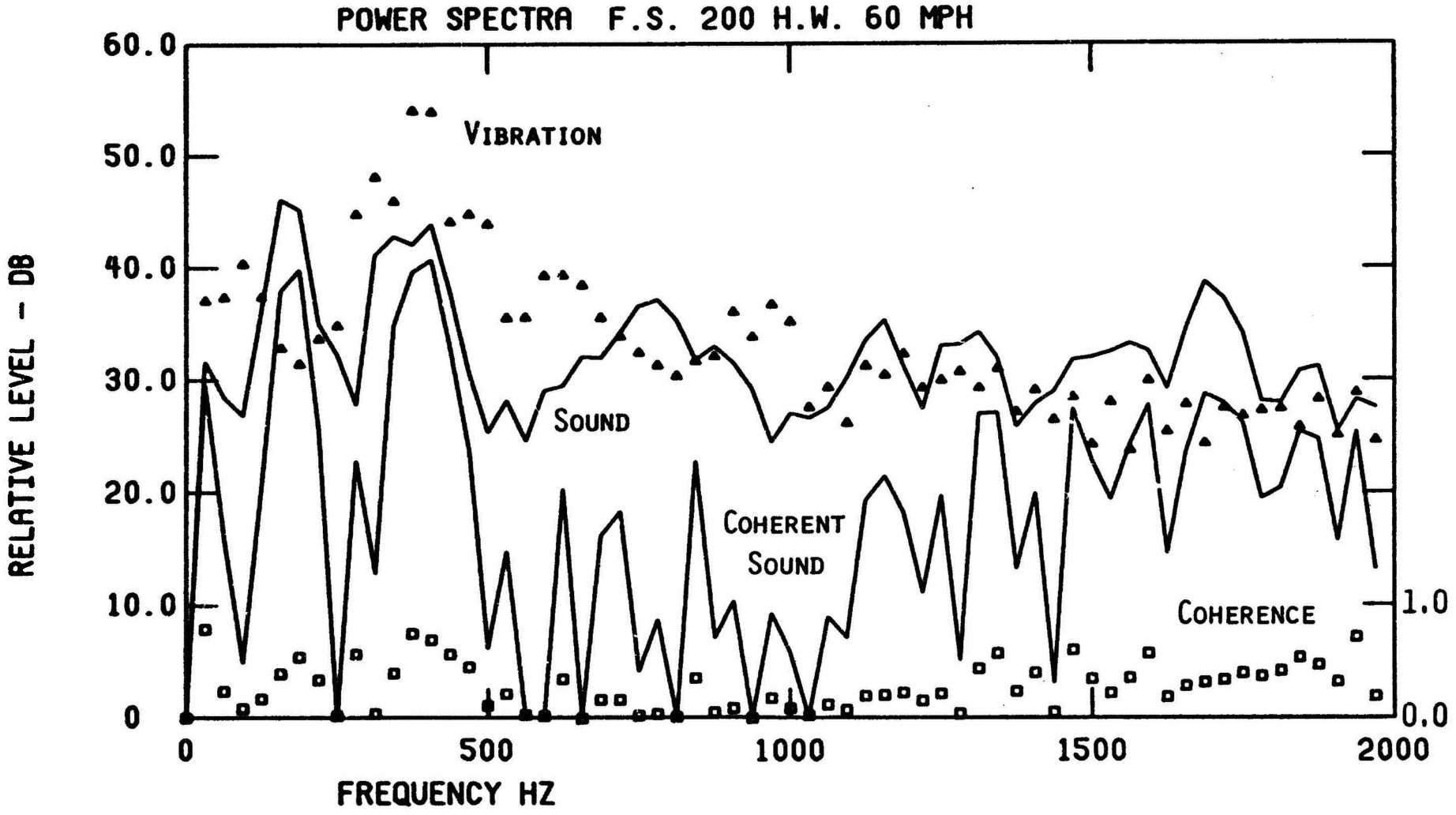

Figure 7. Spectra of sound, vibration, sound coherent with vibration, and coherence for a typical cross bar tire at 60 mph.

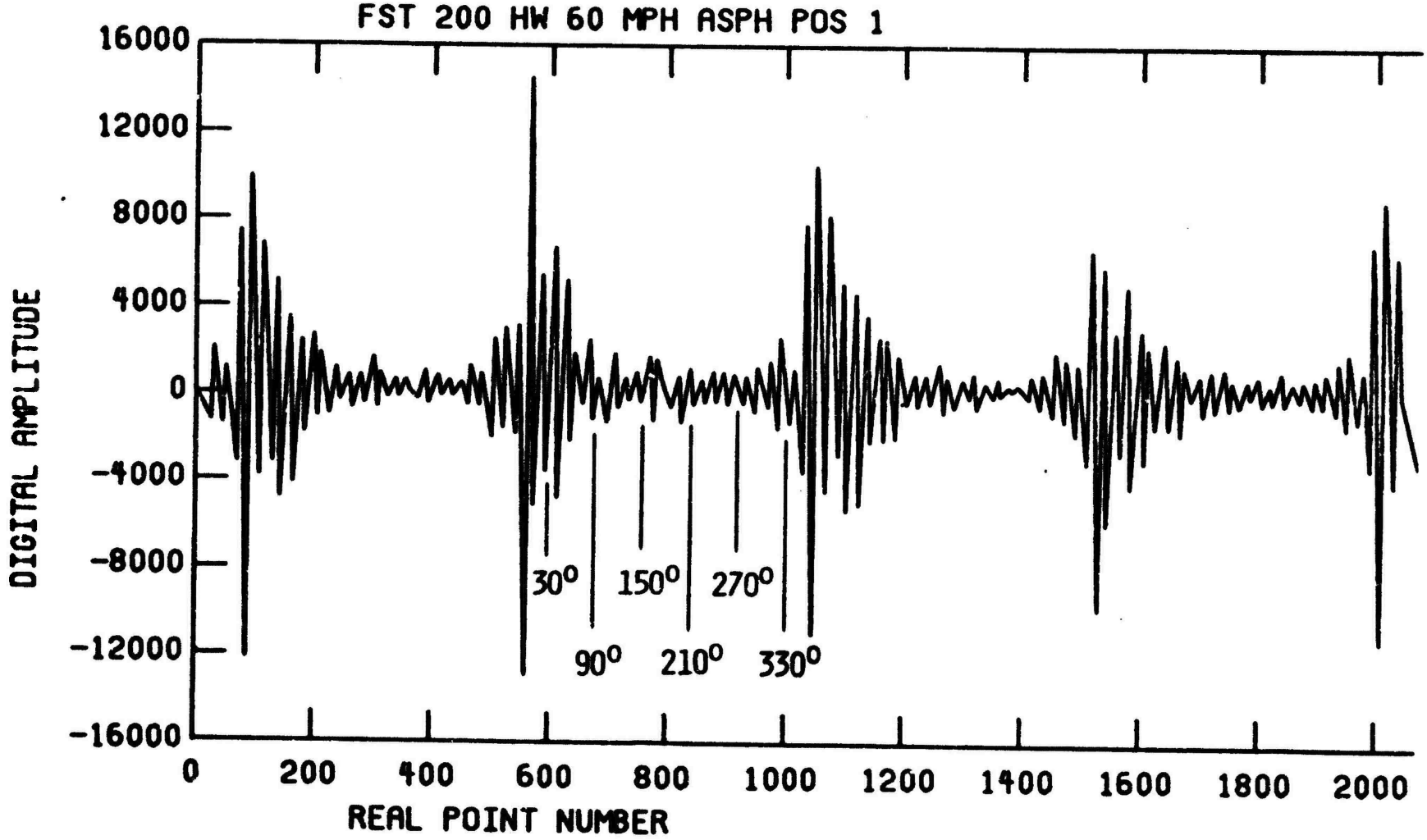

Figure 8. Digital reconstruction of the sampled acceleration signal. The segments of the signal used for the analysis are shown.

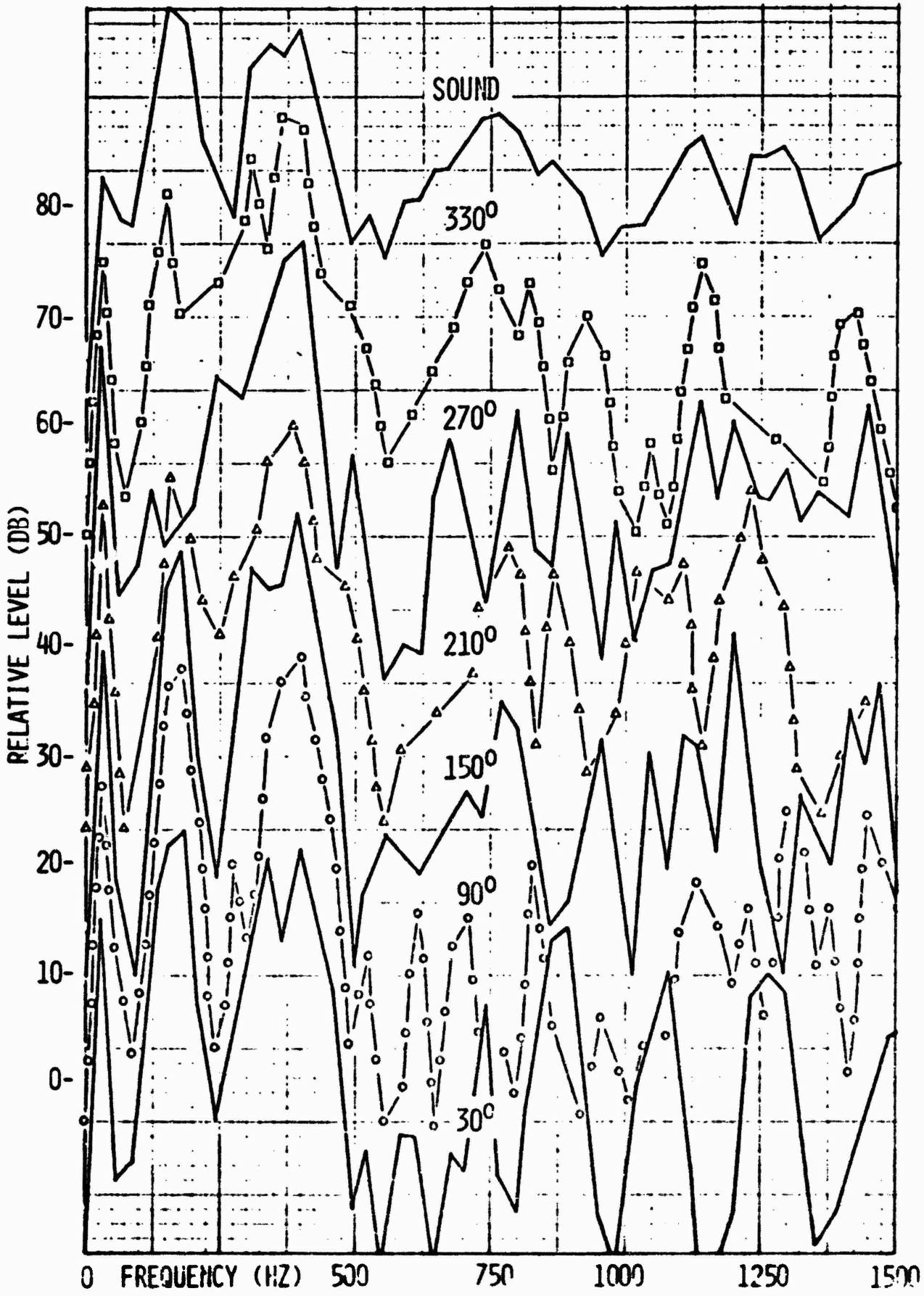

Figure 5. Sound spectrum and [illegible] vibration [illegible] single tire [illegible].

EXPERIMENTAL-ANALYTICAL PREDICTION OF URBAN NOISE

by

S. Slutsky, Polytechnic Institute of New York
Brooklyn, N.Y.
L. Arnold, New York University, New York, N.Y.

Summary

An experimental model procedure has been considered to determine the spectral response character of a neighborhood using transient input and response measurements. Frequency responses were calculated by taking the ratio of the input and response fourier transforms, and third octive energy responses calculated therefrom using several alternative procedures. Third octave responses were fairly similar for all procedures, but all showed fluctuations of from 1 to 2 dB between results from successive experiments.

Introduction

An experimental procedure has been under study whose purpose is the development of techniques for precise prediction of noise in urban environments of complex architectural configuration, which are not well suited to purely analytical approaches.

The basic concept entailed the construction of a geometrically scaled model, the generation of a spherically symmetric acoustic pulse, measurement of the pulse shape in time, and of the response of the system at a single spatial point. The pair of signals (input and response) were recorded, played back at reduced speed into an analog to digital converter, and recorded on magnetic tape in Fortran compatible notation. Each signal was then Fourier analyzed and several alternative procedures used to obtain the power ratios corresponding to the third octave spectral bands. The next step in this procedure would be to use the third octave power spectral data available for various urban noise sources in conjunction with the model response data to calculate responses of interest in the prototype system.

Experimental Procedure

Model Construction

The model for the tests was chosen in order to exemplify the problem of urban canyon type environments. One of the best examples of this type of neighborhood is the financial district in lower Manhattan. A representative area which could be built up in a scale model is that bordering Exchange Place, between Broad and Hanover Streets, Fig. 1. The model was built of 3/4 inch plywood, to a scale of 1 : 100. Choice of plywood as a construction material was tested by comparing incident and reflected pulse shapes for alternative

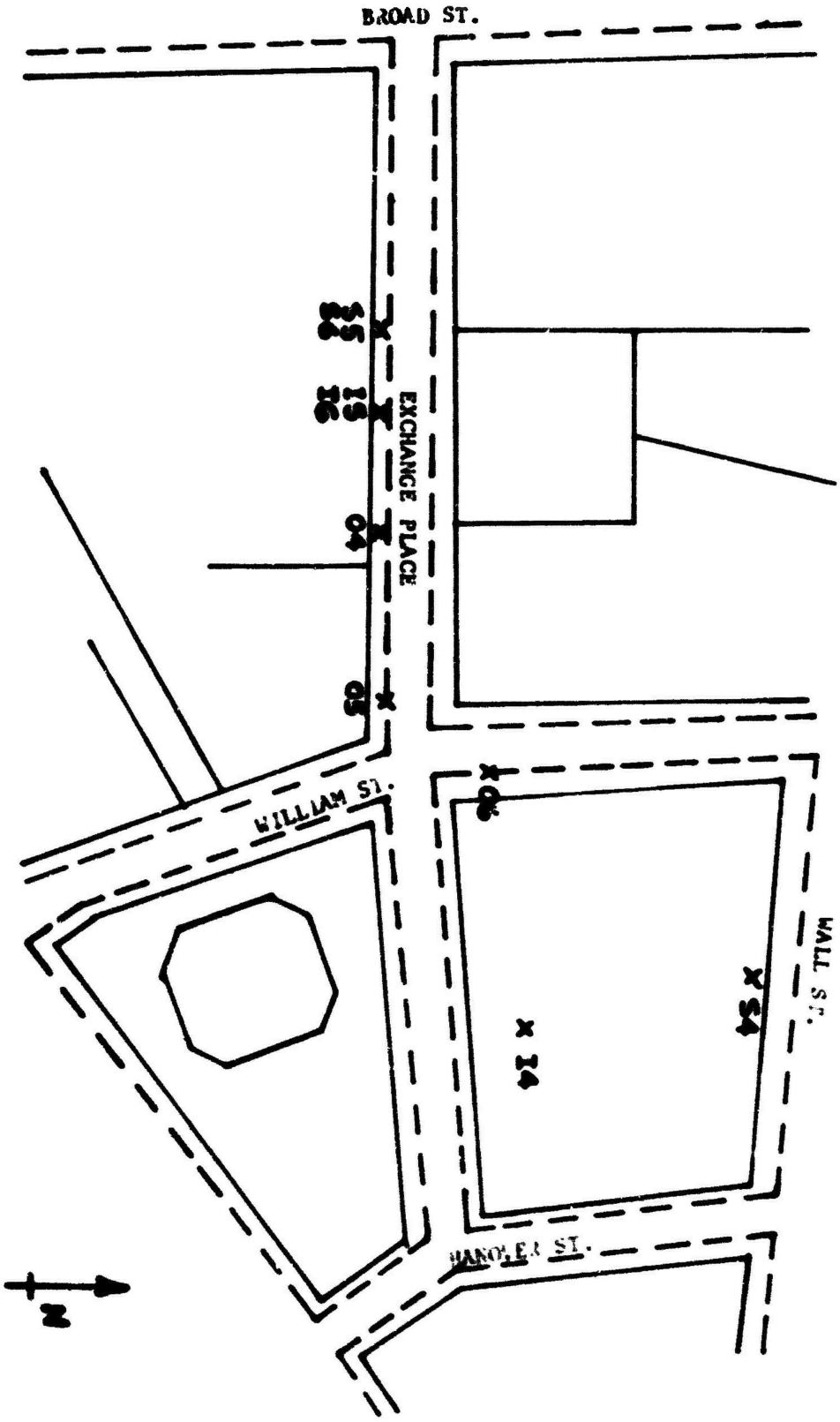

Figure 1 - Area Plan
Scale 1" = 9' Model
1" = 75' Prototype

surfaces. Thus, as anticipated, a steel plate produced no apparent change in shape, whereas styrafoam produced considerable change. A clean, hard wood surface appeared to differ insignificantly from the steel surface in its effect. The plywood, therefore, appeared adequate, as long as careful construction procedures and a sealer coat of enamel were applied. Dimensions of the buildings were obtained from records of the New York City Departmnet of Buildings and from photographs and on site visual estimates. The finished model is shown in Figure 2.

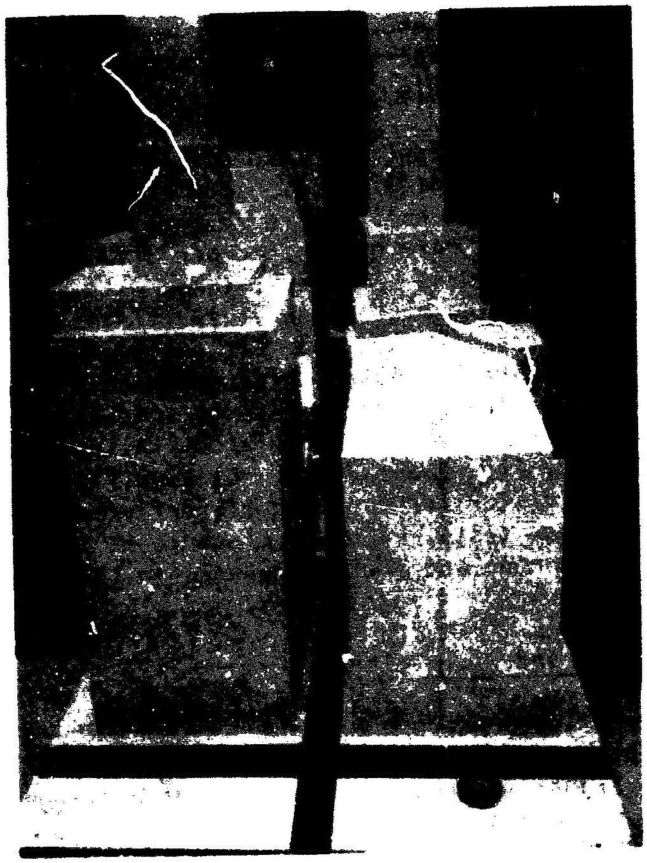

Figure 2 - Model

The Sound Source

The sound source used for these experiments was a small shock tube built of half inch tubing, with diaphragms made of either aluminum foil or cellophane. Breaking pressures ranged from 15 psi to 50 psi, depending on the diaphragm material and the number of layers loaded together. For a given choice of material, the pulse shape reproducibility was good, as seen from some of the oscilloscope traces discussed below. Although the basic disturbance pulse shape within the shock tube is rectangular, the shape radiated from the end

of the tube is roughly like the derivative of the exit mass flow, so that the radiated field consists of a pulse of about 50-100 μsec duration followed after four milliseconds by a second pulse. The second pulse can be considerably weaker than the first by adding a few feet of tubing between the compression chamber and the radiating end.

It was found that there was reasonable spherical symmetry around the source exit. The imperfect directionality was not believed to constitute much of a handicap in our experiment because the source was placed in our model near the intersection of the ground and a wall, pointing towards the ground. (In addition, a flow diffusing surface built up around the source exit tube was believed to result in some smoothing of the field).

Figures 3 to 8 show the basic behavior of the source signal. Thus Fig. 3 shows the pulse shape at a point 12 inches from the source, and far from any reflecting surface. The peak amplitude represents a pressure of about 152 dB, and at an oscilloscope sweep rate of 50 μsec per div. The duration of the main pulse is about 100 microseconds. Figure 4, taken with the source located 1/4" from the ground plane, and the microphone at 10" distance and 1/4" off the ground, shows ground-source interaction. Figures 5 and 6 are similar except that the microphone position is along a line from the source oriented at 45° and 70°, respectively, to the ground. There is some change, but the gross assumption of symmetry is not overmuch violated. Also, change of microphone distance from 5" to 20", Fig. 7 and 8, did not significantly change the observed shapes, so that distortion due to nonlinear steepening could be considered unimportant in these tests. (The 5" distance is the standard distance between the input microphone and the source used in these tests).

Measurement, Recording and Digitizing

The instrumentation procedure entailed use of two 1/8 inch condenser microphones with their appropriate preamplifiers and amplifiers. In addition, a third microphone signal was required to serve as a trigger whether for oscilloscope monitoring or for magnetic recording. A 1/4 inch condenser microphone was used for this purpose. Signals from the 1/8 inch microphones were recorded on both FM and direct record channels of a Honeywell 5600 tape recorder. The trigger signal was input to a pulse generator whose output was then recorded on an additional direct record channel of the tape recorder. Both recording modes were used because the FM channel frequency response extended only to 40 KHz (400 Hz when corrected for scale) while the direct record channels were limited at the low frequency end and also were noisier. It was further found that the direct record channels exhibited a sizeable overshoot, which did not respond to adjustment. The high frequency end of the D/R channel response was limited by the microphones, which extended from between 150 KHz for normal incidence to 70 KHz for grazing incidence.

The tape recordings were digitized by playback at reduced speed into an Adage digital computer, using the trigger signal to initiate the digitization. The digitization operation must be repeated four times for each experiment; for the input on FM, for the input on D/R, for the output on FM and for the output on D/R. The maximum record length was limited by the computer to 4000 points, so that a minimum digitization interval of .766 microseconds per point could be used in the short non-reverberant experiments (Cases 1,2 and 3), whereas 2.06 microseconds per point was required for the longer time records, Cases 5 and 6. An interval of 1.344 μsec was used in Case 4.

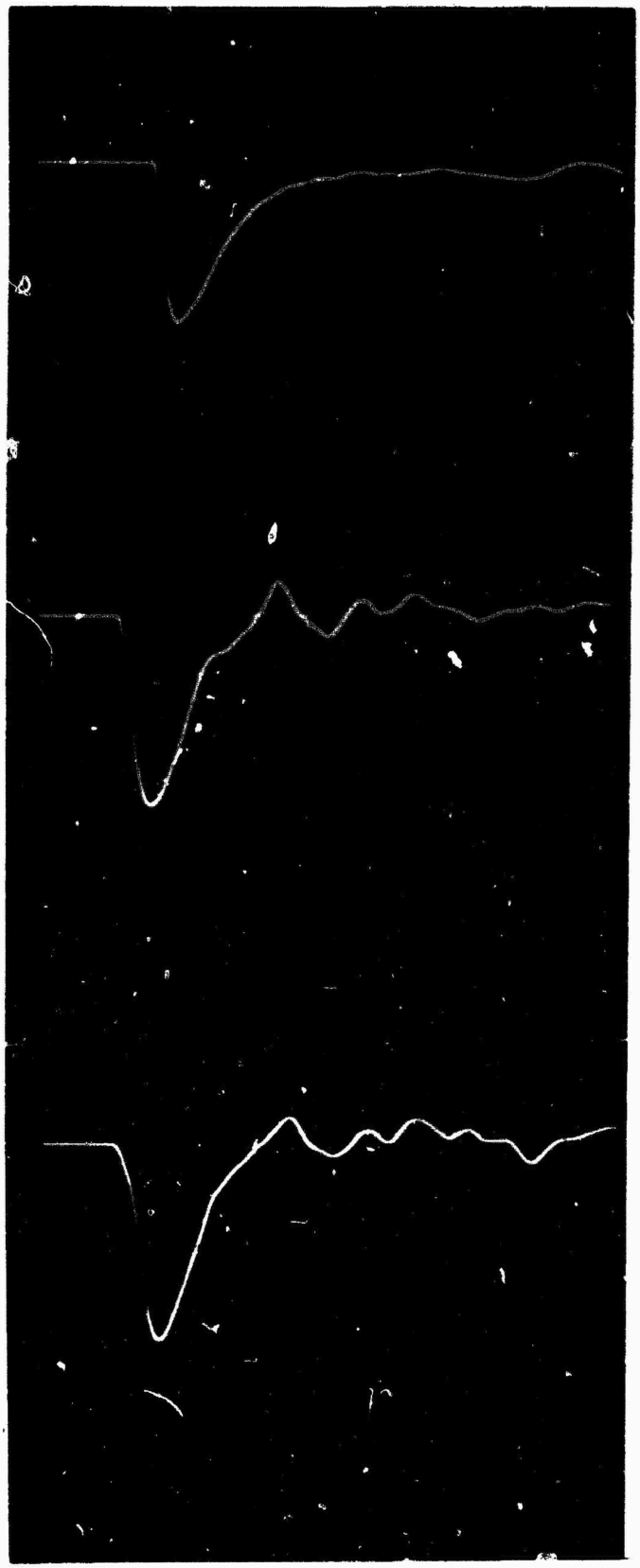

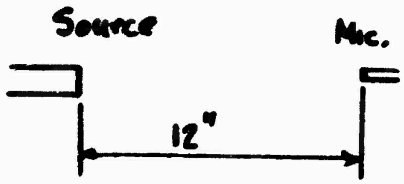

Fig. 3

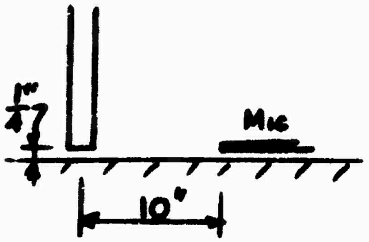

Fig. 4

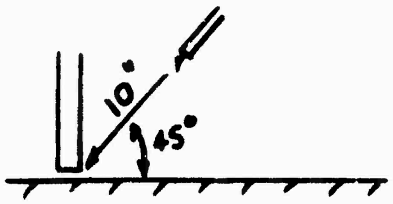

Fig. 5

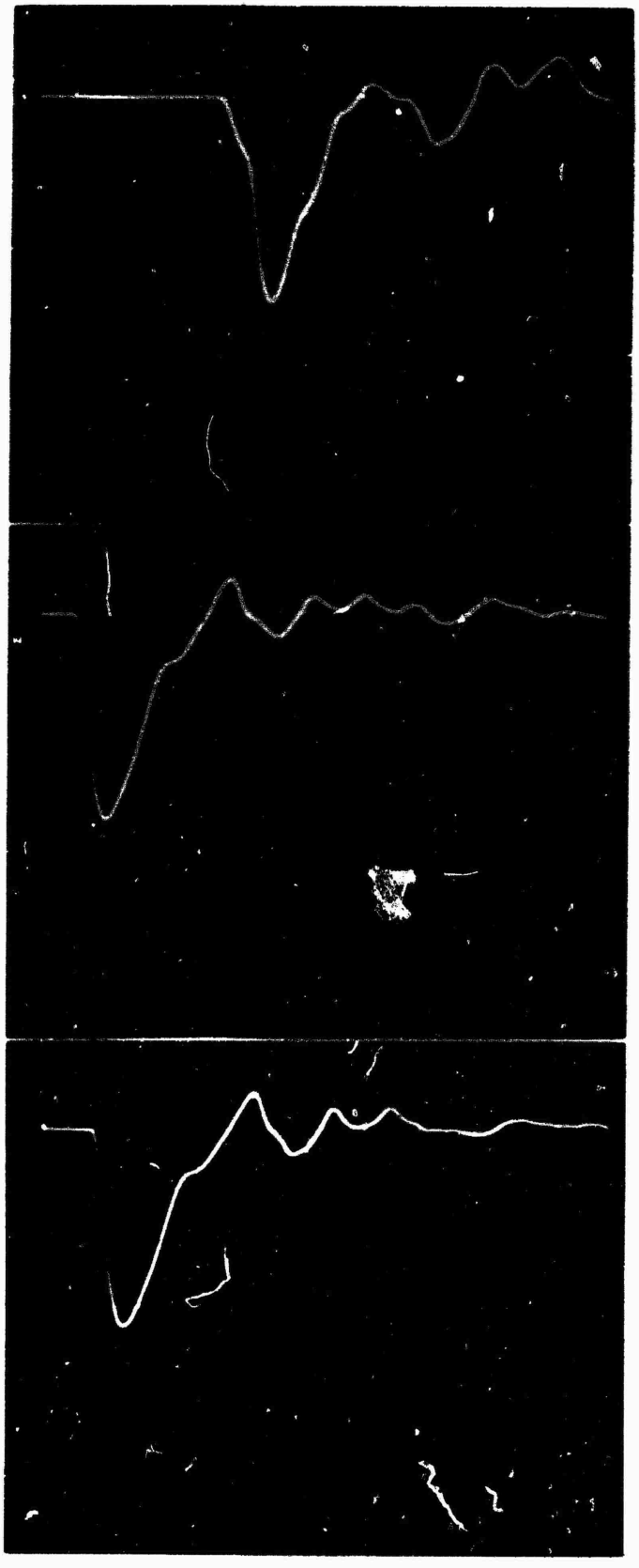

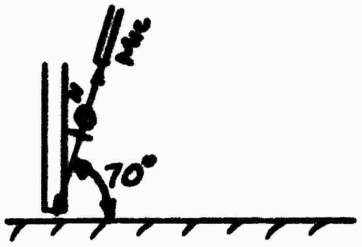

Fig. 6

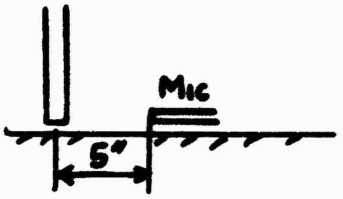

Fig. 7

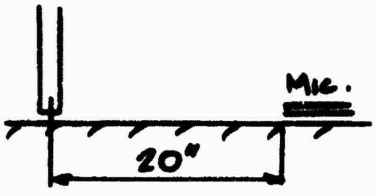

Fig. 8

Test Configurations

Six configurations were studied. (1) The first and simplest involved the source, S, and two microphones; input microphone I at two feet and the output, O, at three feet from the source. An angle of 30° was set for ISO in order to avoid scattering or shadow interaction between the microphones. Microphone and source axes were parallel. (2) The second was similar to the first except that the output microphone was 8" above the ground plane so that a reflected wave was picked up, and the input microphone was 18" from the source. (3) The third test was identical with test 2 except that a foam diffuser surface was built up around the end of the source tube. (4) The source was held in the air about 52 inches above the ground over Wall Street halfway between William and Hanover (Fig. 1). The source tube was horizontal and pointed southwest. The output microphone was one inch off the ground on the south sidewalk of Exchange Place, 12" west of William, and well out of the direct line of sight from the source. The input microphone was about sixteen inches from the source, and clear of any reflecting surfaces. (5) The source was held over the point on Exchange Place marked S5 on Fig. 1 (a distance of 15" from the southeast building corner). The source was oriented vertically, with the exit at 1/4 inch off the ground, and as close to the wall as possible. The input microphone was placed 5" further east along Exchange Place, pointed vertically down, cartridge about 1/8 " above the ground and almost touching the wall (Point I-5 of Fig. 1). The output microphone was placed at the intersection of Exchange Place and William Street, 1/2' above the edge of the sidewalk (Point O-5 of Fig. 1). (6) The source and input microphone locations were identical with those of test 5. The output microphone was moved diagonally across the intersection and slightly north along William Street until it was several inches out of the direct line of sight of the source.

The reason for placing the input microphone so close to the ground-wall intersection in tests 5 and 6 was that this position minimized the formation of discrete incident and wall reflected signals. The output microphones, on the other hand, was placed at normal listener position (scaled).

Figures 9 to 11 are representations of the digital data as stored on the magnetic disc of the Adage computer. Two independent repetitions of each configuration were run, labeled A and B in the figures. The upper trace is always the input trace, the lower the output. The prefixes D and FM represent the direct record and FM traces respectively. Comparison of the FM with the direct record traces of Test 1 show the effect of overshoot in the direct record mode. The overshoot does not automatically disqualify the tape recorder for this application, because both input and output channels behave the same way, and therefore the ratio of the frequency responses should be free of this overshoot effect. Test 1 traces also clearly show a relatively large level of signal fluctuation after the passage of the first pulse. It might seem that this is random noise and due perhaps to jet or boundary layer air turbulence, except that the fluctuation patterns of cases A and B are very similar, and hence not random.

In general, comparison of cases A with B show that the system is highly repeatable. Case 6 and case 5 direct record histories were not photographed.

D-1A

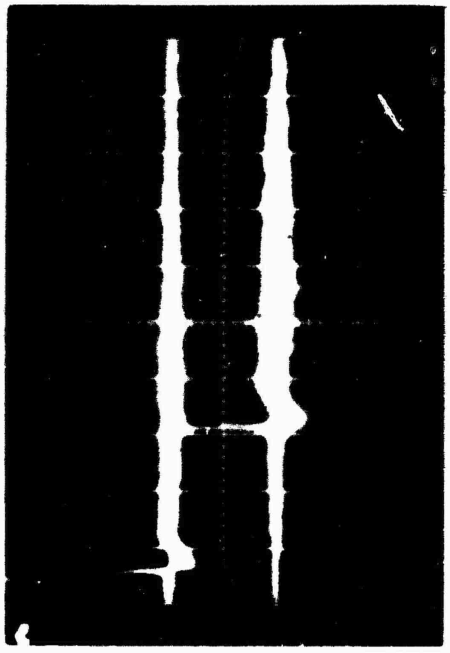

D-1B

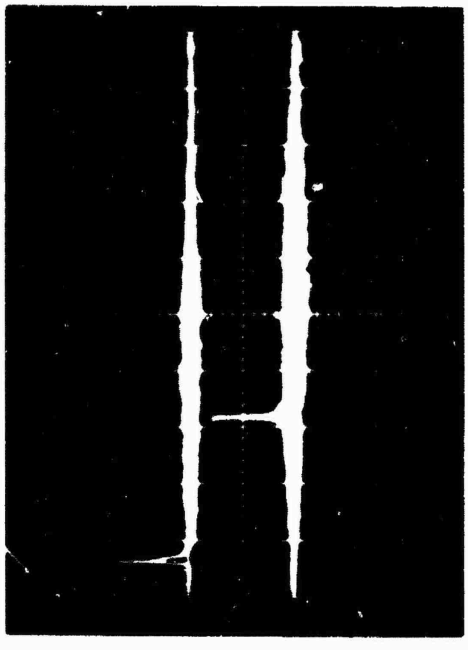

FM-1A

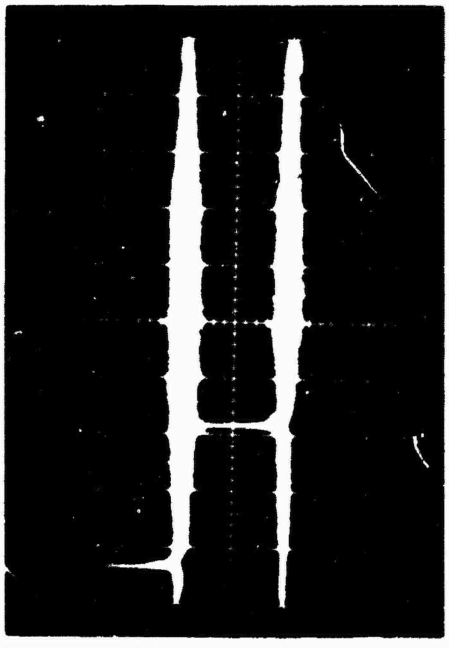

FM-1B

Figure 9

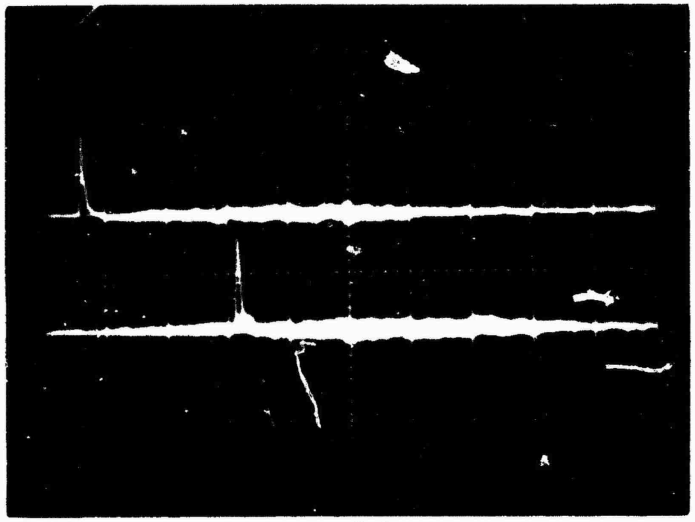

FM - 1A

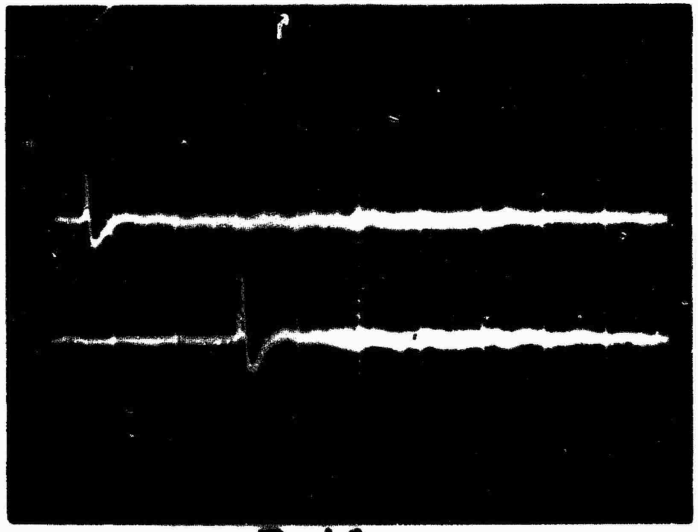

D - 1A

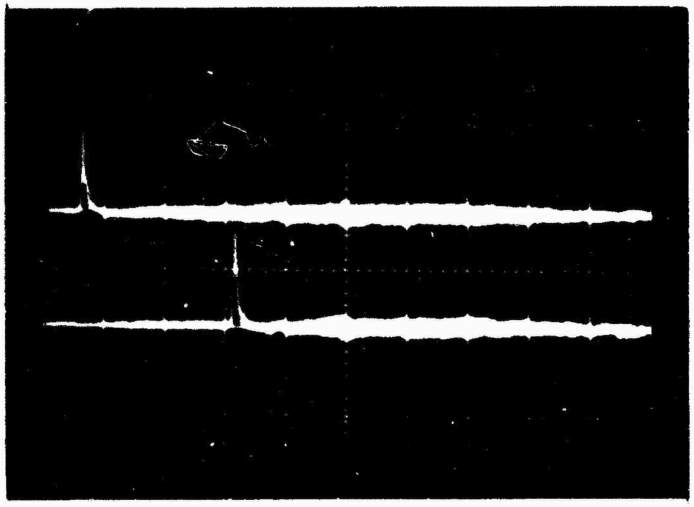

FM - 1B

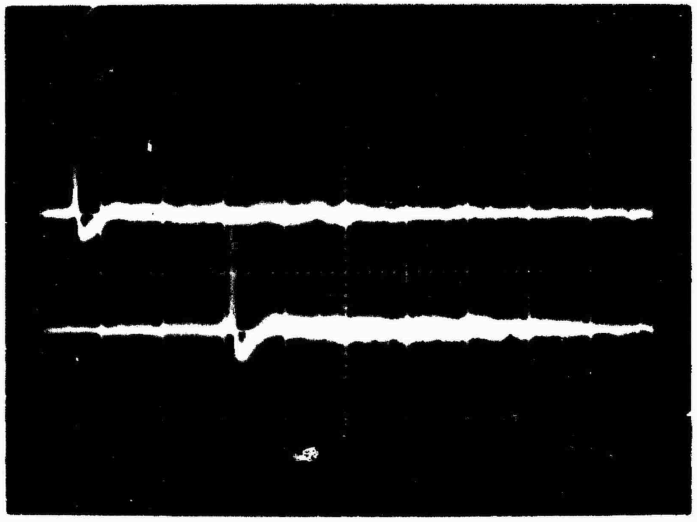

D - 1B

FIG. 9

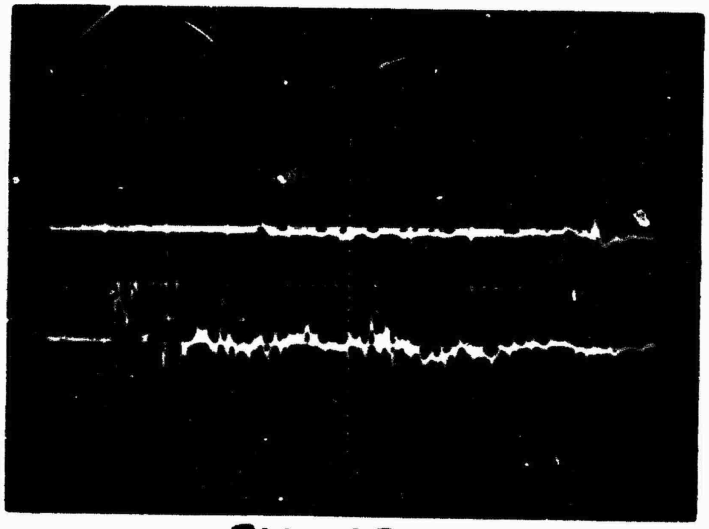

FM-4B

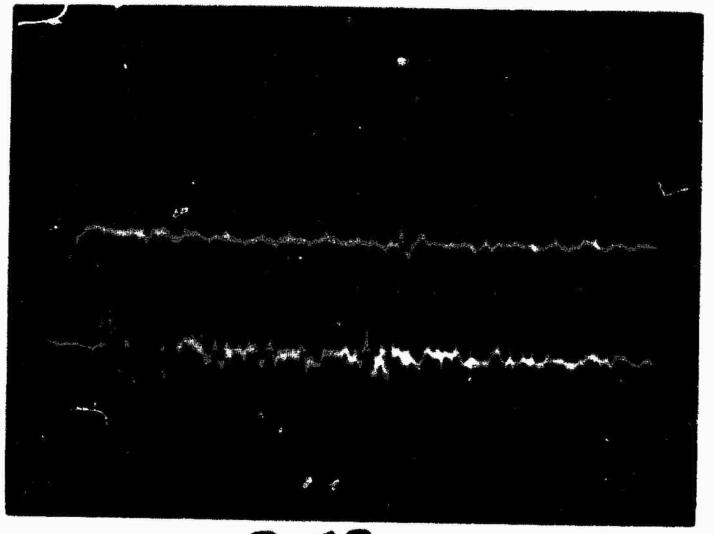

D-4B

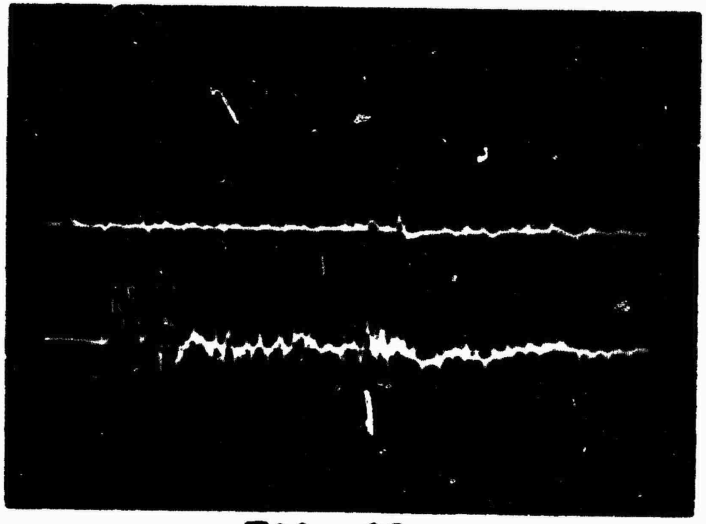

FM-4C

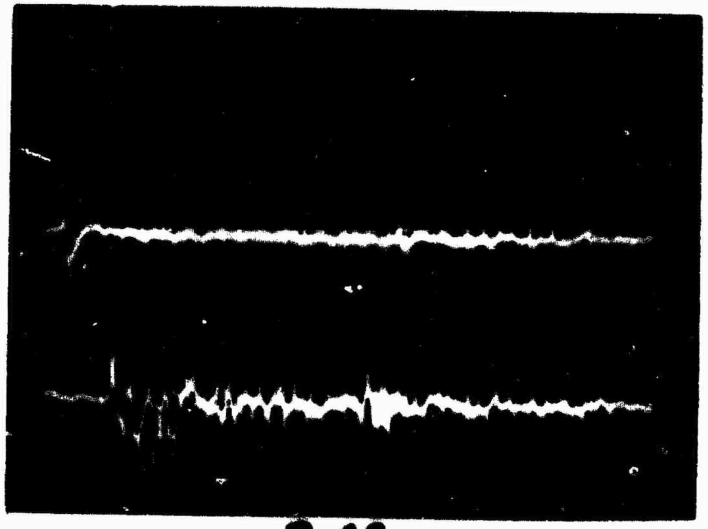

D-4C

FIG. 10

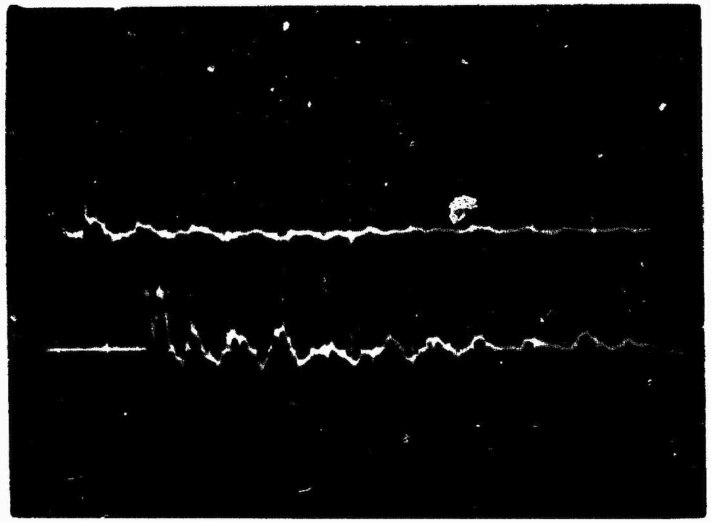

FM-8D

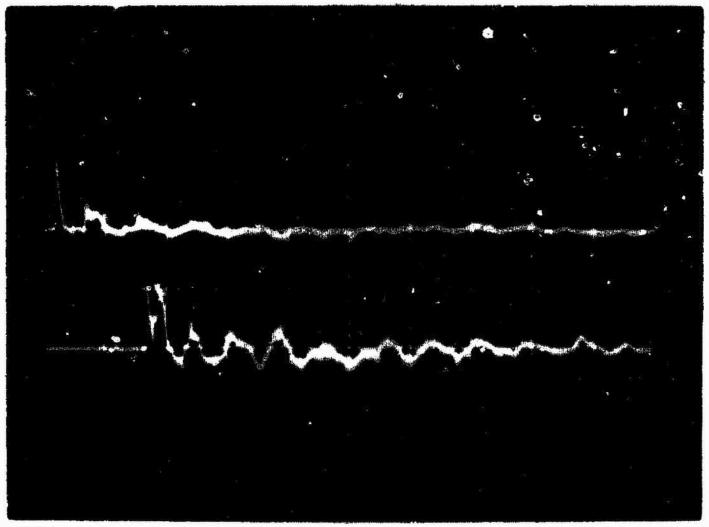

FM-8E

FIG. 11

Numerical Procedure

The digital data stored on the Adage magnetic disc was first transferred to a magnetic tape format which was compatible with the Univac 1108 available at the University Heights campus of N.Y.U. Each trace was then Fourier analyzed, using a Fast Fourier Transform routine (basically the Cooley-Tukey formulation). Thus, the input frequency response $\bar{I}(k)$ was calculated from the input time data $I(n)$, and similarly for the output;

$$\begin{Bmatrix} \bar{I}(k) \\ \bar{O}(k) \end{Bmatrix} = \sum_{n=0}^{N-1} \begin{Bmatrix} I(n) \\ O(n) \end{Bmatrix} \exp\left[-i\frac{2\pi nk}{N}\right]$$

The number of points, N, used in the calculation was 4096. In the input calculations 600 to 700 were data points in cases 1 to 4 and the rest were zeros. In cases 5 and 6 only 200 input points were used in order to suppress reflected pulses, which relate to the model, not the source. In the output calculations, from 3200 to 3600 data points were used, the rest zeros; except for case 1 in which the same number of data points as for the input were used.

The longest time increment used was 2 μsec for cases 5 and 6. Therefore no aliasing problems should arise provided our data frequency cutoff is less than the Nyquist frequency, $f_N = 1/(2\Delta t) = 250$ Hz. In tests 5 and 6 the probable microphone cutoff is about 70 KHz (for 90° incidence). In other configurations (where the microphone cutoff could reach 200 KHz at normal incidence) the Nyquist frequency is greater than 250 KHz. In the FM recording mode the recorder cutoff is 40 KHz. In view of the foregoing no difficulty was anticipated in the computation of the transforms, and of their ratio $A(k)^2$:

$$|A(k)|^2 = \left|\frac{O(k)}{I(k)}\right|^2 \qquad (2)$$

We were consequently surprised when the values of $A(k)^2$ calculated for repetitions A and B were not in agreement with each other. In fact, both sets of spectra looked like responses to signals with sizeable random components. This frequency domain behavior was first noted in connection with input-output pairs which had in a previous study, Ref. 1, been used very successfully to compute time domain responses. The FFT program used in that study to calculate the transforms $O(k)$ $I(k)$ and their complex ratio $A(k)$ (Eq 2), is the same one used in the current work.

A series of examples were devised based on analytically defined input, output and impulse response functions to compare the calculated transfer power spectrum with the analytical one. These pinpointed the need for care in the neighborhood of zeros of the input power spectrum. Use of a smoothing operation on the input and output power spectra removed these spurious singularities.

The sequence of six repeated tests listed above were then devised in order to proceed systematically from a "simple" physical system (Tests 1, 2 and 3) to the more complex (Tests 4, 5, 6). The test 1 results which involved comparison of a simple pulse at different distances from the source, should theoretically result in a constant value of the transfer power spectrum $|A(k)|^2$ for all frequencies $\leq f_o$. Instead, the inputs $\bar{I}(k)$, outputs $\bar{O}(k)$ and transfer power spectra $|A(k)|^2$ showed considerable fluctuation with frequency, and from test to test.

Summation of the $|A(k)|^2$ into third octave band groups (required for the basic methodology) resulted in considerable improvement of test to test variation. Results for test 1 are presented graphically in Fig. 14. It is seen that the FM data are fairly flat from 16 Hz to 250 Hz (corresponding to experimental model data between 1600 Hz and 25 KHz), and the variations between the independent tests are also small. The direct record data have no real significance beyond 700 Hz, or 1 KHz at most. Internal self consistency seems good, but the drooping tendency is not well understood. Case 1 also gave us a suggestion as to the source of some of the noise. Thus, it was found that the input power spectrum was reasonably flat out to 10 KHz (model scale) and dropped rapidly thereafter, at a final rate of 24 dB per octave, and was 30 dB below peak value at 60 KHz. Since the tape recorder S/N specification is 42 dB for direct record and 46 dB for FM, it is seen that electronic noise becomes very important at higher frequencies, and sooner for the direct record. Results for tests 4, 5, 6 are similarly plotted in figures 15, 16, 17.

Some preliminary tests taken full scale on the actual site are not in good agreement with the calculated data. A number of effects which were not yet taken into account include wall absorption and atmospheric absorption may be responsible, in part, for the discrepancy. Additional improvements are needed in the noise handling aspects of the experimental and numerical procedures and in the high frequency recording capability.

Ref. (1) S. Slutsky and L. Arnold, "Numerical Prediction of Interior and Structural Response of Buildings to Sonic Boom Overflights" FAA-RD-72-116, September 1972.

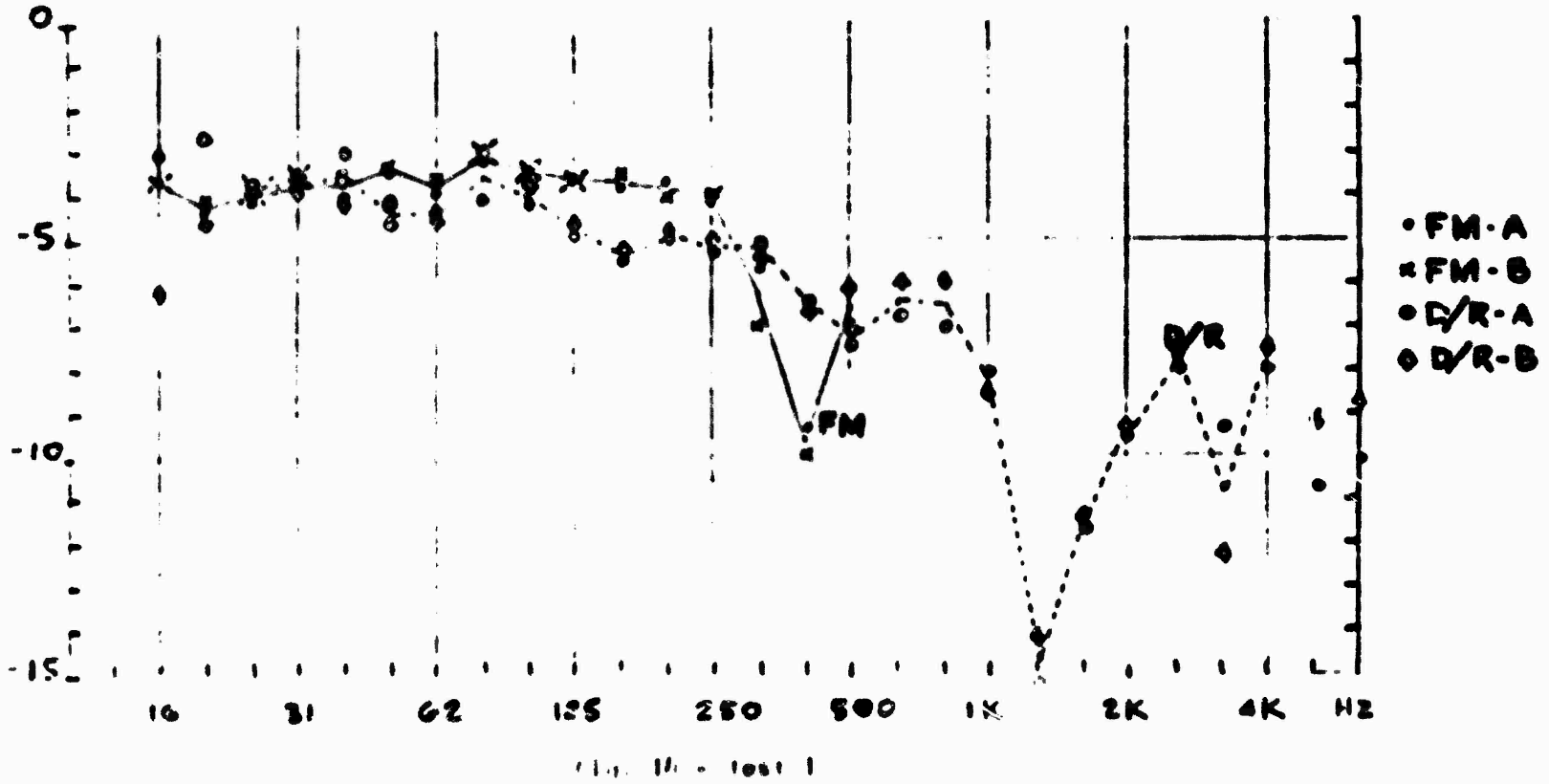
0
-5
-10
-15
16
31
62
125
250
500
1K
2K
4K
HZ
FM
D/R
• FM-A
× FM-B
• D/R-A
• D/R-B

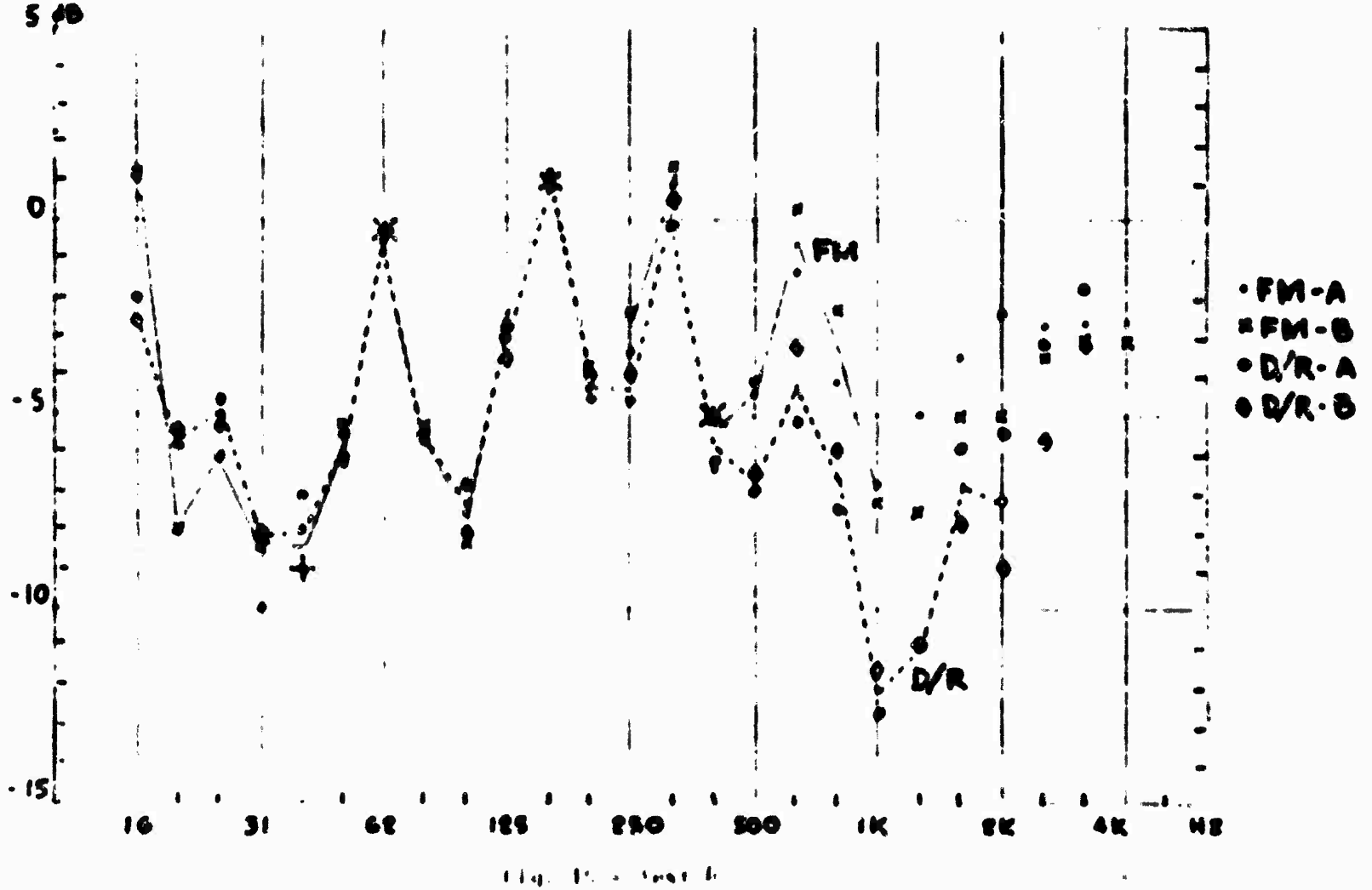
5 dB
0
-5
-10
-15
16
31
62
125
250
500
1K
2K
4K
HZ
FM
D/R
FM-A
FM-B
D/R-A
D/R-B

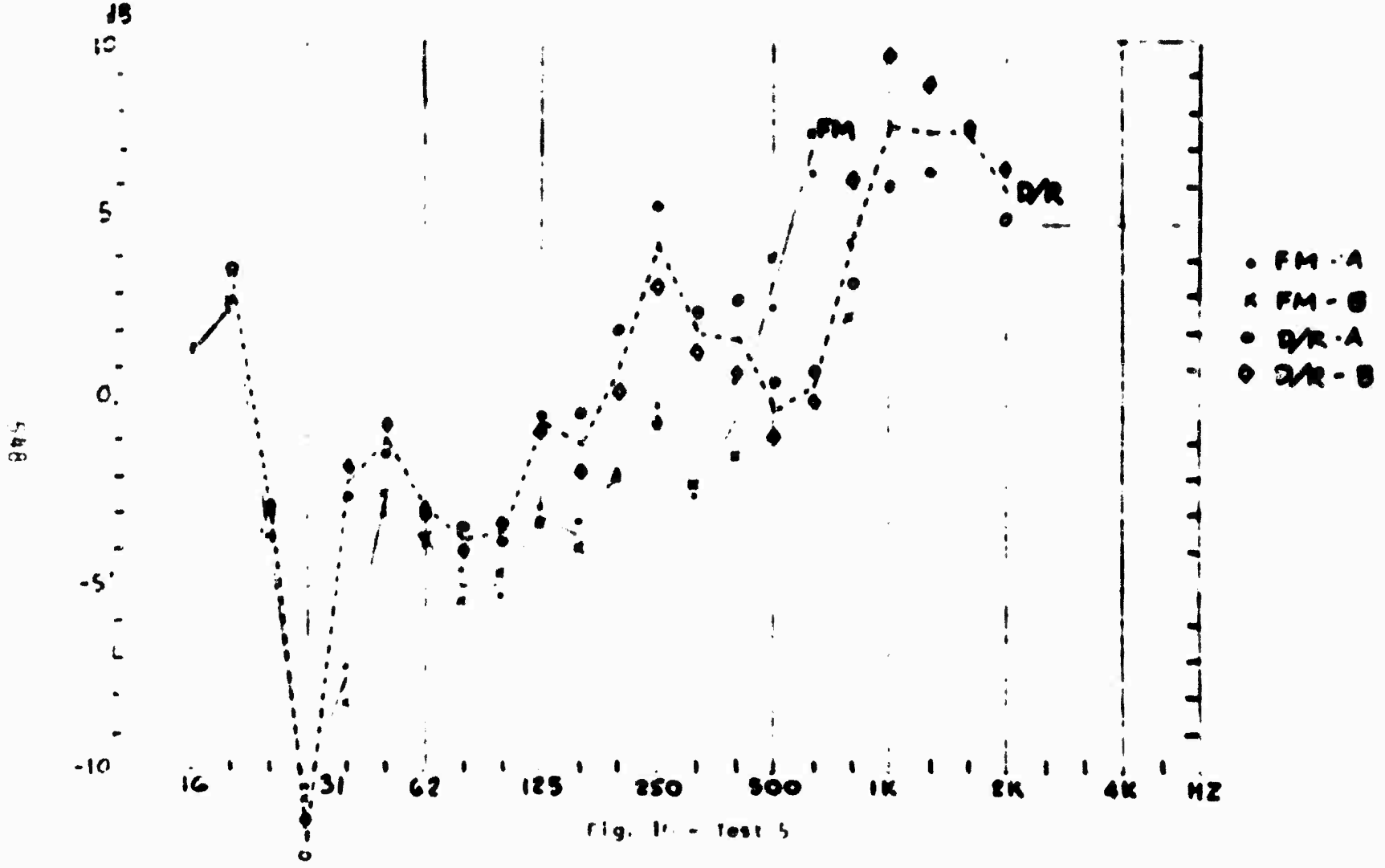
dB
10
5
0
-5
-10
dB
16
31
62
125
250
500
1K
2K
4K
HZ
FM
D/R
FM - A
FM - B
D/R - A
D/R - B

Fig. 1[illegible] - Test 5

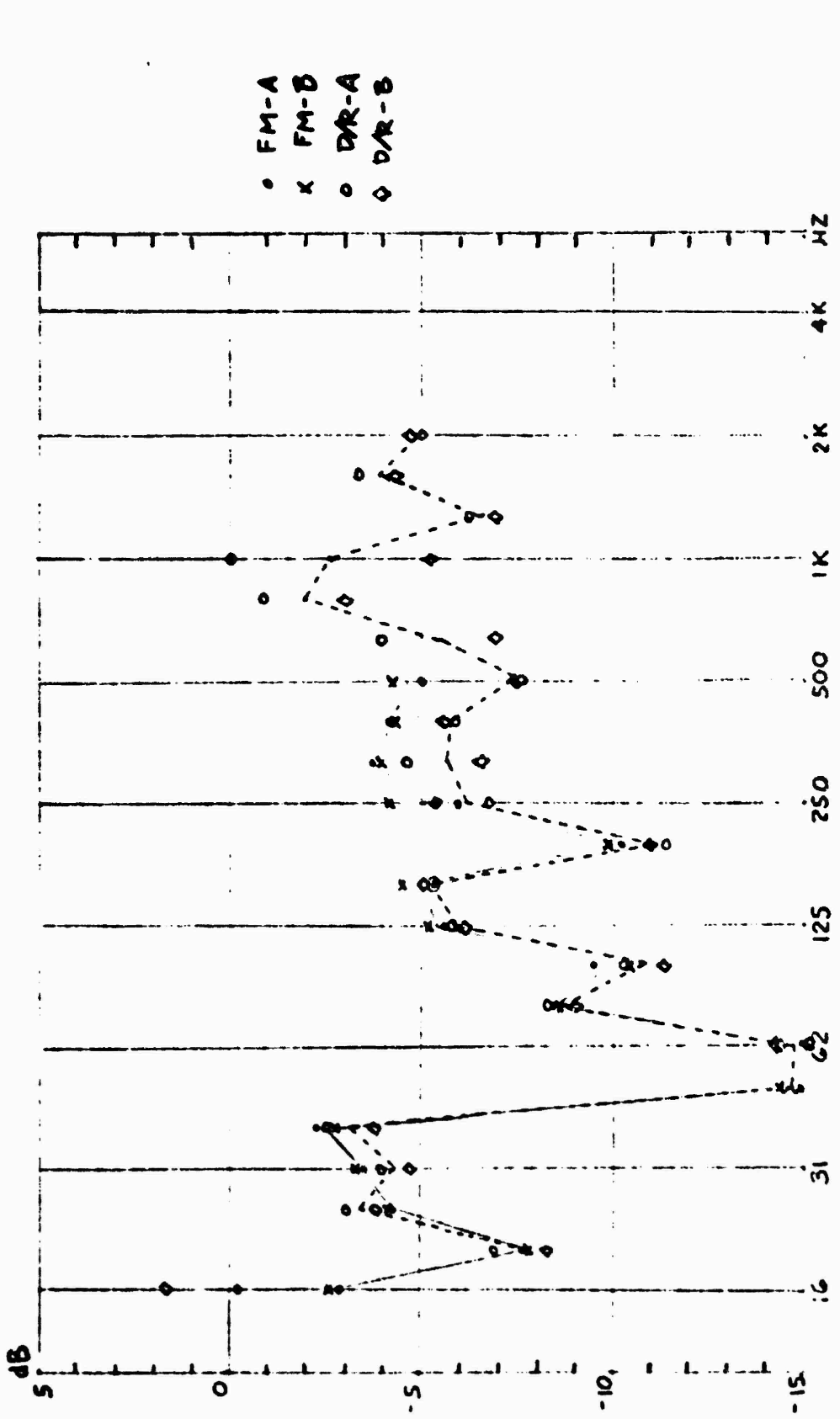

Fig. 17 - Test f.

NOISE AND VIBRATION ASSESSMENT OF THE NEW YORK CITY TRANSIT SYSTEM: A STATUS REPORT

by

Simon Slutsky
William R. McShane
Louis J. Pignataro

Polytechnic Institute of New York
333 Jay Street
Brooklyn, New York 11201

This paper reports on a project now underway at the Polytechnic Institute of New York, an Urban Mass Transportation Administration sponsored effort on "Noise and Vibration Assessment of the New York City Transit System." The Transportation Systems Center (TSC) of the U.S. Department of Transportation is the technical monitor on the work.

The effort is divided into the following tasks:

- Assessment of the existing noise situation on the rail transit system;
- Preparation of cost analyses information, generally from secondary sources, leading to costing and cost-effectiveness methodologies serving the function of the methodology presented therein;
- Development of a modeling priorities and concepts which are outgrowths of the preceding tasks, as a secondary effort and as consistent with the overall assessment and cost methodology objectives.

The third task will be pursued only to the extent dictated by developments of the first two, and the awareness that certain data might be collected with a minimal incremental effort beyond the Task 1 requirement.

This paper addresses only the first task in detail.

1. OVERVIEW

Four types of measurements are being taken:

- In-Train
- In-Station
- Community Noise
- Employee Exposure

In addition to a standard measurement program, some special baseline data will be collected. For in-train and some community noise data collection, vibration as well as noise information will be collected. All data is being kept on tape and will be retained after reduction so as to establish a data bank.

Throughout the project, there will be substantial interaction with the New York City Transit Authority. Cooperation from the Authority has been excellent. Extant data in the files of the New York City Environmental Protection Administration, Bureau of Noise Abatement, is being made available by the Director of that Bureau, as are reports from the Bureau.

The following sections present some details on the data collection program.

2. IN-TRAIN

Measurement will be sought on all lines of the New York City Transit Authority (NYCTA) and on the Staten Island Line of the Staten Island Rapid Transit Operating Authority (SIRTOA). Two complete runs will be made on each track (express and local) on the NYCTA and SIRTOA systems. One complete round trip on each line will be made using R-44 cars (where used). If these are not available on a given track section then the most modern equipment on that line will be used. A second complete round trip will be sought on the most frequently operated car model on each line (if the same, then the next one). One round trip will be sought on the PATH line in order to make possible the extrapolation of PATH equipment to IRT track.

Measurement locations will be at the center of the second car, with the microphone at 1.2 meters from the car floor.

A list of "hotspots" (points of unusual noise frequency, intensity or other special character) has been established. These points need special examination and attention.

Data collection periods will be arranged so that car passenger loading are light.

Simultaneously with the in-car sound measurement program, an accelerometer will be fixed to the floor of the car to measure the vertical vibration characteristics of the ride. The accelerometer will be placed in the middle of the car, directly beneath the microphone tripod (for maximum security and protection).

3. IN-STATION

Measurements are being made at 25 stations, chosen to reflect all prevalent subway track layout configurations. The point of measurement is opposite the centers of the train at the platform centerline if the platform is less than 4 meters wide, and at 2 meters from edge if platform is wider than 4 meters. The microphone height is 1.6 meters.

At least 10 train passages on the specified track are being recorded (entry and exit). If there is a great diversity of train models in a given situation, more measurements are being taken.

The data is being run out on strip charts, and the maximum is being recorded on coding forms for each entry and exit, as is the duration t_o that the noise is within 5 dbA of the maximum.

Results to date indicate most levels in the 90 dbA range. The compressor release on the newest cars is a significant source of short-term noise.

Figure 1 illustrates the strip chart output in three situations: (A) a typical train arrival (B) the same arrival with the time scale expanded so as to see t_o better (c) an unusual situation in which high levels are experienced for a very long duration due to station geometry and slow exit.

4. COMMUNITY NOISE

Measurements will be made at the selection of representative locations chosen to fill the elements of a table formed by the column of building construction types and the row of train exposure types.

The pickup microphone will be placed whenever possible at a distance of 25 meters from the nearest track centerline. If that distance is not feasible due to the presence of structures, then 15 meters or 7.5 meters will be the next choices, in that order. In no case will the microphone be placed closer than 2 meters from a building front.

Microphone height will be at 1.2 meters above rail level when feasible (e.g., tracks at grade). On elevated sections of open steel construction, measurements will be made at 1.6 meters above ground height, and selected measurements will be carried out to establish the magnitude of the noise correction required. On the relatively small stretches of NYCTA system where elevated track rests on non-transmitting (acoustically opaque) concrete structure, measurements will be made at 1.2 meters above rail elevation, using extension poles or equivalent support techniques.

Open flat terrain sites will be included insofar as possible to permit comparative measurements to be made for each type of track structure and for each type of car. These measurements will be made at 25 meters from the nearest track centerline.

5. EMPLOYEE EXPOSURE

Efforts will be made to arrange for the placement of noise dosimeters at typical in-train, station and tunnel locations where NYCTA employees are expected to carry out their standard work tasks. The NYCTA has already undertaken such measurements, and review of that data may show that a sufficient amount has already been taken.

6. SPECIAL BASELINE DATA

The following measurements are to be done in support of the above collection program:

1. In-train, short runs will be made on all car types on each significant tunnel or outdoor configuration so that the total noise due to specific car mixes may be estimated.

2. Benchmark measurements of noise variation within the second car and also among cars in the same train will be made.

A) R-32 Withtime scale at 6 sec. per division

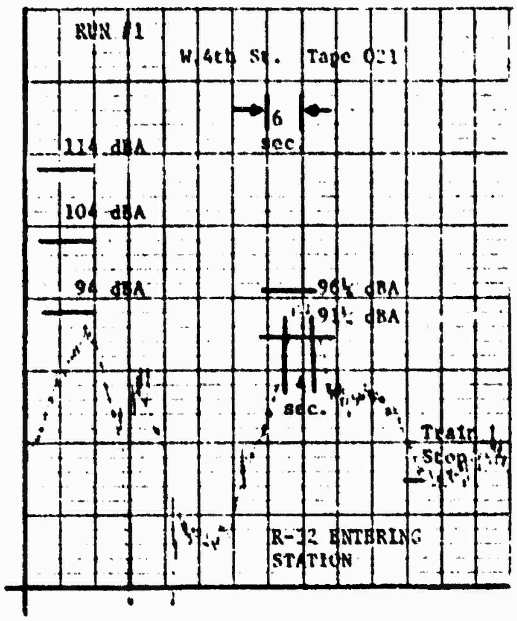

B) Same as (A) only at time scale of 2 sec. per division

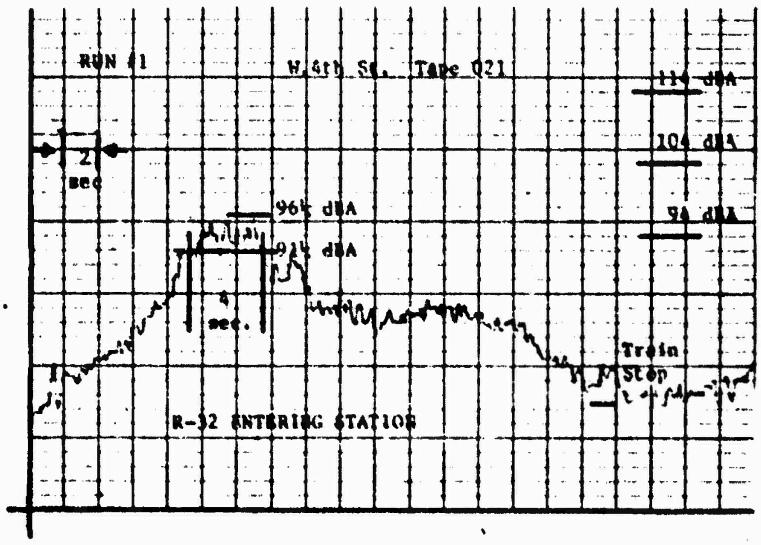

C) R-21 Leaving South Station. 6 sec. per division

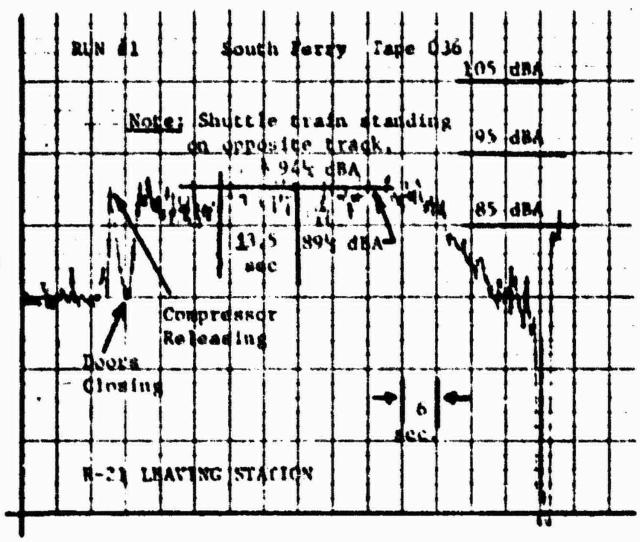

FIGURE 1

3. Two station types have been selected and measurements are to be made in several stations of each type so that the variability within stations of the same type may be studied.

4. Measurements are to be done in the above two station types (one station of each) such that the variation in noise level along the platform may be noted.

5. Measurements will be taken at various heights in the vicinity of a sampling of elevated lines so as to estimate the shielding effect of elevated structures relative to pedestrians and residential structures. Measurements will be made both with buildings nearby and with open areas facing the line.

6. An illustrative set of measurements will be made at various distances from an elevated line in a structurally uniform residential area, so that the propagation through at least one neighborhood may be illustrated.

7. STATUS

The measurement program is now well underway, with most of the in-station data now collected. The data is being reduced within 1-2 days after its collection so as to uncover any difficulties as soon as possible. This not only allows a timely new collection, but also allows for corrections to equipment or personnel as appropriate.

The second task has been initiated, and cost data necessary for the assessment is being acquired.

Meetings have been, and are being, arranged by the technical monitor among various contracting agencies related to the overall rail transit noise assessment program being managed by TSC, of which the present project is a part. These meetings, intended for cross-fertilization and for information have been most beneficial.

SPECTRA OF PAVEMENT MACROTEXTURE PROFILES

by

James M. Lawther and John J. Henry

Applied Research Laboratory and Pennsylvania Transportation Institute
The Pennsylvania State University
University Park, Pennsylvania 16802

In connection with highway vehicle skid resistance research, the Pennsylvania Transportation Institute (PTI) at The Pennsylvania State University has developed techniques for characterizing pavement texture at texture scales within the tire "footprint" area. The scale of particular interest in the present report is that thought to be important in at least some tire noise source mechanisms and is known, in the parlance of pavement texture specialists, as the pavement macrotexture. The macrotexture scale is that appropriate to the overall dimensions of individual stones in the pavement aggregate, generally of the order of one or two centimeters and less. At the small-length end of the scale, which is not closely defined, there is an overlap with the microtexture regime, i.e., with the scale characteristic of the surface texture on the individual stones.

The macrotexture characteristics reported here are wave number spectra of four pavements, stretches of which form part of the PTI Skid Test Facility. A profile tracer of an in-house design was utilized to obtain over 200 profiles of the pavement sites. It is believed that these results will be of interest to the noise control audience for the following reasons:

1. Models of tire-pavement interaction mechanisms in tire noise generation must account for the generally observed variability of this noise [1, 2] as vehicles traverse different pavements. Quantitative pavement texture characterization will almost necessarily be required in such a model.

2. The observed skid resistance properties of pavements also depend on both pavement and tire texture [3]. Noise control and skid control design specialists should speak the same language in discussing texture characterization.

3. Data bases for both skid resistance and tire noise should include a more quantitative description of the pavements involved than such characterizers as "smooth concrete", "partially worn asphalt", and the like.

4. The degree of compliance of motor vehicles with noise standards enforced by roadside monitoring is, and will be, subject to variability from texture differences, until the textures of monitoring sites can be specified quantitatively in noise-related terms.

The data reported here are drawn from a more comprehensive report [4] now in preparation.

Reference To Some Earlier Work

Primarily from the standpoints of ride quality and vehicle structural integrity an interest has been taken in pavement profile characterization by spectrum analysis for some years. The scale of interest has been the so-called "roughness" regime, with wave lengths of a meter or so, and longer. Data have usually been presented as wave number spectra and, at the highest wave numbers reported, show approximately a 6 dB/octave decrease in spectrum level with wave number. Van Deusen [5] suggests that "paved road" roughness texture spectra may be represented approximately by the empirical formula:

$$P(\Omega) = C\Omega^{-n} \qquad (1)$$

where, if $P(\cdot)$ is power spectrum level in $ft^2/(cycle/foot)$ and Ω is cycle wave number in cycles/foot, then C is a constant of the order 1×10^{-6} and n is approximately 2. Other investigators of the roughness texture report similar findings [6, 7]. As will be shown, however, the macrotexture is not just a continuation of road roughness, but is a regime in its own right with a spectrum departing substantially from Equation 1.

Other characteristics of macrotexture, in addition to profile spectra, have been suggested in connection with the problem of specifying pavement surface finishes. Statistics such as profile height standard deviations, cross correlations, and standard deviations of space derivatives of profile height are among the quantitative measures suggested. Some volumetric descriptions have been utilized, including a measure derived from a water outflow test and others from the surface areas covered by a given volume of grease, putty, or sand. Various ingenious methods of copying or replicating the texture have been devised. It is obviously much more convenient to examine replications for characterization purposes than to make measurements in the middle of a well-traveled highway. To date most of the characterizations available are derived from short samples or require very slow traverses over the pavement being examined.

The Profile Tracer Technique

The PTI macrotexture profile tracer employs a motor-driven, texture-scanning stylus attached to a linear variable displacement transducer (LVDT) to generate an electrical signal proportional to instantaneous texture displacement from a reference plane. The reference plane is determined by the profile tracer platform, which is set by three point contact leveling screws. In operation the screws are adjusted to bring the platform nearly parallel to the estimated local mean pavement plane. A twelve inch sample length is scanned at 0.152 inches per second to generate the profile wave form. For some purposes the time rate of change of the scanned profile height, proportional to the first derivative of the profile height, is desired and a velocity sensing element then replaces the LVDT.

In our experiment the electrical output representing a profile is recorded on magnetic tape, using the FM record mode. Calibration of the tape records is accomplished by tracing several calibrate surfaces each of which has a wave form controlled to close tolerances. The controlled surfaces include ramps of known slope and extent, flats, and sinusoids of several spatial periods and peak amplitudes. These surfaces are scanned just as are the actual pavement profiles, and the electrical output of the LVDT is similarly recorded on the magnetic tape. Tape playback, and subsequent spectrum analysis, is accomplished in the facilities of the Applied Research Laboratory (ARL) at Penn State. There, it is convenient to use a 32:1 playback-to-record speed ratio so as to bring the effective profile scan rate to 0.125 meters/second. A wave number of 100 cycles per meter, scanned at this speed, produces a temporal frequency of 12.5 Hertz. Most of the macrostructure regime is then represented around and above this frequency in the playback signal. Equalization of the record-playback system for the runs reported here is flat over the full frequency range of interest. Stylus radius is a principal limiting factor at the highest wave numbers. In addition, the characteristic spectrum drop-off was such as to bring the measured levels into the playback noise threshold in the vicinity of 10,000 cycles/meter. Better response tailoring is under consideration to improve the high wave number signal-to-background ratio.

Pavement and Site Selection

The present program includes data from four pavement types, each consisting of a 200 foot by 6 foot strip and all forming part of the PTI Skid Test Facility. A sketch of the facility is shown in Figure 1. The data reported here are derived from profiles of the sites numbered 3, 5, 6, and 8. Pavement compositions for these sites are:

Site 3 Jennite: Pennsylvania specification ID-2A surface (see Site 6 below) treated with a first coat of Jennite J-16 mixed 3 to 1 with AFR Plus (100 sq. ft./gallon).

Site 5 Concrete (Burlap Drag): Portland Cement Concrete, 8 inch, reinforced; finished with light application of transverse burlap drag.

Site 6 ID-2A Wearing Course: Pennsylvania specification, hot mix bituminous concrete; 5.5% AC2000 asphalt, Pennsylvania Type A limestone aggregate consisting of 42% 1-B (close) graded coarse (1/2" max. size) and 58% crushed stone sand fines.

Site 8 SR-1A (Popcorn): Pennsylvania SR-1A Experimental Hot Mix Plant Seal; 6.5% AC2000 asphalt, crushed river gravel aggregate consisting of 85% 1-B (close) graded coarse, and 15% crushed stone sand fines.

Sample profiles were taken from locations throughout each site and, at each location, profiles were taken at different angles with respect to the long dimensions of the site. The test facility is only one year old and is used only for skid resistance research; hence, it was fairly easy to avoid

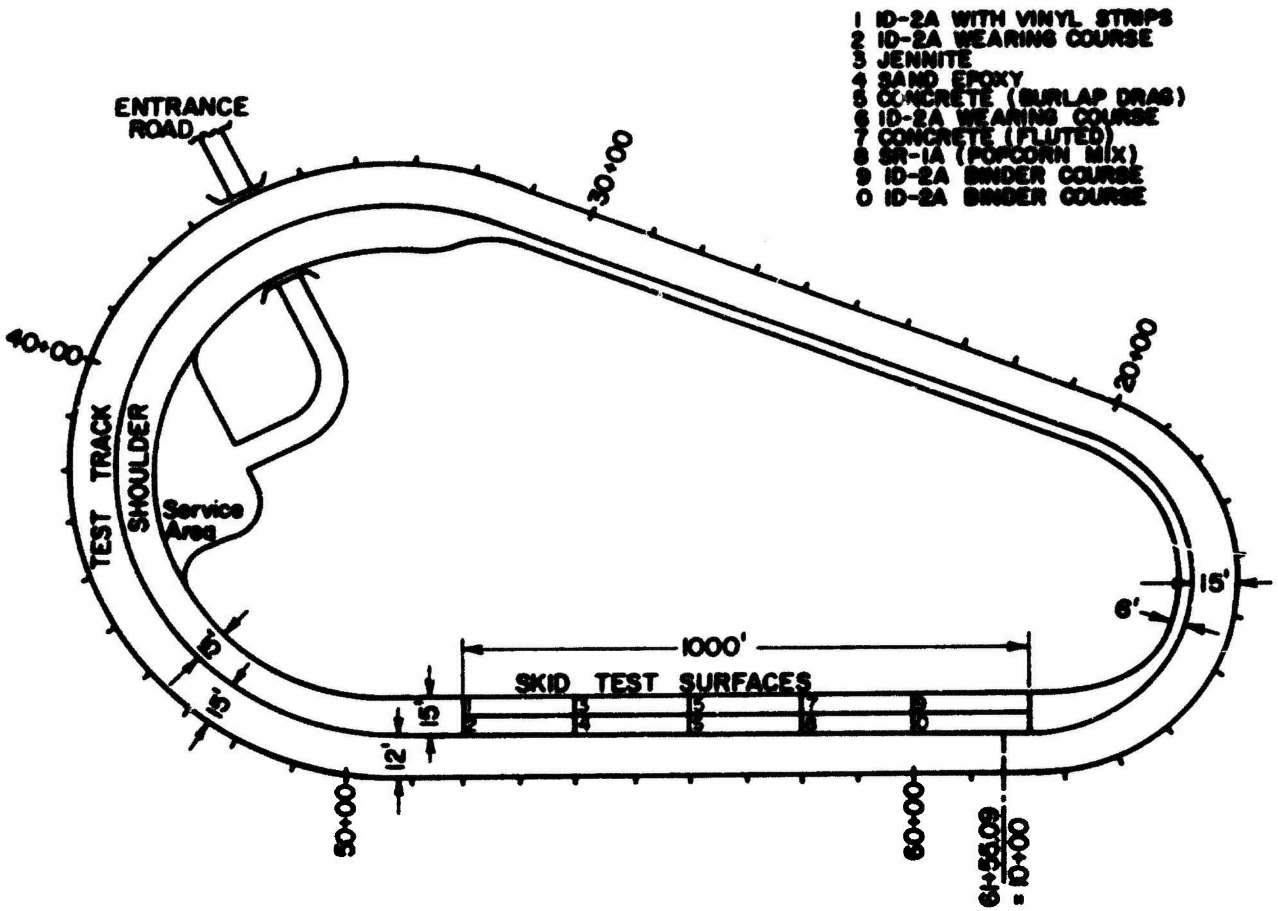

Fig. 1 - The PTI Skid Test Facility

regions strongly abraded by traffic. In apportioning the effort, it was desired to give most attention to pavements close to those in common use on highways today. Thus Sites 5 and 6 were emphasized as being typical of average pavements. Site 3, although artificially prepared, is characteristic of a bleeding asphalt pavement and Site 8 is a coarse-textured pavement of a type gaining popularity due to its good skid resistance properties. The data presented here represent 85 profiles of Site 5, 50 profiles of Site 6, and 25 profiles, each for Sites 3 and 8.

Average Wave Number Spectra

After conducting some preliminary narrow band analyses of profile wave forms to determine that, as anticipated, their spectra evidenced no prominent narrow peaks in the frequency range of interest, the bulk of the analysis effort was devoted to generation and averaging of third-octave band data. Some results are shown in Figure 2. This figure displays the ensemble averages of profiles for each pavement, with all profile directions included.

The only site to exhibit evidence of anisotropy in macrotexture was Site 5, the burlap dragged-concrete surface. For this site, profile spectra taken parallel with the direction of the drag averaged some 2-3 dB lower in band levels up to about 300 cycles per meter. Above this space frequency the anisotropy disappeared.

Figure 3 shows the overall site averages for the two commonly used surfaces (the ID-2A of Site 6 and the concrete of Site 5) displayed together with some of the previously referenced roughness spectrum data (generally those data representing newer roads). The data from the macrotexture profiles have been extended downward two octaves further than shown in Figure 2. The extension for each site was made by analyzing the records of 10 profiles pieced together end to end. The correspondence, in overlapping bands, between temporal and ensemble averaging was good.

It is clear from Figure 3 that the general negative slope which is characteristic of the roughness regime can not extend much higher in wave number than, perhaps, four or five cycles per meter before encountering the macrotexture. Parameters of the latter will, as is seen, depend on pavement composition.

Conclusions

Each of four pavement types has been represented in the macrotexture regime by wave number spectra of a sizeable sample of linear profiles. The macrotexture scale, being the largest within the footprint size of highway vehicle tires, is thought to be important to noise generation mechanism modeling and is certainly important in skid resistance considerations. There are substantial differences in wave number spectra among pavement types, suggesting that wave number characterizers may serve as quantitative identifiers more

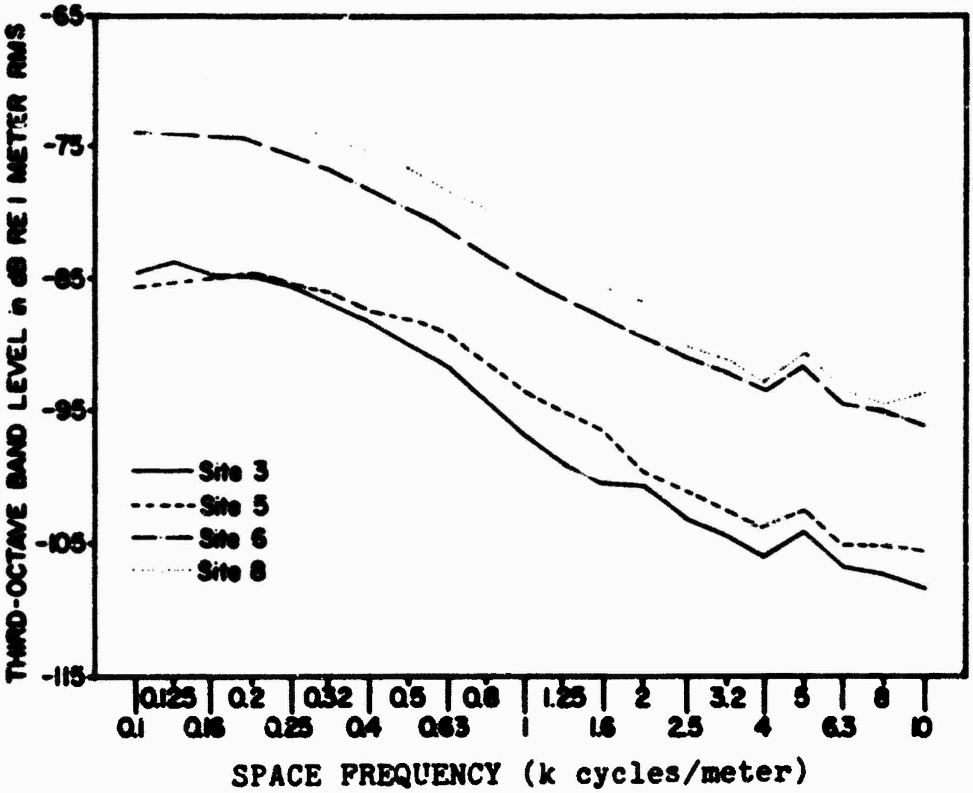

Fig. 2 - Ensemble Averages of Spectra of Profiles of Four Pavements

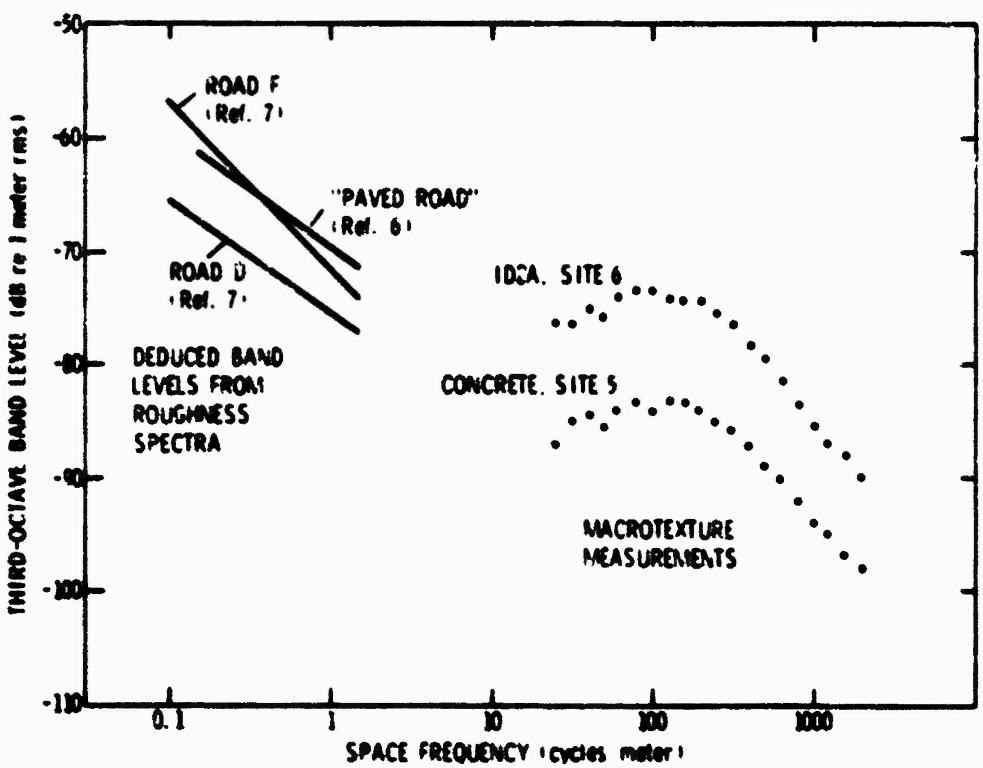

Fig. 3 - Spectra of Pavement Profiles in the Roughness and Macrotexture Regimes

suitable than such word descriptions as "concrete" or "asphalt-based". In the partially conflicting interests of tire noise reduction and skid resistance design, there remains a common need for a more complete characterization of the tire footprint interface.

[Information for this publication was collected (in part) under NBS Contract No. 3-35996 as part of a joint agreement between the NBS and the DOT.]

References

1. Leasure, W. W., Jr., Corley, D. M., Flynn, D. R. and Forrer, D. S., "Truck Noise I. Peak A-Weighted Sound Levels Due To Truck Tires," Report No. OST/TST-72-1, National Bureau of Standards, July 1972.

2. Hillquist, R. K. and Carpenter, P. C., "A Basic Study of Automobile Tire Noise," Sound and Vibration Vol. 8, No. 2, Feb. 1974.

3. Kummer, H. W. and Meyer, W. E., "Tentative Skid Resistance Requirements for Main Rural Highways". NCHRP Rept. 37, 1967.

4. Henry, J. J. and Lawther, J. M., "Characterization of Pavement Macrotexture by Profile Spectral Analysis". Final Report NBS Contract 3-35996, Pending.

5. Van Deusen, B. D., "A Study of Vehicle Ride Dynamics Aspect of Ground Mobility," Chrysler Corp., Contract Report No. 3-114, Vol. 1, under Contract CA 22-079-ang 403, March 1965.

6. Thompson, W. E., "Measurements and Power Spectra of Runway Roughness at Airports in Countries of The North Atlantic Treaty Organization," NACA Technical Note 4303, July 1958.

7. Brickman, A. H., Wambold, J. C. and Zimmerman, J. R., "An Amplitude-Frequency Description of Road Roughness," Highway Research Board Special Report 116, 1971.

MEASUREMENT OF THE MULTIPLE COHERENCE FUNCTION AND THE SEPARATION OF THE COHERENT ENGINE NOISE FROM THE TOTAL NOISE OF A DIESEL ENGINE

by

J. Y. Chung, Malcolm J. Crocker and James F. Hamilton

Ray W. Herrick Laboratories
School of Mechanical Engineering
Purdue University
West Lafayette, Indiana

I. INTRODUCTION

The early investigations on diesel engine noise in the 1930's and early 40's were mainly concerned with reducing "diesel knock" by means of improving the burning characteristics of the cylinder combustion (1-9). Not until the late 40's was more sophisticated research on engine noise problems initiated by Priede and his colleagues at the British Internal Combustion Engine Research Association.

Since the late 1960's "noise pollution control" has become one of the major issues raised by environmentalists and other concerned individuals. As a result of this public awareness, noise legislation has been enacted in the United States as well as in European countries.

One of the major noise sources to be controlled under noise legislation is vehicle noise. There are about 18 million trucks and buses in use in the USA. Most heavy trucks are powered by diesel engines, which are about 6 or 8 dB (A) noisier than similar gasoline engines (10). Today truck noise has become a problem which urgently awaits solution by the engine manufacturers.

In spite of two decades of research on diesel engine noise, a total understanding of the subject matter has not been achieved. The general approach applied to diesel engine noise research involves "noise source identification" in a "qualitative sense." In many cases, a noise source of interest was removed, or replaced by a modified unit. By comparing the original and the new noise spectra, one could decide the contribution of that particular noise source to the total engine noise. So far, some experimental "quiet engines" have been developed. The principles used to build the "quiet engine" are mainly concerned with engine surface structure modifications and the redesign of the basic engine structures. This involves (a) vibration isolation, (b) utilizing highly damped material, (c) utilizing high stiffness material, (d) reducing engine clearances. In a separate category, a total enclosure method has been applied to reduce diesel engine noise (11).

Often, the measurement of engine noise has been made in a so-called "semi-anechoic engine test cell." It has been common to make the measurement at about 3 feet from the engine surface structure. These measurement procedures were firstly used by Priede (12) and then adapted by many other researchers. The "semi-anechoic room" or "3 feet measuring distance," however, have not yet been accepted as a standard measurement procedure.

In recent years, the commercial Fast Fourier Transform (FFT) digital Fourier analyzer has become available. The FFT algorithm, which was published in 1965 by Cooley and Tukey (13) is much faster than the conventional digital Fourier transform algorithms. This makes the digital Fourier analyzer an efficient means for signal analysis. The digital Fourier analyzer makes many acoustical or vibrational measurements possible, which otherwise are very difficult if not impossible. In the present research, a Hewlett Packard Fourier analyzer has been used for the noise and cylinder spectral analysis of a V-6 cylinder diesel engine.

In the present paper the following two areas of research have been discussed:

1. Experimental evaluation of the multiple coherence function between the cylinder pressures of the engine and the engine noise, and

2. Separation of the coherent part of the engine noise from the total engine noise by means of the multiple coherence function.

In a later paper (14) the following two topics will also be described:

1. The experimental evaluation of the frequency responses of the structural acoustical noise generating system with respect to each cylinder, and

2. Coherent engine noise predictions based on assumed cylinder pressure diagrams and experimentally evaluated frequency responses.

None of these topics has been found discussed in literature of acoustics. This paper describes a continuation of the work described in Reference 15 which is also more completely described in the Ph.D. Thesis by Gene Chung (16).

II. MEASUREMENT OF THE MULTIPLE COHERENCE FUNCTION BETWEEN THE CYLINDER PRESSURES AND THE ENGINE NOISE

As previously discussed in Reference 15, the complex structure of a diesel engine can be represented by a lumped spring-mass system (Figure 1). The force due to the cylinder combustion can be treated as the primary excitation to the system. The vibrational response of the engine surface structure can then be treated

as the excitation to the sound propagating medium, i.e., air. If a point in space is chosen there is a single frequency response relating the input cylinder combustion and the output engine noise.

For a multiple input, single output system, if the inputs are mutually uncorrelated, then the frequency response with respect to each input can be evaluated individually, as long as the coherences between the output and the individual inputs are known. However, in the case of a multiple cylinder engine, the multiple inputs (the cylinder pressures) are not mutually uncorrelated. This is because of the fact that the cylinder pressure contains not only the random component but also the deterministic component. Some spectral components of cylinder pressures of different cylinders can be located precisely at the same frequency points on the frequency axis. Should the cylinder pressures be random signals, then the overlapping of the spectral components would not cause correlation. But the cylinder pressure, in fact, has numerous harmonics shown in the spectrum (Figure 2). That means the cylinder pressure cannot be treated as a random signal. This is particularly pronounced for a direct injection engine which has much steadier combustion than an indirect injection engine.

The engine under present investigation is of the direct injection type. A typical coherence function between the cylinder pressures of two different cylinders is shown in Figure 3. The coherence function is defined by equation (1)

$$\gamma^2_{ij}(f) = \frac{|S_{ij}(f)|^2}{S_{ii}(f)\, S_{jj}(f)} , \qquad (1)$$

where S_{ij} is the cross spectral density of the pressure signals from the ith and jth cylinders and S_{ii} and S_{jj} are the spectral densities of the pressure signals from the two cylinders. The coherence function γ^2_{ij} is a measure of the correlation between the two signals. When the coherence function equals 1, the two signals are completely mutually coherent and when the coherence function equals 0, the two signals are mutually incoherent. It is seen from Figure 3 that the cylinder pressures of different cylinders are strongly coherent in the low frequency region. It should be noted that a high pass filter with a 1200 Hz cutoff frequency was used in the measurements of the coherence function given in Figure 3. Theoretically, filtering the two signals will not affect the value of the coherence function. However, in the measurements shown in Figure 3 the spectral components of the signals below about 600 Hz were low enough to be similar to the instrument noise level. Hence low coherence is shown below 600 Hz. One would expect, however, that the coherence function would be higher for frequencies lower than 700 Hz for non-filtered signals.

For a 6 cylinder engine with 6 correlated inputs (cylinder pressures) and a single output (engine noise), the frequency responses between the individual cylinder pressures and the noise cannot be evaluated independently. The correlations between the inputs, in essence, establish mutual transfer relations between the inputs. Hence simultaneous equations must be solved in order to evaluate the 6 complex frequency responses at each frequency of interest.

Experimental evaluation of the frequency responses of the engine structure involves measurement and analysis of the random signals. Hence all the quantities either being directly measured or being evaluated from the measured data, should be in terms of estimations. Necessary random error estimations must be performed after the frequency responses are evaluated.

The multiple coherence function between the cylinder pressure inputs, x, and noise output, y, may be shown to be (14,15)

$$\gamma_{xy}^{2}(f) = \left\{ \sum_{i=1}^{6} \sum_{j=1}^{6} H_i(f)\, H_j^{*}(f)\, G_{ij}(f) \right\} \Big/ G_{yy}(f),$$

$$= G'_{yy}(f) \Big/ G_{yy}(f) \quad . \qquad (2)$$

Here H(f), and G(f) are the frequency responses, and one-sided spectral densities, respectively. Thus $G_{yy}(f)$ and $G'_{yy}(f)$ are the one-sided densities of the total noise y and of the coherent (correlated)engine noise, respectively.

The following instruments were used in the course of the experimental evaluation of the multiple coherence function of the V-6 diesel engine.

1. Six Kistler 603A quartz pressure transducers and two Kistler charge amplifiers (models 504 and 504E).

2. A 1/2", B & K 4133 condenser microphone, a B & K 2612 cathode follower and a B & K 2603 microphone amplifier.

3. A Hewlett Packard system 5450A digital Fourier analyzer and a teleprinter.

4. Two SKL high-pass, low-pass variable electronic filters (model 302)

5. A Spectral Dynamics signal generator, an oscilloscope and a frequency counter.

6. A Honeywell type 580 X - Y recorder.

7. A Midwest Dynamic Dynamometer of the eddy-current type (Type 1014), thermocouples and other engine auxiliary equipment.

Figure 4 is a schematic diagram showing the arrangement of the experiment. 21 cross spectral densities and 7 auto spectral densities were measured, i.e.,

$$\begin{array}{ccccccc} G_{yy} & G_{y1} & G_{y2} & G_{y3} & G_{y4} & G_{y5} & G_{y6} \\ & G_{11} & G_{12} & G_{13} & G_{14} & G_{15} & G_{16} \\ & & G_{22} & G_{23} & G_{24} & G_{25} & G_{26} \\ & & & G_{33} & G_{34} & G_{35} & G_{36} \\ & & & & G_{44} & G_{45} & G_{46} \\ & & & & & G_{55} & G_{56} \\ & & & & & & G_{66} \end{array} ,$$

and then using the conjugate symmetry, i.e.

$$G_{ji} = G_{ij}^{*} \ , \ i, j = y, 1, 2, 3,... \qquad (3)$$

the rest of the off diagonal elements were calculated.

The multiple coherence function was evaluated firstly based on equation (2). The same multiple coherence function was also checked based on a method utilizing all the cylinder cross and auto spectral densities (16). The results turned out to be precisely the same. In the former method, the multiple coherence function was evaluated based on the calculated frequency responses, while in the latter method, the multiple coherence function was evaluated directly from the measured spectral densities. The agreement of the results from the two different methods suggested that the computer programs for evaluating both the multiple coherence function and the frequency responses were working properly. Figure 5 shows the multiple coherence function obtained from the experimental runs using 1050 equivalent ensemble averages. In each coherence function plot, the random error estimation based on theory (16) and a 95% confidence interval is plotted as an upper and a lower-bound to the coherence function curve. Figure 6 shows the engine noise coherent to the cylinder pressures.

III. DISCUSSION

It is seen from Figure 6 that the coherent engine noise is almost equal to the total engine noise except at high frequency. In terms of overall level, there is less than one decibel dif-

ference between the coherent and total engine noise. However it should be noted that piston slap contributes to the coherent engine noise. It would be necessary to evaluate the partial coherence function in order to separate the piston slap noise.

IV. ACKNOWLEDGEMENTS

This work was supported by a grant from the National Science Foundation, Washington, D. C.

V. REFERENCES

1. R. N.Janeway, "Combustion Control by Cylinder Head Design," S.A.E. Journal, 24-498, 1929.

2. G. D. Borelage and J. J. Broeze, "The Ignition Quality of Fuel in Compression Ignition Engine," Engineering, 132-602, 1931.

3. L. J. LeMesurier and R. Stansfield, "Fuel Testing in Slow and High Speed Diesel Engines," J. Petrol Tech., 17-387, 1931.

4. A. M. Rothrock, NACA Report No. 401, 1931.

5. L. J. LeMesurier and R. Stanfield, "Combustion in Heavy Oil Engines," Paper read at North East Coast Institution of Engineers and Shipbuilders, England, February 26, 1932.

6. P. H. Schweitzer, "Combustion Knock in Diesel Engines," Technical Bulletin, Pennsylvania State College School of Engineering, 1935.

7. W. Joachim, "The Characteristics of Diesel Fuel Oil," Diesel Power, 13-283, 1935.

8. C. C. Minter, "Flame Movement and Pressure Development in Gasoline Engines," S.A.E. Journal, 30-80, 1935.

9. W. Wilke, "Investigation Concerning the Burning of Diesel Fuels," M.T.Z., 1-43, 1939.

10. M. J. Crocker, "Noise Control in the USA - The Present State of Affairs," Purdue Noise Control Conference Proceedings,July 14-16, 1971.

11. M. J. Crocker, D. R. Tree, S. R. Jones, and D. A. Towers, "Acoustic Enclosures for Diesel Engines in Trucks," Proceedings of the Interagency Symposium on University Research in Transportation Noise, March, 1973.

12. T. Priede, "Noise of Internal Combustion Engines," National Physical Laboratory Symposium No. 12, London, 1962.

13. J. W. Cooley and J. Tuckey, "An Algorithm for the Machine Calculation of Complex Fourier Series," Mathematics of Computation, Vol. 19, No. 90, April, 1965.

14. J. Y. Chung, M. J. Crocker and J. F. Hamilton,"Prediction of Diesel Engine Coherent Noise Using Frequency Responses and the Multiple Coherence Function," paper to be submitted to JASA, 1974.

15. J. Y. Chung, M. J. Crocker and J. F. Hamilton "Noise Measurement on a V-6 Diesel Engine," NOISE-CON 73 Proceedings pp. 86-91, Washington D. C., October 15-17, 1973.

16. J. Y. Chung, "Measurement and Analysis of Diesel Engine Noise", Ph.D. thesis, Purdue University, May, 1974.

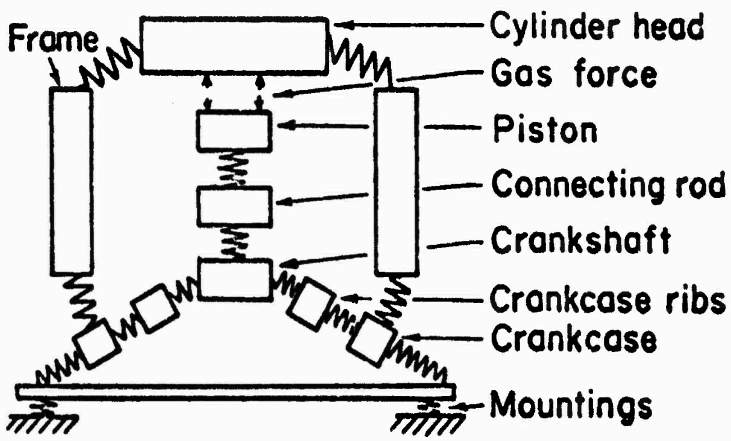

Figure 1. A spring-mass system representation of the engine structure.

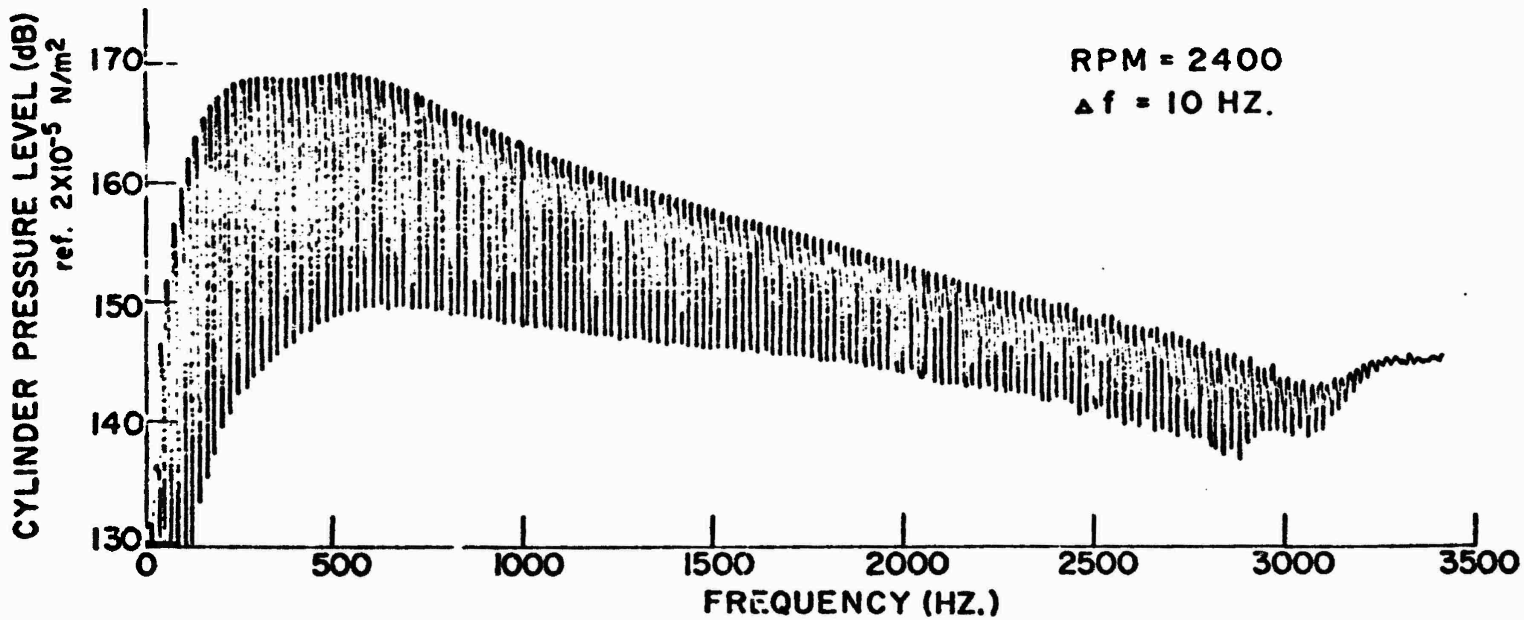

Figure 2. Details of the harmonics of the cylinder pressure-time history.

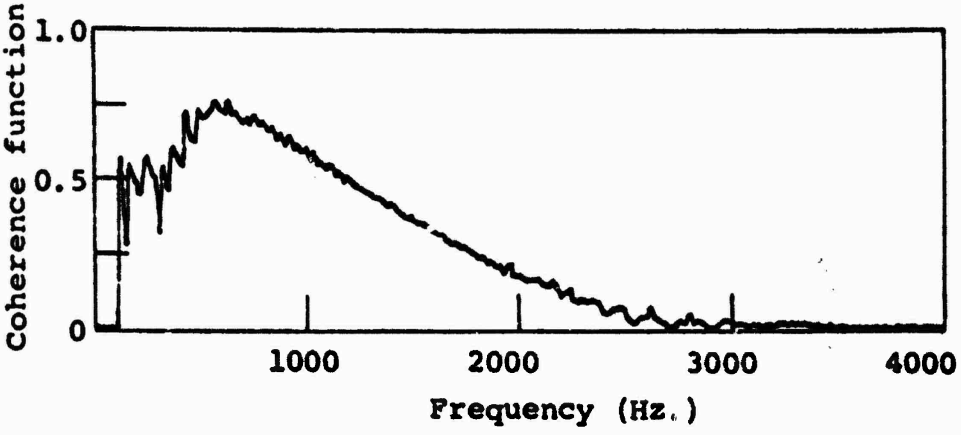

Figure 3. Typical coherence function between two cylinder pressures.

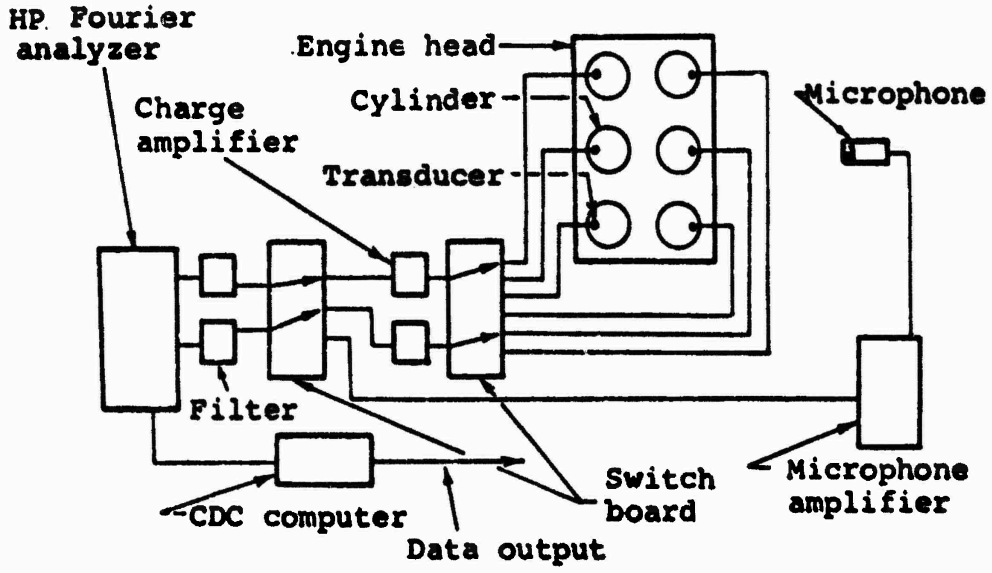

Figure 4. Schematic diagram for the experimental evaluation of the multiple coherence function of the V-6 diesel engine.

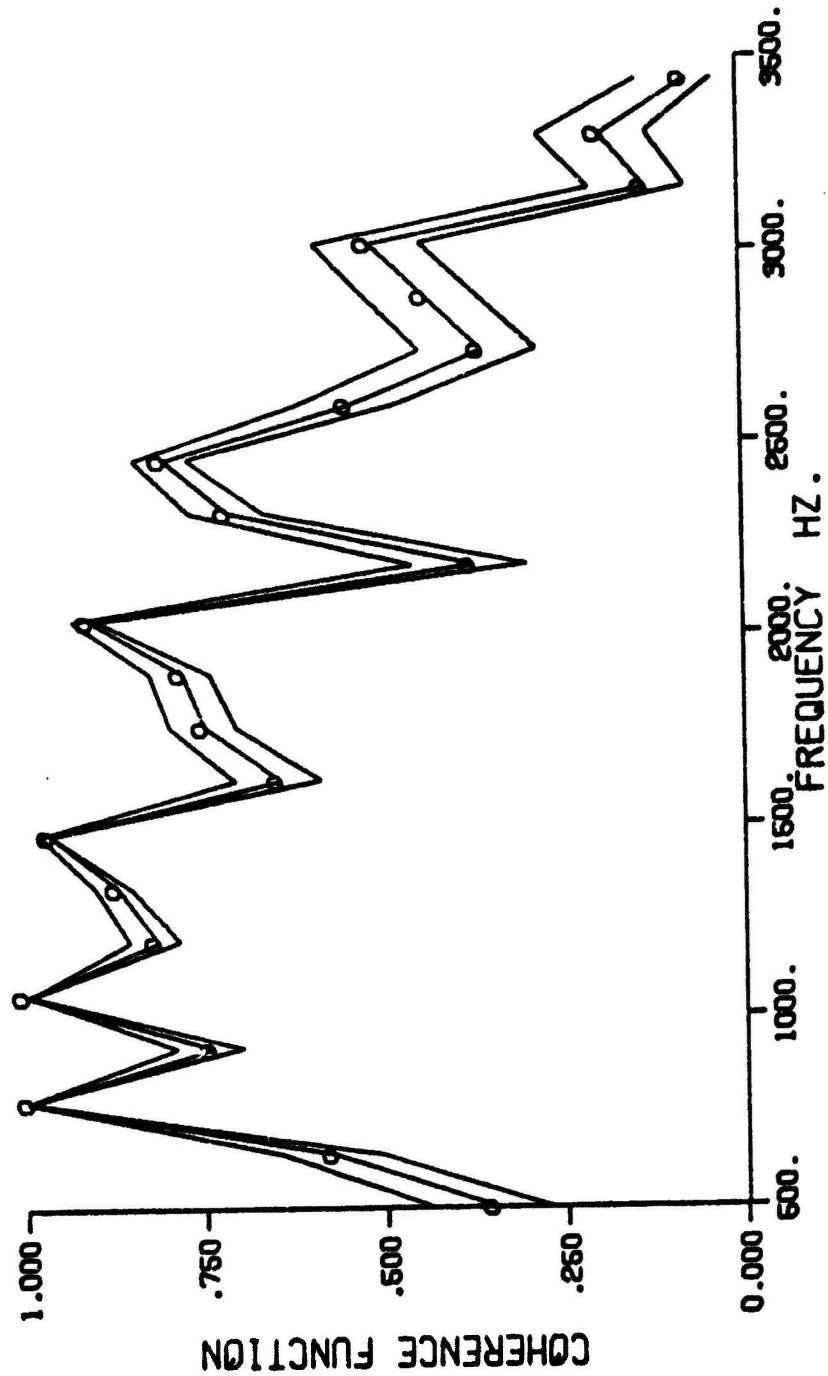

Figure 5. The multiple coherence function.

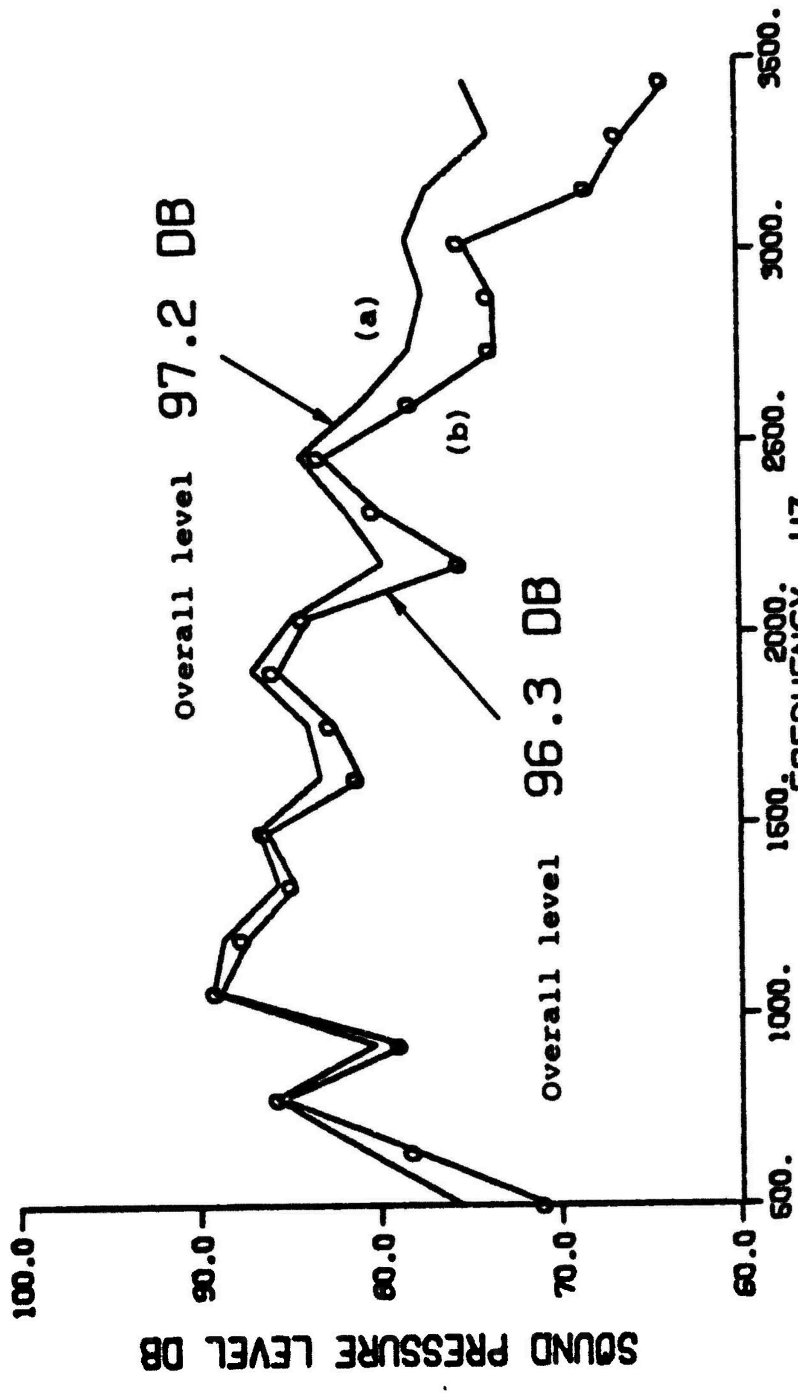

Figure 6. The engine noise spectrum at 2400 rpm, (a) total noise, (b) coherent noise.

THE ACOUSTIC RESISTOR

by

Herbert V. Hillery

Applied Research Laboratories
The University of Texas at Austin
Austin, Texas

It is well known that the similarity between the differential equations describing the motions of a driven linear mechanical oscillator and describing the movement of charge in a driven electrical oscillator allows several different dynamical analogies to be drawn between mechanical circuit and electrical circuit component reactions.

According to the impedance or "classical" analogy, the inertia of a mass is regarded as analogous to the inductance of an inductor, the compliance of a spring is regarded as analogous to the capacitance of a capacitor, and frictional losses in a mechanical circuit are regarded as analogous to electrical losses in an electrical circuit.

Using this analogy, acoustical engineers familiar with electrical circuits can readily predict the performance of many acoustical circuits by regarding masses as inductors, springs as capacitors, and dashpots or shock absorbers as resistors. Because this procedure has proven effective for many acoustical circuits, there has been little awareness that a true acoustical analog to the electrical resistor has not been available. The main difference between the functioning of electrical resistors and of presently available mechanical resistance devices is shown by the following.

It is well known that an electrical transmission line is analogous to an acoustical waveguide.[1] The input impedance of an infinitely long lossless transmission line is a pure resistance, R_{CE}, called the characteristic resistance of the line. Similarly, the longitudinal wave mechanical input impedance of an infinitely long lossless straight solid rod of diameter d, small relative to a wavelength of the sound waves propagating along the rod, is a pure resistance, R_{CM}, called the characteristic mechanical resistance of the rod.

If an electrical transmission line of finite length has an open circuit or short circuit at its remote end, or if the remote end is terminated with an inductor or capacitor or with a resistor having a resistance unequal to R_{CE}, any electrical wave applied to the near end of the line is partially or totally reflected from the remote termination. Because of the reflection, the line is said to be improperly terminated.

If the remote end is properly terminated, that is, if it is terminated in an electrical resistor of resistance $R=R_{CE}$, no reflection occurs even if all dimensions of the resistor are many orders of magnitude smaller than the wavelength on the transmission line.

For this properly terminated case, regardless of the length of the transmission line relative to the wavelength, the input impedance of the line is the pure resistance R_{CE}. No alternating voltage or current measurements at the input end of the line will reveal whether the line is infinitely long or has a finite length that may even be extremely short relative to a wavelength.

Three characteristics of the electrical terminating resistor have particular significance relative to the problem of obtaining a description of the characteristics of a true acoustic analog to an electrical resistor.

First, the electrical resistor is an electro-thermal transducer which converts electron vibrations into the random molecular vibrations defined as heat. In this respect, the resistor acts as a radiation impedance just as though it were a perfect antenna radiating into infinite space. It acts as a radiation resistance even though it is exceedingly small relative to the wavelength on the transmission line. Second, the resistor does not have to be directly or indirectly connected to an inductor in order to perform its function. Third, the electrical resistor exhibits a resistance that appears to be a fundamental property of the material of which it is constructed. Although the characteristic resistance of a transmission line can be expressed as a function of the inductance and capacitance per unit length of the line, the resistance of the resistor cannot be expressed as some function of inductance and capacitance. Indeed, a well constructed electrical resistor exhibits almost no inductive and capacitive reactance, regardless of frequency.

Because of this third characteristic of an electrical resistor, and because the effect of a proper terminating resistor on the input impedance of a transmission line is independent of the length of the line, there appears to be no reason for assuming that the characteristic resistance of a lossless transmission line is any less a fundamental property of the line than its inductance and capacitance per unit length. In fact, it appears possible, for a lossless line, to regard R_{CE} as the primary function of the dimensions and material of the line and to regard the inductance and capacitance of the line as merely the effects on the input impedance of the line that arise from improper termination.

From the three characteristics of an electrical resistor acting as a proper termination for a transmission line, it can be seen that a true acoustical analog to an electrical resistor should exhibit the following characteristics if it is used as the proper termination for a straight lossless solid rod carrying longitudinal sound waves.

First, the acoustical resistor should act as an acoustic-thermal transducer, transforming acoustic particle vibrations into the random molecular vibrations defined as heat. It this respect, an acoustic resistor, when used to properly terminate a solid longitudinal wave waveguide, should act as an acoustic radiation resistance just as though

it were a perfect radiator of sound that is radiating into an infinite medium. It should act as a radiation resistance even though it is exceedingly small relative to the wavelength on the waveguide.

Second, the acoustic resistor should perform its function without having to be directly or indirectly connected to a mass (analogous to an inductor).

Third, the resistance of the acoustic resistor should be a fundamental property of the material from which the resistor is constructed or of the configuration of the material. The resistance should not be some function of the mass or stiffness of the resistor. In fact, the acoustic resistor should exhibit, regardless of frequency, almost no mass reactance or stiffness reactance.

The input resistance of a lossless straight rod properly terminated with an acoustic resistor should be R_{CM}, regardless of the length of the rod relative to a wavelength and regardless of the dimensions of the resistor. Despite its weight, the properly terminated rod should exhibit no longitudinal inertia or springiness. This suggests that the qualities of mass and stiffness commonly attributed to material objects are merely the effects on the input impedance of the objects produced by the reflections caused by improper termination of the objects.

Since it was evident that no acoustic component in common use fitted this derived description of an acoustic resistor, the acoustics literature was searched to determine whether any component fitting the description had been described earlier. No evidence could be located that an acoustic resistor has ever been constructed or that anyone previously has suggested that such a component might be feasible or useful. Consequently, the research now in progress was undertaken.

Additional consideration of analogous lumped impedance electrical and acoustical circuits suggested that the various lumped impedances belong to two classes which might be called natural and artificial.

Among the electrical impedances, resistance is the only natural impedance. A wide range of values of resistance can be obtained from simple shapes of more or less natural materials. On the other hand, inductance and capacitance are artificial--only very small values of these impedances are available from simple shapes of natural materials. In order to obtain large values, science has had to learn to shape and arrange materials into previously unknown configurations such as coils with cores, and alternated layers of conductors and insulators.

Contrastingly, among the acoustical impedances, inertance and compliance are natural--wide ranges of values are available from simple shapes of more or less natural objects. Acoustical resistance, on the other hand, appeared

to belong in the artificial class. Certainly only small values of acoustical resistance have been obtained from simple shapes of common materials. Although no assurance was available that some configuration of materials could yield high values of acoustical resistance, the examples of inductance and capacitance suggested that a search for suitable configuration might be rewarding.

One solid structure was known that could theoretically provide at least a small value of pure acoustical resistance. This is the transversely vibrating finite string that is terminated in resistive supports having a resistance equal to the transverse wave impedance.[2] It appeared also that perhaps a finite flat plate could be provided with resistive edges to make its flexural wave impedance equal to the impedance of an infinite flat plate, which is known to be resistive.[3] It was felt that resistive end supports for strings and resistive edges for flat plates might be achieved with one of the polymers known to exhibit high shear losses. Using the predicted and surmised characteristics of resistance terminated, transversely vibrating strings and plates for guidance, various sample acoustic resistors have been assembled from a wide variety of materials. These sample resistors are now being tested.

The tests are made by mounting the sample resistors on the remote end of a 48.5 m long, 5.7 mm diam solid aluminum rod having a characteristic mechanical impedance R_{CM}=289 kg/sec. The near end of the rod is driven with longitudinal tone bursts that are shorter on the rod than the length of the rod. The outgoing and reflected tone burst signals are detected by a displacement probe resting on the rod 31 m from the input end. A more detailed description of this tone burst rod apparatus has been given in an earlier paper.[4]

Results of the tests performed so far show that an acoustic resistor can be constructed that absorbs more than 90% of the acoustic energy incident upon it from the 289 kg/sec output impedance of the aluminum rod over the 2 1/2 octave band from 500 Hz to 2800 Hz and that absorbs more than 98% from 800 Hz to 2000 Hz. The frequency dependence of the absorption shows that resonant behavior has not been totally eliminated.

The thickness of the resistor which has given the best absorption is 2.2 cm or 4.3/1000 of the wavelength at 1 kHz on the rod. The transverse dimensions are 8 cm by 12 cm. The resistor consists centrally of a stack of three round 0.081 cm thick aluminum disks separated by round disks of Scotchcast 221 polyurethane. Two of the aluminum disks are 2.5 cm diam and the third is 6.1 cm diam. One of the polyurethane disks is 0.18 cm thick and 3.8 cm diam. The other two main polyurethane disks are 7.6 cm diam. One is 0.56 cm thick and the other is 0.48 cm thick. Near the circumference of the latter, two 0.165 cm thick, 3.8 cm diam disks, one of the polyurethane and one of polypropylene are attached. The plane of the small disks is parallel to the plane of the large disk. The axis of the large disk is midway between the axes of the small disks. The small disks are mounted between 0.051 cm thick, 2.54 cm diam aluminum disks and attached to the large disk with 4-40 brass screws and nuts. Radial cuts into the edges of these small plastic disks divide the disks into fan shaped segments. The entire resistor structure is attached to the aluminum rod with a 4-40 nylon screw.

Although this acoustic resistor is totally lacking in beauty, it is so effective that virtually no sound radiates from it. The results achieved with the resistor are regarded as providing a strong indication that a practical solid lumped acoustic resistor can be achieved. The research is now directed toward fully defining the physical principles that produce the high absorption, so that the principles can be applied to the construction of resistors of predictable resistance that are more compact and more practical for application in reducing sound propagation in transportation structures and other structures.

(This research is supported by NSF Grant GK-34367.)

REFERENCES

1. R. K. Moore, Traveling-wave Engineering (McGraw-Hill, New York, 1960), pp. 25-6.

2. J. C. Slater and N. H. Frank, Mechanics (McGraw-Hill, New York, 1947), p. 172.

3. L. Cremer, "Calculation of Sound Propagation in Structures," Acustica Vol. 3, No. 5, 1953, p. 324.

4. H. V. Hillery, "Investigation of Acoustic Propagation in Branched Solids," Proceedings, Interagency Symposium on University Research in Transportation Noise, Stanford University, 28-30 March 1973, Vol. 2, p. 674.

RELATIONSHIPS BETWEEN TREAD PATTERN AND AUTOMOTIVE TIRE NOISE

by

W. C. Reynolds
Department of Mechanical Engineering
Stanford University, Stanford, CA 94305

1. Motivation and objectives

It is known[1] that tires are a major contributor to passenger automobile noise at freeway speeds. The tread features contribute significantly to this noise, as evidenced by experiments on smooth tires and tires with straight circumferential grooves (aircraft type tires).[2] Modern tires employ variable-pitch wavy grooves, or pitch-sequencing, which produces acoustic signatures found to be less annoying than the pure-tone uniform-pitch wavy grooves. More sophisticated tires, such as General Motors' new special tires, also employ phase-shifting between grooves in an effort to obtain some cancellation. There are many other tread features, such as cross-grooves and sipes, all of which contribute in some unknown way to the complex acoustic signature of the tread pattern. In addition, there is a "random" noise component produced by irregularities in the road surface and the tire motion.

The present work deals primarily with the tread-related portion of the acoustic signature. The objectives of the current state of this work are

1) to determine the acoustic signature of individual tread features
2) to explore the possibility of prediction of the tread-related signature of complex patterns by superposition of these elementary components
3) to investigate the potential for reducing the tread-related component by designing a tread pattern for optimum cancellation and acoustic beam directional characteristics.

The ease and success of (3) will depend on our success in (2). If (3) can be achieved, the next step will involve study of systematic approaches to pitch-sequencing with regard to both acoustics and aural perception. An additional future objective might be the development of standardized laboratory testing procedures for evaluation of commercial automotive tires with respect to state and federal noise standards.

The basic approach involves study of special tires under controlled laboratory conditions. Although there has been considerable controversy about the relationship of tests on rotating roadway-wheels to tests on flat road surfaces, there is really no evidence to indicate that the objectives described above can not be met using a laboratory wheel. We chose the wheel approach over field testing for a variety of reasons, perhaps the most important being our ability to carefully control the test conditions. We have had some discussions with General Motors about the possibility of some joint experiments to obtain definitive answers to the flat-curved surface controversy, and if these can be arranged a resolution of this controversy will become an additional objective of this program.

2. Basic approach and status

a) roadway wheel

We have constructed a special roadway-simulation wheel for these tests. The wheel has a circumference of 1/300th of a mile, which seems to be a standard of the tire industry. It is eight inches wide and can support loads of up to 1500 lbs. A solid-web construction was used to eliminate aerodynamic noise from webs. The wheel was cast in aluminum and machined over its entire surface, and hence required only minor balancing. It is driven through a 3-inch diameter shrunk-fit shaft, and runs true to within 0.003" vertically and 0.010" horizontally.

The driving motor is a large DC motor, obtained from government surplus at no cost. The motor is rated at 15 hp at 1150 rpm, 220 V, but is operated at a fraction of its capacity. This direct-drive system is very quiet and vibration-free. A solid-state control system is being constructed, which will permit accurate control of the wheel speed under varying load.

The tire is mounted on a special wheel supported from below. The support is connected to the roadway-wheel frame through a load control system. Load is supplied through a hydraulic piston, and the hydraulic pressure is controlled by the supply pressure of bottled nitrogen. Needle valves provide for some control of the stiffness of the suspension system. It is our initial intention to operate with a very stiff suspension in order to obtain a steady contact patch footprint.

The head on which the wheel is mounted has sufficient freedom to permit a proper alignment of the tire with the roadway-wheel. Alignment is accomplished using appropriate machinists rules and gauges. Camber can be adjusted by tilting the loading system at the point where it attaches to the roadway-wheel frame. The initial tests will be without camber.

Aluminum is not a satisfactory working surface, but at the suggestion of workers at Ford and General Motors we are using a surface of 3-M medium grade Safety-Walk, normally used to provide traction on stairways and ramps. This surface has a roughness characteristic somewhat like asphalt. We have found that it does not load up with rubber, and believe it will be an excellent surface for our first experiments.

b) test laboratory

A special laboratory has been prepared for this experiment. A pit was dug in the floor, large enough to accomodate the roadway-wheel and the proper depth to set the contact patch a fraction of an inch above the floor level of the room. Plywood plates will be used to cover most of the pit, and special aluminum plates will be used to extend the surface to within a fraction of an inch of the roadway-wheel. When complete, the tire will appear to be running on the floor of the test room, supported from below.

The pit has been provided with a quieted exhaust fan, which will suck air out of the pit. Make-up air will in part be sucked through the slots where the roadway-wheel meets the stationary floor, and this will serve to control the boundary layer on the rotating surface. Additional make-up air is supplied to the pit through a separate duct from the roof. The exhausted air will carry with it heat developed by the motor and roadway-wheel system, and also will romove the vorticity that would tend to develop in the pit if the wheel were allowed to operate in an enclosed pit for a long period of time. Without this vorticity removal, winds of up to 50 mph could develop in the pit with prolonged operation.

Power and instrumentation is carried to the pit from an adjacent room in a covered trench. Controls and instrumentation may be located in the pit area where this is deemed desirable. The roadway-wheel and pit cover plates will be treated as necessary to remove undesirable system vibrations that might interfere with the acoustic experiments.

The idea is to do the tests in a "hemianechoic" environment, with the solid floor of the room providing acoustic reflections representative of the highway surface. Initially it was planned to line the walls and ceiling of the test room with acoustic wedges. However, after some experimentation with fiberglass in an acoustic wave tube, and upon consideration of the fact that the tread-related features generate frequencies typically in the range 500-1500 hz, it was decided to take a simpler approach. The walls and ceiling are now being lined with 6 inches of medium density (3 lbm/ft^3) fiberglass covered with a 3/8 inch layer of open-cell foam [100 pores per linear inch fire retardant Scott Industrial Foam]. Manufacturers information indicates that this combination should have a random (Sabin) absorption coefficient of .99 at frequencies above 250 Hz. The inside dimensions of the finished room will be 18'-6" by 13'-6" by 7'-9" high. Thus normal modes of room resonance will occur at multiples of 30, 42, and 73 Hz. The wall treatment is such that we anticipate no difficulties with room resonance in the frequency range of interest.

Two walls and a false ceiling within the room were covered with two layers of cross-lapped sheetrock, and special solid-core double-doors were installed. With these modifications the room will enjoy excellent isolation from external sounds. Room ventilation is provided through acoustically treated ducts by special quiet fans. Lighting is provided by special quiet-ballast fluorscent bulbs. The level of background sound, with both blowers and all lights operating, is expected to be less than 30 dbA.

A special device for moving a microphone around the vertical axis of the contact patch has been constructed as a "design project" by a team of first-year graduate students. The drive motor and support system for this unit are mounted in the ceiling directly above the tire. This system will allow us to scan the radial acoustic field around our test tires on a radium up to about eight feet over a 90° sector, and over partial sectors in "curbside" areas for up to fifteen feet.

c) special tires

Arrangements were made with Firestone for construction of special test tires, and the first group was delivered early this year. These tires are made by cutting the tread pattern on blank tires using their electric knife device. All test tires are 600:13 with identical carcasses. Tire #1 is a blank tire for reference. The remaining tires will all carry four grooves of the same depth cut into identical blank tires, and tire #2 is a straight-groove reference tire. Tires #1 and #2 will be used primarily to determine the level of the "random" portion of the noise. Tire #3 has one uniformly-pitched wavy groove and three straight grooves. The first tread-signature studies will be carried out with this tire. It has been run on the wheel, and produces a distinct pure-tone noise. Subsequent tires will involve multiple grooves, optimally phased, for testing of the superposition, cancellation, and acoustic beaming concepts. The designs for these will be determined using data from the experiments on tire #3.

We expect to place microphones near the leading and trailing edges of the contact patch, in an effort to educe the contributions of both regions (it is not believed that sidewall vibration contributes significantly to the tread-related noise). This will be part of a total survey of the directional characteristics of the tread-related noise. These surveys will be carried out over a range of speeds under a variety of loads. It is hoped that the single wavy groove can be represented as an acoustic monopole at the center of the contact patch, or perhaps as the sum of a monopole at the leading edge and another (with different phase) at the trailing edge. The velocity dependence of the tread-related sound should correspond to 12 dB per doubling of speed, for a monopole source. This behavior is close to that observed for total tire noise.[1] The directional characteristics will also be useful in fitting the acoustic signature on tire #3 to this simple model.

Tools from our turbulence work that might very likely be useful in this study are flow visualization and the hot-wire anemometer. It may be useful in illuminating the mechanisms of tread-related noise generation to try to visualize or measure with hot wires the "jetting" of air from the tread grooves, if indeed this occurs. The exact nature of these experiments, or whether or not they should be done, can not be decided at this point. But we do have the capacity to carry them out, and will do so if this will add to our understanding of the processes of sound generation in a manner pertinent to the stated objectives of the program.

d) tread-related sound determination

Special signal processing procedures, developed in our long research programs in turbulence[3] will be employed to sort out the tread-related signal from the total acoustic signature. A pulse signal will be generated each time that a particular point on the tire enters the contact patch. This will be generated using a small light source and a thin slit on a disc attached to the wheel carrying the tire. This pulse will be used to initiate a signal reduction process. By taking an average over a large ensemble of such events, the "noise" portion of the sound is rejected and the tread-related portion is "educed." We have a PAR waveform educator and a HP digital cross-correlator/eductor available for this purpose. The noise portion can be determined by a separate measurement of the spectrum of the total signal.

e) work schedule

The construction forecast now plans completion of the room by May 1 and installation of the wheel by June 1. It is expected that initial tests on special tires will be conducted in the summer.

References

1. Groening, J. A., "Characteristics and Control of Car, Truck, and Bus Noise," Proc. Purdue Noise Control Conf. July, 1971, p. 29.

2. Hayden, R. E., "Roadside Noise from the Interaction of a Rolling Tire with the Road Surface," Proc. Purdue Noise Contorl Conf., July, 1971, p. 62.

3. Hussain, A.K.M.F. and Reynolds, W. C., J. Fluid Mech., 41, 421, 1970.

ACOUSTIC ATTENUATION BY VAPORIZATION OF LIQUID DROPLETS*

by

Frank E. Marble**

Daniel and Florence Guggenheim Jet Propulsion Center
California Institute of Technology
Pasadena, California

Summary

The acoustic attenuation properties of clouds of small solid particles have been relatively well understood since the work of Epstein[1] and Epstein and Carhart[2]. These papers examined for the first time in a consistent manner, the attenuation of acoustic fields caused by viscous drag of the small spheres and thermal heat conduction to and from the spheres during the passage of a wave. Recently, in connection with investigations into the flows of multiphase mixtures, Wooten[3], Marble[4,5], and Marble and Wooten[6] explored the acoustic effects of phase change between the liquid droplets and the vapor in which they were suspended. The unique features of the attenuation associated with the condensation and vaporization phenomena were confirmed in a splendid experimental work of Cole and Dobbins[7].

The attenuation associated with a cloud of solid particles, each of mass m, radius σ, and number n per unit volume, corresponds to that of continuously distributed dipoles whose strength is proportional to the force per unit volume exerted upon the gas as the particles attempt to follow the gas motion. This dipole strength is proportional to $\varkappa_p\left(\frac{i\omega\tau}{1+i\omega\tau}\right)$ where $\varkappa_p = \frac{mn}{\rho}$ is the fraction of mass per unit volume due to the particulate phase, ω is the angular frequency of acoustic disturbance, and $\tau \equiv \frac{m}{6\pi\sigma\mu}$ is the velocity relaxation time for the particle in a medium of viscosity μ, according to Stokes law. The acoustic disturbance is attenuated as $\exp\left[-\frac{\varkappa_p}{2}\left(\frac{\omega\tau}{1+\omega^2\tau^2}\right)\varkappa x\right]$ where $\varkappa \equiv \omega/c$ is the wave number. This absorption band is centered about the frequency $\frac{1}{\tau} = \frac{6\pi\sigma\mu}{m}$, which depends upon the particle size and composition but is independent of particle concentration.

The attenuation caused by thermal exchange between the gas and the particle cloud corresponds to that for a continuously distributed field of sources whose strength is proportional to the head absorbed from the gas per unit volume by the particles. The form is, of course, the same as that for the viscous attenuation but now the thermal relaxation time $\frac{mc_p}{4\pi\sigma k}$ replaces

*Supported by Department of Air Force, AFOSR Aeromechanics Division, Grant AFOSR-71-2068.

**Professor of Engineering.

the Stokes relaxation time above, where c_p and k are the specific heat and thermal conductivity of the gas. For most gases, the difference between these times is negligible, and we shall not differentiate here. The thermal attenuation then behaves as $\exp\left\{-\frac{\gamma-1}{2}\varkappa_p\left(\frac{\omega\tau}{1+\omega^2\tau^2}\right)\varkappa x\right\}$, generally less than half that caused by the viscous losses. The absorption band is centered on essentially the same frequency, $1/\tau$.

When one examines the response of a medium consisting largely of inert gas, a small mass fraction $\varkappa_p$ of liquid droplets and small mass fraction $\varkappa_v$ of vapor corresponding to the liquid, the behavior[4-6] is much more complex. In general, and with very good accuracy when the $\varkappa_p$ and $\varkappa_v$ are not large, the response may be divided into a fast portion in which the droplet temperature adjusts to a value intermediate between its original temperature and the local gas temperature and a much slower relaxation time during which the larger portion of the phase equilibrium is achieved. The fast portion, which takes place with a relaxation time $\approx \tau$, leads to an attenuation corresponding to the thermal attenuation discussed above -- exactly so when the latent heat of vaporization is very large. The slow portion takes place with a relaxation time $\approx \tau/\varkappa_p \gg \tau$ and is a process[4-6] in which the droplets exchange vapor and heat with the gas, retaining essentially the same temperature.

The attenuation band corresponding to this slow relaxation process may easily be at a frequency of 1000 Hz, instead of 10^4 - 10^5 Hz for the other absorption bands we have discussed, and has the form

$$\exp\left\{-\frac{\gamma}{2}\varkappa_v\left[\frac{(\eta-1)^2}{1+\frac{\gamma}{\gamma-1}\eta^2\varkappa_v}\right]\left[\frac{\omega\tau/\varkappa_p}{1+(\omega\tau/\varkappa_p)^2}\right]\varkappa x\right\}$$

where $\eta \equiv \frac{h_\ell}{c_p T}$, h_ℓ is the latent heat of vaporization of the liquid. The fact that the location of the absorption band may be strongly altered by changes in droplet size, and the magnitude of the attenuation altered by changes to the partial pressure of the vapor and to the liquid properties, makes this phenomenon interesting for technical applications.

Investigations have been carried out concerning application to fan noise and duct modes; these will be reported in detail in reference 8.

References

1. Epstein, P.S. Contributions to Applied Mechanics, Theodore von Karman Anniversary Volume, California Institute of Technology (1941), pp. 162-188.

2. Epstein, P.S. and Carhart, R. R. J. Acoust. Soc. Amer., 25 (1955), pp. 555-565.

3. Wooten, D. C. The Attenuation and Dispersion of Sound in a Condensing Medium, Part I. Ph. D. Thesis, California Institute of Technology (1966), pp. 1-72.

4. Marble, F.E. Astronautica Acta, 14, 6 (1969), pp. 585-614.

5. Marble, F.E. Dynamics of Dusty Gases, Annual Review of Fluid Mechanics, 2 (1970), pp. 397-446.

6. Marble, F.E. and Wooten, D.C. Physics of Fluids, 13, 11 (1970), pp. 2657-2664.

7. Cole, J.E. III and Dobbins, R.A. Measurement of the Attenuation of Sound by a Warm Air Fog, Jour. Atm. Sci., 28, 2 (1970), pp. 202-209.

8. Marble, F.E. and Candel, S.M. Acoustic Attenuation by Vaporization of Liquid Droplets -- Application to Noise Reduction in Powerplants and Ducts. To be presented at the AIAA Fluid and Plasma Dynamics Conference, Palo Alto, Calif., 17-19 June 1974.

SOCIETAL PROBLEMS

The Application of the CNEL Methodology to Investigate the Transportation Noise Environment Around a British Airport

by
P.J. Dickinson, J.B. Large
Institute of Sound and Vibration Research,
Southampton University.

Next to London, Birmingham is England's second city and one of the busiest in the country. As usual with all such high concentrations of urbanisation, Birmingham has severe community noise problems. It is the center of England's rail network, the heart of the British car industry, and other light engineering concerns and has a fairly busy international airport although the latter is perhaps small by American standards. England is a small country with a large population and residential areas encroach on much of the countryside. Airports that were once in the heart of the country are now surrounded by urban development. Up to about 1950 planners had no thoughts of noise problems, with the result that at Birmingham some residential properties are situated almost on the end of the runway. Not only do these properties receive high noise levels from aircraft, but they also have running alongside, on an embankment, one of the busiest main railway lines in the country. In the near vicinity too are busy main roads and local industry. One large manufacturing plant runs several unsilenced gas turbine installations in the area. The local noise environment caused concern to the local Health Committee and the Institute of Sound and Vibration Research was asked to assess the noise environment and recommend an insulation scheme to protect against aircraft noise intrusion (ref. 1).

England, in common with most other countries, has individual noise units, and an attempt at legislation for each individual noise source. For aircraft, the Noise and Number Index is the recognised unit based on a social survey of London (Heathrow) Airport in 1961 (ref. 2). It includes the measure of the average peak received noise level above 80 PNdB over 12 hours from 0600 GMT on an average summer's day, and on the number of movements heard in the period. Road traffic noise is characterised by a 10 percentile 'A' weighted level over an 18 hour period starting at 0600 GMT. For railway noise there are no units with any precedence, as the study of this source type has only recently commenced (ref. 3). For industry again percentile levels are used. None of these units can be summated for the entire noise environment. Nor can the component effect of one source be compared with another. In assessing the noise environment in an area, such a comparison is essential. When this comparison is not made we have the sort of situation that has recently occurred around London (Heathrow) Airport where many householders obtaining a grant to protect their properties from aircraft noise have used the grant to soundproof rooms receiving road traffic noise and have left unprotected the rooms facing the airport. Much thought was given to how such an assessment (and comparison) could be made in the Birmingham area. After considering the

units in use in other countries, and taking account of subjective studies taking place in the Operational Acoustics Group at the Institute, it was decided that a Night Weighted Equivalent Level was probably the best unit to use. It may not be as accurate as the units developed for each individual noise source, but when used in the context of this study, it seemed superior to any other. In considering the family life style in the area, and the importance of evening rest and relaxation, it was decided that an evening weighting too should be incorporated. Thus the Community Noise Equivalent Level (CNEL) developed for the State of California to describe all forms of transportation noise, was used in the study.

Perhaps at this point some comment on 'accuracy' of measurement is in order. With the present concerted effort to bring all noise sources within a single rating that will somehow take into account subjective reactions, there are difficulties. Aircraft, for instance, are less socially accepted than most other forms of transportation noise (e.g. trains) and therefore even if one takes a relation that somehow physically lumps all these together, the result is unlikely to be as accurate as a subjective accumulation of some sort. However, perhaps too much emphasis is placed on the accuracy of measurement and description of the noise, when in practice there are large variations in the received noise over a period of time and in the subjective response of recipients. A 3 deciBel change in noise levels is just perceptible when the initial and changed levels are heard consecutively. With an interval of time between them (say 5 minutes) it requires 5 deciBels or more difference to be noticeable. On the subjective side, this one factor alone makes attempts to describe environmental noise in units accurate to fractions of a deciBel, rather pointless. The CNEL is accurate certainly to within this margin and has many advantages over some of the other units, not least of which is its ease of measurement.

For a period of three weeks in the summer of 1973 noise was sampled day and night in random rotation at a large number of locations around Birmingham Airport; complete case histories being compiled at 44 specific locations. The noise exposure was measured, for each transportation mode, in CNEL and in the unit with legal precedence (NNI, L_{10}, etc.). For the aircraft noise exposure contours were plotted from the measurements with computer interpolation. Noise contours over one area of the district is shown in Figures 1 and 2.

In the comparison of NNI and CNEL contours, one can see a marked difference in shape, particularly at the ends of the cross runway. Birmingham has a thriving light aircraft fraternity and this runway is used only for this type of aircraft. Whereas the CNEL contour does accurately locate an area of disturbance from this type of traffic, the NNI does not. This is a distinct fault in the NNI system of noise exposure rating. When the NNI was developed a lower limit of 80 PNdB was selected as a level causing zero annoyance, i.e. 1000 aircraft at 79 dBA cause no annoyance,

but 1 at 81 PNdB would. In practice, such a difference of 2 PNdB would pass unnoticed, as mentioned above. Why such a lower limit was set is not fully understood, but it is understood that the apparatus used in the survey measured noise in dBA (it would have been a mammoth task to compute PNdB levels) and that the apparatus had a limited dynamic range with a lower cut off at about 67 dBA. This, for the large jet aircraft of those days, would have been about 80 PNdB, and perhaps this is the reason. However, the people living near the small cross runway at Birmingham have no uncertainty about the annoyance they feel for the approximately 60 movements of light aircraft a day they experience at about 66 dBA.

From the flight and air logs kept by the airport, noise exposure contours were also plotted using standard prediction methodology, Fig. 3. These differ from measured levels being about 5 deciBels lower near the airport and about the same amount higher farther out. The cause of this discrepancy is the weather. Predictions of noise exposure can be made really for standard average conditions only, and cannot allow for the existing conditions at any particular time. In a study at Gatwick Airport in 1970 (ref. 4) noise level attenuations varied from 7 to 22 deciBels over a period of 3 weeks, when one would predict 29 deciBels using recognised methodology. This latter discrepancy was caused by the prevalence of temperature inversions to which southern England is subjected for more than 55% of the time. Thus it must be recognised that although methodology exists for fairly accurate prediction of aircraft noise levels in standard conditions we may have a variation of 20 deciBels or more on any one specific occasion. At Birmingham the increase in noise level measured over that predicted was caused by a spell of fairly warm, windless weather in which the aircraft on the whole could not reach optimum climb-out speed without a short accelerating run at fairly low altitude. During the measurement period a simple polaroid camera was used in a vertical plane to photograph each flight, during daylight hours, hence enabling the position and altitude of the aircraft to be calculated. The 5 deciBel increase in noise is directly attributable to this low altitude run. Another study at Gatwick Airport in 1972 (ref. 5) photographed the same B707 flight on 4 different days with the results shown in Figure 4. Reiterating: one can predict aircraft noise exposure for standard average conditions only, and it must be realised especially by planners and lawyers, that individual daily exposures may vary considerably from these predictions. There is of course, another problem. The Birmingham study asked for a delimitation of a sound insulation scheme and the question arises: Which should take precedence, a prediction or a measurement? The prediction may be a good average over a period of time, but may never occur in practice. The measurement records a condition that has happened, but may never do so again. Perhaps the logical way is to plan always for worst conditions.

In the United Kingdom the Department of Employment has issued a code of practice for the Protection of Employed Persons to Noise (ref. 6). A maximum limit of 90 dBA for 8 hours is set and above this level/time hearing protection must be given. In the Birmingham study (conducted before the Environmental Protection Agency drafted its regulations) this was converted to CNEL and is equivalent to 85 CNEL. The limit was developed from the work of Burns and Robinson (ref. 7) and at this level there is a 10% chance of hearing damage (albeit for exposure over a period of some years), 1% of which may be to such an extent that social handicap results (ref. 8). One area in Birmingham from measurements would seem to have a noise environment closely approaching this limit. In the circumstances one must question again the validity of measurements over a short period of time; the predicted average level being 5 deciBels less. However, for the protection of residents, can one take the chance that predictions are correct? The margin for error is too small, and thus the team involved had to suggest this small area of about 100 prefabricated houses be seriously considered for sterilisation (noise-wise).

So far the paper has dealt with the discussion of aircraft noise and no doubt for a study of noise around an airport, this is what one would expect. However, we are not really being fair to the air transportation industry. During the measurement part of the study, in all but a few locations it was not aircraft noise that predominated. Perhaps also rather surprisingly the several unsilenced gas turbine installations, mentioned above, did not really intrude even when close to the establishment concerned, which latter had an acreage sufficiently large to keep the turbine well away from the nearby residential area. The noise from road traffic predominated almost everywhere. Railway noise too was high in some places although perhaps not reaching such a level as to be 'hazardous' from a health point of view. However, one case history at a local school (Figure 5) showed that the number of interruptions to classes should cause concern. A study at Stansted Airport in 1969 (ref. 9) concluded that 4 interruptions per hour would be quite sufficient for children to lose the entire content of the lesson. Thus making learning, and of course the teaching, very difficult. Classes in this small school were being interrupted at least 10 times an hour by trains alone. Yet the whole school had come to accept this and to live with the problem. It was an extremely happy little community upset only by - aircraft noise. This in general was of a lower noise level except on just one or two occasions; and the noise exposure was decidedly less. Perhaps in-built was the fear that one day an aircraft, slightly off course, might crash and hence even a lower level of noise caused some concern.

In many areas road traffic noise was far greater than ever imagined by the local authorities. The case history shown in Fig. 6 is not by any means exceptional for the area. The measurements were taken as near as possible to the standard measuring position, in the United Kingdom, of 1m away from the facade of residences and 1.6m above ground. The noise exposure levels received from road traffic are as great, or greater, in many areas than the level received from aircraft noise in the

small area near the runway - the small area considered "hazardous" from a health point of view and recommended for sterilisation. We thus have the iniquitous situation of recommending an area be penalised for receiving aircraft noise, when very much larger areas in the city are receiving much more noise exposure from surface traffic. It must also be remembered that the measured noise from the aircraft may be greater than the average over the year, because of the weather conditions. Such weather conditions have much less effect on the spread of noise from surface temperature and measurements are unlikely to pick out exceptional conditions only. Schemes for sound insulation grants to protect against aircraft noise are in operation at many airports, but there are no schemes and no real resources in the United Kingdom to provide sound insulation grants for homes affected by road traffic noise - unless the road, or some construction associated therewith, was not completed until 1969 or after.

Many people are living in conditions approaching the Department of Employment's health limits, and the noise source is road traffic. Yet if asked about the noise, most people quote aircraft as the source of their noise disturbance. Other people living in areas clear from heavy road traffic and experiencing aircraft noise only seem quite happy with the area.

Since this paper was conceived a study has been conducted by the ISVR team at Britain's busiest airport - Manchester (Ringway) Airport (ref. 10). In this study a social survey was conducted concurrently with noise and noise exposure measurement. The Social Survey shows that a night weighted noise equivalent level (CNEL) has a better correlation than Noise and Number Index in all conditions. Although the correlation for Noise and Number Index was not as low as initially anticipated, there is no validity for its retention as the unit of Aircraft Noise Exposure. A simple unit such as CNEL (or Night Weighted L_{eq}) which gives a better correlation with annoyance, is not limited to aircraft but can be used for any transportation noise exposure and can be directly related to public health considerations, is superior in every respect.

The overall response of the population of the district was estimated by applying suitable weighting factors to the raw survey results. The surveyed population was 43,000. The corresponding Heathrow percentages are given for comparison thus | |.

Noisiness	22,000 (52%)	|34|	consider their area at least noisy
Aircraft Noise Annoyance	25,000 (58%)	| -|	consider aircraft noise to be the noise that bothers them the most
	12,000 (28%)	|15|	consider themselves very much annoyed
	15,000 (34%)	|26|	consider themselves moderately annoyed
	11,000 (26%)	|27|	consider themselves a little annoyed.

Activities disturbed by aircraft noise:

Interference with Communications	29,000 (68%)	|37|	report that aircraft noise interferes with conversations
	20,000 (46%)	|53|	report that aircraft noise interferes with listening to T.V. or radio
Sleep and Relaxation	22,000 (51%)	| -|	report that aircraft noise disturbs their rest and relaxation
	22,000 (51%)	|36|	report that aircraft noise wakes them up
	12,000 (27%)	| -|	report that aircraft noise keeps them from going to sleep
Other effects	17,000 (42%)	|24|	report that they are startled by aircraft noise
	21,000 (49%)	|38|	report that aircraft noise makes their house vibrate and shake.

Again at this airport, planners had not foreseen the oncoming noise exposure threat and development had been allowed right up to the airport boundary. This airport too was once in the heart of the countryside but is now in almost an urban area. Here again some areas are receiving noise exposure levels so great that people are potentially at risk, and in the summer of 1973 no part of the Urban District containing more than 43,000 people to the north of the airport received levels as low as the EPA recommendation of 55 L_{DN}. No road traffic noise measurements were conducted in the study and this may be a bad omission,for once again fairly heavy traffic is evident.

More and more we are finding that areas are receiving high noise exposure levels from road traffic, but inhabitants place the blame for their noise annoyance on aircraft, even though noise exposure levels from the aircraft, and sometimes the peak noise levels themselves, are lower. When one is faced with the problem of defining areas eligible for sound proofing schemes, noise constituents must not be confused. The scheme must allow for protection from the main source of noise exposure and one must not fall into the trap of assuming that at an airport, aircraft must be the main source of noise.

References

1. Environmental Noise at Birmingham (Elmdon) Airport
   P.J. Dickinson, ISVR.Wolfson Report No. 1569 (B2)

2. Noise. Final Report by the Committee on the Problem of Noise. HMSO London. Cmnd. 2056.

3. Planning and Railway Noise. J.G. Walker. Institute of Sound and Vibration Research, University of Southampton.

4. Aircraft Noise at Horley, Surrey
   ISVR Wolfson Report 1970

5. Aircraft Noise Exposure at London (Gatwick) Airport
   R. Lam. M.Sc. Thesis, ISVR. 1972.

6. Code of Practice for Reducing the Exposure of Employed Persons to Noise. Department of Employment 1973.

7. Burns W. and Robinson D.W. 'Hearing and Noise in Industry' HMSO, London.

8. Hygiene Standard for Wide Band Noise. The British Occupational Hygiene Society, 1971. Pergamon Press.

9. Report of Proceedings. Stansted Airport Inquiry 1969
   Evidence of W.A. Allen.

10. Assessment of Aircraft Noise at Cheadle and Gatley
    P.J. Dickinson, ISVR Wolfson Report No. 1608.

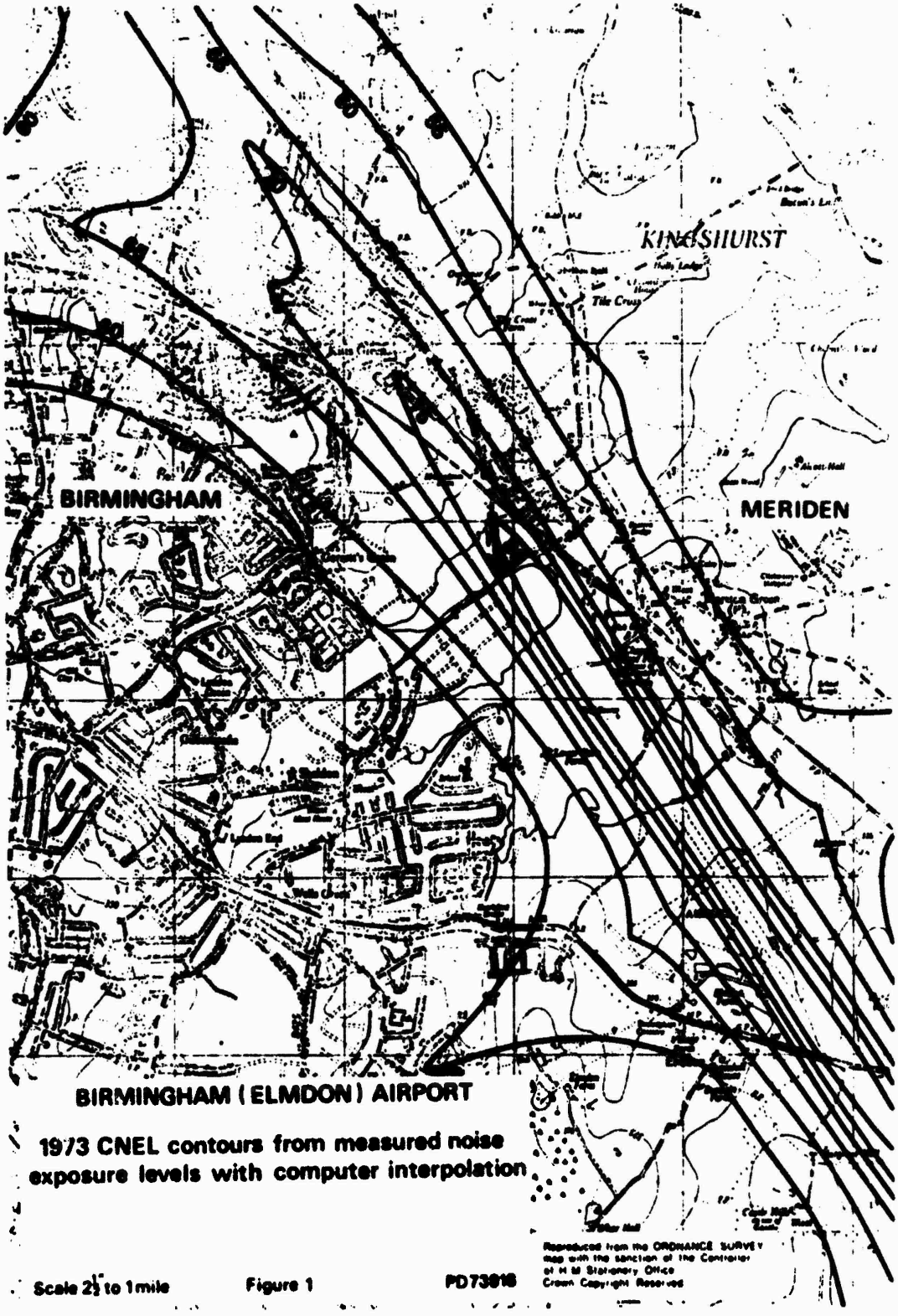
KINGSHURST
BIRMINGHAM
MERIDEN
BIRMINGHAM (ELMDON) AIRPORT
1973 CNEL contours from measured noise exposure levels with computer interpolation
Scale 2½" to 1 mile
Figure 1
PD73918
Reproduced from the ORDNANCE SURVEY map with the sanction of the Controller of H M Stationery Office
Crown Copyright Reserved

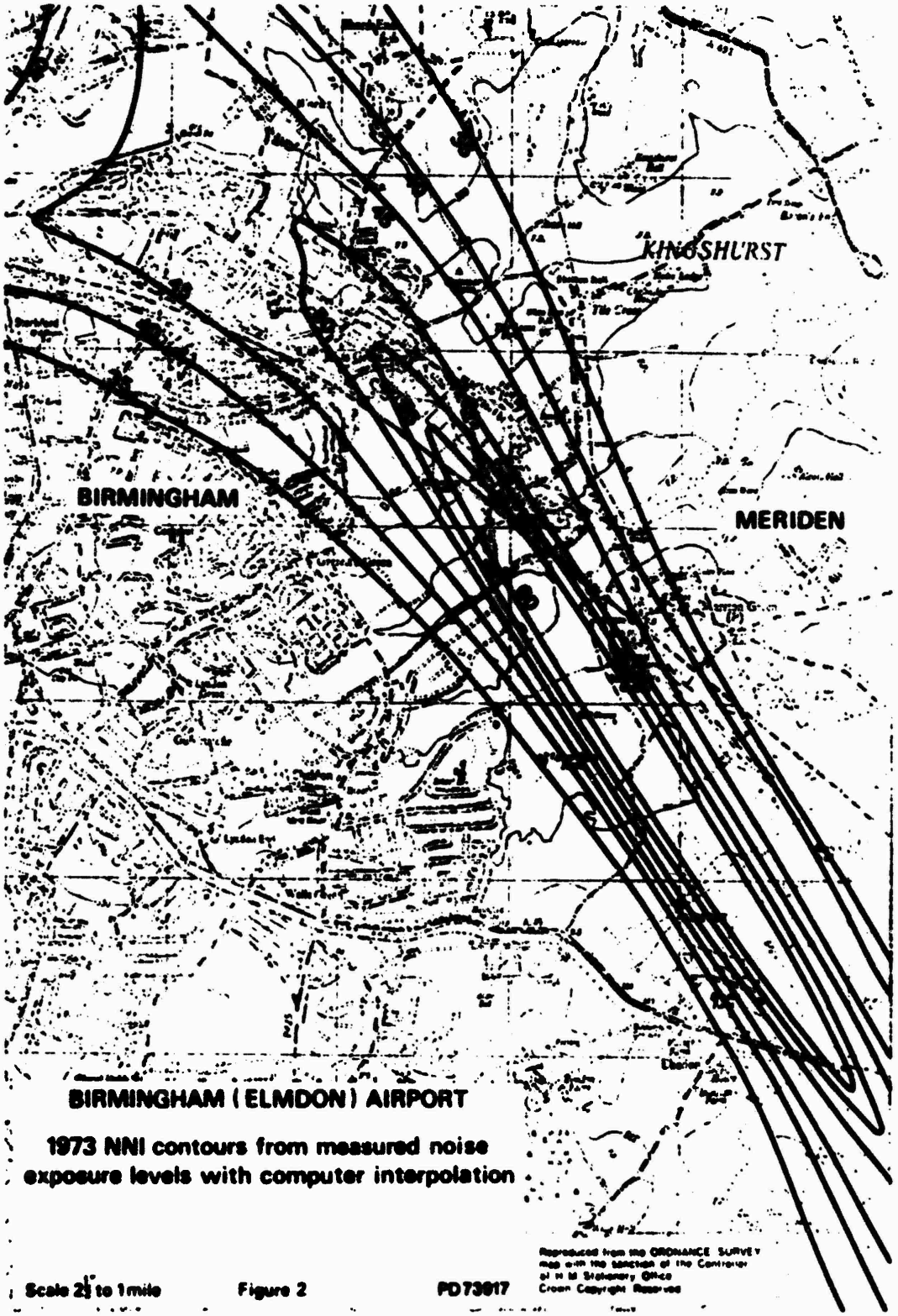
KINGSHURST
BIRMINGHAM
MERIDEN
BIRMINGHAM (ELMDON) AIRPORT
1973 NNI contours from measured noise exposure levels with computer interpolation
Scale 2½ to 1 mile
Figure 2
PD73817
Reproduced from the ORDNANCE SURVEY map with the sanction of the Controller of H M Stationery Office
Crown Copyright Reserved

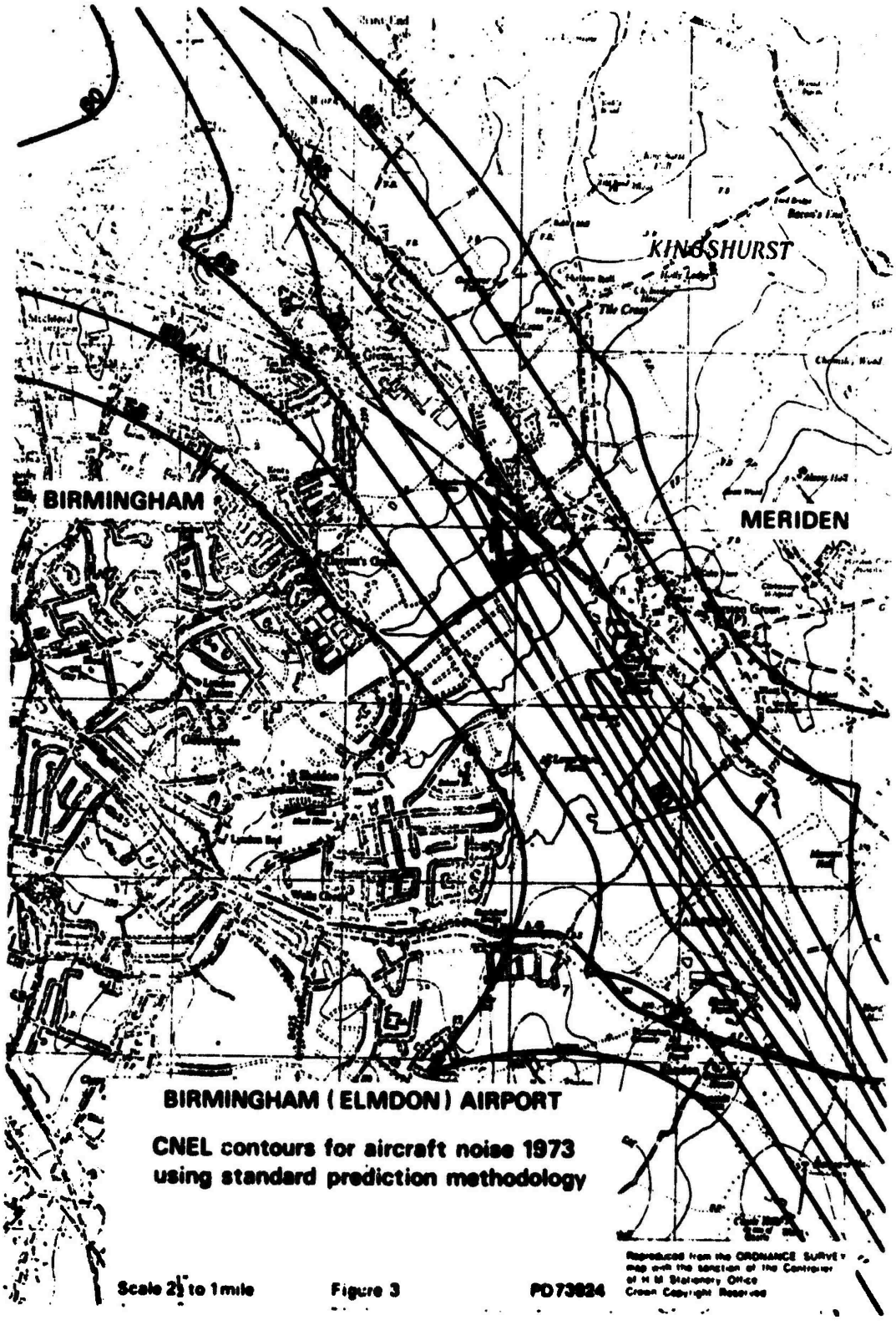
KINGSHURST
BIRMINGHAM
MERIDEN
BIRMINGHAM (ELMDON) AIRPORT
CNEL contours for aircraft noise 1973
using standard prediction methodology
Scale 2½ to 1 mile
Figure 3
PD73824
Reproduced from the ORDNANCE SURVEY map with the sanction of the Controller of H M Stationery Office
Crown Copyright Reserved

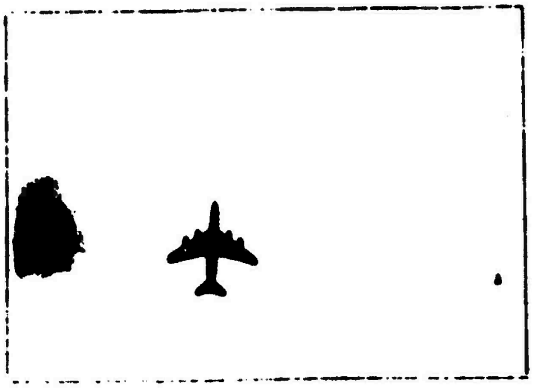

HT. = 1231 FT.

HT. = 704 FT.

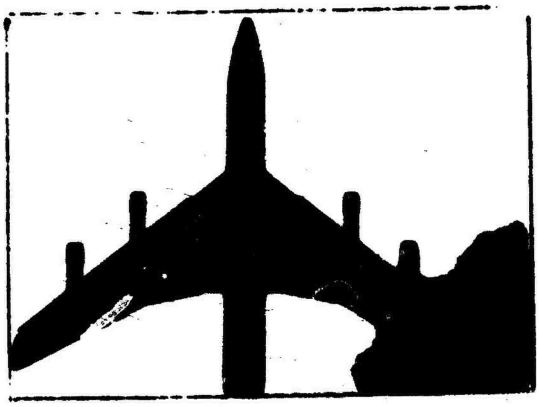

HT. = 234 FT.

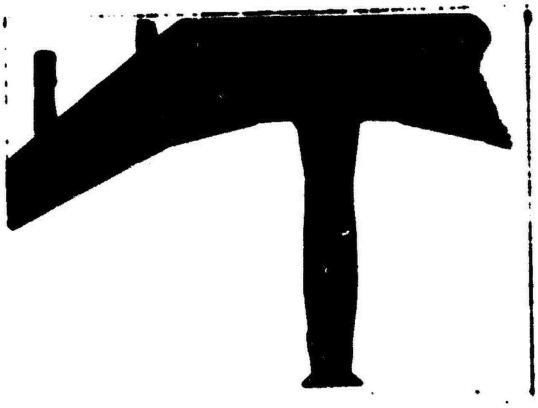

HT. = 122 FT.

Figure 4 VARIATION IN AIRCRAFT HEIGHT MEASURED AT POSITION E — AIRCRAFT: B707

POSITION: 9 PLACE: Marston Green County Infants School, Elm Farm Avenue, Marston Green

TRANSPORT TYPE	CNEL
ROAD TRAFFIC	62
AIRCRAFT Large	57
AIRCRAFT Light	nil
RAILWAY	>71

OVERALL COMMUNITY REACTION related to CNEL

> 75 Almost intolerable noise disturbance. Vigorous protests.
70-75 Pronounced noise annoyance. Organised protests.
60-69 Some noise annoyance. Sporadic complaints.
50-59 Noise noticeable but causes few complaints.
< 50 None.

TRANSPORT TYPE		NOISE LEVEL DESCRIPTIONS					
		PEAK PERIODS (ROAD TRAFFIC) OR DAY (AIR & RAIL TRAFFIC)		OFF PEAK PERIODS (ROAD TRAFFIC) OR EVENING (AIR & RAIL TRAFFIC)		NIGHT (ALL TRAFFIC)	
		LEVELS	*UK STANDARD	LEVELS	* UK STANDARD	LEVELS	* UK STANDARD
ROAD TRAFFIC	L_{10} dBA	60	68 (18 hr L_{10})	59	68 (18 hr L_{10})	nm	none
AIRCRAFT	NNI	35	DOE >60,50,40	not applicable		not applicable	
	TOTAL FLIGHTS	46	none	~12	none	~4	London only
	AV. PEAK dBA LARGE A/C	77	none	nm	none	nm	none
	A/C PRODUCING MAX dBA	Trident	99 dBA at Heathrow monitors	Trident	99 dBA at Heathrow monitors	Vis	89 dBA at Heathrow monitors
	MAX dBA	93		82		81	
RAILWAY	PEAK dBA	88	none	88	none	88	none
	MOVEMENTS	122	none	23	none	26	none
BACKGROUND LEVEL dBA		51		51		40	

Comments:- During the day a significant noise contribution from the school children, but with extremely high noise from the adjacent railway line. This far exceeded the noise from aircraft and road traffic and must cause considerable disturbance to the school. (The recording position was shielded from the railway, and levels may be higher than listed. A 4 dB allowance on the 84 dBA peak measured, has been used.) It is suggested that this school should have remedial measures taken immediately.

la = not measured above other noise sources nm = not measured * see text

FIGURE 5

POSITION: 14 PLACE: The Meadway, Kitts Green

TRANSPORT TYPE	CNEL
ROAD TRAFFIC	80
AIRCRAFT Large	74
AIRCRAFT Light	nil
RAILWAY	43

OVERALL COMMUNITY REACTION related to CNEL

> 75 Almost intolerable noise disturbance. Vigorous protests.
70-75 Pronounced noise annoyance. Organised protests.
60-69 Some noise annoyance. Sporadic complaints.
50-59 Noise noticeable but causes few complaints.
< 50 None.

		NOISE LEVEL DESCRIPTIONS					
		PEAK PERIODS (ROAD TRAFFIC) OR DAY (AIR & RAIL TRAFFIC)		OFF PEAK PERIODS (ROAD TRAFFIC) OR EVENING (AIR & RAIL TRAFFIC)		NIGHT (ALL TRAFFIC)	
TRANSPORT TYPE		LEVELS	*UK STANDARD	LEVELS	* UK STANDARD	LEVELS	* UK STANDARD
ROAD TRAFFIC	L_{10} dBA	75	68 (18 hr L_{10})	76	68 (18 hr L_{10})	58	none
AIRCRAFT	NNI	55	DOE >60,50,40	not applicable		not applicable	
	TOTAL FLIGHTS	37	none	4	none	1	London only
	AV. PEAK dBA LARGE A/C	98	none	nm	none	nm	none
	A/C PRODUCING MAX dBA	BAC1-11	99 dBA at Heathrow monitors	Tu 134A	99 dBA at Heathrow monitors	Vis	89 dBA at Heathrow monitors
	MAX dBA	98		97		89	
RAILWAY	PEAK dBA	59	none	59	none	59	none
	MOVEMENTS	122	none	23	none	26	none
BACKGROUND LEVEL dBA		64		69		42	

Comments:- A remarkably noisy area with an almost continuous high traffic noise. This exceeds the aircraft noise exposure, which itself is high. Of the aircraft overflying this location, the DC8 is predicted the noisiest at 105 dBA, but was not recorded. Only one aircraft overflew the area at night during the measurement period.

la = not measured above other noise sources nm = not measured * see text

FIGURE 6

PLANNING AND RAILWAY NOISE

by

J.G. Walker, G. Allen* and J.B. Large

Institute of Sound and Vibration Research

The University, Southampton, England

INTRODUCTION

There is no doubt that transportation noise is the major source of noise nuisance in the world today. The most serious offenders are road traffic which has grown rapidly over the last twenty years, and air traffic which has also increased dramatically and which was revolutionised by the introduction of the commercial jet airliner in the late 1950s. This growth has led to increases in noise levels in towns, alongside motorways and close to airports to a point where a significant percentage of the population is disturbed. Indeed in the United Kingdom at least 14 million people are exposed to road traffic noise that may be disturbing to some extent, and ½ million people are seriously disturbed by aircraft noise. Numerous studies throughout the world have investigated the relationships between noise exposure patterns and the community reaction. The environmental disturbance has grown to such an extent that research has been directed at producing engines for both road and air transport that generate less noise. The latest generation of jet engines has reduced noise levels by a significant amount and prototype truck engines have been designed that reduce noise levels to around one-half the loudness of present engines.

These efforts illustrate the importance that is placed on the intrusion of noise into the environment. The community as a whole is becoming more "noise conscious" and more vigorous in its protests about noise pollution.

In contrast to the growth of road and air traffic, railways have not developed in the same way. Indeed in many countries the railway system has been in a state of decline. Recently, however, there have been indications that railways will assume a new role. Following the success of high speed trains in Japan, many European countries have decided to increase the speed and numbers of their passenger services and many countries have plans to operate trains running at speeds up to 300 or 400 Km/hr, thus offering inter-city services that are more competitive than air travel. In addition, many new rail links are planned and new construction is also anticipated in the form of "rapid transit" schemes within many urban areas.

Hence with the advent of increased traffic and speeds, both of which result in increased noise levels, new railway construction

* present address: Feasibility Planning Office, Ministry of Transportation and Communications, Province of Ontario, Downsview, Ontario, Canada

and pressure for land in the conurbations forcing residential development closer to existing railway lines it is probable that the railways will have to be considered as a noise intruder in the environment. This situation has already arisen in Japan where a wave of public protest against high speed train noise followed the opening of the new Sanyo extension to the existing high speed Shinkansen network in 1972. As a result of these protests Japanese National Railways delayed the construction of a rail link to the new Tokyo Airport at Narita and, in addition, announced ambitious plans for reducing wayside noise levels along the whole 676 kM of the Shinkansen route.

Railway noise is therefore likely to pose an environmental problem in many countries. At the present time there is little information available that enables the noise levels alongside railway lines to be predicted and there have been very few surveys that relate noise levels to community response.

This paper reports data collected for a variety of British Rail trains, compares this data with that from other sources and presents a simple method of predicting railway noise based on the data in several acoustical units. It is intended to be a practical method that will assist engineers and planners in designing new lines and residential developments close to railways.

2. REVIEW OF MAJOR STUDIES UNDERTAKEN TO DATE

2.1 Noise measurements.

In most of the papers on the physical measurement of railway noise the source of the noise and the parameters affecting its propagation are examined. The findings are summarised in Tables I and II respectively, on pages 3 and 4.

2.2 Prediction methods.

Serendipity Inc. in 1970 produced a method of predicting railway noise (10). They incorporated data from the Japanese high speed train, Embleton and Thiessen's data, European subway data and measurements on the BART system. It is open to question whether for instance their data on high speed trains which use screening aprons and running on concrete sleepers and welded rails can be used without corrections. Their data on freight trains would be difficult to apply to European-style freight trains which are shorter but generally operate at higher speeds.

In Britain, British Rail have developed their own method of predicting noise levels interms of peak dB(A) because they felt that existing prediction methods may not apply to their proposed new train types (2, 6). They assumed rail/wheel noise to be the predominant source of noise beyond 20m from the track. Each rail/wheel interface is considered as a dipole source and the train is assumed to be made up of a line of these sources. A

TABLE I

Sources of railway noise

	Rolling stock
Sub-source	Comments
Propulsion system	Significant only in the case of diesel locomotives especially where engine is working hard, e.g. in overcoming gradients or accelerating (Refs. 1,2,3,6)
Auxiliary equipment	Cooling fans, air compressors, etc. Not found to be significant noise source (Refs. 3,4,5,6). Engine casing noise is significant (Ref. 3) in some trains
Power collector system	Aerodynamic noise from overhead pantograph not significant (Refs. 4,5). Third rail pick-up - no data
	Track
Rail/wheel interaction	Generally accepted to be the predominant noise source although opinion differs as to whether rail or wheel is the main compcnent (Refs. 2,4,5,6)
Structure	Vibration from train transmitted tc substructure which in turn radiates as secondary noise. Not significant except in the case of steel bridges which leads to higher wayside noise levels (Refs. 4,7)

TABLE II

Parameters which influence noise levels from railways

Parameter	Effect
Distance from track	Sound level decreases as a combination of point source and line source models depending on type and length of train (Refs. 2,3,4,6,8)
Speed	Relation between speed (V) and sound pressure level (L) in form $L_1 - L_2 = K \log_{10} \frac{V_1}{V_2}$ where K is a constant. Value of K ranges from 20 to 33. (Refs. 2,3,4,6,7)
Rail: Type	Welded rail quieter than jointed by 4 - 10 dB(A) (Refs. 7,8)
Condition	Corrugations can add up to 15 dB(A) to noise (Ref. 7)
Fastening	Resilient fastening can reduce vibration of rail and hence resultant noise level. No figures available (Ref. 9)
Sleeper (tie) type	Concrete as opposed to wooden sleeper (tie) reduces vibration of rail and hence noise level about 2 dB(A) less (Ref. 7)

relationship between the peak dB(A) and train make-up and speed is given.

In Sweden, Ljunggren and Benjegard (11) formulated values of energy equivalent (Leq) over an hourly period for three different train types at different distances from the track and different speeds. They have provided a simple method of predicting the noise climate in terms of Leq once the traffic mix and speeds are known.

Several other prediction methods exist but details are contained in reports that are not widely available.

3. COLLECTION OF DATA

A series of measurements was carried out alongside the main Waterloo-Bournemouth line in the Southern Region of the British Rail network. Whilst data was collected for only a limited number of British Rail train types it will be seen later that the data might be applied to a much wider range of train types.

Two measuring sites were chosen where the line was level and the surrounding terrain was open and relatively flat. One site (site 1) sloped gradually upwards away from the track; the other (site 2) was level to about 130m when the ground fell slightly to beyond 200m. At site 1, there were two tracks of continuously welded rails on concrete sleepers. At site 2 there were four tracks, the central two of which were continuously welded rail on concrete sleepers whilst the outer pair were jointed rails on wooden sleepers.

Tape recordings of each train pass-by were made simultaneously at 50, 100 and 200m. For each pass-by the locomotive type, train make-up, length and speed and the track on which the train travelled were noted. Complete data were obtained for 72 train pass bys.

The trains consisted of the following categories:

1) Electric multiple units (EMU). These consist of units of 4 coaches with one coach containing a set of electric power units supplied from a 750v DC third rail. 8 and 12 coach units are made up from four coach units. Very few 8-car units were observed and hence are not included in the analysis.

2) Diesel-electric locomotives hauling freight or passenger trains.

3) Electro-diesel locomotives which can use either electricity supplied by the third rail or diesel power on non-electrified routes.

The traffic at the two sites consisted mainly of passenger traffic (12 car EMU, 4 car EMU and loco-hauled passenger) and 20% freight (mainly 5-10m wagons, 20m oil tankers, 20m flat wagons).

The noise levels for both lines at site 1 and the central lines at site 2 were identical. The outer tracks at site 2 give differences of about 8 dB(A) between the near and far tracks which were used exclusively by 4 car EMU.

Analysis of the train pass-by profiles showed that the A-weighted noise profile was in general similar for all trains, being of a symmetrical "bell" shape which tended towards a triangular shape for shorter trains or trains moving at higher speeds. The peak levels (L_A) for passenger trains were higher than the slower freight trains, although freight trains would no doubt have higher levels at similar speeds, and the peak levels for identical trains at both sites were approximately the same at 50m and 100m. However, the peak dB(A) at site 1 at 200m was always higher than the level at site 2 at 200m. This difference could well be due to the dip at site 2, between 130m and 200m. At site 1, the change in L_A between 50m and 100m and between 100m and 200m was the same whilst at site 2 the fall-off between 100m and 200m was double that between 50m and 100m.

It was observed that the peak dB(A) values were not dependent on the number of wagons or coaches hauled for a particular train category but solely on the speed of the train.

All express passenger trains, whether loco-hauled or EMU gave similar levels and are thus treated together as "long-haul passenger". 4-car EMUs are called "short-haul passenger".

It was clear that the A-weighted level was the same for similar trains hauled by both diesel or electric locomotives. The low frequency energy produced by the diesel locomotive is not evaluated on the A-scale although in some cases it was clearly audible. The fact that the diesel locomotive does produce low frequency energy that is audible may affect the subjective response to this noise and indeed it may be more important when the noise is attenuated by a house structure and is heard indoors.

4. RESULTS

4.1 Peak dB(A)/velocity relationship

Using the 50m and 100m at both sites (the scatter at 200m was too large) it was possible to obtain representative values of K in the relationship

$$L_{A_1} - L_{A_2} = K \log_{10} \frac{V_1}{V_2}$$

where L_{A_1}, L_{A_2} are the peak dB(A) values at speeds V_1, V_2 respectively. The values are shown in the Table III below, and are "rounded" off to the nearest 5 units. Any errors thus involved would be very slight (much less than 1dB) over the speed range of interest.

TABLE III

Values of K for passenger and freight trains for peak dB(A)

Train type	K	Speed range km/hr
Long-haul passenger Freight (all)	25	95-175 65-90
Short-haul passenger	40	95-140

4.2 Normalisation of data

Using the values for K given above it is possible to normalise all the data to a speed of 140 km/hr for long haul passengers, 75 km/hr for all freight trains (except trains of containers on flat wagons which were observed to be faster but quieter than other freight trains) and to 120 km/hr for short haul passenger trains.

The data for the different categories of train are summarised in Table IV. The values for 200m are those at site 1 where the fall-off in peak dB(A) is constant between 50m and 100m and 100m and 200m.

TABLE IV

Representative values of peak dB(A) for passenger and freight trains normalised to their respective mean speeds.

Train type	Speed km/hr	Peak dB(A)		
		50m	100m	200m
Long distance passenger	140	88	82	76
Freight	75	82	75	68
Short-haul passenger	120	84	76	68
Container train	107-122	78	72	66

4.3 Measurement of equivalent continuous energy level (L_{eq})

The A-weighted energy level (L_{eq}) was measured for each pass-by by use of a noise dosemeter. Unlike peak dB(A) L_{eq} was found to depend on the number of wagons/coaches hauled. There was found to be a relationship of the form $L_{eq} = L_A - B$ where L_{eq} is the energy equivalent assuming 1 train pass-by per hour, L_A is peak dB(A) and B is a constant which depends on the length of the train. Values of B for different trains are given in Table V.

L_{eq} will increase by 3 dB for each doubling of train movements.

It is clear that the value of L_{eq} is dependent on the speed and length of the train. The data given in Table V may be

summarised in Table V(a) which gives the value of the constant B for different train lengths. The change in L_{eq} with speed is allowed for in the change in L_A with speed.

TABLE V

Representative values of B, for different train types

Type of train	Length of wagon or coach (m)	Number of wagons or coaches	Approximate length of train (m)	B
Long-haul passenger	20	8-12	160-240	28
Short-haul passenger	20	4	80	30
Freight	5-10	20 30 40	100-200 150-300 200-400	28 26 24
	20	10	200	28

TABLE V(a)

Train length (m)	80-160	160-260	250-300	300-400
B (dB)	30	28	26	24

4.4 Measurement of perceived noise level (PNL).

From the original tape recordings values of the PNL were calculated using computing facilities. PNL was found to be related to peak dB(A) by:

$$\text{Max PNL} = L_A + 12 \pm 2.5$$

for all trains.

5. COMPARISON WITH DATA FROM OTHER SOURCES

Comparisons between the present data and data available from other sources are summarised in tabular form in this section.

TABLE VI

Values of K relating L_A with speed

Train type	Present data	Ref.4	Ref.6	Ref.7	Ref.11*
Long-haul passenger	25	20	25	33	20
Short-haul "	40	-	25	33	20
Freight	25	-	25	-	20

(*Calculated for L_{eq})

TABLE VII

Comparison of peak dB(A) from several sources for long-haul passenger trains normalised to 140km/hr.

Distance (m)	Peak dB(A)				
	Present study[1]	Ref 7[2]	Ref 6[3]	Ref 4[4]	Ref 12[5]
25	-	92	85	84	93
50	88	87	82	-	89
100	82	82	78	-	85
200	76	-	74	-	81

Notes:
1. Only data at site 1 at 200m quoted.
2. Original results normalised to 140 km/hr.
3. Predicted values.
4. JNR used screening aprons and resilient fastening on tracks.
5. Original measurements taken in front of facade so reduced by 3 dB for "free-field" condition.

TABLE VIII

Comparison of peak dB(A) from several sources for short-haul passenger trains normalised to 120km/hr.

Distance (m)	Peak		
	Present study[1]	Ref 7[2]	Ref 6[3]
25	-	85	82
50	84	81	78
100	76	76	75
200	68	-	69

Notes:
1. Data from site 1 only.
2. Trains use screening aprons over wheels.
3. Predicted values

TABLE IX

Comparison of peak dB(A) from the present study with BR predicted values for freight trains excluding containers normalised to 75km/hr (Ref.6).

Distance	Present Study	Peak dB(A) BR predicted values		
		5-10m wagons		20m wagons
		20 wagons	40 wagons	10 wagons
50	82	75-78	76-78	75
100	75	73	72-75	72
200	68	68	69-71	68

6. METHOD FOR PREDICTION OF RAILWAY NOISE BASED ON DATA COLLECTED

It has been shown that the present data compares well with other studies on trains running under similar operating conditions. It is also clear that similar trains operating on a given stretch of line generate very similar noise levels; that is, there is very little scatter between the noise levels measured. These two points suggest that although the data reported in this study were collected at only two sites and covered a limited range of train types the data can be applied to a wide range of train types and situations with little loss in accuracy.

It is also shown that the propulsion system has no effect on the peak A-weighted noise levels produced; that is rail/wheel noise is predominant when railway noise is measured in peak dB(A). However, subjective reaction to the diesel locomotive may be influenced by the low frequency energy in the noise.

In the following prediction method noise levels will be given in such a way as to enable several different units to be defined. This has been done because the unit that best describes the nuisance caused by railway noise has not been defined. Thus, until such a unit is defined, users of the method can use the unit that is most applicable to their requirements.

The basic conditions assumed are:

i) Trains are described in four categories

a) Long-haul passenger trains of over 8 coaches
b) Short-haul passenger trains of up to 4 coaches
c) Container trains of 20m wagons
d) All other freight.

ii) Any new trains designed to operate at high speeds will probably use sophisticated suspension systems. In the absence of data it must be assumed that the noise level will increase with speed in the same way as for present day trains.

iii) The track is level, of continuous welded rail on concrete sleepers, and surrounding terrain is flat.

iv) The base noise level from which all others are derived is taken at 50m. Whilst measurements have been carried out at distances up to 200m from the track and the predicted values compare well with measured levels, the levels at distances greater than 200m are extrapolated, assuming that there is no unusual attenuation effect present at any site.

STEP 1

Use Figure 1 to obtain noise level in peak dB(A) (L_A) for each train type at different speeds at 50m from track. For corrections to other distances use Step 3.

STEP 2

If it is necessary to obtain values of L_{eq} for each train type use this step (Figure 2). Data are given for 50m from the track at any speed. Values of L_A obtained from Step 1 are corrected by the value shown to give L_{eq}. To determine values of L_{eq} at other distances use Step 3.

STEP 3

Corrections to L_A and L_{eq} for various distances from track for each train type are given in Figure 3.

STEP 4

To add the values of L_{eq} for each train category use chart shown in Figure 4.

STEP 5

If it is necessary to use the perceived noise level to describe railway noise the following relationship applies to all trains:

$$PNL = L_A + 12.$$

From this relationship units such as the noise and number index (NNI) can be calculated, where NNI = Average L_A + 15 $\log_{10}$ N - 68.

STEP 6

Corrections to allow for changes in the track type. These data are based on results of the present study and data reported elsewhere.

a) If wooden sleepers are used add 2 dB(A) to the above levels.

b) If jointed rails are used add 3 dB(A) to the above levels.

NOTE: The effects of embankments and cuttings and the gradient of the track are not yet known and therefore no allowance can be made for them. The use of screening walls alongside the track and the shielding of the wheels by aprons is very dependent on the type of shield employed. It is not therefore possible to provide corrections to the basic values.

7. SUMMARY

A simple method for predicting the noise from railway operations has been provided from empirical data. The predicted values agree well with data from French, German and Swedish sources. This suggests that the method can be applied to a wider range of railway operations than was originally studied.

The method is based on the use of the peak A-weighted sound level, which can easily be measured and from this unit several other units that describe the noise climate can be derived.

Limitations of the method are that allowances for cuttings and embankments and track gradient cannot yet be made, and that the levels at distances greater than 200m from the track have been extrapolated.

The effect of the surrounding topography will affect the noise level also. The generation and propagation of railway noise must be studied more fully before the effect of terrain, ballast type, screening walls etc. can be fully understood.

REFERENCES

1. T.F.W. EMBLETON and G.J. THIESSEN 1962. Sound, 10-16. Train noises and use of adjacent land.

2. S. PETERS, B. WOODWARD, N.A. SHELLEY and K. BUNTING 1972 British Railways Research Department, Internal Memo. IMPHYS 7236. The prediction of rail-wheel noise from passing trains.

3. R.A. ELY, 1973 BBN Rept: 2623 submitted to U.S. E.P.A. Measurement and evaluation of the impact of railroad noise upon communities.

4. JAPANESE NATIONAL RAILWAYS 1973. Shinkansen Noise.

5. T. NIMURA, T. SONE and S. KONO 1973. Inter-noise 73 Copenhagen. Paper D22Y17. Some considerations on noise problems of high-speed railways in Japan.

6. S. PETERS 1974. Journal of Sound & Vibration 32 87-99. The prediction of railway noise profiles.

7. C. STUBER 1973. German Federal Railways, Munich Testing Laboratory Report P1/1973. Noise generation of rail vehicles.

8. D. AUBREE 1973. CSTB Nantes, France. Acoustical and Sociological Survey to define a scale of annoyance felt by people in their homes due to the noise of railroad trains.

9. M.J. COCKRELL and R.A. WALLER 1972. Railway Gazette International 249-254. Noise from the urban railway.

10. SERENDIPITY INC. 1971. Report No. OST-ONA-71 Vol. 5. A study of the magnitude of transportation noise generation and abatement.

11. S. LJUNGGREN and S-O BENJEGARD 1972. Byggmastaren, 1. Train noise from the point of view of planning.

12. D. WALTERS 1969. Proc. conf. at Dalhandui, University of Strathclyde. Annoyance due to railway noise in residential areas.

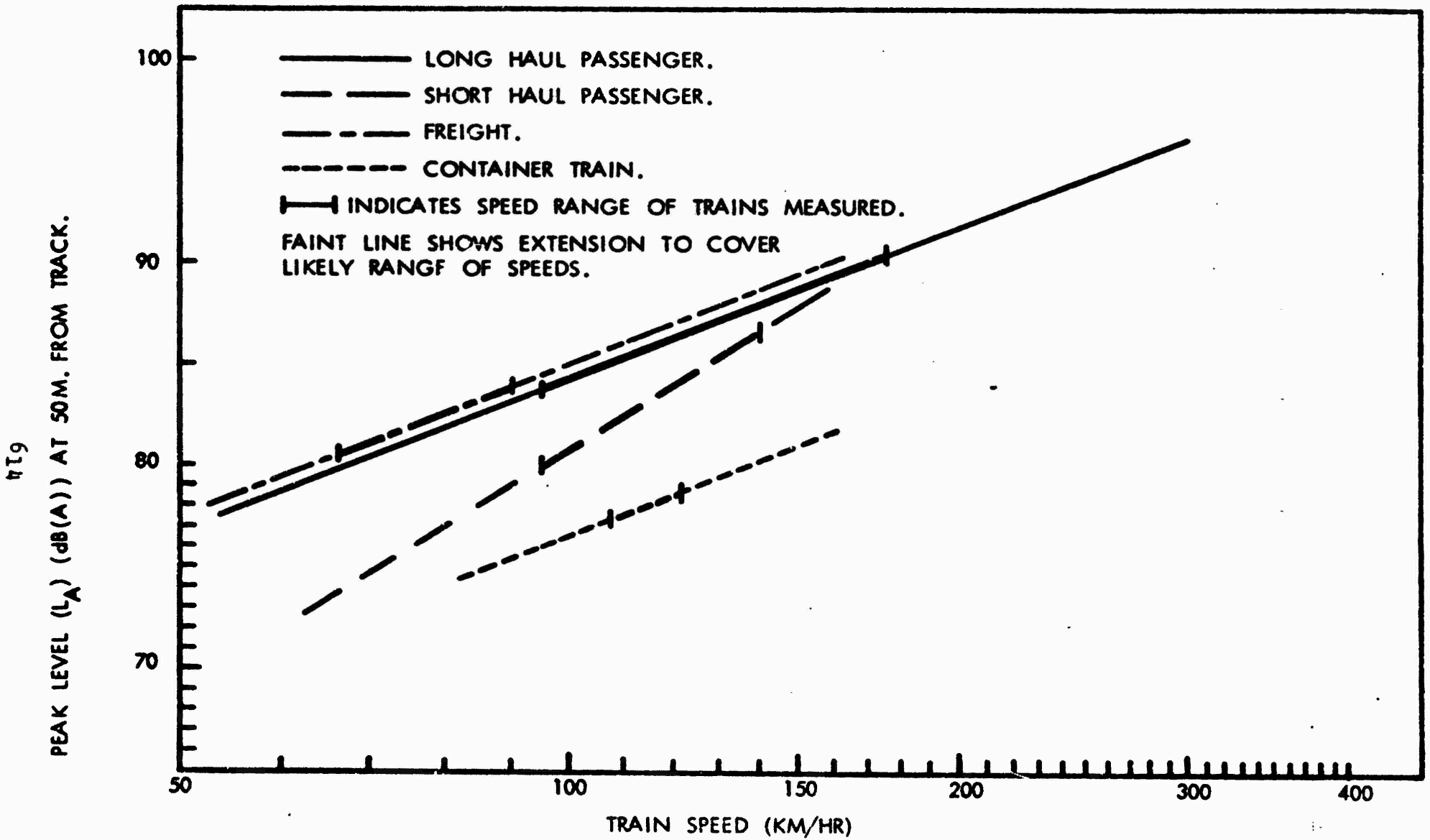

FIG. 1: STEP 1: RELATION BETWEEN TRAIN SPEED AND PEAK LEVEL (dB(A)).

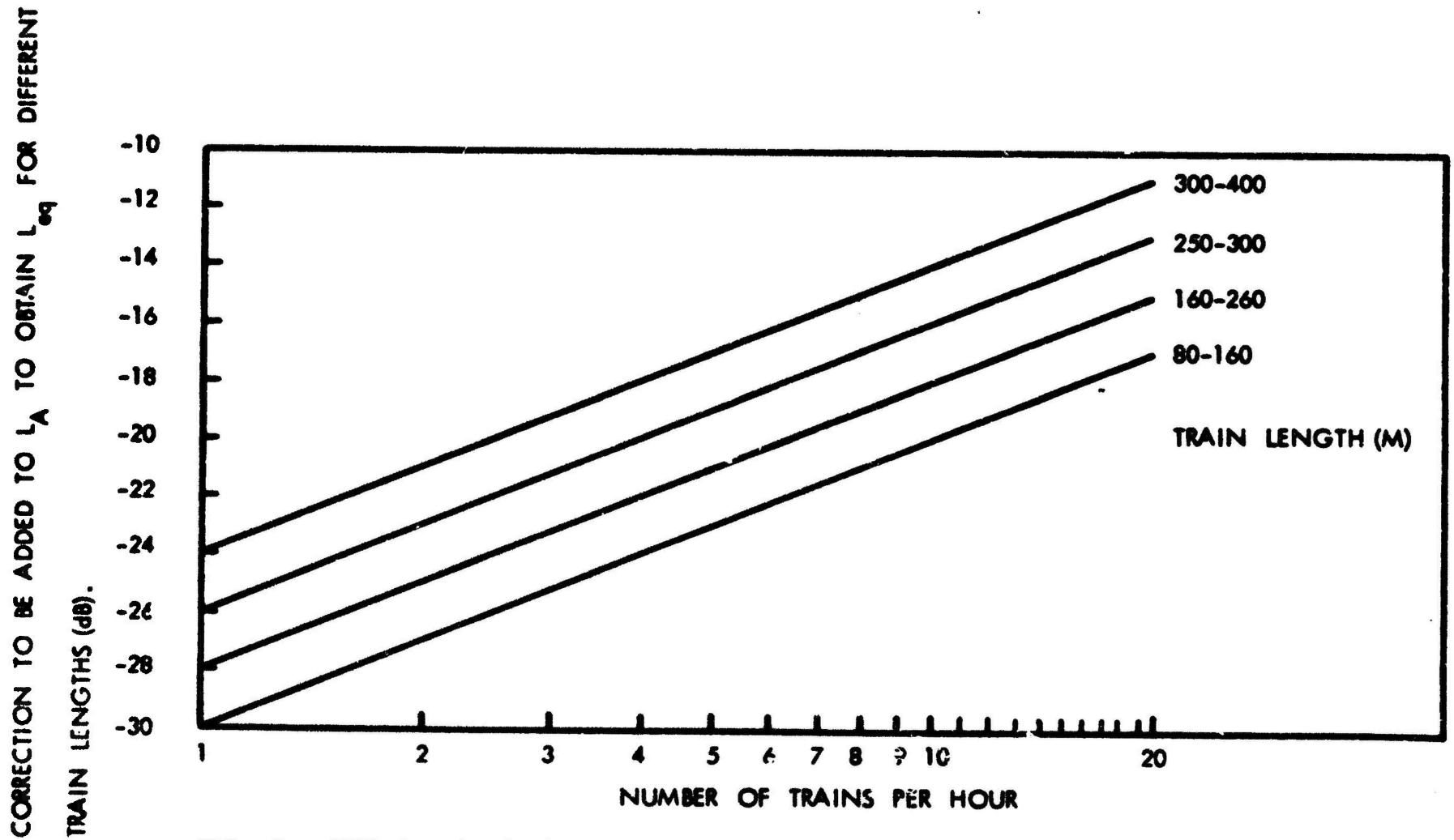

FIG. 2: STEP 2: ALLOWANCES TO BE ADDED TO L_A TO OBTAIN L_{eq} FOR DIFFERENT TRAIN LENGTHS AND NUMBERS OF MOVEMENTS.

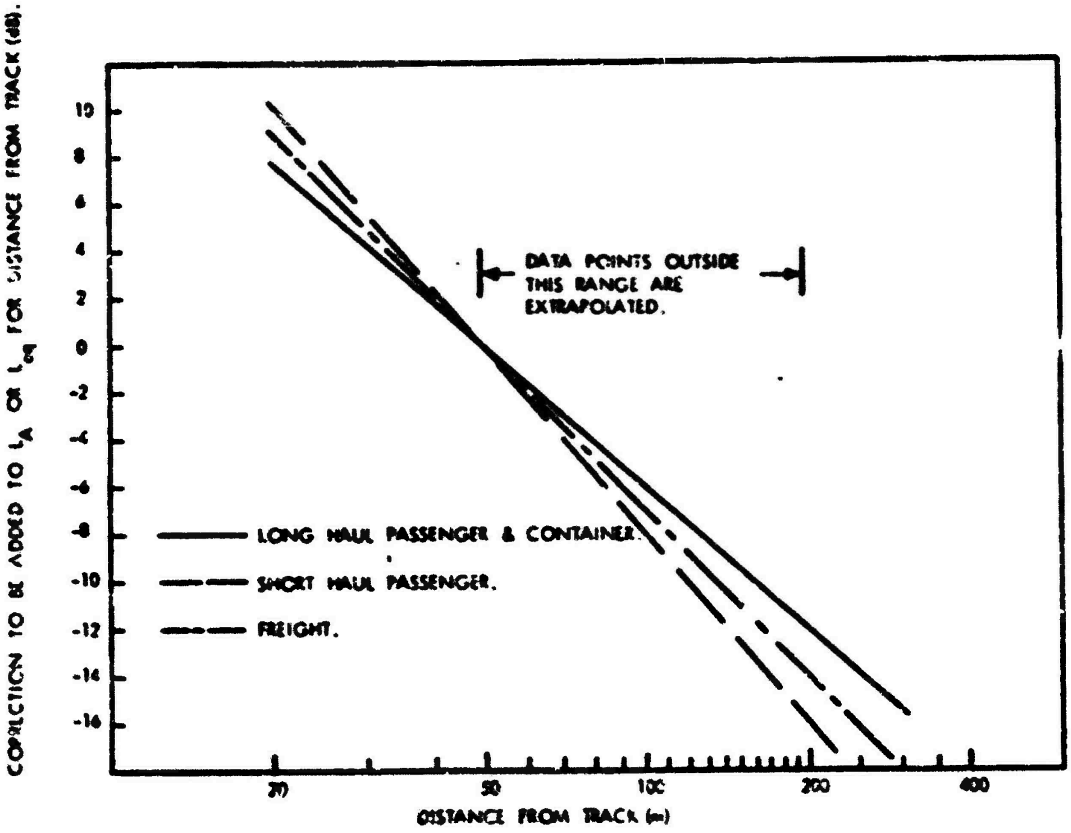

FIG. 3: STEP 3: RELATION BETWEEN L_A AND L_{eq} AND DISTANCE FROM TRACK.

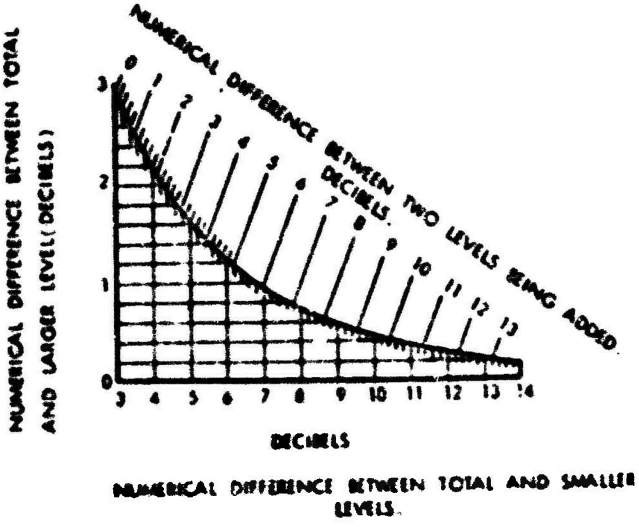

FIG. 4: STEP 4: CHART FOR COMBINING DECIBELS (AFTER R. MUSA).

THE EFFECT OF NUMBER OF FLIGHTS PRIOR TO JUDGEMENT ON ANNOYANCE TO AIRCRAFT FLYOVER NOISE

by

Walter J. Gunn
Senior Research Psychologist
Noise Effects Branch
Acoustics and Noise Reduction Division
NASA Langley Research Center
Hampton, Virginia

and

John L. Fletcher
Project Director
Professor, Memphis State University
Audio and Speech Pathology
Memphis, Tennessee

Past laboratory studies dealing with the subjective feelings of annoyance towards recorded aircraft sounds have traditionally been conducted in relatively unrealistic test situations. While subjects are usually asked to report their annoyance reactions toward each and every flyover heard (1) some researchers prefer to allow subjects to listen to several flights prior to making annoyance judgements (2). A reasonable question, in light of the different procedures employed by various researchers, would be whether the results from the different laboratories can be compared directly. That is to say, does a subject report the same level of annoyance to a specific aircraft sound when he is making judgements of each and every flight as when he is judging only selected flights, i.e., every other flight, every 4th flight, 8th flight, or 16th flight?

While it is important to establish comparability of laboratory results, it is also important from the standpoint of efficiency of laboratory procedure to establish the minimum number of unjudged flights required before stabilization of annoyance responses to specific stimuli. This is especially important because of the limited period of time subjects are willing to serve in laboratory experiments of this nature, usually one to two hours at best. If stable responses can be obtained when subjects judge every flight, rather than every three, four, or more, then the length of the test session can be reduced proportionally without losing or distorting data.

Therefore, this study is concerned with the effect of the rate of making annoyance judgements on one's reaction to specific flyover noises. The subjects in this experiment are required to participate in five

specific sessions. In one session, they judge the annoyance value of each aircraft flight they hear, while in other sessions they make judgements of every second, fourth, eighth, or sixteenth flight. Their annoyance responses to each specific level of noise can then be compared under the five different rates of making judgements.

In a study of community reaction to aircraft noise (3) it was reported that the most important psychological variable influencing one's annoyance reaction to aircraft noise was "Fear of airplane crashes in the neighborhood." A recent study by NBS (4) explored the need for further investigation of the importance of fear. Furthermore, there may be other psychological factors that influence the individual's reactions to noise. In order to test this notion, subjects in the present experiment were required to answer questions on the Taylor Manifest Anxiety Scale (5), which provides a measure of individual anxiety level. In this way, individual annoyance responses can be compared with individual anxiety scores to determine the extent to which individual anxiety level effects one's annoyance reaction to aircraft noises, at least in a laboratory situation.

Method

The subjects (S's) used in this study were obtained through Memphis State University and were either students or staff and ranged in age from 20-50 with the average age 25.7 years. There were 14 male and 11 female S's. They were paid $10.00 for their participation in the study. All S's were screened for conventional hearing (500-6,000 Hz) with no one accepted as a S with hearing loss at any of those frequencies of 20 dB or higher. Hearing was also tested for high frequency tones (8,000-18,000 Hz) but no criterion level was set for high frequency hearing. All testing was done in an Industrial Acoustics Co. model 1203 sound treated room by a graduate student in audiology from the Memphis Speech and Hearing Center. Conventional hearing was tested using a Rudmose ARJ-4A audiometer while high frequency hearing was tested using a Rudmose ARJ-4F audiometer. Both audiometers were within acceptable calibration limits.

All S's were also administered the Taylor Manifest Anxiety Scale (TMAS) as part of their pre-experiment screening.

The research was conducted in a quiet room 15 x 24', set up to be similar to a living room, with wall-to-wall carpeting, drapes on three of the four walls, and acoustic tile on the ceiling. (See Appendix A for picture of the test room.) Ambient sound pressure level in the room was 43 dBA.

The S's were divided into five groups of five as they were screened and found qualified for the experiment. The groups were then called in one group at a time, given the instructions necessary to perform in the

experiment, and the study was begun. Subjects were not allowed to smoke or to talk to each other during actual running of the experiment. During the course of the experiment the S's were presented five different tape recordings of aircraft flyovers recorded with four different maximum levels of noise, 80, 85, 90, and 95 dB. Tape #1 called for an annoyance judgement after every flight, #2 after every other flight #3 after every fourth flight, #4 after every eighth flight, and #5 after the sixteenth (and last) flight. Each tape took approximately 30 min. to run. Table I shows the order of tape presentations while Table II shows the stimulus order within tapes.

The order of running of the five tapes was counterbalanced and the sequence of presentation of the four levels of flyover noise was determined by a Latin square order of presentation.

A Bruel and Kjaer model 2203 sound level meter, set on the slow meter reading, A scale, was used to adjust the SPL of the stimuli on the tapes at the S's chair position with the S not present, the tape was run to the 1,000 Hz calibration tone, and the pre-amplifier gain control was adjusted until the meter read 95 dB(A). The voltage across the speaker necessary to obtain 95 dB(A) was found to be 4 volts. Thereafter, each time a tape was run, voltage to the speaker was checked on the VTVM, set at exactly 4 volts if it was not, and the tape run. In practice, little or no change in voltage was noted from tape to tape or session to session. A block diagram of the apparatus may be seen in Fig. 1.

Each group of S's was brought into the testing room, seated, then handed the aircraft flyover noise annoyance rating sheet (see Fig. 2). They were told to read the instructions on the sheet carefully and follow them exactly throughout the experiment. If there were any questions about the procedure or the task required of them, they were answered at that time. As soon as the Experimenter (E) could see that all the S's understood the job they were to do, he left the room and put on the first tape recorded stimuli they were to listen to and started the experiment. There was a 5 min. break between playing of each of the five tapes to enable the E to rewind the tape presented and put the next tape on the recorder. The S's were allowed to get up, talk, smoke, and move around until the next tape was ready. Thus the overall length of each experimental group session was about 3 hrs.

Results

Results of the study of the effect of number of flights prior to judgements and the ratio of judgements to number of overflights on annoyance are depicted in Fig. 3. Essentially, judgements made of individual stimuli within a tape appear not to be based upon number of flights heard prior to that particular stimulus. Additionally, annoyance judgements of individual stimuli do not appear to be affected by the ratio of judgements to number of stimuli presented, i.e., the

judgements of the overflight with a 95 dB(A) peak as presented in Tape 1 where every flight is rated by the S's are not significantly different from ratings of the same flights from Tape 2 where judgements are made every other flight. Likewise, judgements of annoyance at a peak level of 85 dB(A) do not differ significantly whether judged every time, every other time, after every fourth, eighth, or sixteenth flight.

As expected, specific annoyance increases with level of noise. In fact, a doubling of annoyance, i.e., increasing the annoyance score from about 2 to 4, results where the SPL of the overflight goes from 80 dB(A) to 90 dB(A). This is consistent with Stevens' (6) finding that doubling or halving of loudness occurs with a change in stimulus level of about 10 dB and also with Kryter's (7) finding with respect to annoyance.

Fig. 4 shows the relationship between mean general annoyance summed across all stimuli and anxiety, as measured by scores on the TMAS for each S. Surprisingly, there appears to be a strong negative correlation between general annoyance to the aircraft noise used in this experiment and anxiety level. The Pearson product-moment correlation coefficient (r) was found to be -.56, significant beyond the .01 level. The r for specific annoyance was also calculated (see Fig. 5) and found to be -.53, also significant beyond the .01 level, substantiating the results found for general annoyance. These results, then, apparently indicate that anxious people, defined as those scoring high on the TMAS, tend not to be as annoyed by recorded aircraft flyover noise in the laboratory as less anxious (lower scoring on the TMAS) persons.

Figure 6 shows the relation between specific annoyance and general annoyance over trials. It appears that general annoyance does not grow over the 16 flight session but does reflect the level of the specific flight preceding the general annoyance judgement.

Discussion

The fact that number of flights heard prior to judging the annoyance of the flights was not significantly related to annoyance is important in the design of future laboratory studies of annoyance to aircraft flyover noise. Individual flyovers can be presented and directly compared to results of other researchers who may use different procedures.

The finding in this study that a doubling of annoyance occurred with a 10 dB(A) increase in the peak level of the overflight substantiates findings of other researchers regarding loudness changes as a function of changes in intensity and indicate that loudness and annoyance are rather directly linked.

Additionally, a considerable shortening of test session length can be achieved by having S's judge each flight, rather than every third flight without degrading the results.

At first the negative correlation of the TMAS scores and aircraft flyover noise annoyance scores would seem to be startling. Without thinking about the problem too deeply the first thought would probably be that anxious people would also be easily annoyed because they are probably more aroused and driven by their anxieties. From one point of view, perhaps the anxieties - whatever they are - distract the person and occupy his thoughts such that at least minor, non-threatening stimuli in the laboratory environment are not as noticed and annoying as they might be if he were not so distracted. On the other hand, the result may be an artifact induced by the artificial laboratory setting, and therefore not valid in a real-life setting such as at the subject's home.

Another possibility should be considered. A study by Glickstein (8) of the response to stress of S's rated as either high or low anxious persons found that the various physiological indices studies changed less in high anxious than in low anxious S's. These findings would appear to support the findings of the present study and suggest that the low anxious S's respond to their subjective feelings (blood pressure, heart rate, etc.) which in turn change more and would be more noticeable than they do for high anxious S's.

The implications of this finding are rather clear. Results of annoyance studies using anxious S's may show artificially low annoyance to stimuli. Therefore, S's should be screened for annoyance so that those with high anxiety levels do not unduly influence the results of the study. It would appear to be more than worthwhile to investigate further the relations between anxiety and annoyance to aircraft flyover noise both in the laboratory and in the community.

References

1. Clarke, Frank R. and Kryter, Karl D. The methods of paired comparisons and magnitude estimation in judging the noisiness of aircraft. NASA Report CR-2107, Aug., 1972, 31 pp.

2. Borsky, Paul N. and Leonard, Skipton. Annoyance judgements of aircraft with and without acoustically treated nacelles, NASA Report CR-2261, Aug., 1973, 70 pp.

3. Connor, William and Patterson, Harold. Community reaction to airport noise. NASA Rept. NASW-1549, Tracor Co., Austin, Texas, 1970.

4. U.S. National Bur. Standards study of the fear component in reactions to aircraft noise. Unpubl. Interim Report, NASA Order L-88318, Aug., 1973, 10 pp.

5. Taylor, Janet A. A personality scale of manifest anxiety. J. Abn. and Soc. Psych., 1953, 48, 285-290.

6. Stevens, S. S. Concerning the form of the loudness function. J. Acoust. Soc. Amer., 1957, 29, 603-606

7. Kryter, Karl D. Scaling human reactions to the sound from aircraft. J. Acoust. Soc. Amer., 1959, 31, 1415-1429.

8. Glickstein, M., Chevalier, J. A., Karchen, S. J., Basowits, H., Sabshin, M., Hamburg, D. A., and Grinker, R. R. Temporal heart rate patterns in anxious patients. AMA, Arch. Neur. Psychist., 78, 101-106, 1957.

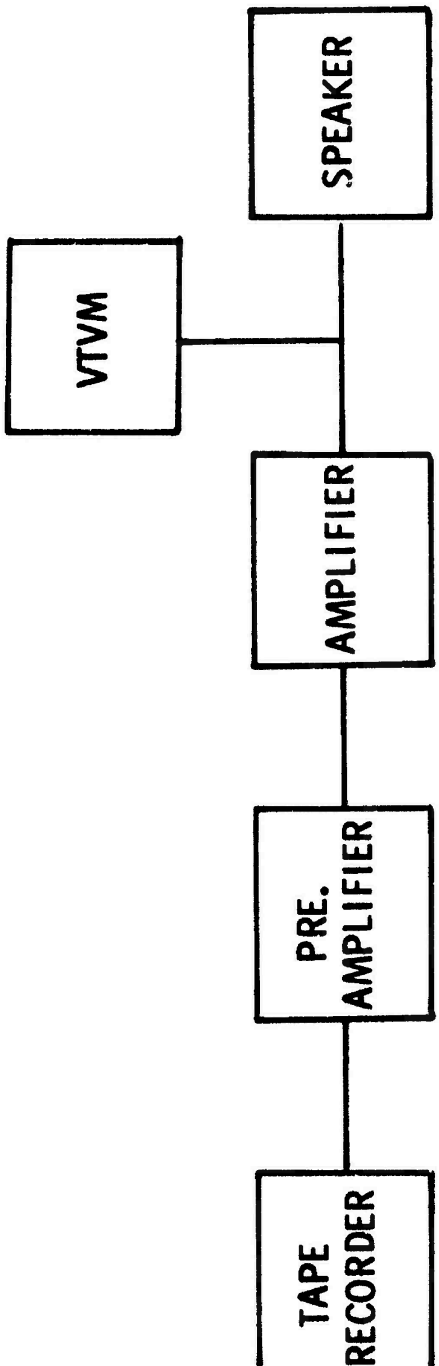

FIGURE 1

FIGURE 2

EXPERIMENT NO. METHOD NO.

(Subjects Instruction and Data Sheet)

ANSWER SHEET

Name _____ Date _____

Sex _____ Age _____ Session _____ Listening Position _____

INSTRUCTIONS

We are going to ask you to help in an experiment about aircraft noise. You will hear a series of aircraft noises and we would like to know your feelings about how noisy, annoying, unwanted, or objectionable certain sounds are. Try to imagine that you are hearing these sounds at home in your living room and that the planes fly this way on most days.

We would like you to record your response each time you hear a "beep" after certain flights. When you hear the beep, record your response to (a) the flight immediately before the beep, and (b) your overall reaction to all of the flights in general up to this point. Use the thermometer-like scale at the right as a guide to rating the sounds.

BEEP	IMMEDIATELY PRECEDING NOISE	NOISE IN GENERAL
1		
2		
3		
4		
5		
6		
7		
8		
9		
10		
11		
12		
13		
14		
15		
1		

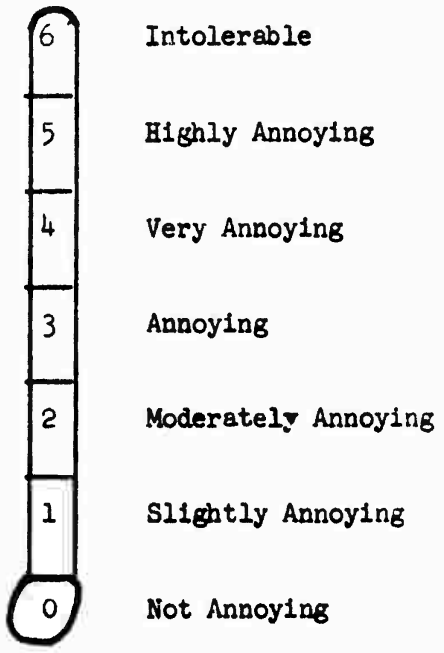

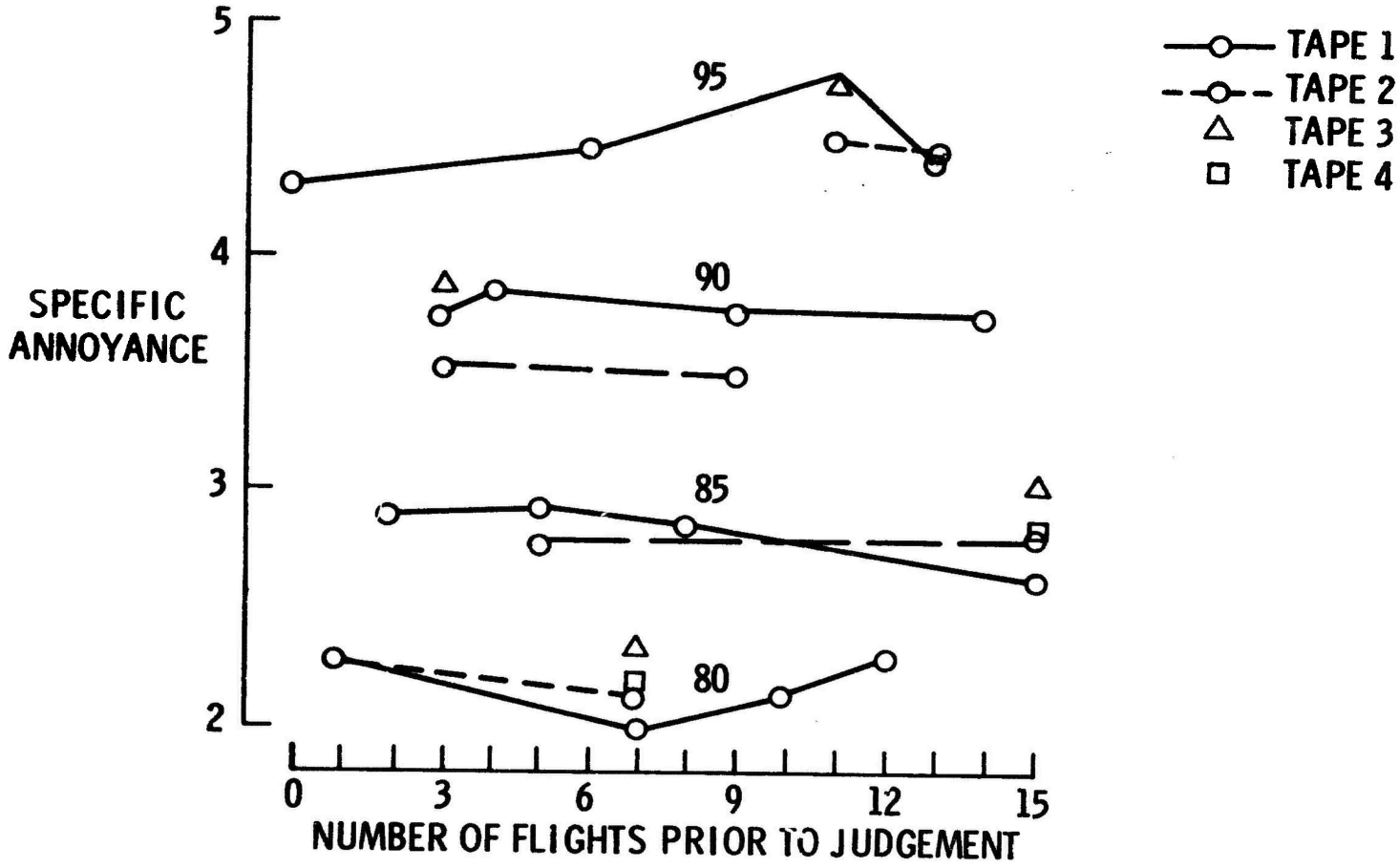
5
4
3
2
SPECIFIC ANNOYANCE
95
90
85
80
TAPE 1
TAPE 2
TAPE 3
TAPE 4
0
3
6
9
12
15
NUMBER OF FLIGHTS PRIOR TO JUDGEMENT

Figure 3

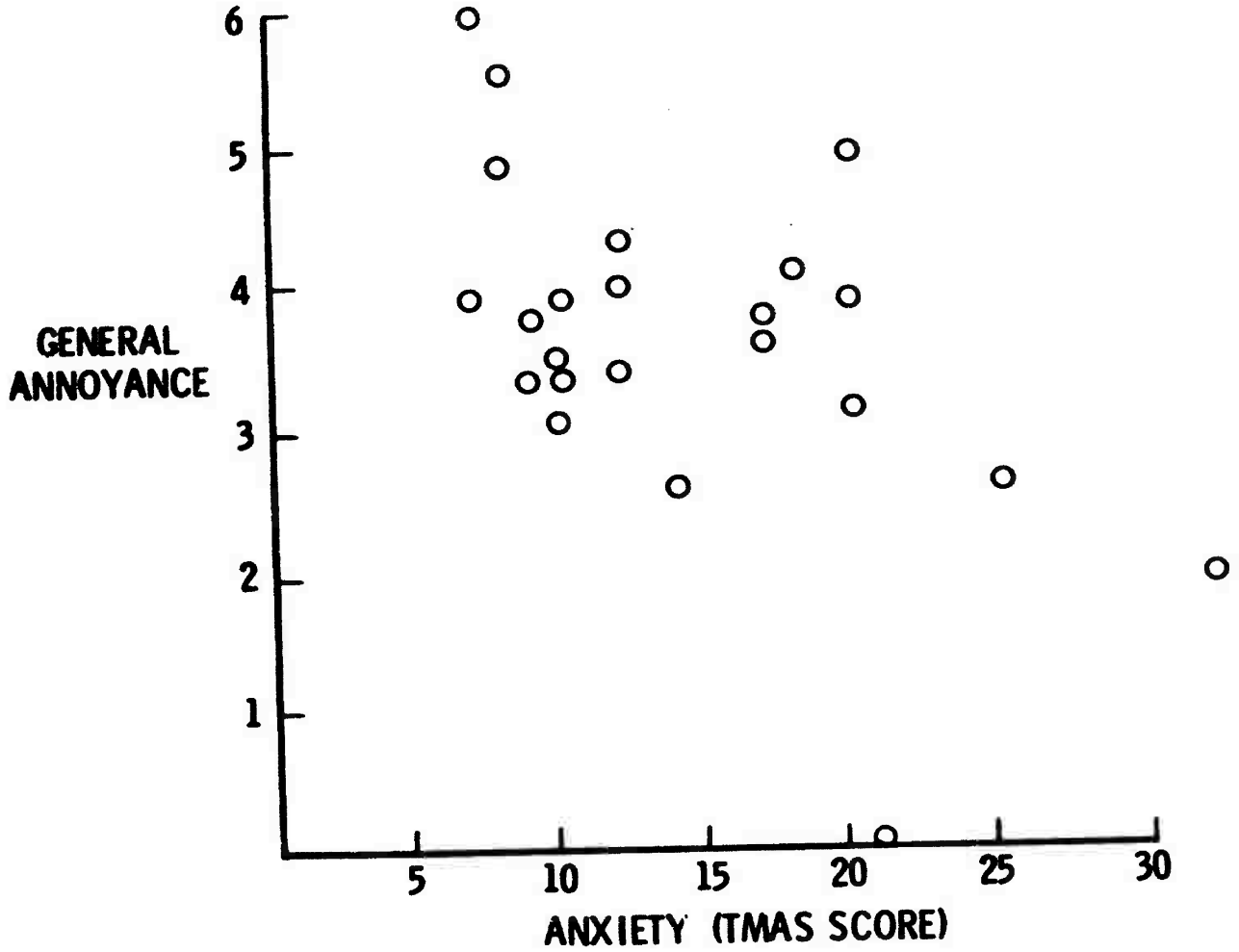

Figure 4

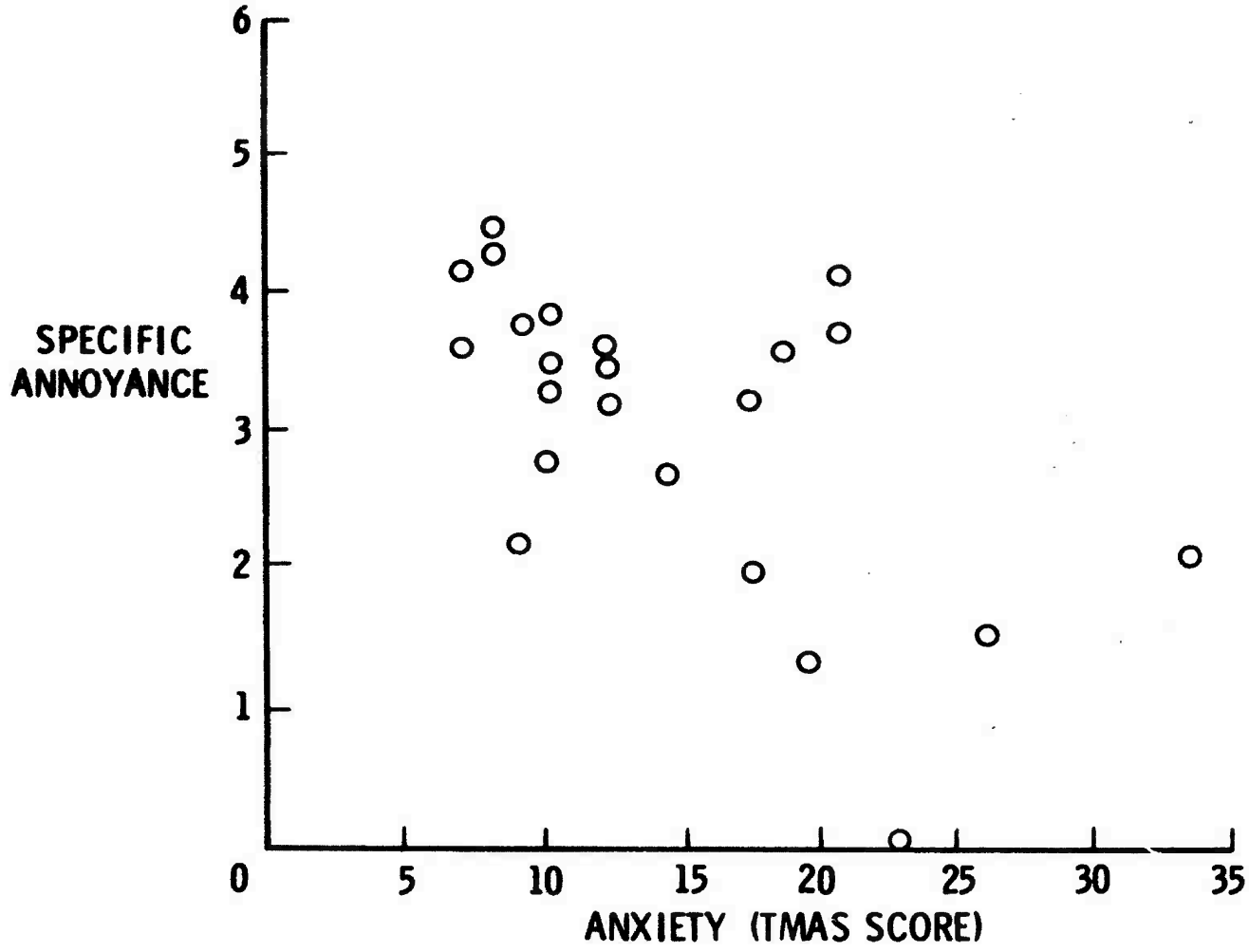
SPECIFIC ANNOYANCE
6
5
4
3
2
1
0
5
10
15
20
25
30
35
ANXIETY (TMAS SCORE)

Figure 5

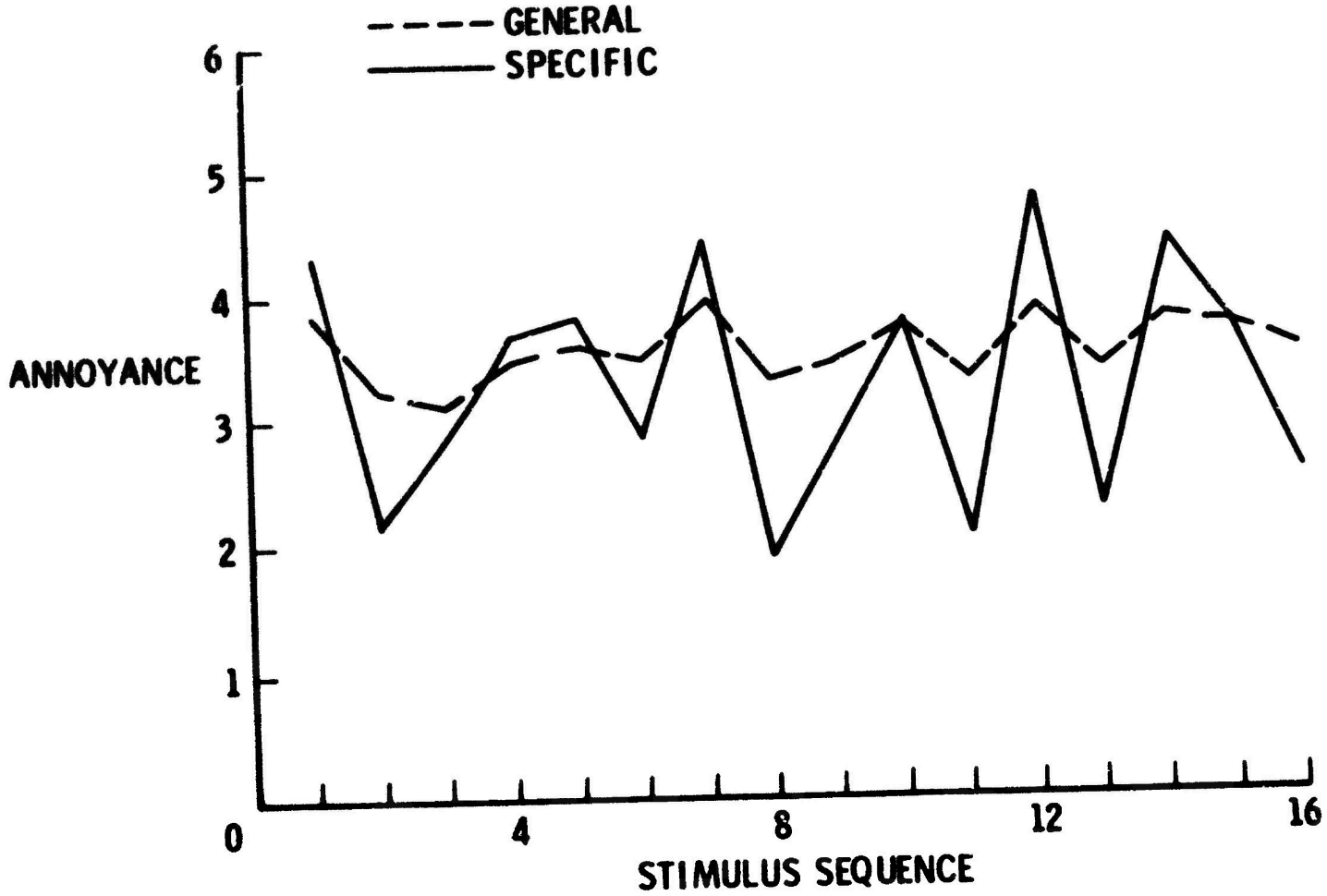
GENERAL
SPECIFIC
ANNOYANCE
6
5
4
3
2
1
0
4
8
12
16
STIMULUS SEQUENCE

Figure 6

TABLE I

SUBJECT GROUP	TAPE PRESENTATION ORDER				
1	2	5	3	1	4
2	3	1	4	2	5
3	4	2	5	3	1
4	5	3	1	4	2
5	1	4	2	5	3

TABLE II

TAPE	STIMULUS PRESENTATION ORDER															
1	A_b	D_b	C_b	B_b	B_b	C_b	A_b	D_b	C_b	B_b	D_b	A_b	D_b	A_b	B_b	C_b
2	A	D_b	C	B_b	B	C_b	A	D_b	C	B_b	D	A_b	D	A_b	B	C_b
3	A	D	C	B_b	B	C	A	D_b	D	B	D	A_b	D	A	B	C_b
4	A	D	C	B	B	C	A	D_b	C	B	D	A	D	A	B	C_b
5	A	D	C	B	B	C	A	D	C	B	D	A	D	A	B	C_b

"B" - BEEP IMMEDIATELY FOLLOWING LAST FLIGHT

A = 95 dB(A) PEAK
B = 90 dB(A) PEAK
C = 85 dB(A) PEAK
D = 80 dB(A) PEAK

APPENDIX B

ANSWER SHEET

Name_____ Date_____

Sex____ Age____ Session_____ Listening Position_____

INSTRUCTIONS FOR THERMOMETER SCALE JUDGEMENTS

We are going to ask you to help in an experiment about aircraft noise. You will hear a series of aircraft noises and we would like to know your feelings about how noisy, annoying, unwanted, or objectionable certain sounds are. Try to imagine that you are hearing these sounds at home in your living room and that the planes fly this way on most days.

We would like you to record your responses to each flight in the left column and your general response to all of the flights up to that point in the right column. Use the thermometer-like scale on the right as a guide to rating the sounds.

FLIGHT	IMMEDIATELY PRECEDING NOISE	NOISE IN GENERAL
1		
2		
3		
4		
5		
6		
7		
8		
9		
10		
11		
12		
13		
14		
15		
16		

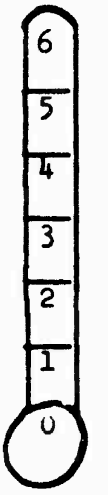

Intolerable

Highly Annoying

Very Annoying

Annoying

Moderately Annoying

Slightly Annoying

Not Annoying

APPENDIX C

EXPERIMENT NO. METHOD NO.

ANSWER SHEET

Name _____ Date _____

Sex _____ Age _____ Session _____ Listening Position _____

INSTRUCTIONS

We are asking you to help us solve a problem concerned with noise: How annoying or disturbing are various kinds of sound when heard in your home? You will be asked to give a score to each sound.

First, we will produce a sound whose noisiness score is 10. Use that sound as a standard, and judge each succeeding sound in relation to that standard. For example, if a sound seem twice as noisy as the standard, you will write 20 in the appropriate box on the answer sheet. If it seems only one-quarter as noisy, write 2.5. If it seems three times as noisy, write 30, and so on.

Please try to judge each sound carefully, and give it a score that tells how strong the annoyance seems to you. There are no right or wrong answers. The important thing is to say how you rate each of the sounds.

1.	_____	11.	_____
2.	_____	12.	_____
3.	_____	13.	_____
4.	_____	14.	_____
5.	_____	15.	_____
6.	_____	16.	_____
7.	_____	17.	_____
8.	_____	18.	_____
9.	_____	19.	_____
10.	_____	20.	_____

ANNOYANCE OF AIRCRAFT FLYOVER NOISE AS A FUNCTION OF THE PRESENCE OF STRANGERS

by

John L. Fletcher
Project Director
Professor, Memphis State University
Department of Psychology
Memphis, Tennessee

and

Walter J. Gunn
Senior Research Psychologist
Noise Effects Branch
Acoustics and Noise Reduction Division
NASA Langley Research Center
Hampton, Virginia

Many researchers (1), (2), use test procedures in which groups of subjects listen to recordings of aircraft flyovers and record their annoyance response for each flight, using various psychophysical procedures. The results are then used in an attempt to predict individual response to noise. It seemed possible that if the presence of others tends to alter one's response to aircraft noise, the practice of testing groups of subjects simultaneously, while efficient, might introduce needless errors into attempts to predict individual response to aircraft noise. In order to determine the comparability of results derived by testing individuals alone or individuals when in groups, the following experiment was designed.

Subjects were tested in groups of six, in one condition, or as individuals in the other condition. Each subject was asked to evaluate the annoyance value of various recorded aircraft sounds, using either a magnitude estimation method or a thermometer-like numerical category scale, after Connor and Patterson (3).

Method

The subjects (S's) used in this study were obtained from Memphis State University and were either students or staff and ranged in age from 20 to 43 with the average age 27.3 years. There were 8 male and 16 female S's. They were paid $10.00 for their participation in the study. All S's were screened for conventional hearing (500-6,000 Hz) with no one accepted as a S with hearing loss at any of those frequencies of 20 dB or higher. Hearing was also tested for high frequency tones (8,000-18,000 Hz) but no criterion level was set for high frequency

hearing. All testing was done in an Industrial Acoustics Co. Model 1203 sound treated room by a graduate student in audiology from the Memphis Speech and Hearing Center. conventional hearing was tested using a Rudmose ARJ-4A audiometer while high frequency hearing was tested using a Rudmose ARJ-4HF audiometer. Both audiometers were within acceptable calibration limits.

All S's were also administered the Taylor Manifest Anxiety Scale (TMAS) as part of their pre-experiment screening.

The research was conducted in a quiet room 15' x 24', set up to be similar to a living room, with wall-to-wall carpeting, drapes on three of the four walls, and acoustical tile on the ceiling. (See Appendix A for pictures of the test room.) Average ambient sound pressure level in the room was 43 dB(A).

A Bruel and Kjaer Model 2203 sound level meter, set on the slow meter reading, A scale, was used to adjust the SPL of the stimuli on the tapes at the S's ear. The meter was placed at ear level at the S's chair position with the S not present, the tape was run to the 1,000 Hz calibration tone, and the preamplifier gain control was adjusted until the meter read 95 dB(A). The voltage across the speaker necessary to obtain 95 dB(A) was found to be 4 volts. Thereafter, each time a tape was run, voltage to the speaker was checked on the VTVM, set at exactly 4 volts if it was not, and the tape run. In practice, little or no change in voltage was noted from tape to tape or session to session. A block diagram of the apparatus may be seen in Fig. 1.

The S's were divided into four groups of six persons per group as they were screened and found qualified for the experiment. The S's were then tested, first either individually or in a group in counterbalanced order, judged annoyance to the aircraft flyover noise either using the "thermometer-like" numerical category scale or the magnitude estimation method (see Appendix C) (5). When tested (Appendix B) as individuals, the S's were called in and given their instructions, and the study began. In similar fashion when they were tested in groups they were called into the room, seated, given their instructions, any questions about task or procedure were answered, and the study begun.

The stimuli on Tape I, 16 in number, were presented and the S rated annoyance to the sound on the "thermometer" scale. There was a 2 min. interval between onset of each stimulus and onset of the next stimulus. Thus, the S's made an annoyance judgement every 2 min. Likewise, on Tape II, there were also 16 aircraft noises, 2 min. apart, and four "standard" noises interspersed, with a magnitude estimation judgement required after each stimulus. On that particular tape, the standard appeared four times or before the first experimental stimulus, and preceeding every group of four stimuli thereafter. (See Table I.)

Results

Fig. 2 shows mean specific annoyance responses for each of the four peak levels of flyover noise for subjects tested as individuals, on one condition, and the same subjects when tested in groups of six. The differences between responses of individuals when tested alone or in groups of six did not reach the 0.05 level of significance. It is therefore concluded that the presence of others does not significantly influence one's annoyance reaction to recorded aircraft noise, in this particular test situation, and when this particular category scale (thermometer scale) is used as an index of annoyance.

Fig. 3 presents mean specific annoyance responses utilizing the magnitude estimation technique for each of the four peak levels of flyover noise for S's tested as individuals, then again in a group of six. Again, as with the "thermometer" scale, the differences between annoyance scores when tested as individuals did not differ significantly (.05 level of significance) from those found for S's tested in groups of six. This suggests strongly that the presence of others does not influence the annoyance reaction to recorded aircraft noise.

Fig. 4 depicts mean specific annoyance as measured by the thermometer scale versus anxiety for each subject in this experiment. No significant correlation was found to exist between annoyance and anxiety, as had been found in a previous study (4). These results were not totally unexpected since the range of anxiety of subjects in this experiment was severly restricted relative to the anxiety levels found in the previous study. Since the subjects in this experiment listened to exactly the same tape as the subjects in the previous experiment and rated the annoyance value of the same aircraft noises using the same thermometer-like numerical category scale, it seems justifiable to combine the data from both experiments into one composite plot. Fig. 5 shows the combined data of both experiments. In this figure, mean specific annoyance is plotted versus anxiety for each of the 43 subjects for whom data were available. The Pearson Product moment correlation coefficient was found to be -0.39 which was significant beyond the 0.01 level.

Discussion

The findings indicate that at least for similar test situations (where the subjects sit and evaluate each recorded flyover noise) and for the two psychophysical methods used, the presence of other does not appear to influence one's annoyance response to aircraft noise. The implications for future laboratory research are that groups of subjects can be tested simultaneously for maximum procedural efficiency with confidence that the procedures do not alter the individual responses significantly.

Although the limited range of anxiety scores may have obscured any possible correlation of anxiety and annoyance in this experiment, the data of this experiment when combined with similar data from a previous study (4) do indicate a significant ($p < .05$) negative correlation between anxiety scores and annoyance ratings for individuals. As suggested in the Gunn and Fletcher study (4), this result may be a laboratory artifact resulting from the laboratory-induced stress of the test situation having a "saturating" effect on one's emotional response to noxious stimuli and therefore not valid in a real life situation, or it may in fact be an important factor governing one's annoyance to aircraft noise. Further research in this area seems indicated in order to verify this effect in the laboratory and in airport communities.

References

1. Kryter, Karl D. Scaling human reactions to the sound from aircraft. J. Acoustic. Soc. Amer. 31, 1415-1429, 1959.

2. Pearsons, K. S. Noisiness judgements of helicopter flyovers. Rept. DS 67-1, Contract FA65WH-1260, Bolt Beranek and Newman, Inc., Van Nuys, California, 1967.

3 Connor, William and Patterson, Harold. Community reaction to airport noise. NASA Rept. NASW-1549, Tracor Co., Austin, Texas, 1970.

4. Gunn, Walter J. and Fletcher, John L. The effect of number of flights prior to judgement on annoyance to aircraft flyover noise, NASA Rept. in press, April 1974.

5. Clarke, Frank R. and Kryter, Karl D. The methods of paired comparisons and magnitude estimation in judging the noisiness of aircraft. NASA Rept. CR-2107, Aug., 1972.

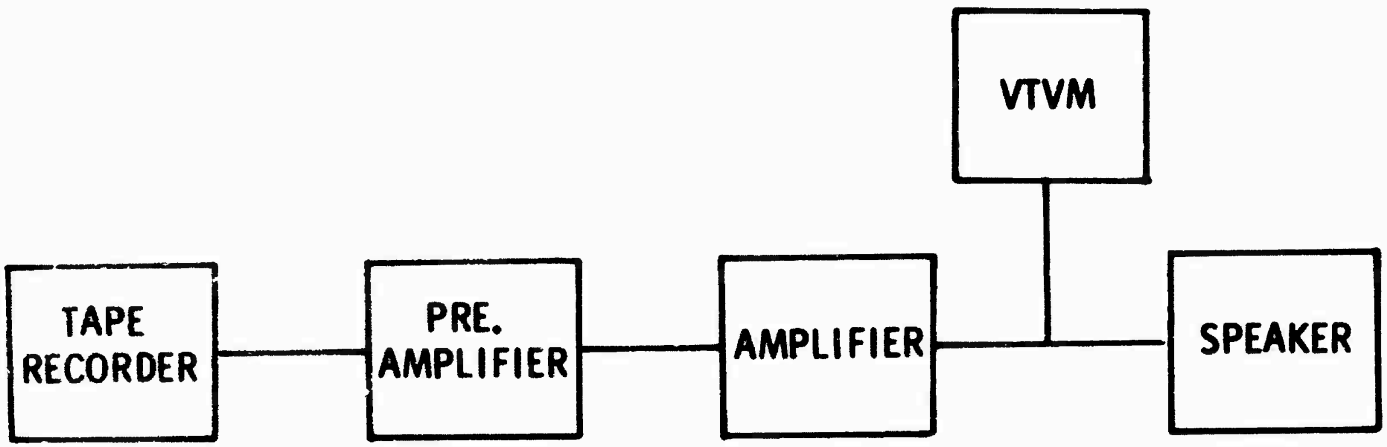

FIGURE 1

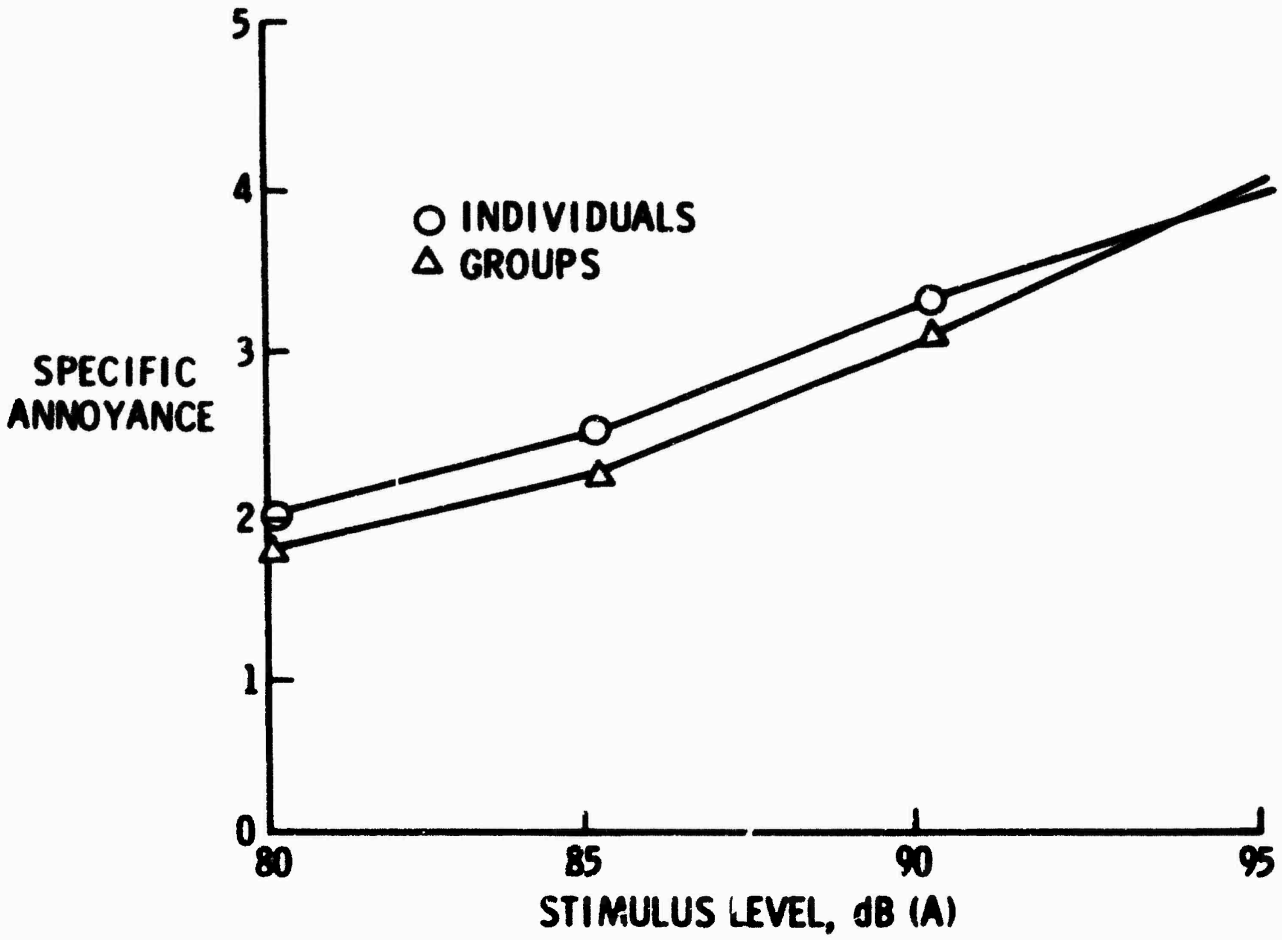
5
4
3
2
1
0
SPECIFIC ANNOYANCE
O INDIVIDUALS
Δ GROUPS
80
85
90
95
STIMULUS LEVEL, dB (A)

FIGURE 2

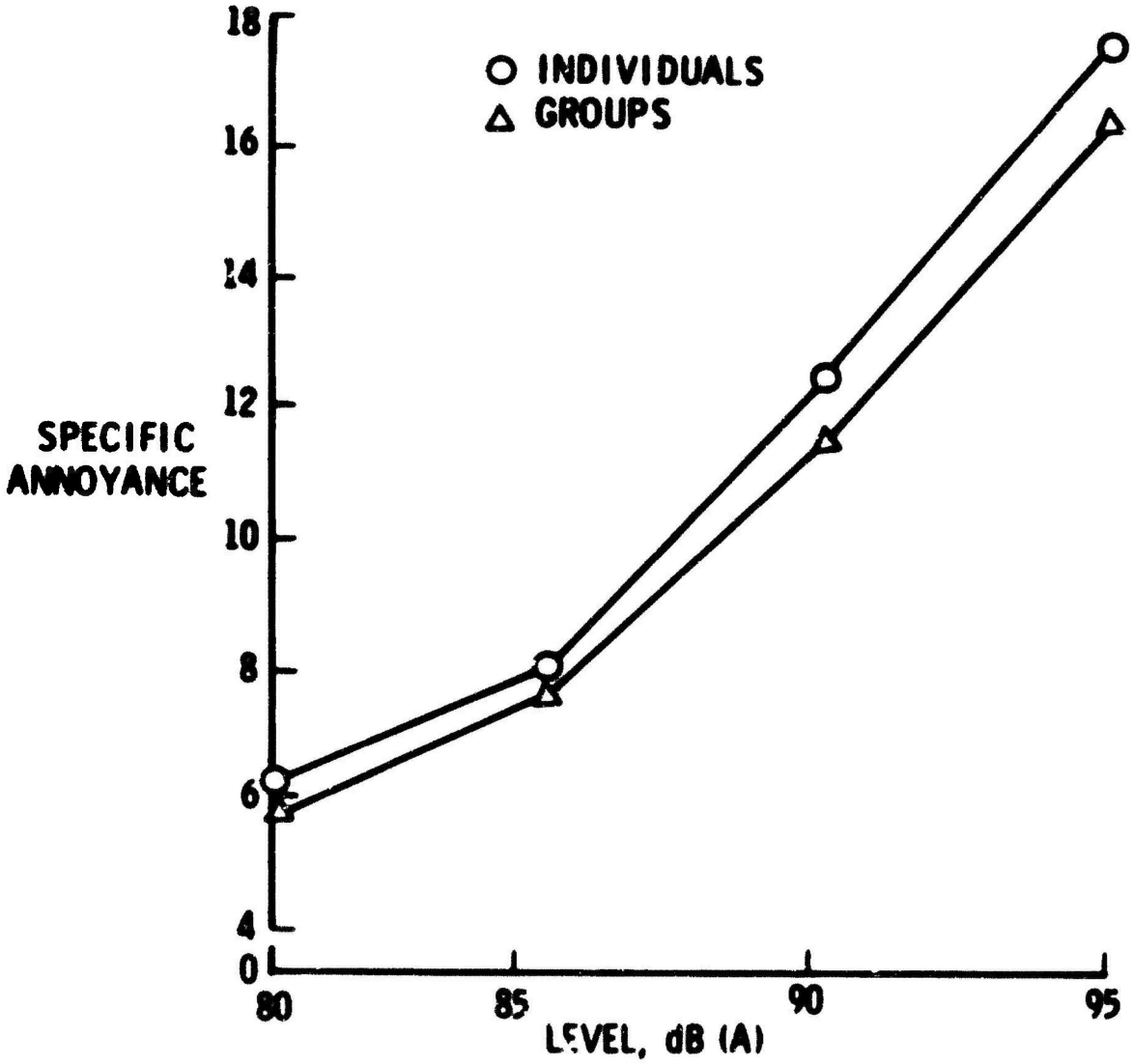
18
16
14
12
10
8
6
4
0
80
85
90
95
SPECIFIC ANNOYANCE
LEVEL, dB (A)
INDIVIDUALS
GROUPS

FIGURE 3

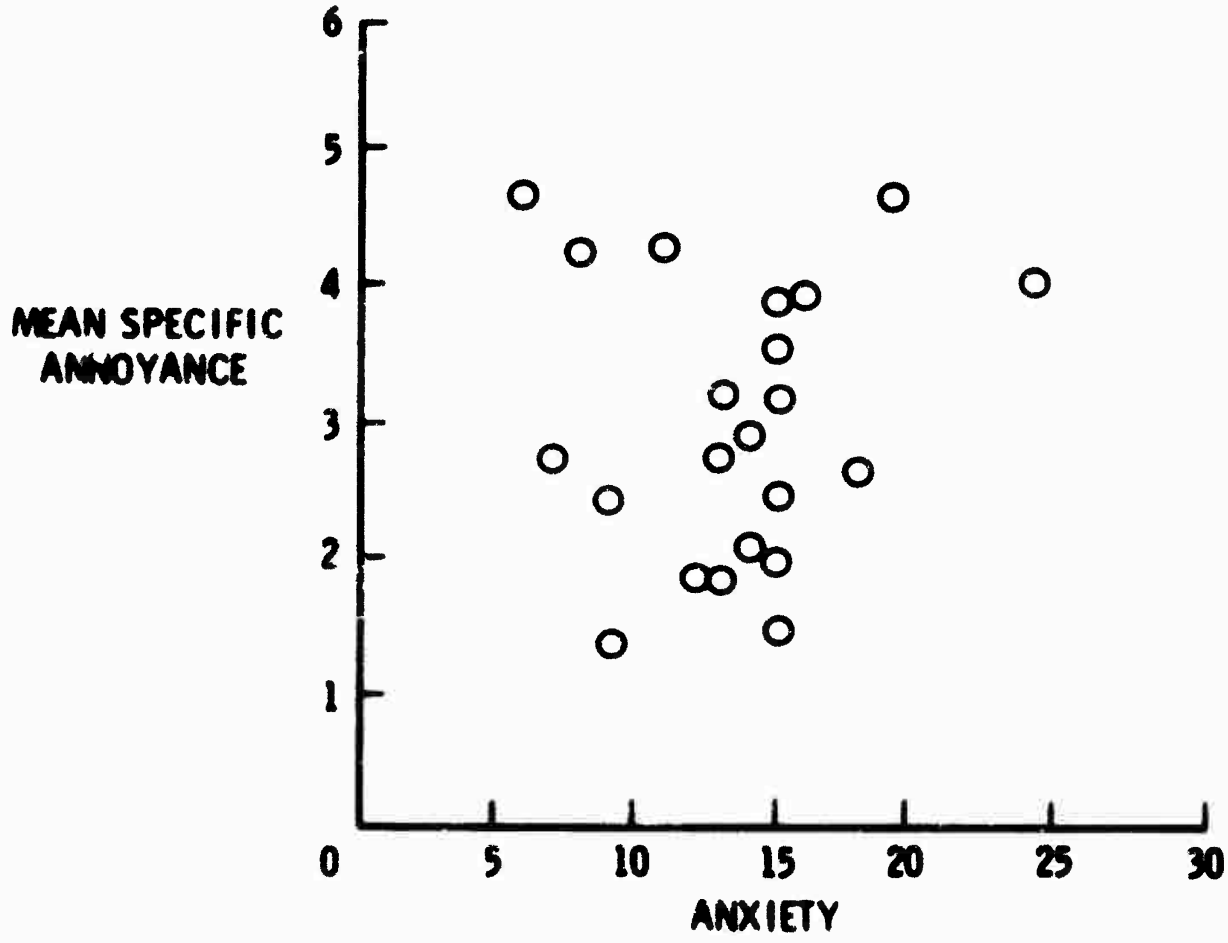

FIGURE 4

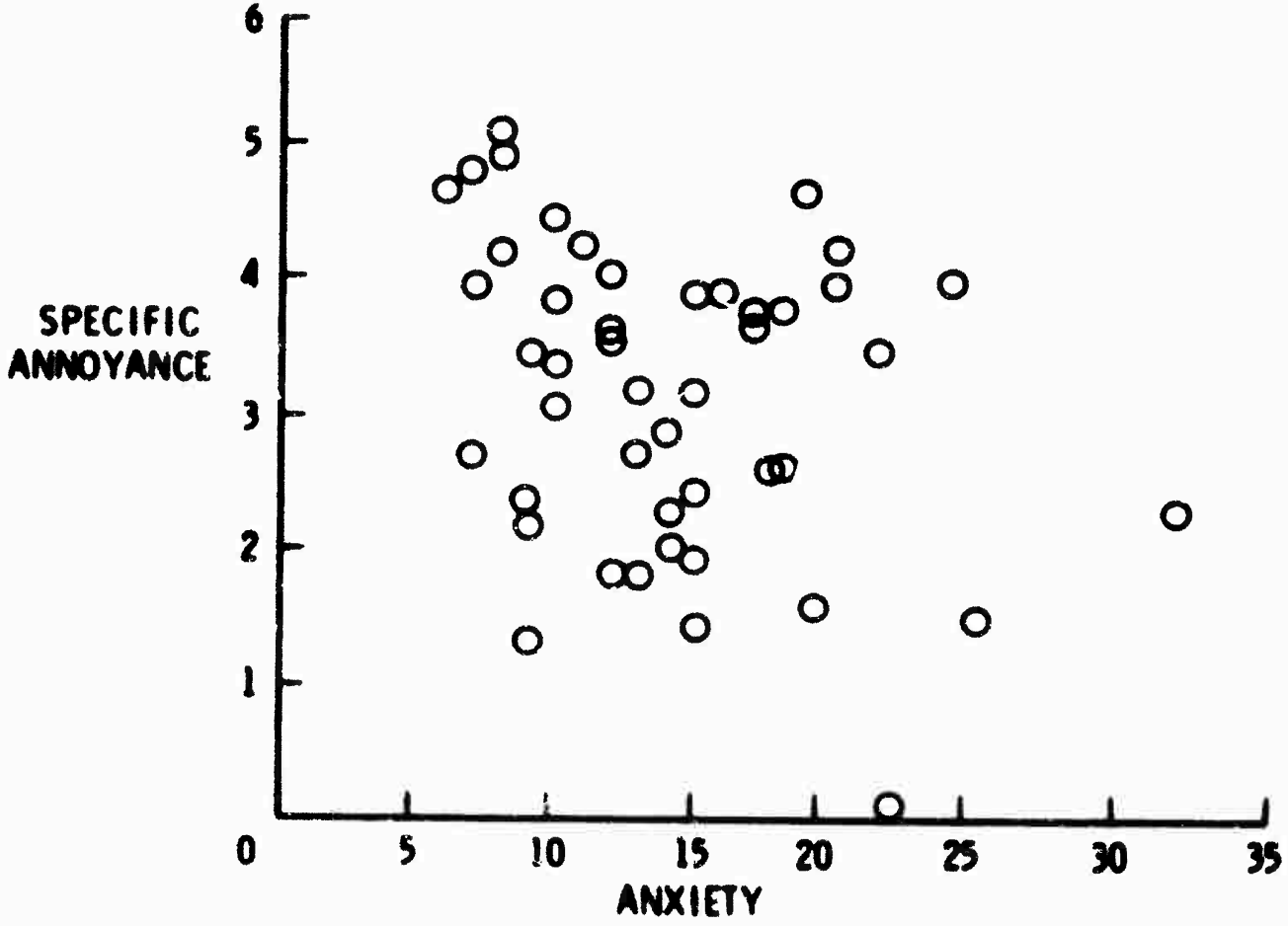

FIGURE 5

TABLE I

STIMULUS LEVELS AND ORDER

The tape for Method II consists of a series of recorded aircraft (747) flyovers (landings). There are 4 presentations of each of four levels of noise.

Stimulus	Peak Level dB (A)
A	95
B	90
C	85
D	80

The flyovers were recorded in the following sequence (according to a Lat. Sq. design) with two minute intervals from onset to onset:

TAPE I

Flight numbers	1	2	3	4	5	6	7	8	9	10	11	12	13	14	15	16
Stimuli	A	D	C	B	B	C	A	D	C	B	D	A	D	A	B	C

The tape for Method I consists of the same series of flights as recorded on Tape I. [illegible] with a "standard" noise (a) [illegible] pink noise at [illegible] dB(A) for [illegible] seconds with [illegible] repeated [illegible] times [illegible] inserted between flights as shown:

Tape II

Flight No.	1	2	3	4	5	6	7	8	9	10	11	12	13	14	15	16	17	18	19	20	21
Stimuli	S	A	D	C	B	S	B	C	A	D	S	C	B	D	A	S	D	A	B	C	S

Since Tape II is a copy of Tape I with standards inserted as shown above, the length of the recordings is approximately equal.

APPENDIX A

APPENDIX B

ANSWER SHEET

Name _____ Date _____

Sex___ Age ___ Session _____ Listening Position_____

INSTRUCTIONS FOR THERMOMETER SCALE JUDGEMENTS

We are going to ask you to help in an experiment about aircraft noise. You will hear a series of aircraft noises and we would like to know your feelings about how noisy, annoying, unwanted, or objectionable certain sounds are. Try to imagine that you are hearing these sounds at home in your living room and that the planes fly this way on most days.

We would like you to record your response to each flight in the left column and your general response to all of the flights up to that point in the right column. Use the thermometer-like scale on the right as a guide to rating the sounds.

FLIGHT	IMMEDIATELY PRECEDING NOISE	NOISE IN GENERAL
1		
2		
3		
4		
5		
6		
7		
8		
9		
10		
11		
12		
13		
14		
15		
16		

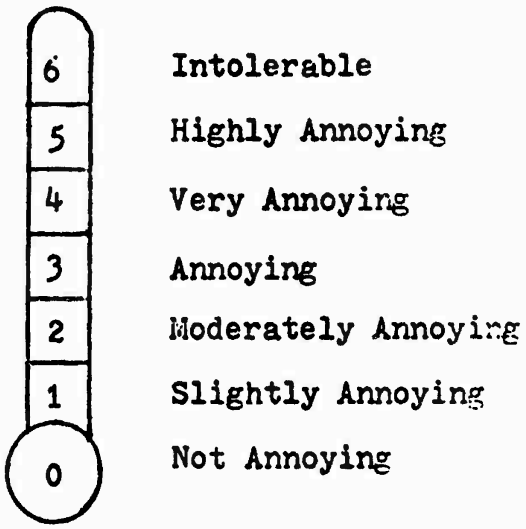

APPENDIX C

EXPERIMENT # METHOD #

ANSWER SHEET

Name_____ Date_____

Sex_____ Age_____ Session _____ Listening Position_____

INSTRUCTIONS

We are asking you to help us solve a problem concerned with noise: How annoying or disturbing are various kinds of sound when heard in your home? You will be asked to give a score to each sound.

First, we will produce a sound whose noisiness score is 10. Use that sound as a standard, and judge each succeeding sound in relation to that standard. For example, if a sound seems twice as noisy as the standard, you will write 20 in the appropriate box on the answer sheet. If it seems only one-quarter as noisy, write 2.5. If it seems three times as noisy, write 30, and so on.

Please try to judge each sound carefully, and give it a score that tells how strong the annoyance seems to you. There are no right or wrong answers. The important thing is to say how you rate each of the sounds.

1.	_____	11.	_____
2.	_____	12.	_____
3.	_____	13.	_____
4.	_____	14.	_____
5.	_____	15.	_____
6.	_____	16.	_____
7.	_____	17.	_____
8.	_____	18.	_____
9.	_____	19.	_____
10.	_____	20.	_____

SLEEP-DISTURBING EFFECTS OF AUDITORY STIMULI AND EFFECTS ON CERTAIN WAKING PERFORMANCES*

by

T. E. LeVere

Neuropsychology Laboratory
Department of Psychology
North Carolina State University
Raleigh, North Carolina 27607

ABSTRACT

Previous data from our laboratory indicated that the way an individual reacts to auditory stimuli during wakefulness does not necessarily predict the way in which the individual will respond to similar auditory stimuli during sleep. Specifically, these data demonstrated that auditory stimuli in the low frequency ranges between 50 and 250 Hz were more disruptive to an individual's sleep than stimuli in the range of 1k Hz even though the stimuli were equated for psychological loudness. The interpretation of these data suggested that whatever neural processes are operative during the waking state were not so operative during the sleeping state and that this qualitative difference should be taken into account when attempting to predict the disruptive effects of auditory noise during sleep. The data which is presently reported extend these results by suggesting that the sleep disruption caused by these auditory stimuli can influence certain waking behaviors. Consideration of our preliminary results with other data concerned with the effects of sleep disruption on waking behavior suggests that the behaviors which are most susceptible to sleep disturbances are those behaviors involving higher cognitive processes as opposed to more simple repetitive performances.

* This research was supported by Research Grant NGL 34-002-095 from the National Aeronautics and Space Administration.

Introduction

The present report assumes the validity of the commonly held and empirically verifiable notion that sleep can be interfered with by auditory noise. From this starting point, we presently address two major issues. Firstly, are the disturbances produced by auditory noise during sleep restricted to the sleep state or is there some carry-over degradation of waking behavior? And secondly, if there is carry-over to the waking state, what parameters of nocturnal stimulation are most effective in producing the carry-over?

General Methodology

The procedures which we generally employ [9,10,11] to investigate these issues involve human male volunteers between the ages of 18 and 35 who sleep, depending upon the experimental procedures, for three or more consecutive nights in our laboratory bedroom setting. During each of these nights, the individual's scalp-recorded electroencephalographic (EEG) activity is continuously monitored to provide both a measure of the subject's sleep as well as a dependent measure of the arousal produced by the auditory stimulation. The auditory stimulation which we employ to disturb the subjects' sleep during some of the nights which they spend in our laboratory (stimulus nights) consists of between nine and twenty-four 15-sec. stimulus presentations set at an intensity of 80 dB measured with an A-weighted scale. For obvious acoustical reasons, these auditory stimuli are produced by filtering white noise to exclude all frequencies save a one-third octave band centered on the frequency of interest. For the presently reported researches, most of the auditory stimuli had a rapid onset and rapid offset.

The individual's response during sleep to these auditory stimuli is assessed in terms of a change in the dominant frequency pattern of the subject's sleeping electroencephalographic activity as computed over 1-min. analysis epochs. Virtually without exception, this change has been a shift to lower amplitude, higher frequency patterns of activity, or what is traditionally termed cortical desynchronization. This kind of response has been classically labeled as "arousal" by numerous researchers [1, 12, 13, 16] who have noted the correlation between this sort of electroencephalographic activity and overt behavioral alerting. In all of the experiments which we will currently report, the assessment of the individual's electroencephalogram was performed by a Digital Equipment Corporation PDP 12A computer system. Most recently, this system has been upgraded to enable on-line, real-time analyses so that the stimulus presentations may be precisely related to the subject's ongoing pattern of sleep as indexed by the electroencephalogram. In a recent experiment [11], the validity of our computer analysis program, a zero-crossings procedure, was determined by computing Kendall's coefficient of concordance with respect to the output of the computer program and two separate individual visual analyses utilizing conventional Rechtschaffen and Kales criteria. This statistic yielded a Chi Square of 1168.2 which is significant at better than the 0.001 level of confidence and suggests that the independent observers, the computer and humans, were essentially applying similar criteria in making their judgments.

To evaluate an individual's waking behavior, the subjects were required

to perform a behavioral task before retiring at night and upon arising in the morning. The task is illustrated in Figure 1 and consists of three individual stimulus lights and three response buttons. The physical configuration of the task thus presented the subject with three vertically oriented 5/8-in. diameter stimulus lights separated by approximately 1 in. center to center. Immediately above these lights is an Industrial Electronic Engineer readout display with the capability of presenting any of the 6 combinations of the numbers 1, 2, 3. Some 4 in. below the stimulus lights were three 5/8-in. in diameter response buttons mounted to a sloping panel and separated by a distance of 1-3/4 in. center to center. These buttons were arranged in a horizontal line at right angles to the stimulus lights. Approximately 2 in. below the center response button was a 1-in. long x 1/2-in. wide registration lever used by the subject to indicate that a response button had been pressed. The subject's task in this situation is to monitor the three vertical stimulus lights and when one is illuminated to press the "correct" response button and then register this choice by pressing the registration lever. If the response is "correct", the stimulus light is extinguished and the inter-trial interval started. If, however, the response is "incorrect" the stimulus light remains illuminated and the subject is required to correct the error by pressing the correct response button and then registering this choice. The particular response button which a given stimulus light indicates as being "correct" is determined by the 3-digit code presented above the stimulus lights. The manner in which a particular code is related to, or defines, the correct response buttons is quite straightforward and easily visualized if the individual code numbers from left to right are superimposed upon the individual stimulus lights from top to bottom. The particular code number associated with a particular stimulus light then indicates the left to right position of the "correct" response button. For example, the code 123 indicates that the left-most response button is correct if the top-most light is illuminated, the middle response button is correct if the middle light is illuminated and the right-most response button is correct if the bottom-most light is illuminated. However, it must be remembered and emphasized that a given code appears on only the first trial of the series of trials that it serves to define the correct response buttons. Thus, in order for the subject to respond optimally, he must, after the first trial of a given series, remember which code is in effect. The number of trials during which a code is in effect varies over the performance session in a random fashion but always remains in the bounds of 5 and 20 trials. It goes without saying that individual performance sessions are balanced with respect to the number of trial series containing particular numbers of trials and particular codes so that an experimental condition cannot be biased by the operation of the task itself. Additionally, since the subject is allowed as much time as needed to respond to the correct response button, the task is essentially subject-paced. However, once the correct response is accomplished, the next trial is programed to occur, i.e. the next stimulus light will come on after a standard inter-trial interval independent of the subject's behavior.

The basic dependent measure used with this task is mean response latency, as measured from stimulus light onset until the subject has responded to the correct response button and is computed over a standard 10-min. performance session. We have also measured errors, percent errors, errors of commission, and percent errors of commission but have not found these to be related to the

Figure 1. Photograph of the behavioral task used to assess the waking effects of disturbed sleep. The picture illustrates the configuration of the task on the first trial of a series where the code "123" would be in effect. In the particular instance shown, the left-most response button would be "correct".

occurrence of nocturnal sleep-disturbing auditory stimuli. Finally, it should be mentioned that in the experiments discussed below, we were interested in the effects of sleep disruption on performance and not acquisition. To realize this interest, the data which we used to assess waking behavior was always that obtained after the subject's performance of the task had stabilized. In certain situations, we accomplished this by requiring the subjects to come to the laboratory in each day of the week preceding their serving as a sleep subject in order to practice the task and become proficient at its operation.

Carry-Over Effects to Waking Performance

Before discussing the particulars of how sleep disturbed by auditory noise may carry over and influence waking performance, it is perhaps best to establish that the effect can occur. To accomplish this, we may cite certain of our early research [9] concerned with the sleep disturbing effects of broad-band auditory noise. In this procedure, subjects were required to sleep in our laboratory bedroom setting for 14 consecutive nights, 7 of which were randomly designated as stimulus nights. During these stimulus nights, the subject was exposed to nine 15-sec. presentations of broad-band auditory noise having a relatively gradual onset and offset as compared to our more recent researches. The subject's overt waking behavior was assessed by a behavioral task essentially similar to that described above. The subject was required to perform this task before retiring each night and upon arising on the next morning. It is perhaps worth mentioning that the subject was required to perform the morning session only after he alone had determined that he was fully awake and able to operate the behavioral task. While this, of course, introduced some variability into our procedures, it was felt that this variability would be less detrimental to the purpose of our experiment than standardizing, and perhaps requiring, certain of the subjects to perform the task before they were ready.

Considering first the sleep-disturbing effects of the auditory stimulation the results indicated that the stimuli produced reliable and significant changes in the subjects' scalp-recorded electroencephalographic activity. As noted above, these changes consisted of a shift to a higher frequency pattern in the scalp recorded electroencephalogram. While this aoursal effect was noted within each subject, it should be pointed out that it was not consistently associated with behavioral awakening nor was it confined to the period of time when the stimulus occurred. Moreover, none of the subjects were able to recall the number of stimuli that occurred during the night and all stressed that they considered their sleep to be normal, i.e. little or not at all affected by the auditory noise.

Figure 2 summarizes the waking effects of this nocturnal stimulation. The insert in the upper right-hand corner indicates the subjects' error score (response latency) as recorded during the morning performance sessions of the experimental procedure without respect to whether or not the subjects received auditory stimulation during the preceding night. As obvious from this insert, the subjects showed a considerable amount of learning during the first portion of the experiment, and since we were not interested in acquisition, this data is not considered in the analysis. Rather, the major

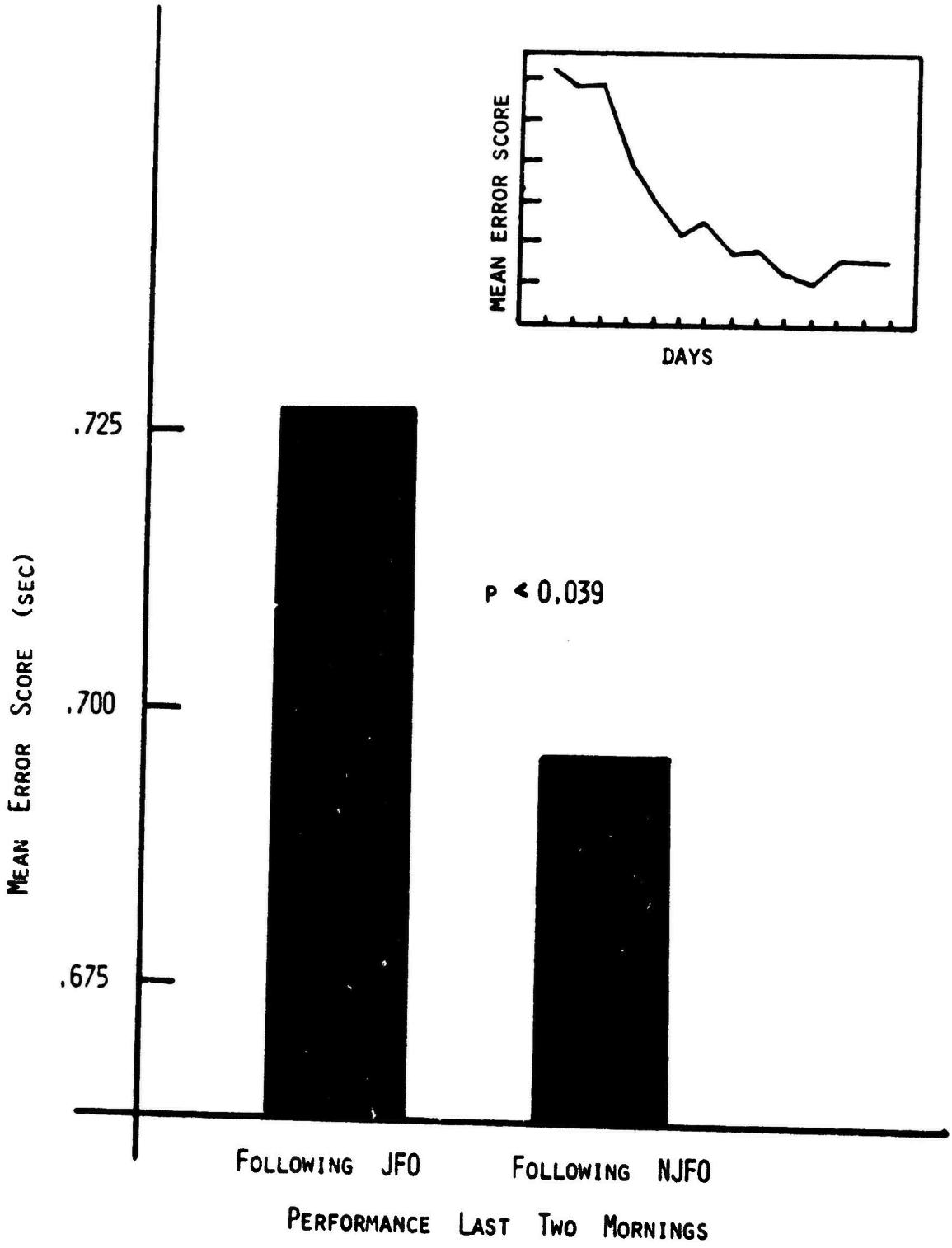

Figure 2. Bar graph illustrating the mean error score (response latency) following nights disturbed by broadband auditory noise (JFO) and following undisturbed sleep (NJFO). The insert at the top right of the figure illustrates the response latency computed over days without regard to whether auditory stimuli were presented during the night.

portion of the figure indicates the morning performance on the last two sessions which followed undisturbed sleep and the morning performance on the last two sessions following sleep disturbed by the auditory stimulation. As the figure indicates, the mean response latency following nights disturbed by auditory stimulation was significantly longer than the mean response latency recorded during performance following undisturbed sleep. It should be pointed out that our randomization precluded attributing this decrement in performance to any order effect since the chronological occurrence of stimulus nights and control nights was not consistent over the subject population.

One very basic and important question concerning the presently observed waking behavioral deficit is why it should occur following the minimal sleep disruptions employed in the present procedures. At the onset, it should be emphasized that the question is not one of whether or not disruptions of sleep have effects on waking behavior. As numerous researches have demonstrated, sleep disturbances can and do, often severely, affect waking behavior. The question is one of degree and involves why seemingly minimal sleep disruptions should influence waking behavior. One perhaps fruitful tack would be to suggest that if one is interested in evaluating the subtle effects of sleep disruption, one should not sample waking behaviors that can occur during sleep. That is, borrowing from the classic restorative conceptualization of sleep, it would seem possible to speculate that any behavior that can operate during sleep may not be dependent upon, or influenced by, sleep or its disruption. Contrariwise, any behavior which does not adequately function during sleep may be critically dependent upon the occurrence of sleep for its optimal waking expression. This distinction is, of course, analogous to the neurophysiological concept that these behaviors which can occur after the ablation of certain neural areas are not dependent for their expression upon the functional operation of the ablated neural tissue.

From this point of view, the rather ample evidence indicating that an individual may respond to extrinsic stimuli and may even discriminate between different types of extrinsic stimuli during sleep [14, 17, 19, 20, 21] would suggest that any task involving a simple response or even a discriminative response, i.e. the usual vigilance procedures, might not be expected to reflect minimal sleep disturbances. This expectation is, in fact, supported by numerous researches. Since there is no reason to assume that the vigilance aspect of the present behavioral task is unique or critically different from those previously reported, it would seem that vigilance is not the parameter which is sensitive to minimal sleep disturbance.

In contradistinction to the subject's ability to simply respond to extrinsic stimuli during sleep, it would appear that memory processes are, at best, most inefficient during sleep [3, 8, 13]. In line with the above speculations and the present data, it might be thus suggested that any waking behavioral task involving memory might be expected to be related quite closely to the quality of an individual's sleep. In fact, this suggestion is not without certain experimental support. Firstly, there are numerous researchers who suggest that memory function may be degraded by sleep loss [2, 4]. The more important of these is the work by Williams, Gieseking and Lubin [18] who demonstrated that the recall of verbal material was impaired

following one night of sleep loss even when it was assured that episodes of microsleep did not prevent the registration of the verbal material. Additionally, data presented by Goodnow, Rubinstein and Shanks [5] indicate that sleep loss may precipitate stereotyped behavior patterns. Stereotyped behavior patterns are here interpreted as indicating that the individuals suffering from sleep loss may not be able to utilize previous experience; and one reason why this might be so is that the individual might not remember what he had previously done. Moreover, there are numerous animal researches summarized by Holdstock and Verschoor [6] suggesting that learning and memory, particularly memory consolidation, may be disrupted by selective sleep deprivation. Thus, the data would clearly suggest that whatever processes are involved in memory, its restoration or retrieval, these processes may be sensitive to sleep loss. In consideration of this data then, a specific speculation concerning the sensitivity of the present behavioral task may be made. This speculation suggests that it may be the memory aspect of the present task which is sensitive to minimal sleep disruption. That is, while it is obvious that the optimal performance of the present task, for that matter any behavior task, may involve many factors, the one factor which would seem critical in the present situation is the facility which the subject remembers the code after its initial (and only) presentation. Whatever else may be involved in pressing the appropriate response button when a particular stimulus light is illuminated, it would appear obvious to even the most casual consideration of the task that the subject must remember which button the stimulus light signifies is "correct". Moreover, if this memory aspect of the present task were eliminated, this situation would reduce to a simple vigilance procedure which is notoriously insensitive to all but the most severe deprivations of sleep. In other words, it is possible to suggest that the present research is but another demonstration of the susceptibility of waking processes to sleep disturbances. This is, of course, nothing dramatically new,and the most noteworthy aspect of the present situation is its sensitivity.

With respect to the present discussion, it should finally be pointed out that Kramer, Roth, Trindar, and Cohen [8] have recently provided data suggesting that sleep disturbances not quantitatively dissimilar to the ones used in the present procedures, can affect mnemonic processes. Moreover, and perhaps more importantly, these researchers utilized a battery of waking behavioral tests and found that only a verbal-recall test could be consistently related to the occurrence of the sleep-disturbing auditory stimulation. These data then are quite compatible to the presently reported results.

Sleep Parameters Affecting Waking Performance

Whether or not one enthusiastically espouses the speculation that sleep disruption degrades higher cognitive processes, the fact still remains that minimal sleep disruption can be detected as a decrement in certain waking performances. Given this,it is of importance to provide some preliminary specification of the parameters of nocturnal auditory stimulation which may precipitate these carry-over effects which influence waking behavior. As an initial and elementary query, we have questioned whether a large number of stimuli may be less debilitating for waking performance than a fewer number of stimuli. That this might occur is because the sleep disruption or arousal produced by the individual stimulus occurrences when a large number are

presented, should be less. In other words, will habituation during sleep attenuate the disrupting effects of nocturnally presented auditory noise?

Specifically, the research involved 6 male subject volunteers who each spent three successive nights in our laboratory bedroom. On different nights, each subject received either no stimuli, 6 occurrences, or 24 occurrences of a one-third octave band burst of noise centered on the frequency of 125 Hz. Each stimulus presentation was 15 sec. in duration and had an intensity of 80 dB(A). The stimulus presentations were in accord with a schedule which distributed the presentations randomly over a night's sleep but with the restriction that half of the stimuli were to occur when the subject's pattern of electroencephalographic activity indicated predominantly fast-wave activity and half were to occur when the subject's pattern of electroencephalographic activity indicated predominantly slow-wave activity. The sequential order of the single no-stimulus control night, the 6-stimulus experimental night, and the 24-stimulus experimental night, was of course balanced across the 6 subjects to control for first-night effects and order effects which might bias the treatment conditions.

Considering first the sleep-disturbing effects of the auditory noise, we present the data in Figure 3. Following our standard procedures, the figure depicts the mean cortical desynchronization as computed over 1-min. EEG epochs during the epoch preceding the occurrence of a stimulus, the epoch when a stimulus occurred, and three succeeding 1 min. EEG epochs. These are further partitioned on the basis of whether the stimuli occurred during sleep dominated by fast-wave EEG activity (left-half of the figure) or during sleep dominated by slow-wave EEG activity (right-half of the figure) and whether there were 6 stimuli or 24 stimuli during the night. The solid line at the top of the figure labeled "wakefulness" is computed on the basis of the mean number of half-wave occurrences (cortical desynchronization) recorded by the computer just prior to the subjects falling asleep. The dashed lines around this value represent the 0.05 confidence intervals for the estimate. As can be seen from the figure, the mean amount of cortical desynchronization produced by the auditory stimuli was significantly greater when only 6 stimuli occurred during the night as compared to when 24 stimuli occurred during the night. This, of course, indicates that the subjects will, so far as their response to individual stimulus presentations is concerned, habituate to the nocturnally presented auditory noise.

However, even though a significant amount of habituation occurred relative to the subject's response to the individual stimulus presentations, this habituation did not mitigate the disruptive effects which these stimuli had relative to morning waking performance. That is, even though the subjects responded less to the individual stimulus presentations when 24 stimuli were presented during the night, there was nonetheless a greater disruption of waking performance following these nights as compared to when either 6 stimuli occurred during the night or sleep was undisturbed. This data is graphically illustrated in Figure 4 which presents the mean response latency which was recorded during the morning performances when sleep was undisturbed, when 6 stimuli occurred, and when 24 stimuli occurred during the night.

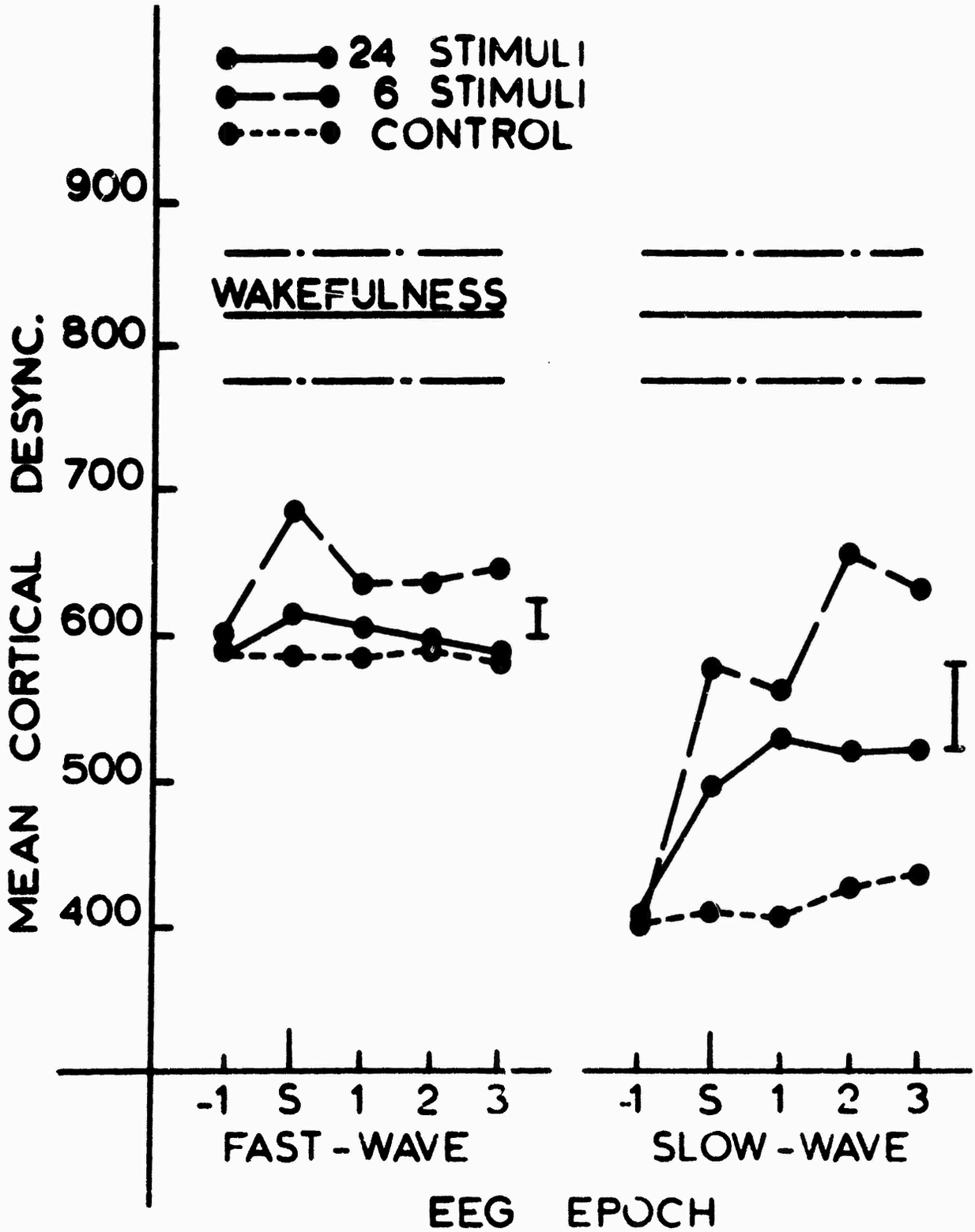

Figure 3. Mean cortical desynchronization (arousal) recorded one minute prior to the occurrence of a stimulus, during the presentation of the stimulus, and for three succeeding minutes following the stimulus occurrence. The figure separates the data on the basis of whether no stimuli were presented, 6 stimuli were presented, or 24 stimuli were presented and whether the stimuli occurred during fast- or slow-wave sleep.

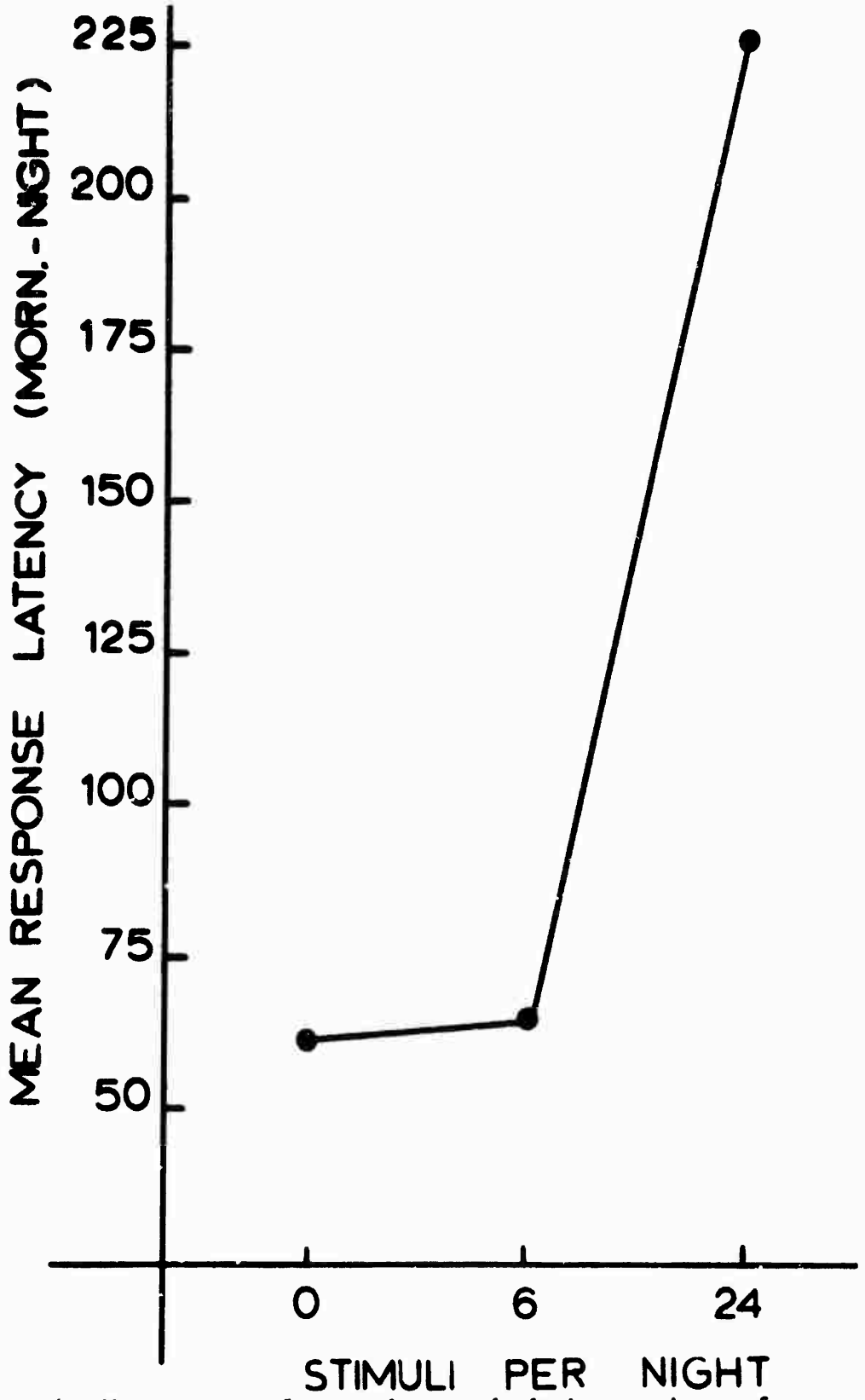

Figure 4. Mean response latency in seconds during morning performance sessions following nights undisturbed by auditory stimuli, following nights disturbed by 6 stimuli and following nights disturbed by 24 stimuli. To control for acquisition effects the presented data are difference scores, i.e. the difference between the previous night's performance and the morning performance.

There are two points which must be made concerning these results. Firstly, it must be noted that even though the subjects' mean response to the individual stimuli on the nights when 24 stimuli were presented was significantly less than the subjects' mean response to the individual siimuli when only 6 stimuli were presented, the total amount of sleep disruption was considerably greater when 24 stimuli occurred. This statement is based upon an analysis of the data which computed the arousal effects of each stimulus by determining, relative to the minute preceding a stimulus, the change in the cortical desynchronization during the 1-min. analysis epoch when the stimulus occurred and the three succeeding 1-min. analysis epochs. These difference values were then summated to provide an estimate of the total effect of each particular stimulus. This was then done for each of the other stimulus occurrences during the night and these values summated together to provide an estimate of tht total sleep disruption which occurred during the nights when 6 stimuli were presented and during the nights when 24 stimuli were presented. The results of this analysis indicated that even though the subjects' mean response to the auditory stimuli was significantly greater when only 6 stimuli occurred during the night, there was considerably less total sleep disruption (total cortical desynchronization) during this night as compared to when 24 stimuli occurred during the night. Specifically, the total sleep disruption when 6 stimuli occurred during the night averaged out acrossed the 6 subjects to be a shift toward cortical desynchronization (arousal) which averaged out at 333 half-waves when 6 stimuli occurred, but jumped to 601 half-waves when 24 stimuli occurred. The difference between these values is of course statistically significant. This then suggests that independent of the greater arousal produced by the individual stimuli, sleep was in fact less disrupted when 6 stimuli occurred as compared to when 24 stimuli occurred during the night. In regard to the waking performance decrement, total sleep disruption appears to be a better predictor of waking performance than the level of arousal precipitated by an individual's response to a single stimulus presentation.

While the above results may simply reaffirm the obvious, what is not so obvious is the fact that this correlation between total sleep disruption and waking performance was not equally valid during sleep characterized by fast-wave electroencephalographic activity and sleep characterized by slow-wave electroencephalographic activity. Consider Figure 5 which presents the total sleep disruption computed as previously described but segregates the data on the basis of fast-wave sleep and slow-wave sleep. As can be seen from the figure, the total amount of sleep disruption occurring in response to 6 stimuli and 24 stimuli was virtually identical during sleep characterized by fast-wave electroencephalographic activity. In contradistinction, during sleep characterized by slow-wave electroencephalographic activity, the total sleep disruption was significantly greater when 24 stimuli occurred as compared to when 6 stimuli occurred. The interaction depicted by this figure is significant beyond the .01 level of confidence. Thus, the tentative conclusion which one might reach on the basis of this data is that the disruption of sleep characterized by slow-wave electroencephalographic activity is more critically related to waking performance than the disruption of sleep characterized by fast-wave electroencephalographic activity. Whether or not this tentative speculation will be borne out by future research is, of course, unanswerable at this point. However, it is perhaps of some interest to note that if one should accept the arguments previously presented that sleep dis-

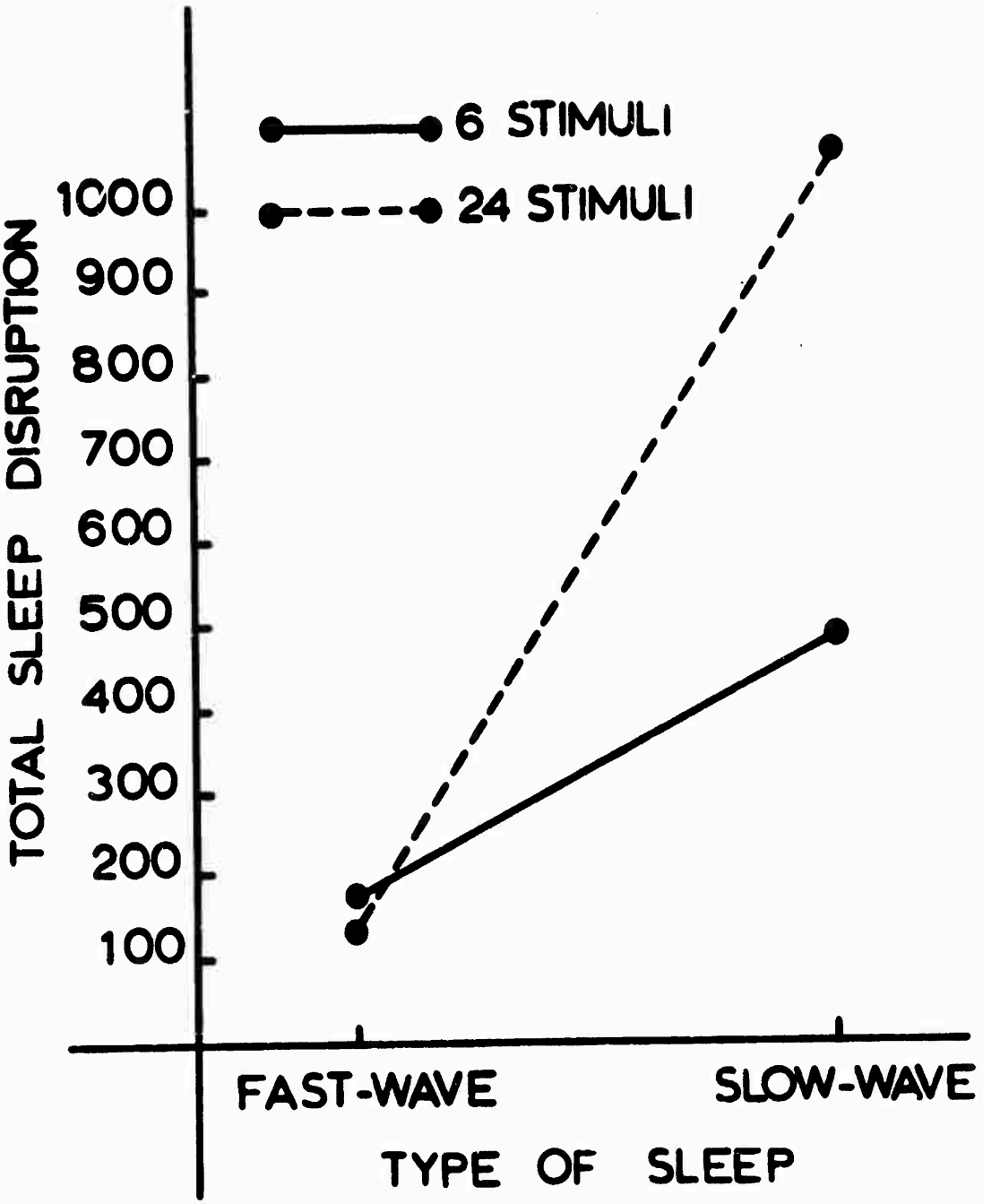

Figure 5. Illustration of the differential amounts of total sleep disruption occurring during fast-wave sleep and during slow-wave sleep when 6 and when 24 stimuli were presented during the night.

ruption most critically effects those behaviors which do not occur during sleep it is important to realize that it is during sleep characterized by slow-wave electroencephalographic activity when mnemonic and higher cognitive processes are virtually nonfunctional [7].

Thus, the commonly held and empirically verifiable notion that the most severe effects of auditory noise is its disruption of sleep would appear to have the added significance that this sleep disruption may not be restricted to the annoyance produced by behavioral awakening,but may, in fact, precipitate nonoptimal waking performance. This then, of course, provides considerable emphasis to our efforts to control this form of environmental pollution.

REFERENCES

1. Adrian, E. D. and Matthews, B. H. C. The Berger Rhythm: Potential changes from the occipital lobes in man. Brain, 57, 355-385, 1934.

2. Edward, A. S. Effects of the loss of 100 hours of sleep. American Journal of Psychology, 1941, 54, 80-91.

3. Emmons, W. H. and Simon, C. W. Responses to material presented during various levels of sleep. Journal of Experimental Psychology, 1956, 51, 89-97.

4. Gieseking, C. M., Williams, H. W. and Lubin, A. The effect of sleep deprivation upon information learning. American Psychologist, 1957, 12, 406 (Abstract).

5. Goodnow, J. J., Rubinstein, I. and Shanks, B. L. The role of past events in problem solving. Journal of Experimental Psychology, 1959, 58, 456-461.

6. Holdstock, T. L. and Verschoor, G. J. Retention of maze learning following paradoxical sleep deprivation in rats. Physiological Psychology, 1973, 1, 29-33.

7. Koukkou, M. and Lehmann, D. EEG and memory storage in sleep experiments with humans. Electroencephalography and Clinical Neurophysiology, 1968, 25, 455-462.

8. Kramer, M., Roth, T., Trindar, K. and Cohen, A. Noise disturbance and sleep. Department of Transportation Final Report No. FAA-NO-70-16, 1971.

9. LeVere, T.E., Bartus, R. T. and Hart, F. D. Electroencephalographic and behavioral effects of nocturnally occurring jet aircraft sounds. Journal of Aerospace Medicine, 1972, 43, 384-389.

10. LeVere, T. E., Bartus, R. T., Morlock, G. W. and Hart, F. D. Arousal from sleep: Responsiveness to different auditory frequencies equated for loudness. Physiology and Behavior, 1973, 10, 53-57.

11. LeVere, T. E., Morlock G. W., Thomas, L. P. and Hart, F. D. Arousal from sleep: The differential effect of frequencies equated for loudness. Physiology and Behavior, 1974, 12, 573-582.

12. Moruzzi, G. and Magoun, H. W. Brain stem reticular formation and activation of the EEG. Electroencephalography and Clinical Neurophysiology, 1949, 1, 455-473.

13. Okuma, T., Nakamura, K., Hayashi, A. and Fujimori, M. Psycho-physiological study of the depth of sleep in normal human subjects. Electroencephalography and Clinical Neurophysiology, 1966, 21, 140-147.

14. Oswald, I. Sleeping and Waking. Amsterdam, Elsevier Publishing Company, 1962.

15. Rheinberger, M. and Jasper, H. H. Electrical activity of the cerebral cortex in the unanesthetized cat. American Journal of Physiology, 1937, 119, 186-196.

16. Sokolov, E. N. Neuronal models in orienting reflex. In: The Cerebral Nervous System in Behavior: Transactions of the 3rd Conference, Ed. by M. A. B. Brazier, New York: Josiah Macy, Jr. Foundation, 1960.

17. Weitzman, E. B. and Kreman, H. Auditory evoked responses during different stages of sleep in man. Electroencephalography and Clinical Neurophysiology, 1965, 18, 65-70.

18. Williams, H. L., Gieseking, C. F. and Lubin, A. Some effects of sleep loss on memory. Perceptual and Motor Skills, 1966, 23, 1287-1293.

19. Williams, H. L., Morlock, H. C. and Morlock, J. Instrumental behavior during sleep. Psychophysiology, 1966, 2, 208-216.

20. Williams, H. L., Tepas, D. I. and Morlock, H. C. Evoked responses to clicks and electroencephalographic stages of sleep in man. Science, 1962, 138, 685-686.

21. Zung, W. W. K. and Wilson, W. P. Response to auditory stimulation during sleep. Archives of General Psychiatry, 1961, 4, 40-44.

HUMAN ANNOYANCE WITHIN NOISE AND VIBRATION ENVIRONMENTS

by

Michael J. Goodman and Richard G. Pearson

Center for Acoustical Studies
North Carolina State University, Raleigh

Contemporary concern for the environment has placed the problem of human response to noise within the context of environmental pollution. As a pollutant noise joins any number of other environmental factors in determining the physical and psychological well being of an individual. Within such a framework noise, vibration, temperature, air composition, etc., may often occur together in such a fashion as to enhance total discomfort to an extent greater than that due to any factor acting alone -- or the opposite may be true; total discomfort may be less than that due to any factor acting alone. It follows that criteria imposed upon a single aspect of the environment may be insufficient in its elimination as a problem — in the presence of other stimulation, as individual's susceptibility to that aspect may be changed.

For those concerned specifically with transportation noise, consideration of the total environment is particularly important, whether from the standpoint of the environment within the vehicle, or the area surrounding the vehicle. In either case an individual is exposed simultaneously to numerous, potentially harmful stimuli. Within this context perhaps the most obvious factor supplementing noise is vibration. Despite the fact that noise and vibration are frequently associated in the home, work and transportation environments, research has typically treated the two as separate entities. While recent concern for the joint effects of noise and vibration has developed, the resulting research has generally concentrated on task performance and physiological effects; little effort has been directed towards subjective response. In fact, a span of more than three decades has produced little more than casual observation in this regard. Consider, for example, the following comments.

Bruderlin, in 1937, within the context of aircraft noise and vibration stated:

> It is well known that noise sounds louder to the ear when it is accompanied by physical vibration, and that vibration is more annoying in the presence of noise (p. 181).

Also with regard to aircraft, Best, in 1945, made the following observation:

> It was found that in flight more vibration was required at propeller frequency to produce a given reaction than on the ground because the other vibration and noise tended to desensitize the subject (p. 654).

Finally, Jansen, in 1969, referring to noise and vibration on ships, related the following:

> On board ships noise and vibration annoyance usually do occur simultaneously. There is ample evidence that the general public find it very hard to separate these influences when asked to judge their environment. Mostly one single judgment is given for sound and vibration together. Moreover, sometimes when comparing two environments people call one noisier, when in fact vibration levels differ but sound levels are equal and conversely (p. 9).

The preceding passages are but a sample of comments characteristic of the last 30 years. Although those working within the noise and vibration disciplines have recognized the relevance and complexity of the problem, little empirical effort has been realized. In 1970, Pearson and Hart reported on a study in which the effects of various combinations of airborne noise and structure-borne vibration were evaluated within the context of human annoyance. The results of their study indicated that annoyance to a "very annoying" level of noise increased only under a high amplitude of vibration. For a lesser annoying noise, however, both the high and low amplitudes of vibration increased annoyance.

The study to be described represents an attempt to explore some basic questions regarding the joint effects of noise and vibration. Specifically, the influence of noise upon annoyance to vibration, and of vibration upon annoyance to noise was considered. In addition, total annoyance to combinations of the two stimuli was evaluated.

Method

Testing was conducted in a 4' by 4' acoustic chamber in which a noise-vibration environment was constructed. This system consisted of an electro-mechanical shaker centered beneath a plywood platform on which a hard-surfaced chair was secured. Acoustic stimuli were presented over a pair of speakers located in front of the chair-shaker system. The floor of the chamber (the area beneath the chair platform and the shaker) were heavily weighted with sandbags, and an extensive effort was made to minimize the level of noise produced by vibration of the chair. An adjustable foot rest was utilized to support the subject's feet and a seat belt-shoulder harness combination was used to secure the subject comfortably in the chair.

The subjects used in the study consisted of male and female undergraduate students who received class credit for their participation. In addition, each subject was compensated at a rate of $2.00 per hour. The research was carried out in two experimental sessions. During the first session 56 subjects were individually subjected to nine levels of noise and nine levels of vibration. Noise stimuli consisted of random noise presented at 45 dB through 85 dB in 5 dB steps. For vibration a 30 Hz sine wave input served as a stimulus. Due to the low power capacity of the chair-shaker system utilized, a subject's body weight was a determining factor of the maximum level of vibration that could be obtained. It was thus impossible to specify absolute levels for vibration stimuli. Rather, for each subject, the maximum power was provided for the highest level of vibration, and the additional eight levels were achieved by attenuating the maximum in steps of 3 dB.

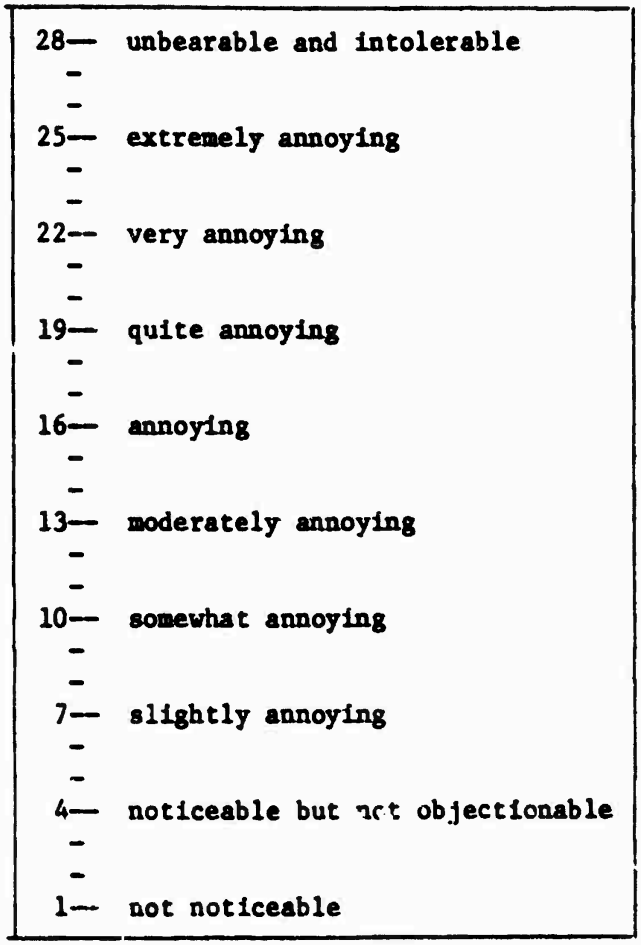

Figure 1. Sample Annoyance Rating Scale

Subjective evaluation of the noise and vibration was accomplished using a modified version of the rating scale developed by Pearson and Hart (1968). Figure 1 illustrates the scale utilized. The addition of a "not noticeable" category at the bottom of the Pearson-Hart version increased the point value of the scale from 25 to 28. In the first session each subject was presented with two blocks of the nine noise and nine vibration stimuli. Within each block the eighteen stimuli were randomized. During each stimulus presentation subjects were required to indicate their annoyance by placing a pencil mark along the scale. After each judgment, the subject terminated the stimulus by activating a switch located on the chair frame.

Immediately following the first session, the ratings of each subject were plotted on a stimulus sensitivity graph. Figure 2 illustrates such a plot for noise. A smooth curve was drawn through the points and the stimulus levels at which a subject was "slightly annoyed" and "annoyed" were extrapolated. In this way, for each subject, the approximate physical levels of noise and vibration at which he or she was "annoyed" or "slightly annoyed" was determined. Where a subject's ratings were either too high or too low to fall within the two subjective categories for either noise or vibration, the subject was eliminated from further participation in the study. From a subject population of 56, 20 males and 20 females were selected on the basis of this procedure.

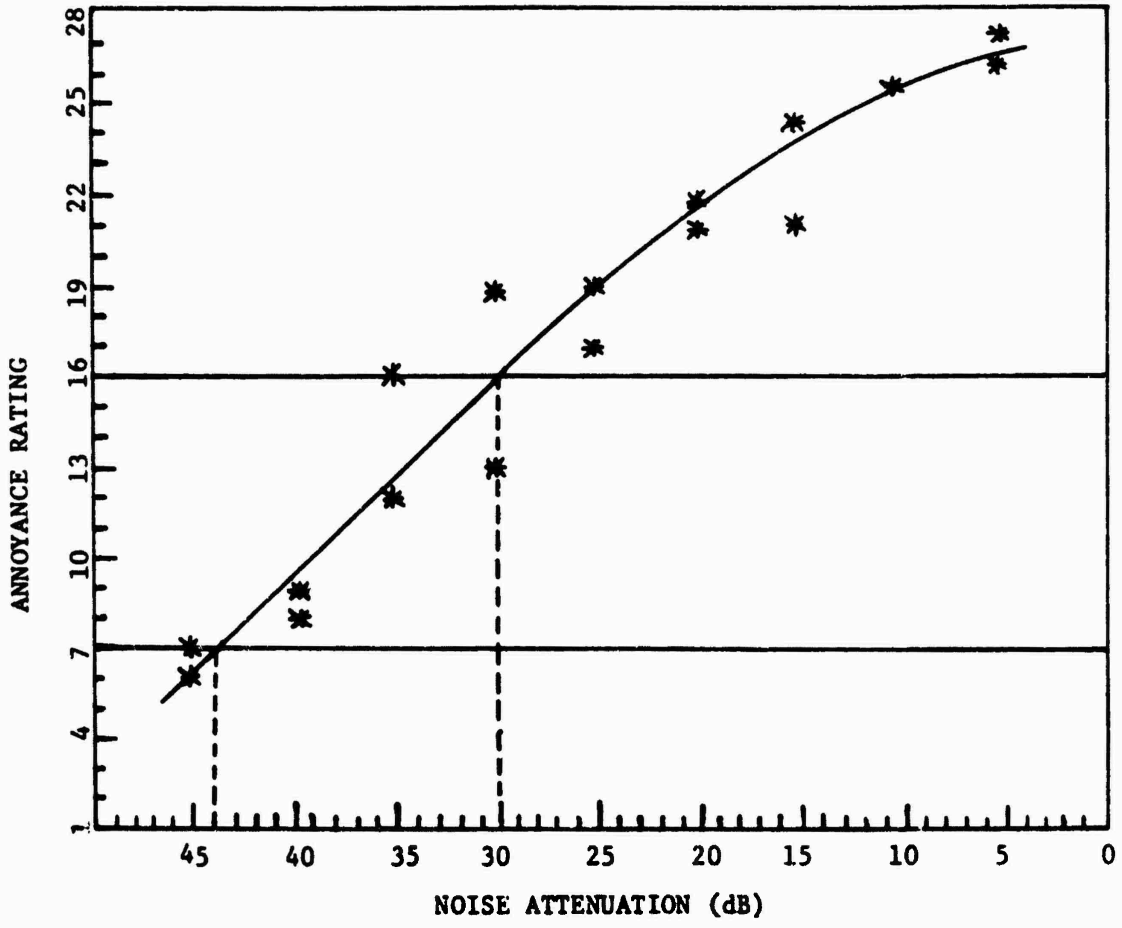

Figure 2. Sample Noise Sensitivity Graph

For the second experimental session those subjects meeting the criteria described earlier received a total of sixteen experimental treatments and eight control treatments. These treatments are described in Tables 1 and 2. The control treatments were included to assess the extent of any noise produced by the vibration as well as any vibration produced by the noise. Although every effort was made to minimize the magnitude of noise produced by vibration of the chair-shaker system, where subject weight and stimulus sensitivity were low, it was possible for vibration to produce a clearly perceptible noise. Similarly, high levels of noise were capable of producing a perceptible vibration of the chair.

Each of the 24 treatments consisted of a noise, vibration, or combination of noise and vibration, and a question; how annoying was the noise--how annoying was the vibration, or how annoying was the combination? Subjects received 72 trials in three consecutive blocks of 24 randomly-ordered treatments. Thus, each treatment was presented three times. The duration of each stimulus presentation was 9.5 seconds with a 10.5 second interstimulus interval. Annoyance judgments were made in a 72 page booklet of rating scales for which the appropriate question was printed on the top of each page.

Table 1. Experimental Treatments

No.	Question	Stimulus Condition
1	How annoying was the noise?	A-N
2	How annoying was the noise?	SA-N
3	How annoying was the noise?	A-N+SA-V
4	How annoying was the noise?	A-N+A-V
5	How annoying was the noise?	SA-N+SA-V
6	How annoying was the noise?	SA-N+A-V
7	How annoying was the vibration?	A-V
8	How annoying was the vibration?	SA-V
9	How annoying was the vibration?	A-N+SA-V
10	How annoying was the vibration?	A-N+A-V
11	How annoying was the vibration?	SA-N+SA-V
12	How annoying was the vibration?	SA-N+A-V
13	How annoying was the combination?	A-N+SA-V
14	How annoying was the combination?	A-N+A-V
15	How annoying was the combination?	SA-N+SA-V
16	How annoying was the combination?	SA-N+A-V

A = annoying SA = slightly annoying V = vibration N = noise

Table 2. Control Treatments

No.	Question	Stimulus Condition
1	How annoying was the noise?	A-V
2	How annoying was the noise?	SA-V
3	How annoying was the vibration?	A-N
4	How annoying was the vibration?	SA-N
5	How annoying was the combination?	A-N
6	How annoying was the combination?	SA-N
7	How annoying was the combination?	A-V
8	How annoying was the combination?	SA-V

A = annoying SA = slightly annoying N = noise V = vibration

Results

Examination of the control data revealed that neither the noise produced by the vibration or the vibration produced by the noise was sufficiently intense to result in noticeable judgments. Table 3 presents the mean annoyance scores for each experimental treatment evaluated across the entire subject population and broken down by sex. Note the mean annoyance scores for treatments 1, 2, 7 and 8 — the single stimulus conditions. These scores reveal an increase in annoyance over that expected on the basis of the first experimental session. Recall that the "slightly annoying" and "annoying" scale positions corresponded to scale values of 7 and 16 respectively. In addition, examination of the mean annoyance scores for males and females reveals consistently greater annoyance judgments for females over those of the males across all experimental treatments.

Table 3. Mean Annoyance for Experimental Treatments

No.	Stimulus	Question	Mean Annoyance	Mean Annoyance Males	Mean Annoyance Females
1	A-N	Noise	18.33	18.10	18.57
2	SA-N	Noise	8.19	8.12	8.27
3	A-N+SA-V	Noise	17.72	17.28	18.15
4	A-N+A-V	Noise	18.00	17.70	18.30
5	SA-N+SA-V	Noise	9.03	8.48	9.58
6	SA-N+A-V	Noise	8.60	7.90	9.30
7	A-V	Vibration	16.61	15.67	17.55
8	SA-V	Vibration	7.67	7.08	8.25
9	A-N+SA-V	Vibration	6.96	6.80	7.12
10	A-N+A-V	Vibration	16.85	15.92	17.78
11	SA-N+SA-V	Vibration	7.63	6.65	8.60
12	SA-N+A-V	Vibration	15.86	15.00	16.70
13	A-N+SA-V	Combination	17.51	17.18	17.83
14	A-N+A-V	Combination	20.97	20.40	21.53
15	SA-N+SA-V	Combination	11.00	10.03	11.97
16	SA-N+A-V	Combination	16.54	15.63	17.45

A = annoying SA = slightly annoying N = Noise V = vibration

A series of sixteen analyses were carried out in order to evaluate any influence the presence of noise or vibration had on judgments of annoyance to vibration and noise respectively. In addition these analyses permitted comparisons between the single-stimulus conditions, and the two-stimulus conditions for which total annoyance was obtained. Each analysis involved a comparison of mean annoyance scores for pairs of experimental treatments. Table 4 describes the 16 comparisons made. The first eight comparisons contrast total annoyance to combinations of noise and vibration with annoyance to noise or vibration presented alone. Consider comparison number 2. Testing for a significant difference between the mean annoyance scores for these treatments would determine whether total annoyance to an "annoying" noise and an "annoying" vibration

was significantly different from that of an "annoying" noise presented alone. The second set of eight comparisons were designed to evaluate any influence the presence of one stimulus would have on annoyance to a second stimulus. Consider comparison number 10. This contrast would determine whether the presence of an "annoying" level of vibration influenced annoyance to an "annoying" level of noise.

Table 4. Treatment Comparisons

No.	Stimulus	Question	Trt.	Stimulus	Question	Trt.
1	A-N	Noise	1	A-N+SA-V	Combination	13
2	A-N	Noise	1	A-N+A-V	Combination	14
3	SA-N	Noise	2	SA-N+SA-V	Combination	15
4	SA-N	Noise	2	SA-N+A-V	Combination	16
5	A-V	Vibration	7	A-N+A-V	Combination	14
6	A-V	Vibration	7	SA-N+A-V	Combination	16
7	SA-V	Vibration	8	A-N+SA-V	Combination	13
8	SA-V	Vibration	8	SA-N+SA-V	Combination	15
9	A-N	Noise	1	A-N+SA-V	Noise	3
10	A-N	Noise	1	A-N+A-V	Noise	4
11	SA-N	Noise	2	SA-N+SA-V	Noise	5
12	SA-N	Noise	2	SA-N+A-V	Noise	6
13	A-V	Vibration	7	A-N+A-V	Vibration	10
14	A-V	Vibration	7	SA-N+A-V	Vibration	12
15	SA-V	Vibration	8	A-N+SA-V	Vibration	9
16	SA-V	Vibration	8	SA-N+SA-V	Vibration	11

A = annoying SA = slightly annoying V = vibration N = noise

Table 5 summarizes the results of the sixteen treatment comparisons. For the first eight comparisons significance was indicated in seven cases. As a general conclusion it can be stated that total annoyance to a combination of noise and vibration is greater than annoyance to either noise or vibration presented alone. However, for comparison 6, where a "slightly annoying" noise accompanied an "annoying" vibration, total annoyance was no different than that due to the vibration alone. Furthermore, for the first comparison, total annoyance to a combination of a "slightly annoying" vibration and an "annoying" noise was significantly less than annoyance to an "annoying" noise by itself. Thus, it appears that the low level of vibration had some positive aspect associated with it. This suggestion was borne out by a number of subjects who indicated that low levels of vibration were at times pleasant and soothing. In several instances similar comments were made with regard to noise.

The remaining eight comparisons yielded only one significant finding; for comparison 11, when "slightly annoying" levels of noise and vibration were combined, annoyance to the noise was significantly greater than when noise was judged by itself. The apparent inconsistency between the outcomes of comparisons 1 and 11 may be reconciled by considering the differences in the subject's task as well as the relative differences between the levels of noise and

vibration for each comparison.

Table 5. Results of Treatment Comparisons

Comparison No.	Treatments Compared	F Statistic	P > F
1	1 & 13	4.95	.03
2	1 & 14	103.84	.0001
3	2 & 15	63.94	.0001
4	2 & 16	212.81	.0001
5	7 & 14	97.02	.0001
6	7 & 16	0.02	.88
7	8 & 13	184.37	.0001
8	8 & 15	63.06	.0001
9	1 & 3	3.22	.08
10	1 & 4	1.30	.26
11	2 & 5	10.47	.0028
12	2 & 6	1.01	.32
13	7 & 10	0.33	.58
14	7 & 12	2.70	.10
15	8 & 9	3.08	.08
16	8 & 11	0.02	.88

Although the results of the latter eight comparisons indicated no great influence of one stimulus upon annoyance to a second stimulus, further analysis of the data revealed that a subject's noise and vibration sensitivity was at least partially responsible for the lack of significant effects. Utilizing the stimulus sensitivity graphs obtained for each subject in the first experimental session, subjects were classified as sensitive or insensitive for both noise and vibration. An analysis was carried out in which noise and vibration sensitivity were evaluated with regard to the sixteen comparisons described in Table 4. Results of this analysis indicated that stimulus sensitivity was an important determinant of both the magnitude and direction of the influence of one stimulus upon annoyance to a second stimulus.

Thus, for example, with regard to comparison 16, noise sensitive subjects demonstrated an increase in annoyance to a "slightly annoying" vibration when it was accompanied by a "slightly annoying" level of noise. Noise insensitive subjects, however, demonstrated a decrease in annoyance under the same conditions. Similarly, for comparison 14, while both high and low noise sensitives demonstrated greater total annoyance to a combination of a "slightly annoying" level of noise and a "slightly annoying" level of vibration, than to a "slightly annoying" level of vibration alone, the noise sensitive subjects demonstrated a greater increase in annoyance than the noise insensitive subjects.

Discussion

It is unfortunate that the laboratory environment utilized could not adequately represent a real world situation. One important aspect of a real

world noise-vibration environment is the frequent correspondence, in the physical domain, between the two stimuli. Thus, component frequencies, changes in amplitude, and changes in duration often correspond very closely. Had such an environment been achieved here, perhaps the results would be more clearcut and hence more meaningful. The findings do point out, however, the potential importance of stimulus, situational, and individual factors in determining how noise and vibration interact subjectively. It is also clear that greater attention should be paid to the positive aspects of noise and vibration exposure.

The general finding that noise and vibration do interact subjectively has important implications for earlier research for which individual stimuli were subjectively evaluated within complex environments. This is particularly true for research which has investigated human response to vibration; the production of vibration has in many instances had high levels of noise associated with it. Finally the need for a single measure for evaluating the total environment is clearly indicated.

List of References

1. Best, S. G. Propeller balancing problems. SAE Journal, 1945, 53, 648.

2. Bruderlin, H. H. Developments in aircraft sound control. Acoustical Society of America - Journal, 1937, 8, 181.

3. Janssen, J. H. A proposal for standardized measurements and annoyance rating of simultaneous noise and vibration in ships. Report 126S, June 1969, Nederlands Scheepsstudiecentrum T.N.O.

4. Pearson, R. G., and Hart, F. D. Annoyance effects of noise-vibration exposures. Paper presented at the meeting of the Aerospace Medical Association, St. Louis, April 1970.

5. Pearson, R. G., and Hart, F. D. Studies relating the individual characteristics of people with their responses to noise. Conference on Progress of NASA Research Relating to Noise Alleviation of Large Subsonic Jet Aircraft, NASA SP-189, paper 35, October 1968.

Acknowledgments

This research was supported by NASA grant NGL-34-002-055 and the NASA Graduate Traineeship Program in Aerospace Acoustics - NGT-34-002-097.

THE INFLUENCE OF FEAR ON COMMUNITY ANNOYANCE WITH AIRCRAFT NOISE

by

Prof. Paul N. Borsky

School of Public Health
Columbia University
New York, N. Y.

Fear of possible aircraft crashes has been found a crucial factor in determining the intensity of annoyance with aircraft noise. Every social survey in this country and abroad has found a high correlation between respondents' reported feelings of fear and annoyance. Since there actually is a higher probability that crashes will occur close to the boundries of an airport on approach or departure operations, feelings of fear have some basis of reality. It is logical, therefore, to hypothesize that persons with feelings of high fear who live close to an airport are not necessarily generally fearful or neurotic, but are responding to a perceived specific danger.

Another important implication of the fear-annoyance relationships is the effect on adaptation. When a person is highly fearful, the noise is a warning signal. Each and every aircraft noise must be separately decoded as to whether or not there is danger involved. Regardless of how many past experiences were safe, this noise of an approaching or departing airplane may be the unsafe one. Therefore, the fearful go through a continuous experience of awareness, tension and emotional release after the plane has passed safely. The cumulative effect of such constant tensions over time generally increases the unwantedness or annoyance with aircraft operations.

In a field study of almost 1500 residents conducted by trained Columbia University interviewers in the summer of 1972, new insights were obtained into the dynamic effects of fear on annoyance. A follow-up study of over 1000 other residents in the summer of 1973 confirmed the findings of the previous year. In the 1972 study, almost equal samples were randomly selected from communities directly under landing flight paths; 1.1, 2.5, and 5.2 miles from touchdown. In the 1973 study, areas under departure flight paths were studied in which 707-320B aircraft were approximately 800 feet (close),1500 feet (middle) and 3000 feet (distant) above the residential areas. In both surveys the response rate was about 85% of the random assignments, with the refusal rate accounting for about 10% of the non-response. Thus, it can be concluded that the surveys were fully representative of the populations sampled. First, some basic definitions:

Fear - The measure of intensity of fear was based on a summation of answers to four questions located in different positions of the hour-long interviews. Respondents were asked to rate; Q.5, their dislike of unsafe low-flying airplanes; Q.22, how much the noise from airplanes startle or frighten them; Q.27, how often they felt airplanes were flying too low for the safety of the residents; Q.28, how often they felt there was some danger that they might crash nearby.

These items have strong face validity as well as high item intercorrelation. In addition, a number of the items have been shown to be related to annoyance in

previous research (Borsky, 1961; McKennell, 1963; TRACOR, 1970). The coefficient of reliability (alpha) for the fear scale is .84. Each item was scored 0-4 with highest fear rating being 4. This produced a possible range of fear scores of 0-16.

Annoyance - The annoyance scale was based on 11 activity items. Based upon a factor analysis (Principal Components, Varimax rotation), it was determined that these items formed a general factor. A simple summation of annoyance ratings was used since TRACOR had demonstrated that an unequal weighting system based on factor loadings contributed little. Each item was scored 0-4, with 4 representing the highest annoyance. This produced a range of annoyance scores of 0-44. A measure of consistency or reliability of the scale is provided by coefficient alpha, which was 0.91. The eleven items were:

1. Interferes with listening to radio or TV.
2. Makes the TV picture flicker.
3. Startles or frightens anyone in family.
4. Disturbs family's sleep.
5. Makes house rattle or shake.
6. Interferes with family's rest and relaxation.
7. Interferes with conversation.
8. Makes you keep your windows shut during the day.
9. Makes you keep your windows shut during the night.
10. Makes you feel tense and edgy.
11. Gives you a headache.

Misfeasance - The concept of misfeasance is an outgrowth of Borsky's (1961) concept of "considerateness", McKennell's (1963) concept of "preventability", and TRACOR's (1970) concept of "misfeasance". This scale was intended to measure the respondents' belief that various agents connected with aircraft noise production are capable of reducing the noise but for some insufficient reason are not. The agents in the present scale include "the people who run the airlines", the airport officials', "the other governmental officials:, "the pilots", "the designers and makers of airplanes", and "the community leaders". The coefficient of reliability (alpha) for the misfeasance scale is .76.

Health Attitudes - McKennell (1963) reported a strong relationship between the belief that aircraft exposure effected the respondent's health and annoyance. In the present questionnaire, respondents were asked "how harmful do you feel the airplane noise is to your health?" This item was scored 0-4 with 4 being very much.

Table 1 presents the zero-order or simple correlation coefficients. The fear and health altitudes variables are highly correlated with reported annoyance with respective correlation coefficients of .72 and .63. The acoustic exposure measures of CNR and misfeasance are moderately related to annoyance with correlation coefficients of .32. A small relationship also exists between belief in the importance of aircraft operations and annoyance ($r = -.22$). The more important a respondent believed aircraft to be, the less annoying he rated the noise.

TABLE I

	June Annoy.	CNR June	Fear	Misf.	Health Attit.	A/C Import.
June Annoyance	1.00					
CNR June	.32	1.00				
Fear	.72	.41	1.00			
Misfeasance	.32	.10	.30	1.00		
Health Attitudes	.63	.24	.64	.31	1.00	
A/C Importance	-.22	-.14	-.19	-.14	-.18	1.00

A multiple correlation analysis of fear, health attitudes, misfeasance and CNR as a predictor set explained 58% of the total annoyance variance. A causal model of these variables was also developed.

The first step in developing a causal model is to identify those relationships in which the causal direction can clearly be inferred on an *a priori* basis. Our model assumes that aircraft noise annoyance is caused by some combination of antecedent variables such as CNR, fear, health attitudes and misfeasance, and not vice versa. It is also clear that CNR cannot be caused by any combination of the other variables. It is not so clear as to the "natural" causal directions between the other variables.

Figure 1 presents the possible causal relationships based upon the above assumptions and the simple or zero-order correlations. One way arrows represent possible causation from the variable at the tail of the arrow to the variable at the point of the arrow. Double-ended arrows indicate indeterminate causal relationships at this stage of the analysis.

The goal of further analyses is to validate each of these possible causal relations, i.e., to identify each as real or spurious. This validation can be accomplished by the use of partial correlations. A partial correlation is the relationship between two variables that exists when the effects of one or more other variables have been held constant or "partialled" out.

For instance, if a direct causal link exists between CNR and annoyance, the partial correlation between CNR and annoyance should not be near zero when the effects of fear, health attitudes and misfeasance are partialled out. In fact, the correlation between CNR and annoyance shrinks from .32 to .06. We conclude, therefore, that there is little direct causal effect of CNR upon annoyance and remove that arrow from the model.

Similar procedures will produce a simplified model as presented in Figure 2. Three causal links have been substantiated; CNR→fear, fear→annoyance, health attitudes→annoyance. The two remaining double arrow relationships, fear↔health attitudes and health attitudes↔misfeasance, require further clarification in order to establish causal direction.

Double-ended arrows in a causal model imply reciprocal causation, i.e., that the pair of variables are causally dependent upon each other. This situation does not lend itself easily to a simple "path analysis" of causation (Simon, 1960). If possible, one would like to establish whether these relationships are really bi-directional since the implications for reciprocal causation situations are quite different than for the unidirectional case.

In the absence of *a* priori knowledge as to causal direction between two variables one may analyze the data to see if both points of the arrow are required to explain the data. If not, that point not required will be dropped from the model. For instance, since the zero-order correlation of .24 between CNR and health attitudes is reduced to .01 when the effects of fear are partialled out, we infer that a fear→health attitudes link exists. In the absence of other variables not measured, there is no other way to explain the zero-order correlation between CNR and health attitudes without including fear as an intervening variable.

In a similar fashion it is observed that the zero-order correlation between misfeasance and annoyance of .32 is reduced to .10 when the effects of health attitudes are partialled out. This indicates that health attitudes are an intervening variable between misfeasance and annoyance and that a misfeasance→health attitudes link exists.

The reduction of the zero-order correlation between fear and misfeasance of .30 to .14 when the effects of health attitudes are partialled out necessitates the existence of at least one more arrow of causation. If health attitudes are an intervening variable between fear and misfeasance either a health attitudes→fear link or a health attitudes→misfeasance link must exist. Both of these links, of course, may exist.

It would seem quite likely that concern with the health of one's family could increase one's fear concerning aircraft operations. On a common sense basis it also would be logical to expect a reciprocal relationship to exist between health attitudes and misfeasance. The sequence might be as follows: I'm concerned about aircraft noise and my family's health; I wish something would be done about the noise; If they can put a man on the moon they can reduce the noise; therefore, the aircraft people aren't doing enough to reduce the noise (are being misfeasant). These proposed links are pure conjecture, however, and the most one can say is that at least one of these links must exist in order to explain the simple relationships between this set of variables.

Figure 3 presents a scheme based upon the causal inferences made so far in the discussion. The dotted arrows represent reciprocal relationships which this investigator believes exist but which must remain tentative at this time.

Fear of aircraft operations and concern with the harmful effects of aircraft noise are the major intervening variables in the proposed causal model. Increases in noise exposure or misfeasance beliefs can be expected to result in significant increases in aircraft annoyance to the extent that fear and health concerns are also increased. Since fear and noise level are related ($r = .41$), an increase in noise usually will produce greater fear and thus, indirectly produce greater annoyance.

Results of the 1973 survey further confirm the strong relationships between fear and annoyance. Each scale category of fear is cross-tabulated by the mean

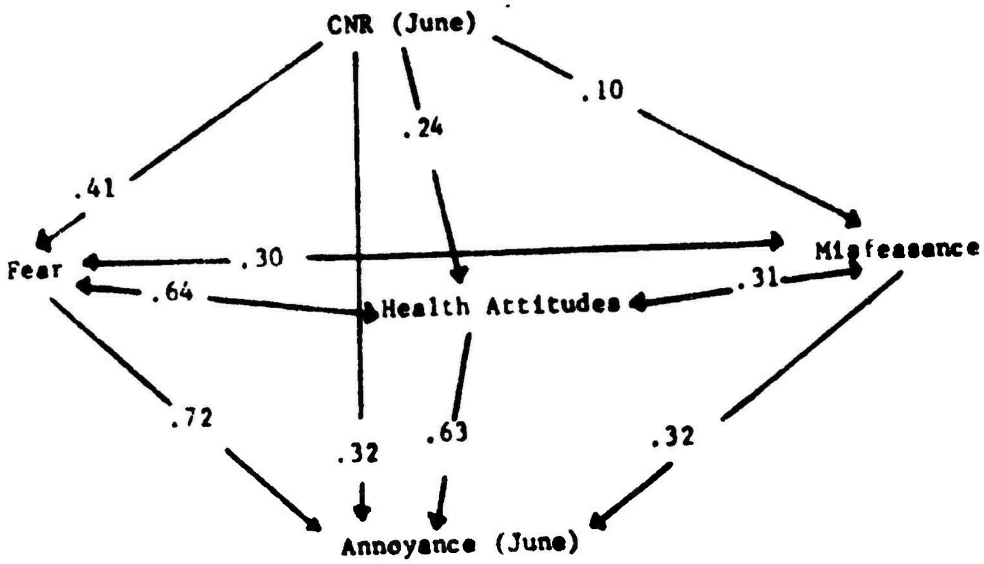

Figure 1: Possible causal relationships based upon a priori assumptions and zero-order (Pearson) correlation coefficients

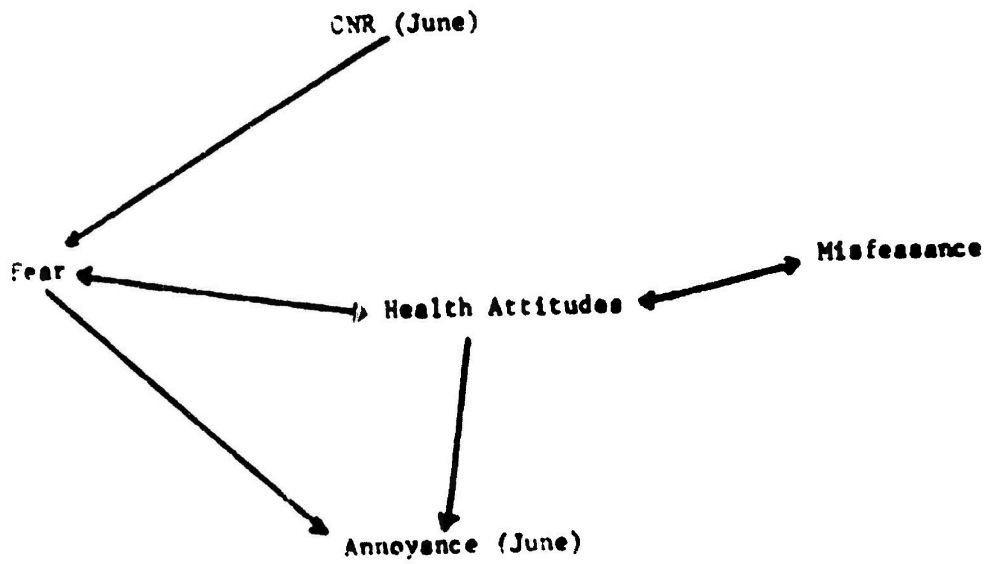

Figure 2: Empirically established causal relationships

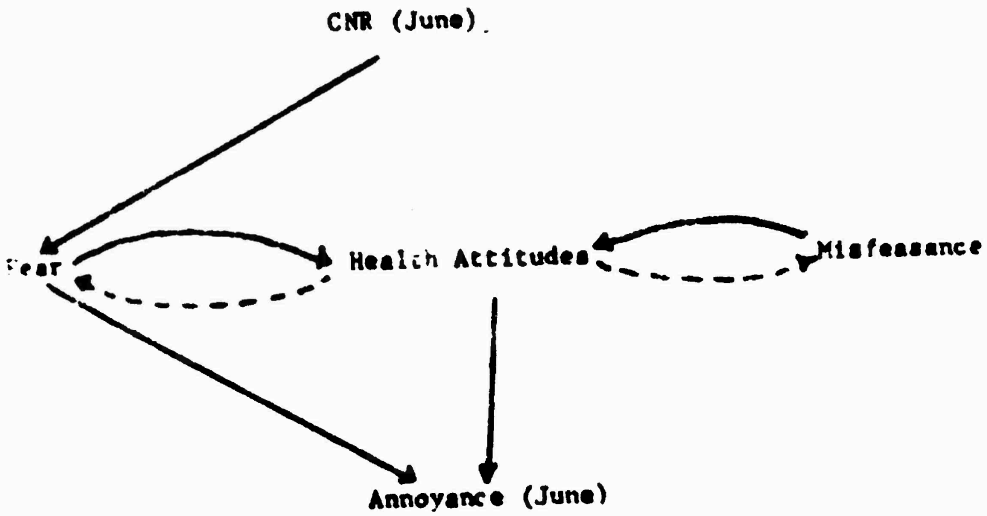

Figure 3: Final causal model for the June CNR and annoyance data

annoyance response ($\bar{X}$) for each distance group of residents. The fear groups are divided into three categories; low, medium and high fear, to facilitate analysis. Table 2 shows that almost half of all close residents are highly fearful, while only 15% of the distant residents report high fear. This verifies the relationship between physical exposure and fear.

TABLE 2

Relationship Between Reported Fear and Distance of Residence from Airport - 1973

Reported Fear	Distance of Residence					
	Close		Middle		Distant	
	N	%	N	%	N	%
Low (0-1)	70	19	111	32	162	48
Medium (2-7)	126	34	129	36	127	37
High (8-16)	170	47	113	32	51	15
	366	100	353	100	340	100

Table 3 shows the detailed fear classifications, the mean fear score and sampling error for each group.

TABLE 3

Reported Number Respondents by Fear and Distance of Resident

	Fear Score	Total	Distance		
			Close	Middle	Distant
A. Low Fear (0-1)	0	234	47	68	119
	1	109	23	43	43
	Total	343	70	111	162
	$\bar{X}$ fear	.32	.33	.39	.27
	S	.47	.47	.49	.44
B. Medium Fear (2-7)	2	101	26	34	41
	3	93	31	31	31
	4	60	15	25	20
	5	46	18	17	11
	6	49	19	17	13
	7	33	17	5	11
	Total	382	126	129	127
	$\bar{X}$ fear	3.86	4.19	3.74	3.66
	S	1.64	1.74	1.50	1.65
C. High Fear (8-16)	8	45	16	17	12
	9	49	21	19	9
	10	37	19	12	6
	11	36	19	11	6
	12	46	27	14	5
	13	28	14	11	3
	14	40	20	14	6
	15	20	14	6	0
	16	33	20	9	4
	Total	334	170	113	51
	$\bar{X}$	11.59	11.95	11.41	10.78
	S	2.56	2.53	2.55	2.52

Table 4 shows the detailed relationships between fear, annoyance and distance of residence.

TABLE 4

Annoyance Scale Scores by Fear and Distance of Residence

		Total		Close		Middle		Distant	
	Fear Score	$\bar{X}$	S_T	$\bar{X}$	S_C	$\bar{X}$	S_M	$\bar{X}$	S_D
A. Low Fear	0	4.5	5.8	5.9	8.0	4.6	5.6	4.0	4.8
	1	7.3	6.2	8.6	7.2	7.2	6.1	6.7	5.8
	Total	5.41	6.1	6.7	7.8	5.9	5.9	4.7	5.2
B. Medium Fear	2	9.7	9.1	13.9	9.8	7.3	6.1	9.1	9.8
	3	9.9	7.7	11.6	9.3	10.2	8.1	7.8	4.9
	4	13.3	8.2	17.2	7.9	11.6	8.4	12.4	7.4
	5	12.0	7.4	12.1	6.9	13.5	8.8	9.4	5.6
	6	15.7	10.3	19.3	9.9	15.1	11.9	11.3	6.6
	7	17.6	10.7	20.8	11.4	18.4	6.7	12.3	9.6
	Total	12.03	9.1	15.2	9.8	11.1	8.7	9.8	7.8
C. High Fear	8	19.0	9.4	21.9	8.6	16.3	8.9	18.9	10.8
	9	20.5	11.2	22.7	10.3	21.5	12.4	13.2	8.1
	10	20.5	9.2	21.8	7.7	23.3	9.5	11.0	8.2
	11	24.1	9.6	24.2	9.5	22.1	11.1	27.3	7.7
	12	24.3	10.8	25.2	10.5	26.1	11.2	14.4	7.2
	13	30.7	9.0	35.2	6.4	26.4	9.9	25.3	6.1
	14	26.5	10.5	29.7	11.0	25.0	9.7	19.3	7.2
	15	32.7	7.5	33.4	8.7	31.0	3.6	--	--
	16	32.6	8.3	35.4	8.5	30.8	5.1	22.8	4.6
	Total	24.7	10.8	27.3	10.5	23.7	10.5	18.3	9.4
Grand Total		13.9	11.8	19.2	12.7	13.4	11.4	8.7	8.4

A series of "t" tests indicates that annoyance for each fear class is significantly greater as fear increases. The low fear residents who live close to the airport have a significantly higher annoyance than the distant group ($p=.05$), but the annoyance for the middle and distant low fear groups are not statistically significant. For the medium fear group, average annoyance is more than double the low fear residents in every distance group. The close medium fear residents report much more annoyance than the middle or distant residents ($p = .01$), but the middle and distant medium fear residents report about the same annoyance. The high fear residents report about double the annoyance of the medium fear and four times the annoyance of the low fear groups. Among the high fear residents, each distance group is significantly different in annoyance responses ($p=.01$). The close residents have greater annoyance than the middle group which has greater annoyance than the distant high fear residents.

The extreme importance of fear in determining annoyance responses is shown in tables 2-4. If all respondents are pooled and fear and location of residence are disregarded, average annoyance is 13.9. But, if fear and distance (noise level) are considered, the close high fear residents report an annoyance of 24.7, while the distant low fear group reports annoyance of only 6.7. Subsamples of each fear group are now being tested under controlled realistic laboratory environments. Future reports will indicate whether controlled aircraft noise exposure also evoke differential annoyance responses in accordance with difference in fear of aircraft.

A correlation analysis of the 1973 data provides additional statistical support for the above conclusions. The simple zero-order correlations between fear and annoyance is r=.64, between fear and distance of residence (measure of physical stimulus) r=-.30. With the effects of distance partialled out, the correlation between fear and annoyance remains at r=.60.

The simple correlation between distance and annoyance is r=-.36, but when fear is partialled out, the correlation between the physical stimulus and annoyance drops to r=-.22. This is a moderate, but significant independent relationship. A more refined measure of the aircraft stimulus will be tested in further analyses of these data, but, even this gross measure of distance suggests a small independent causal relationship between aircraft stimulus and annoyance. A dotted line should, therefore, be drawn between CNR and Annoyance in Figure 3.

Research supported by NASA Grant
NGL 33-008-118

COMBUSTION NOISE

SOME EXPERIMENTAL RESULTS FOR NOISE GENERATION AND STRUCTURE OF OPEN JET FLAMES*

by

R. N. Kumar** and F. E. C. Culick†

Daniel and Florence Guggenheim Jet Propulsion Center
California Institute of Technology
Pasadena, California

The main purpose of the work reported here is to study some of the differences in the noise generation and the structure for one example of premixed and non-premixed flames. Only the single configuration shown in Figure 1 has been used to date. For premixed flames, a fuel/oxidizer mixture flows through both tubes; for the non-premixed flames, fuel flows through the inner tube and oxidizer through the outer tube. Because of the high Reynolds numbers and the large values of length/diameter (173 for the outer tube, 470 for the inner tube), the flow is turbulent and fully developed at the exit. Flow velocities up to 325 ft/sec have been used. The upper limit attained is set by the system for gas supply presently used, not by blow-off limits. No external pilot flame or flame holders have been used in the work. The results which will be discussed here are incomplete, but show some interesting differences between premixed and non-premixed flames.

Figure 2 shows examples of premixed and non-premixed flames, taken with an exposure of 1/60 sec on Kodak Ektachrome transparencies. The visible total lengths of the flames were nearly constant for the non-premixed flames over the velocity range 150 - 325 ft/sec. Invariance of flame length with flow speed has been previously noted for diffusion flames by Hottel and Hawthorne (1949) and by others, e. g. Kotake and Hatta (1965). The visible length of the premixed flame increases with increasing flow speed as others, for example Strahle and Shivashankara (1973), have observed.

A summary of the experimental conditions covered to date in this work appears in Table I. Note that the geometry is fixed throughout. The mixture ratio is very nearly stoichiometric for all tests, but broadly there are two classes distinguished by the shear between the coaxial flows for the non-premixed flames. In the S series, the shear, defined as twice the difference in velocities divided by the sum, is around .19 - .20; in the O series, the shear is nearly zero except for one case (O9) for which the shear is 0.149. For the conditions covered in these experiment, no important influence of shear is obvious.

Acoustic data were taken in an enclosure 21 ft × 17 ft without a roof.

---

*Work supported in part by the Jet Propulsion Laboratory, CIT, under contract NAS 7-100.

**Research Fellow in Jet Propulsion

†Professor of Engineering

The walls and floor were cement. Consequently, the results cannot have the same validity as those taken in anechoic chambers. Comparisons between premixed and non-premixed should, however, be meaningful. The measurements were made with a $\frac{1}{2}$ in microphone (B&K 4134) mounted on a beam which pivoted about an axis passing through the centerline of the burner at the exit. The distance d of the microphone from the exit is shown in Table I. Data were recorded continuously on an Ampex FR-600 tape recorder at a tape speed of 60 inches per second. The data were subsequently played back through an oscilloscope either in the normal time base or through a Tektronix 3L5 spectrum analyzer.

Figure 3 shows a spectrum for a cold jet. The distinct peak in the vicinity of 7 - 8 kHz also shows obviously in the spectra for the premixed flame also (Figure 4). Other peaks seem to be present, but owing to the relatively large amount of electronic noise in the instrumentation used, no definite conclusions can be drawn. No attempt has been made to obtain good data for cold jets. At the average speeds used in this work, the acoustic power emitted by a cold jet is of course very small.

Figures 4 and 5 show results for premixed and non-premixed flames. The pictures labelled "Amplitudes" and "Waveshapes" have been formed by superposing segments from the continuous records. Note that the vertical scales are not the same for all velocities. Also, owing to the rather high sweep rates used, there is some error in the spectra. How large this error is may be inferred from the spectra of pure sinusoids shown at the bottom of the figures.

In Figure 6, the measured amplitudes of the pressure field are plotted as functions of the total mass flow rate. "Amplitude" here means the full width of the bands shown in the left hand columns of Figures 4 and 5. The acoustic power is proportional to the square of the pressure. Hence, the present experimental results show that the acoustic power is proportional to the third power of the average speed for premixed flames and to the fourth power for non-premixed flames. The first is in agreement with the result found by Strahle and Shivashankara (1973) for an open premixed jet. Knott (1971) found the acoustic power to be proportional to the square of the average speed of the fuel gas for non-premixed flames, and to the fourth power of the speed for premixed flames. However, the short length of tube used in that work may not have produced fully-developed pipe flow; and the removal of a short length of the inner tube, in the coaxial geometry, may not have been sufficient to ensure complete premixing. Knott's work seems to be the only previous effort to study non-premixed flames with a coaxial burner.

The premixed and non-premixed flames also exhibit different directionality of the noise produced. Although the non-premixed flames appear to emit almost uniformly in direction, the noise from the premixed flames is largest in the direction normal to the axis (0°), drops off noticeably in the vicinity of 45°, and gradually reaches a minimum along the axis of the burner. (The large signals at 90° are due to the flow of hot gases over the microphone.) This behavior is qualitatively like that reported by previous workers: for a recent summary of this and other aspects of combustion noise, see Strahle (1973).

Perhaps the most striking differences appear in the wave shapes and spectra. The waveforms emitted by the non-premixed flames seem to be considerably more distorted. This is reflected also in the spectra. Comparison of the last columns of Figures 4 and 5 show clearly that there is more energy in the high frequency range for the non-premixed flames. The well-defined peaks shown in the spectra for the premixed flames are almost entirely smeared out in the spectra for the non-premixed flames. In earlier work -- Smith and Kilham (1963), Hurle, et al. (1968), and Strahle and Shivashankara (1973) -- rather broad peaks were found in the spectra for premixed flames. In all of those works, some form of external pilot flame was used. Here, the peaks seem to be associated with three characteristic dimensions of the apparatus: the inner and outer diameters of the inner tube, and the inner diameter of the outer tube.

Calculated Strouhal numbers -- frequency times length divided by the mean flow speed -- for the peak frequencies and the three diameters are shown in Figure 7. That the Strouhal number remains nearly constant over the range of flow speeds used, suggests that the noise production at the frequencies near the peaks may be associated with eddies whose scales are set by the dimensions noted. In the earlier works cited above, not only was an external pilot flame used, but only a single tube was present. Thus, it is not surprising that the spectra should be qualitatively different.

High-speed motion pictures show even more obvious differences between the two cases. For the premixed flames, quite well-defined oscillations of the visible flame surface (near the exit of the tube) are apparent. These may cause "wrinkling" of the flame surface, and fluctuations of the local volumetric reaction rate. Consequently, noise may be generated in accord with the model of the flame as a collection of monopoles [Bragg (1963), Strahle (1971)]. But the distribution in frequency is strongly influenced by the geometry of the exit of the tube. It seems reasonable that a pilot flame placed near the exit might strongly interfere with these processes and alter the observed spectra.

On the other hand, pictures of the non-premixed flames show a discrete structure which appears as a diffuse luminois jet in time-averaged photographs. A series of frames from a high-speed movie ($\sim$ 2500 frames per second) is shown in Figure 8. Evidently, the details of the geometry at the tube exit cannot be important to the behavior of the eddies, after they move downstream. But certain gross features surely depend on geometry. For example, the diameter of the outer tube must, in any case, impose a characteristic scale. The associated characteristic frequency, equal to the mean flow speed divided by the diameter, is around 7000 Hz for a speed of 300 ft/sec. Note that a mild peak appears at about that frequency in the spectra shown in Figure 5. Otherwise, the spectra are rather more as one would expect for the noise produced by a field of sources distributed smoothly (but not uniformly, of course) in frequency. The large eddies shown in Figure 8 obviously encompass a distribution of smaller eddies which must have much to do with the noise generated.

REFERENCES

Bragg, S. L. (1963) "Combustion Noise," J. Inst. Fuel, V. 36, p. 12.

Giammar, R. D. and Putnam, A. A. (1970) "Combustion Roar of Turbulent Diffusion Flames," J. Eng. for Power, V. 92A, p. 157.

Hottel, H. C. and Hawthorne, W. R. (1949) "Diffusion in Laminar Flame Jets," Third Symposium (International) on Combustion, Williams and Wilkins, p. 636.

Hurle, I. R., et al. (1968) "Sound Emission from Open Turbulent Premixed Flames," Proc. Roy. Soc., V. A303, p. 409.

Knott, P. R. (1971) "Noise Generated by Turbulent Non-Premixed Flames" AIAA/SAE 7th Propulsion Joint Specialist Conference, AIAA Paper No. 71-732.

Kotake, S. and Hatta, K. (1965) "On the Noise of Diffusion Flames," JSME, V. 8, no. 30, p. 211.

Smith, T. B. J. and Kilham, J. K. (1963) "Noise Generated by Open Turbulent Flames," J. Acoust. Soc. Amer., V. 35 , p. 715.

Strahle, W. C. (1971) "On Combustion Generated Noise," J. Fl. Mech., V. 49, p. 399.

Strahle, W. C. (1973) "A Review of Combustion Generated Noise," AIAA Paper No. 73-1023.

Strahle, W. C. and Shivashankara, B. N. (1973) "Experiments on Combustion Generated Noise," Interagency Symposium on University Research in Transportation Noise, Stanford University (March 1973), p. 536.

TABLE I. EXPERIMENTAL CONDITIONS OF THE RUNS

Run No.	Type	Fuel Q 10^{-2} cfs	Fuel U fps	Air Q 10^{-2} cfs	Oxygen Q 10^{-2} cfs	Total Oxidiser Q 10^{-2} cfs	Oxidiser, U fps	Total Flow, Q 10^{-2} cfs	Total Flow U fps	Oxidiser Composition Mole Fractions	$\frac{Q_{oxidiser}}{Q_{fuel}}$	$\frac{Q_o}{Q_f}$ for $\phi=1$	ϕ	Shear $=\frac{2\Delta U}{U_o+U_f}$	$\bar{d}$ in.	P_{dB} ref. 0.0002μB
S1	NP	1.9	150	4.03	2.6	6.63	123	8.53	-	$0.52O_2+0.48N_2$	3.49	3.85	1.1	0.198	26	87
S2	P	1.9	-	4.03	2.6	6.63	-	8.53	128	$0.52O_2+0.48N_2$	3.49	3.85	1.1	-	26	93
S3	NP	2.53	200	5.35	3.5	8.85	162	11.38	-	$0.523O_2+0.477N_2$	3.50	3.82	1.09	0.21	26	93
S4	P	2.53	-	5.35	3.5	8.85	-	11.38	171	$0.523O_2+0.477N_2$	3.50	3.82	1.09	-	26	98
S5	NP	3.17	250	6.68	4.4	11.08	205	14.25	-	$0.525O_2+0.475N_2$	3.50	3.81	1.09	0.196	26	97
S6	P	3.17	-	6.68	4.4	11.08	-	14.25	214	$0.525O_2+0.475N_2$	3.50	3.81	1.09	-	26	99
S7	NP	3.8	300	8.05	5.26	13.31	246	17.11	-	$0.523O_2+0.477N_2$	3.50	3.82	1.09	0.198	26	100
S8	P	3.8	-	8.05	5.26	13.31	-	17.11	257	$0.523O_2+0.477N_2$	3.50	3.82	1.09	-	26	102
S9	NP	4.13	326	8.68	5.95	14.63	270	18.76	-	$0.532O_2+0.468N_2$	3.55	3.76	1.06	0.188	26	101
S10	P	4.13	-	8.68	5.95	14.63	-	18.76	281	$0.532O_2+0.468N_2$	3.55	3.76	1.06	-	26	103
S11	NP	1.9	150	4.03	2.6	6.63	123	8.53	-	$0.52O_2+0.48N_2$	3.49	3.85	1.1	0.198	55.7	86
S12	NP	2.53	200	5.35	3.5	8.85	162	11.38	-	$0.523O_2+0.477N_2$	3.50	3.82	1.09	0.21	55.7	90
S13	NP	3.17	250	6.68	4.4	11.08	205	14.25	-	$0.525O_2+0.475N_2$	3.50	3.81	1.09	0.196	55.7	93
S14	NP	3.8	300	8.05	5.26	13.31	246	17.11	-	$0.523O_2+0.477N_2$	3.50	3.82	1.09	0.198	55.7	95
S15	NP	4.13	326	8.68	5.95	14.63	270	18.76	-	$0.532O_2+0.468N_2$	3.55	3.76	1.06	0.188	55.7	96
S16	P	1.9	-	4.03	2.6	6.63	-	8.53	128	$0.52O_2+0.48N_2$	3.49	3.85	1.1	-	55.7	89
S17	P	2.53	-	5.35	3.5	8.85	-	11.38	171	$0.523O_2+0.477N_2$	3.50	3.82	1.09	-	55.7	94

TABLE I (Continued) EXPERIMENTAL CONDITIONS OF THE RUNS

Run No.	Type	Fuel Q 10^{-2} cfs	Fuel U fps	Air Q 10^{-2} cfs	Oxygen Q 10^{-2} cfs	Total Oxidizer, Q 10^{-2} cfs	Oxidizer, U fps	Total Flow, Q 10^{-2} cfs	Total Flow U fps	Oxidizer Composition Mole Fractions	$\frac{Q_{oxidizer}}{Q_{fuel}}$	$\frac{Q_o}{Q_f}$ for $\phi=1$	ϕ	Shear $=\frac{2\Delta U}{U_o+U_f}$	$\bar{d}$ in.	P_{dB} ref. 0.0002μb
O1	NP	1.89	150	5.475	2.625	8.1	150	9.99	-	$0.465O_2+0.535N_2$	4.3	4.3	1	zero	32.7	88
O2	P	1.89	-	5.475	2.625	8.1	-	9.99	150	$0.465O_2+0.535N_2$	4.3	4.3	1	-	32.7	94
O3	NP	2.52	200	6.475	3.75	10.225	189.5	12.745	-	$0.5O_2+0.5N_2$	4.06	4.0	0.986	.054	32.7	90
O4	P	2.52	-	6.475	3.75	10.225	-	12.745	191	$0.5O_2+0.5N_2$	4.06	4.0	0.986	-	32.7	96
O5	NP	3.15	250	8.05	4.92	12.97	240	16.12	-	$0.51O_2+0.49N_2$	4.12	3.92	0.952	.0408	32.7	96
O6	P	3.15	-	8.05	4.92	12.97	-	16.12	242	$0.51O_2+0.49N_2$	4.12	3.92	0.952	-	32.7	100
O7	NP	3.775	300	8.9	5.80	14.70	271	18.475	-	$0.521O_2+0.479N_2$	3.89	3.84	0.987	.084	32.7	99
O8	P	3.775	-	8.9	5.80	14.70	-	18.475	277	$0.521O_2+0.479N_2$	3.89	3.84	0.987	-	32.7	102
O9	NP	4.1	325	9.15	6.05	15.2	280	19.3	-	$0.525O_2+0.475N_2$	3.71	3.81	1.028	.149	32.7	100
O10	P	4.1	-	9.15	6.05	15.2	-	19.3	290	$0.525O_2+0.475N_2$	3.71	3.81	1.028	-	32.7	102
O11	P	4.1	-	11.9	5.7	17.6	-	21.7	325	$0.465O_2+0.535N_2$	4.3	4.3	1	-	32.7	105
O12	P	3.775	-	11.0	5.25	16.25	-	20.025	300	$0.465O_2+0.535N_2$	4.3	4.3	1	-	32.7	104

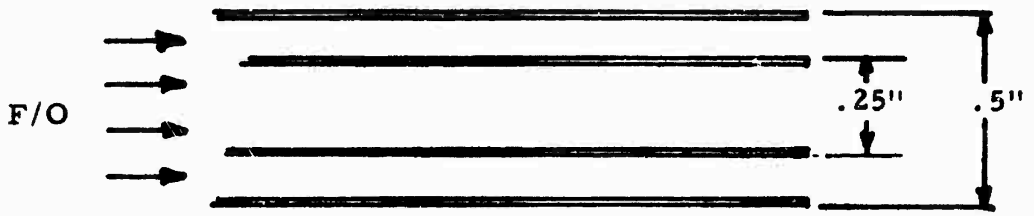

Premixed

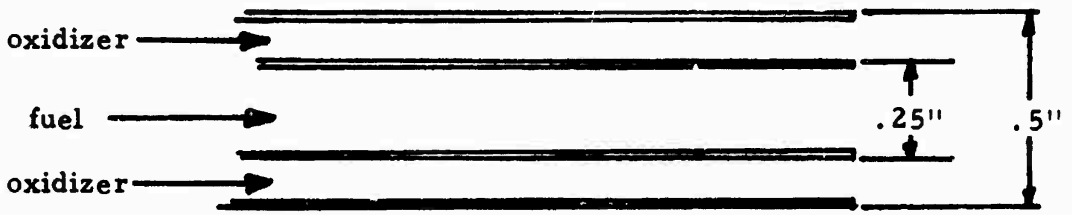

Non-Premixed

	Wall thickness (inch)	Length (inches)
outer tube	.049	69.5
inner tube	.049	71.5

Figure 1. Configuration of the Coaxial Burner.

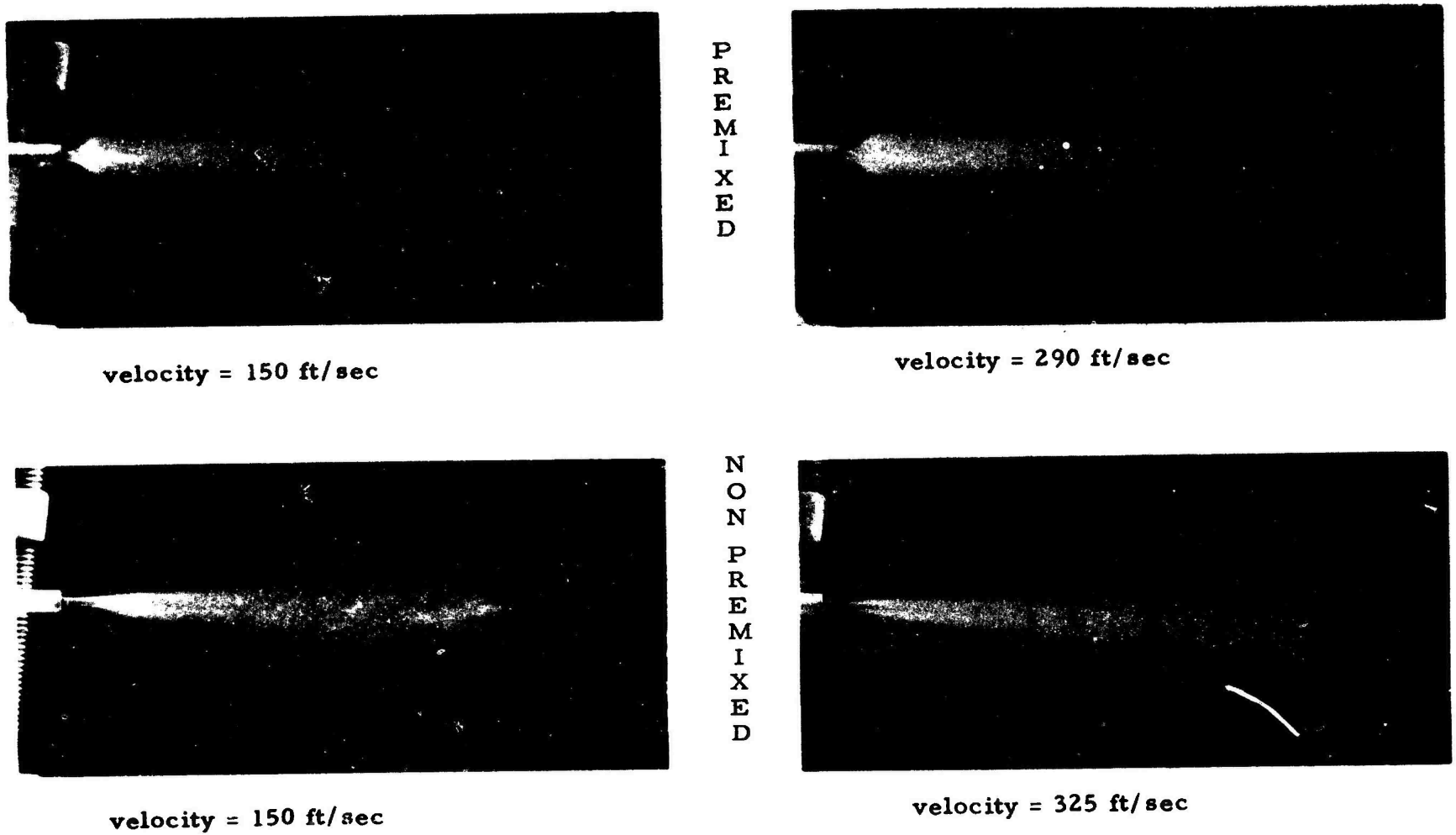

Figure 2. Time-Averaged Appearance of the Jet Flames.

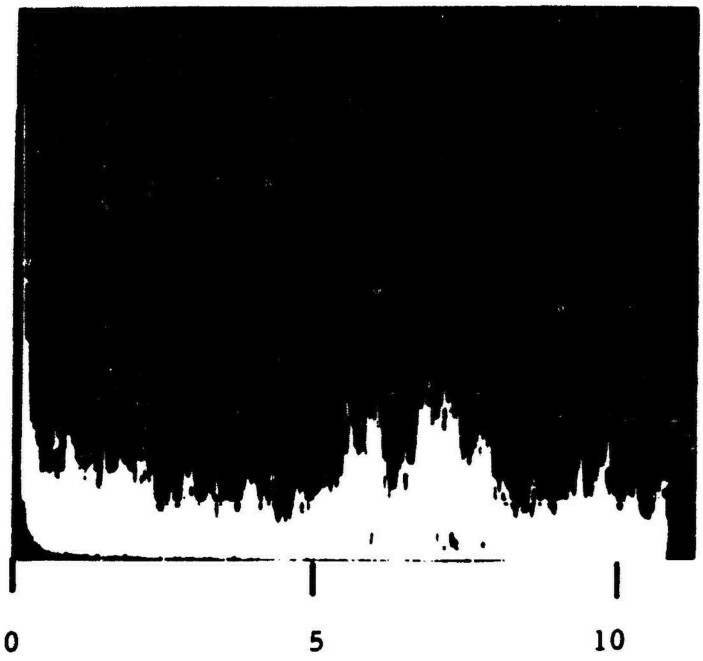

Figure 3. Frequency Spectrum of a Cold Jet.

central tube:	N_2 flow	323 ft/sec
outer tube:	air flow	280 ft/sec

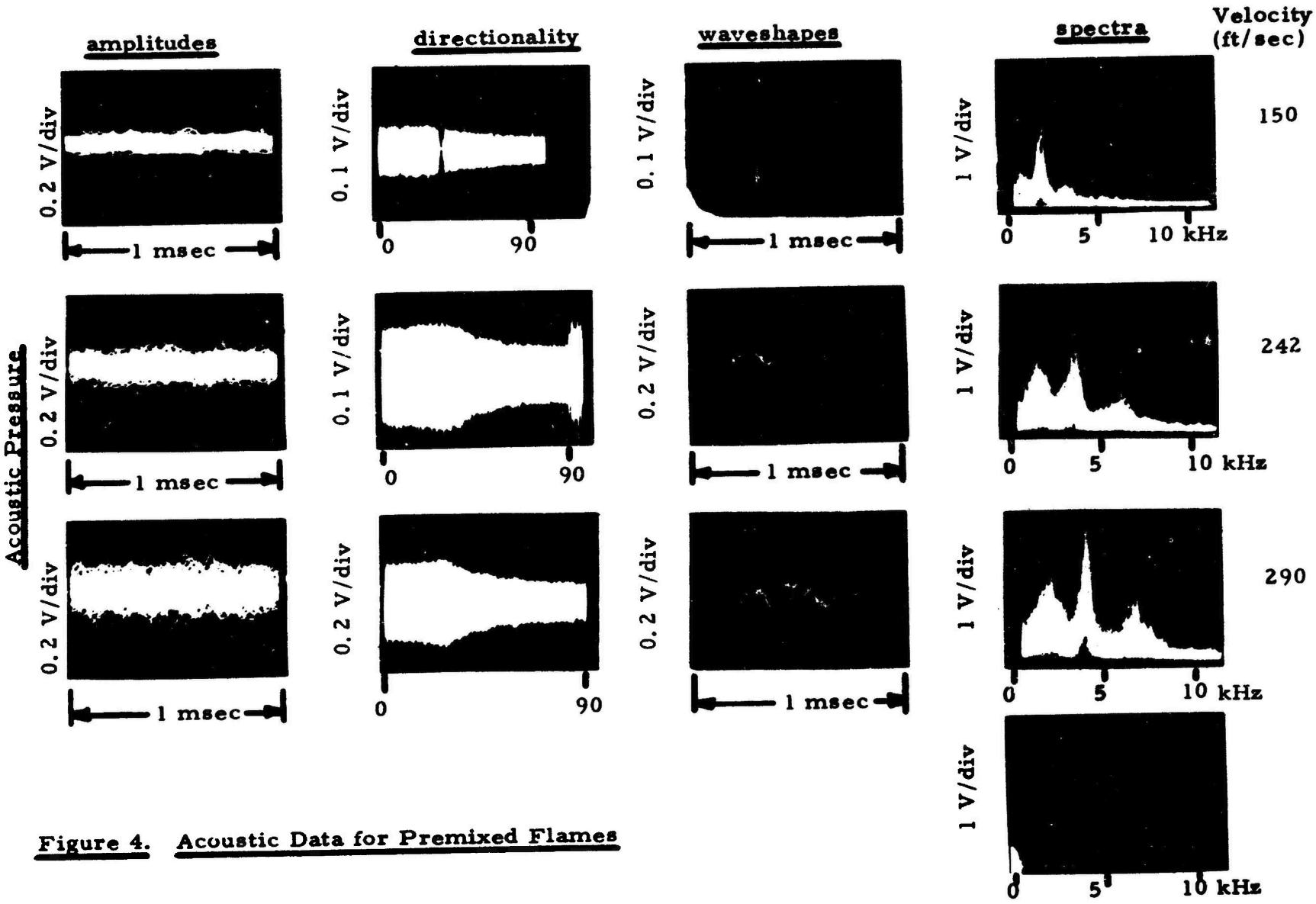

Figure 4. Acoustic Data for Premixed Flames

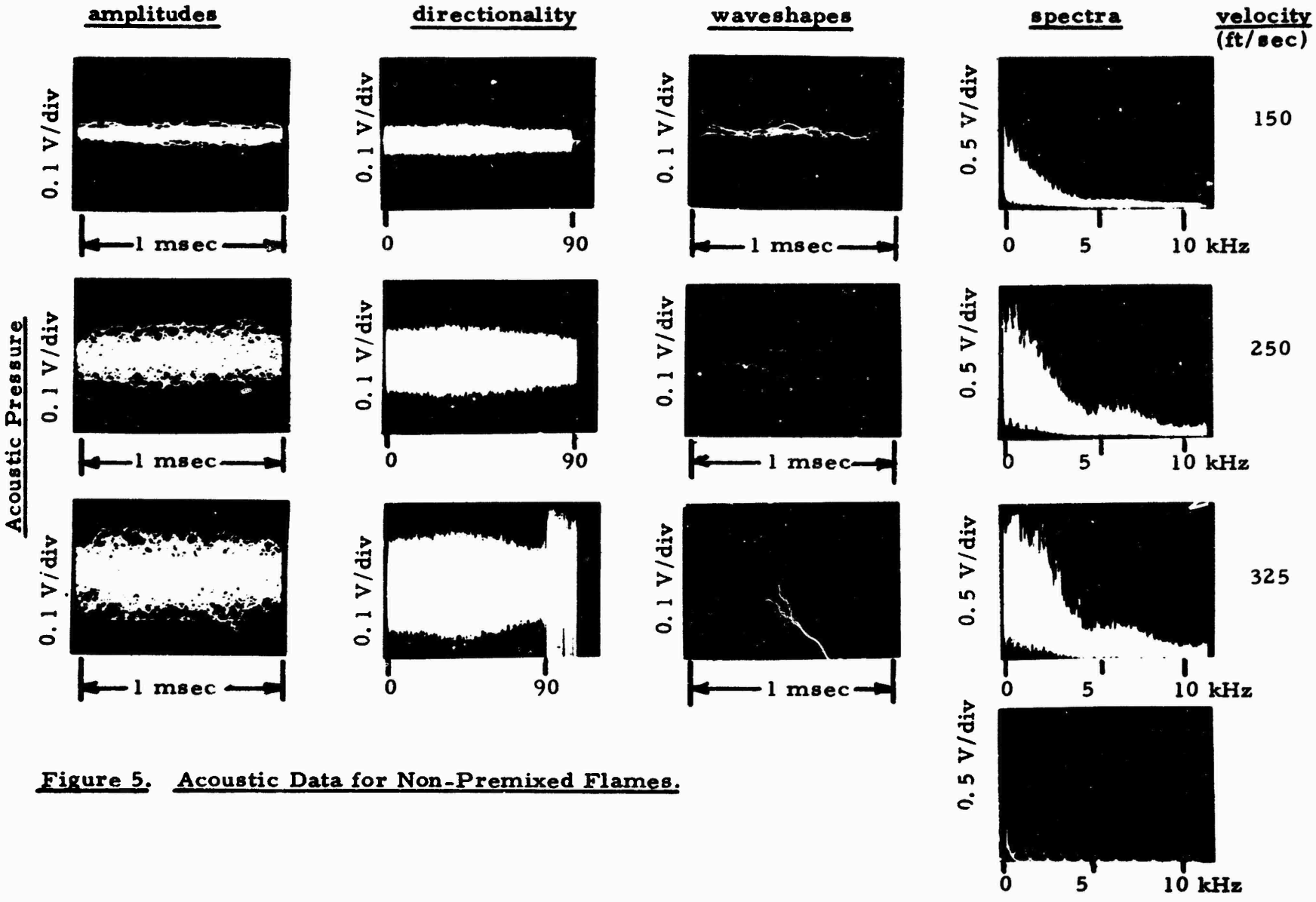

Figure 5. Acoustic Data for Non-Premixed Flames.

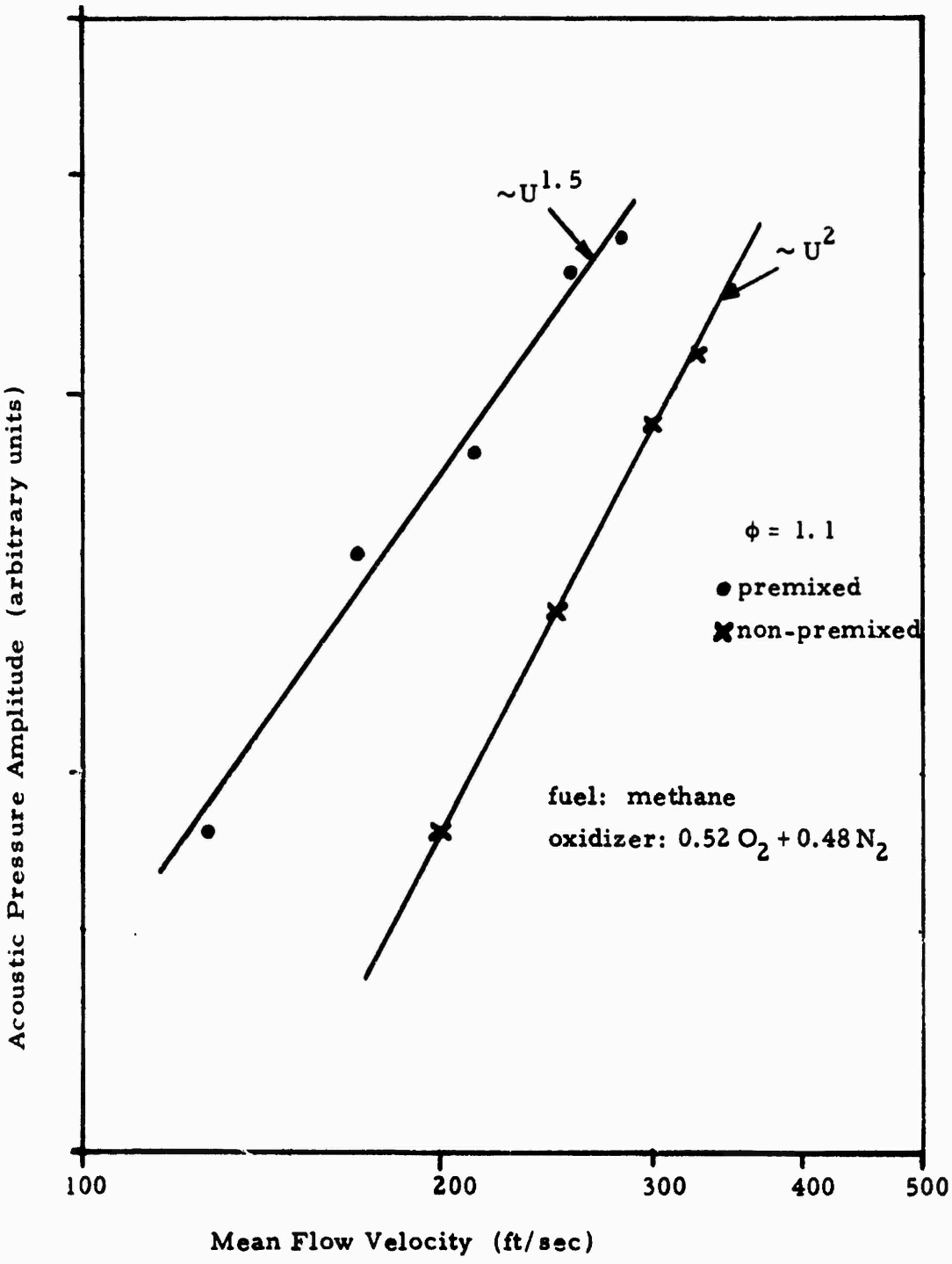

Figure 6. Pressure Amplitude Versus Flow Velocity.

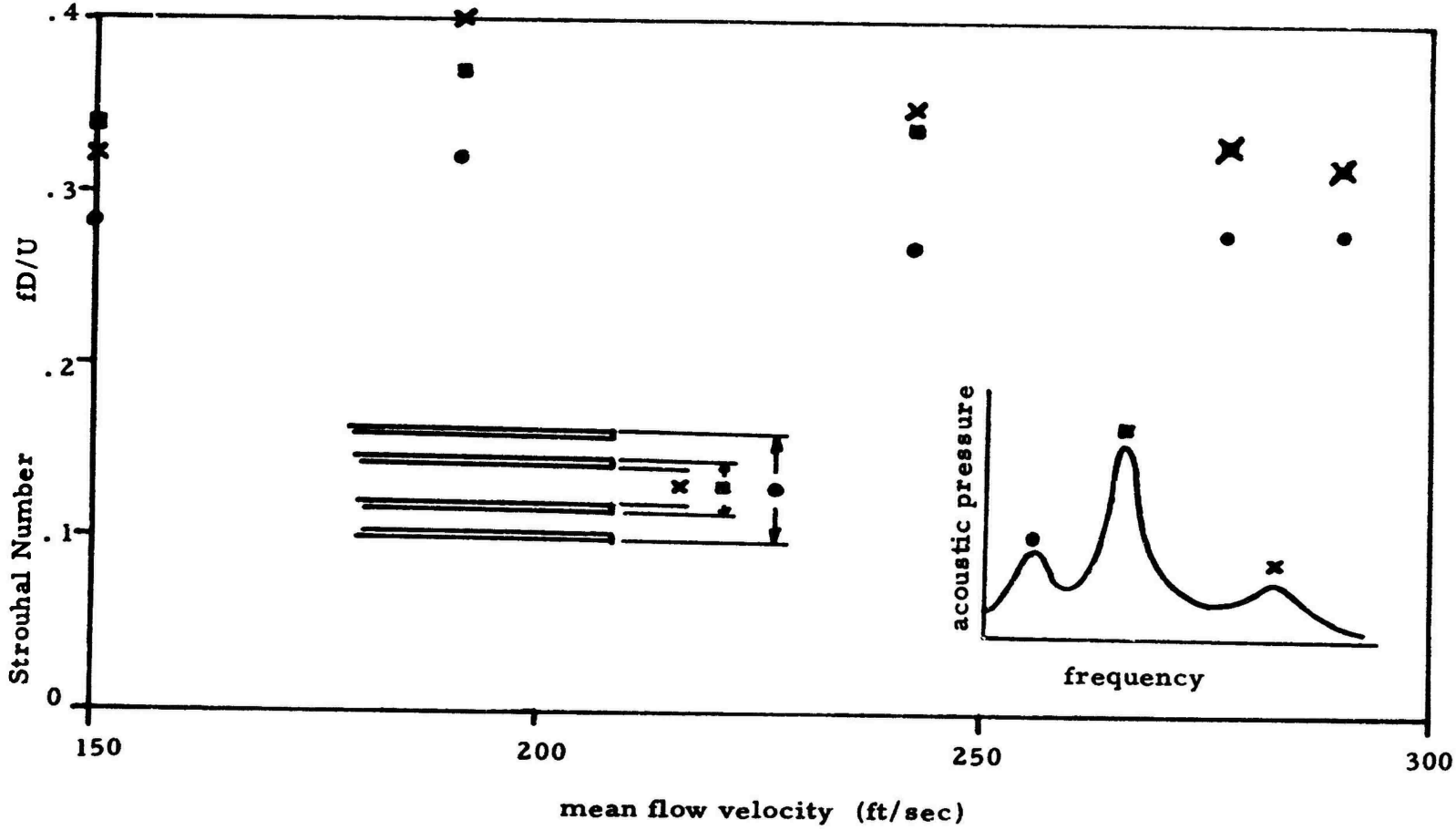

Figure 7. Calculated Strouhal Numbers for Premixed Flames.

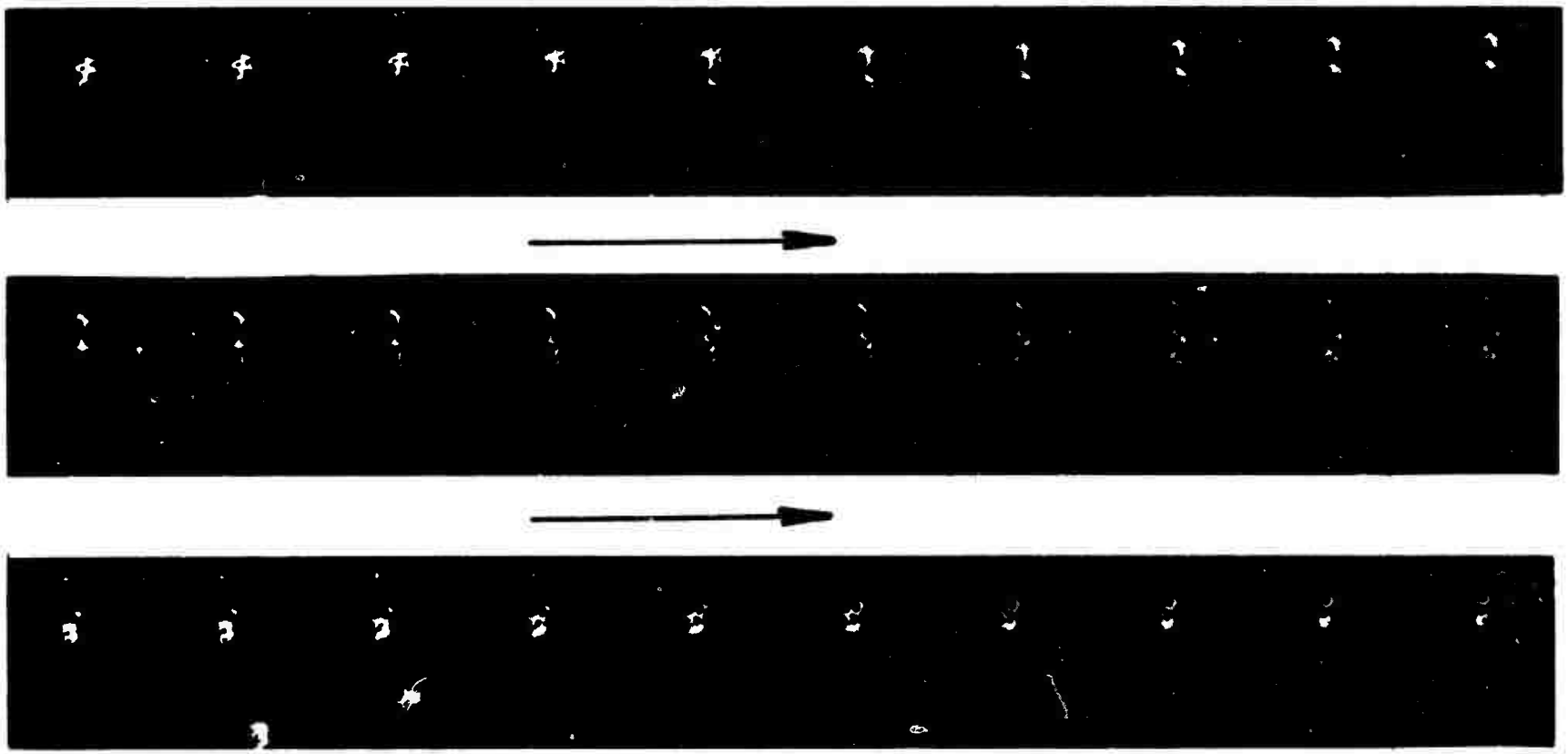

Figure 8. **A Sequence of Pictures Showing the Structure of a Non-Premixed Turbulent Flame.**

fuel (CH_4) speed 177.5 ft/sec oxidizer (.72 O_2 + .28 N_2) speed 137.5 ft/sec

SCALING OF COMBUSTION GENERATED NOISE

by

H. A. Hassan

Department of Mechanical and Aerospace Engineering
North Carolina State University
Raleigh, North Carolina

Using the framework of Lighthill's acoustic analogy, a theory has been developed for combustion generated noise. The theory is used to derive the scaling laws for combustion generated noise in open turbulent flames. It is shown that the scaling laws for both power and frequency are in good agreement with experiment.

1. Introduction

In a recent review of combustion generated noise, Strahle (1973) stressed the need for additional theoretical and experimental efforts to explain discrepancies between theory and experiment. In particular, he indicated that, for open turbulent flames, available theory is unable to explain the exact scaling laws and frequency content of combustion generated noise. Thus, by using the theory and non-dimensionalization procedure of Chiu and Summerfield (1973), he was able to predict the scaling and order of magnitude of observed acoustic power. However, the same procedure resulted in a scaling law for the frequency which was not observed in experiment. Another feature of combustion noise which is not explained by theory is the fact that, for all hydrocarbon-air flames, combustion noise is a broad-band noise with a single peak in the range 300-500 Hz.

The object of this investigation is to reexamine the theory of combustion noise using the framework of Lighthill's acoustic analogy (1952) as modified by Doak (1972). The source term in the wave equation for the pressure is manipulated using appropriate thermodynamic relations and the conservation of energy and species equations. The resulting expression is used as a basis for deriving scaling laws for both acoustic power and frequency. The results of the theory are shown to be in good agreement with available measurements for open turbulent flames.

2. Expression for the Pressure Fluctuation

Ignoring viscous effects, Doak's (1972) modified form of the acoustic analogy equation may be expressed as

$$\frac{1}{a_\infty^2}\frac{\partial^2 p}{\partial t^2} - \nabla^2 p = \frac{\partial^2 (\rho u_i u_j)}{\partial x_i \partial x_j} - \frac{\partial^2}{\partial t^2}\left(\rho - \frac{p}{a_\infty^2}\right) \equiv q_o \qquad (1)$$

where p is the pressure, ρ is the density, u_i is the velocity and a_∞ is the speed of sound of the quiescent fluid. For a reacting gas mixture, the density may be expressed as

$$\rho = \rho(s,p,Y_k) \tag{2}$$

where s is the entropy and Y_k is the mass fraction of species k. After some rather lengthy manipulations it is shown in the Appendix that, for a perfect gas with no molecular weight change during the chemical reaction, (2) gives

$$d\rho = \frac{1}{a^2}\left(dp + (\gamma-1)\rho \sum h_k dY_k\right) - \frac{\rho}{C_p}\left(ds + \frac{1}{T}\sum \frac{\mu_k}{M_k} dY_k\right), \tag{3}$$

where a and C_p are the frozen speed of sound and specific heat, respectively

$$a^2 = \left(\frac{\partial p}{\partial \rho}\right)_{s,Y_k} \equiv \gamma \frac{R_o}{M_o} T = \gamma \frac{p}{\rho}, \quad C_p = \left(\frac{\partial h}{\partial T}\right)_{p,Y_k}, \tag{4}$$

T is the temperature, h and h_k are the specific enthalpies of the mixture and species k, respectively, μ is the chemical potential, R_o is the universal gas constant, and M_k and M_o are the molecular weights of species k and the mixture.

Equation (3) together with the conservation of species and energy equations will be used to manipulate $\frac{\partial^2}{\partial t^2}\left(\rho - \frac{p}{a_\infty^2}\right)$. Thus, from (3)

$$\frac{\partial}{\partial t}\left(\rho - \frac{p}{a_\infty^2}\right) = \left(\frac{1}{a^2} - \frac{1}{a_\infty^2}\right)\frac{\partial p}{\partial t} + \frac{(\gamma-1)}{a^2}\rho \sum h_k \frac{\partial Y_k}{\partial t} - \frac{\rho}{C_p}\left(\frac{\partial s}{\partial t} + \frac{1}{T}\sum \frac{\mu_k}{M_k}\frac{\partial Y_k}{\partial t}\right). \tag{5}$$

Next, (5) can be simplified by using the energy equation (Williams, 1965)

$$\frac{Ds}{Dt} + \frac{1}{T}\sum \frac{\mu_k}{M_k}\frac{DY_k}{Dt} = 0 \tag{6}$$

and the conservation of species equations

$$\rho \frac{DY_k}{Dt} = W_k \tag{7}$$

where W_k is the production rate of species k. Thus (3) and (6) give

$$-\frac{\rho}{C_p}\left(\frac{\partial s}{\partial t} + \frac{1}{T}\sum \frac{\mu_k}{M_k}\frac{\partial Y_k}{\partial t}\right) = -u_i \frac{\partial \rho}{\partial x_i} + \frac{1}{a^2}u_i \frac{\partial p}{\partial x_i} + \frac{(\gamma-1)\rho}{a^2} u_i \sum h_k \frac{\partial Y_k}{\partial x_i} \tag{8}$$

Using (4), (7) and (8), (5) reduces to

$$\frac{\partial}{\partial t}\left(\rho - \frac{p}{a_\infty^2}\right) = \left(\frac{1}{a^2} - \frac{1}{a_\infty^2}\right)\frac{\partial p}{\partial t} - (\gamma-1)\frac{\partial}{\partial x_i}\left(\frac{u_i p}{a^2}\right) + (\gamma-1)\frac{p}{a^2}\frac{\partial u_i}{\partial x_i} - p u_i \frac{\partial}{\partial x_i}\left(\frac{1}{a^2}\right) + \frac{(\gamma-1)}{a^2}\Sigma\, h_k W_k \tag{9}$$

or,

$$\frac{\partial}{\partial t}\left(\rho - \frac{p}{a_\infty^2}\right) = \left(\frac{1}{a^2} - \frac{1}{a_\infty^2}\right)\frac{\partial p}{\partial t} - \frac{\partial}{\partial x_i}(\rho_e u_i) + \rho_e \frac{\partial u_i}{\partial x_i} - (p - p_\infty)\, u_i \frac{\partial}{\partial x_i}\left(\frac{1}{a^2}\right) + \frac{(\gamma-1)}{a^2}\Sigma\, h_k W_k \tag{10}$$

where

$$\rho_e = \rho - \rho_\infty - \frac{(p-p_\infty)}{a^2} \tag{11}$$

Equation (10) gives

$$\frac{\partial^2}{\partial t^2}\left(\rho - \frac{p}{a_\infty^2}\right) = \left(\frac{1}{a^2} - \frac{1}{a_\infty^2}\right)\frac{\partial^2 p}{\partial t^2} - \frac{\partial}{\partial x_i}\left[\frac{\partial}{\partial t}(\rho_e u_i)\right] + \frac{\gamma-1}{a^2}\frac{\partial}{\partial t}\Sigma\, h_k W_k + O(a^{-3})$$

and higher order terms (11)

The ordering with respect to inverse powers of a introduced above is similar to that carried out by Morfey (1973). It is employed here because we are interested in combustion noise at low Mach numbers.

Introducing (11) into (1), the wave equation for the pressure reduces to

$$\frac{1}{a_\infty^2}\frac{\partial^2 p}{\partial t^2} - \nabla^2 p = q_o = -\left(\frac{1}{a^2} - \frac{1}{a_\infty^2}\right)\frac{\partial^2 p}{\partial t^2} - \frac{(\gamma-1)}{a^2}\frac{\partial}{\partial t}\Sigma\, h_k W_k + \frac{\partial}{\partial x_i}\left[\frac{\partial}{\partial t}(\rho_e u_i)\right] + \frac{\partial^2(\rho u_i u_j)}{\partial x_i \partial x_j} + O(a^{-3}) \text{ and higher order terms} \tag{12}$$

Thus, the source term in (12) consists of two simple sources, one resulting from the non-uniform temperature distribution and the other resulting from combustion, together with a dipole term which may explain the weak directionality associated with combustion noise, and the usual quadrupole term.

It is to be noted that if the heating in the system is carried out by external means such as an arc jet and not by a chemical reaction, then (6) is replaced by

$$T \frac{Ds}{Dt} = Q \tag{13}$$

where Q is the energy added per unit mass and unit time. Because Q is related to the stagnation temperature rise, (12) will contain a simple source term which depends on the rise in the stagnation temperature.

Formal solution of (12) yields

$$p - p_\infty = \frac{1}{4\pi} \int \frac{q_o(\vec{\xi},\eta)}{r} \, d\vec{\xi}$$

$$\simeq \frac{1}{4\pi} \{ \int \frac{1}{r} \frac{\partial^2 (\rho v_i v_j)}{\partial \xi_i \partial \xi_j} \, d\vec{\xi} - \int \frac{1}{r} \left(\frac{1}{a^2} - \frac{1}{a_\infty^2} \right) \frac{\partial^2 p}{\partial t^2} \, d\vec{\xi}$$

$$+ \int \frac{1}{r} \frac{\partial}{\partial \xi_i} \left[\frac{\partial}{\partial t} (\rho_e u_i) \right] d\vec{\xi} - (\gamma - 1) \int \frac{1}{a^2 r} \left[\frac{\partial}{\partial t} \Sigma \, h_k \, W_k \right] d\vec{\xi} \} \tag{14}$$

where

$$\eta = t - \frac{r}{a_o} \, , \quad r = |\vec{x} - \vec{\xi}| \tag{15}$$

The far field sound pressure for a compact source follows from (14) as

$$p - p_\infty \simeq - \frac{1}{4\pi x} \{ \int \left(\frac{1}{a^2} - \frac{1}{a_\infty^2} \right) \frac{\partial^2 p}{\partial t^2} \, d\vec{\xi} + (\gamma - 1) \int \frac{1}{a^2} \left[\frac{\partial}{\partial t} \Sigma \, h_k \, W_k \right] d\vec{\xi}$$

$$+ \frac{1}{a_\infty} \frac{x_i}{x} \int \frac{\partial}{\partial t} (\rho_e u_i) \, d\vec{\xi} - \frac{1}{a_\infty^2} \frac{x_i x_j}{x^2} \int \frac{\partial^2 (\rho u_i u_j)}{\partial t^2} \, d\vec{\xi} \} \tag{16}$$

If (13) is used instead of (6), then (16) takes the form

$$p - p_\infty \simeq - \frac{1}{4\pi x} \{ \int \left(\frac{1}{a^2} - \frac{1}{a_\infty^2} \right) \frac{\partial^2 p}{\partial t^2} \, d\vec{\xi} - \int \frac{\partial}{\partial t} \left(\frac{\rho Q}{C_p T} \right) d\vec{\xi}$$

$$+ \frac{1}{a_\infty} \frac{x_i}{x} \int \frac{\partial}{\partial t} (\rho_e u_i) \, d\vec{\xi} - \frac{1}{a_\infty^2} \frac{x_i x_j}{x^2} \int \frac{\partial^2 (\rho u_i u_j)}{\partial t^2} \, d\vec{\xi} \} \tag{17}$$

3. Scaling Laws

As a first step in deriving appropriate scaling laws the following dimensionless quantities are introduced:

$$p' = \frac{p}{p_\infty} , \quad u_i' = \frac{u_i}{u} , \quad t' = t/(\ell/u) , \quad \xi' = \xi/\ell , \quad x_i' = x_i/R , \quad \rho_e' = \frac{\rho_e}{\rho_\infty} ,$$

$$(\Sigma\, h_k\, W_k)' = \frac{\Sigma\, h_k\, W_k}{qw} \tag{18}$$

where q is the heat release per unit mass of mixture, w is a characteristic production rate (Williams, 1965), ℓ is a characteristic dimension, u is the mean velocity and R is a typical far field distance. When (18) is used in (16), one finds

$$\Delta p' = \frac{\Delta p}{p_\infty} \simeq -\frac{1}{4\pi x'} \frac{\ell}{R} M^2 \left\{ \int \left[\left(\frac{a_\infty}{a}\right)^2 - 1 \right] \frac{\partial^2 p'}{\partial t'^2}\, d\vec{\xi}' \right.$$

$$+ \lambda \int \left(\frac{a_\infty}{a}\right)^2 \frac{\partial}{\partial t'} (\Sigma\, h_k\, W_k)'\, d\vec{\xi}' + \gamma \frac{x_i'}{x'} M \int \frac{\partial^2}{\partial t'^2} (\rho_e' u_i')\, d\vec{\xi}'$$

$$\left. - \gamma \frac{x_i' x_j'}{x'^2} M^2 \int \frac{\partial^2}{\partial t'^2} (\rho' u_i' u_j')\, d\vec{\xi}' \right\} \tag{19}$$

where

$$\lambda = (\gamma - 1) \frac{qw\ell}{p_\infty u} , \quad M = \frac{u}{a_\infty} \tag{20}$$

Equation (19) shows that the pressure fluctuation depends, in addition to the ratio of specific heats which is essentially constant, on the two dimensionless numbers λ and M. Therefore, from dimensional considerations (Kline, 1965) one concludes that any dimensionless quantity characterizing combustion noise must be a function of both λ and M. Thus, if ν is the characteristic frequency, then

$$\nu \frac{\ell}{u} = G(\lambda, M) \tag{21}$$

Similarly, at low Mach numbers where combustion noise is expected to be dominant, and thus

$$\Delta p \simeq -\frac{1}{4\pi x'} \left(\frac{\ell}{R}\right) M^2 p_\infty \lambda \int \left(\frac{a_\infty}{a}\right)^2 \frac{\partial}{\partial t'} (\Sigma\, h_k\, W_k)'\, d\vec{\xi}' \tag{22}$$

the far field power output can be written as

$$P = K \frac{(\gamma-1)^2 q^2 w^2 \ell^4 u^2}{4\pi \rho_\infty a_\infty^5} , \quad K = K(\lambda, M) \tag{23}$$

At higher Mach numbers other terms in (19) have to be included. In spite of this, the representation indicated in (23) for the far field power output may be employed.

The choice of G and K is usually guided by experiment. Examination of the measurements of Smith and Kilham (1963) and Shivashankara, Strahle and Handley (1973) (later referred to as SSH) shows that, at low Mach numbers, the results of experiment are well correlated if one assumes

$$\ell = (\ell_f D)^{1/2} \quad , \quad G(\lambda, M) = A\,\lambda$$

$$K = K(M) = K_o(1 + a_1 M + a_2 M^2 + ..) \tag{24}$$

where D is the burner diameter and A, K_o, a_1, a_2 ... are constants to be determined from experiment. Using (24), one obtains

$$\nu = (\gamma - 1)\frac{Aqw}{p_\infty} \tag{25}$$

$$P = K(M)\frac{(\gamma-1)^2 q^2 w^2 \ell_f^2 D^2 u^2}{4\pi \rho_\infty a_\infty^2} \tag{26}$$

Equation (24) will be justified by showing that K is of order unity and that (25) and (26) lead to adequate scaling laws.

Using the relation (Williams, 1965)

$$w = \rho_\infty \frac{S_t}{\ell_f} \tag{27}$$

where S_t is the turbulent flame velocity, (25) and (26) take the form

$$\nu = (\gamma - 1)\,A\frac{\rho_\infty q S_t}{p_\infty \ell_f} \tag{28}$$

and

$$P = K\frac{(\gamma-1)^2}{4\pi a_\infty^5}\rho_\infty q^2 u^2 D^2 S_t^2 \tag{29}$$

There are a number of relations (Williams, 1965) relating S_t to S_ℓ, the laminar flame velocity. Thus, as an example, Bollinger and Williams (1949) give

$$S_t = C_1 u^{1/4} D^{1/2} S_\ell \tag{30}$$

therefore

$$P = K_s \frac{(\gamma-1)^2}{4\pi a_\infty^5} \rho_\infty q^2 u^{2.5} D^3 S_\ell^2 \ , \ K_s = C_1 K \tag{31}$$

4. Discussion of the Results

We proceed now to show that K is of order unity and that (28) and (29) give good agreement with available experiment. For the sake of estimating K it will be assumed that the numerical value of S_t is approximately that of S_ℓ at low velocities (of the order of 50 ft/sec) and that (30) may be used to estimate S_t at the higher velocities. Values of S_ℓ are taken from Dugger (1952). The quantity q is related to the heat of combustion per unit mass of fuel, H, by the relation

$$q = \frac{f}{1+f} H \simeq fH \quad \text{when } f \ll 1 \tag{32}$$

where f is the fuel to air ratio. Values of H are taken from Keenan and Kaye (1948).

Using the ethylene data shown in Figure 5 of Smith and Kilham (1963) and assuming S_ℓ to be 63 cm, H = - 20,276 Btu/lbm, $\rho_\infty = 1.293 \times 10^{-3}$ g/cm^3 , $a_\infty = 3.41 \times 10^4$ cm/sec, $\gamma = 1.3$, one finds

$$K \simeq .72 \quad \text{for ethylene} \tag{33}$$

Similarly, utilizing the propylene data of Smith and Kilham with $S_\ell = 42$ cm/sec and H = - 19,683 Btu/lbm, one obtains

$$K \simeq 1.4 \quad \text{for propylene} \tag{34}$$

Finally, using table 1 in SSH (1973) one finds for $S_\ell = 30$ cm/sec, u = 100 ft/sec, H = - 19,929 Btu/lbm

$$K \simeq 1.3 \quad \text{for propane} \tag{35}$$

Because other terms in (19) become important at the higher velocities, some variation of K with Mach number, such as indicated in (24), is expected. Thus, the data in SSH results in $K \simeq 1.9$ for u = 200 ft/sec and $K \simeq 3.1$ for u = 600 ft/sec. It is seen that the above estimates support the earlier contention that K is of order unity.

Comparison of (31) and (32) with (4) in SSH shows that, with the exception of the dependance on the fuel to air ratio, the predictions of the theory are in good agreement with the measurements for fuel-lean mixtures. Because S_ℓ increases and then decreases with fuel to air ratio (Dugger, 1952), the present theory which gives

$$P \alpha \frac{f^2 S_\ell^2}{(1+f)^2} \tag{36}$$

predicts the trends indicated for propane and propylene in Figure 17 in SSH.

As was pointed out by Strahle, a successful scaling law must predict the scaling of both the power output and the frequency. The characteristic frequency is given by (28), or using (32)

$$\nu = (\gamma - 1)\, A\, \frac{\rho_\infty f H S_t}{p_\infty \ell_f} \tag{37}$$

Because H, and to a lesser extent S_t and ℓ_f, are essentially the same for hydrocarbon fuels and hydrocarbon-air flames, one concludes from (37) that the characteristic frequency is essentially the same for hydrocarbon-air flames (SSH, 1973). Assuming $\ell_f = .1$ and using the data of SSH one finds that $A = -0.1$, (A is negative because, by convention, H is negative). As may be seen from (37), flames other than hydrocarbon-air flames which are characterized by different S_t and H will have different characteristics frequencies (Knott, 1971).

Substituting for S_t from (30) and assuming that $\ell_f \alpha \mathcal{D}$, one recovers a formula which, with the exception of the dependence on the fuel to air ratio, is in fair agreement with (7) in SSH.

Acknowledgement

The author would like to acknowledge many helpful discussions with Professor T. H. Hodgson. The work was supported, in part, by the Department of Transportation.

Appendix

From

$$\rho = \rho(p, s, Y_k) \tag{A.1}$$

one can write

$$d\rho = \left(\frac{\partial \rho}{\partial p}\right)_{s,Y_k} dp + \left(\frac{\partial \rho}{\partial s}\right)_{p,Y_k} ds + \Sigma \left(\frac{\partial \rho}{\partial Y_k}\right)_{s,p,Y_j} dY_k \tag{A.2}$$

At constant pressure and density, (A.2) gives

$$\left(\frac{\partial \rho}{\partial s}\right)_{p,Y_k} \left(\frac{\partial s}{\partial Y_k}\right)_{p,\rho,Y_j} + \left(\frac{\partial \rho}{\partial Y_k}\right)_{s,p,Y_j} = 0 \tag{A.3}$$

thus, (A.2) can be written as

$$d\rho = \left(\frac{\partial \rho}{\partial p}\right)_{s,Y_k} dp + \left(\frac{\partial \rho}{\partial s}\right)_{p,Y_k} \left[ds - \Sigma \left(\frac{\partial s}{\partial Y_k}\right)_{p,\rho,Y_j} dY_k\right] \tag{A.4}$$

The quantity $(\frac{\partial \rho}{\partial s})_{p,Y_k}$ can be expressed as

$$(\frac{\partial \rho}{\partial s})_{p,Y_k} = (\frac{\partial \rho}{\partial T})_{p,Y_k} (\frac{\partial T}{\partial s})_{p,Y_k} \tag{A.5}$$

Using the equation of state

$$p = R_o \rho T \Sigma \frac{Y_k}{M_k} \equiv \frac{R_o}{M_o} \rho T \tag{A.6}$$

where R_o is the universal gas constant, M_o is the molecular weight of the mixture and M_k is the molecular weight of species k, one finds

$$(\frac{\partial \rho}{\partial T})_{p,Y_k} = - \frac{\rho}{T} \tag{A.7}$$

Similarly, from the equation for the differential change of the specific enthalpy h (Williams, 1965)

$$dh = Tds + \frac{dp}{\rho} + \Sigma \frac{\mu_k}{M_k} dY_k \tag{A.8}$$

where μ_k is the chemical potential, one finds

$$C_p = (\frac{\partial h}{\partial T})_{p,Y_k} = T (\frac{\partial s}{\partial T})_{p,Y_k} \tag{A.9}$$

where C_p is the frozen specific heat. Thus, from (A.7) and (A.9) one obtains

$$(\frac{\partial \rho}{\partial s})_{p,Y_k} = - \frac{\rho}{C_p} \tag{A.10}$$

The quantity $(\frac{\partial s}{\partial Y_k})_{p,\rho,Y_j}$ is considered next. From

$$ds = (\frac{\partial s}{\partial p})_{T,Y_k} dp + (\frac{\partial s}{\partial T})_{p,Y_k} dT + \Sigma (\frac{\partial s}{\partial Y_k})_{p,T,Y_j} dY_k \tag{A.11}$$

one obtains

$$\begin{aligned} (\frac{\partial s}{\partial Y_k})_{p,\rho,Y_j} &= (\frac{\partial s}{\partial T})_{p,Y_k} (\frac{\partial T}{\partial Y_k})_{p,\rho,Y_j} + (\frac{\partial s}{\partial Y_k})_{p,T,Y_j} \\ &= (\frac{\partial s}{\partial \rho})_{p,Y_k} (\frac{\partial \rho}{\partial T})_{p,Y_k} (\frac{\partial T}{\partial Y_k})_{p,\rho,Y_j} + (\frac{\partial s}{\partial Y_k})_{p,T,Y_j} \end{aligned} \tag{A.12}$$

Again, writing $d\rho$ as

$$d\rho = \left(\frac{\partial \rho}{\partial p}\right)_{T,Y_k} dp + \left(\frac{\partial \rho}{\partial T}\right)_{p,Y_k} dT + \Sigma \left(\frac{\partial \rho}{\partial Y_k}\right)_{p,T,Y_j} dY_k$$

one obtains

$$\left(\frac{\partial \rho}{\partial T}\right)_{p,Y_k} \left(\frac{\partial T}{\partial Y_k}\right)_{p,\rho,Y_j} + \left(\frac{\partial \rho}{\partial Y_k}\right)_{p,T,Y_j} = 0 \qquad \text{(A.13)}$$

Using (A.13), (A.12) takes the form

$$\left(\frac{\partial s}{\partial Y_k}\right)_{p,\rho,Y_j} = - \left(\frac{\partial s}{\partial \rho}\right)_{p,Y_k} \left(\frac{\partial \rho}{\partial Y_k}\right)_{p,T,Y_j} + \left(\frac{\partial s}{\partial Y_k}\right)_{p,T,Y_j} \qquad \text{(A.14)}$$

However, (A.8) gives

$$\left(\frac{\partial h}{\partial Y_k}\right)_{p,T,Y_j} = T \left(\frac{\partial s}{\partial Y_k}\right)_{p,T,Y_j} + \frac{\mu_k}{M_k}$$

therefore,

$$\left(\frac{\partial s}{\partial Y_k}\right)_{p,\rho,Y_j} = \frac{C_p}{\rho} \left(\frac{\partial \rho}{\partial Y_k}\right)_{p,T,Y_j} + \frac{1}{T} \left[\left(\frac{\partial h}{\partial Y_k}\right)_{p,T,Y_j} - \frac{\mu_k}{M_k}\right] \qquad \text{(A.15)}$$

Noting that

$$h_k = \left(\frac{\partial h}{\partial Y_k}\right)_{p,T,Y_j}, \quad \left(\frac{\partial \rho}{\partial Y_k}\right)_{p,T,Y_j} = - \frac{M_o}{M_k} \rho$$

and substituting (A.15) into (A.4), one finds

$$d\rho = \frac{dp}{a^2} - \frac{\rho}{C_p} \left\{ds - \Sigma \left[-C_p \frac{M_o}{M_k} + \frac{1}{T} \left(h_k - \frac{\mu_k}{M_k}\right)\right] dY_k\right\} \qquad \text{(A.16)}$$

If the molecular weight remains constant during the chemical reactions, then (A.16) reduces to

$$d\rho = \frac{1}{a^2} \left[dp + (\gamma - 1) \rho \Sigma h_k \, dY_k\right] - \frac{\rho}{C_p} \left[ds + \frac{1}{T} \Sigma \frac{\mu_k}{M_k} dY_k\right] \qquad \text{(A.17)}$$

REFERENCES

Bollinger, L. M. and Williams, D. T. 1949. NACA Report 932.

Chiu, H. H. and Summerfield, M. 1973. Fourth International Colloquium on Gasdynamics of Explosions and Reactive Systems.

Dugger, G. L. 1952. NACA Report 1061.

Keenan, J. H. and Kaye, J. 1948. Gas Tables. Wiley.

Kline, S. J. 1965. Similitude and Approximation Theory, McGraw-Hill.

Knott, P. R. 1971. AIAA Paper No. 71-732.

Lighthill, M. J. 1952. Proc. Roy. Soc. A 211, 564.

Morfey, C. L. 1973. J. Sound Vib. 31, 391.

Shivashankara, B. N., Strahle, W. C. and Handley, J. C. 1973. AIAA Paper No. 73-1025.

Smith, T. J. B. and Kilham, J. S. 1963. J. Acoust. Soc. Am. 35, 715.

Strahle, W. C. 1973. AIAA Paper No. 73-1023.

Williams, F. A. 1965. Combustion Theory. Addison-Wesley.

COMBUSTION GENERATED NOISE

by

B. N. Shivashankara, W. C. Strahle, J. C. Handley and M. Muthukrishnan

School of Aerospace Engineering, Georgia Institute of Technology
Atlanta, Georgia 30332

This expanded abstract summarizes work completed since the first symposium under Air Force Office of Scientific Research Grant No. AFOSR-72-2365 and National Science Foundation Grant No. GK-32544. This program consists of fundamental flame research aimed at understanding of the origin, magnitude, and scaling behavior of combustion generated noise.

There are six major tasks which have been completed during the past year. These are:

1) Completion of sound power, directionality and spectra measurements on open turbulent flames anchored on burner tubes in anechoic surroundings with the fuels acetylene, ethylene, propane and propylene.
2) Correlation of the results for sound power and frequency of maximum spectral output with regard to Reynolds number, Mach number, fuel mass fraction and Dämkohler's first similarity group.
3) Construction of a theory of combustion noise capable of recovering the observed correlation.
4) Optical measurements of CH-C_2 emission from the flame as correlated with far field pressure signals to verify the theoretical approach to combustion noise.
5) Measurement of the pressure generated by the same flame types as in 1) but enclosed in a simulated infinite tube to measure the effects of wall reflection and possible feedback behavior on enclosed flames.
6) Construction of a theory to explain and interpret the results of 5).

The results of Tasks 1), 2) and 3) above will be presented in Reference (1); partial results are located in Reference (2). Within the range of variables listed the flame behaves as an equivalent monopole with very little directionality to the observed noise. The experimental correlation for thermoacoustic efficiency, η_{ta}, is

$$\eta_{ta} \equiv \frac{P}{\dot{m}_f H} = 5.48 \times 10^{-7}\ Da_1^{.92}\ Re^{-.14}\ F^{-1.4}\ M^{2.72} \qquad (1)$$

where P is the noise power, $\dot{m}_f$ the fuel flow rate, H the fuel heating value, $Da_1 = S_L^2 D/U\alpha_o$ is Dämkohler's first similarity group (flow time/chemical time), Re is the Reynolds number based upon pipe diameter, D, and flow velocity, U, F is the fuel mass fraction, M is the Mach number, S_L is the laminar flame speed and α_o is the thermal diffusivity. Equation (1) is valid for open, fuel lean, turbulent hydrocarbon-air flames anchored on burner tubes.

The dimensional correlation obtained for frequency of maximum radiated sound power is

$$f_c = 2.3\ U^{.18}\ S_L^{.88}\ F^{-1.21}\ D^{-.13} \qquad (2)$$

where f_c is in Hz, U in ft/sec, S_L in ft/sec, and D in ft. Equations (1) and (2) are based upon 63 tests with standard deviations of 41% for sound power and 16% for frequency. The sound power range covered was 10^4:1.

Using the basic theory of Reference (3), but with a different approach to estimating the necessary quantities in the sound power formula, as outlined in Reference (1), the theoretical laws obtained are

$$\eta_{ta} \propto Da_1^{.800}\ Re^0\ M^{2.584}\ F^{-.4} \qquad (3)$$

$$f_c \propto U^{.54}\ S_L^{.60}\ D^{-.70}\ F^{-1.2} \qquad (4)$$

Equations (3) and (4) are to be compared with Equations (1) and (2) and the agreement is quite good. In developing Equations (3) and (4) use is made of a) the empirical fact that f_c is determined by the frequency of the energy containing eddies of the turbulence, b) known laws for the decay of turbulence between the burner exit and the flame tip, where most of the noise is generated, c) turbulent flame speed and geometric data from References (4) and (5) and d) the empirical dependence of f_c on F from Equation (2), for which there is no theoretical explanation.

The results of Task 4) are presented in Reference (6). Figure 1 shows typical results of cross-correlations of the far field pressure signature and the time derivative of the C_2 emission intensity when the entire flame is viewed through an optical filter. The strong cross-correlation peak occurs at a time delay corresponding to the time required for a pressure wave to travel from the flame to the microphone. Since the time derivative of the emission intensity directly measures the time derivative of the global heat release rate, the cross correlation proves the deduction of Reference (3) that the far field sound pressure is directly proportional to the volume integral of the Eulerian time derivative of the reaction rate. This fact is used in construction of the theory mentioned above.

Task 5) is carried out by use of the apparatus of Figure 2. The same burners as used in the open flame experiments are enclosed by a 4 inch diameter duct terminated by "mufflers" intended to make the apparatus simulate an infinite tube. Visual observation shows that, although there exists aspirated flow, there is no change in the flame aerodynamics with the enclosure

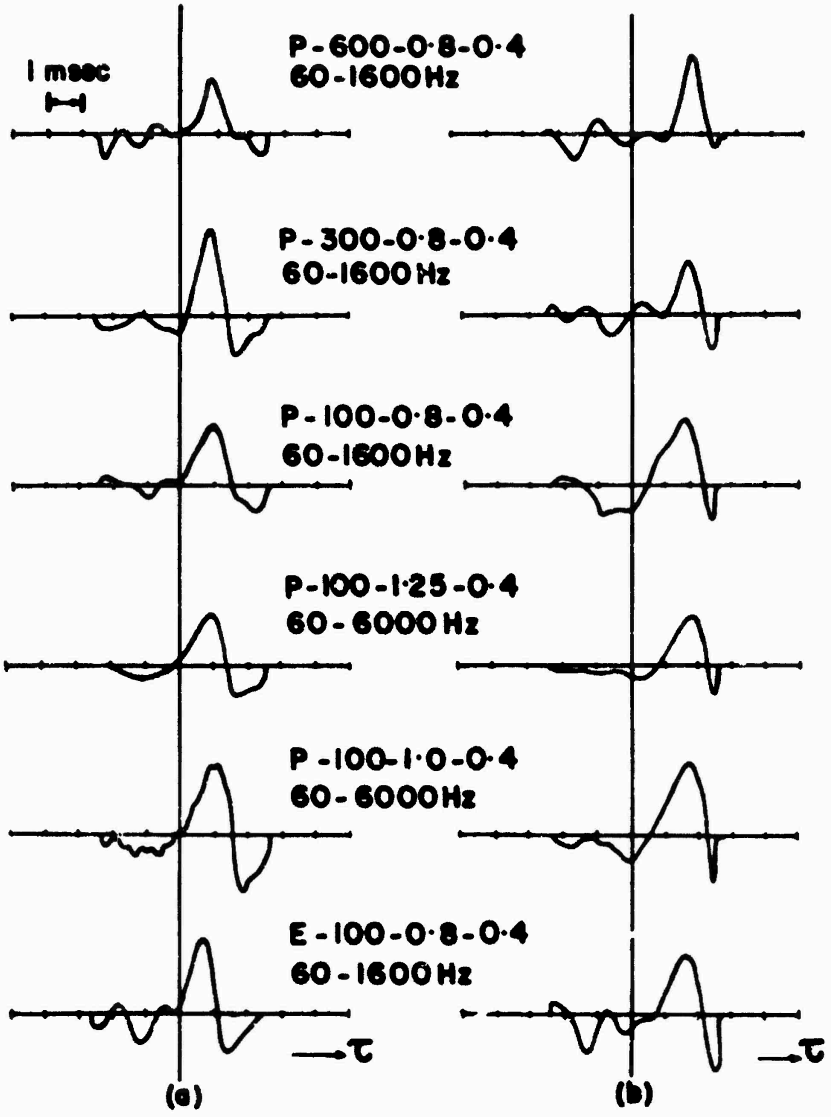

Figure 1. Cross-Correlation Curves. Cross-Correlations between Sound Pressure p(t) and the Time Derivative of the Emission Intensity $\dot{I}(t)$ are Shown. Microphone to Flame Distances were 14" for (a) and 2-" for (b) Cases. The Cross-Correlations can be Seen to Maximize at Time Delays τ Corresponding to the Time Taken by Sound to Travel from the Flame to the Microphone.

Figure 2. Photograph of Burner in Tube. Tube Has Two Sections; One Half is Made of Glass to Allow Observation and the Other Half is a Metal Tube. Both Ends of the Tube Are Fitted with Specially Designed Mufflers which are Intended to Simulate Infinite Tube Situation.

so that the flame, as a noise radiator, is expected to be unchanged as compared to its behavior when open. Two things may happen upon enclosing the flame: a) the radiation impedance will change due to wall reflections and b) there may be feedback between the reflected waves and the combustion process, altering the noise output. This is experimentally checked by measuring the wall pressure and comparing this with calculations from the theory of Task 6). The theory is a quasi-one dimensional theory for a hard wall tube with an imbedded monopole source with the tube terminated by known impedance material. The impedances of the "mufflers" have been measured with a classical impedance tube method. Shown in Figure 3 are a) the flame spectrum when in the open, b) the wall pressure spectrum when the flame is enclosed and c) the computed spectrum assuming no feedback interactions and with the flame behaving as though it were in a free field. It is seen that there is excellent agreement on the basis of a no-interaction theory. Furthermore, the calculated rms pressure and the theoretical pressure differ by less than 1 db. This has been repeated for several other conditions than shown in Figure 3. Consequently, for noise calculations the feedback effect appears negligible.

In summary, it now appears that the noise characteristics of at least one simple flame type may be explained theoretically. Consequently, the theory may be used with confidence in other situations. For actual installations the acoustics of the enclosure must be known. Using the theory of combustion noise together with calculated or measured acoustic properties of the enclosure should yield a satisfactory answer for the noise radiation characteristic, and the feedback effect between wall reflections and the combustion process may be neglected, at least in sufficiently damped configurations.

References

1. Strahle, W. C., "A Rational Correlation of Combustion Noise Results from Open Turbulent Flames," to be published in Fifteenth Symposium (International) on Combustion, August, 1974.

2. Shivashankara, B. N., Strahle, W. C. and Handley, J. C., "Combustion Noise Radiation by Open Turbulent Flames," AIAA Paper No. 73-1025 (1973).

3. Strahle, W. C., "Some Results in Combustion Generated Noise," Journal of Sound and Vibration, 23, p. 113 (1972).

4. Dollinger, L. M. and Williams, D. T., "Effect of Reynolds Number in the Turbulent Flow Range on Flame Speeds of Bunsen Burner Flames," NACA TN 1707 (1948).

5. Shivashankara, B. N., Strahle, W. C. and Handley, J. C., "Decomposition of Combustion Noise Scaling Rules by Direct Flame Photography," Presented at the 4th International Colloquium on Gasdynamics of Explosions and Reactive Systems, San Diego (1973).

6. Shivashankara, B. N., Strahle, W. C. and Handley, J. C., "An Evaluation of Combustion Noise Scaling Laws by an Optical Technique," AIAA Paper No. 74-47 (1974).

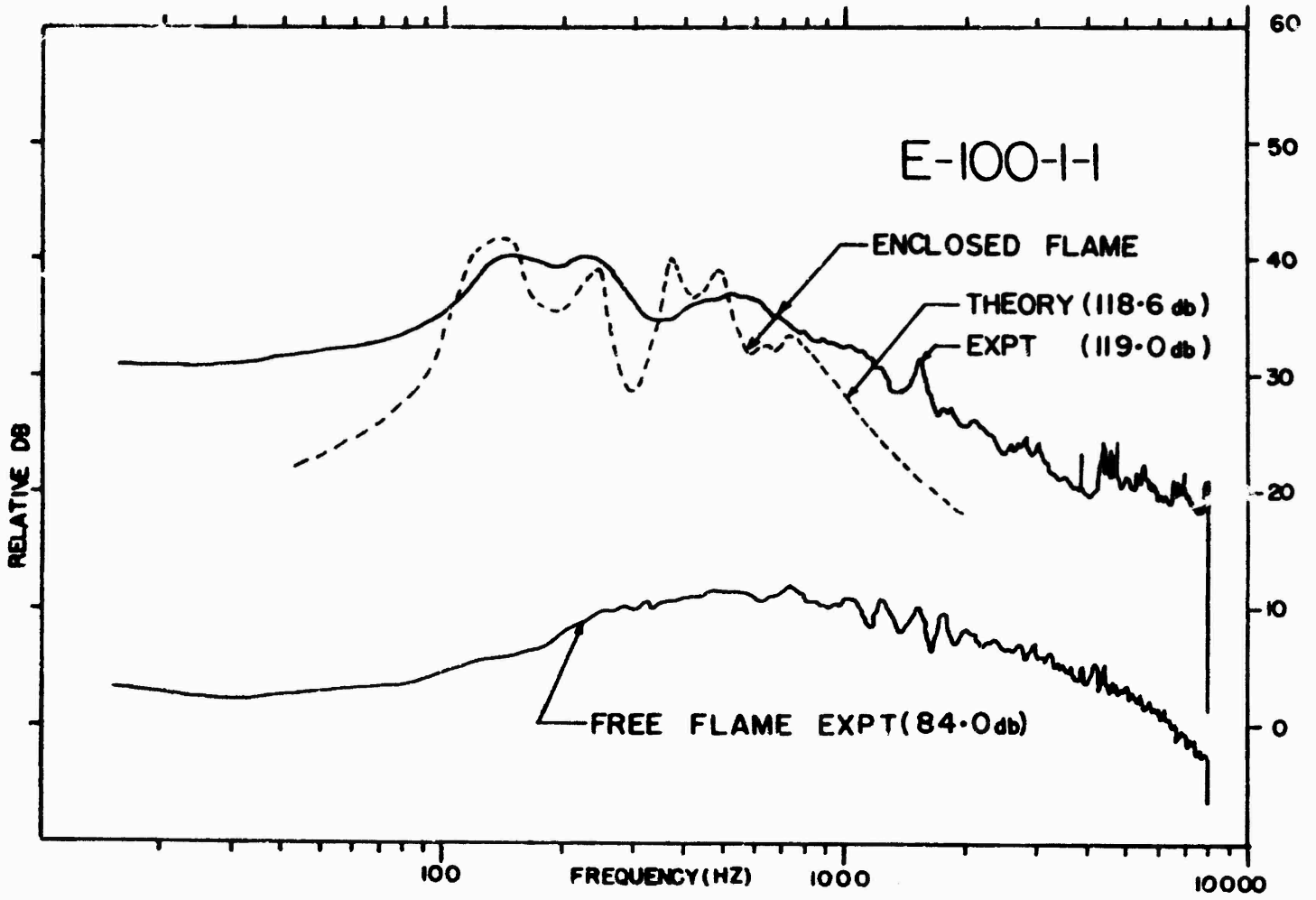

Figure 3. Comparison between Experimental and Theoretical Spectra.

COMBUSTION GENERATED NOISE IN TURBOPROPULSION SYSTEMS

by

B. N. Shivashankara, W. C. Strahle and Tai-Chen Cho

School of Aerospace Engineering, Georgia Institute of Technology
Atlanta, Georgia 30332

The work presented in this expanded abstract has been supported by the National Aeronautics and Space Administration under Contract No. NAS3-17861. This program is designed to investigate the noise produced by the combustion process in a can-type combustor.

The major tasks are to a) measure the sound power output and noise spectra radiated from a typical combustor with JP-4 fuel terminated by the atmosphere and varying the air flow and fuel flow rates over as wide a range as possible, b) correlate the noise power output and frequency of maximum radiated power with the test variables, c) apply theoretical acoustics to account for any duct wall modification of the basic sound generation capacity of the flame and d) theoretically explain the correlations achieved.

The combustor used in this study is shown in Figure 1. It is a can-type combustor taken out of a Boeing 502-7D gas turbine unit with its air inlet slightly modified to adapt to the present experimental set-up. Liquid fuel is sprayed inside the burner liner. The liner has slots at both the head end and the walls for air to flow into the combustion region. Ignition of the combustor is achieved by a spark plug. The spark is necessary only during starting. Once the combustor is operating the combustion process is self-sustaining.

The flow system is schematically shown in Figure 2. Air is supplied from a 125 psi air reservoir, regulated by a valve and metered by an orifice meter. A muffler is included in the air piping just upstream of the combustor to reduce flow noises. The liquid fuel is pumped by gas pressurization. A turbine flow meter is used to measure the flow rate of fuel through the system.

The combustor, fuel tank and the air muffler are mounted on a test stand. The test stand is placed on a platform outside the laboratory in such a way that the burner axis is horizontal and at about 8 feet above the ground level in the forward half-circle. All the flow control valves, flow display units and instrumentation are placed inside the laboratory.

Sound pressures are measured by five B and K type 4134 half-inch condenser microphones mounted on stands and in the same horizontal plane as the burner axis. The microphones are provided with wind shields. The radius of the microphones in all the experiments is chosen as 10 feet with the angular locations varying between 15° and 120° to the flow direction. It has been verified that at this distance the sound pressure measurements would correspond to the acoustic far-field. The output from the microphones are read out one by one on a B and K type 2604 microphone amplifier. Also all the five signals are recorded simultaneously on an AMPEX FR1300 magnetic tape recorder. Calibration signals are also included on the tape for reference

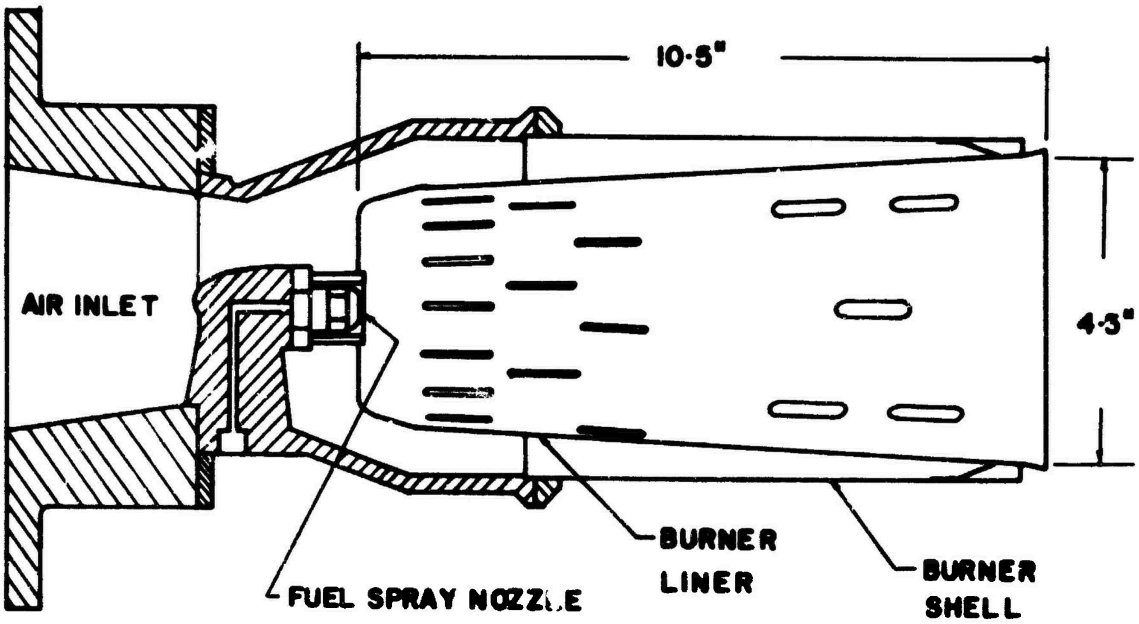

Figure 1. Cross-Sectional View of the Combustor.

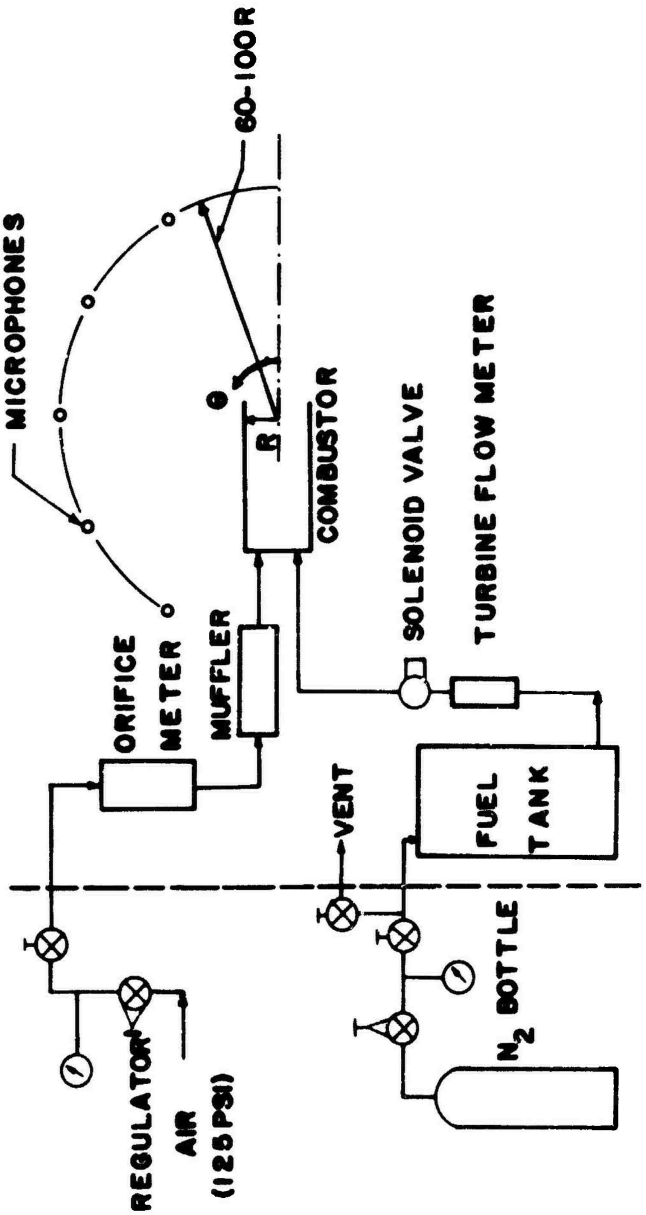

Figure 2. Flow System Schematic.

when reproducing data. The frequency spectra of noise are obtained using a Hewlett-Packard Model 5645 digital fourier analyzer.

Figure 3 shows the directionality pattern obtained at various air flow rates through the combustor. It can be seen that the directionality is quite weak. Further, there is no apparent trend for the directionality pattern with changes in air flow rate. This weak directionality is similar to that obtained for open turbulent flames,[1,2] because of the low frequencies involved. From the sound pressure measured the radiated sound power is calculated by integration of the intensity over a spherical surface around the combustor. Figure 4 shows the variation of radiated sound power with total air flow rate through the combustor. The sound power is found to scale to an exponent between 2.3 and 2.7 with the total air flow rate. The effect of changing the fuel flow rate at a constant value of air flow rate is presented in Figure 5. Figure 5 also shows the variation of thermo-acoustic efficiency, the ratio of radiated sound power to the total heat input rate. The radiated sound power appears to be virtually insensitive to fuel flow rate over a wide range of fuel flow rates. Also, a thermo-acoustic efficiency as high as 3×10^{-5} is seen which shows that the combustor has a considerable capacity to convert the heat input to noise.

Figure 6 shows a frequency spectrum of the noise. The curve shown is a smooth line drawn through the mid-points of the x-y plot obtained from the fourier analyzer. The spectrum shows that the combustor output is a broad-band noise with a marked peak around 400 Hz. Also, weak secondary peaks can be seen at frequencies of 1200, 2400, 3600, 4800 Hz etc. Further, almost identical frequency spectra were obtained over the entire sequence of experiments in which flow rates of air were varied between 1000 and 400 SCFM and fuel flow rates between 0.0091 and 0.082 gpm. No significant effect of the microphone azimuth could be observed either. The repeatability of the experiment has been found to be excellent.

The high values of thermo-acoustic efficiency obtained indicate that the can walls are only slightly absorbent, as may be expected from the small open area of the can walls compared to the total surface area and the fact that a high flow velocity enters the can from these holes. The lack of any strong resonances in the spectra indicate that the end plane impedance differs substantially from a cold unflanged circular pipe and that virtually all sound is transmitted which impinges upon the end plane. This appears to be a fortuitous occurrence for the data reduction. Although data reduction has not been completed at this time, the equivalent free flame noise output will be obtained assuming a hard wall can with an end plane impedance equal to the local characteristic impedance of the medium.

The theory of Reference (3) as modified in Reference (4) produces the following estimate for the noise power output of the equivalent free flame when operating fuel lean overall:

$$P \propto \frac{1}{4\pi\rho_o c_o S_{can}} F_{st}^2 \left(\frac{H}{c_o}\right)^2 \dot{m}_a^2 u'^2 \qquad (1)$$

Here ρ_o and c_o are the cold density and speed of sound, respectively. S_{can}

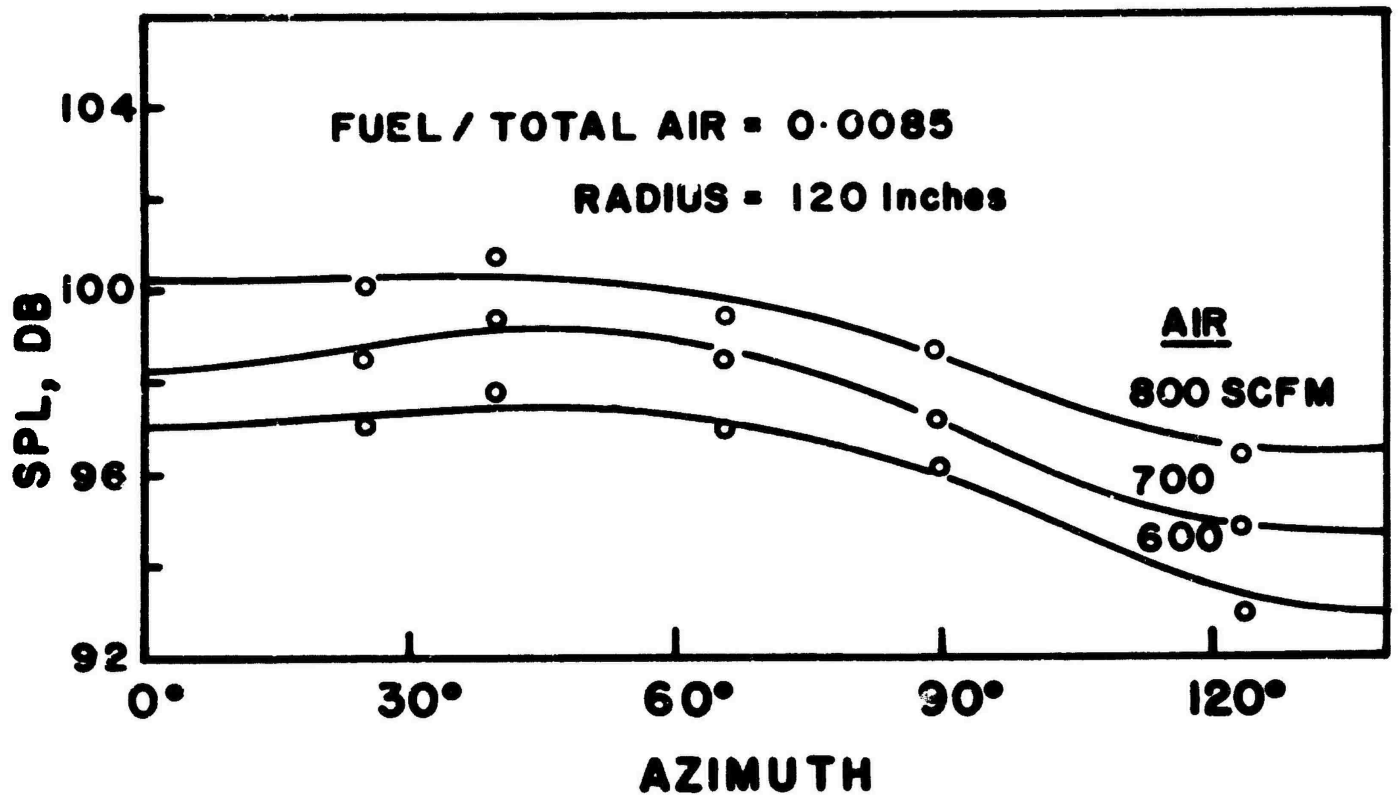

Figure 3. Directionality of Far-Field Noise Radiated by the Combustor. The Smooth Lines Shown are Cubics in Cos θ Fitted to the Experimental Data Points by a Least Square Method.

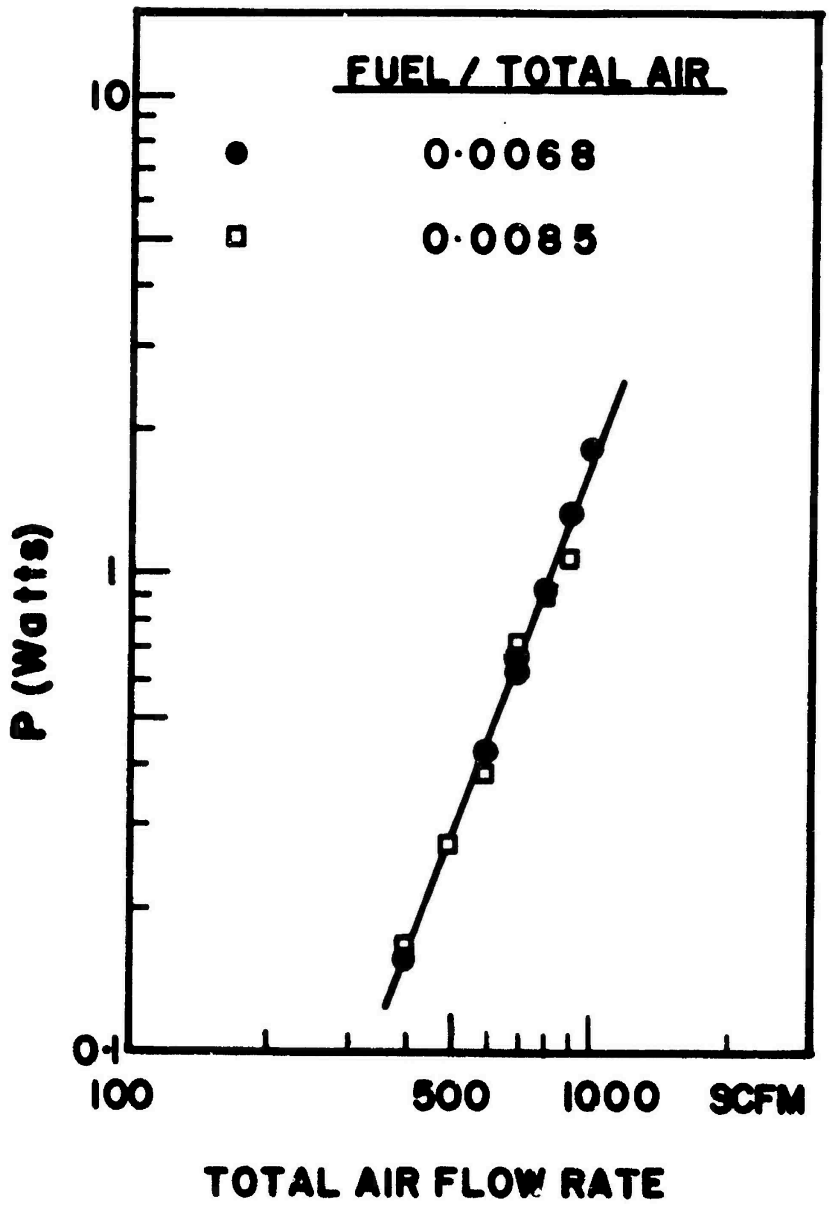

Figure 4. Radiated Sound Power P as a Function of Total Air Flow Rate at Two Different Mixture Ratios.

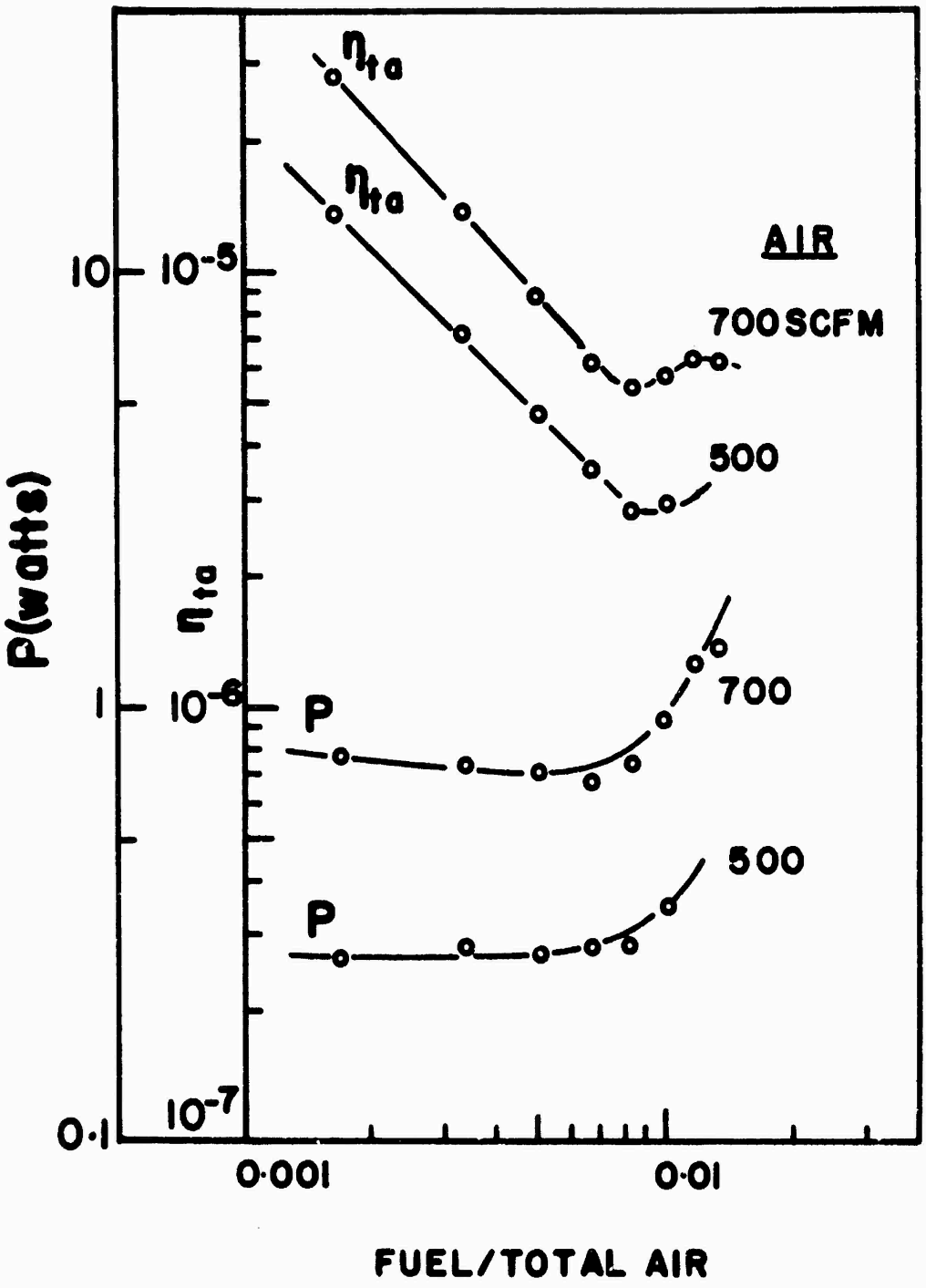

Figure 5. Radiated Sound Power P and Thermo-Acoustic Efficiency η_{ta} as a Function of Mixture Ratio.

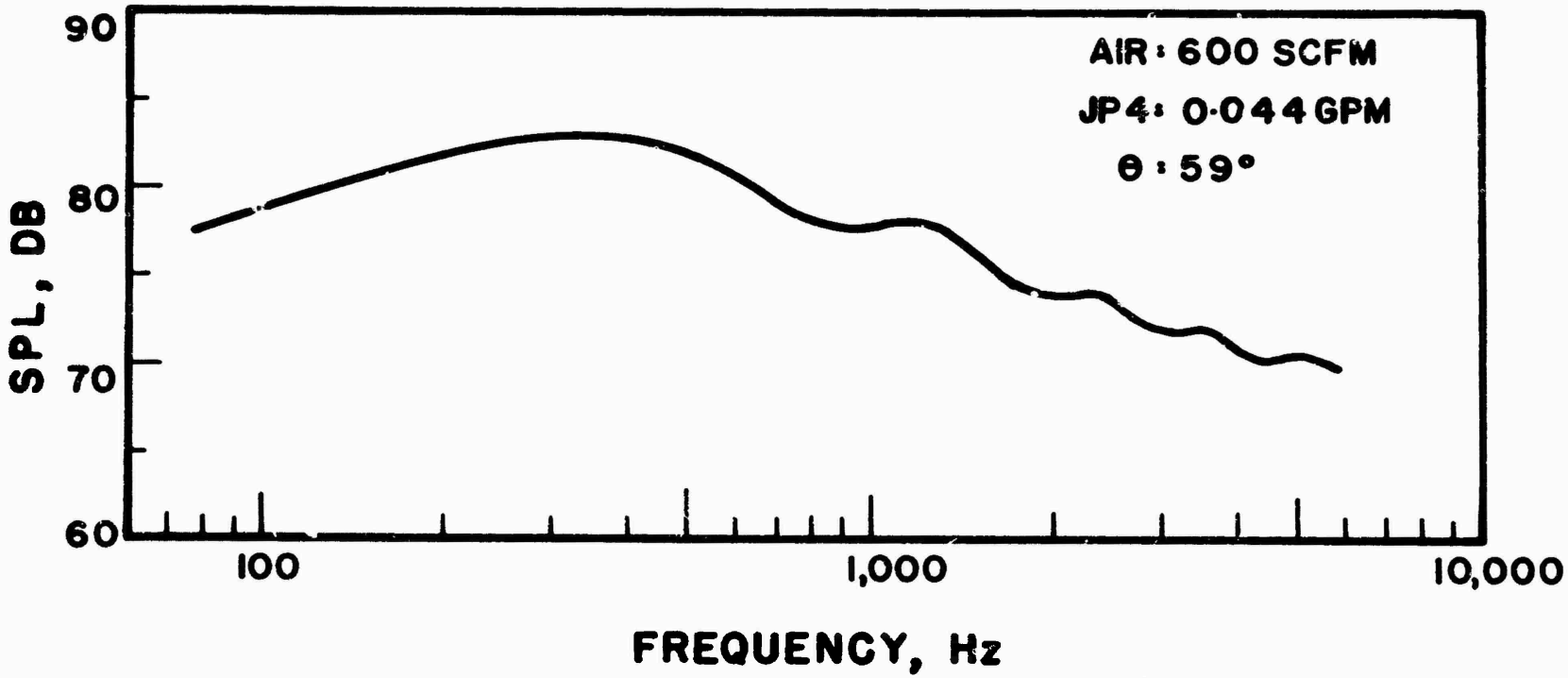

Figure 6. Frequency Spectrum of Noise Radiated by the Combustor. Spectrum Shown is a Smooth Curve Drawn through the Mid-Points of the x-y Plot Obtained from the Fourier Analyzer.

is the can crossection area, F_{st} is the stoichiometric fuel fraction, H is the fuel heating value, $\dot{m}_a$ is the air flow rate through the can and u' is the intensity of turbulence in the can. u' arises in an estimate of the frequency; empirically the frequency of maximum radiated power is seen to be independent of the test variables. Consequently, Equation (1) predicts

$$P \propto \dot{m}_f^0 \, \dot{m}_a^2 \tag{2}$$

where $\dot{m}_f$ is the fuel flow rate. Equation (2) recovers the observed power scaling law quite accurately.

The can used has the characteristic of a large bypass flow rate of air. Consequently, $\dot{m}_a$ in Equation (1), being the flow rate through the inner can, is inaccurately known at this time. Current efforts center about fully characterizing the ratio of bypass to total air flow.

References

1. Shivashankara, B. N., Strahle, W. C. and Handley, J. C., "Combustion Noise Radiation by Open Turbulent Flames," AIAA Paper No. 73-1025 (1973).

2. Smith, T. B. J. and Kilham, J. K., "Noise Generated by Open Turbulent Flames," Journal of the Acoustical Society of America, 35, p. 715 (1963).

3. Strahle, W. C., "Some Results in Combustion Generated Noise," Journal of Sound and Vibration, 23, p. 113 (1972).

4. Strahle, W. C., "A Rational Correlation of Combustion Noise Results from Open Turbulent Flames," to be published in Fifteenth Symposium (International) on Combustion, August, 1974.

COMBUSTOR GEOMETRY AND COMBUSTION ROUGHNESS RELATION TO NOISE GENERATION*

by

E. G. Plett,[1] M. D. Leshner,[2] and M. Summerfield[3]

Guggenheim Aerospace Propulsion Laboratories
Aerospace and Mechanical Sciences Department
Princeton University
Princeton, New Jersey

ABSTRACT

Some results of a study of the importance of geometrical features of the combustor to combustion roughness and resulting noise are presented. Comparison is made among a perforated can flame holder, a plane slotted flame holder and a plane slotted flame holder which introduces two counter swirling streams. The latter is found to permit the most stable, quiet combustion. Crosscorrelations between the time derivative of chamber pressure fluctuations and far field noise are found to be stronger than between the far field noise and the direct chamber pressure signal. Temperature fluctuations in the combustor nozzle are also found to have a reasonably strong crosscorrelation with far field sound. Indications are given of areas where further work is planned relating to these findings.

INTRODUCTION

Earlier studies of the relative importance of combustion as a source of noise in jet engines[1,2] revealed that the intensity of combustion roughness, which generates noise, was affected by the type of flame holder and the air/fuel mixture used, as well as on the flow rate through the combustor. Approximate relationships were derived to predict the far field noise due to the combustor pressure oscillations, and it was found experimentally, that there was a correlation between pressure and temperature fluctuations in the combustor and far field noise. The present research is a continuation of that earlier work.

In the present work we are studying, over a broader operating range, the relative importance of

(a) burning characteristics of the fuel; how burning rate, diffusion rate of the fuel into the air, intensity of combustion, flame distribution and flame roughness affect the noise generated.

*This paper is based on work sponsored by NASA under Grants NGR31-001-241 issued by the Acoustics Division of the Langley Research Center, and Grant NGR31-001-307 issued by the V/STOL and Noise Division of Lewis Research Center.

[1]Research Staff Member

[2]Graduate Student

[3]Professor of Aerospace Propulsion, Principal Investigator

(b) geometrical features of the combustor; effect of fuel injector configuration and type, the method of air admission -- whether swirling, highly turbulent or smooth, stratification of air and fuel and insertion of obstacles to modify the flame.

In addition to the above objectives, we are seeking to develop better means of measuring the important parameters, such as pressure, temperature and velocity fluctuations in the combustor and exhaust flow, and to improve analytical schemes to predict the contribution to far field noise made by these internal sources.

This paper presents some results obtained with several flame holder geometries in which fuel/air mixing was varied by the use of a perforated can burner, a plane, slotted flame holder and a plane slotted flame holder with turning vanes to introduce swirl. Some further interpretations and correlations of internal pressure with far field sound are included. In addition, results of temperature fluctuation measurements and their correlation with far field sound are presented.

FLAME HOLDER GEOMETRY EFFECTS

Details of Combustors

Figure 1 is a schematic of the combustor apparatus showing the perforated can and the plane slotted, swirl vane flame holders. The perforated can was used previously,[1,2] and simply consists of a 2.5" O.D., 13.5" long can concentrically placed within the 3" I.D. main tube with 0.40" diameter perforations beginning about 3.25" from the closed front end where the fuel is injected. Isooctane fuel is injected as a conical spray. Hydrogen and air are injected at the gap of a spark plug which ignites the gaseous mixture which in turn ignites the spray combustion. Recirculation of the secondary air (there is no primary air) which enters through the perforations serves to stabilize the flame reasonably well.

The second configuration shown in Fig. 1 has both primary and secondary air. Primary air enters through the outer 0.2" periphery of the 1.3" diameter inner ring. Fuel is injected through a hole at the center of this inner ring. A second ring, 2.375" O.D., fits around this inner cylinder. In the configuration shown, the inner ring has vanes set at about 60° to the flow axis, which create a clockwise swirl when looking downstream. The outer ring has similar swirl vanes set to generate a counter clockwise swirl. A 2.5" diameter sleeve fits over this assembly which is mounted concentrically within the 3" diameter main combustor tube. The fuel/air mixture is ignited as with the perforated can, but the flame is now stabilized only by the small scale recirculation due to the flow over the sharp edges of the vanes.

A third configuration, not shown in Fig. 1, is geometrically similar to the swirl vane assembly, except that the vanes are simply slotted, and do not cause a swirl. This flame holder was intended to give about the same air flow distribution and similar local recirculation flows around the vanes but without the swirl generated by the above described assembly. With these three flame holders, we can compare the effect of flow distribution, with and without swirl in one of the two flow distributions, to determine whether the

unsteady nature of the combustion region which is responsible for the noise generation, can be significantly altered by these changes.

Roughness Characteristics of Combustors

Figure 2 shows the roughness level of pressure fluctuations in the three combustors for a range of mass flow rates through the system. At the low end of the range of mass flow rates, the can combustor exhibits very rough, intermittent burning, almost to the extent that the flame is blown off. As the flow rate is increased slightly, the combustion becomes smoother in the can combustor, so that at the upper end of the range shown, it has smoother burning than is found in the case with the plane, slotted flame holder. Over this entire range of flow conditions, the plane slotted flame holder with swirl vanes exhibits the smoothest burning of the three. To an observer standing near the combustor, the difference between the swirling combustor noise and the can combustor noise is dramatically different.

Detailed acoustic far field measurements have not been obtained for each of these combustor configurations to date. The spectral content of the flame roughness has, however, been examined, and power spectral density distributions are included here for comparisons.

Figures 3 through 5 show the power spectral density distributions for the three combustor configurations, for the highest flow rate condition shown on Fig. 2. Figure 3 is for the can combustor, and exhibits very strong oscillations at low frequencies. This low frequency rumble was more pronounced at lower flow rates with this combustor, especially at the lowest condition shown on Fig. 2. At that lowest condition, the 164 dB bursts would last for several seconds, then the oscillation would drop to a level of about 145 dB for a second or two, followed by another loud burst, and so on. Clearly, this kind of intermittent, rough burning is not desirable in an aircraft engine combustor. The relatively smoother burning in the other two cases at this low flow rate by comparison with the rough burning case illustrate the big improvements that are possible in terms of noise levels when appropriate changes are made in combustor designs.

Comparisons of Figs. 3, 4, and 5 reveal at least two strong spectral peaks at frequencies above 100 Hz. In Fig. 3 these peaks are at about 150 and 400 Hz, in Fig. 4 they are at about 350 and 550 Hz and in Fig. 5 they occur at about 300 and 475 Hz. These peaks are probably related to duct resonances excited by the unsteady combustion.[3] More detailed measurements of the conditions in the combustor corresponding to each of these cases is needed to explain why these spectral peaks appear at these particular frequencies at these flow conditions.

It is evident from the results obtained with these three combustors, that swirl in the flow is desirable. The swirling promotes better mixing between the fuel and air, resulting in a more smoothly burning flame. Not only does this result in less noise outside the combustion region, but it results in more stable combustion over a broader range of operating conditions.

Far Field Noise Correlation with Chamber Pressure

It was shown earlier[1,2] that there is a strong correlation between the chamber pressure fluctuations and the far field noise, as obtained from real time crosscorrelations. The maximum value obtained for the normalized crosscorrelation coefficient was never more than about 0.7 in spite of the fact that the dominant frequencies in the combustor pressure spectrum also appeared in the far field noise spectrum. One point was noted. In each case, the higher frequency components were relatively stronger in the far field than in the combustor spectrum. This was attributed to the fact that high frequency fluctuations are more efficient sources of noise than are low frequency fluctuations.

This is true, and the reason it is so is that the noise produced is proportional to the time rate of change of velocity of the source, while the velocity at the exit plane is directly related to the chamber pressure. Therefore, a more meaningful correlation is obtained by crosscorrelating the far field sound with the time derivative of the chamber pressure fluctuation. Taking the time derivative of a harmonic function has the effect of multiplying by the angular velocity, thus giving larger contributions at high frequencies, as was observed in experiments. This may be seen in the following.

The far field sound due to the mass flow fluctuation at the nozzle exit plane is, following Curle[4]

$$p_f' \sim \oint_S \frac{\partial}{\partial t}(\rho u)_{exit} \cdot dS \tag{1}$$

and

$$\frac{\partial (\rho u)_{exit}}{\partial t} \sim \frac{\partial p_c}{\partial t} \tag{2}$$

where sub f denotes far field, and sub c the chamber.

This second expression is most accurate for incompressible quasi-steady flow. As compressibility effects become important, the fluctuations in temperature must be incorporated into the analysis. We have examined the effect of temperature fluctuations, as described in the next section. First, however, it is of interest to examine the pressure effect alone.

Figure 6 shows the function obtained by crosscorrelating the time derivative of the chamber pressure with the far field sound, and Fig. 7 shows a similar trace for which the chamber pressure itself was crosscorrelated with the far field sound. Since both are dominated by the 170 Hz narrow band sound, there is little difference between them. Close examination reveals that Fig. 6 has its peak at about 44 msec while Fig. 7 has its peak at about 48 msec. The 44 msec corresponds to the travel time to the far field microphone, 50 ft away. The 48 msec is equivalent to the travel time to 50 ft plus about half a wave length of the dominant signal (its peak is on the negative side while the first has a positive peak) corresponding to a 180° phase shift. Other similar experiments reveal peaks at times close to the correct delay but never as exactly at the correct delay as when the time derivative of the pressure is crosscorrelated with the far field sound. When the normalized crosscorrela-

tion coefficient is obtained, the value for the case in Fig. 6 is 1.01 while that for Fig. 7 is 0.94, again emphasizing the closer correspondence between the far field sound and the time derivative of the chamber pressure than between the far field sound and the chamber pressure directly.

TEMPERATURE FLUCTUATION EFFECTS

It was pointed out in the previous section that in compressible flows, the temperature fluctuation would enter as a parameter affecting noise generation. To obtain meaningful measurements of temperature fluctuations in the combustion gases is considerably more difficult than to obtain pressure fluctuations, as reported earlier.[1] The basic reason for the greater difficulty is the fact that the temperature probe must be immersed in the hot, reacting flow, while the pressure probe can be mounted on the wall where it can be cooled and insulated from the flow.

A hot wire anemometer system in conjunction with a 0.001" diameter platinum wire was used to make the measurements reported herein. The velocity sensitivity of the probe was minimized by maintaining a low probe current (1.5 ma) which kept the wire just above the ambient temperature. Therefore, as the ambient temperature fluctuates, the wire temperature follows, and the anemometer circuit gives an output proportional to wire resistance which is temperature dependent.

Difficulties were encountered due to the high temperature, reactive flow. A metal's strength is generally reduced as its temperature is raised, so although the wire may not melt, it is more easily broken at elevated temperatures. In addition, certain metals such as tungsten catalyze recombination reactions which can result in large errors as the probe temperature is raised, due to additional energy deposition at its surface. Thus, early attempts with tungsten wires yielded unreliable data, and platinum was adopted, in spite of its lower strength.

The maximum temperature recommended for this probe was about 1500°F, which was considerably lower than the mean temperature in previous runs.[1,3] An air/fuel ratio of 70 was adopted for this purpose, which should give a mean temperature of about 1090°F, in the nozzle, but since hot spots can occur in such a system, this seemed a safe condition at which to operate.

The probe used for the temperature measurements was a Thermo Systems Model 1226 High Temperature probe with a 0.001" diameter platinum wire. It was used in conjunction with a TSI Model 1050 Anemometer. The probe was inserted through the nozzle wall so that the wire was held at the duct centerline about 1.25 in. upstream of the nozzle exit. The combustor can configuration, Fig. 1, and a 2" diameter nozzle were used in these experiments.

Spectrum and Level of Temperature Fluctuations

Figure 8 shows the power spectral density of the nozzle temperature fluctuations. A very low frequency fluctuation is dominant with the first peak at 5 Hz, which is the lower limit of the spectral analysis. Relative peaks next occur at 125 and 165 Hz, with a subsequent intensity decrease to the instrumentation noise levels. Figure 9 shows the corresponding far field noise spectrum which exhibits the 165 Hz peak, but does not exhibit the

strong low frequency content seen in the temperature spectrum; instead it shows approximate higher harmonics of the 165 Hz peak. The power spectrum of the temperature signal with low frequencies suppressed by a 100 Hz high pass filter is shown in Fig. 10. The 165 Hz peak is now dominant, with another relative peak at 330 Hz. At frequencies above that peak, the noise level of the electronics is dominant over any temperature signals. This may be expected, since tht thermal time constant of the wire under these operating conditions is about 2.5 msec, having the effect of filtering out frequencies above about 400 Hz. Either the circuitry does not compensate for this decrease of response with increased frequency, or there is negligible fluctuation in temperature above this frequency. Further experiments with smaller wires are required and planned to explore this further.

The absolute, rms level of temperature fluctuation in the 125-160 Hz, 1/3 octave band was measured to be about 12.5 Fahrenheit degrees, or a little more than 1% of the mean temperature. The overall rms temperature fluctuation in the frequency range from 22 Hz to 22 kHz was measured to be about 20% of the mean temperature, with peak to peak variation considerably higher. This large temperature fluctuation level appears to be somewhat characteristic of jet engine combustors, as evidenced by recent measurements, in which rms temperature fluctuations of several hundred degrees have been measured downstream of the combustor in engine tests.[5] The results presented here do not show a strong relationship between this temperature unsteadiness and noise possibly due to crude measurements. Further studies with more refined instrumentation are required to establish its relative importance.

Crosscorrelations of Temperature Fluctuations and Far Field Sound.

Figure 11 shows the cross spectral density of the nozzle temperature fluctuation and the far field sound, for each signal taken directly as recorded. The dominant low frequencies noted in the individual frequency spectra are evident in this cross spectrum. The normalized crosscorrelation coefficient was found to be 0.05 for this case.

It would seem, on comparing Figs. 8 and 9, that the very low frequency (below 100 Hz) temperature fluctuations do not substantially contribute to the far field noise. A second crosscorrelation between these same two signals was obtained, this time with a 100 Hz highpass filter cutting out the low frequency content of each signal. The resulting cross spectral density is shown in Fig. 12. The normalized crosscorrelation coefficient in this case is 0.276, or more than five times as large as for the unfiltered signal. This higher correlation after filtering out the intense fluctuations at ultra low frequencies illustrates that a simple overall crosscorrelation coefficient is not sufficient information to determine the percentage of far field noise which originated at the source being probed.

It is of interest to note further, that these data in which the normalized temperature-far field crosscorrelation coefficient is 0.276 are the same data for which the normalized pressure time derivative-far field sound crosscorrelation coefficient was 1.01, as discussed earlier. This implies that the temperature and pressure fluctuations are related, as was verified by direct crosscorrelations. It further tells us that the normalized crosscorrelation coefficient alone is not sufficient information to use to describe the)

relative importance of various thermodynamic variables in describing the source strength. Before taking the temperature data, it appeared that the time derivative of pressure contained all the necessary information about the source, neglecting compressibility effects. The temperature data has some merits of its own, however, as evidenced by the normalized crosscorrelation coefficient of 0.276. A more complete study of the interrelations of these variables is needed, and how each contributes to the noise must be ascertained. More detailed studies of this are planned.

CONCLUSIONS AND FUTURE PLANS

It has been demonstrated that geometrical changes in the combustor which affect the flame distribution and method of flame stabilization have a pronounced effect on the flame roughness and associated external noise generation. Of the methods examined to date, counter swirling air streams have been found to produce the smoothest combustion. Further probing with pressure and temperature probes in the combustor to learn more about the mechanisms by which these geometric changes affect the combustion roughness are planned.

It has further been demonstrated that the time derivative of the chamber pressure more strongly crosscorrelates with the far field noise than does the chamber pressure directly. This is expected from theoretical considerations. Temperature fluctuations in the exhaust nozzle of the combustion chamber are also found to have a fairly strong crosscorrelation with the far field sound, and with the chamber pressure fluctuations. Further analysis and diagnostic experiments are needed and planned to separate the importance of each of these thermodynamic properties of the source region for the purpose of completely describing the physical processes responsible for sound generation by a region of unsteady combustion and its exhaust flow.

References

1. Abdelhamid, A. N., Harrje, D. T., Plett, E. G. and Summerfield, M., "Noise Characteristics of Combustion Augmented Jets at Midsubsonic Speeds," AIAA J., 12, 336-392 (1974).

2. Plett, E. G., Abdelhamid, A. N., Harrje, D. T. and Summerfield, M., "Combustion Contribution to Noise in Jet Engines," Final Report on NASA Grant NGR31-001-241, Princeton University, Princeton, New Jersey (1974).

3. Chiu, H. H., Plett, E. G. and Summerfield, M., "Noise Generation by Ducted Combustion Systems," AIAA Paper No. 73-1024, October, 1973.

4. Curle, N., "The Influence of Solid Boundaries Upon Aerodynamic Sound," Proc. Roy. Soc., Vol. 231A, 505-514 (1955).

5. Mathews, D. C., Private Communication, Pratt and Whitney Aircraft, East Hartford, Conn. (1973).

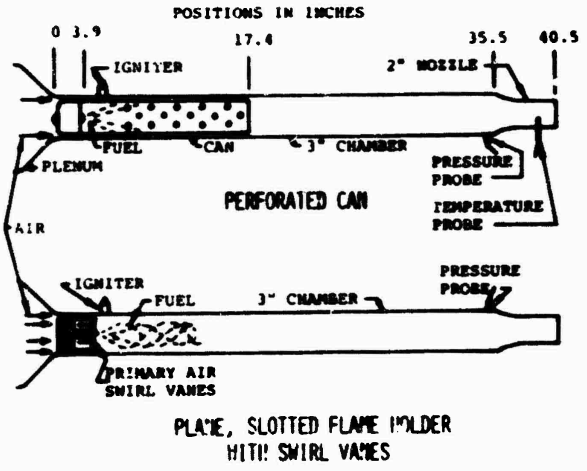

Fig. 1 Schematic of flame holding methods used in combustors to investigate effects of geometry and flame intensity on combustion roughness.

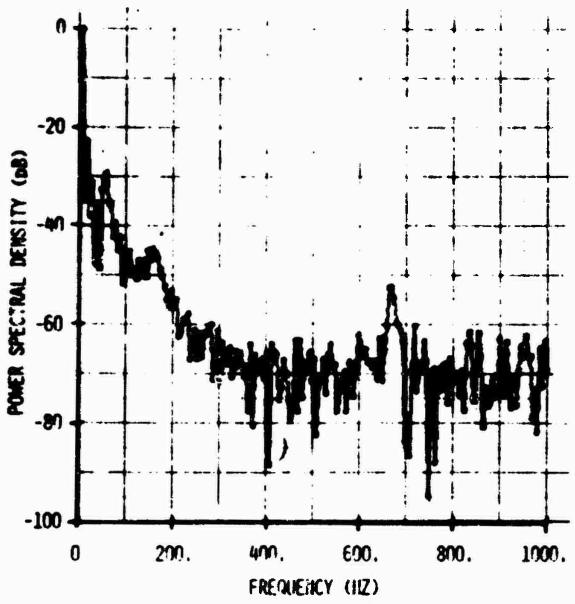

Fig. 3 Power spectral density distribution of pressure fluctuation in combustor with perforated can flame holder at a mass flow rate of 0.27 lb/sec.

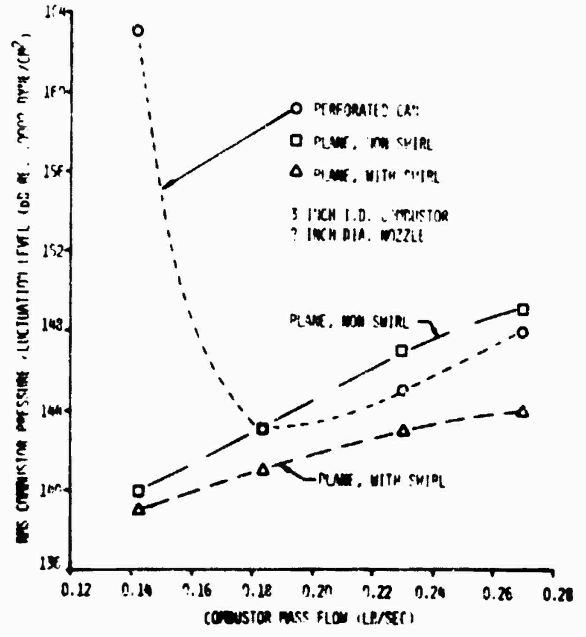

Fig. 2 Pressure fluctuation levels in combustors for a range of mass flow rates, with air/fuel ratios of 52.

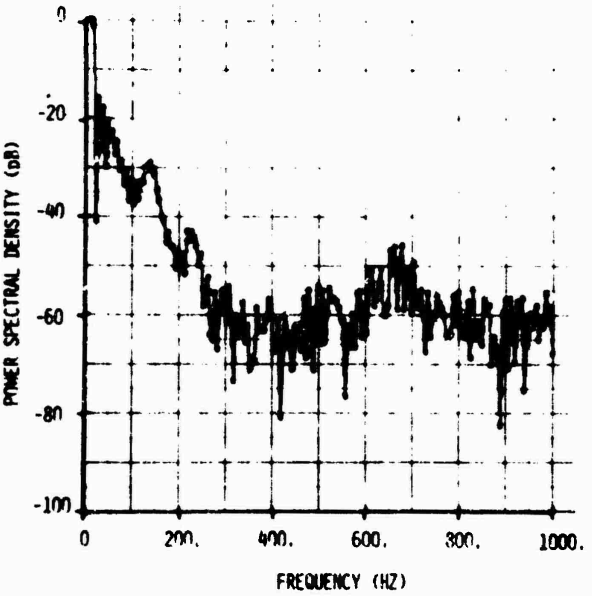

Fig. 4 Power spectral density distribution of pressure fluctuation in combustor with plane, slotted flame holder at a mass flow rate of 0.27 lb/sec.

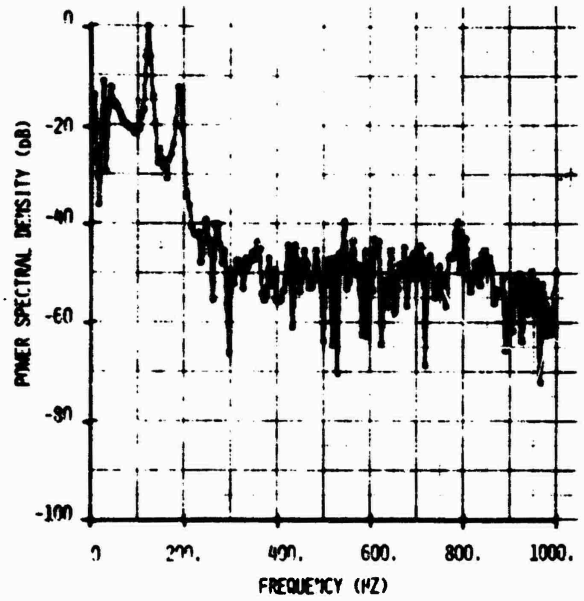

Fig. 5 Power spectral density distribution of pressure fluctuation in combustor with plane, slotted flame holder with swirl vanes, at a mass flow rate of 0.27 lb/sec

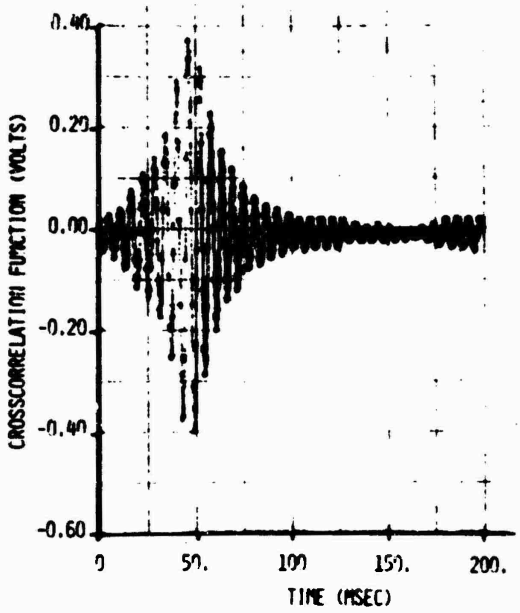

Fig. 7 Crosscorrelation of chamber pressure with far field sound at 30° to duct axis.

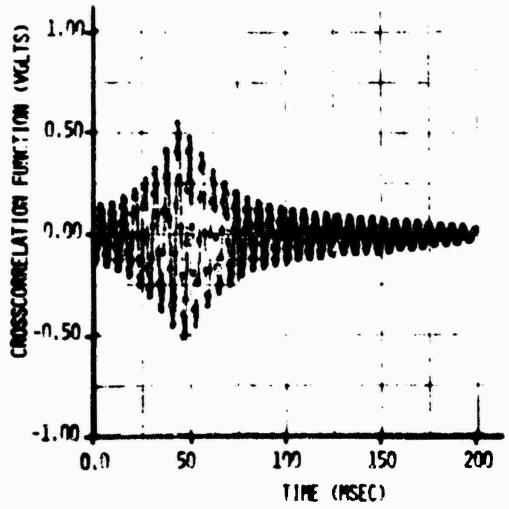

Fig. 6 Crosscorrelation of time derivative of chamber pressure with far field sound at 30° to duct axis.

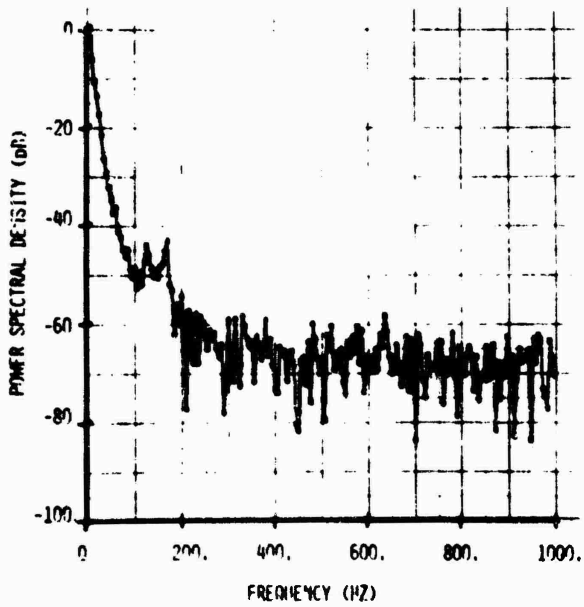

Fig. 3 Power spectral density distribution of the temperature fluctuation in the exhaust nozzle.

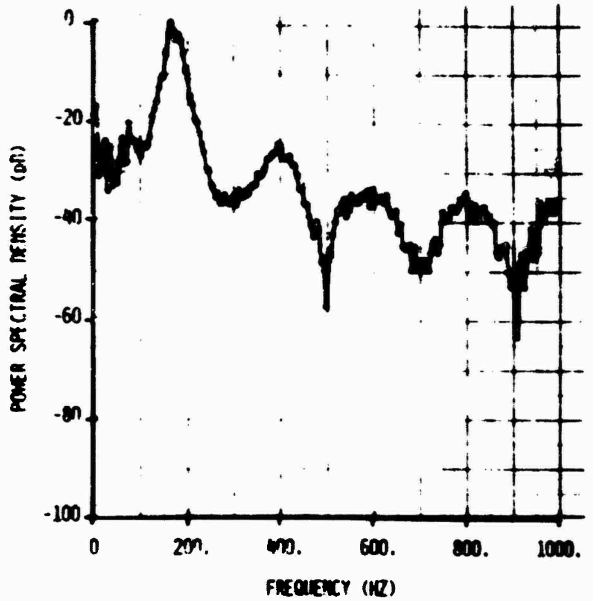

Fig. 9 Far field noise power spectral density for same case as in Fig. 8, for microphone at 60° to duct axis.

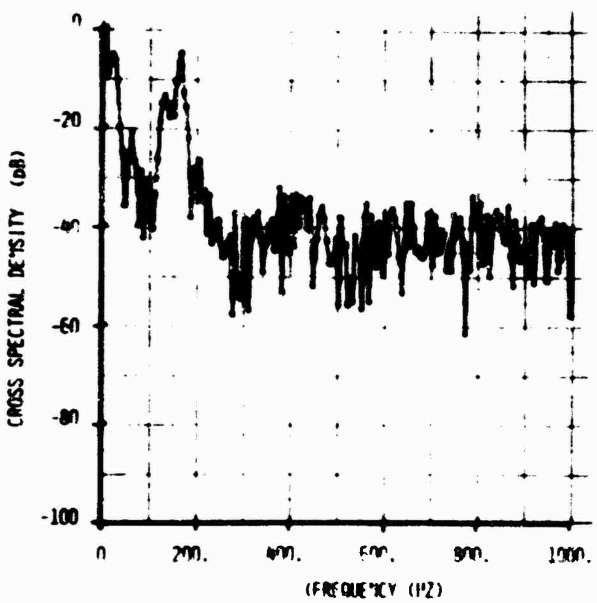

Fig. 11 Cross spectral density of nozzle temperature fluctuation and far field noise at 60° to duct axis.

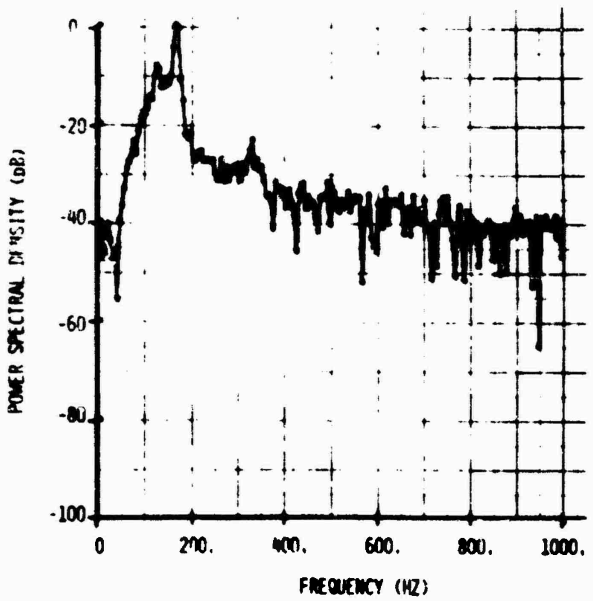

Fig. 10 Power spectral density of temperature, as Fig. 8 except that a 100 Hz highpass filter reduced the low frequency content in this record.

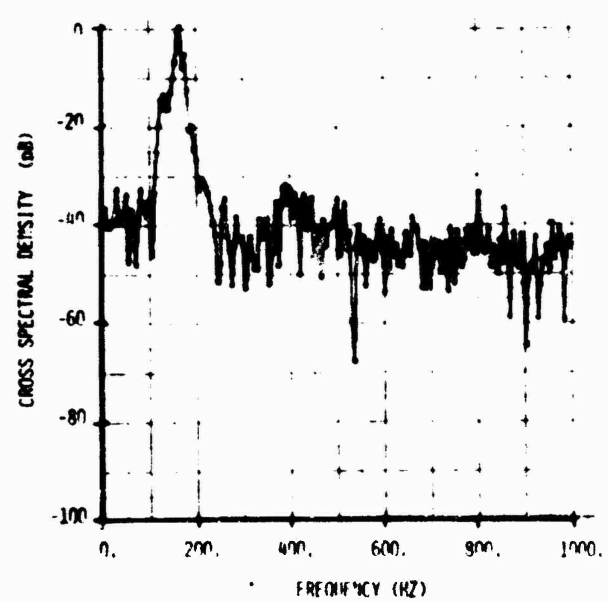

Fig. 12 Cross spectral density of nozzle temperature fluctuation and far field noise at 60° to duct axis, with 100 Hz highpass on each signal.

COMBUSTION NOISE THEORY*

by

H. H. Chiu,[1] and M. Summerfield[2]

Guggenheim Aerospace Propulsion Laboratories
Aerospace and Mechanical Sciences Department
Princeton University
Princeton, New Jersey

ABSTRACT

Mechanisms of sound generation, amplification and scattering by various combustion systems are described on theoretical bases compatible with the contemporary understanding of unsteady burning processes. Sound generation mechanisms are classified into categories relating to the Smith-Kilham emission mechanism and the turbulent driven Rijke-Riess emission mechanism. The intensity of the generated sound is found to be proportional to the combustion sound number and the flame structural factor which depend on detailed structure of a flame. Experimental correlation of the intensities of the sound emitted and the light radiated from free radicals is also discussed. Analytical and experimental investigations revealed that the noise generation by ducted burners depends on the nature of the rough burning and the duct resonance which is identified as the source of the observed multiple peak structure in sound spectra. Interactions within the flow through the combustor-turbomachinery components within a gas turbine are predicted to produce similar multiple peak noise spectra. Scattering of the plane sound wave by a flame is also discussed. Quantitative correlations between the intensity of the scattered sound wave and the physical parameters of the flame are obtained.

INTRODUCTION

Current interest in combustion noise has focused our attention on the mechanisms of sound emission and amplification by various combustion systems operating at different conditions. Earlier investigations[1-4] were largely concerned with the overall physical description of the acoustic properties of combustion systems aimed at providing quantitative links between the combustion system and its sound field. The results of these earlier investigations furnished a physical basis for the understanding of combustion noise. Further extensions have been made to investigate the effect of coupling of flow and chemical reaction to allow predictions to be made about noise generated by combustors in jet engines.

In a jet engine combustor, the fluid mechanical processes which have a high intensity of turbulence at a high mean convective speed, are expected to

*This paper is based on research performed under contract N00014-67-A-0151-0029 issued by the Power Branch of the Office of Naval Research

[1]Research Scientist

[2]Professor of Aerospace Propulsion

alter the nature of the sound emission and the resulting acoustic power. Consequently these fluid mechanical aspects need be taken into consideration along with other factors such as the effect of the flame enclosure. Recent studies on sound emissions by open flames [5-9,11] and ducted flames[10-13] accomodate these aspects.

The present paper summarizes the mechanisms of sound emission by open flames, liquid fuel spray combustion processes and by the combustion in a ducted system. Attention has been focused upon (1) the quantitative correlation between the flame structure and the sound field of an open flame and (2) the prediction of the sound field produced by turbulent combustion confined in a cylindrical duct. The experimental correlation between the spectra of emitted sound and the radiation of light from radicals in the flame zone has been discussed and a modified correlation is suggested. In addition, some aspects of sound scattering and amplification by temperature gradients due to combustion are also discussed on the basis of Born's approximate solutions.[14]

SOUND EMISSION BY COMBUSTION PROCESSES

Within a turbulent reaction zone there are three unsteady modes; the turbulent vortex mode, a sound mode and an entropy mode which are aerothermochemically coupled. It has been shown that the behavior of these modes may be described by the following system of equations:

$$\nabla^2\phi = -\frac{1}{\gamma}\frac{D\Omega}{D\tau} + \Lambda\frac{\dot{Q}}{\bar{\rho}} \tag{1}$$

$$\frac{D\vec{W}}{D\tau} = -\frac{1}{\gamma M^2}\frac{\nabla p}{\bar{\rho}} - \frac{D}{D\tau}(\nabla\phi) \tag{2}$$

$$\frac{D\Omega}{D\tau} = \gamma\frac{D\sigma}{D\tau} + \gamma\Lambda\frac{\dot{Q}}{\bar{\rho}} \tag{3}$$

$$\bar{\rho}\frac{DY_i}{D\tau} = \frac{C_p T_1}{\Delta H}\omega_i \tag{4}$$

where $\Omega = \ln p/p_1$, $\sigma = \ln \rho/\rho_1$, $\Lambda = \frac{\Delta H}{C_p T_1}\left(\frac{\omega_1 l_f}{\rho_1 U_1}\right)$, ω_i is the rate of the reaction of i th speicies, ϕ is the velocity potential of the perturbative solenoidal velocity component, $\vec{W}$ is the rotational field, $\dot{Q}$ is the rate of the heat release by chemical reaction, M is the Mach number, and Λ is the Damköhler number. The wave equation governing the sound field is derived from the system of equations (1) to (4), and is given by

$$M^2\frac{\partial^2\Omega}{D\tau^2} - \frac{\partial}{\partial x_i}\left(a_j^2\frac{\partial\Omega}{\partial x_i}\right) = \gamma M^2\frac{\partial u_i}{\partial x_j}\frac{\partial u_j}{\partial x_i} + \gamma\Lambda M^2\frac{D}{D\tau}\left(\frac{\rho_0}{\bar{\rho}}\dot{Q}\right) \tag{5}$$

where

$$\dot{Q} = \Sigma\omega_i h_i + \frac{\partial}{\partial x_i}K\frac{\partial\theta}{\partial x_i} + \Phi$$

and h_i is the heat of formation of ith species, θ is the non-dimensional temperature, K is the non-dimensional turbulent heat conductivity, and Φ represents other heat sources. The convected wave equation describes the acoustic field

produced by convected noise sources. This equation has been previously applied to the investigation of the noise generated by turbulent eddies, and by turbulent combustion processes. An alternate approach to the analytical investigation of sound generation is to use Lighthill's formulation:[5]

$$\frac{1}{a_\infty^2}\frac{\partial^2 p'}{\partial \tau^2} - \frac{\partial^2 p'}{\partial x_i^2} = q'(x_i, t) \tag{6}$$

where p' is the pressure and a_∞ is the reference speed of sound. It should be emphasized that the overall sound source, $q(x_i,t)$, appearing on the right side of Eq. (6), includes all sound generating mechanisms and must account for the effect of convection as well as refraction of sound in the flow. Despite its apparent simplicity in form, its solution involves determining appropriate source terms $q(x_i,t)$ which account for the turbulent convection and dispersion in a non-isentropic regime which is often quite complicated.

An analytical procedure useful in identifying appropriate noise sources in the presence of convection is to apply the following transformation to the convected wave equation (5)

$$\frac{\partial}{\partial \tau} = \frac{\partial}{\partial \tau} + \bar{u}\frac{\partial}{\partial x} \qquad \frac{\partial}{\partial x_i'} = \frac{\partial}{\partial x_i} \tag{7a}$$

$$\tau = \tau' - \int \frac{dx'}{\bar{u}} \qquad x_i = x_i' \tag{7b}$$

where $\bar{u}$ is the mean velocity and X is the coordinate along the stream line direction. It is evident that in the frame of reference moving with mean velocity, $\bar{u}$, along the stream line, the wave equation (5) is reduced to the following form

$$M^2\frac{\partial^2 \rho'}{\partial \tau'^2} - \frac{\partial}{\partial x_i'}\left(a_\infty^2\frac{\partial \rho'}{\partial x_i'}\right) = \gamma M^2\left(\frac{\partial \dot{Q}'}{\partial \tau'} + u_i'\frac{\partial \bar{\dot{Q}}}{\partial x_i'}\right) - \gamma M^2 \bar{\dot{Q}}\frac{\partial \rho'}{\partial \tau'} \tag{8}$$

where primed quantities refer to fluctuating flow variables. The effect of mean convection is removed and the essential sound generation mechanisms are now self evident. The first term which appears at the right hand side of Eq. (8), i.e. $\partial \dot{Q}'/\partial \tau'$ is the source of combustion noise due to the temporal variation of heat release of the hot reacting spots convected with the mean stream. This sound source, $\partial \dot{Q}'/\partial \tau'$ corresponds to the monopole sound source described by Smith and Kilham in their modeling of combustion noise, and is therefore termed as the Smith-Kilham sound source. The order of magnitude of the frequencies of the S-K sound field is, to a large extent, determined by the chemical reaction times. The second term which appears at the right hand side of Eq. (8) represents the sound generation by a fluctuating flow passing through the reacting spots. The sound emission by a similar process was demonstrated by Rijke and Riess.[15] In their experiment, the fluctuating velocity field was an acoustically induced periodic flow which was amplified by a properly tuned duct. In an open flame, however, the velocity u' appearing in Eq. (8) is that provoked by turbulent fluctuations. Despite this difference in the driving velocity fields between the present case and Rijke's experiment, the basic mechanisms of the local emission remain essentially the same. Hence, we shall refer to this sound source as the turbulent driven Rijke-Riess noise source. It is evident that the frequencies of the sound emitted by the turbulent driven R-R mechanism are determined primarily by the frequencies of the turbulent fluctuations. The third term represents the amplification of the sound waves passing through

the flame zone. It has been known for some time that a laminar flame, which itself does not generate sound, will amplify sound. While the sound emission by the first and second mechanisms previously described are the dominant mechanisms of combustion noise generation, at least for low subsonic Mach numbers, the effects of the sound amplification by combustion in high speed flows through primary combustion chambers or afterburners are not well understood.

Making a distinction between these two mechanisms of sound emission and sound amplification is useful for the purpose of describing the nature of the sound generation. It is, however, difficult to distinguish between them in practical combustion processes unless special experimental techniques are designed for such a purpose.

SOUND FIELD GENERATED BY OPEN FLAMES

The detailed mechanism of sound emission by the S-K monopole sound source, and turbulent driven R-R sound sources follow similar gasdynamic processes which are described in the following. Firstly, the gas in the vicinity of S-K and R-R sources is heated periodically resulting in local gas expansion and compression. At a low Mach number the fractional variation of the density by the non-isentropic heating processes is proportional to the Damköhler number which represents the ratio of the chemical heat release to the heat convection. Since the fractional variation in the gas density is equal to the negative of the dilatation of the induced gas motion, the magnitude of the velocity induced is equal to Λ and the amplitude of the corresponding pressure wave is equal to $M^2 \Lambda$. In view of this physical significance we shall refer to $M^2 \Lambda$ as combustion sound number, C_s.

The combustion sound number[11] is given explicitly as follows:

$$C_s = \Lambda M^2 = \left(\frac{\Delta H}{c_p T_1}\right)\left(\frac{\omega_1 \ell_f}{\rho_1 U_1}\right)\left(\frac{U_1}{a_1}\right)^2 \qquad (9)$$

the total sound emitted by a flame is therefore proportional to the combustion sound number times the total volume of the flame and the flame structural factor which is to be discussed later.

In a hot non-reacting zone, the turbulent heat transport may also generate sound by both S-K and turbulent driven R-R mechanisms. The non-dimensional parameter C_K representing the intensity of the sound generation is given by:

$$C_K = \frac{M^2}{Re_K Pr_T} = \left(\frac{\nu_T}{\ell_K U_1}\right)\left(\frac{K_T}{c_p \mu_T}\right)\left(\frac{U_1}{a_1}\right)^2 \qquad (10)$$

where ν_t is the turbulent diffusivity, K_t is the turbulent heat conductivity, l_k is the size of a typical thermal eddy. The ratio of the combustion noise to that of the thermal noise emitted by a flame is thus given by

$$\epsilon = (\Lambda Re_K Pr_T) V_f / V_K \qquad (11)$$

where V_f and V_k are the volumes of the reacting zone and that of the hot zone dominated by thermal eddies. The pressure waves generated within the combustion zone, the dimensions of which are smaller than acoustic wave lengths, are identified as pseudosound waves[11]. The thermoacoustic efficiency of generation of the pseudosound waves was found, in general to be lower than the efficiency

of generation of true sound waves in a ducted burner of larger dimensions. These sound waves generated within the combustion zone are transmitted through the non-isothermal wake and finally propagate in free space as true sound waves, Fig. (1).

An asymptotic analysis of sound generation and transmission in the reaction zone, thermal wake, and wave zone revealed that the far field sound pressure is given by the following expression[11]

$$p' = \frac{1}{4\pi R}\left\{\frac{\gamma C_s}{C_k}\right\}\left(\frac{A_1}{\lambda_\infty}\right)^2 \iiint \frac{1}{A^2}\left\{ \frac{\bar{D}}{D\tau}\left[\begin{matrix}\dot{Q}_s' \\ \dot{q}_k'\end{matrix}\right] + \left(u' - \frac{\theta'}{\bar{\theta}}\bar{u}\right)_i \frac{\partial}{\partial y_i}\left[\begin{matrix}\dot{\bar{Q}}_c \\ \dot{\bar{Q}}_k\end{matrix}\right]\right\} dV(\eta) \qquad (12)$$

Smith-Kilham Emission Mechanism — Turbulent Dirven Pijke-Riess Emission Mechanism

where $\dot{Q}_c'$ is the fluctuating heat release due to the convecting parcels, $\dot{\bar{Q}}_c$ is the steady heat release rate, $\dot{Q}_k'$, and $\dot{\bar{Q}}_k$ are the similar heat sources due to turbulent heat transport.

The far field sound intensity due to combustion noise is calculated to be

$$I = \frac{\gamma^2 C_i^2}{16\pi^2 \bar{T}_\infty Q^2 R^2}\left(\frac{A_1}{\lambda_\infty}\right)^4 \left\{ R_{SK} + R_{RR} + R_{SK-RR} \right\} \qquad (13)$$

where R_{ij} is refered to as a flame structural factor, given by

$$R_{ij} = \int_{V(\alpha)} \int_{V(\beta)} \bar{S}_{ij}(\alpha,\beta)\, dV(\alpha)\, dV(\beta) \qquad (14a)$$

α and β denote the positions of two correlation volume elements. The integrands $S_{ij}(\alpha,\beta)$ are

$$S_{SK} = \frac{1}{A^2} \frac{\bar{D}\dot{q}'(\alpha)}{D\tau} \frac{\bar{D}\dot{q}'(\beta)}{D\tau} \qquad (14b)$$

$$S_{RR} = \frac{1}{A^2}\left[u_i'(\alpha) - \frac{\theta'(\alpha)}{\bar{\theta}(\alpha)}\bar{u}_i(\alpha)\right]\left[u_j'(\beta) - \frac{\theta'(\beta)}{\bar{\theta}(\beta)}\bar{u}_j(\beta)\right] \frac{\partial \dot{\bar{Q}}(\alpha)}{\partial y_i} \frac{\partial \dot{\bar{Q}}(\beta)}{\partial y_j} \qquad (14c)$$

$$S_{SK-RR} = \frac{2}{A^2}\left[u_i'(\alpha) - \frac{\theta'(\alpha)}{\bar{\theta}(\alpha)}\bar{u}_i(\alpha)\right] \frac{\partial \dot{\bar{Q}}(\alpha)}{\partial y_i} \frac{D\dot{q}'(\beta)}{D\tau} \qquad (14d)$$

R_{SK} is the structural factor for S-K emission mechanism, R_{RR} is that due to R-R mechanisms and R_{SK-RR} is attributed to the combination of the S-K and R-R mechanisms.

The central problem of predicting the intensity of flame noise lies in the determination of the double correlation functions, R_{ij}, which depend on the non-steady structure of turbulent flames.

CORRELATION OF THE SOUND PRESSURE AND THE EMISSION OF LIGHT BY FREE RADICALS

Structural surveys of turbulent flames through the measurement of radiation emitted by free radicals which serve as diagnostic tracers, have been conducted by various authors[16,17] during past decades. One such optical technique was adopted by Smith and Kilham for the purpose of studying the relationship between sound emission and the radiation emitted by free radicals produced in the combustion zone. The experimental investigation was further advanced by a group at Shell Research,[2] and more recently by Strahle and his associates.[3]

Their results reveal that the sound pressure vs time curves agree reasonably well with the corresponding time rate of change of the radiative intensity, but the frequency spectra of measured and derived sound pressures may differ by factors of 2 to 3 in some frequency intervals, even after the measured radiation spectra are corrected for electronic noise contributed by the measuring circuitry. It should be pointed out that in these experiments the sound pressure is compared with the rate of the change of the intensity of the light emitted measured by a stationary observer. In the above experiments the effects of the non-steady convection of the reacting spots were not detected by light emission from free radicals. A modified quantitative correlation between sound pressure and the radiation spectra, can be obtained from the results of the present analysis. It will be shown that this modified view point provides proper correlation and also suggests a practical method for the classification of flames according to their turbulent structure. This is described in the following.

In general the rate of fluctuation of the local heat release rate, $\dot{Q}$, and the intensity of the light emission, J, are related by

$$\dot{Q} = \frac{W}{\Pi} J \tag{15}$$

where W and Π are the non-dimensional rate of heat release[15] and the rate of production of free radicals respectively. Note that W/Π is not necessarily constant, but depends, in general, on both x and t. Substituting Eq. (15) into Eq. (12) yields

$$P \simeq \frac{\rho\gamma c_s}{4\pi R_0} \iiint \frac{1}{R^2}\left\{\alpha \frac{\partial J}{\partial \tau} + \left(\frac{W}{\Pi} - \alpha\right)\frac{\partial J}{\partial \tau} + \left[\frac{R}{c_s}\left(\frac{W}{\Pi}\right)\right] J\right\} dV \tag{16a}$$

or

$$P_\omega \simeq P_{i_\omega} + \frac{\rho\gamma c_s}{4\pi} \iiint \frac{1}{R^2}\left\{\alpha u_r \frac{\partial J_\omega}{\partial r} + \left(\frac{W}{\Pi} - \alpha\right)\frac{\partial J_\omega}{\partial \tau} + \left[\frac{R}{c_s}\left(\frac{W}{\Pi}\right)\right] J_\omega\right\} dV \tag{16b}$$

where

$$P_{i_\omega} \simeq \frac{\rho\gamma c_s}{4\pi} \iiint \frac{\alpha}{R^2} \frac{\partial J_\omega}{\partial \tau} dV \qquad \rho \simeq (A_1/A_\omega)^2 \tag{16c}$$

α is an appropriate constant proportionality factor determined from experimental observations. The physical significance of each term appearing in the integrand of Eq. (16b) is described as follows. The second and third terms represent the deviation from the presumed proportionality between the rate of production of the free radicals and the overall heat release rate. The magnitudes of these terms depend primarily on the equivalence ratio. The first term represents the effects of convection of reacting spots and the turbulent driven R-F sound emission. The magnitude of this term depends on the sizes and frequencies of the reacting hot spots and of the turbulent eddies.

Appropriate non-dimensionalization reveals that the order of magnitude of this term is proportional to the non-dimensional parameter ($K = U'l_t/S_L$), proposed by Kovasznay[18], and is also equal to the ratio of two characteristic times $\tau = \tau_{chem}/\tau_{mix}$ defined by John and Summerfield.[17] Large values of K or τ could lead to the break up of the flame, i.e. distributed reaction model[18], whereas lower values of K or τ would lead to a continuous wrinkled laminar flame.

This indicates, that for a flame with a large value of K or τ, the sound spectra should correlate with P_{i_ω} plus the first term appearing in the integrand of Eq. (16b) which represents the convection of reacting spots. If K is of the

order of unity, the above additional term is the same order of magnitude as the F_{jw}. This may account for the difference in the sound intensity spectrum and the light emission spectrum. On the other hand, for a flame with small K or J number, the sound spectrum should correlate well with light intensity spectrum. This suggest that by comparing the spectra of the sound intensity and the light intensity, it may be possible to determine the nature of the combustion in a turbulent flame. When the two spectra show a high degree of correlation the combustion regime is that of the wrinkled laminar flame. Lack of correlation of the two spectra would indicate that the flame is dominated by small scale turbulence and the combustion is in the distributed reaction regime. Confirmation of this conjecture will require detailed measurements of time and space distribution of the light intensity emitted from all parts of the flame.

SOUND GENERATION BY LIQUID FUEL SPRAY COMBUSTION

The process of sound generation by liquid fuel spray combustion is of practical interest in view of the wide application of spray combustors. Analysis of this problem is complicated by various non-steady processes associated with many-particle statistics, and turbulent two phase interactions involving the exchange of the mass, momentum and energy. It can be shown from the convected wave equation applied to liquid spray combustion, that the sound pressure generated by such a non-steady burning process is given by

$$p' \simeq \frac{\gamma \Lambda M^2}{4\pi r} \iiint \left\{ \frac{\bar{f}}{\bar{\rho}} \bar{\phi} \left(\frac{D\dot{M}'}{Dt} + \frac{D'\dot{\bar{M}}}{Dt} \right) + \frac{\bar{\phi}}{\bar{\rho}} \dot{\bar{M}} \left[\left(\frac{Df'}{Dt} + \frac{D'\bar{f}}{Dt} \right) - \frac{\bar{f}}{\bar{\rho}} \left(\frac{D\rho'}{Dt} + \frac{D'\bar{\rho}}{Dt} \right) \right] \right.$$

$$\left. + \frac{\bar{f}}{\bar{\rho}} \dot{\bar{M}} (\bar{\phi} - 1) \left(\frac{D\theta'}{Dt} + \frac{D'\bar{\theta}}{Dt} \right) \right\} dV \qquad (17)$$

where $\phi = 1 + \frac{L}{\Delta H} \frac{\bar{\theta}_1}{\theta_1} + \frac{c_p T_1}{\Delta H} \bar{\theta}_1$, $f = n/N_0$, $M^2 \Lambda = \frac{\dot{M}_0 \bar{m}_0}{\rho_1} \frac{\Delta \gamma}{c_p T_1} \left(\frac{u_1}{a_1} \right)^2$

$\dot{M}_0$ is the reference burning rate of a droplet, $\dot{m}$ is the fluctuating burning rate, f' is the fluctuation in the droplet number density, L is the latent heat of vaporization.

Evaluation of the contribution by sound sources that appear in the above equation requires detailed knowledge of the gas and liquid phases. It appears that the phenomenological model based on the distributed droplet combustion provides a relationship between the droplet parameters and the emitted sound. To this end the experimentally obtained droplet burning law is used to evaluate the rate of combustion. By assuming a droplet size vs time relation to be $d^2 = 1 - t$, the sound intensity due to combustion of a spray of uniform sized liquid droplets may be expressed by

$$I = \frac{(\gamma - 1)^2 (N_0 m_0 \Delta H)^2}{64 \pi^2 \rho_0 a_\infty h^2} \left(\frac{B}{a_\infty \tau_{life}} \right)^{\alpha} g^2 \phi^2 \qquad (18)$$

where h is the characteristic dimension of the combustion zone, V is the total volume of the flame, g is a statistical factor τ_{life} is the mean life-time and M_0 is the mass of the liquid droplet. This relation is valid when τ_{life} is greater than the characteristic time for the reaction of the gas phase.

NOISE GENERATION BY DUCTED COMBUSTORS

Recent studies of the noise generation in ducted burners reported by the Princeton group[10] revealed a good correlation at low frequencies (10-1000 H_z) between the sound spectra recorded by pressure generated by the non-steady combustion, and the sound spectra recorded in far field. Furthermore, it was disclosed that unlike the sound spectrum that pertains to an open flame, the sound spectra generated by a ducted burner revealed a multiple peak structure at certain frequency intervals. This was subsequently identified by Chiu et al. as oscillations occurring at some resonant frequency and its harmonics, which depend on the geometry and the aeroacoustic parameters of the duct. This aspect was verified by comparing the critical frequencies predicted by theory with experimentally observed frequencies for ducts of different length. This section describes the essential factors contributing to duct noise generation and the features of their sound spectra.

For a cylindrical duct combustor with radius, R, axial length, L, and the combustion zone extending from X = 0 to X = L_F, (shown in Fig. 2) the solutions of the wave equations in two zones are obtained by standard mathematical procedures. The sound waves consist of axial, radial and circumferential modes, as ordinary duct acoustic modes. The sound pressure in the far field can be calculated from the velocity or pressure fluctuation at the exit plane and it is given by the following expression

$$P_{nm} \simeq -\frac{1}{\phi \pi k_{nm}} \iiint \frac{\rho_E}{\Sigma_{nm}} \frac{\bar{\rho}_E}{r} \int^{\infty} (1 + \frac{\bar{u}_E}{a \bar{\rho}_E} Z_{\omega E}) D_{nm}(t,\theta) \dot{Q}_{nm} \, dS_E \, d\omega \qquad (19)$$

where subscript E refers to the properties measured at the exit plane of the duct, $Z_{\omega E}$ is the acoustic impedance, subscript n, represents circumferential mode numbers and m radial mode numbers. The quantity D_{nm} is termed the duct noise factor representing the exit plane pressure induced by a non-steady heat source of unit strength in the burning zone, i.e.

$$D_{nm\omega} = \frac{-i}{\Delta} \left\{ \frac{\pi \Lambda [\omega - M\lambda(1-M^2)^{\frac{1}{2}}]}{k_{nm}^2 - (\lambda_{nm} - \beta)^2} \right\} \left\{ a_{nm} e^{i(\phi + k_{nm})L} + b_{nm} e^{i(\phi - k_{nm})L} \right\} e^{in\theta} J_n(k_{nm} \Lambda) \qquad (20)$$

where K_{nm}, is the axial mode number $\beta = M\omega/(1 - M^2)^{\frac{1}{2}}$ $\dot{Q}_{nm}$ is the amplitude of the fluctuating heat release given by

$$\dot{Q}_{nm\omega} = \frac{1}{2\pi \Lambda_{nm}} \int_0^{2\pi} \int_0^1 \dot{Q}'_{\omega}(\vec{r}) J_n(k_{nm} \lambda) e^{in\theta'} \, d\lambda' \, d\theta' \qquad (21)$$

a_{nm} and b_{nm} are constants depending on L, L_F and other parameters. The duct noise factor D_{nm} has a significant feature described in the following.

Observation of Eq. (20) reveals that the duct noise factor becomes infinity when $\Delta = 0$. This physically corresponds to the duct resonance, which occurs if the duct length is equal to the critical length determined by the following expression[11]

$$L_{cr} = (N + \tfrac{1}{2}) \frac{\pi}{k_{nm}} - \frac{i}{k_{nm}} \tan^{-1} \left[\frac{I\psi_{nm}}{R\psi_{nm}} \right] \qquad (22)$$

where N is an integer, $I\psi_{nm}$ and $R\psi_{nm}$ are the imaginary and real parts of the function ψ_{nm}, given by

$$\psi_{nm} = -\frac{(1 - Z_{\omega E} M^-_{nm})(1 - Z_{\omega E} M^+_{nm})}{(1 - Z_{\omega E} M^+_{nm})(1 - Z_{\omega E} M^-_{nm})} \qquad (23)$$

and $$\mathcal{M}_{nm}^{\pm} = a(\beta \pm K_{nm})\{\gamma M[n\omega(1-M^2)^{\frac{1}{2}} - (\beta \pm K_{nm})M]\}^{-1}$$

It is evident that for a duct open on one end and closed on the other end i.e. $Z_{\omega I} = \infty$, $Z_{\omega E} = 0$, the first critical length L_{cr} for $N = 0$, is equal to the quater wave length. For $N \geq 1$, Eq. (22) gives the critical length of higher harmonics. For a finite terminal acoustic impedance, $Z_{\omega E}$, taken to be that given for unflanged ducts, natural frequencies for resonant ascillation at various duct length L/R can be computed. The result of such computations have been compared with a series of ducted burner experiments, as shown in Fig. 3 . It may be pointed out that the frequency of the first peak falls between the values obtained for an open and closed inlet. This is physically expected because the inlet of the duct used in the experiments was partially closed.

For a burning zone length of approximately 5 times the radius of the duct and with the non-steady heat release spectrum shown in the inset of Fig. 3, the sound spectra invariably exhibit multiple peak structure irrespective of the shape of the combustion spectra. Qualitative agreement between the analytical predictions and experimental observations are quite good, Figs. 4 and 5.

What has been discussed above has been based on the assumption that the size of the fluctuating reacting spot is substantially different from the acoustic wave length of the corresponding acoustic wave mode. If the sizes of the reacting spots are comparable to that of the sound wave length the acoustic oscillation is enhanced. The phenomonon may be classified as an acoustic modal instability by which the thermal energy contained in the reacting gas pockets is completely deposited into a whole sound wave. This direct energy transfer into true acoustic waves results in higher thermoacoustic efficiencies than in the case of energy transport into a pseudosound wave.

The pressure waves in a duct include propagating and non-propagating modes. The propagating mode includes plane waves at any frequency and spinning waves at frequencies above the critical frequency, $f_{nm_{cr}}$ given by

$$f_{nm_{cr}} = (1-M^2)^{\frac{1}{2}} K_{nm} a / 2\pi R \qquad (24)$$

Waves at frequencies below the cut-off value cease to propagate but decay exponentially along the duct.

In the theory just discussed, neither acoustic damping mechanisms nor nonlinear effects are considered. Furthermore, the response of the burning rate to the pressure or combustion instability and its effects on the duct noise emission are not completely understood to date.

SOUND GENERATION BY TURBO-MACHINERY - COMBUSTION SYSTEMS

The assembly of components such as in a turbojet engine generate sounds by various means. The sound spectrum of rotating machinery is composed of a background of white noise with tones superposed at discrete frequencies, corresponding to the blade passing frequency. When these sound waves pass through the combustion chamber, they may interact with combustion processes and thus further generate what has been termed combustion noise.

It is expected that the sound generated by such a system can be described in terms of engine parameters, such as tangentical and axial forces generated by the fan, compressor and turbine and the fluctuating heat release rate in the combustion chamber. By assuming that the compressor, combustion chamber and turbine are located as shown in Fig. 6, one may solve the wave equations with appropriate boundary conditions at the interface between the rotating machinery and the burning zone. For example, the boundary conditions at the compressor are the system of conservation laws including mass and momentum equations. Detailed analysis reveals that the pressure fluctuation at the end of the duct can be represented by the following expression[12]

$$p'_{nm} = \Delta_T^{-1} \Sigma \left[D_{nm} \dot{Q}'_{nm} + G_{nm,x} f^{(c)}_{nm,x} + G_{nm,\theta} f^{(c)}_{nm,\theta} + \mathcal{T}_{nm,x} f^{(T)}_{nm,x} + \mathcal{T}_{nm,\theta} f^{(T)}_{nm,\theta} \right] \tag{25}$$

where D_{nm}, $G_{nm,x}$, $G_{nm,\theta}$, $\mathcal{T}_{nm,x}$, and $\mathcal{T}_{nm,\theta}$ are coefficients associated with various noise sources. These expressions are given in terms of the geometry and other aeroacoustic parameters, and their detailed expressions are given in ref. 12. The resonant oscillation occurs when Δ_T vanishes. The overall resonance occur as a result of local resonant oscillation in the combustion chamber. Since the complete system consists of four different zones (see Fig. 6) there are four possible local resonance conditions for the overall system. In view of these various conditions for possible resonant oscillations, it is very likely that the complete noise spectrum will show a multiple peak structure with certain discrete tones. The acoustic instability may also provoke resonant oscillations of a given acoustic mode when the sizes of the fluctuating reacting spots become comparable with the acoustic wave length.

SCATTERING AND AMPLIFICATION OF SOUND BY FLAMES

It has been known for some time that flames have ability to scatter sound, but a detailed description of these phenomena is not available to date. The problem is complicated by the interaction of the flame with the incident sound waves of various wave lengths, and by the refraction of the sound by non-isothermal zones in which the sound speed changes. This section presents some essential features of the scattering of the sound wave by flames and in particular, the relation existing between the scattered sound and physical parameters of the flame.

The wave equation describing the scattering of sound waves by an open flame is given by the following non-dimensional equation

$$\frac{1}{A_f^2} \frac{\partial^2 \Omega}{\partial \tau^2} - \nabla^2 \Omega - \nabla \ln A_f^2 \cdot \nabla \Omega + \epsilon \frac{\dot{Q}}{A_f^2} \frac{\partial \Omega}{\partial \tau} = 0 \tag{26}$$

where the spatial coordinate is non-dimensionalized by wave length with

$$A_f^2 = a_f^2 / a_1^2, \quad \tau = a_1 t / \lambda, \quad \text{and} \quad \epsilon = (\gamma - 1) \lambda \dot{Q}_0 / a_1 p_1$$

The subscript 1 refers to the properties immediately downstream of the reaction zone, Q_0 is the reference rate of heat release.

We consider a plane wave incident on a flame located at the origin of the spatial coordinates. The sound wave in the far field may be expressed

as the superposition of a plane wave propagating in the z direction and a scattered spherical wave

$$\Omega \simeq e^{-i\omega A_{f\infty}\tau}\left[e^{iKz} + e^{iKr} f(\theta,K)/r\right] \tag{27}$$

where $A_{f\infty}$ is the ratio of the speed of sound at infinity to that of the flame, K is the wave number of the incident wave and f represents the amplitude of the scattered wave given by

$$f(\theta,K)=\frac{-1}{4\pi}\iiint e^{iqz'}\left[i\epsilon\omega A_{f\infty}\dot{Q}/A_f^2 + \omega^2(1-A_{f\infty}^2/A_f^2)-(\nabla' \ln A_f^2)\cdot iK\nabla z'\right]dV' \tag{28}$$

in which θ is the angular position of the field point and $q = \frac{K}{2}\sin\theta/2$

To illustrate the explicit scattering amplitude due to the heat release rate $\dot{Q}$, i.e., the first term appearing in the integral of Eq. (28), we assume the following distributions for the heat release rate and the speed of the sound.

$$\dot{Q} = B\exp\left[-r^2/R_c^2\right] \tag{29a}$$

$$\frac{1}{A_f^2} = \frac{1}{A_{f\infty}^2} - \left(\frac{1}{A_{f\infty}^2} - \frac{1}{A_{f1}^2}\right)\exp\left[-r^2/R_c^2\right] \tag{29b}$$

where R_c and R_T are the sizes of the combustion zone and non-isothermal zone respectively.

Substituting the above expression into Eq. (28), yields

$$f(\theta,K)=\frac{\epsilon\omega B}{4A_{f\infty}}\sqrt{\pi}R_c^3 e^{-\left(\frac{R_c}{K}\sin\frac{\theta}{2}\right)^2}\left\{1-(1-A_{f\infty}^2)\left[1+\left(\frac{R_T}{R_c}\right)^3\right]^{-\frac{1}{3}} e^{-KR_c^2\left\{\left[1+\left(\frac{R_T}{R_c}\right)^3\right]^{\frac{1}{3}}-1\right\}\sin^2\theta/2}\right\} \tag{30}$$

It is interesting to note that the amplitude of the scattered wave is proportional to the total heat realese rate, $\epsilon B R_c^3$ and to the frequency of the wave. The distribution of amplitudes, f, is not independent of angular position. The maximum in f occurs in the direction of the wave propagation, $\theta = 0$, $\theta = 180°$ propagation $\theta = 90°$. It is also clear that the longer waves are scattered more efficiently than the shorter waves, as may be expected from physical reasoning.

CONCLUSION

The physical theory of combustion noise is presented with attention focused on the mechanism of the sound emission and the acoustic power of the sound fields generated by open flames and ducted combustion systems. Sound emission mechanisms of an open flame are classified into Smith-Kilham emission mechanisms and turbulent driven Rijke-Riess emission mechanism. The total sound emitted is proportional to the combustion sound number and the structural factors which depend on the structure of the flame. The analysis also suggests that a high degree of correlation should exit between the spectra of sound pressure and the light emitted from the free radicals for a flame dominated by large scale turbulence. On the other hand, lack of correlation of the two spectra would indicate that the combustion is in the distributed reaction regime. The difference in the measured pressure and the sound pressure is proportional to the non-dimensional parameter $K = u'l_f/S_L\lambda$. Confirmation of this conjecture, by detailed flame survey, is essential fo the understanding of the flame noise. The scattering of the sound wave by a flame is found to

depend on the total heat release rate, and the temperature difference between the flame and the surroundings. Present analysis indicates that the relative size of the flame zone and the wave length are important parameters determining the angular distribution of the scattered waves.

ACKNOWLEDGEMENT

The authors wish to thank Doctor E. G. Plett and Professor H. J. Shafer for their suggestions pertaining to technical matters.

References

1. Smith, T. J. B. and Kilham, J. K., "Noise Generated by Open Turbulent Flames," J. Acoust. Soc. Amer. 35, 715-724 (1963).

2. Hurle, I. R., Price, R. B., Sugden, T. M., and Thomas A.,"Sound Emission from Open Turbulent Premixed Flame", Proc. R. Soc. A303, 409-427 (1969).

3. Giammar, R. D. and Putnam, A. A.,"Combustion Roar of Premix Burners, Singly and in Pairs," Combustion and Flame 18, 435-438 (1972).

4. Bragg, S. L., "Combustion Noise," J. Inst. Fuel 36, 12-17 (1963).

5. Strahle, W. C.,"On Combustion Generated Noise", J. Fluid Mech. 49, 399-414 (1971).

6. Strahle, W. C., "Some Results in Combustion Generated Noise", Journal of Sound and Vibration 23 p 113 (1972)

7. Shivashankara, B. N., Strahle, W. C., and Handley, J. C., "Combustion Noise Radiation by Open Turbulent Flames", AIAA Paper No. 73-1025 (1973)

8. Strahle, W. C., "A Review of Combustion Generated Noise", AIAA Paper No. 73-1023

9. Shivashankara, B. N., Strahle, W. C., "An Evaluation of Combustion Noise Scaling Laws by an Optical Technique", AIAA Paper No. 74-47 (1974)

10. Abdelhamid, A. N., Harrje, D.T., Plett, E. G., and Summerfield, M., "Noise Characteristics of Combustion Augmented High Speed Jets", AIAA Paper No. 73-189 (1973), also AIAA Journal 12 336-392 (1974).

11. Chiu, H. H., and Summerfield, M., "Theory of Combustion Noise", Paper Presented at the 4th International Colloquium on Gasdynamics of explosions and Reactive Systems, San Diego, Calif. (1973). To appear in Astronautica Acta.

12. Chiu, H. H., Plett, E. G., and Summerfield, M., "Noise Generation by Ducted Combustion Systems", AIAA paper No 73-1024 (1973)

13. Plett, E. G. Leshner, M. D., and Summerfield, M., "Combustor Geometry and Combustion Roughness Relation to Noise Generation", Symposium on University Research in Transportation Noise, North Carolina State Univ., June 5-7 (1974)

14. Morse, P. M., and Ingard, U. K., "Theoretical Acoustics", p.154 McGraw-Hill, N. Y., (1968)

15. Rayleigh, J. B., The Theory of Sound , Vol II, pp. 232-235, Pover publication, N. Y. (1945)

16. Gaydon, A. C., and Wolfhard, H. G., "Comparison of the Spectra of Turbulent and Laminar Flames", Fuel Vol 33 (1954)

17. John, R. R., and Summerfield, M., "Effect of Turbulence on Radiation Intensity From Propane-Air Flames", Jet Propulsion 27, 16a (1957)

18. Kovasznay, L.,"A comment on Turbulent Combustion", Jet Propulsion, Vol. 26 485, (1956)

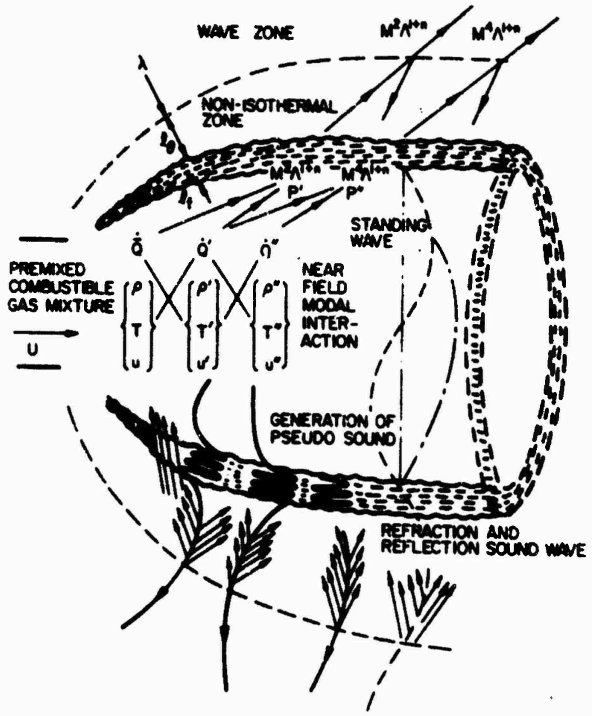

FIG. 1 Schematic diagram of sound generation by open flame: distributed reaction model.

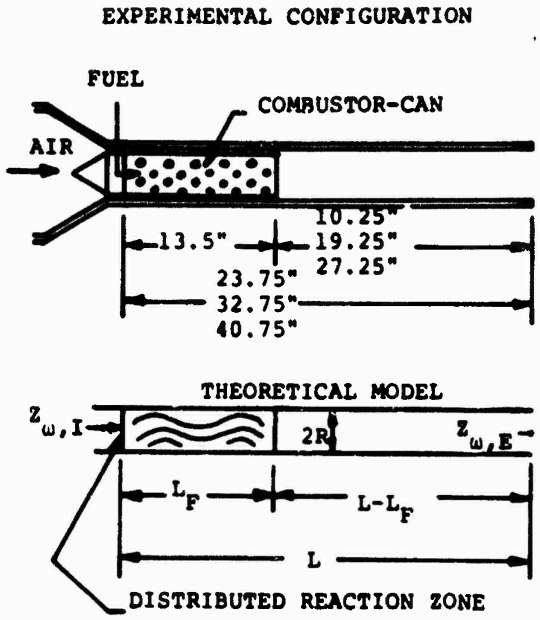

FIG. 2 Schematic of combustor configuration used in experiments, with corresponding theoretical model representation.

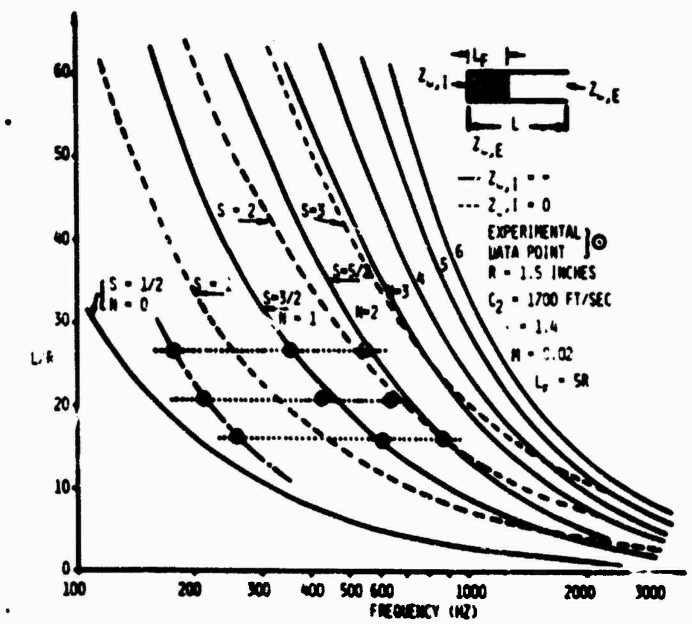

FIG 3 Frequency of resonance for a range of duct length showing fundamental and harmonics.

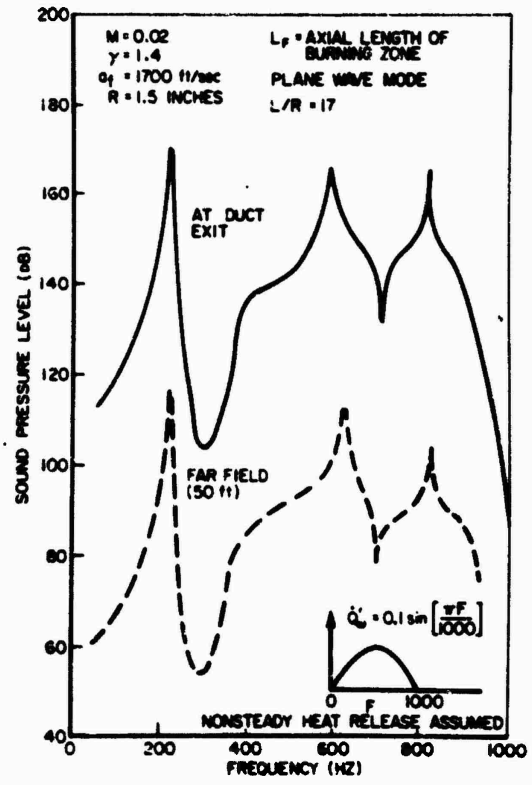

FIG. 4 Predicted sound pressure sprectrum levels at duct exit and corresponding levels in far field at 50 ft.

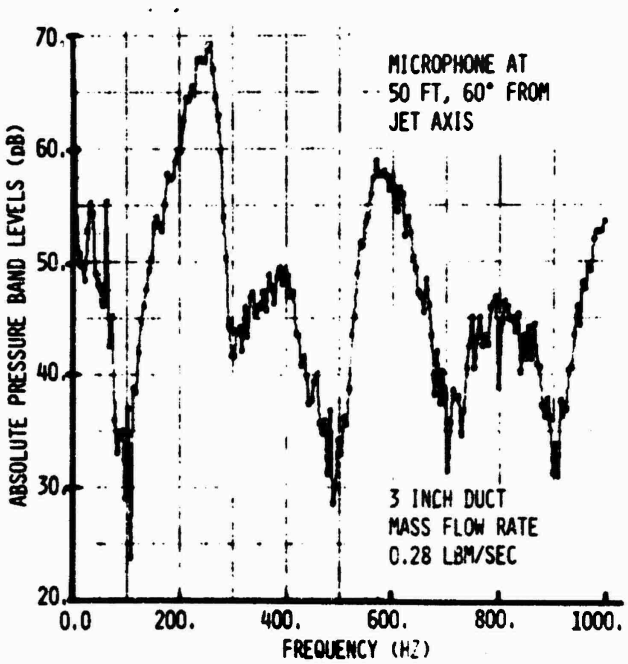

FIG. 5 Far field sound spectrum levels for combustor length of 23.5 inches, with 10.25 inch length downstream of combustor can.

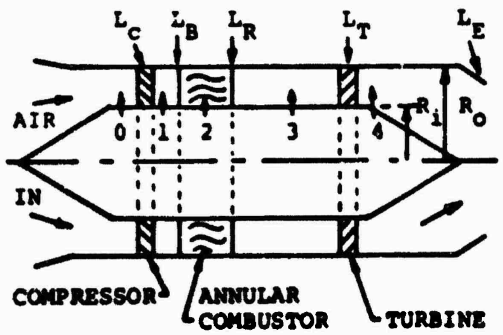

FIG. 6 Schematic representation of turbo-jet engine as modeled in analysis.

COMBUSTION NOISE: CROSS-CORRELATION OF SOURCE SIGNAL (HOT WIRE) WITH SOUND SIGNAL

W. G. Richarz[1], H. S. Ribner[2], G. W. Johnston[3].

Institute for Aerospace Studies, University of Toronto, Toronto, Canada.

ABSTRACT

Fluctuation of entropy is known to be the dominant source of flame noise. The source term for the wave equation can be approximated in terms of local temperature as $\rho/T \; D^2T/Dt^2$. The assumption that the eddy scales and speeds are such that $\partial^2/\partial t^2$ is statistically proportional to D^2/Dt^2 is justified as posteriori. As in an earlier jet noise study (H. K. Lee and H. S. Ribner, J.A.S.A. (1972) 52, No.5 (Part 1) 1280-1290), the cross-correlation technique has been applied. An unheated "hot wire" probe of iridium (melting point 2700°K) is used as a sensor of local flame temperature. The probe signal ($\sim T$) and the microphone signal ($\sim \partial^2T/\partial t^2$ in part if the theory is correct) are cross-correlated. The theory implies that the cross-correlation should have a shape similar to that of the second derivative of the temperature rate autocorrelation ($R_{TT}^{\bullet\bullet}(\tau)$). The calculated and measured correlograms are in good agreement.* (Research supported by National Research Council (Canada) and Air Force Office of Scientific Research (U.S.A.)).

---

*

1. Research Fellow - Institute for Aerospace Studies, U. of T. Toronto, Canada.
2. Professor - " " " " " "
3. Associate Professor " " " " " "

INTRODUCTION

Noise generated by open, premixed turbulent flames has been described by several investigators (1,2), and their theoretical models have been verified to some degree. Hurle et al (3) and recently Shivashankara and Strahle (4) have cross-correlated light radiation - an integrated property of the flame with flame generated sound. However, no direct correlation of the assumed local source term with the radiated sound has been made. In the present investigation local temperature measurements in the flame and radiated sound are cross-correlated in a manner similar to the one used by Lee and Ribner (5).

THEORETICAL CONSIDERATIONS

The most comprehensive analytical flame noise model is one due to Chiu and Summerfield (6). A simpler formalism results if one follows along the lines of the jet noise analysis by Phillips (7) and neglects differences between the burned and unburned gases in the combustion case. The simplified wave equation

$$\frac{D^2}{Dt^2} \ln \frac{p}{p_o} - \frac{\partial}{\partial x_i} a^2 \frac{\partial}{\partial x_i} \ln \frac{p}{p_o} = \gamma \frac{D}{Dt} \frac{1}{C_p} \frac{DS}{Dt} \tag{1}$$

serves as a model for the flame-generated noise. For an air-fed burner only a fraction of the gases react, allowing the entropy to be expressed in terms of temperature and pressure.

We may linearize $\ln p/p_o$ as $1 + (p-p_o)/p_o$. Moreover the speeds are so low (typically $M<,02$) that the mean flow effects (source convection, refraction by velocity gradients) are small. This permits approximating the convected wave equation (1) as an unconvected wave equation.

$$\frac{\partial^2 p}{\partial t^2} - a_o^2 \frac{\partial^2}{\partial x_i^2} p = \frac{\gamma p_o}{\bar{T}_f} \frac{D^2 T_f}{Dt^2} + (\bar{a}^2 - a_o^2) \frac{\partial^2 p}{\partial x_i^2} \tag{2}$$

The second term on the RHS merely accounts for refraction of the sound field by the flame temperature gradients; this will be small owing to the large ratio of typical wavelength/flame dimension; so that this term may be neglected for our purposes.

A dimensional argument based on typical eddy time and length scales indicates that we cannot safely take the further step of approximating D^2T_f/Dt^2 on the R.H.S. by $\partial^2 T_f/\partial^2 t^2$. (However, it will be seen later - from the experiment - that $\partial^2 T_f/\partial t^2$ behaves similarly to D^2T_f/Dt^2 in its contribution to correlations. The far-field solution for the acoustic pressure is then given by

$$p(\underline{x},t) = \frac{1}{4\pi|\underline{x}|} \int_{-\infty}^{\infty} \int_{V_f} \frac{\gamma p_o}{a_o^2 \bar{T}_f} \frac{D^2}{Dt^2} T_f(\underline{z},t') \delta(t'-t+\frac{r}{a}) \, dt' d^3z \tag{3}$$

and the cross-correlation of the acoustic pressure at $\underline{x}$ and the flame temperature at $\underline{y}$ is

$$R_{TP}(\underline{x},\underline{y},\tau) = \frac{1}{4\pi|\underline{x}|}\int_V \frac{\gamma p_o}{a_o^2 \bar{T}_f}\,\frac{D^2}{D\tau^2}\,R_{TT}(\underline{y},\underline{z},t-\frac{r}{a})\,d^3z \qquad (4)$$

where $D/D\tau \equiv \partial/\partial\tau + u_i\,\partial/\partial\eta_i$; $\eta_i = z_i - y_i$ and R_{TT} is a two point correlation. A scaling argument (8) suggests that

$$R_{TP}(\underline{x},\underline{y},r/a) \tilde{-} \frac{1}{4\pi|\underline{x}|}\,\frac{\gamma p_o}{a_o^2 \bar{T}_f}\,w^2 k\,R_{TT}(\underline{y},\underline{y},0)\,L^3 \qquad (5)$$

with

$$k = \left(1 + 2\,\frac{u}{L'}\,\frac{1}{w} + \left(\frac{u}{L'}\right)^2 \frac{1}{w^2}\right) \qquad (6)$$

where u is the mean local flow velocity, L' a scale length, w a characteristic frequency (reciprocal of a time scale) and L^3 the correlation volume. Thus the theory provides an explicit connection, equation (5), between the peak of the local flame temperature autocorrelation R_{TT} and the peak of the temperature-sound pressure cross-correlation R_{TP}. This connection can be tested experimentally.

EXPERIMENTAL PROCEDURE

The experiment was conducted in the UTIAS 420 x 290 x 210 cm^3 anechoic chamber. The experimental arrangement is shown schematically in figure 1. The 1.27 cm. diameter burner was fuelled by a mixture of air and methane (CH_4). A probe, similar in construction to a hot wire anemometer probe, made of iridium wire (Melting point ~ 2700°K) served as a temperature sensor (9). The probe was placed in one arm of a Wheatstone bridge that was driven by a constant current source. A high gain amplifier detected the bridge unbalance, the probe acting as a resistance thermometer. The unbalance voltage (proportional to temperature fluctuations) and the acoustic signal of the flame were cross-correlated by a P.A.R. Model 101 Correlation Function Computer and the correlograms were plotted on an x-y plotter.

RESULTS AND DISCUSSION

The instrumentation permitted several correlation functions to be computed. They were the temperature autocorrelation $R_{TT}(\tau)$ the acoustic pressure autocorrelation $R_{pp}(\tau)$, the second time derivative of the temperature autocorrelation $\partial^2/\partial\tau^2\,R_{TT}(\tau)$, and the cross-correlation function of the temperature and acoustic pressure $R_{TP}(\tau)$. Figures 2 and 3 show some of the correlograms obtained. The autocorrelation $\partial^2/\partial\tau^2 R_{TT}(\tau)$ was computed by autocorrelating the first time derivative of the temperature, using the relation $\partial^2/\partial\tau^2 R_{TT}(\tau) = -R_{\dot{T}\dot{T}}(\tau)$. The differentiation was performed by an electronic differentiator.

Nondimensional correlations eliminate the need for conversion factors that are required if a dimensional correlation is desired. For the purpose of being able to compare $R_{TP}(\tau)$ and $R_{TT}(\tau)$, these factors must be known. As both signals passed through linear systems only, a simple scaling applied. The flame volume V_f was estimated from the flame dimensions. For the flow setting used, the flame volume was 120. cm^3.

If the proposed theory is correct, then the maximum value of the cross-correlation $R_{TP}(\tau)$ must be related to $R_{TT}(0)$ as shown in equation (5). This was confirmed (Fig. 4) but more than that, a remarkable similarity was found between the shape of the cross-correlation $R_{TP}(\tau)$ and that of the auto-correlation $R_{TT}(\tau)$. When the measured correlations were replotted and matched at their maxima, little deviation could be found. Thus the equation

$$R_{TP}(\tau) = \frac{1}{4\pi|\underline{x}|} \frac{\gamma p_o}{a_o^2 \bar{T}_f} k_{exp} \frac{\partial^2}{\partial t^2} R_{TT}(\tau - \frac{r}{a}) L^3 \qquad (7)$$

applies everywhere. On the other hand the theory dictates an equation similar to (7) but with $D^2R_{TT}/D\tau^2$ replacing $k_{exp}\partial^2 R_{TT}/\partial\tau^2$. The experimental confirmation of the form (7) appears to imply that the temporal and spatial parts of the two-point correlation $R_{TT}(\tau,\eta)$ have a similar functional dependence.

For comparison with the experimental value k_{exp}, the value of k predicted by equation (6) can be evaluated also from experimental data. A source of characteristic length L (a volume of high or low temperature) passes an observer in L/u seconds. This passing has associated with it a frequency w' such that the duration of the pulse corresponds to the duration of one half cycle of frequency w'. From $w' = \pi u/L$ the magnitude of k can be extracted. Laser Doppler Anemometer measurements by Durst et al (10) have shown that u equals the upstream orifice velocity u_o.

The scaling may be summarized as follows:

$$R_{TP}(\tau^*) = \frac{\dot{}}{4\pi|\underline{x}|} \frac{\gamma p_o}{a_o^2 \bar{T}_f} k \frac{\partial^2}{\partial\tau^2} R_{TT}(0) \qquad (a)$$

$$\frac{R_{TP}^2(\tau^*)}{R_{TT}(0)R_{PP}(0)} \sim \frac{L^3}{V_f} = \frac{1}{N} \; ; \; \tau^* = \frac{r}{a} \qquad (b) \qquad (8)$$

Here N is the number of sources on an equal strength basis. The measured and normalized correlations of $R_{TP}(\tau)$ indicated that there were some 1200 sources on the average, corresponding to a characteristic source size of L = .464 cm.

From the above data it was found that the predicted value of k = 12.8 for the flow speed u_o = 600 cm/sec. From a number of runs the average experimental value $\bar{k}_{exp}$ = 12.4. Figure 4 illustrates the measured cross-correlation $R_{TP}(\tau)$ and the estimate of $R_{TP}(\tau)$ based on the value of k and $R_{TT}(\tau)$. The agreement is very good. The measured cross-correlations $R_{PT}(\tau)$ ranged from 6.5 to 12.5 mV in maximum value, while the base noise voltage of

the correlator was of the order of 1 mV. The poor signal to noise ratio explains the often jagged appearance of a single correlogram. Where several correlograms of the same signals were superimposed, they were found to average to a smooth curve.

ACKNOWLEDGEMENT

This research was sponsored by the National Research Council of Canada under N.R.C. Grant A-2003 and by the Air Force Office of Scientific Research, USAF, under Grant AF-AFOSR-70-1885A.

REFERENCES

1) Smith, T. J. B., Kilham, J. K. Noise Generation by Open Turbulent Flames. JASA Vol. 35, No.5, pp.715-724 (1963).

2) Strahle, W. C. Some Results in Combustion Generated Noise, AIAA Paper No. 72-198.

3) Hurle, I. R., Price, R. B., Smudgen, T. M., Thomas, A., Sound Emission From Open Turbulent Pressurized Flames. Proc. Roy. Soc. 303, pp-409-427, (1968).

4) Shivashankara, B. N., Strahle, W. C., Handley, J. C. An Evaluation of Combustion Noise Scaling Laws by an Optical Technique. AIAA Paper No.74-47.

5) Lee, H. K., Ribner, H. S. Direct Correlation of Noise and Flow of a Jet. JASA Vol. 52, No.5, pp.1280-1290 (1972).

6) Chiu, H. H., Summerfield, M. Theory of Combustion Noise, 4th. Internat. Colloq. on Gas Dynamics of Explosions and Reactive Systems, San Diego, July 10-13, (1973).

7) Phillips, O. M. On The Generation of Sound by Supersonic Turbulent Shear Layers. J. Fluid. Mech. Vol. 9, pp.1-28 (1960).

8) Richarz, W. G. Correlation of Temperature and Noise of a Flame. M.A.Sc. Thesis (unpublished). University of Toronto, 1974.

9) Parker, K. H., Guillon, O. Local Measurement in a Turbulent Flame by Hot Wire Anemometry. 13th Symp. on Combustion, pp.667-674 (1972).

10) Durst, F., Melling, A., Whitelaw, J. H., The Application of Optical Anemometry to Measurement in Combustion Systems. Combustion and Flame, 18, pp.197-201 (1972).

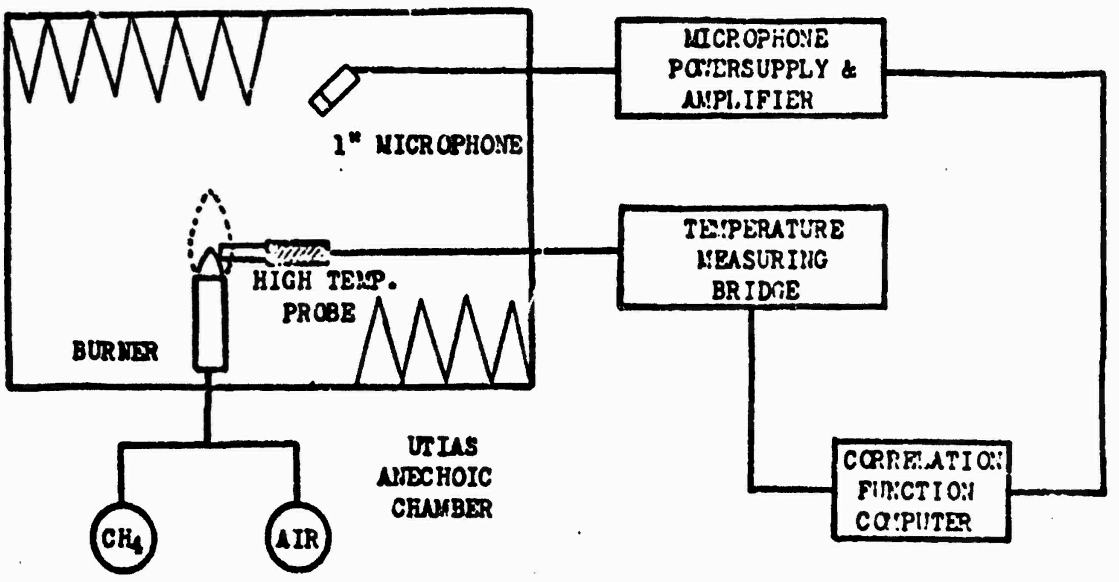

FIG. 1. GENERAL ARRANGEMENT OF FLAME NOISE CORRELATION EXPERIMENT

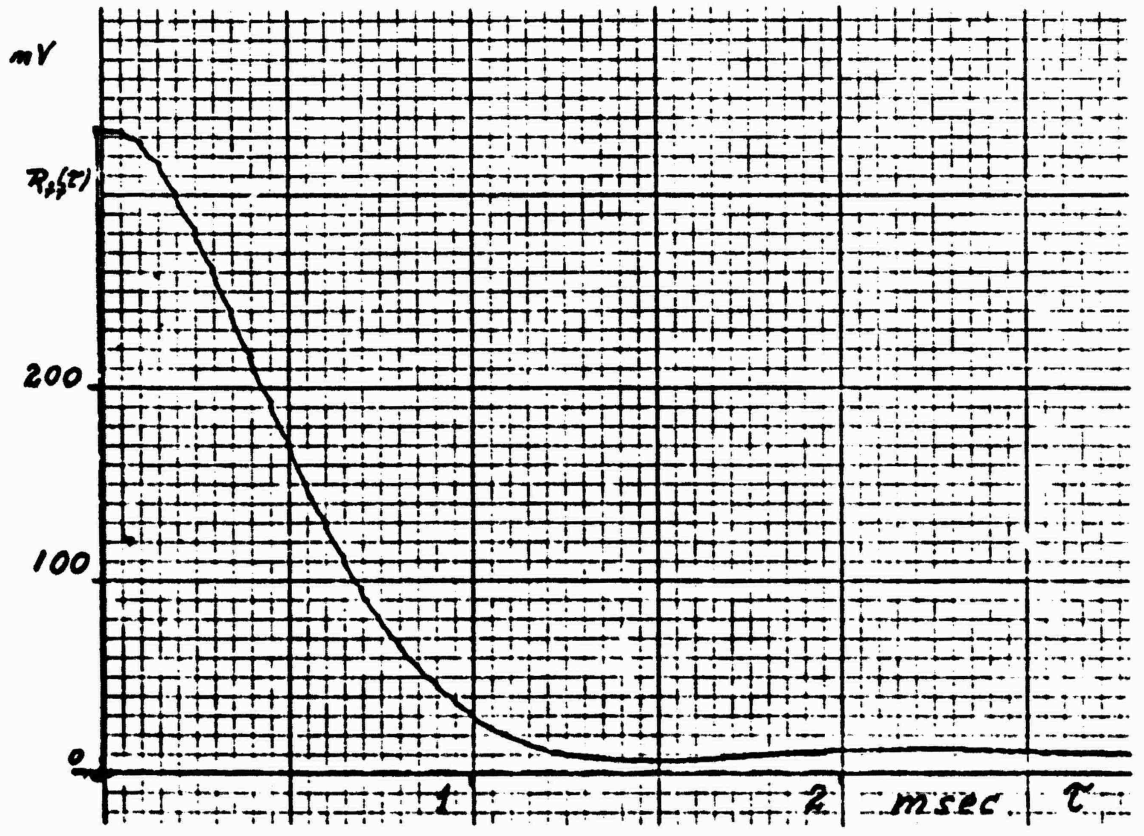

FIG. 2: AUTOCORRELATION OF $\partial/\partial t$ (local flame temperature T_f); $R_{\dot{T}\dot{T}}(\tau)$; THE ACOUSTIC RADIATION EFFECTIVENESS IS CLOSELY RELATED TO THIS QUANTITY.

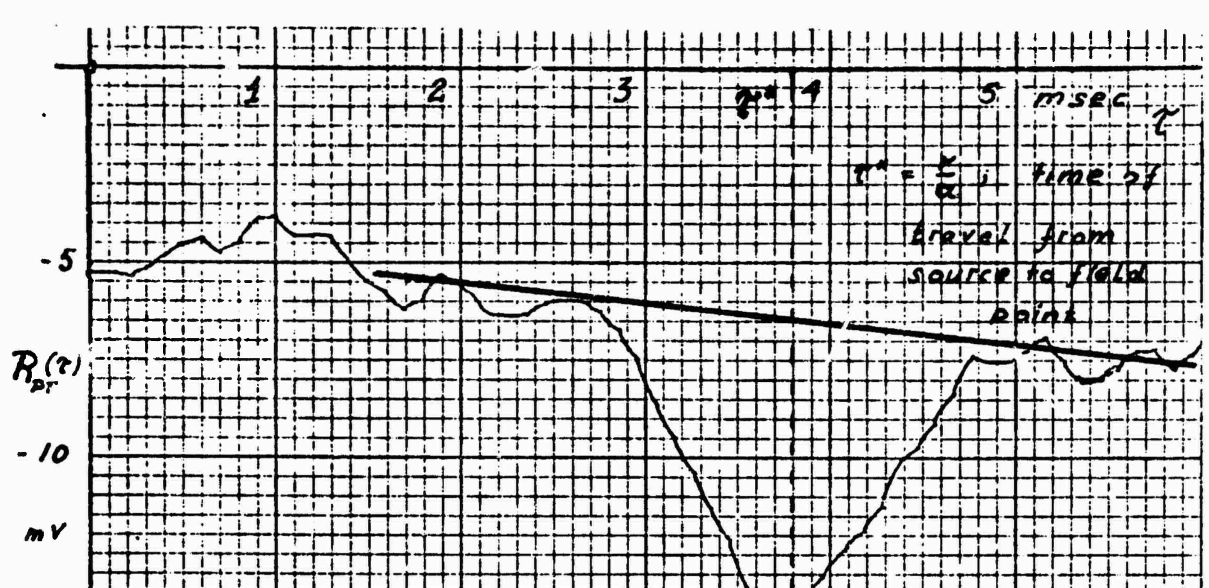

FIG. 3: MEASURED CAUSE-EFFECT CORRELATION $R_{PT}(\tau)$ BETWEEN LOCAL FLAME TEMPERATURE AND RADIATED SOUND PRESSURE. (SKEW REFERENCE LINE IS DUE TO HUM AND INHERENT INSTRUMENTATION OFFSET).

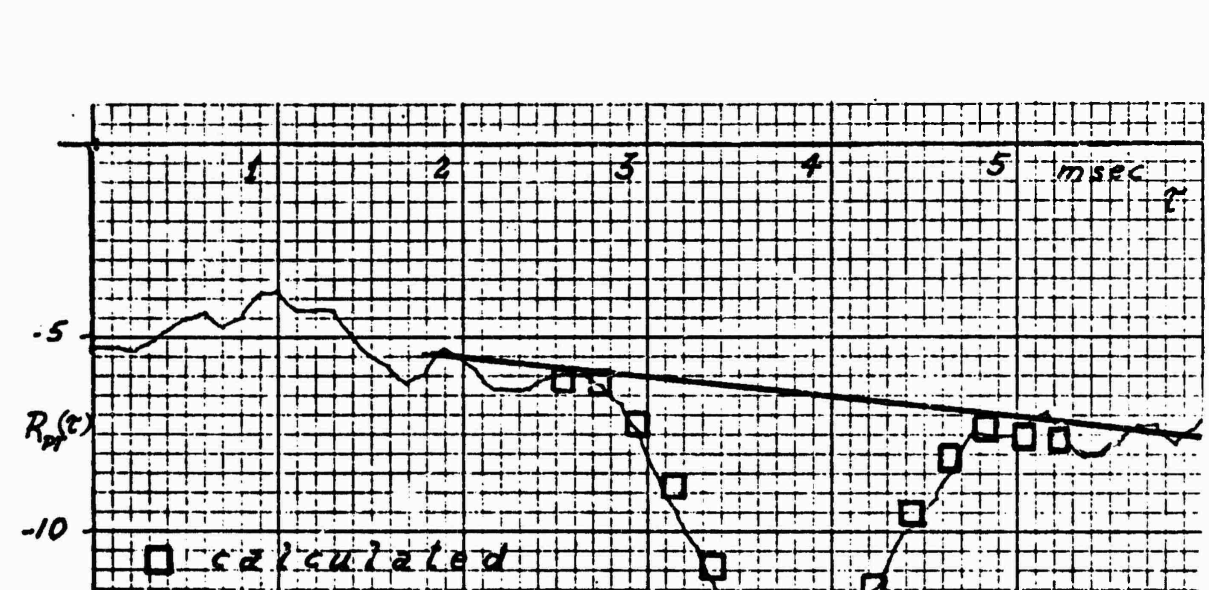

FIG. 4: COMPARISON OF THE MEASURED CROSS-CORRELATION $R_{PT}(\tau)$ WITH VALUES CALCULATED ACCORDING TO THEORY FROM THE AUTOCORRELATION $R_{TT}(\tau)$. THE AGREEMENT TENDS TO CONFIRM $\partial^2 T/\partial t^2$ AS MODELLING THE EFFECTIVE ACOUSTIC SOURCE TERM IN A FLAME.

DUCT ACOUSTICS

SHOCK WAVE PROPAGATION THROUGH A TURBULENT PIPE FLOW

by
Ho, Chih-ming and Leslie S. G. Kovasznay
Department of Mechanics and Materials Science
The Johns Hopkins University
Baltimore, Maryland 21218

ABSTRACT

An experimental study was carried out on a solitary weak pressure discontinuity propagating through a fully developed turbulent pipe flow. The shape of the wave front, the propagation velocity, the effective rise time were all measured as functions of the flow velocity (Mach number) both for upstream and downstream propagation.

INTRODUCTION

Sound wave propagation in ducts was considered as an important problem for a long time and there is a great deal of theoretical work in the literature. Here an experimental study is presented dealing with the propagation of a weak shock wave through a fully developed turbulent pipe flow. The propagation of a pressure discontinuity as contrasted with the propagation of pure sine waves can give a complementary picture about the propagation and scattering through turbulent shear flows. Turbulent pipe flow was chosen as a turbulent shear flow that is both homogeneous in one direction (axial) and stationary in time. Wave propagation in real time was chosen instead of frequency domain analysis. This was deliberate as the concept of first arrival is lost when the data is converted into frequency domain. The wave transmitted was not a true shock wave only a sharp pressure rise with a finite gradient. The emphasis is rather on the solitary wave aspect of the experiment so that the first arrival of the signal is clearly detectable.

The results of the experiments are applicable to the assessment of the sound wave propagation through ducts with turbulent flow as well as to sonic boom signatures after passage through the turbulent atmospheric boundary layer.

EQUIPMENT

A shock wave generator was located at one end of the 15 cm diameter 1800 cm long plastic pipe (Fig. 1). The pipe was

mechanically isolated from the generator by a soft foam-rubber coupling. The air flow through the pipe was produced by a centrifugal blower. The air first passes through a plenum chamber (a wooden box of 120 cm x 90 cm x 90 cm) then it enters the pipe through a 3.8 cm annular slot, 127 cm away from the shock wave generator. Using such a configuration, the shock generator operates in still air and it is not disturbed by the turbulent flow field. The flow leaves the pipe through a second annular slot (3.8 cm) about 330 cm from the opposite end of the pipe. The length of the pipe section with turbulent flow between the entrance and exit slots is approximately 1,275 cm (the length diametric ratio $\approx$ 85). The maximum velocity in the pipe was 2,320 cm/sec and the Reynolds number

$$\frac{U(0)\,D}{\nu} = 2.43 \times 10^5$$

The flow velocity was varied by changing the amount of bleeding near the outlet of the blower.

The direction of wave propagation was defined as the positive direction correspondingly when the flow direction coincided with the wave propagation direction, it was referred as "downstream" propagation and the Mach number $M = U(0)/a_0$ of the flow was also defined as positive. In the opposite case we shall refer to "upstream" propagation and the Mach number is defined as negative. Here $U(0)$ is the centerline mean velocity of the flow and a_0 is the wave propagation velocity in still air.

Small microphones (1/8" = .3175 cm; B&K Type 4138) were used to detect pressure waves. The microphones were placed at different locations both inside the flow field and also in the still air at either end sections. Along the pipe, 25 static pressure holes were provided. The measured static pressure decreased linearly with distance as evidence of fully developed pipe flow. The detailed flow field was measured by hot-wire anemometers at four stations, located 300 cm apart. All conventional flow parameters (mean velocity profile, turbulent intensity) behaved as expected.

The weak transient pressure wave was produced by an electromagnetic shock wave generator (Fig. 2) originally suggested for liquids by Eisenmenger (1964) then adapted to gasses by Nakamura and Takeuchi (1969). The generator consists of a circular metal disk (in our case an aluminum plate 0.119 cm thick) driven by a single layer 78 turn flat spiral coil of 17 cm in diameter. The coil was made of enamaled wire of 0.075 cm nestled in the spiral grove of a heavy plastic disk. The coil is energized by the discharge of a

storage condenser (2.5 microfarad, applied voltage 10 KV). No external trigger was used as the air gap acted as a switch when the breakdown voltage was reached.

When the air gap breakes down, the magnetic "pressure" developed in the coil repelles the aluminum disk. A rubber ring cushions the aluminum disk and it served as an elastic element to restore the plate to its original position after the shock. A shock wave is produced in the pipe following the sudden motion of the aluminum disk.

DATA PROCESSING

The transient signal representing the shock wave signatures was obtained by the condenser microphones (Fig. 3). The signal first was recorded and stored in a dual channel transient recorder (Physical Data Model 512 A) that sampled the signal at 20 microsecond intervals up to 1,000 samples in each channel or alternately a single channel operation with samples at each 10 microseconds. The recorder was triggered by the electric discharge in the shock wave generator. The total sweep of the transient recorder was 20 msec, but the interesting portion of the shock wave generator signature was only about 1 millisec. This 1 millisec portion of the recorded signal was replayed many times and fed into the input of a wave form eductor (PAR Model TDH-9) in order to "magnify" the relevant details such as accurate arrival time. The maximum error in timing is contributed by the following resources. The uncertainty of the trigger 0.1 microsecond, the time base of the transient recorder $\pm$ 0.01 % amounting to typically 2 microsecond. Error in delay of the eductor 1 microseconds so the total error is less then 4 microsecond. The relative error is of course much less, estimated to be the order 0.0003 % of the total elapased time. The output of the eductor was recorded on an X - Y plotter (Moseley Model 135) for further data analysis.

As an alternate route the record stored in the transient recorder was displayed in a cathode ray oscilloscope and pol roid pictures were taken of the traces (e.g. Fig. 5).

EXPERIMENTAL RESULTS

The curvature of the wave front was determined by taking two simultaneous records from the two microphones placed at the same axial location (1430 cm from the shock wave generator) but at different radii. The difference in arrival time indicated the cur-

vature of wave front. Both microphones were oriented perpendicular to the axis and they were within the flow field. Naturally there is some contamination of the traces by the velocity in addition to the pressure transient. The magnitude of the parasitic signal from the turbulent velocity fluctuations ($\approx \rho U u$) was estimated to be below 1% of the shock wave signal and it was concluded that the parasitic signal cannot effect the arrival time only add some "noise" to the signal. The arrival time was defined by extrapolating the maximum slope to the base line (Fig. 5-a). First at zero Mach number (no flow), the weak shock wave was found to be a plane wave. In case of finite flow velocity, the shape of the shock wave was found again to be a plane wave within the resolution limit of the transient recorder (10 microsec or 0.36 cm). In other words, the wave front arrived at the same time at all different radial portion in the pipe. If one imagines the pipe to be subdivided into annular channels without mutual interaction, then the propagation velocity in each one would be $a_o + U(r)$, where $U(r)$ is the local mean flow velocity at the different radii. In such a hypothetical case the wave front would be increasingly curved with time or distance travelled. Since experimentally, a uniform propagation velocity was found, it follows that scattering must be responsible for the radial exchange of wave components, resulting in a distinct plane wavefront.

The propagation velocity of the wavefront was determined by measuring the difference of arrival time at two microphone stations along the axis, separated by ΔX = 1,082 cm. The propagation velocity of the weak shock wave was measured at different positive and negative Mach numbers of the pipe flow, corresponding to both upstream and downstream propagation. An interesting non-symmetrical behavior was observed. The difference between the shock wave propagation in the flow and in still air was plotted against the Mach number of the flow (Fig. 4). In the case of positive Mach number (downstream propagation), all the data points were on the straight line representing $a - a_o = U(o)$, therefore the wavefront appears to propagate at the velocity of $a_o + U(o)$. For negative Mach numbers (upstream propagation), the wavefront propagation velocity was not exactly $a_o - U(o)$, but slightly faster, with a small but conclusive difference about $0.13\, U(o)$. The plausible explanation is that a portion of the wave propagates near the wall of the pipe, where the counter flow in the pipe is much less than at the center. This portion of the wave appears to be scattered by the high turbulence (see e.g. Ho, Chih-ming and Kovasznay 1974), back to the center region and it arrives ahead of the wave component propagated upstream in the center . In the case of positive Mach number, the wave propagation in the boundary layer is also scattered

into central portion of the pipe, but in this case, it fell behind the earliest wavefront, so the velocity of the first arrival is not affected by the contribution from the scattered wave.

The detailed shape of the wavefront was examined by taking microphone records at the other end of the pipe within the still air but still away from the conical absorber at the end of the pipe. After recording, high resolution traces were taken using polaroid pictures from selecting small portions on the oscillogram and these are shown in Fig. 5. A precursor wave can be observed, it may be due to the bending wave propagating in the pipe wall excited by the shock wave and it is observed as "pumping" the air in the pipe. For $M=0$ (no flow), the maximum slope of the pressure rise is still finite and the rise time is about 20 microseconds. This is the reason why the shock wave was termed as weak since it is not a true discontinuity. The 20 microseconds time is well within the response time limit of the microphone, whose rise time is estimated to be only 1-2 microseconds. In the case of downstream propagation, the slope of the wave front was the same as for still air. At the very beginning rise, the "corner" rounded off probably due to scattering by the low intensity turbulence within the central portion of the pipe, where the fast arriving signal propagated. In case of $M<0$ (upstream propagation), the maximum slope of the first arriving wave front decreases with increasing flow velocity. This is most likely due to the role of scatter-propagation outside the center core. The propagation through turbulence may be viewed as a turbulent diffusion of the wave front or even as an effective turbulent viscosity increasing the wave front thickness. The results presented here appear to disagree somewhat with Ribner's (1973) results obtained when a turbulent jet was placed into a horn type duct. One must keep in mind however that the two flow configurations were so different that a direct comparison is really not possible.

To sum it up present experiments gave clear quantitative data on pressure discontunity travelling through a well defined shear flow that is both homogeneous in the axial direction and stationary in time.

ACKNOWLEDGEMENT

The work reported here was supported by the Air Force Office of Scientific Research under contract No. F44620-69-C-0023.

REFERENCES

Eisenmenger, W. (1964) Acoustica 14 p. 187.

Ho, C. M. and Kovasznay, L. S. G. (1974) AFSOR Report, AFSOR-TR-74-0365.

Nakamura, A. and Takeuchi, R. (1969) Acoustica 22, p. 88.

Ribner, H. S., Morris, P. J., and Chu, W. H., (1973) J. of Acous. Soc. of Amer. 53, p. 926.

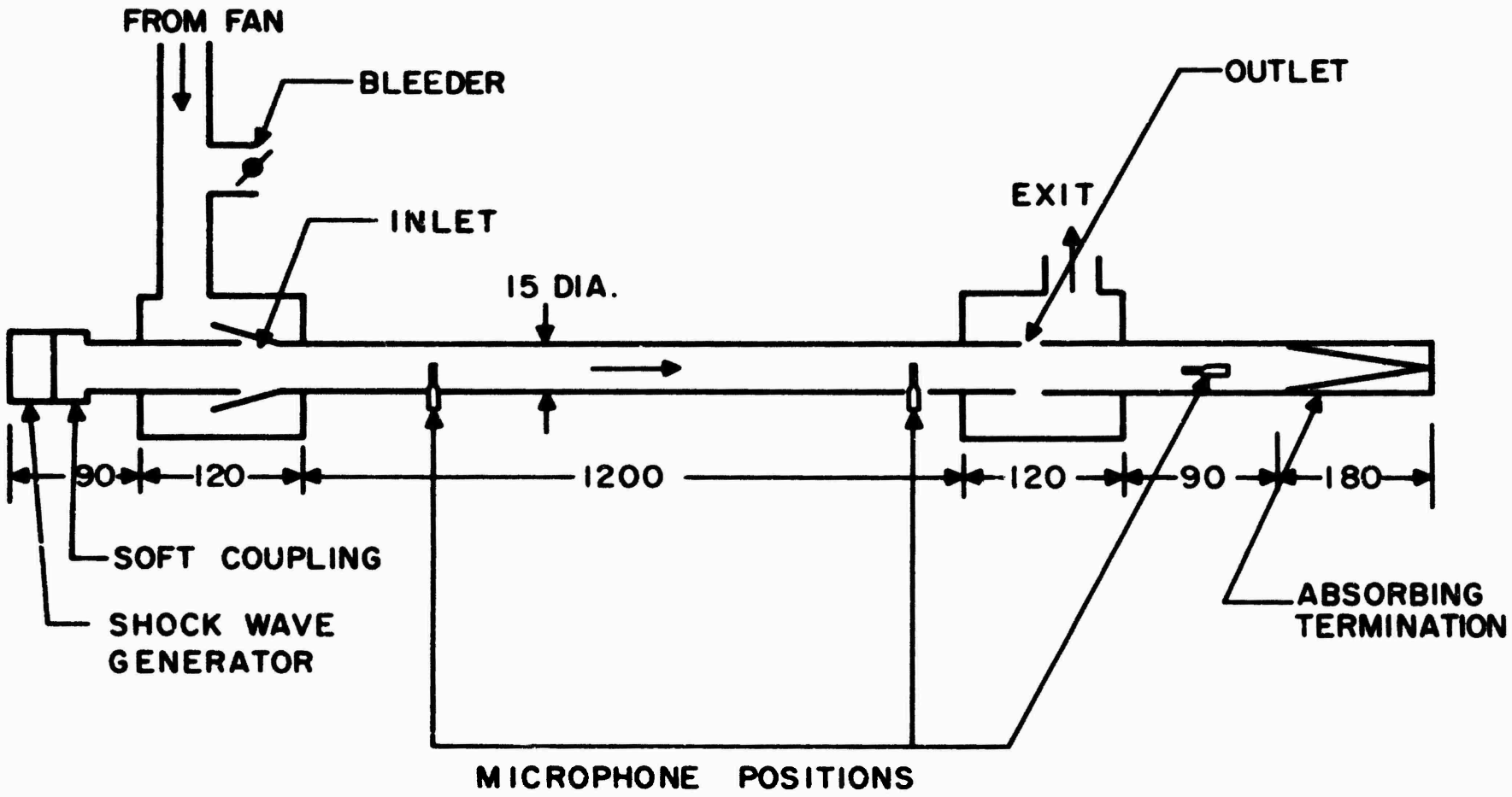

Fig. 1: Experimental Configuration (Dimension : cm)

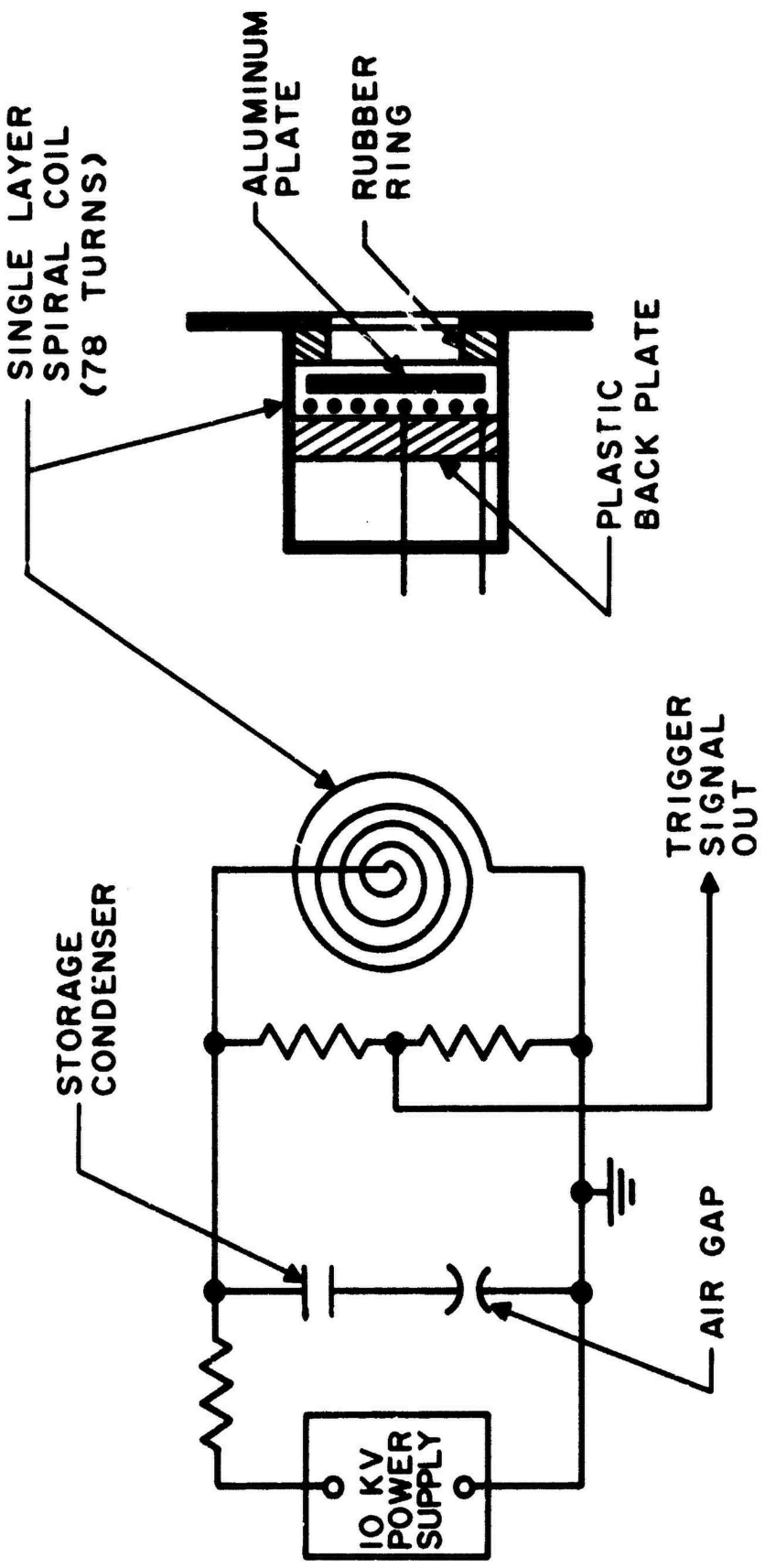

Fig. 2: Details of the Shock Wave Generator

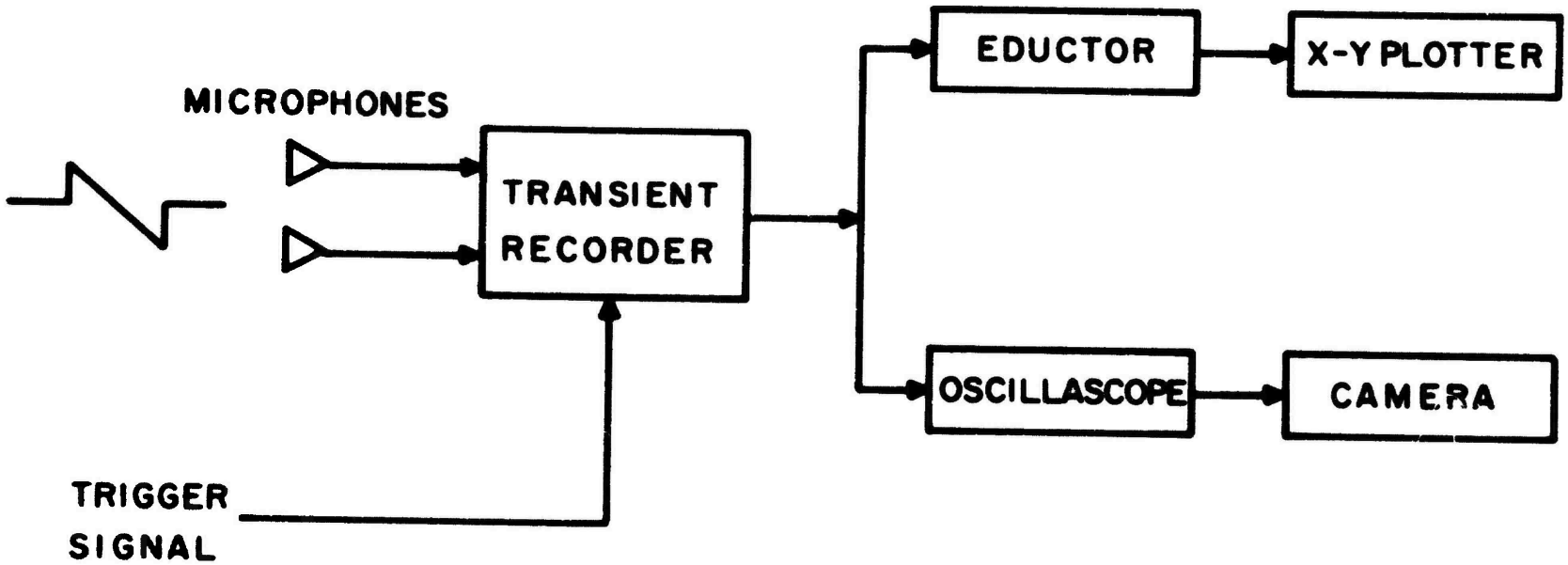

Fig. 3: Data Processing

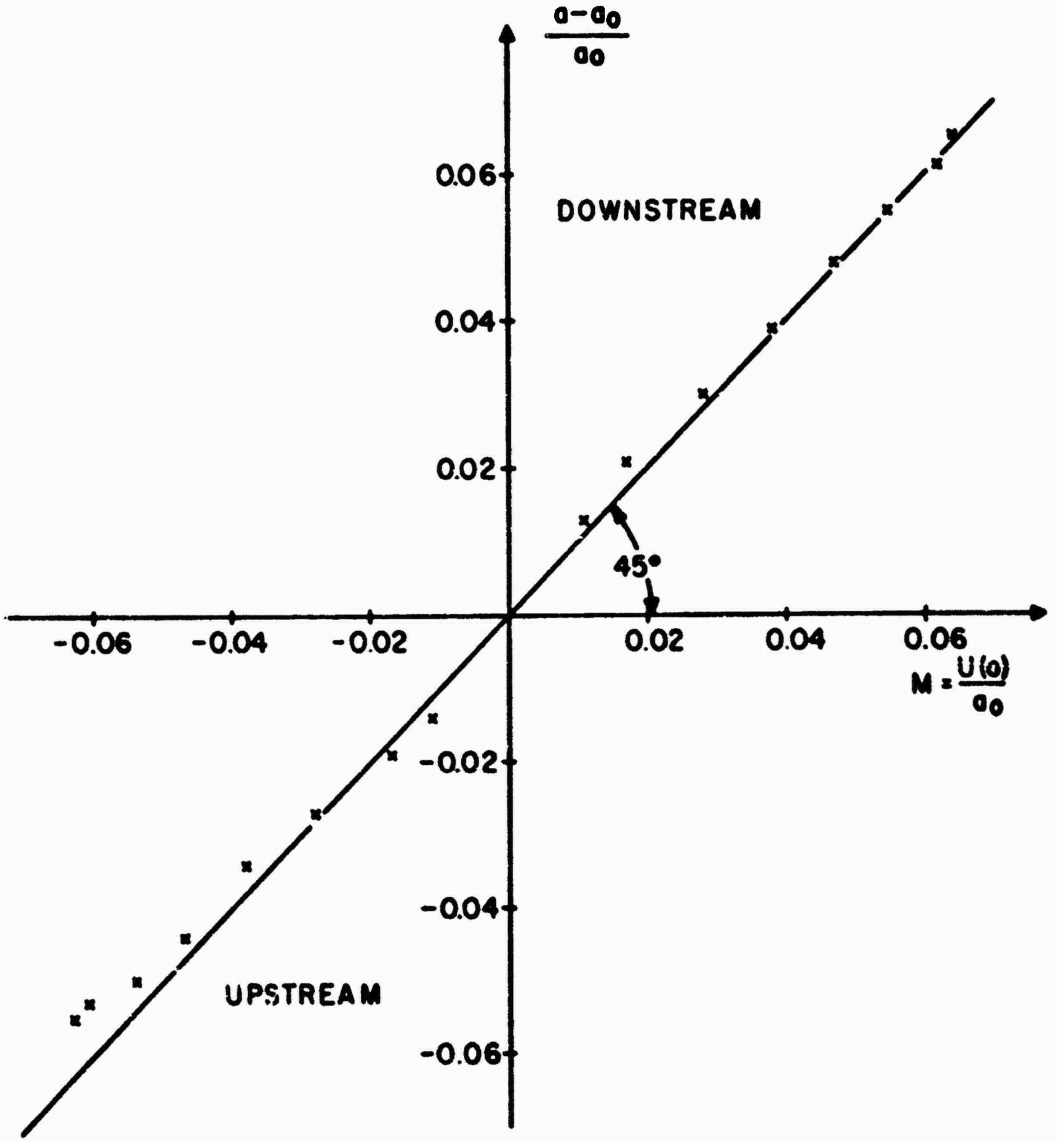

Fig. 4: The propagation velocity of the wave front as a function of flow velocity

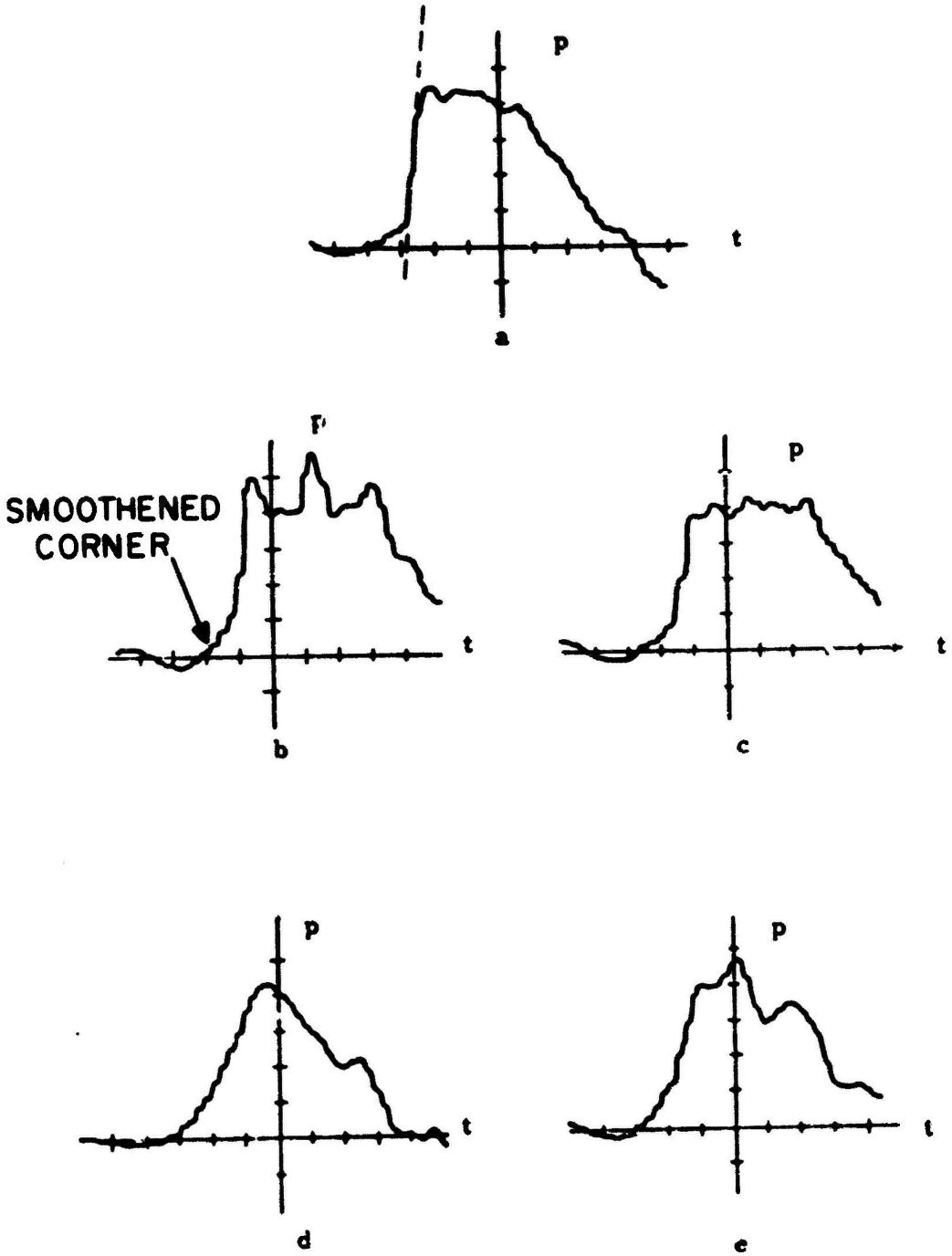

Fig. 5: Details of the wave front

(a) M = 0 (b) M = 0.0638
(c) M = 0.038 (d) M = -0.0638
(e) M = -0.038
Pressure p = 650 (dyne/cm^2)/Div.
Time t = 40 Microsecond/Div.

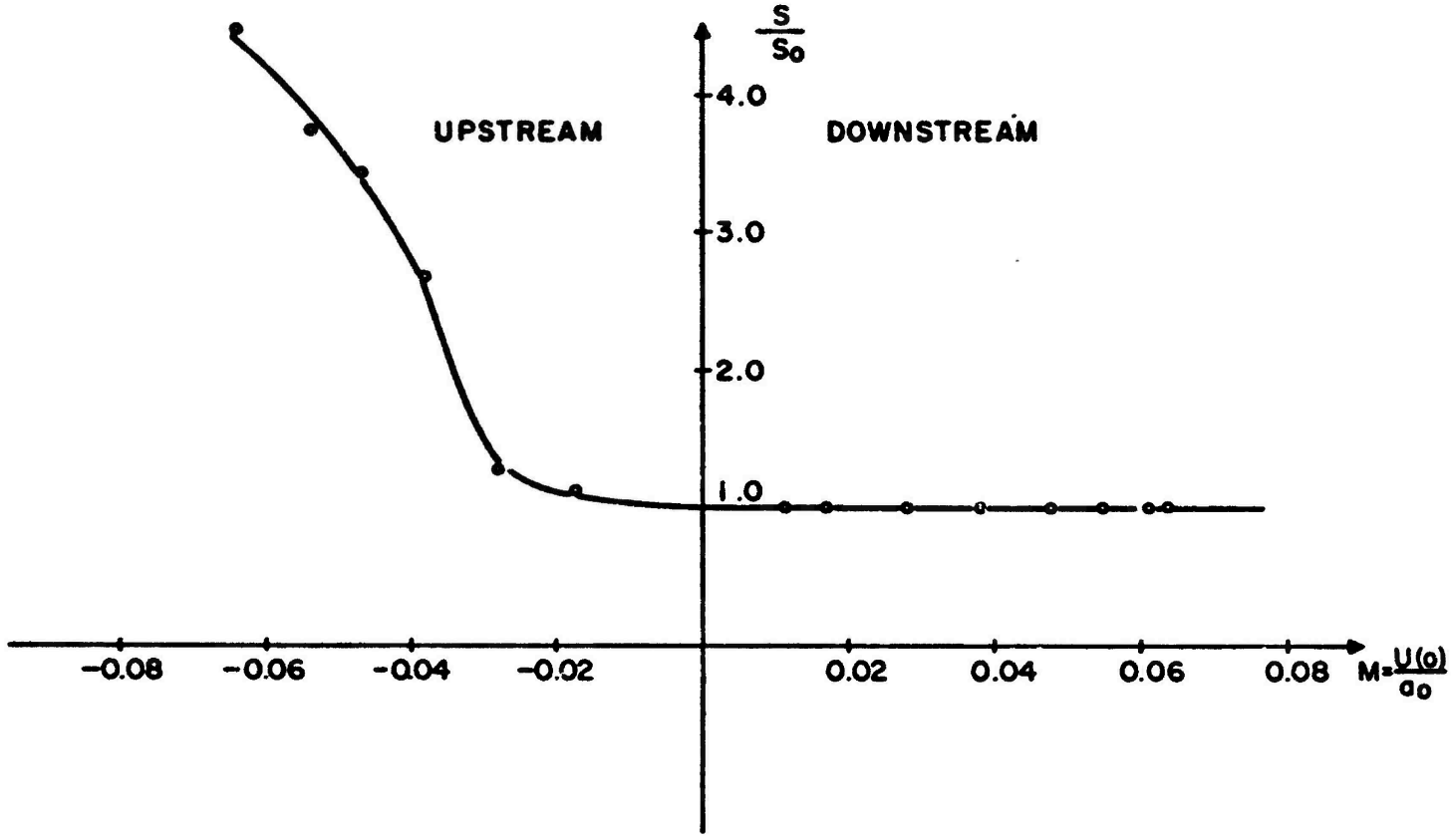

Fig. 6: The rise time of the wave front as function of flow velocity

S. Slope of the wave front
So: Slope of the wave front as M = 0

FLOW DUCT NOISE STUDIES INVOLVING SPATIAL FILTERING TECHNIQUES

by

F. A. Aupperle and R. F. Lambert
Institute of Technology
University of Minnesots
Minneapolis, Minnesota

INTRODUCTION

A number of investigators (1,2) have examined the utility of a directional probe tube for extracting acoustic signals from flow noise in a duct. These probes can be used for acoustic power monitoring and have been proposed for measurement standards. To date probe tubes have been built as extensions of the microphone itself and inserted directly in the flow stream. Proposed here is a directional coupler, which operates on the same principle as the probe tube, but can be mounted on the wall. By mounting the device on the wall of the duct conceivably one can reduce flow disturbance and in addition, one can enhance via ρc terminations certain wave filtering properties of the coupler. Such terminations actually facilitate better rejection of the unwanted noise components and in addition make possible the direct measurement of both upstream and downstream acoustic signal components. Hence, this device is also capable of monitoring acoustic power radiation by directional wave filtering and in addition can be used for sensing standing wave patterns in the flow duct.

Ignoring for the moment signal attenuation or internal reflections the coupler consists of an array of coupling ports (tranducers) and a delay line. Signal sampling is done by microphones mounted at both ends (Fig. 1). If, for example, one assumes that there are N identical coupling ports aligned in the axial direction each of length b, width w and center to center separation a, and there is perfect pressure coupling, then one can mathematically model the coupler by an array of finite size transducers, the outputs of which are summed with an equal time delay between transducers of $\tau = a/c$. The basic frequency-wavenumber filtering properties of such an array have been discussed at length by Maidanik (3). If one applies shading principles (4) to the coupling of such an array, then theoretically more that 40 dB attenuation of the level of certain frequency-wavenumber components of the noise can be obtained. Obviously with a realizable device, there are internal reflections, attenuation, and imperfect pressure coupling. However, it appears on the basis of a computer simulated model and limited experimental studies, that a directional coupler can be realized that closely approximates the ideal coupler.

In this paper we first briefly discuss the important design parameters assuming an ideal model for the coupler. Next, we present some design considerations for an operational directional coupler and discuss results obtained to date.

FILTERING PROPERTIES OF THE IDEAL DIRECTIONAL COUPLER

If the total pressure signal is stationary in both time and space, one can show using spatial filtering arguments developed by Aupperle and Lambert (5) that the output signal of the coupler will be

$$S_o(\omega) = \int_{-\infty}^{\infty} P(K_x, \omega) \left|G(K_x, \omega)\right|^2 dK_x/2\pi \qquad (1)$$

where $P(K_x, \omega)$ is the wavenumber spectral density of the stationary pressure fluctuations detected at the wall of the flow duct, $G(K_x, \omega)$ is the Fourier transform of the impulse response function of the coupler, and K_x is the axial wavenumber. The dependence on the lateral wavenumber K_y is excluded since it is assumed that the coupling port width is sufficiently small that no lateral filtering is provided. This formulation is then directly applicable to flow noise excitation of any one-dimensional spatially distributed linear system.

However, in many situations of interest in flow duct acoustics, the acoustic pressure signal components propagating upstream and downstream are highly correlated. Thus, in general, the acoustic signal plus flow noise terms will not obey Eq. (1) and $S_o(\omega)$ must be reformulated. It can be shown that the output of the coupler can be written as the sum of a stationary and non-stationary component, viz.

$$S_o(\omega) = \int_{-\infty}^{\infty} P_1(K_x, \omega) \left|G(K_x, \omega)\right|^2 dK_x/2\pi \qquad (2)$$

$$+ \int_{-\infty}^{\infty} P_2(K_x, \omega)\, G\left[-K_x(1 - M_c)\,,\ \omega\right] G\left[K_x(1 + M_c)\,,\ -\omega\right] dK_x/2\pi$$

where $M_c = U_c/c$ is the convective mach number, $P_1(K_x, \omega)$ is the spectral density function for the stationary components of the excitation, and $P_2(K_x, \omega)$ is the spectral density of the non-stationary components of the excitation. Basically $P_2(K_x, \omega)$ comprises a cross correlation term between the upstream and downstream propagating acoustic signals. The second term in Eq. (2) does introduce an element of mathematical complexity but does not alter the essential characteristics of the filtering action by the coupler. This term can be minimized by design and actually may be negligible in many applications. For example, the second term in Eq. (2) may be negligible compared with the first if the acoustic signals are broadband noise since upstream and downstream signal components become uncorrelated if there is sufficient time delay between them. More importantly this term can be made negligible for pure tone excitation if the spatial filter itself has sufficient wavenumber selectivity. For example, assuming $M_c = 0$ for simplification, the level of the second term is 17 dB below the first for measurement of a downstream signal provided the product

$$\Gamma \left|G^d(-\omega/c, \omega)\right| < 0.01 \qquad (3)$$

Here the superscript d indicates the transfer function at the downstream microphone position and Γ is the magnitude of the pressure reflection coefficient of the acoustic signal in the flow duct. In this paper it is assumed that only the dominant mode propagates in the flow duct.

In order to illustrate graphically various filtering properties of the coupler, modeled by an array of transducers, a typical measurement situation is sketched in Figure 2. Figure 2a illustrates the anticipated excitation spectra consisting of superimposed flow noise and both upstream and downstream acoustic signals for a particular excitation frequency ω. Figure 2b illustrates the filtering properties of the array of N identical coupling ports aligned along the axial direction of length b and center to center separation a. Actually the periodic component of this filter function in the illustration is determined assuming point transducers. The function

$$|H^d(K_x, \omega)|^2 = \left[\sin(\omega/c - K_x)b/2/(\omega/c - K_x)b/2\right]^2 \quad (4)$$

is the Fourier transform of the pressure impulse response function of an individual coupling port. This function is determined by assuming that the pressure fluctuations are transmitted uniformly through the coupling port and by accounting for the time delay along the port length. Figures 2a and 2b superimposed then illustrate a particular measurement situation where downstream acoustic signal information is wanted and the filter is set to reject both the upstream acoustical signal and the flow noise component. A comparable situation for upstream signal excitation is illustrated in Figure 3.

Examination of both Figures 2 and 3 reveal that the axial length of the coupling port b should be as large as possible to eliminate response maxima other than those at $\pm \omega/c$. If for example, b ~ a, then only maxima at $\pm \omega/c$ would appear. The filtering function for a continuous port of length $L = Na$ would be identical to that for multible ports with b = a. That is, for the continuous port only one response maxima located at $\pm \omega/c$ would be present. Thus, ideally one would choose a continuous coupling port in order to eliminate any unwanted maxima. However, multiple coupling ports improve the possibility of shading the response and if they are used one would choose the separation distance, a, such that the unwanted maxima fall beyond the wave-number range of interest.

It is evident upon further examination of Figures 2 and 3 that the inherent filtering properties of the coupler can be enhanced by reducing the side lobe contribution to the response. This can be accomplished by proper coupling design thereby improving both acoustic signal discrimination and flow noise reflection properties. Reduction of side lobe response is a common problem in array design and one technique is to employ shading principles (4). In this case by shading one chooses the coupler response to be maxima at the geometrical center of the array and tapers it to zero at both ends in some prescribed manner. Shading principles are commonly used when one wishes to obtain the signal spectal density of a signal sampled over either a finite time or spatial duration. For example, if one samples a signal f(x) over the interval (-L/2,L/2) the resulting signal is $s(x) = f(x)q(x)$ where $q(x) = 0$ for $|x| > L/2$. The Fourier transform of s(x) is then

$$S(K_x) = \int_{-\infty}^{\infty} Q(\beta)\, F(K_x - \beta)\, d\beta \qquad (5)$$

Here F(K) is the Fourier transform of f(x) and Q(K) of q(x).

Obviously in order to ascertain the spectra of f(x) from spectral measurements of s(x) one would prefer Q(K) to be narrow band and low pass. Thus one would choose the sampling window such that Q(K) contained no high wavenumber components. In order to reduce the level of such components one shades or rounds off the corners of the sampling window. (Fig. 4)

The above formulation is directly applicable to a directional coupler which samples a signal over a finite distance and from which one wishes to obtain the signal spectra at the wavenumbers $K_x = \pm \omega/c$. In order to numerically illustrate the inherent advantages of shading the coupling, the logrithmic expression:

$$F(K_o, \omega) = 20\ \mathrm{Log}_{10} \left[|G^d(K_o + \omega/c, \omega)| \,/\, |G^d(\omega/c, \omega)| \right] \qquad (6)$$

is plotted in Figure 5 as a function of the dimensionless variable $K_o L$. Curves a) and b) clearly illustrate the advantages of shading. Here $K_o = K_x - \omega/c$ and L is the total length of the continuous coupling port. Observe the marked difference between the spatial filtering function for the uniform port (curve a) and the filtering function for the port using the weighting function of Tukey and Hamming (curve b). As predicted, the side lobe response is reduced considerably, however, the center lobe is slightly broadened.

In order to examine flow noise rejection capabilities, the output of the filter was calculated using Eq. (1) with the wavenumber spectra of the flow noise $P(K_x, \omega)$ modeled after Corcos' approximation of the cross spectral density function, i.e.

$$P(K_x, \omega) = \int_{-\infty}^{\infty} \mathrm{Exp}\left(-\left|\frac{\omega\xi}{U_c \alpha_1}\right| + j\left(K_x - \frac{\omega}{U_c}\right)\xi\right) d\xi \qquad (7)$$

Here α_1 is a decay constant and for purposes of these calculations $\alpha_1 = 7.4$. The results are plotted in Figure 6 as a function of $\omega L/U_c$. Curves b) and c) were obtained from reference (2). The output for a coupler with a uniform port is given by curve b). Observe that the noise reduction increases with an increase in the parameter $\omega L/U_c$.

In recent years there has been considerable discussion about the magnitude of the low-wavenumber spectra of the wall turbulence in the range $K_x < \omega/U_c$. Measurements by Jameson (6) indicate that for some flow conditions this level can be as much as 30 dB below that predicted by the Corcos approximation. This observation takes on great importance if it is observed

(Figs. 2 and 3) that when the side lobe contributions are negligible, the flow noise captured by the spatial filter is due primarily to the low-wavenumber components falling in the range of the primary lobe.

Calculations assuming Corcos' approximation indicate that the side lobe contribution is negligible even for a uniform array. However, with a decrease in the level of the low-wavenumber spectra eventually the side lobe contribution due to the convective wavenumbers will dominate the noise terms. In curve c)(Fig. 6) the envelope of the output of a filter incorporating a uniform continuous coupling port assuming the level of the low-wavenumber flow noise spectra is zero is plotted as a function of $\omega L/U_c$ and in curve d) the envelope of a filter with Tukey-Hamming shading is plotted. Observe for zero low-wavenumber contributions, that the shaded coupling port provides considerably more noise rejection than a uniform port. In fact, such a device could be used to measure the wavenumber wall pressure spectra of turbulent air flow.

Since the level of the low-wavenumber spectra is not zero, one should assume that the actual noise reduction of the filter with a shaded coupling port excited by flow noise lies somewhere between curves a) and d). At present there is not sufficient data on the low-wavenumber spectra of turbulence for more accurate predictions. Thus, it is concluded that flow noise rejection by the spatial filter depends in a very significant way on the level of the low-wavenumber spectra of the flow noise and will depend on the array shading only if the level of the low-wavenumber spectra is sufficiently low.

DESIGN CONSIDERATIONS FOR THE DIRECTIONAL COUPLER

It is here propcsed to realize the spatial filter by a broadband directional coupler attached to the wall of the flow duct as illustrated in Figure 1. Pressure coupling to the flow duct is achieved either by one long continuous slit of length L or by N short slits or holes aligned along the axial direction. Here we will assume the ports (or slits) are covered with a flow resistant material since better filtering response appears to be realizable than with open ports. The basic coupler consists of a uniform tube whose internal dimensions permit only plane wave propagation over the frequency range of interest and with ρc terminations at each end.

In order to formulate the response of this coupler the approached presented by Wang and Crocker (1) will be employed for the pressure fluctuations in the coupler along the port. For their model the pressure fluctuations satisfy the differential equation

$$\frac{d^2 p(x,\omega)}{dx^2} + (\omega^2/c^2 - j\omega\rho_o w/AZ)\, p(x,\omega) = -j\omega\rho_o w/AZ\; p^1(x,\omega) \qquad (8)$$

Where $p^1(K_x, \omega)$ is the pressure fluctuation in the flow duct at a frequency ω and position x, w is the slit width, A is the cross sectional area of the coupler ρ_o is the density of air and

$$Z = d(\phi + j\omega\rho_p). \qquad (9)$$

Here d is the slit depth, Φ is the flow resistance of the material in the port and ρ_p is the effective density of air in the porous material.

For the coupler with multiple ports it is assumed that over the length of each port the pressure fluctuations in the coupler satisfy Eq. 8. Between ports it is assumed that the pressure fluctuations satisfy the homogeneous wave equation, i.e.

$$\frac{d^2p(x,\omega)}{dx^2} + (\omega^2/c^2)\, p(x,\omega) = 0 \qquad (10)$$

By matching boundary conditions at each port one can calculate the wave-number filtering characteristics for the filter with N ports. The frequency wavenumber transfer function can be written in the form below,

$$|G(K_x,\omega)|^2 = \frac{|T|^2}{4} \sum_{n=1}^{N} \sum_{m=1}^{N} U_n U_m^* H_n(K_x,\omega) H_m^*(K_x,\omega)\, e^{-j(K_x-\omega/c)(X_n-X_m)} \qquad (11)$$

Here $H_n(K_x,\omega)$ is the Fourier transform of the impulse response of an individual port, U_n are weighting functions which indicate how strong the signal from the n th port is weighted at the receiving microphone, and T is an amplitude scaling factor dependent on microphone location and coupling tube terminations. For ρc terminations T = 1.

Observe, that if the weighting functions U_n are constant so that the signal from each port is weighted equally and if the port filtering functions $H_n(K_x,\omega)$ are independent of n then the effective filtering function is that of a uniform array. In order to shade the array one need only to design the spatial filter such that the weighting functions U_n are of the required amplitude for the shading scheme desired. For multiple port coupling the individual U_n can be expressed

$$U_n = w_n b_n F_n / d_n (\Phi + j\omega\rho_p) A \qquad (12)$$

where F_n is a function dependent on the internal reflections and attenuation in the coupler. For the ratio $w_n b_n / d_n \Phi A$ sufficiently small it turns out that the internal reflections and attenuation are reduced and F_n becomes nearly independent of position. For this situation one can shade the array of ports by selecting either the individual length, width, depth, or flow resistance independently or in combinations.

Calculations of the side lobe response using this model assuming 25 ports uniformly spaced with a total array length of 22 cm. are presented in Figure 5. Observe that the theory predicts that more than 40 dB attenuation of the side lobe response is possible. The frequency response of the filter for waves propagating downstream is constant to the nearest 0.1 dB from 600 - 4000HZ. Experimental results have not been completed, however, an

initial measurement of the rejection of the unwanted acoustical component indicates that for the array of 25 slits with a total array length of 22 cm, one can obtain between 5-10 dB more attenuation of the reflected wave with a shaded array than with a uniform array of the same length in the frequency range 2-3KHZ. (Fig. 5).

As indicated in the introduction, enhanced filtering is obtained by virtue of ρc terminations on the ends of the coupling tube. This makes attenuation along the tube unnecessary and, therefore, reduces the required amount of energy coupling between the flow duct and the coupler. In fact, the filtering capabilities of the coupler are enhanced by reduction of attenuation of the signal in the coupler and by removal of any signals reflected from the ends of the coupler. This observation is illustrated in Figures 7 and 8. In these figures the filtering rejection properties of a continuous port are plotted as a function of $K_o L$ with port width or equivalently flow resistance as a parameter. In Figure 7, ρc terminations were assumed and in Figure 8, it was assumed that the signal was totally reflected at each effective end of the coupling tube. For the situation with ρc terminations, decreasing the port width and, therefore, the attenuation improves the inherent rejection properties of the filter by reducing the level of the side lobes. In fact, the filtering properties of this design theoretically approach that of a uniform transducer array as the port width is decreased. With end reflections accounted for, one observes that if sufficient attenuation is present the effect of the end reflections is negated (curve c) Figs. 7 and 8. Observe as the width of the port is decreased the filtering capability rapidly deteriorates as a result of serious end reflections. One sees that in order to minimize side lobe response and enhance the filtering capabilities of the coupler, end reflections should be eliminated and, in addition, attenuation should be reduced in so far as possible.

CONCLUSION

The filtering properties of a directional coupler mounted on the wall of the flow duct have been examined. For ideal conditions the coupler is modeled by an array of finite sized coupling ports and the important spatial filtering properties examined. A more realistic model is also presented and discussed in order to obtain design criteria.

It was concluded from a spatial filtering viewpoint that a continuous coupling port is preferable and also that for detecting either upstream or downstream propagating acoustic signals one would shade the port coupling in order to enhance the front to back selectivity of the spatial filter. The shaded coupling port may provide superior flow noise reduction properties depending on the level of the low-wavenumber spectra of the flow noise.

Calculations of the response of a multiple port coupling tube indicate that theoretically shading facilitates side lobe response more than 40 dB below the peak response. Experimentally we have been able to realize 25-30dB side lobe attenuation. It was also demonstrated that both attenuation in the coupling tube and reflections from the ends of the tube decrease the effective filtering capabilities of the coupler. Another advantage of mounting the coupler on the wall of the flow duct is that one may provide ρc terminations thereby reducing end reflections and eliminating the need for large attenuation along the length of the coupler.

ACKNOWLEDGEMENTS

This work was supported by a grant from the NSF. G34043

REFERENCES

1) J. S. Wang and M. J. Crocker, Proceedings of Noise Con 73, October, 1973, Washington, D. C., Library of Congress Catalogue Number 72-91606. Investigation of the Characteristics of Tubular Microphone Windscreens for In-Duct Fan Sound Power Measurements.

2) W. Neise, Symposium, Acoustics of Flow Ducts, University of Southampton, Jan., 1972. The Flow Around the Microphone as an obstacle for Sound Measurements in Flow Ducts.

3) G. Maidanik, 1967. Journal of the Acoustical Society of America, 42, 1017-1024. Flush-Mounted Pressure Transducer Systems as Spatial and Spectral Filters.

4) E. Parzen, 1964, Proceedings of Symposia in Applied Mathematics, XVI, 221-246, Library of Congress Catalog Number 64-18128. On Statistical Spectral Analysis.

5) F. A. Aupperle and R. F. Lambert, 1972, Journal of Sound and Vibration 24, 249-267. On the Utilization of a Flexible Beam as a Spatial Filter.

6) P. W. Jameson, 1970, Bolt Beranek and Newman Report No. 1937. Measurements of Low-wavenumber Component of Turbulent Boundary Layer Wall Pressure Spectrum.

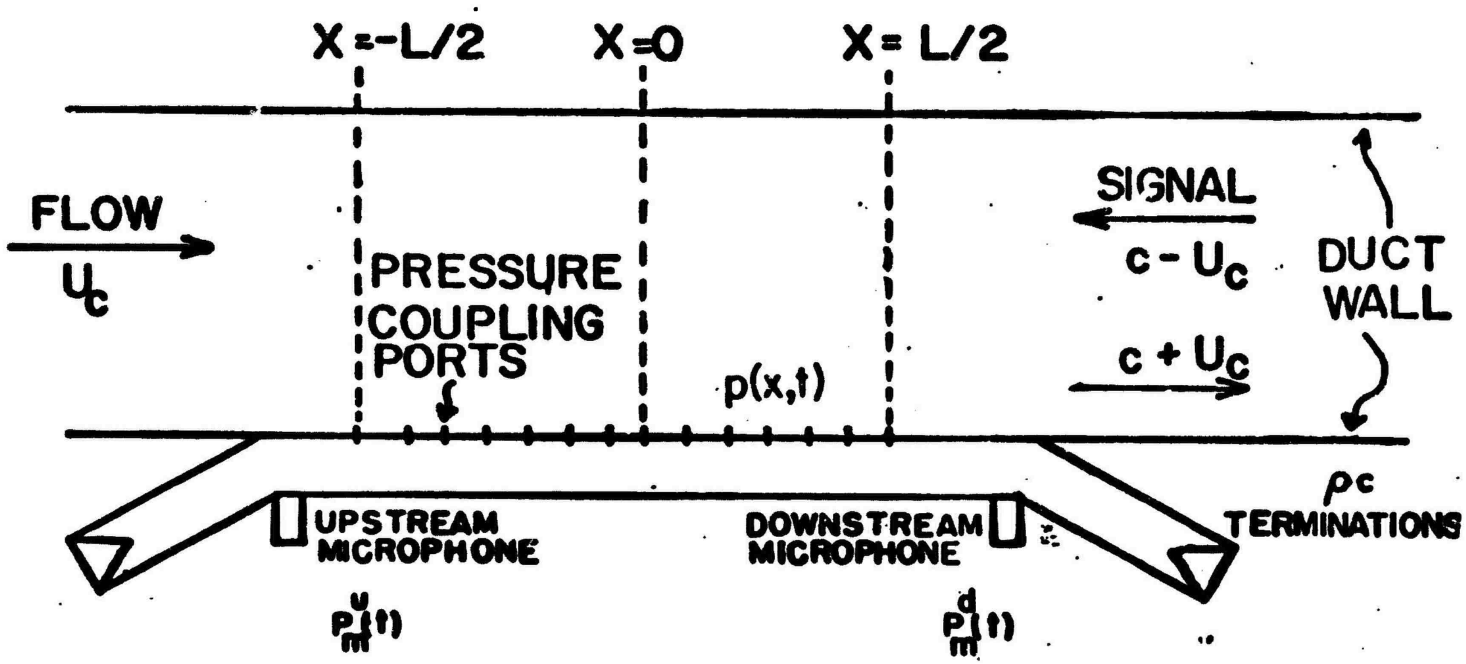

Figure 1. Schematic diagram of directional coupler and coordinate system.

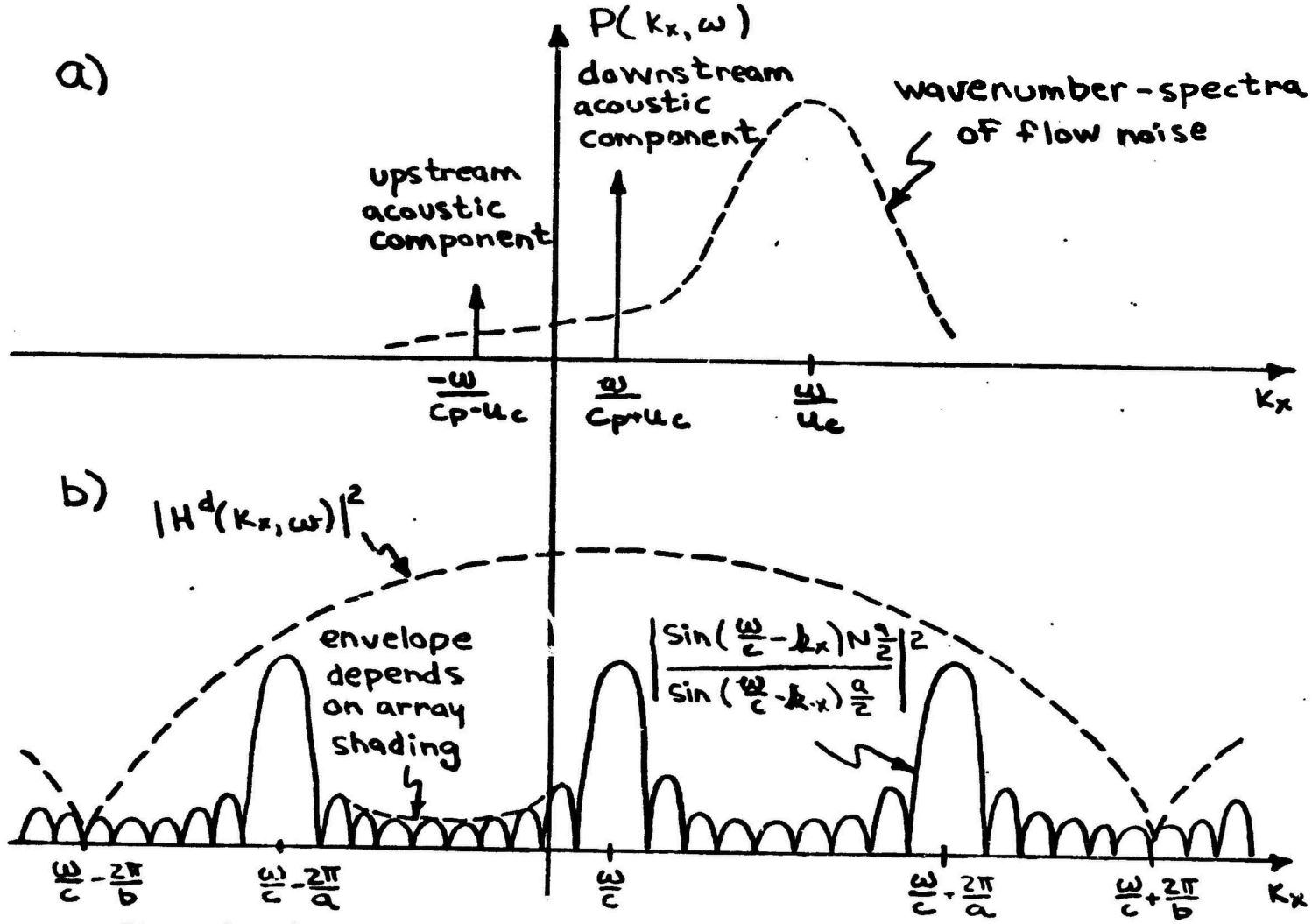

Figure 2. a) Wavenumber spectra of the acoustic signals plus the spectra of the flow noise. b) Wavenumber filter characteristics of the coupler with the output downstream of the ports.

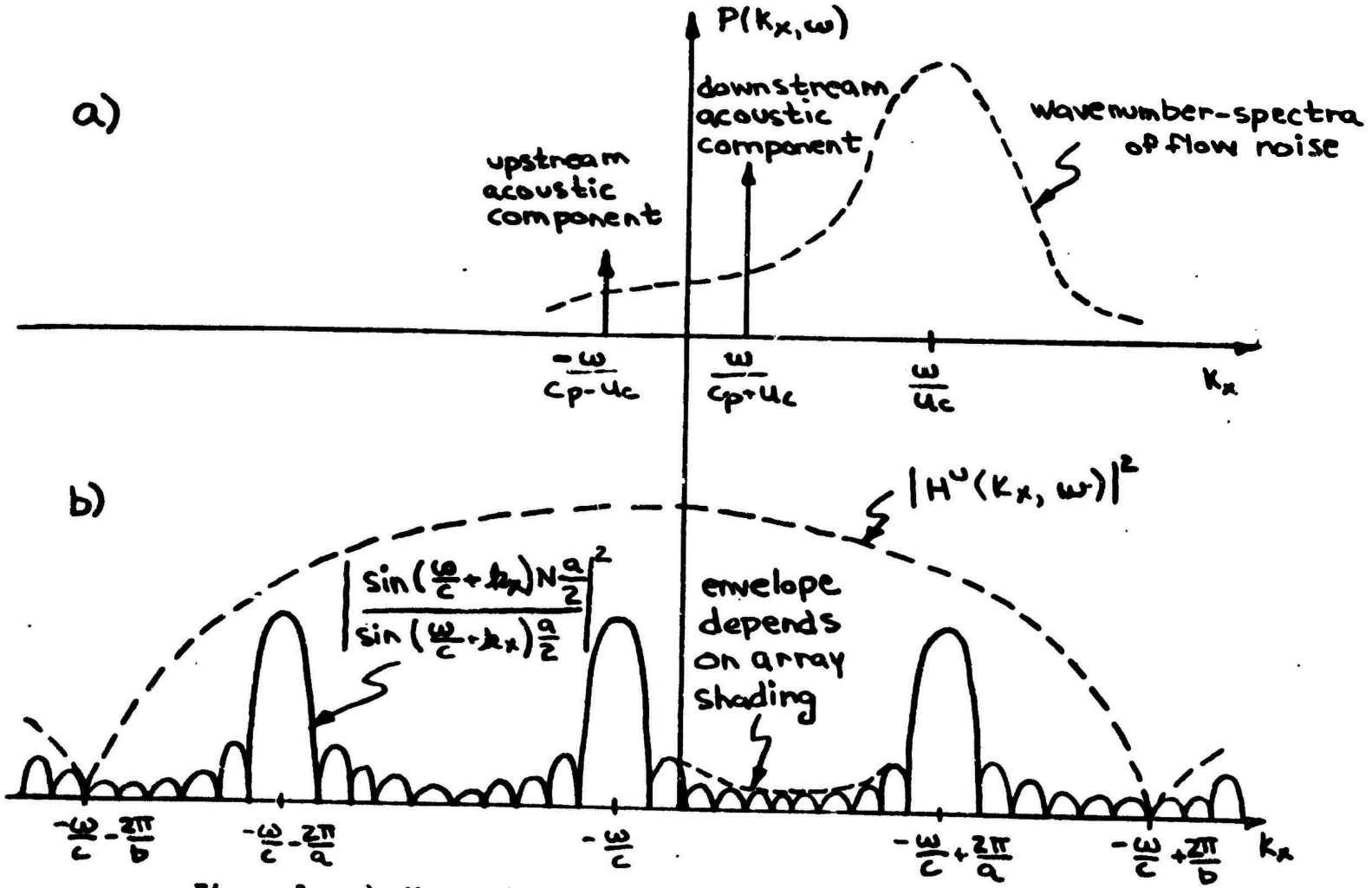

Figure 3. a) Wavenumber spectra of the acoustic signals plus the spectra of the flow noise. b) Wavenumber filter characteristics of the coupler with the output upstream of the ports.

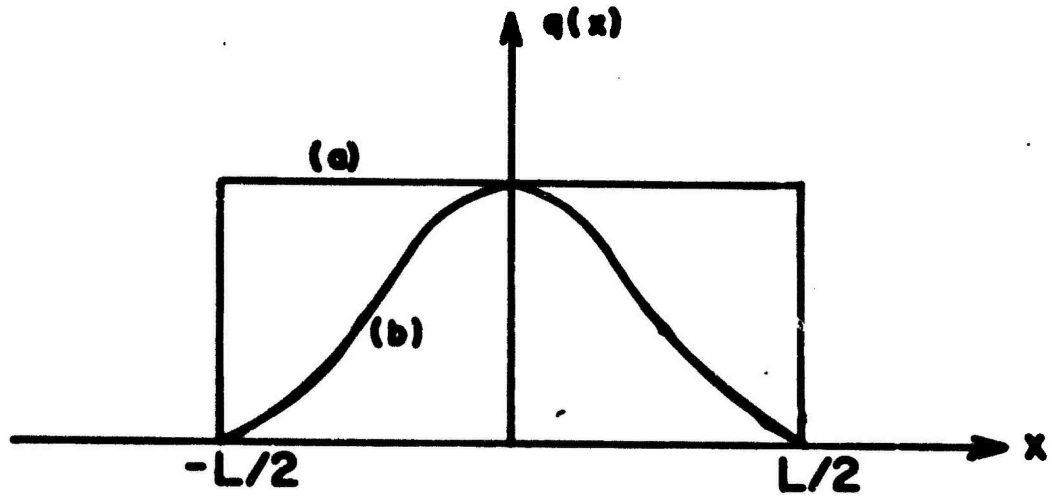

Figure 4. Weighting function for signal sampled for a finite duration. a) Uniform weighting function, b) Tukey-Hamming weighting function, $q(x) = \sin^2(\pi/L(x-L/2))$.

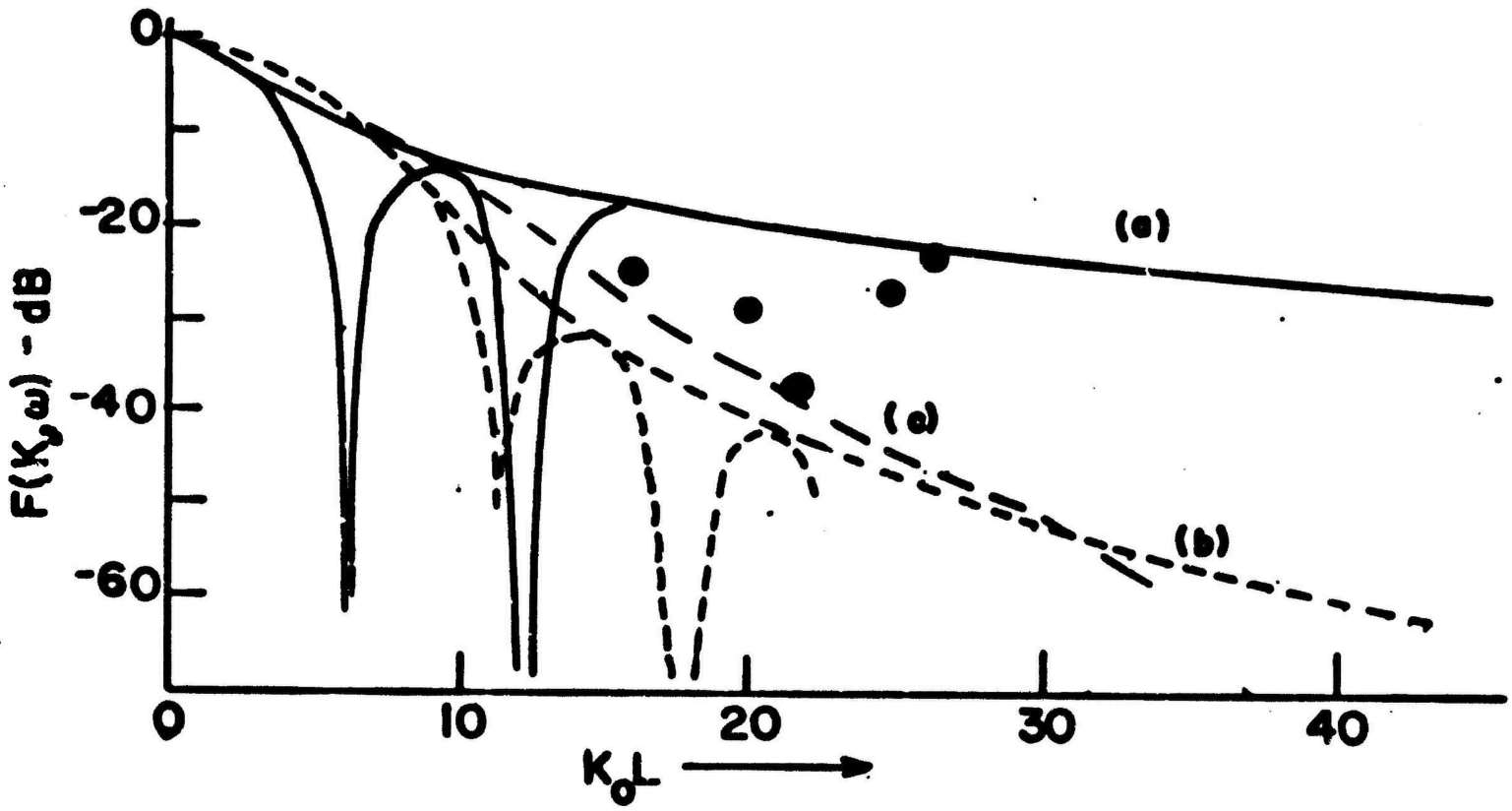

Figure 5. Wavenumber spectra of spatial filter. a) Ideal model with a uniform weighting function. b) Ideal model with Tukey-Hamming weighting function. c) Corrected model with Tukey-Hamming shading of port area. N = 25, $b_p = w_p = 0.254$ cm. ● , Experimental data with Tukey-Hamming shading of port area. Center port is a hole of radius $r_1 = 0.127$ cm.

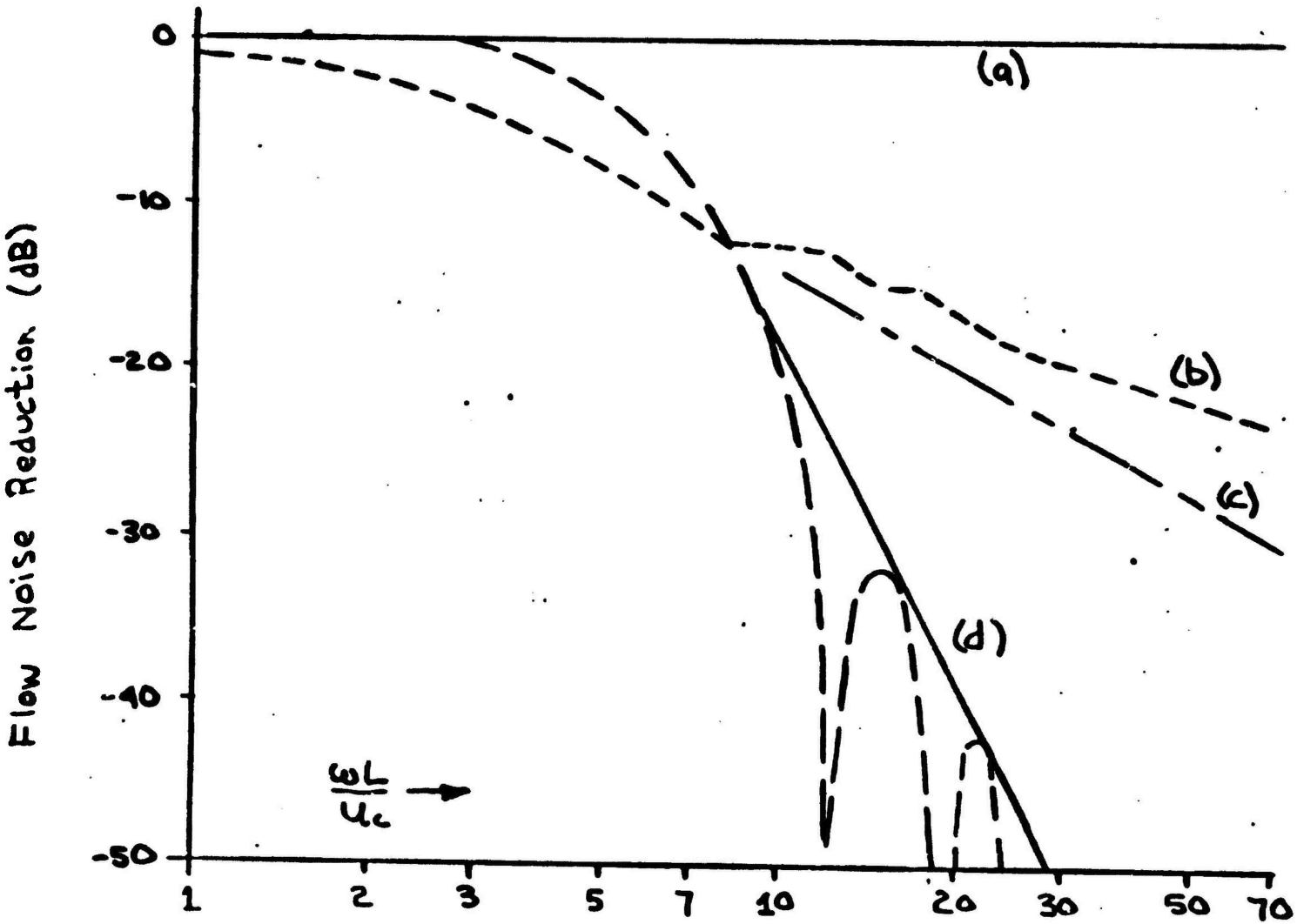

Figure 6. Comparison of flow noise rejection. a) $M_c = 1$, $\alpha_1 = \infty$. b) $M_c << 1$, $\alpha_1 = 7.4$, uniform weighting function. c) $M_c << 1$, $\alpha_1 = \infty$, uniform weighting function. d) $M_c << 1$, $\alpha_1 = \infty$, Tukey-Hamming weighting function.

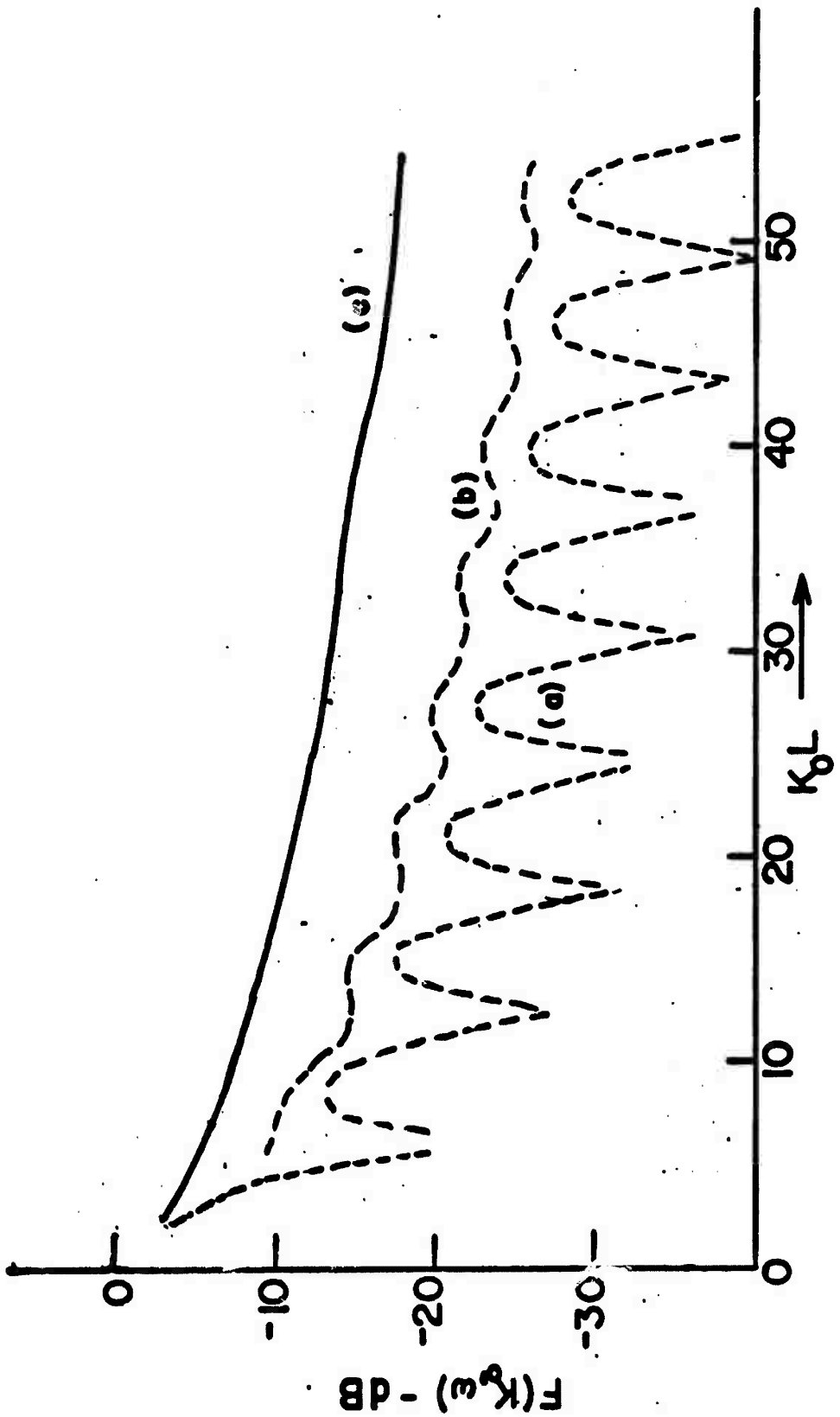

Figure 7. Wavenumber spectra of spatial filter for continuous port. ϕ_d = 350 Rayls, A = 0.542 cm.^{2}, ρc terminations. a) w = 0.254 mm. b) w = 1.27 mm. c) w = 3.81 mm.

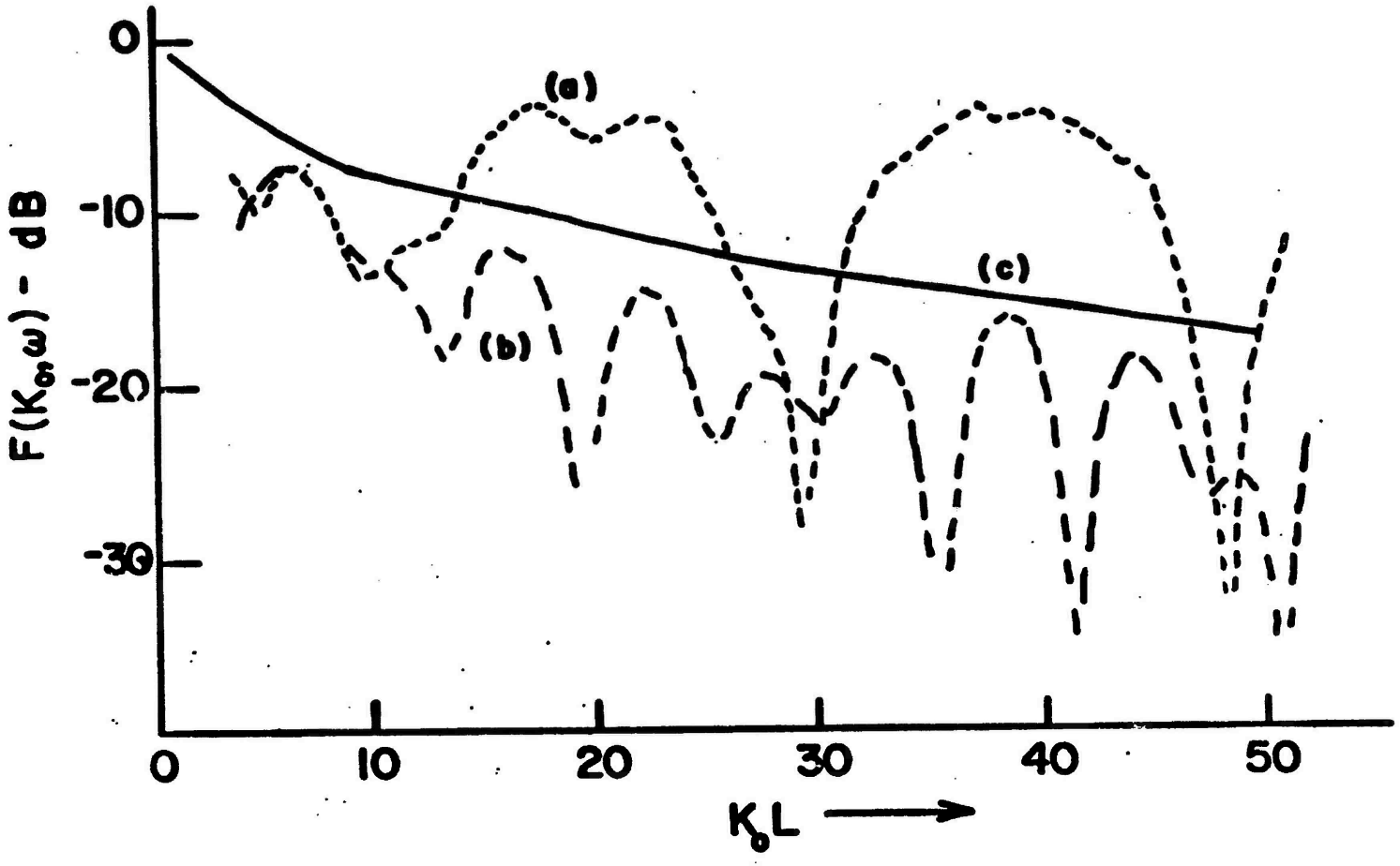

Figure 6. Wavenumber spectra of spatial filter for continuous port. Φd = 350 Rayls, A = 0.542 cm^2, total reflection at terminations. a) w = 0.254 mm. b) w = 1.27 mm. c) w = 3.81 mm.

NOISE IN INTERNAL FLOWS

by

J. P. Johnston, D. W. Roberts, W. E. Schmidt

Department of Mechanical Engineering
Stanford University, Stanford, CA. 94305

ABSTRACT

A novel air flow apparatus for study of noise generation and sound wave propagation in pipes with flow has been constructed. The principal objectives of the program for which it was designed are to: (i) study propagation of sound through restrictions (orifices, nozzles, valves, etc.) in a pipe with and without flow, (ii) investigate the sound generation mechanisms and their relationship to the fluid flow patterns resulting from the restrictions, (iii) compile useful engineering data on acoustic power generated and radiated from various standard types of restrictions and (iv) develop a cross-correlation wall pressure measurement technique that allows the decoupling of plane acoustic wave signals from the pseudo-sound resulting from flow convected fluctuations. The apparatus is described, some of its measured acoustic characteristics are presented, and preliminary results on overall SPL levels measured downstream of four different sized ASME metering orifices are given.

INTRODUCTION AND OBJECTIVES

The problem of noise generation and sound propagation in the presence of high-speed gas flow through restrictions (orifices, nozzles, valves, etc.) in pipe lines is a vital area for basic research[1,2,3,4,5,6]. As pointed out by Heymann[1], it is particularly important, in order to lay a proper basis for design analysis, to separate the internal aeroacoustic effects from the separate problems of acoustic wave transmission along, and through the pipe wall material. Our research centers upon internal flow aeroacoustics.

The most common technique for study of control valve or orifice noise is to place the valve with, or without, a short length of discharge pipe in a reverberant chamber where a microphone, placed far from the valve's discharge jet, picks up the radiated acoustic energy. In reference 1 this technique is used in a chamber with a low frequency limit of about 800 Hz for 1/3-octave band analysis. A larger, but similar facility was seen during a recent trip by the first author to the Institute of Sound and Vibration Research, Southampton University, England.

The apparatus devised for our research is quite different, and is believed to have a number of advantages over the reverberation chamber method. Details of our method are outlined below and in Figs. 1, 2 and 3. Acoustically its main advantage is that pressures are measured right on the inside of the pipe wall. Thus one obtains the total fluctuating forces on the pipe, as well as the acoustic component propagated along the pipe from the main noise sources close to the restriction (test element, Fig. 2). A major part of our future research will concentrate on techniques* for separating acoustic wave magnitudes

*NSF Proposal , MET-27-72, August 1972 from Stanford Univ., Mech. Engrg. Dept.

from the part of the measured pressure signal due to pseudo-sound. The main fluid dynamic advantage of our new apparatus is that it can model the actual geometry of restriction and downstream pipe line much more realistically than can the reverberation chamber method. Finally, our apparatus, because it requires no large chamber may be considerably cheaper to build than equipment for other methods.

Many different uses may be envisioned for our new apparatus, but the principal objectives of the program for which it was designed are to: (i) study propagation of sound through restrictions (orifices, nozzles, valves, etc.) in a pipe with and without flow, (ii) investigate the sound generation mechanisms and their relationship to the fluid flow patterns resulting from the restrictions, (iii) compile useful engineering data on acoustic power generated and radiated from various standard types of restrictions and (iv) develop a cross-correlation wall pressure measurement technique that allows the decoupling of plane acoustic wave signals from the pseudo-sound resulting from flow convected fluctuations.

DESCRIPTION OF APPARATUS

Basically, the apparatus is a long, 4 inch diameter, plastic (PVC), schedule 80 pipe made up in flanged sections as shown in Figs. 1 and 2. Both ends of the pipe are closed by anechoic terminations, Fig. 3.

Flow, at controlled rates, enters and leaves the pipe through 16 inch long, 1/8 inch thick, porous cylinders of sintered bronze particles. These cylinders have the same inside diameter as the pipe, 3.83 inches. Flow feeds into and out of the porous cylinders through short annular, 8 inch diameter, pipe segments that form plenum chambers. At peak flow rates of 300 SCFM, the radial speed of the air through the porous cylinders is about 1.5 ft/sec and the mean axial air speed in the pipe is close to 50 ft/sec.

The inlet and outlet plenum chambers are baffled and lined with acoustical grade open-cell foam to reduce some resonant standing waves that showed up in early studies of background noise inside the pipe. However, the porous cylinders are very stiff and transmit very little acoustic energy to the inside of the pipe. Measurements indicated that they attenuate transmitted sound pressure levels by at least 30dB. Thus sound waves propagated into the plenum chamber from far upstream in supply pipes, filter or control valves do not seriously influence pipe background noise levels for our present purposes.

The particular restriction, or test element type, chosen for test is placed between flanges a distance about midway from inlet to outlet. Lengths of pipe, flanged on both ends, can be added up- and downstream of the element as desired. The total length of our test stand* is currently limited to 26 ft, but added lengths of up to 20 ft might be added later if needed. Some of the pipe sections are fitted with wall static pressure taps and special ports for mounting traversing probes** and microphones or other dynamic wall pressure transducers.

---

*A steel channel, shock mounted on posts set in the floor, upon which the 4 inch pipe rests.

**Total pressure tubes, static pressure tubes and hot wire anemometers are to be used later in the experimental program.

Our first test element type is a set of standard ASME, square edged, flow metering orifice plates. Their hole diameters are 1/2, 3/4, 1 and 2 inches respectively. This geometry was chosen for three reasons: (i) It is the most common class of flow meter in practical pipe systems, (ii) it gives a high fluid power loss and produces a high internal noise level and (iii) most important, it is geometrically the simplest and most easily replicated restrictive element one can devise. Should standards for internal aeroacoustic measurements ever be established, the orifice is an excellent choice for the standardizing flow element.

Currently we have measured only a few flow parameters: pressure drop across the orifice, upstream pressures and temperature and mass flow rate. Two B and K (Type 4134) half-inch condenser microphones, with shields removed so that their diaphrams may be held flush at the inside of the pipe wall, are the principal acoustic transducers. The microphones are mounted in especially designed holders that allow them to operate safely under base pressures up to 30 psig. Shortly, we will also have two Kistler Piezotron (204M) pressure transducers (SPL 70 to 176dB, flat to 3dB from 8 to 20000 Hz) which are more rugged than the B and K microphones. The latter transducers will be particularly useful in the pipe wall regions that are close to the developing jet; just downstream of the orifice where pressure fluctuation levels above the useful range of the B and K microphones are anticipated.

Because objective (i) of our program is to study sound propagation through the pipe restrictions and to measure their acoustic impedences with flow, we have constructed a special insert that holds a 3 inch loudspeaker perpendicular to the pipe axis. The speaker, which can generate acoustic waves, slips between flanges that connect one, or the other, anechoic termination to its plenum. As shown in Fig. 2 it may be used to broadcast in the downstream direction, or alternatively, it may be placed by the outlet plenum to broadcast upstream. No tests with this feature have been made to date.

Even though we have just started operations, a few preliminary results are presented below to indicate the possible value, and some of the capabilities, of this new apparatus for internal aeroacoustics research.

PRELIMINARY RESULTS

The initial development of the anechoic terminations was done as part of a series of absorption coefficient experiments on a variety of configurations. The commercial, B and K standing wave apparatus of the acoustics laboratory in the Stanford Department of Aeronautics and Astronautics was used. Tests on models closely identical to our final design gave absorption coefficients of 80% at 100 Hz, 94% at 200 Hz, 98% at 300 Hz and above 99% from 400 to 2000 Hz, the upper limit of the experiment.

A series of experiments conducted in the actual apparatus set up without any flow restriction (test element) established one measure of background noise as a function of air flow rate. In Fig. 4 are shown two typical background noise spectra taken at the downstream microphone port, see Fig. 2 for its location. The peak values of SPL, sound pressure level, were recorded at lowest frequency. Levels higher than those shown were obtained below 200 Hz. Without doubt, the high level of noise at low frequency is caused by strong

standing waves that develop below 200 Hz where the termination absorption coefficients drop sharply lower than 94%. Two-hundred Hz is the lower useful frequency, and thus all reported overall sound pressure levels were obtained by linear integration after high-pass filtering of the microphone output to remove signal below 200 Hz.

A full set of data on background noise for the full range of possible flow rates is shown as the no-orifice curve in Fig. 6. Noise floor levels at zero flow vary randomly depending on conditions in the laboratory building at time of test. However, the typical noise floor level inside the pipe is an overall SPL of 50bB, well below the 80bB obtained at lowest flow rate during orifice tests. Figure 6 also shows that, except for the 2 inch orifice, all measured noise levels are 30dB or more above the background so that background noise was not a serious problem.

Figure 5 gives some characteristic downstream SPL spectra for the orifice with the 3/4 inch diameter hole. The upper two curves are very similar to each other, but different than the lower curve. The reason for this behavior probably lies in the fact that the flow was supercritical for the curve labeled 143.1dB. The flow for the middle curve, labeled 133.5dB, is just barely choked or slightly supercritical. However the flow for the lower curve, 111.0dB, is totally subcritical. Its orifice jet is all subsonic and contains no supersonic zones or shocks as does the jet formed behind the orifice when it operates supercritically. We are not yet able to offer a detailed interpretation of the spectral curve shapes, yet apparently the supercritical flows generate much more acoustic power in the 400 to 4000 Hz range than does subcritical flow.

When overall, downstream sound pressure levels are plotted against the "indicated" Mach number*, M_i , of the orifice jet, Fig. 7, one sees no distinct change in curve shape as the jet goes from sub- to supercritical flow somewhere near $M_i = 1$. However, the SPL curves do appear to approach an upper limit of about 147dB. This result is yet to be explained. But, if overall SPL does in fact attain an upper limit once full supercritical flow is reached, then the acoustic efficiency, η_a , will rise to a maximum in the supercritical zone and then decrease as orifice pressure drop continues to increase. This fact, if true, could have considerable value to the design engineer who wishes to optimize pipe and valve cost and size, and at the same time is required to keep noise below recommended levels.

---

*M_i obtained by assuming isentropic flow from upstream stagnation, p_1, ahead of orifice to downstream static, p_2 . p_1 and p_2 measured at standard flange tap locations.

$$M_i = \frac{2}{\gamma-1}\left[\left(\frac{p_1}{p_2}\right)^{\frac{\gamma-1}{\gamma}} - 1\right]$$

Acoustic efficiency, defined as in Ref. 1, is $\eta_a = W_a/W_f$ where W_a is the acoustic power transmitted down the pipe from the orifice jet region. W_f is the flow power defined as $W_f = (1/2)U_i^2\dot{m}$. $\dot{m}$ is the mass rate of flow and U_i is a defined theoretical "indicated" isentropic jet velocity obtained from $U_i = M_i c_o$. c_o is the upstream, stagnation speed of sound.

Measured overall, downstream SPL values, converted to W_a, gave us a rough measure of η_a. It was found that η_a increased as the (5/4) power of M_i, for subcritical orifice jet flow. This rate of increase is very slow compared to the 8th power law of "quadrupole" free jet flow. It is even well below the 3rd power law that one might expect to obtain if most of the acoustic power were generated by "dipole" mechanisms through interaction of the jet with the orifice plate and pipe walls. The fact that higher values of acoustic efficiency were obtained for the orifices with larger holes relative to pipe diameter indicates that jet - pipe wall interactions are probably quite important.

Finally, we note that the magnitudes of η_a were not unreasonable. Maximum values of $\eta_a \approx 1.3 \times 10^{-4}$ occurred at M_i values slightly above unity, in the supercritical jet flow regime. η_a decreased slightly for higher M_i in the region where overall SPL is limiting out to about 145 to 147db. The lowest values of η_a observed in these tests were between 1.5 to 2.5 x 10^{-5} for M_i values between 0.2 and 0.6 .

CONCLUSION

These data and conclusions are very recent. They should be treated as preliminary until backed up by more research.

There are a number of measurement problems and questions about the measurements that must be studied in the coming months. Most vital is the question of refraction effects due to radial and axial flow field velocity profiles in the region where the jet mixes out and refraction in the region where the flow exits from the pipe through the porous cylinder. SPL is easily measured downstream of the outlet plenum, but its value upstream of this outlet is that which we really desire.

When we measure upstream of the outlet the main problem is the separation of acoustic wave pressure fluctuations from the total signal which includes the pseudo-sound generated by flow convected eddies. Both real and pseudo-sound are of interest. A technique for this measurement which entails the use of two wall pressure transducers displaced in the axial direction is to be attempted. The method is similar to that of Ref. 7. Time shifted correlations between the two signals can, it is hoped, separate plane (200 to 2000 Hz range) acoustic wave pressures from the pseudo-sound even when signal-to-noise ratio is as small as 1, or perhaps even lower.

[Work is supported by NSF Grant GK-37294. Particular thanks for needed assistance in the early stages goes to Professor I. Kavrak of Bogazici University, Turkey, a visitor in our department in 1973. Professor W. C. Reynolds had the initial idea for the main design features of the current test apparatus as outlined in the grant proposal.]

REFERENCES

1. Heymann, F. J., "Some experiments concerning control valve noise", NOISE-CON 73 Proceedings, Wash. D.C., Oct. 15-17 (1973), pp. 383-388.

2. Baumann, H. D., "On the pressure level of aerodynamically created sound pressure level of control valves", ASME Paper 70-WA/FE-28, (1970).

3. Schuder, C. B., "Coping with control valve noise", Chemical Engineering, Oct. 19 (1970).

4. Reethof, G. and A. V. Karvelis, "Control valve noise and its reduction", Inter-Noise 72 Proceedings, (1972), pp. 146-153.

5. Nakano, A., "Characteristics of noise emitted by valves", 6th International Cong. on Acoustics, Tokyo (1968), Paper F-5-7, pp. F-169/F-172.

6. Katra, T. S. and D. B. King, "Noise-control design using scale model tests", ASME Paper No. 71-WA/Pwr-7, (1971).

7. Thornton, W. R. and M. Crocker, "Pressure cross-correlation of white noise in a turbulent flowing medium in a cylindrical duct", ASME Paper No. 71-WA/FE-5, (1971).

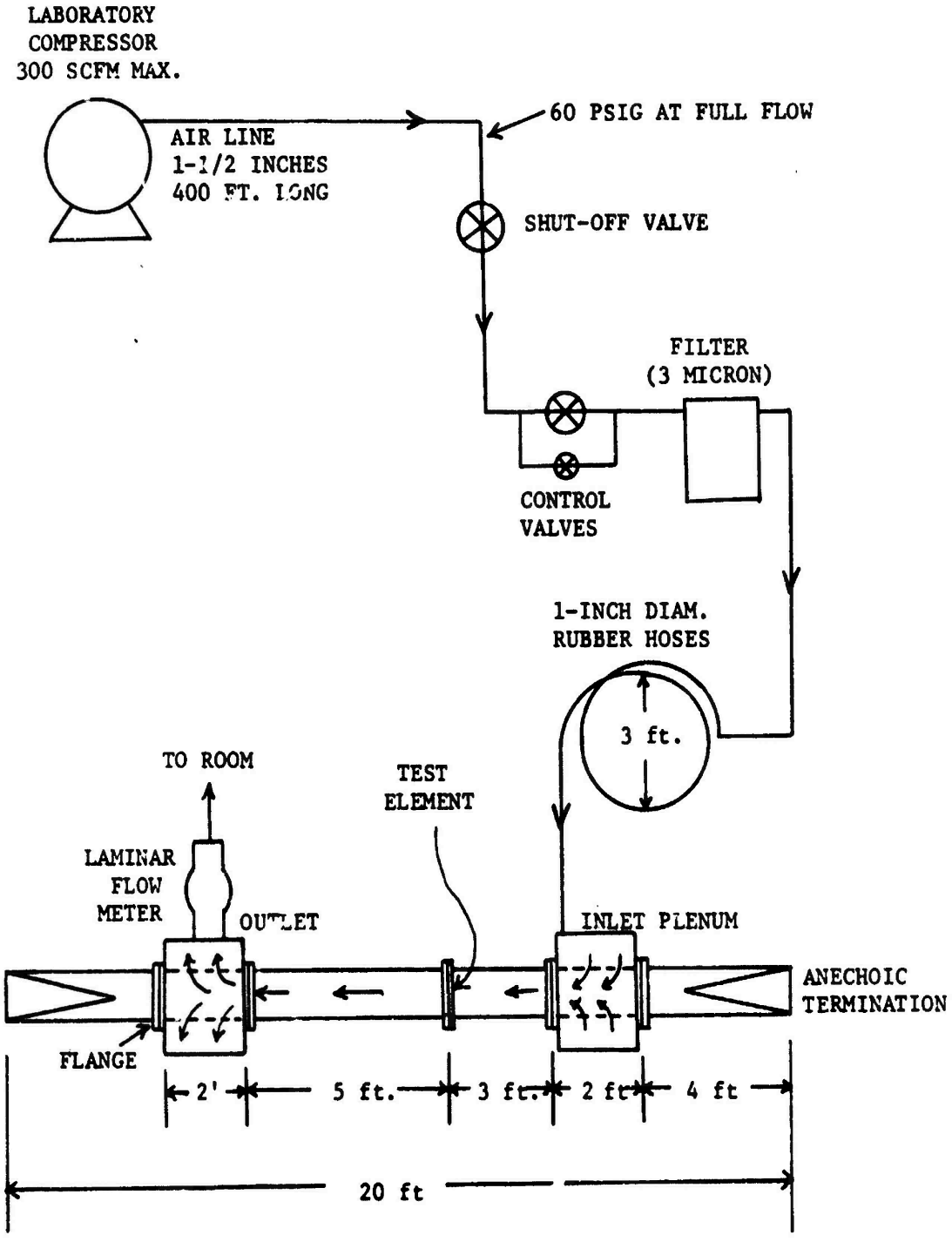

Fig. 1. SCHEMATIC OF TEST APPARATUS

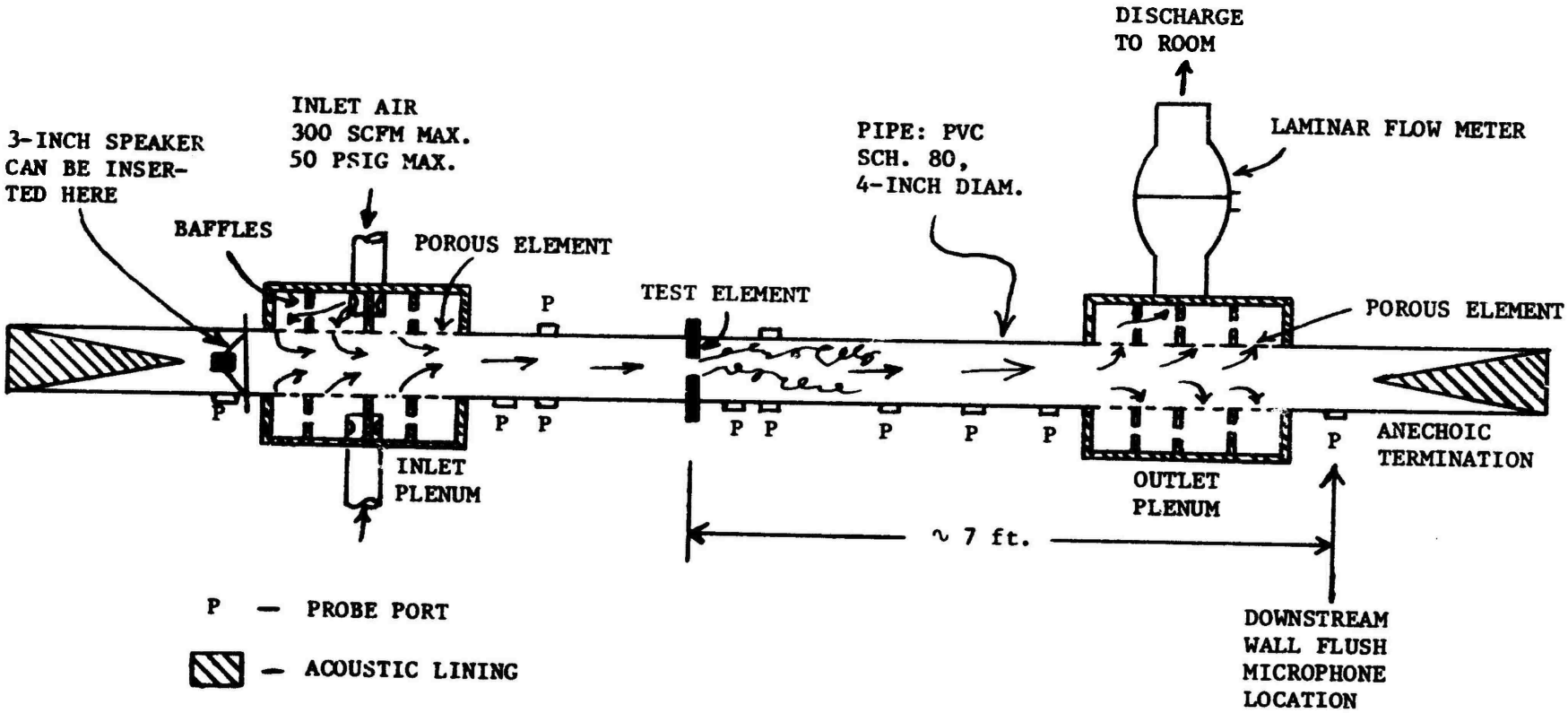

FIG. 2. DETAILS OF THE PIPE

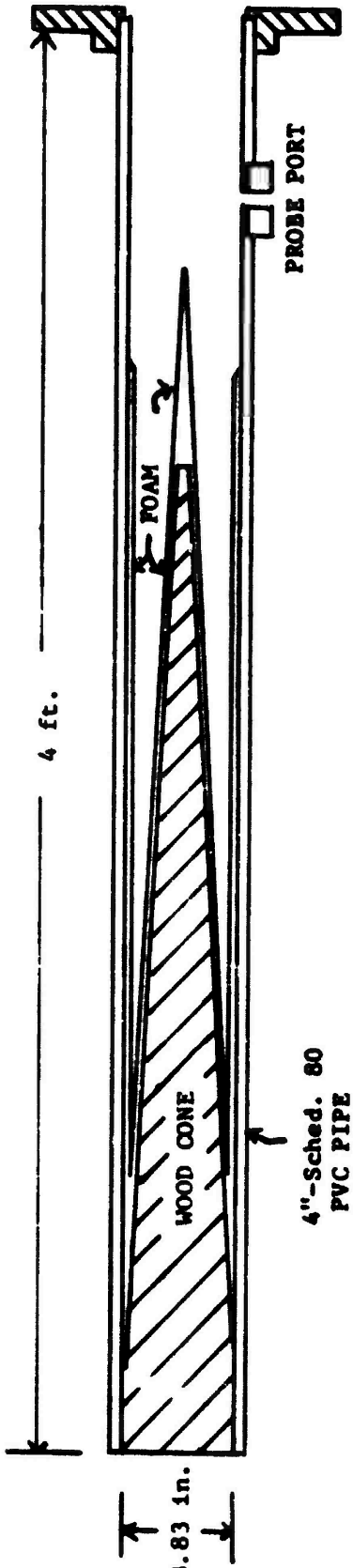

Fig. 3. THE ANECHOIC TERMINATION

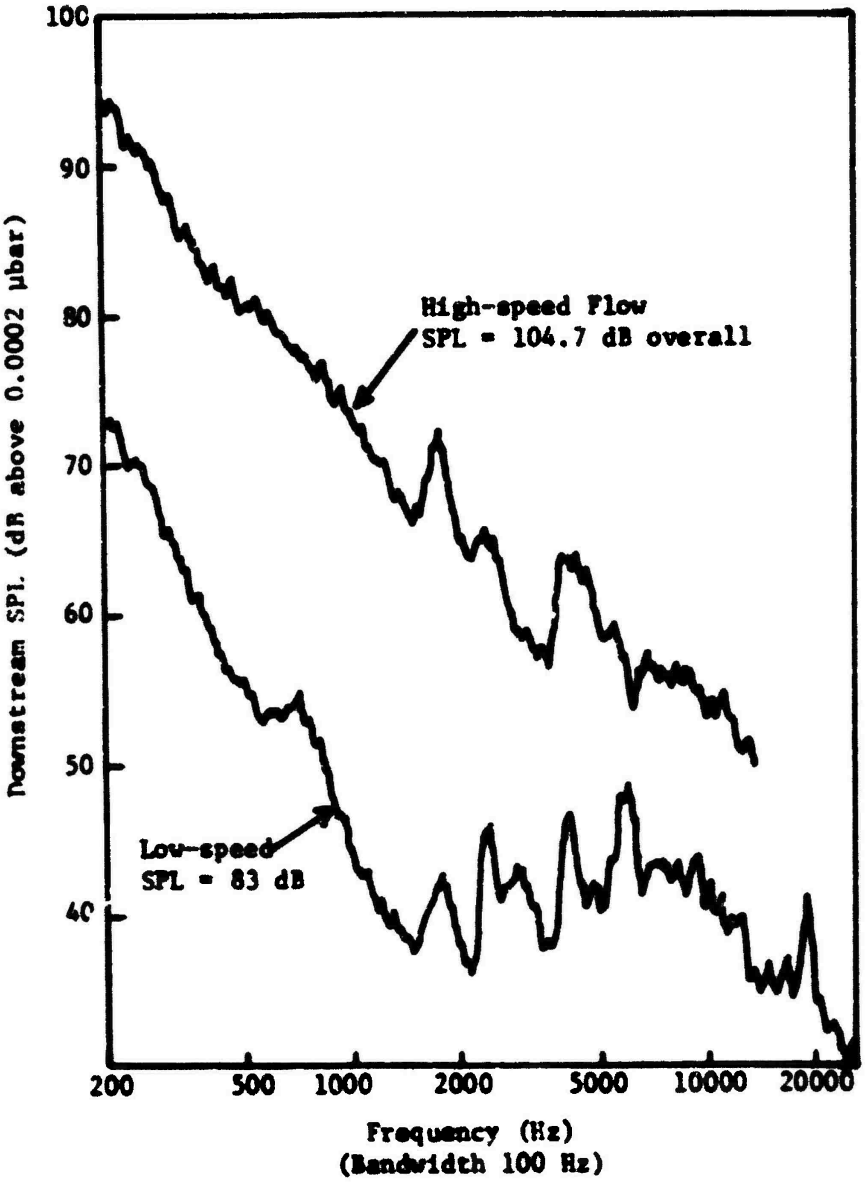

Fig. 4. Background noise spectra in pipe without obstruction.

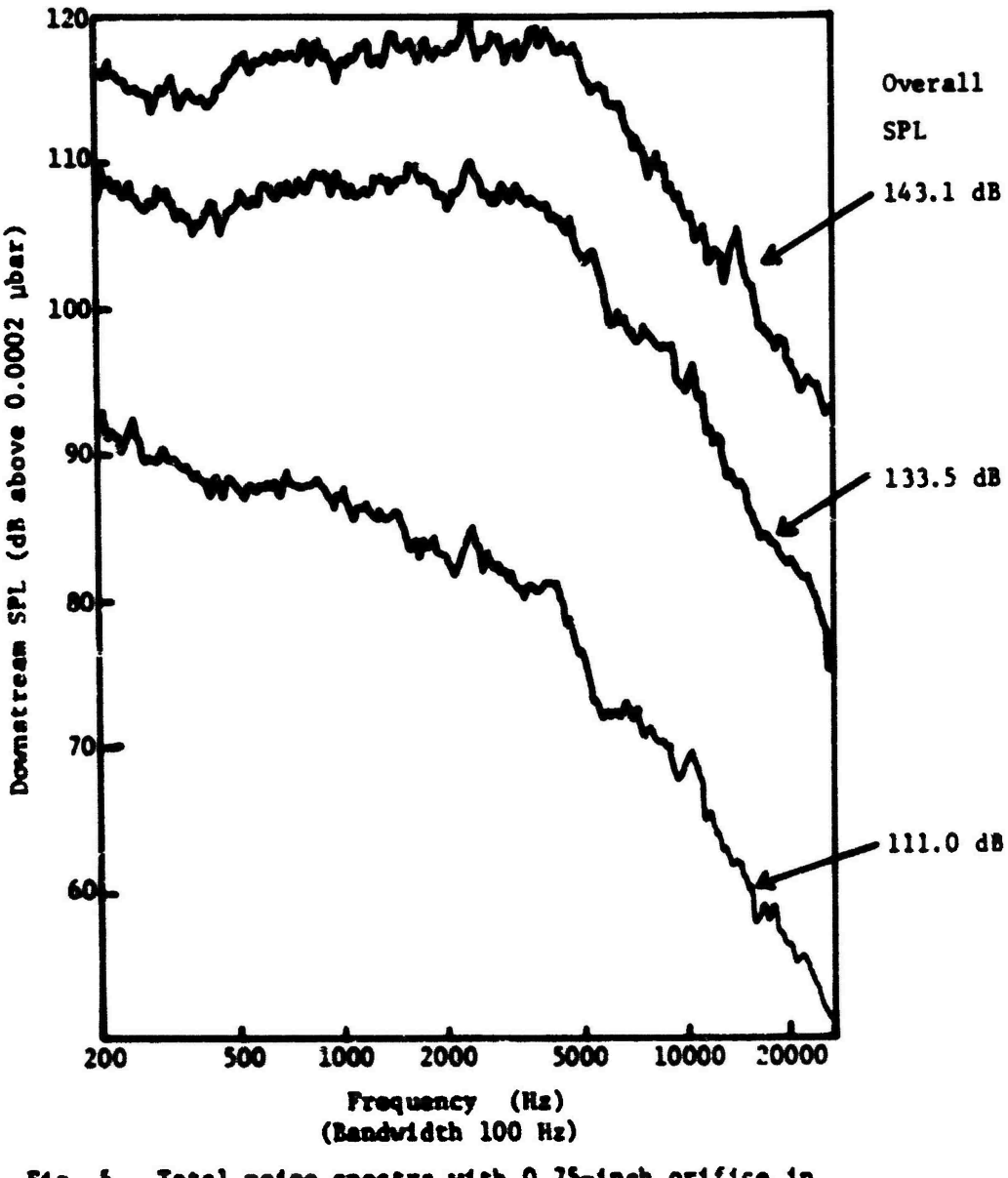

Fig. 5. Total noise spectra with 0.75-inch orifice in pipe at three flow rates.

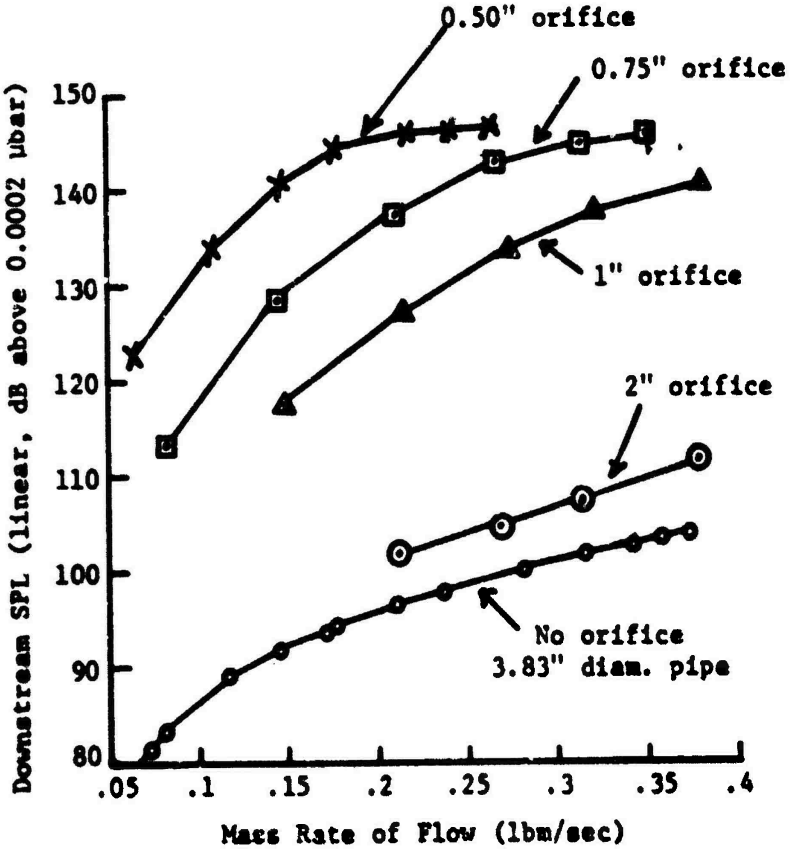

Fig. 6. Orifice overall SPL versus experimental mass rate of flow.

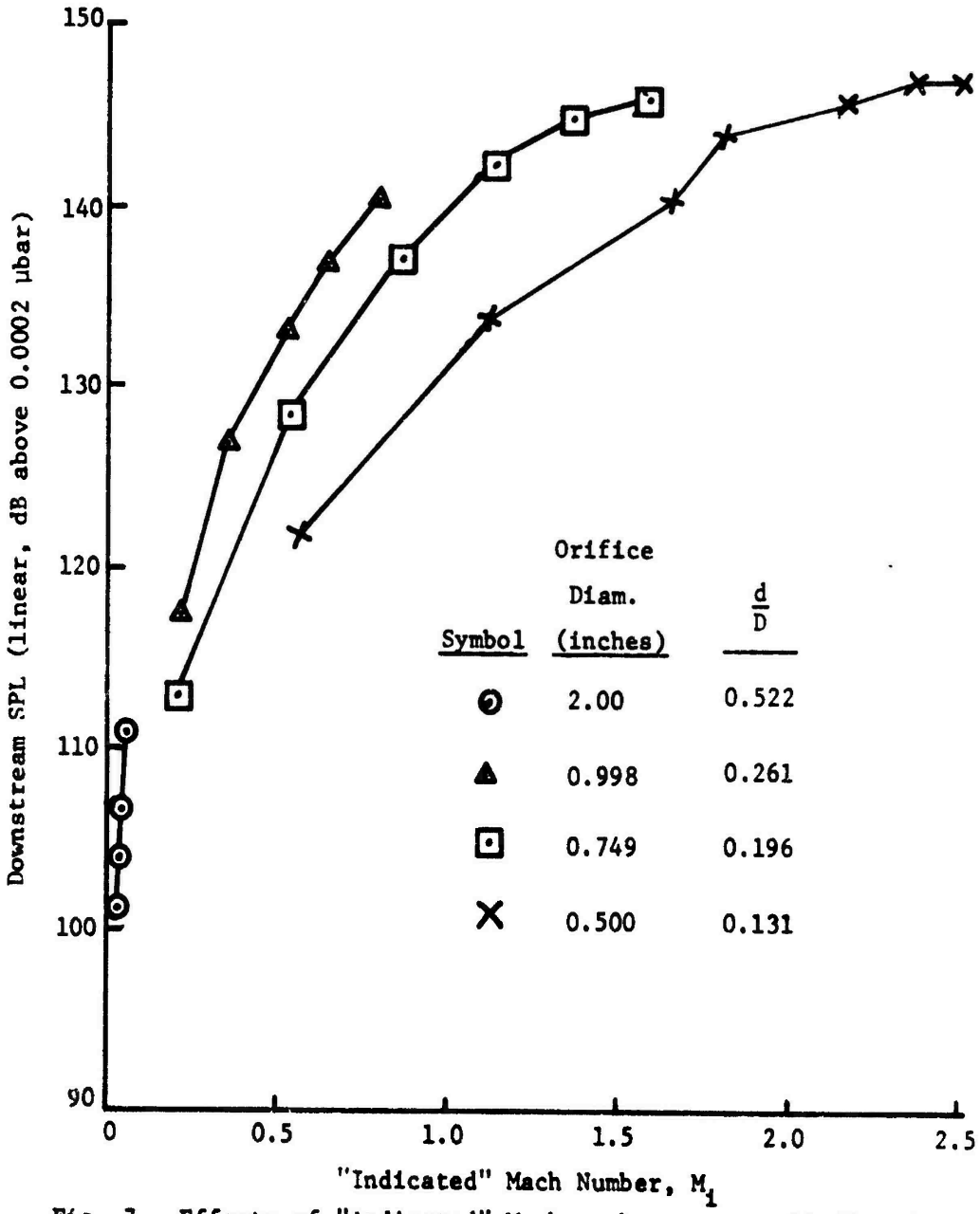

Fig. 7. Effects of "indicated" Mach number on overall SPL of orifices.

MULTIPLE PURE TONE NOISE RADIATION FROM A SUPERSONIC ROTOR PROPAGATING IN AN ACOUSTICALLY TREATED DUCT

by

P. G. Vaidya, R. Shashaani, L. Kisner, & J. Sullivan
Ray W. Herrick Laboratories
Purdue University
West Lafayette, Indiana 47907

1. INTRODUCTION

Under the support of NASA-Lewis, a program to conduct research on "Multiple Pure Tone Noise Radiation from a Supersonic Rotor propagating in an Acoustically Treated Duct", has begun. The long term aim of this program is to improve the basic understanding of the mechanisms involved, to lead to improved design and prediction techniques.

The program involves both theoretical and experimental investigations. In both of these, a choice of two strategies is available: the total system could be analyzed at once, or each component of the system could be separately analyzed.

It is felt that both these strategies should complement one another. Thus, in case of the theoretical approach, basic analysis can be carried out for some idealized cases to explore in detail a specific phenomenon and this should lead to improvements in the total system of design and prediction techniques. In the absence of such feedback, numerical computational procedures lead to 'canned' programs which are used beyond the range of validity of their input assumptions. Similarly, controlled basic experiments should complement full scale testing procedures.

In the research program at Purdue University, we have planned to carry out the basic analytical investigations which, as the program advances, would lead to a computational procedure for the prediction of the total system. We are also carrying out controlled laboratory experiments. It is hoped that at a later stage full scale testing could be carried out at the NASA-Lewis Research Center.

In what follows, a description of the Multiple Pure Tone radiation problem is presented. In Section 3, the Method of Acoustic Modules is presented and in Section 4 is included a brief outline of the supplimentary studies. These two taken together, represent our efforts to seek analytical models for the problem. In Section 5, details of the experimental investigations is presented. Conclusions are included in Section 6.

2. CHARACTERISTICS OF MULTIPLE PURE TONES

The most striking feature of noise from a high speed fan is

a change from the shrill, high pitched scream of blade passing frequency to the low frequency buzzing sound characteristic of M.P.T.'s, as the fan tangential Mach numbers become supersonic. Figure 1 shows a typical far field M.P.T. spectra. There remains some controversy as to the relative subjective response of listeners to these two types of spectra; however, it is evident from the examination of most of the published noise data that fans with M.P.T.'s present are noiser than subsonic fans at equivalent pressure ratios and mass flows (1). It therefore becomes essential to develop improved suppression concepts for the reduction of multiple pure tones.

There are several interesting acoustic characteristics of multiple pure tones that suggest mechanisms for their generation. Data from actual fans reveal the following (2):

a) M.P.T.'s are only detected in the inlet duct and forward arc far field noise data,

b) they propagate only when the rotor tangential tip Mach number is greater than unity,

c) the highest sound pressure levels exist, in general, below the blade passage frequency at integral multiples of shaft rotational frequency,

d) as the fan speed is increased successively, lower orders of shaft frequency propagate, suggesting a cutoff phenomena,

e) M.P.T. noise levels tend to increase rapidly up to Mach numbers of 1.2-1.3 dominated by frequencies near half the blade passing frequency, then decrease in intensity as the Mach number increases partly due to convective effects, partly due to changes in shock patterns.

The above acoustic characteristics of M.P.T.'s suggest strongly that the noise mechanism is related to the supersonic aerodynamics of the fan upstream of the rotor. Spectral analysis indicates the wave form should be of the form of a nonuniformity, rotating at shaft speed.

Multiple pure tone noise generation is governed by the aerodynamics of the fan shock system, more specifically by the unsteady flow effects of irregularities in the shock amplitudes and spacing. The strengths and positions of these shocks are sensitive to small blade to blade differences, thus the detailed spectral characteristics are unique to each fan. Data has shown that these irregularities amplify upstream of the rotor and persist out into the radiated far field (3), (4).

Several investigators have analyzed M.P.T. noise through the application of finite amplitude wave theories given in re-

ferences (5) - (11). A one dimensional analysis by Hawkings (12) shows how some of the basic features of M.P.T's can be explained. Two dimensional extensions of the theory have also been made (13), (14). Pickett (15) developed a method for the prediction of the spectral content of M.P.T.'s in terms of almost periodic pulse trains.

3. THE METHOD OF ACOUSTIC MODULES

3.1 Concept of Acoustic Modules

Most theoretical studies, in the field of duct acoustics understandably concentrate upon idealized conditions. Thus sound propagation in semi-infinite absorbent ducts is considered, or radiation from a rigid duct termination is analyzed. Very little consideration is given, in general, to matching these subproblems together to solve a specific practical problem.

The concept of the Acoustic Modules is a first step in resolution of such discrepancies. Effort has been made to solve all these problems in terms of the same (rigid duct) eigenfunctions. Each of the modules is assumed to have an input (pressure and velocity distribution) which uniquely determines the output. Thus a cascade of modules could be considered and if the source distribution (pressure or velocity) of the first module and the termination impedance of the last module are known, the entire problem should be solvable. (See Figure 4).

In Section 3.3, expressions for a rectangular module with a uniform but arbitrary lining are described. These results are now extended to circular ducts carrying mean flow. Preliminary analysis has indicated that this concept could be extended to modules with variations in their cross-sectional area.

3.2 Eigenfunctions for Absorbent Ducts

Sound propagation in rigid ducts is analyzed in terms of rigid duct eigenfunctions (modes). Field at the entrance of a duct is expressed as a summation of these modes and each of these modes are allowed to propagate separately. Total field at any point is simply the sum of the contributions due to each of these modes. In this manner, all the relevent quantities of pressure, velocity, and intensity could be calculated.

When the duct is uniformly lined with a layer of an absorbant material, the boundary conditions at the walls are altered. A straight forward approach would be to choose eigenfunctions which obey the wave equation and the soft wall boundary conditions.

A controversy about the 'orthogonality' of such modes has arisen. It appears that this might be a matter of semantics. It has been shown (references 16, 17) that for two soft wall

eigenfunctions, (if they are normalized),

$$\int_S \psi_n \psi_m \, dS = \delta_{n,m} \qquad (1)$$

that is, their produce integrated over the cross-sectional area identically vanishes if $n \neq m$.

Furthermore, equation (1) can be used to obtain the expansions of any input distribution in terms of these eigenfunctions.

However, when the wall impedance has a non zero resistive part; both ψ_n and ψ_m are complex and although equation (1) still remains valid, but

$$\int_S \psi_n \psi_m^* \, dS \neq 0, \text{ if } n \neq m \qquad (2)$$

the integral in equation (2) should vanish if the intensity is to remain separately calculable in each mode. This condition should, therefore, be considered to be the proper definition of 'orthogonality'. In this sense the modes which satisfy the absorbent boundary condition are not 'orthogonal'.

In addition, these modes violate the concept of compatability of Acoustic Modules. Therefore a Green's function formulation, based on the rigid duct eigenfunctions, has been developed. Details of this formulation could be found in the Herrick Laboratory Technical Report, mentioned above (reference 16).

3.3 Propagation of Sound in a Uniformly Lined Duct

The method of Green's function is used to obtain expression for pressure and velocity at any point in a rectangular duct, in terms of the pressure and velocity at the entrance to the duct. A homogenous solution was added to the semi-infinite duct Green's function to obtain a 'finite length' Green's function. The Green's function does not have to obey the wall boundary conditions. In view of the discussion in Sections 3.1 and 3.2, the rigid wall boundary conditions were chosen. The specific problem posed by Figure 3 leads to an integral equation which was solved by means of Laplace Transforms. Only the final results are presented here, (for details, please refer to reference 16).

From $p(y,o)$ and $v(y,o)$ coefficients C_m and D_m are calculated as follows:

$$C_m = \frac{(-1)^m (2-\delta o,m)}{i\omega\rho_o b} \int_o^b \text{Cos } \frac{m\pi y}{b}\, p(y,o)dy \qquad (3)$$

and

$$D_m = \frac{(-1)^m (2-\delta o,m)}{bK_m} \int_o^b \text{Cos } \frac{m\pi y}{b}\, v(y,o)dy \qquad (4)$$

where

$$K_m = \sqrt{\frac{m^2\pi^2}{b^2} - 1} \qquad (5)$$

From these it is shown that, at any point (y,z)

$$p(y,z) = \sum_m \sum_n p_{n,m} \text{ Cos } \frac{n\pi y}{b} (-1)^n \qquad (6)$$

and

$$v(y,z) = \sum_m \sum_n v_{n,m} \text{ Cos } \frac{n\pi y}{b} (-1)^n \qquad (7)$$

where

$$p_{n,m} = \frac{\omega^2\rho^2(2-\delta o,n)}{bZ_t} \sum_q \frac{s_q^2 - K_q^2}{(s_q^2 - K_m^2)(s_q^2 - K_n^2)} x$$

$$x \left[\frac{K_m D_m}{s_q} \text{ Sinh } s_q z + C_m \text{ Cosh } s_q z \right] \qquad (8)$$

and

$$v_{n,m} = \frac{-i\rho\omega(2-\delta o,n)}{bZ_t} \sum_q \frac{s_q^2 - K_q^2}{(s_q^2 - K_m^2)(s_q^2 - K_n^2)} x \qquad (9)$$

$$x \left[K_m D_m \text{ Cosh } s_q z + C_m s_q \text{ Sinh } s_q z \right]$$

where Z_t is the wall impedance and s_q is the $(q + 1)^{st}$ root of

$$\sqrt{s^2 + k^2} \quad \tan \; b \sqrt{s^2 + k^2} = \frac{-i\rho\omega}{Z_t} \tag{10}$$

In particular, when z = D, one obtains the output for the module from the given input.

Equations 8 and 9 simplify considerably when $Z_t >> 1$. In that case most significant contribution is obtained when m = n = q.

4. SUPPLIMENTARY STUDIES

4.1 Introduction

The Method of Acoustic Modules is to be used, in the long term, to analyze the core problem described in Figure 3. This analysis is supplimented by several basic studies which would indicate the limitations involved in the core problem and also suggest its modifications. A brief description of these studies is included in the next subsections.

4.2 Near Field Aerodynamics of Blades

This involves studying various models which explain the generation of Multiple Pure Tones. A physical description of the field is sought so as to serve as the initial conditions to the transmission problem in the next subsection.

4.3 Transmission of Weak Shock Waves in Ducts

The transmission of various shapes of pulses, in ducts, is being investigated. It is assumed that the assumption of "Quasi-Linearity" is justified. This would indeed be the case for shocks of small amplitude, propagating over small distances. For longer distances. repeated application of this method could be used and for higher amplitudes, other techniques, such as the one in the previous section, will have to be used.

To obtain "Quasi-Linear" solution to a given problem, a corresponding steady state problem is solved, at first. This is follwed by a Fourier or Laplace transform technique, described in reference (18), to obtain the time domain responses.

Two sets of problems for infinite long ducts with "rigid wall" and with "lined wall" are considered. Specific application is made to the transmission of a Buzz-Saw form in slightly absorbent ducts. For details see reference (19).

4.4 Propagation of Sound in Duct with Nonuniform Lining

It would be highly unlikely that the optimum lining configuration for a given problem happens to be a uniform one. In any case, due to the high intensities of sound encountered, even the treatments of uniform thickness would lead to an axially non-uniform impedance for the lining.

It was shown (references 20, 21) that sound fields under these conditions can be analyzed in terms of the extraneous modes. It was found that for an exponential variation of the duct impedance, coefficients of the extraneous modes could be readily calculated. Experimental work, related to this problem is briefly described in the section and is presented in detail in reference (22).

5. EXPERIMENTAL STUDIES

5.1 Design and Construction of the Spinning Mode Facility

In what follows, a brief discussion of the experimental set-up whose construction is completed at this date is presented. Details of the design may be found in a Herrick Laboratory Report (reference (23)).

The system consists of seven distinct parts as follows:

i) Horn drivers and horns: There are eight E-V drivers each having 90 watts input power continuous sine wave used in order to produce the acoustical signals. The horns are of the conical type, and transform the small-area diaphragm of the drivers into large area while avoiding the problems of resonance.

ii) Transition section: The unwanted patterns of higher order modes are to be diminished through this section before reaching the measurement section. This section can also be used to introduce a mean flow accompanying the acoustic signals; the mean flow is accelerated due to the geometry of this section, and thus a more uniform flow distribution is reached at the measurement section.

iii) Measurement section: In this section the type of higher order modes generated by the drivers will be investigated and verified. This is done by cross correlating signals from two microphones.

iv) Test section: The 6 ft. long test tube provides means of investigating propagation of spinning modes in a cylindrical duct with or without lining. The study of attenuation of the pressure fluctuations

along the duct axis as well as radially can thus be performed by means of a traversing probe in this section.

v) Anechoic termination: This part of the system is basically an exponential horn which gradually matches the two impedances of the test section and the free space. It is hoped that the reflecting waves into the test section are thus minimized.

vi) Center Body Cylinder: This component of the facility constitutes the inner cylinder of the duct as well as being the housing for the traversing probe of the test section. A set of center bodies varying in dimensions provide the desirable hub to tip ratios in the test section.

vii) Electronic instruments: A set of electronic devices provide means for generating proper input functions to the acoustic drivers, measurement and correlation of signals, monitoring inputs and outputs and plotting of data. These instruments may be outlined as follows:

a. Function generator

b. Operational amplifier circuit to produce desired phase differences for the inputs to the driving units.

c. two 400 watts phaselinear amplifiers

d. two 1/4" B & K microphones

e. B & K microphone amplifier

f. B & K narrow band analyzer

g. Hewlett-Packard real time analyzer

h. Cathod Ray Oscilloscope

A sketch of this facility is seen in Figure 5 and that of the planned modification of the facility is seen in Figure 6.

5.2 Measurements in a Duct with Nonuniform Lining

A previously existing facility at the Herrick Laboratory has been modified to carry out preliminary investigation of the effect of axially nonuniform lining on sound propagation. Figure 7 shows a sketch of the facility. Four speakers can be driven, all in phase or with any number of them with a phase shift of 180°. A simple traverse of the microphone measures the field in the test section, lined with an exponentially varying

material and the anechoic termination keeps the back reflections to a minimum. Experimental results show that at least for some specific range of frequencies, the material arranged in this fashion, absorbs move sound. (see for example, Figure 8)

An interesting phenonenon is the increase in the sound pressure level aong the axis, at some of the frequencies. One of the explanations for this behavior is a possibility of modal conversion. A detailed report of these results was made at the Acoustical Society's meeting in April '74. (22)

6. CONCLUSIONS

The problem of the Multiple Pure Tone radiation is seen to be a complex one. It is being modelled in an idealized form and being analyzed by means of the Method of Acoustic Modules. This analysis is being supplimented by several other basic studies to check its validity. Experimental testing of the basic problems involved has begun.

7. ACKNOWLEDGMENTS

The work is supported by the National Aeronautics and Space Administration, Lewis Research Center, Contract No. NAS 3-18010. Special thanks are due to Dr. Gene Minner, NASA's project manager for this contract, and to Dr. Raymond Cohen and Mr. Arthur Smith of the Herrick Laboratories, for their guidance and assistance for the program.

8. REFERENCES

1. C. E. Feiler and W. Conrad, 1973, "Noise from Turbomachinery", AIAA Paper No. 73-815.

2. M. J. Benzakein, et. al., 1972, "Fan/Compressor Noise Research", FAA Contract Final Report FAA-RD-71-35, General Electric Co.

3. M. G. Philpot, 1970, "The Buzz-Saw Noise Generated by a High Duty Transonic Compressor", ASME Paper No. 70-GT-54.

4. M. J. Benzakein, 1972, "Research on Fan Noise Generation", Journal of the Acoustical Society of America, 51, No. 5 (Part 1), p. 1427-1438.

5. G. B. Whitham, 1952, "The Flow Pattern of a Supersonic Projectile (Appendix)", Comm. on Pure and Applied Math, Vol. V, No. 3, p. 301-348.

6. M. J. Lighthill, 1956, "Viscosity Effects in Sound Waves of Finite Amplitudes", Surveys in Mechanics, G. I. Taylor

7th Anniversary Volume, Cambridge, University Press, p. 250-351.

7. D. T. Blackstock, 1966, "Connection Between the Fay and Fubini Solutions for Plane Sound Waves of Finite Amplitude", Journal of the Acoustical Society of America, 39, No. 6, p. 1019-1026.

8. C. L. Morfey, 1968, "A Review of the Sound-Generating Mechanisms in Aircraft-Engine Fans and Compressors", Aerodynamic Noise, Proc. of the AFOSR-UTIAS Symposium, Toronto, University of Toronto Press, p. 299-330.

9. B. D. Mugridge and C. L. Morfey, 1971, "Sources of Noise in Axial Flow Fans", 85th Meeting of the Acoustical Society of America.

10. P. M. Morse and K. U. Ingard, 1968, Methods of Theoretical Acoustics, McGraw Hill, New York, P. 874-882.

11. Anon., 1973, Symposium on Finite Amplitude Wave Effects in Fluids, Technical University of Denmark.

12. D. Hawkings, 1970, "Multiple Pure Tone Generation by Transonic Compressors", Aerodynamic Noise Symposium, Loughborough University of Technology, Paper No. E. 4.

13. R. A. Kantola and M. Kurosaka, 1971, "The Theoretical and Experimental Investigatior of Multiple Pure Tone Noise - Part I", NASA CR-1831.

14. C. L. Morfey and M. J. Fisher, 1970, "Shock-Wave Radiation from a Supersonic Ducted Rotor", The Aeronautical Journal of the Royal Aeronautical Society (London), 74, p. 579-585.

15. G. G. Pickett, 1972, "Prediction of the Spectral Content of Combination Tone Noise", Journal of Aircraft, Vol. 9, No. 9, p. 658-663.

16. P. G. Vaidya, 1973, "Propagation of Sound in a Rectangular Duct with Uniform but Arbitrary Lining", NASA T. Report 1, HL 73-38, December 1973.

17. P. G. Vaidya, 1974, "Method of Acoustic Modules", presented at the 87th Meeting of the Acoustical Society of America, New York.

18. P. G. Vaidya, 1972, "The Acoustic Response of Rooms with Open Window to Airborne Sounds", Journal of Sound and Vibration 25, p. 505-532.

19. R. Shashaani, P. G. Vaidya, 1974, "Propagation of Shock Waves in Ducts:, Herrick Laboratory Technical Report, to be prepared.

20. P. G. Vaidya, 1972, "Some Developments in the Theory of Sound Attenuation", Symposium on the Acoustics of Flow Ducts, I.S.V.R. University of Southampton, England.

21. P. G. Vaidya and A. St. Hilaive, 1972, "Extraneous Modes in Sound Absorbing Ducts", Inter-Noise 72, Washington, D.C.

22. P. G. Vaidya and J. Ridd, 1974, "Use of Nonuniform Liners as Sound Suppressors", presented at the 87th Meeting of the Acoustical Society of America, New York.

23. R. Shashaani, J. Sullivan, L. S. Kisner, and P. G. Vaidya, 1974, "Design of the Spinning Mode Facility", NASA T. Report 2, HL 74-3, January 1974.

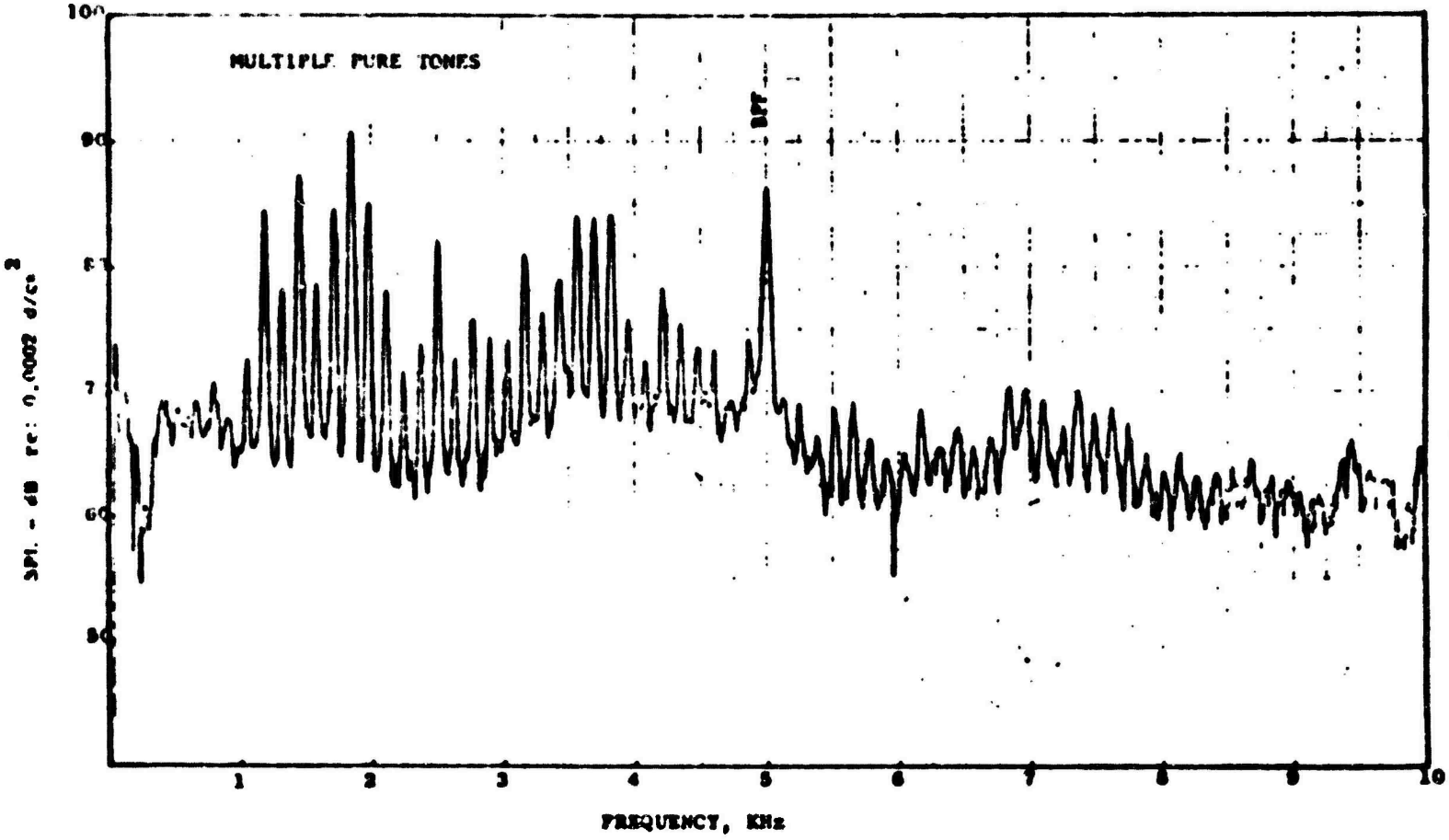

TYPICAL SPECTRUM CONTAINING MULTIPLE PURE TONES
FROM REFERENCE (2)

FIGURE 1

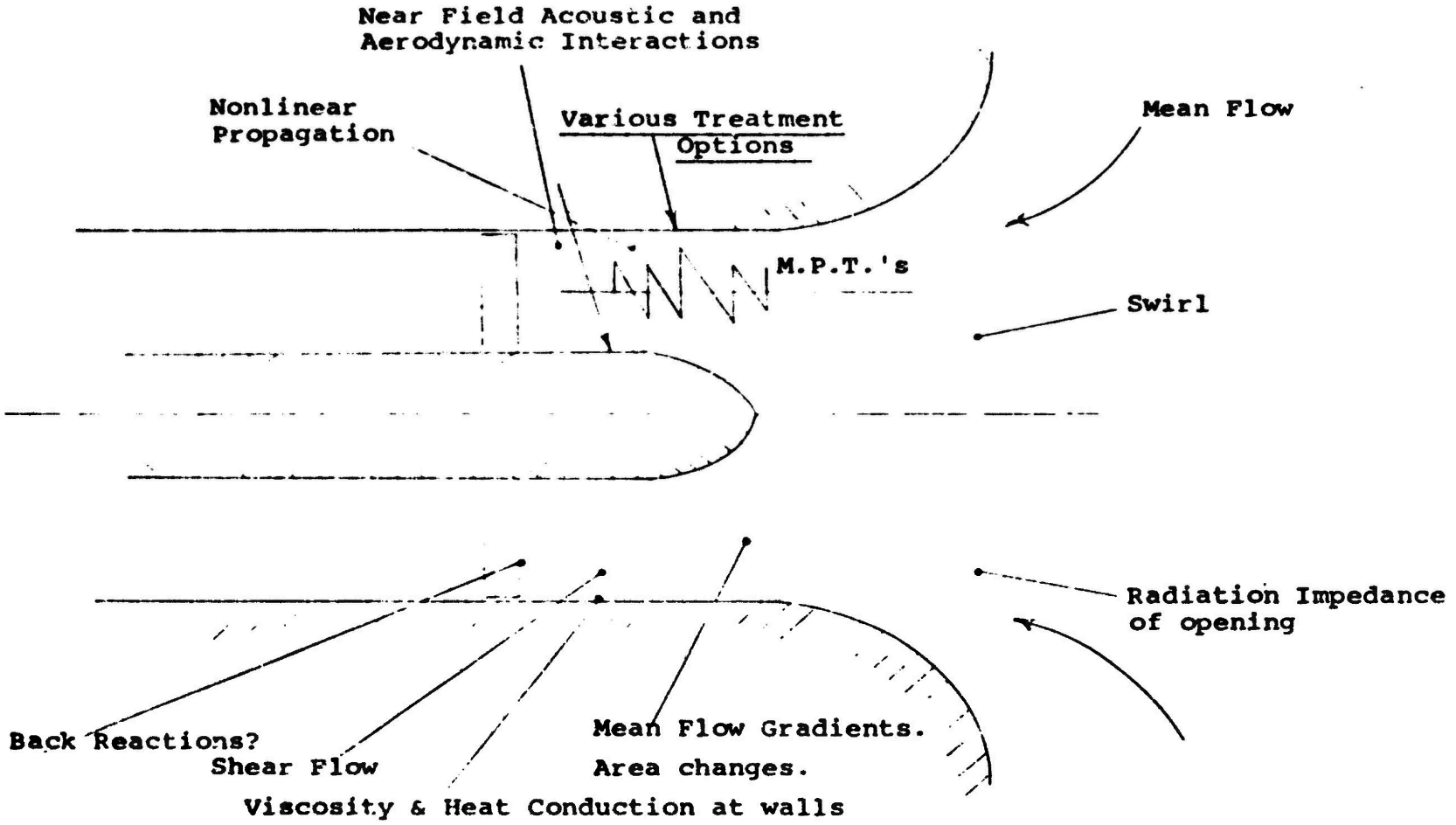

FIGURE 2 - THE ACTUAL MULTIPLE PURE TONE PROBLEM.

NEAR FIELD OF ROTOR IS ASSUMED TO BE KNOWN. THIS MODEL WOULD HELP EVALUATE BEST TREATMENT AND ITS' EFFECTIVENESS.

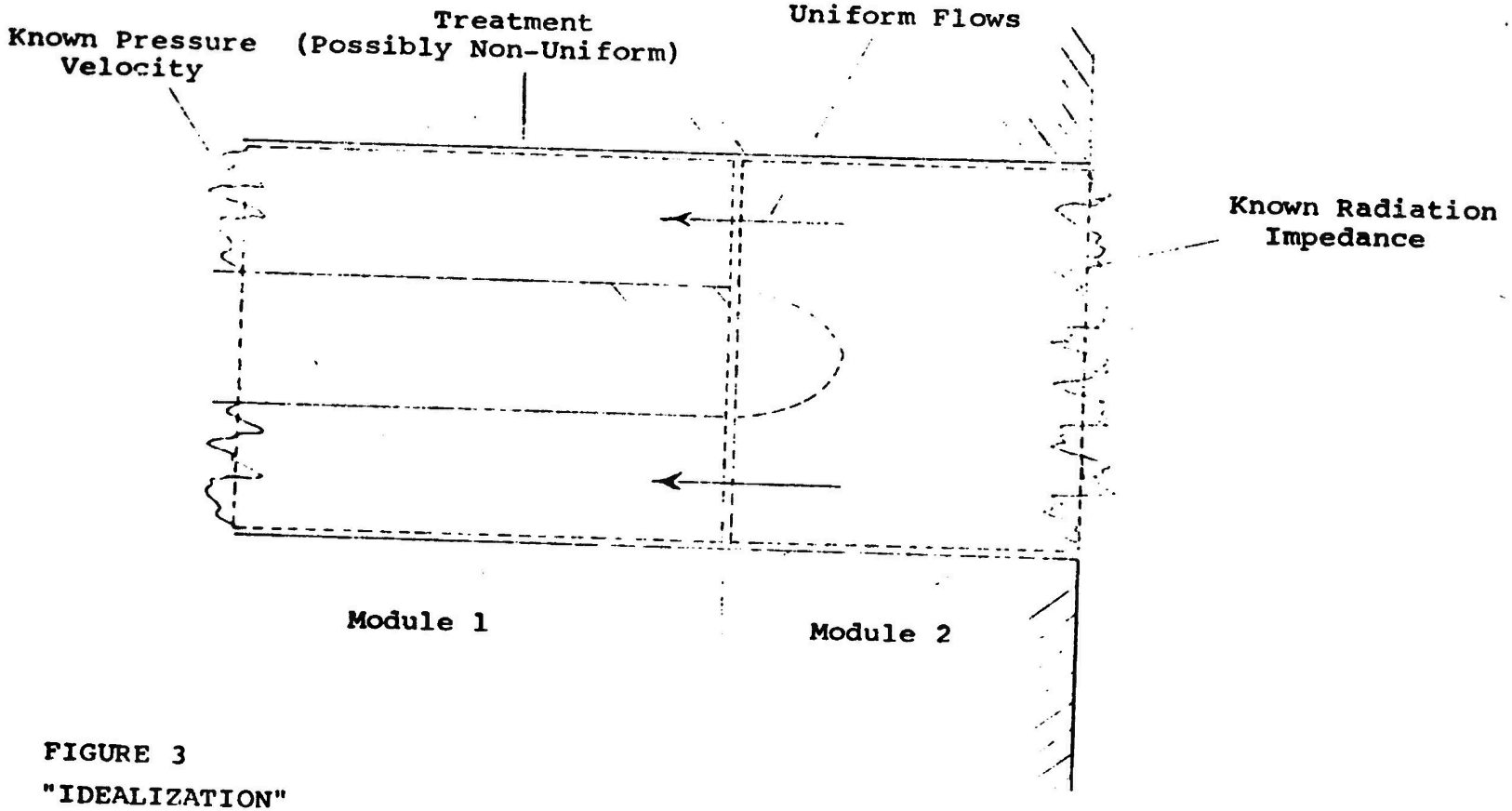

FIGURE 3

"IDEALIZATION"

First Step - Exact solution to the idealized problem.

Second Step - Modification of this solution by means of basic analysis of effects of Shockwaves Transmission, Area Changes, Mean Flow Gradients and Shear, Swirl, and etc.

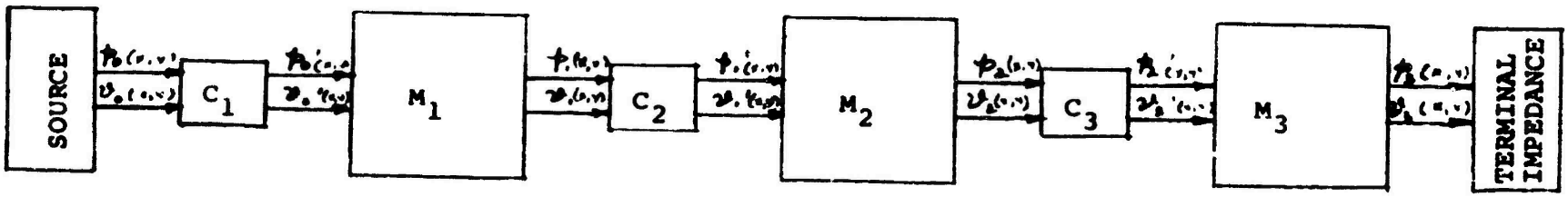

VARIOUS TRANSMISSION ELEMENTS ARE REPRESENTED BY MODULES M_1, M_2, M_3, C_1, C_2, AND C_3 REPRESENT THE COMPATABILITY CONDITIONS AT THEIR INTERFACES. SOURCE IS SPECIFIED IN TERMS OF ITS CHARACTERISTICS (VELOCITY SOURCE, PRESSURE SOURCE, ETC). TERMINATION OF THE CASCADE IS PRESENTED AS AN IMPEDANCE

METHOD OF ACOUSTIC MODULES

FIGURE 4

ASSEMBLY PLAN FOR SPINNING MODE FACILITY

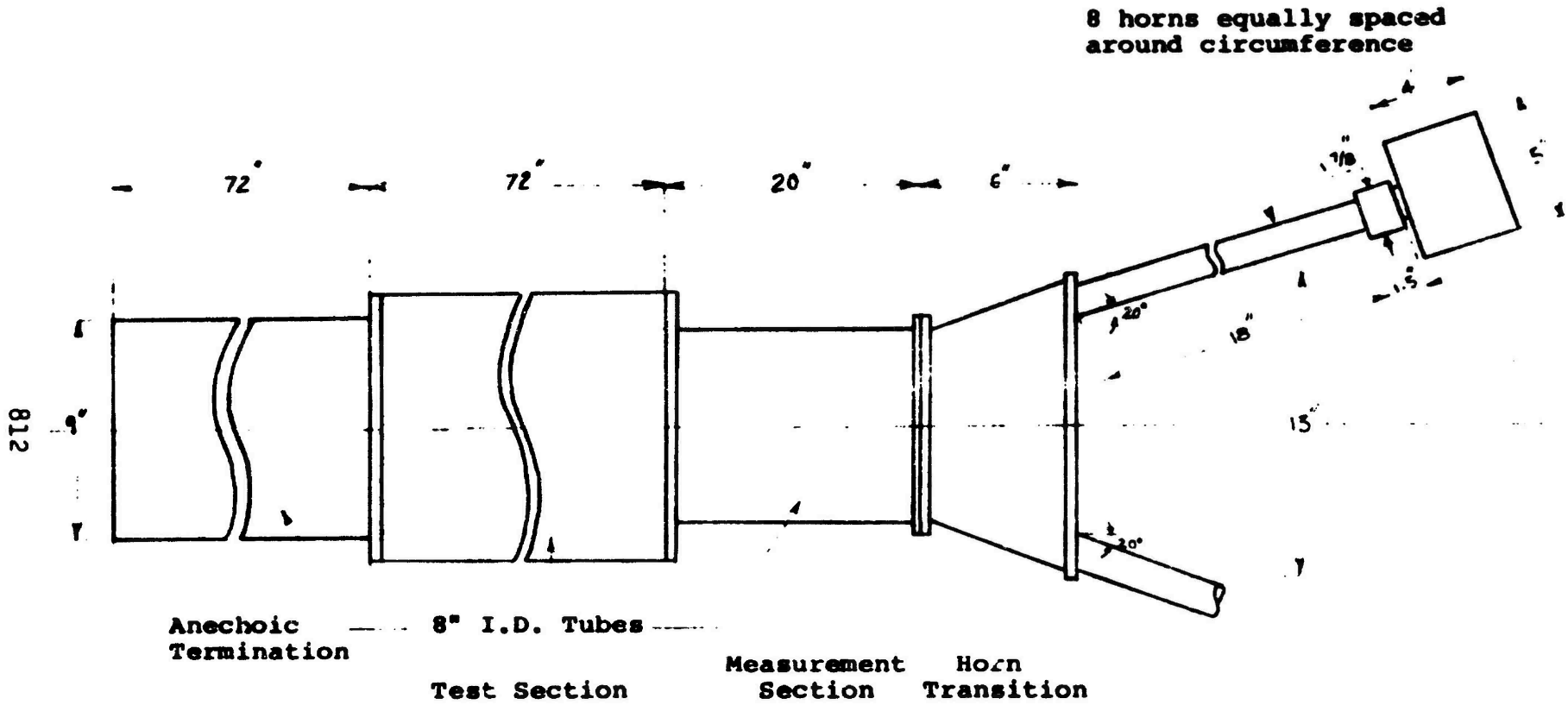

FIGURE 5

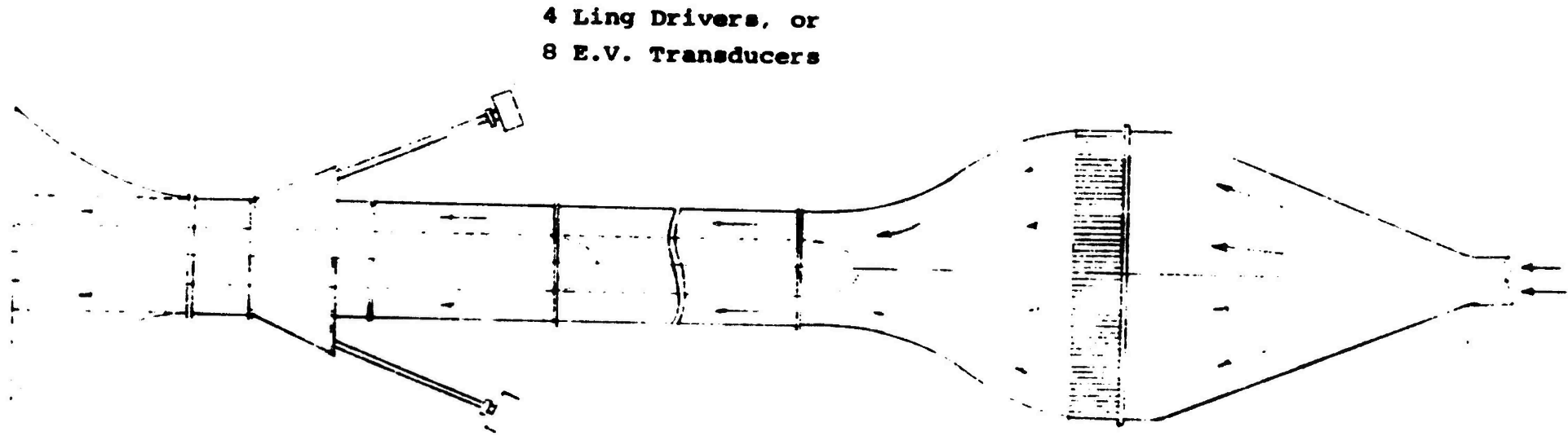

FIGURE 6

Modification of the Facility to Include Flow

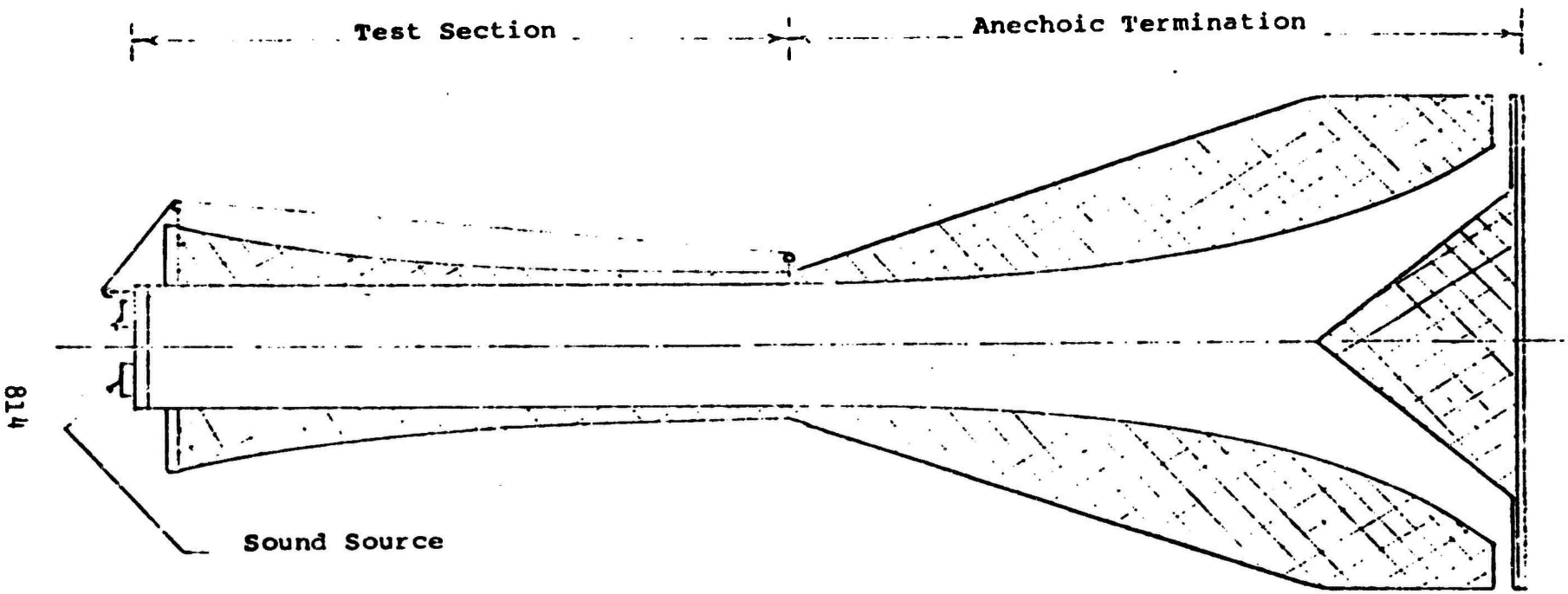

FIGURE 7: SKETCH OF THE NONUNIFORM LINING ANALYSIS FACILITY AT THE HERRICK LABORATORIES

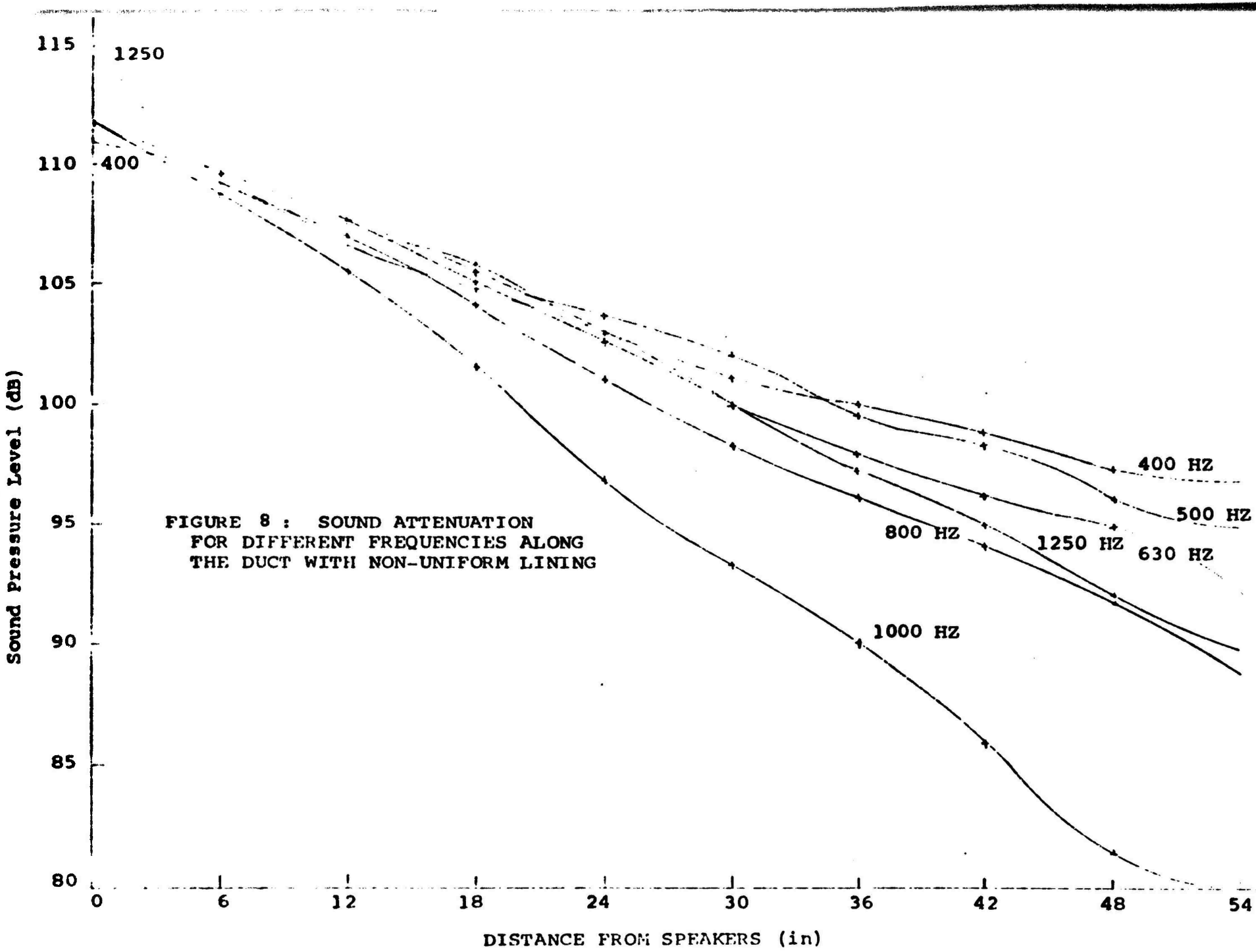

FIGURE 8 : SOUND ATTENUATION FOR DIFFERENT FREQUENCIES ALONG THE DUCT WITH NON-UNIFORM LINING

STUDIES OF SOUND ABSORPTION MATERIALS AND THE ATTENUATION OF SOUND IN DUCTS

by

Uno Ingard, Young-chung Cho, Vijay K. Singhal, George P. Succi, and William P. Patrick
Massachusetts Institute of Technology
Cambridge, Massachusetts 02139

(a) Analytical Studies of Sound Attenuation in Ducts

Extensive calculations of the insertion loss of rectangular and circular lined ducts have been carried out. In many cases of practical interest the octave band insertion loss is used in describing the performance of a duct, and for this reason we have included in the analysis the appropriate integration over frequency to obtain the octave band insertion loss for a variety of situations. The results demonstrate some interesting features that often are overlooked. First, we show explicitly how the octave band insertion loss depends rather markedly on the shape of the input spectrum. Thus we have calculated the octave band insertion loss for spectra with slopes 0, +6 dB per octave, and - 6 dB per octave. The differences can be surprisingly large, and the results indicate that specification of octave band insertion losses for a duct in many cases can be quite misleading unless the shape of the input spectrum is also specified.

Another interesting point is that the octave band insertion loss of a duct does not increase linearly with the duct length even if end reflections are excluded. The reason for this is that the shape of the spectrum varies with location along the duct. It is found that the deviation from linearity depends rather strongly on the boundary impedance. This effect has been examined in some detail as a function of the liner characteristics.

(b) Reflection of Sound from a Single Side Branch Resonator in a Duct with Flow

Measurements of the reflection and transmission characteristics of a single side branch resonator in a duct with flow have been made and compared with a theoretical analysis of the problem. Good agreement is found in the flow regime where the resonator is not excited by the flow. Under conditions of self-oscillations, the "resonance curve" of the reflection coefficient is found to be considerably sharper than it is normally, and the pressure reflection coefficient is found to exceed unity.

(c) Flow Noise in Ducts

Studies of flow noise in ducts have been carried out for

three specific cases, involving a single side branch cavity in a duct, a constriction in a duct, and a cylindrical obstruction in a duct. Conditions for excitation of pure tones in these three cases are presented, together with some attempts to describe these effects theoretically, at least in part.

Included in these studies are experiments on the excitation of an open-ended pipe by jet flow. The conditions for excitation of the axial acoustic modes of the duct are given, and the results are consistent with the theoretical analysis of the acoustics of an open-ended tube with flow. Thus the excitation of the axial modes is found to occur only at comparatively low flow velocities, and the reason for this is largely that the acoustic damping of the tube increases with increasing flow speed. The Mach number dependence of the damping in the tube has been determined and forms a basis for a criterion of flow excitation of axial modes.

[This work was supported in part by DOT Grant Agreement DOT-OS-30011 and in part by NASA Research Grant NGR 22-009-805.]

TRANSMISSION OF SOUND THROUGH DUCTS WITH VARYING CROSS SECTIONS

by

Ali H. Nayfeh, John E. Kaiser and Demetri P. Telionis

Department of Engineering Science and Mechanics
Virginia Polytechnic Institute and State University
Blacksburg, Virginia 24061

The main objective of the project is to analyze the transmission and attenuation of sound in two-dimensional and circular ducts with slowly varying cross sections with or without mean flow, taking into account any slow variations in the wall admittance and the growth of the boundary layer. Approximate solutions for incompressible mean flows have been obtained by using the method of multiple scales. A parametric study is underway to determine the effect of the different flow and liner properties on the attenuation of sound, and the analysis is being extended to compressible mean flows. A secondary objective is to analyze the wave propagation in ducts with sinusoidal wall undulations.

1. Introduction

The design of many physical facilities requires the prediction of acoustic wave propagation and attenuation in ducts with varying cross sections with or without mean flows. These facilities include horns, loudspeakers, central air-conditioning and heating installations, high-speed wind tunnels, rocket nozzles, and aircraft-engine duct systems, with the latter being an area which is currently receiving much attention. The need for techniques that permit the identification of those duct configurations which possess the most favorable sound propagation and attenuation characteristics has prompted numerous investigations into the effects of area variations. A summary and review of several techniques of analysis of this problem may be found in the review article by Nayfeh, Kaiser and Telionis[1]. Of immediate concern in the present discussion are two problems: the effect of small undulations in the duct walls and the modelling of the effect of geometry variations typical of those encountered in aircraft engine-duct systems.

Isakovitch[2], Samuels[3], and Salant[4] obtained perturbation solutions for wave propagation in ducts with no mean flow whose walls vary sinusoidally with distance. The wall variations were taken to be of small amplitude and had a wave length of the same order as the wave length of the sound. Under certain conditions, their solutions predicted disturbances from the small wall variations that were not small; hence, the basic perturbation expansion was invalid under these resonant conditions. They tabulated, from numerical calculations, the resonant frequencies; however, no insight into the nature of the wave propagation at resonant conditions was provided by their analyses since their solutions were not valid at resonance. Nayfeh[5] pointed out that resonance occurs whenever the wavenumber of the wall variations equals the sum or difference of the wave numbers of any two acoustic modes, and he obtained the solution for the wave propagation at resonance. The results of this latter analysis are outlined in section 2 below.

Early studies of the effect of area variations typical of aircraft engine duct systems restricted their scope to the case of no mean flow. Several authors (Zorumski and Clark[6], Lansing and Zorumski[7] and Alfredson[8]) used a discretization technique based on the solution for a single duct discontinuity. Nayfeh and Telionis[9] applied the method of multiple scales to obtain a uniformly-valid perturbation solution for a duct of slowly-varying cross section. Beckemeyer and Eversman[10] used the Ritz minimization of functionals with the governing equations as stationary conditions in order to waive the restriction of slow variation with axial distance; however, it is not known whether their analysis will converge when the variations are large.

The inclusion of the effects of the high-speed mean flow, which possesses streamwise gradients as well as strong transverse gradients in the wall boundary layers, makes the problem considerably more difficult, and most studies have employed one or more simplifying assumptions. The most commonly-used assumption is that of quasi-one-dimensional flow, which eliminates the effect of sound refraction through the boundary layer. Powell[11] studied the propagation of sound discontinuities, while Eisenberg and Kao[12] considered the propagation of the lowest acoustic mode through ducts with variable cross sections. Huerre and Karamcheti[13] and King and Karamcheti[14] investigated the propagation of the lowest acoustic mode, using, respectively, the short-wave approximation (ray acoustics) and the method of characteristics. Hogge and Ritzi[15] assumed that the duct can be broken down into cylindrical and conical sections, and they solved the wave equation for a uniform mean flow by application of the method of finite elements. However, the restrictions to one-dimensional flow and/or propagation of the fundamental mode limits the usefulness of such analyses for realistic situations in which the sound is a combination of numerous modes which propagate through a mean flow that possesses both axial and transverse velocity gradients.

Perhaps the only simplifying factor of the problem is the fact that, in many practical situations, for example in the bypass ducts of high-bypass-ratio jet engines, the duct cross-sectional area depends only mildly on the distance along the axis of the duct. Moreover, the growth of the mean boundary layer at high Reynolds numbers is a slow function of the axial distance, except perhaps at the leading edge of the duct inlet. The above factors indicate that a perturbation method should be appropriate. Such a method could determine the correction due to weak nonuniformities of the duct shape, a mean flow with a small normal velocity component, slow variations of the duct liner properties, and a growing boundary-layer thickness, in addition to including the effects of large transverse velocity gradients.

By using the Born approximation Tam[16] investigated the transmission and scattering of spinning acoustic-wave modes through a duct nonuniformity. With this perturbation solution, he introduced for the first time the effect of the normal component of the mean flow but neglected the refractive effect of transverse velocity gradients. Nayfeh, Telionis and Lekoudis[17] used the method of multiple scales in order to study the propagation of all acoustic modes in a two-dimensional duct with a slowly-varying cross section carrying a sheared incompressible mean flow. Nayfeh, Kaiser and Telionis[18] extended the analysis to the more practical annular-duct configuration. Their analyses included the effects of streamwise variations of the mean velocity, of the liner properties, and of the boundary-layer thickness, and the effect of the mean normal velocity and transverse velocity gradient. These solutions based on the method of multiple

scales provide the most comprehensive description of sound propagation in realistic duct configurations that are available to date. The results of these analyses are summarized in section 3.

2. Effect of Sinusoidal Wall Undulations

The problem discussed here is that of sound propagation in a two-dimensional duct with no mean flow whose rigid upper and lower walls are given by

$$y_u = 1 + \varepsilon \sin(k_w x + \theta) \tag{1a}$$

and

$$y_\ell = \varepsilon \sin k_w x, \tag{1b}$$

respectively; ε is a small dimensionless parameter characterizing the magnitude of the wall undulations, k_w is the wave number of the undulations, and θ is the phase difference between the undulations of the two walls. The gas motion is described by a dimensionless velocity potential of the form

$$\tilde{\phi}(x,y,t) = \phi(x,y) \exp(-i\omega t) \tag{2}$$

where ω is the dimensionless frequency of the sound oscillation.

In straightforward perturbation solutions,[2-5] the potential function

$$\phi(x,y) = \phi_0(x,y) + \varepsilon\phi_1(x,y) \tag{3}$$

is substituted into the governing wave equation and boundary conditions, and the equations are expanded in powers of ε to yield problems for ϕ_0 and for ϕ_1.

The solution for ϕ_0 is simply a wave traveling in a constant-area duct:

$$\phi_0 = A \cos m\pi y \exp(ik_m x) \tag{4a}$$

where

$$k_m^2 = \omega^2 - m^2\pi^2 \tag{4b}$$

The solution for ϕ_1 shows that if the mth mode described above passes through the duct, the wall undulations generate two waves with wavenumbers $k_m + k_w$ and $k_m - k_w$, i.e.,

$$\phi_1(x,y) = B_1(y) \exp[i(k_m + k_w)x] + B_2(y) \exp[i(k_m - k_w)x] \tag{5}$$

where the form of $B_1(y)$ and $B_2(y)$ may be found in reference 5. In general, the two waves generated by the wall undulations are weak; however, if $(k_m \pm k_w)^2$ is equal (or nearly equal) to k_n^2, where k_n is the wave number of the nth mode, then $\phi_1(x,y) \to \infty$, and the straightforward expansion breaks down. Salant[6] has tabulated the frequencies at which such resonances occur but has not examined the nature of the wave propagation when this resonance occurs.

The straightforward solution shows that whenever a wave generated by the

wall undulations propagates at the speed of one of the basic duct modes, such a wave is not a small correction but appears at the first order of approximation, i.e., in the ϕ_0 term of equation (3). Further, the basic duct modes can be expected to modulate and interact slowly as they propagate, and the wave propagation at resonance can be analyzed with the method of multiple scales (see reference 19). Hence, to study the wave propagation near resonance, $k_w \approx k_n + k_m$, one expands the potential function in the form

$$\phi(x,y) = \phi_0(x_0,x_1,y) + \varepsilon\phi_1(x_0,x_1,y) \tag{6}$$

where $x_0 = x$ is a short scale characterizing the wavelengths of the acoustic waves and $x_1 = \varepsilon x$ is a long scale characterizing the amplitude and phase modulations and wave interactions. Equation (6) is substituted into the governing equations which are expanded in powers of ε to yield problems for ϕ_0 and ϕ_1. The solution of the first-order problem must contain the two interacting modes; that is

$$\phi_0(x_0,x_1,y) = A_m(x_1)\cos my \exp(ik_m x_0)$$

$$+ A_n(x_1)\cos ny \exp(ik_n x_0) \tag{7}$$

where the wave amplitudes $A_m(x_1)$ and $A_n(x_1)$ express the slow modulation and interaction of the two modes. The functions $A_m(x_1)$ and $A_n(x_1)$ are determined such that the solution (6) is uniformly valid to $0(\varepsilon)$; that is, by imposing an integrability condition on the problem for ϕ_1, one determines the variation of $A_m(x_1)$ and $A_n(x_1)$. The closeness of the wave propagation to resonance is expressed by the detuning parameter σ according to

$$k_w = k_n + k_m + \varepsilon\sigma, \quad \sigma = 0(1) \tag{8}$$

In the first case, $k_w = k_n - k_m + \varepsilon\sigma$, the integrability condition yields

$$A_m = a_m \exp(sx_1), \quad A_n = a_n \exp[(s + i\sigma)x_1] \tag{9a}$$

where

$$s = \frac{i}{2}[-\sigma \pm (\sigma^2 - 4\Omega)^{1/2}] \tag{9b}$$

and Ω is a constant that depends on the wave numbers k_n, k_m, k_w and the wall phase shift θ. In this case, it can be shown that $\Omega \leq 0$; thus s is purely imaginary and the amplitudes $A_m(x_1)$ and $A_n(x_1)$ are bounded as x_1 varies. As a consequence, in the case $k_w = k_n - k_m$ neither mode can exist without strongly exciting the other and the amplitudes of the two waves slowly modulate according to equation (9) as the waves travel along the duct.

In the case $k_w = k_n + k_m + \varepsilon\sigma$, the integrability condition yields

$$A_m = c_1 \exp(s_1 x_1) + c_2 \exp(s_2 x_1) \tag{10a}$$

where

$$s_{1,2} = \frac{1}{2}[i\sigma \pm (4\Omega - \sigma^2)^{1/2}] \tag{10b}$$

with a similar result for A_n. In this case the constant Ω is greater than zero and the amplitudes are bounded or unbounded as $x_1 \to \infty$ depending on whether $4\Omega \leq \sigma^2$ or $4\Omega > \sigma^2$, i.e., depending on the closeness to resonance. Hence, in the case $k_\nu = k_m + k_n$ neither mode can exist without strongly exciting the other, and the solution admits the possibility of both modes growing exponentially with axial distance.

In future work, these resonant interactions due to small wall undulations need to be examined to determine the influence of a mean flow in the duct and the influence of duct liners.

3. Effect of Slowly-Varying Area

a. No mean flow

Mayfeh and Telionis[9] used the method of multiple scales to determine the propagation of a wave packet in rectangular and circular ducts with slowly varying cross sections and slowly varying wall admittance. For rectangular ducts they assumed the dimensionless acoustic velocity potential to have the form

$$\tilde{\phi}(x,y,z,t) = \phi(x_1,T_1,y,z;\varepsilon)\exp(i\psi) \tag{11}$$

where $x_1 = \varepsilon x$ and $T_1 = \varepsilon t$ are slow scales measuring the modulation of the wave packet due to the area variations; ε is a small parameter the order of the maximum slope of the wall; and

$$\frac{\partial\psi}{\partial t} = -\omega(x_1,T_1) \text{ and } \frac{\partial\psi}{\partial x} = k_e(x_1,T_1) \tag{12}$$

with ω the frequency and k_e the complex wave number. Expanding ϕ in powers of ε according to

$$\phi = \phi_0(x_1,T_1,y,z) + \varepsilon\phi_1(x_1,T_1,y,z) + \ldots, \tag{13}$$

substituting into the wave equation and the boundary conditions, and equating coefficients of like powers of ε, they obtained problems describing ϕ_0 and ϕ_1.

The solution of the first-order problem is

$$\phi_0 = A(x_1,T_1)\,\psi(y,z;x_1) \tag{14}$$

where ψ is the characteristic mode obtained by assuming that the cross section is uniform at each station, and the amplitude function $A(x_1,T_1)$ is still undetermined. Since the dimensions of the duct and the liner properties change along the duct, the eigenfunction ψ varies with x_1.

The second-order problem is an inhomogeneous problem for ϕ_1, and it has a solution if, and only if, a solvability condition is satisfied. This condition yields an equation for A of the form

$$\frac{\partial E}{\partial T} + \frac{\partial}{\partial x_1}\left(\frac{d\omega}{dk}E\right) = 0 \tag{15}$$

where, for two-dimensional ducts,

$$E = \frac{A^2 d}{4}\left(\omega^2 + \frac{k_0^2 \sin 2k_y d}{2k_y d}\right) \tag{16}$$

$d(x_1)$ is the dimensionless duct half width and k_y is the eigenvalue associated with the characteristic mode $\psi(y,z;x_1)$. Thus, k_y is the solution of

$$k_y \tan k_y d = -i\omega\beta \tag{17}$$

where β is the specific admittance of the liner. The complex wave number k_0 is given by

$$k_0^2 = \omega^2 - k_y^2 \tag{18}$$

For rigid walls, $k_y = n\pi/d$, E is the acoustic energy flux and $d\omega/dk$ is the group velocity of the wave packet.

For a monochromatic wave ($\partial\omega/\partial T_1 = \partial A/\partial T_1 = 0$), Eq. (15) integrates to

$$A^2 k\left(d + \frac{\sin 2k_y d}{2k_y}\right) = \text{constant} \tag{19}$$

Thus, for no mean flow the variable area gives rise to an inverse square root behavior of the amplitude function. Combining the above results, one expresses the acoustic velocity potential as

$$\tilde{\Phi} \sim \frac{\text{const.}}{\sqrt{f(x_1)}}\,\psi(y,z;x_1)\,\exp\left[i\int k_0(x_1)dx - i\omega t\right] \tag{20a}$$

$$\text{where } f(x_1) = k_0\left(d + \frac{\sin 2k_y d}{2k_y}\right) \tag{20b}$$

The amplitude function $A(x_1)$ can be interpreted as a correction to the complex wave number by writing equation (20) in the form

$$\tilde{\Phi} = \text{const.}\ \psi(y,z;x_1)\,\exp\left[i\int (k_0 + \varepsilon k_1)dx - i\omega t\right] \tag{21a}$$

$$\text{where } k_1 = i\,f'(x_1)/2f(x_1) \tag{21b}$$

b. With mean flow

Nayfeh, Telionis, and Lekoudis[17] used the method of multiple scales to analyze the propagation of all acoustic modes in a two-dimensional duct with slowly-varying cross section that carries an incompressible, sheared mean flow whose velocity components are u_0 and v_0. The analysis was extended to the case of an annular duct by Nayfeh, Kaiser, and Telionis.[18] A long scale $x_1 = \varepsilon x$ is used to characterize the wave modulations due to the varying cross section where ε is the maximum slope of the wall.

For the two-dimensional case, the acoustic pressure and velocity components

are expanded in the form

$$p = [F_0(y;x_1) + \varepsilon F_1(y;x_1) + \ldots] \exp(i\phi) \tag{22a}$$

$$u = [G_0(y;x_1) + \varepsilon G_1(y;x_1) + \ldots] \exp(i\phi) \tag{22b}$$

$$v = [H_0(y;x_1) + \varepsilon H_1(y;x_1) + \ldots] \exp(k\phi) \tag{22c}$$

where $-\partial\phi/\partial t = \omega$ and $\partial\phi/\partial x = k_0(x_1)$ are the frequency and propagation constant respectively. These expansions are substituted into the governing equations, which are expanded for small ε to yield a sequence of problems for F_n, G_n and H_n; G_n and H_n are eliminated from these problems to yield problems for F_n.

The basic problem,

$$\mathcal{L}(F_0) \equiv \frac{\partial}{\partial y}\left(\frac{1}{\hat{\omega}^2}\ \frac{\partial F_0}{\partial y}\right) + \left(1 - \frac{k_0^2}{\hat{\omega}^2}\right)F_0 = 0 \tag{23a}$$

and

$$\frac{\partial F_0}{\partial y} \mp i\omega\beta F_0 = 0 \quad \text{at} \quad y = \pm d \tag{23b}$$

where $\hat{\omega} = \omega - k_0 u_0$, is identical to the problem that describes acoustic propagation in a constant area duct, except that β and d can take on different values at each axial station. Hence,

$$F_0(y;x_1) = A(x_1)\ \psi(y;x_1) \tag{24}$$

where $\psi(y;x_1)$ is the eigenfunction corresponding to the eigenvalue k_0 and is determined as if the flow and duct walls were parallel at each station. The amplitude function $A(x_1)$ is determined so that the solution is uniformly valid to order $O(\varepsilon)$, i.e., by imposing a solvability condition on the inhomogeneous problem for F_1:

$$\mathcal{L}(F_1) = M(F_0, u_0, v_0, k_0, d) \tag{25a}$$

$$\frac{\partial F_1}{\partial y} \mp i\omega\beta F_1 = B(F_0, u_0, v_0, k_0, d) \quad \text{at } y = \pm d \tag{25b}$$

This solvability condition yields an equation for A of the form

$$f(x_1)\frac{dA}{dx_1} + g(x_1)A = 0 \tag{26}$$

where $f(x_1)$ and $g(x_1)$ are obtained by simple numerical quadratures across the duct width of integrands that are functions of $\psi, k_0, \beta, d, u_0, v_0$ and their axial derivatives. The solution of equation (26) is

$$A(x_1) = A_0 \exp(i\int k_1\, dx_1) = A_0 \exp(i\int \varepsilon k_1\, dx) \tag{27a}$$

where

$$k_1(x_1) = ig(x_1)/f(x_1) \tag{27b}$$

Combining the above results, one writes the dimensionless acoustic pressure in the form

$$p(x,y,t) = A_0\psi(y;x_1)\exp\left[i\int[k_0(x_1) + \varepsilon k_1(x_1)]dx - i\omega t\right] + O(\varepsilon) \qquad (28)$$

The equivalent analysis in annular ducts yields

$$p(r,\theta,x,t) = A_0\psi(r;x_1)\exp\left[i\int[k_0(x_1) + \varepsilon k_1(x_1)]dx - i\omega t + im\theta\right] + O(\varepsilon) \qquad (29)$$

where m is the circumferential mode number and $k_1(x_1)$ is determined by equations of the form of equations (26) and (27). For no mean flow $g(x_1) = f'(x_1)$ and the amplitude functions reduce to the inverse square root behavior found in reference 9.

In the above analyses, the local attenuation rate is obtained in the form $\alpha_0 + \varepsilon\alpha_1 = \mathrm{Im}(k_0 + \varepsilon k_1)$ where α_0 is the "quasi-parallel" attenuation rate, which is calculated at each axial location as if the mean flow and duct walls were parallel; α_1 contains the effect of the wall slope, the refractive effects of the streamwise and transverse derivatives of the mean flow, and the effect of the streamwise derivatives of the quasi-parallel eigenfunction and eigenvalue and of the liner properties. The total attenuation over a finite duct length is the integral of $\alpha_0 + \varepsilon\alpha_1$ over that length. Computer codes have been developed for the numerical evaluation of these effects. The basic eigenvalue problem for $\psi(r;x_1)$ and $k_0(x_1)$ is solved with a Runge-Kutta forward integration procedure at each step along the duct length. The axial derivatives dk_0/dx_1 and $\partial\psi/\partial x_1$ are obtained from an additional application of the Runge-Kutta procedure to the problem defined by taking the x_1 derivative of the basic eigenvalue problem for ψ. Finally, $k_1(x_1)$ is calculated by use of Simpson's rule. The computer codes are operative and are being applied to the analysis of the effect of geometry changes typical of those encountered in aircraft engine-duct systems.

The results of two sample calculations are cited here. Figure 1 shows an

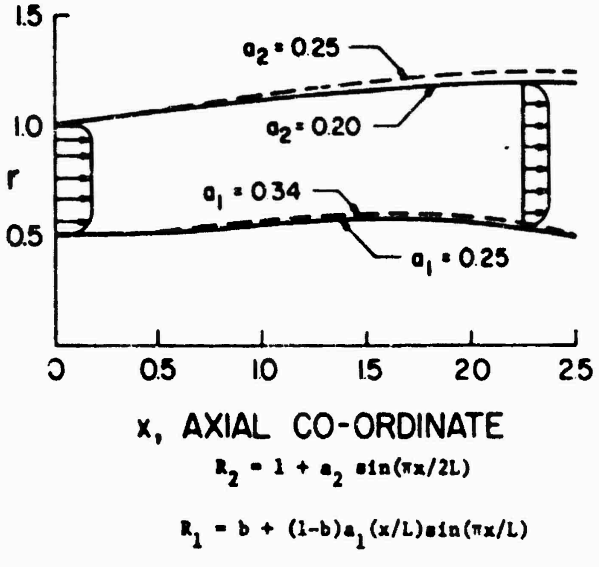

Figure 1. Approximate model of an annular bypass duct.

approximate model of an annular bypass duct whose walls are lined with a porous facing sheet backed by cellular cavities; a_1 and a_2 are parameters in the expressions for the wall radii and are used to vary the duct configuration slightly, the core Mach number at the duct entrance was taken to be 0.4, and the flow was expanded to a lower Mach number at the exit. In Fig. 2(a) a comparison of the effect of two different outer wall variations is made. For the case of $a_2 = 0.25$, the mean flow is expanded to a lower Mach number at the exit than that in the $a_2 = 0.2$ case. The quasi-parallel approximation predicts a lower total attenuation for the $a_2 = 0.25$ case, but inclusion of the non-parallel effects results in a slightly higher attenuation for this case. In Fig. 2(b), the results of two different inner wall variations are shown. The entrance and exit Mach numbers are the same for both configurations, but the $a_1 = 0.34$ case has a slightly higher Mach number within the duct than does the $a_1 = 0.25$ case. The quasi-parallel

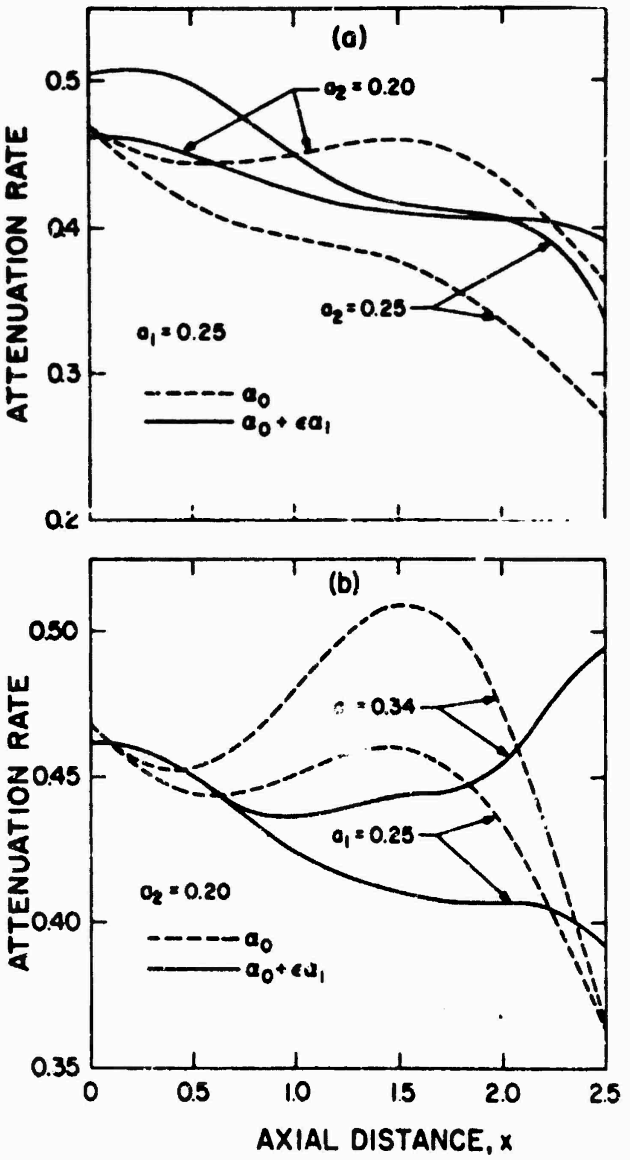

Figure 2. Comparison of the attenuation of the (0,0) mode for various wall configurations and $\omega = 30$.

approximation indicates that the additional constriction of the duct provided by $a_2 = 0.34$ results in a slightly higher attenuation. Inclusion of the effects of the axial derivatives does not change this general conclusion but does result in a lower attenuation level and shifts the point of peak attenuation away from the point of maximum deflection of the inner wall.

The results cited above demonstrate that area variations have a significant influence on the characteristics of the sound propagation and that an accurate prediction of the attenuation must include the influence of axial velocity gradients (i.e., the quasi-parallel approximation is not sufficient).

This analysis is being extended to the case of a compressible mean flow, and further numerical calculations for the incompressible case are being made to study the effect of different flow and liner properties on the attenuation of sound.

Acknowledgement

This work was supported by the NASA-Langley Research Center under Grant NGR 47-004-109.

References

1. Nayfeh, A.H., Kaiser, J.E., and Telionis, D.P., "The Acoustics of Aircraft Engine-Duct Systems," AIAA Paper No. 73-1153 (1973).

2. Isakovich, M.A., "Scattering of Sound Waves on Small Irregularities in a Waveguide," Akusticheskii Zhurmal, Vol. 3, 37-45 (1957).

3. Samuels, J.S., "On Propagation of Waves in Slightly Rough Ducts," the Journal of the Acoustical Society of America, Vol. 31, 319-325 (1959).

4. Salant, R.F., "Acoustic Propagation in Waveguides with Sinusoidal Walls," The Journal of the Acoustical Society of America, Vol. 53, 504-507 (1973).

5. Nayfeh, A.H., "Sound Waves in Two-Dimensional Ducts with Sinusoidal Walls," VPI & SU Report No. E-74-9, Virginia Polytechnic Institute and State University (March 1974).

6. Zorumski, W.E. and Clark, L.R.,"Sound Radiation from a Source in an Acoustically Treated Circular Duct," unpublished, NASA-Langley Research Center (1971).

7. Lansing, D.L. and Zorumski, W.E., "Effects of Wall Admittance Changes on Duct Transmission and Radiation of Sound," Journal of Sound and Vibration, Vol. 27, 85-100 (1973).

8. Alfredson, R.J.,"The Propagation of Sound in a Circular Duct of Continuously Varying Cross-Sectional Area," Journal of Sound and Vibration, Vol. 23, 433-442.(1972).

9. Nayfeh, A.H. and Telionis, D.P.,"Acoustic Propagation in Ducts with Varying Cross Sections," Journal of the Acoustical Society of America, Vol. 54, 1654-1661 (1973).

10. Beckemeyer, R.J. and Eversman, W., "Computational Methods for Studying Acoustic Propagation in Nonuniform Waveguides," AIAA Paper No. 73-1006 (1973).

11. Powell, A., "Theory of Sound Propagation through Ducts Carrying High-Speed Flows," Journal of the Acoustical Society of America, Vol. 32, 1640-1646 (1960).

12. Eisenberg, N.A. and Kao, T.W., "Propagation of Sound Through a Fluid Moving in a Duct of Varying Area," in Interagency Symposium of University Research on Transportation Noise, Stanford, Vol. II, 397-413 (1973).

14. King, L.S. and Karamcheti, K., "Propagation of Plane Waves in the Flow through a Variable Area Duct," AIAA Paper No. 73-1009 (1973).

15. Hogge, H.D. and Ritzi, E.W., "Theoretical Studies of Sound Emission from Aircraft Ducts," AIAA Paper No. 73-1012 (1973).

16. Tam, C.K.W., "Transmission of Spinning Acoustic Modes in a Slightly Nonuniform Duct," Journal of Sound and Vibration, Vol. 18, 339-351 (1971).

17. Nayfeh, A.H., Telionis, D.P. and Lekoudis, S.G., "Acoustic Propagation in Ducts with Varying Cross Sections and Sheared Mean Flow," AIAA Paper No. 73-1008 (1973).

18. Nayfeh, A.H., Kaiser, J.E. and Telionis, D.P., "Transmission of Sound Through Annular Ducts of Varying Cross Sections and Sheared Mean Flow," AIAA Paper No. 74-58 (1974).

19. Nayfeh, A.H., Perturbation Methods, Wiley-Interscience, New York, Chap. 6.

HIGH INTENSITY SOUND IN LINED DUCTS

by

Ali H. Nayfeh and Ming-Shing Tsai

Department of Engineering Science and Mechanics
Virginia Polytechnic Institute and State University
Blacksburg, Virginia 24061

The objective of the project is to analyze the nonlinear effects of the gas motion as well as the acoustic lining material on the transmission and attenuation of sound in two-dimensional and circular ducts with uniform cross sections. Approximate solutions have been obtained for small but finite amplitudes by using the method of multiple scales. The effect of the acoustic material is included either by characterizing the material by an empirical nonlinear impedance or by coupling the waves in the duct with those in the liner. The results show that the nonlinearity flattens and broadens the absorption vs. frequency curves. Moreover, the effect of the gas nonlinearity increases with increasing sound frequency, whereas the effect of the material nonlinearity decreases with increasing sound frequency.

1. Introduction

Measured data in typical jet engines indicate that the sound pressure levels involved may be in excess of 160 dB which corresponds to a pressure fluctuation of the order of 0.01 atmospheres. At these levels, the nonlinear effects play an important role in the attenuation of the sound. These nonlinear effects can be classified into two types: the nonlinearity of the gas itself and the nonlinearity of the acoustic properties of the lining material.

The nonlinearity of the gas was investigated by Maslen and Moore[1], Burns[2], Keller and Millman[3], Coppens[4], Pestorius and Blackstock[5], and Peube and Chasseriaux[6]. Coppens[4] and Pestorius and Blackstock[5] determined the viscous and thermal dissipative effects on the nonlinear propagation of plane waves in hard-walled ducts. Maslen and Moore used the method of strained parameters (e.g., Nayfeh[7], Section 3.1) to analyze strong transverse waves in a circular cylinder. They determined the nonlinear frequency shift and the dissipative effects of the acoustic boundary layer. Burns obtained a straightforward expansion that contains secular terms for nonlinear waves in a hard-walled duct. Peube and Chasseriaux proposed two expansions for nonlinear waves in hard-walled ducts with varying cross sections, one valid for small Mach numbers and the other valid for long waves; no solutions were obtained to assess the nonlinear effects.

Isakovich[8] determined a second-order expansion for the nonlinear wave propagation in a duct lined with a material having linear acoustic properties. He found that the expansion is free of secular terms as opposed to the case of propagation in an unbounded space.

The nonlinearity of the acoustic lining material was investigated, experimentally, by Zorumski and Parrott[9] and Kurze and Allen[10] and, theoretically,

by Ingard[11,12] and Kurze and Allen[10]. Zorumski and Parrott[9] and Kurze and Allen[10] observed that the nonlinear effects tend to flatten and broaden the absorption vs. frequency curve. Ingard used the one-dimensional transmission line approximation in conjunction with the empirical impedance proposed by Ingard and Ising[13] to determine the nonlinear material effects on the attenuation of the lowest mode at low frequencies. Kurze and Allen extended the work of Ingard to the case of resonant frequencies.

The objective of this project is to analyze the nonlinear effects of the gas motion as well as the acoustic lining material on the transmission and attenuation of sound in two-dimensional and circular ducts with uniform cross sections.

2. Problem Formulation

We consider nonlinear waves propagating in a uniform two-dimensional/circular duct whose walls are lined with a nonlinear acoustic material. The gas is assumed to be inviscid, irrotational and initially quiescent with a uniform pressure p_0^* and a uniform density ρ_0^*. The inviscid, irrotational gas assumption is justified provided that $\epsilon > 0(Re^{-1/2})$, where ϵ is a parameter characterizing the dimensionless acoustic pressure and $Re = d^* c_0^* / \nu^*$ with d^* a characteristic dimension of the cross section, c_0^* the ambient speed of sound, and ν^* the gas viscosity. For a duct with $d^* = 1$ ft. at room temperature ($c_0^* = 1150$ ft./sec., $\nu^* = 2.142 \times 10^{-4}$ ft.^{2}/sec.), $Re \sim 5.4 \times 10^6$ and the inviscid gas assumption is valid provided that the sound pressure level $L \geq 130$ dB above 0.0002 dyne/cm^2. For a duct with $d^* = 1$ in., the viscous effects can be neglected for $L \geq 140.5$dB.

Lengths, time, velocities, density, and pressure are made dimensionless by using d^*, d^*/c_0^*, c_0^*, ρ_0^*, and $\rho_0^* c_0^{*2}$. The problem formulation consists of the governing equations and appropriate boundary conditions.

Governing Equations

Since the gas flow is assumed to be inviscid and irrotational, the velocity $\vec{v} = \vec{v}(\vec{r},t)$ in the duct can be derived from a potential function $\phi(\vec{r},t)$ according to

$$\vec{v} = \nabla\phi \tag{1}$$

while the pressure is related to the density by

$$\frac{p^*}{p_0^*} = \left(\frac{\rho^*}{\rho_0^*}\right)^\gamma$$

or in dimensionless quantities by

$$\gamma p = \rho^\gamma \tag{2}$$

where γ is the gas specific heat ratio. Substituting for $\vec{v}$ and p from Eqs. (1) and (2) into the momentum equations and integrating yield the following equation

$$\gamma p = \left\{(1-\gamma)\left[\phi_t + \frac{1}{2}(\nabla\phi)^2\right] + 1\right\}^{\gamma/(\gamma-1)} \tag{3}$$

Eliminating ρ, p, and $\vec{v}$ from the continuity equation gives

$$\phi_{tt} + \frac{\partial}{\partial t}(\nabla\phi)^2 + \frac{1}{2}(\nabla\phi\cdot\nabla)(\nabla\phi)^2$$

$$= \left\{1 + (1-\gamma)[\phi_t + \frac{1}{2}(\nabla\phi)^2]\right\}\nabla^2\phi \qquad (4)$$

Boundary Conditions

The effect of the acoustic lining material on the propagation and attenuation of the waves is treated by two different approaches. First, Nayfeh and Tsai[14,15] represented the effect of the liner by a semi-empirical impedance. Second, Nayfeh and Tsai[16,17] coupled the wave propagation in the duct with the wave propagation in the liner.

Semi-Empirical Wall Impedance

The nonlinear acoustic properties of lining materials are very important in determining the attenuation characteristics of high intensity sound in ducts. A considerable number of formulas that relate the acoustic pressure drop across the liner to the acoustic velocity have appeared in the literature (see, for example Ref. 18 for a review and new results). In references 14 and 15, Nayfeh and Tsai used a modified form of the semi-empirical formula proposed by Zorumski and Parrott[19] to analyze the wave propagation in two-dimensional and circular ducts. In terms of this semi-empirical formula, the boundary condition at the wall is

$$p_0^* - p_0 = [R_0^* + R_n^*(v^*)]v^* + [\chi_0^*(\omega^*) + \chi_n^*(v^*,\omega^*)]\frac{\partial v^*}{\partial t^*} \qquad (5)$$

where p^* and v^* are respectively the gas pressure and velocity normal to the duct walls, R_n^* is the nonlinear part of the liner resistance and χ_n^* is related to the nonlinear part of the liner reactance. This form is based on what Zorumski and Parrott call the "instantaneous acoustic laws" which imply incompressibility across the sheet or plate and include a semi-empirical term in the momentum equation. In terms of the dimensionless variables defined above, Eq. (5) can be rewritten as

$$p - \gamma^{-1} = [R_0 + R_n(v)]v + [\chi_0(\omega) + \chi_n(v,\omega)]\frac{\partial v}{\partial t}$$

$$\text{at duct/liner interface} \qquad (6)$$

Coupling of the Waves in the Duct and Liner

To accomplish this, we need the equations that govern the flow in the porous material and the cavities as well as the boundary conditions at the impervious walls, the porous material/duct interface, and the porous material/cavities interface. The equations governing the wave propagation in the cavities are the same as Eqs. (3) and (4) except for the absence of the x derivatives.

The equations describing conservation of mass and momentum in the porous material are

$$\Omega\frac{\partial\rho}{\partial t} + \frac{\partial}{\partial y}(\rho v) = 0 \qquad (7)$$

$$\rho_e \frac{\partial v}{\partial t} + \sigma v + \frac{\partial p}{\partial y} = 0 \tag{8}$$

where Ω is the material porosity, ρ_e is the effective density, $\sigma = \sigma^* d^*/\rho_0^* c_0^*$, and σ^* is the resistivity of the material. The resistivity is related to the velocity by

$$\sigma = \sigma_0 + \sigma_1 |v| \tag{9}$$

where σ_0 (Darcy's constant) is due to viscous resistance and $\sigma_1 |v|$ (Forchheimer nonlinear part) is due to inertia effects. The pressure is related to the density by

$$\gamma p = \rho^n \tag{10}$$

where n is generally a complex number; it is real only at high frequencies (above 1000 Hz) and at low frequencies (below 100 Hz).

As the gas Reynolds number tends to infinity, viscosity can be neglected in the duct and in the cavities but it cannot be neglected near the boundaries where the viscous effects are important. With very small viscosity, the mean boundary layers can be approximated by vortex sheets across which the pressure and the particle displacement are continuous. For the two-dimensional case, we denote by $y = \eta(x,t)$ and $y = \zeta(x,t)$ the positions of the vortex sheets that separate the flow in the duct from that in the porous material and the flow in the porous material from that in the core. The continuity of pressure and particle displacement gives

$$p = p_p \quad \text{at} \quad y = \eta(x,t) \tag{11}$$

$$\frac{\partial \eta}{\partial t} + \frac{\partial \eta}{\partial x}\frac{\partial \phi}{\partial x} - \frac{\partial \phi}{\partial y} = 0 \quad \text{at} \quad y = \eta(x,t) \tag{12}$$

$$\frac{\partial \eta}{\partial t} - v_p = 0 \quad \text{at} \quad y = \eta(x,t) \tag{13}$$

$$p_p = p_c \quad \text{at} \quad y = \zeta(x,t) \tag{14}$$

$$\frac{\partial \zeta}{\partial t} - v_p = 0 \quad \text{at} \quad y = \zeta(x,t) \tag{15}$$

$$\frac{\partial \zeta}{\partial t} + \frac{\partial \zeta}{\partial x}\frac{\partial \phi}{\partial x} - \frac{\partial \phi}{\partial y} = 0 \quad \text{at} \quad y = \zeta(x,t) \tag{16}$$

where Φ is the potential function describing the flow in the core and the subscripts p and c refer to the porous material and the core, respectively.

3. Two-Dimensional Configuration

To obtain an approximate solution for small but finite amplitudes, Nayfeh and Tsai used the method of multiple scales (see, for example, chapter 6 of Ref. 7). According to this method, the solution is sought in the form

$$\phi(x,y,t) = \sum_{m=1}^{3} \epsilon^m \phi_m(x_0,x_1,x_2,y,t) + O(\epsilon^4) \tag{17}$$

where

$$x_m = \epsilon^m x \tag{18}$$

The short scale $x_0 = x$ characterizes the wavelength of the sound while the long scales $x_1 = \epsilon x$ and $x_2 = \epsilon^2 x$ characterize the evolution of the wave amplitude and phase due to the nonlinearities. The axial derivative transforms according to

$$\frac{\partial}{\partial x} = \frac{\partial}{\partial x_0} + \epsilon \frac{\partial}{\partial x_1} + \epsilon^2 \frac{\partial}{\partial x_2} \tag{19}$$

Substituting Eqs. (17)-(19) into the governing equations and boundary conditions, expanding, and equating coefficients of like powers of ϵ, we obtain

$$\frac{\partial^2 \phi_m}{\partial x_0^2} + \frac{\partial^2 \phi_m}{\partial y^2} - \frac{\partial^2 \phi_m}{\partial t^2} = F_m \tag{20}$$

$$\mathcal{L}(\phi_m) = G_m \quad \text{at duct/liner interface} \tag{21}$$

where $\mathcal{L}$ is a linear known operator and F_m and G_m are known functions of the preceeding terms; that is, $F_1 = G_1 = 0$, F_2 and G_2 are functions of ϕ_1, and F_3 and G_3 are functions of ϕ_1 and ϕ_2. If the liner effects are represented by the semi-empirical formula (6), $\mathcal{L}$ takes the form

$$\mathcal{L} = \frac{\partial}{\partial t} + R_0 \frac{\partial}{\partial y} + \gamma_2 \frac{\partial^2}{\partial y \partial t} \tag{22}$$

When m = 1, the solution of Eqs. (20) and (21) for symmetric waves is written as

$$\phi_1 = A(x_1,x_2) \cos \kappa y \, e^{i(kx_0 - \omega t)} + cc \tag{23}$$

$$\kappa^2 = \omega^2 - k^2 \tag{24}$$

$$\kappa \tan \kappa = -i\omega \hat{B} \tag{25}$$

where cc stands for the complex conjugate of the preceeding terms and the function $A(x_1,x_2)$ is still undetermined at this level of approximation; it is determined by using the so-called solvability condition at the higher levels of approximation. The admittance $\hat{B}$ is related to the liner properties.

With ϕ_1 known, the right-hand sides of Eqs. (20) and (21) are known for the case m=2. The resulting inhomogeneous problem has a solution if, and only if, the inhomogeneous parts are orthogonal to every solution of the adjoint homogeneous problem. This solvability condition leads to an equation describing the evolution of $A(x_1,x_2)$ on the long scale x_1. With this solvability condition, Eqs. (20) and (21) can be solved for ϕ_2. Then, F_3 and G_3 are known functions. Invoking the solvability condition in the inhomogeneous problem consisting of Eqs. (20) and (21) when m=3 yields an equation for the evolution of A on the long scale x_2.

Denoting the amplitude of the wave by a(x) and using the results of the solvability condition, we obtain

$$\frac{da}{dx} = -(\alpha_0 + \alpha_1 a + \alpha_2 a^2)a \tag{26}$$

where α_0 is the linear attenuation rate and $\alpha_1 a$ and $\alpha_2 a^2$ are the nonlinear contributions to the attenuation rate. The effect of the gas nonlinearity is contained in $\alpha_2 a^2$ while the effect of the material nonlinearity is contained in α_1 and α_2. From this equation, it is clear that the material nonlinearity is much more important than the gas nonlinearity. Detailed numerical examination of α_1 and α_2 show that the effect of the gas nonlinearity increases with increasing frequency while the opposite holds for the effect of the material nonlinearity.

Figure 1 shows good agreement between the present results and the experimental data of Kurze and Allen. Note that the nonlinearity tends to increase the attenuation rate at all frequencies except in narrow bandwidths around the resonant frequencies. Figures 2-5 as well as other detailed numerical calculations verify this conclusion irrespective of the mode number or the acoustic properties of the liner. Moreover, Figures 2-5 show that the sharper the tuning is the narrower the frequency bandwidths in which the nonlinearity decreases the attenuation rate.

4. Cylindrical Configuration

In this case, Nayfeh and Tsai[15,17] obtained an approximate solution by letting

$$\Phi(x,r,\theta,t) = \sum_{m=1}^{3} \varepsilon^m \phi_m(x_0,x_1,x_2,r,\theta,t) + O(\varepsilon^4) \tag{27}$$

Substituting Eqs. (27), (18), and (19) into the governing equations and boundary conditions, expanding, and equating coefficients of like powers of ε, we obtain

$$\frac{\partial^2 \phi_m}{\partial x_0^2} + \frac{\partial^2 \phi_m}{\partial r^2} + \frac{1}{r}\frac{\partial \phi_m}{\partial r} + \frac{1}{r}\frac{\partial^2 \phi_m}{\partial \theta^2} - \frac{\partial^2 \phi_m}{\partial t^2} = F_m \tag{28}$$

$$\mathcal{L}(\phi_m) = G_m \quad \text{at duct/liner interface} \tag{29}$$

where F_m and G_m are functions of the preceeding terms and the operator $\mathcal{L}$ depends on the detailed modelling of the effect of the liner as in the two-dimensional case.

The solution of Eqs. (28) and (29) when $m = 1$ that is bounded at the duct axis is taken in the form

$$\phi_1 = A(x_1,x_2)\, J_s(\kappa r)\, e^{i(kx_0 - \omega t + s\theta)} + cc \tag{30}$$

$$\kappa^2 = \omega^2 - k^2 \tag{31}$$

$$\kappa J_s'(\kappa) = is\delta J_s(\kappa) \tag{32}$$

where s is a positive integer and J_s is Bessel's function of order s. Following the procedure described in the previous section, we determine ϕ_2 and ϕ_3 and the function $A(x_1,x_2)$. Denoting the amplitude of the wave by a(x) and using the equation describing $A(x_1,x_2)$, we obtain

$$\frac{da}{dx} = -(\alpha_1 + \alpha_2 a + \alpha_3 a^2)a \tag{33}$$

Detailed numerical calculations show that the nonlinear effects tend to flatten and broaden the absorption vs. frequency curves, in qualitative agreement with the experimental results and the aforementioned two-dimensional analytical results. Moreover, the effects of the gas nonlinearity increase with increasing frequency while the opposite holds for the material nonlinear effects.

5. Conclusions

The propagation and attenuation of high intensity sound in two-dimensional and circular lined ducts of uniform cross sections is analyzed in the absence of mean flow. The duct is lined with a point-reacting acoustic material consisting of a porous sheet or a perforated plate followed by honeycomb cavities and backed by the impervious wall of the duct. The effects of the gas viscosity in the duct and cavities are neglected.

Since a small amount of wave distortion may take place over many wavelengths, multiple length scales can be used to represent the propagation and distortion of these waves; that is a short scale characterizing the wavelength and long scales characterizing the amplitude modulation. Therefore, the method of multiple scales is used to determine the nonlinear effects of both the gas and the acoustic properties of the lining material on the propagation and attenuation of sound waves in the above mentioned ducts. An equation is derived for the variation of the amplitude with the axial distance by invoking the solvability condition in the second- and third-order problems.

The effect of the liner on the wave propagation is treated using two approaches. In the first approach, the acoustic characteristics of the liner are described by a semi-empirical impedance that is a nonlinear function of the acoustic particle velocity. In the second approach, the waves in the duct are coupled with those in the liner, and the wall impedance is obtained as a by-product in terms of the liner geometry and acoustic properties.

The principal conclusions of the present study are:

1) The nonlinearity flattens and broadens the absorption vs. frequency curve, irrespective of the geometrical dimensions or the porous material acoustic properties, in agreement with the experimental observations. Thus, the nonlinearity always has an adverse effect on the attenuation rate in narrow frequency bandwidths about the resonant frequencies. Outside these bandwidths the nonlinearity always has a favorable effect.

2) The effect of the gas nonlinearity increases with increasing sound frequency, whereas the effect of the material nonlinearity decreases with increasing sound frequency. In general, the material nonlinearity is much more important than the gas nonlinearity.

3) The sharper the resonant tuning is the narrower the adverse frequency bandwidth is.

4) Since the resonant frequencies increase with mode number, the frequency corresponding to the onset of the adverse nonlinear effect increases with mode number. Moreover, the adverse frequency bandwidth increases with mode number.

The limitations of the present study are:

1) There is no mean flow.

2) A point-reacting liner is considered when the waves in the duct are coupled with those in the liner. The wavelength of interest must be longer than the thickness of the porous medium, unless there are partitions in the porous material.

3) Viscous effects are neglected.

4) The waves are dispersive; that is waves with different wavelengths travel with different phase speeds.

5) The ducts have uniform cross-sections.

The present analysis is being extended to determine the combined effects of flow and high intensity sound on the attenuation in a lined duct with a uniform cross section.

Acknowledgement

This work was supported by the NASA-Langley Research Center under Grant NGR 47-004-109.

References

1. Maslen, S.H. and Moore, F.K.,"On Strong Transverse Waves without Shocks in a Circular Cylinder," Journal of Aerospace Sciences, Vol. 23,583 (1956).

2. Burns, S.H., "Finite Amplitude Distortion in Air at High Acoustic Pressures," Journal of the Acoustical Society of America, Vol. 41, 1157 (1967).

3. Keller, J.B. and Millman, M.H., "Finite-Amplitude Sound-Wave Propagation in a Waveguide," Journal of the Acoustical Society of America, Vol. 49, 329 (1971).

4. Coppens, A.B., "Theoretical Study of Finite Amplitude Traveling Waves in Rigid-Walled Ducts," Journal of the Acoustical Society of America, Vol. 49, 306 (1971).

5. Pestorius, F.M. and Blackstock, D.T., "Nonlinear Distortion in the Propagation of Intense Acoustic Noise," Interagency Symposium of University Research in Transportation Noise, 565,(1973).

6. Peube, J.L. and Chasseriaux, J., "Nonlinear Acoustics in Ducts with Varying Cross Sections," Journal of Sound and Vibration, Vol. 27, 533 (1973).

7. Nayfeh, A.H., Perturbation Methods, New York, Wiley-Interscience. (1973).

8. Isakovich, M.A., "Nonlinear Effects Involved in Certain Acoustical Problems," Soviet Physics-Acoustics, Vol. 6, 321 (1961).

9. Zorumski, W.E. and Parrott, T.L., "Nonlinear Acoustic Theory for Thin Porous Sheets," NASA SP-189, 17 (1968).

10. Kurze, U.J. and Allen, C.H., "Influence of Flow and High Sound Level on the Attenuation in a Lined Duct," Journal of the Acoustical Society of America, Vol. 49, 1643 (1971).

11. Ingard, U., "Absorption Characteristics of Nonlinear Acoustic Resonators," Journal of the Acoustical Society of America, Vol. 43, 167 (1968a).

12. Ingard, U., "Nonlinear Attenuation of Sound in a Duct," Journal of the Acoustical Society of America, Vol. 42, 6 (1968b).

13. Ingard, U. and Ising, H., "Acoustic Nonlinearity of an Orifice," Journal of The Acoustical Society of America, Vol. 42, 6 (1967).

14. Nayfeh, A.H. and Tsai, M.-S., " Nonlinear Acoustic Propagation in Two-Dimensional Ducts," Journal of the Acoustical Society of America, in press, (1974).

15. Nayfeh, A.H. and Tsai, M.-S., "Nonlinear Wave Propagation in Acoustically Lined Circular Ducts," Journal of Sound and Vibration, in press (1974).

16. Nayfeh, A.H. and Tsai, M.-S., "Finite Amplitude Waves in Two-Dimensional Lined Ducts," Journal of Fluid Mechanics, submitted for publication (1974).

17. Nayfeh, A.H. and Tsai, M.-S., "Finite Amplitude Waves in Circular Lined Ducts," To be presented at the AIAA Fluid and Plasma Dynamics Conference, Palo Alto, California, June 17-19, 1974.

18. Melling, T.H., "Acoustic Impedance of Perforates at Medium and High Sound Pressure Levels," Journal of Sound and Vibration, Vol. 29, 1 (1973)

19. Zorumski, W.E. and Parrott, T.L., "Nonlinear Acoustic Theory for Rigid Porous Material," NASA TN - 6196.

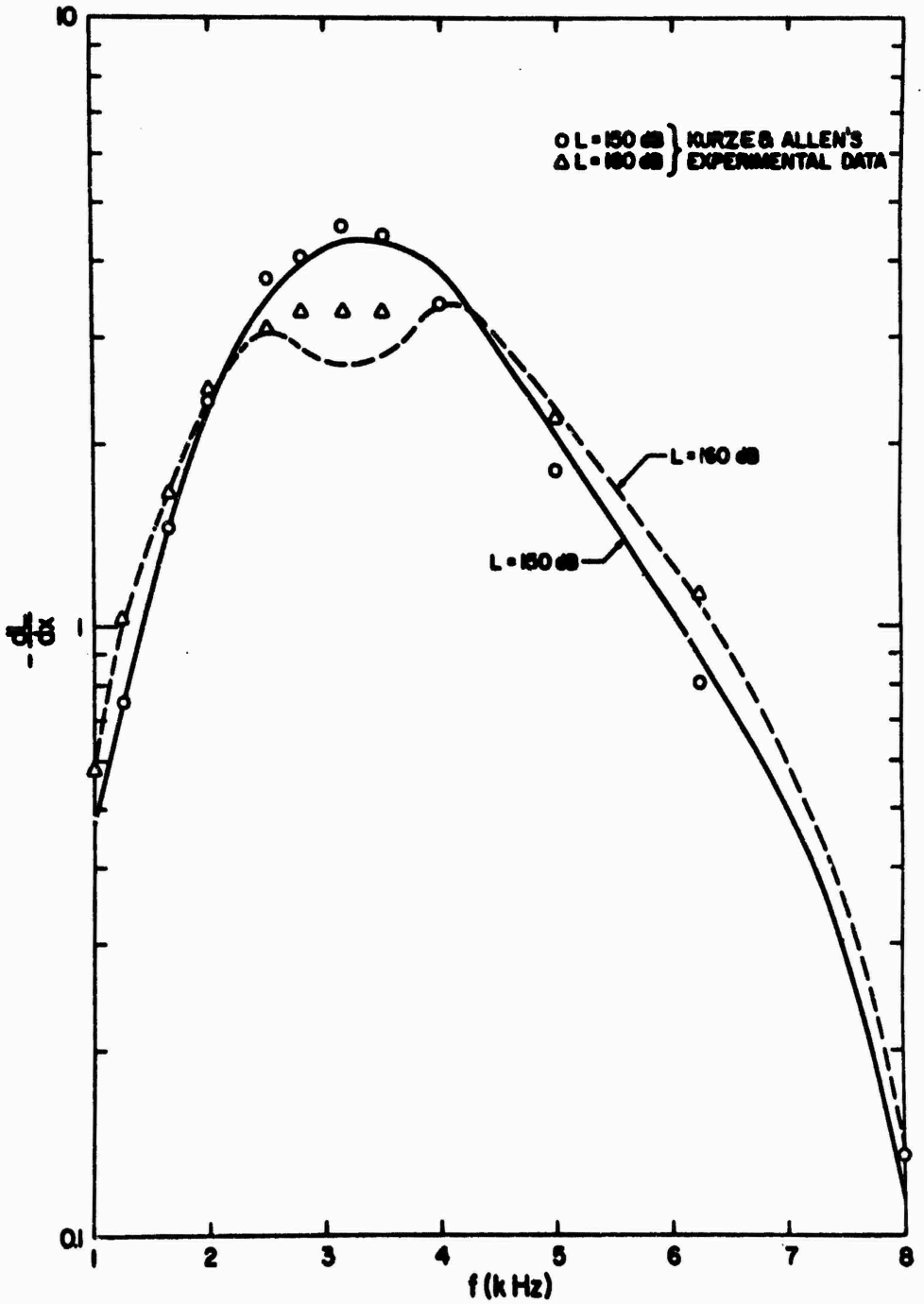

Figure 1. Comparison of the present analytical results with the experimental data of Kurze & Allen (1971) for the lowest mode, $d^*=1"$, $b^*=0.015"$, $h^*=0.75"$, $\Omega=0.95$, $s=1.15$, $\sigma_1=2293$ or $\hat{\sigma}_1 = 3.8675 \times 10^6$.

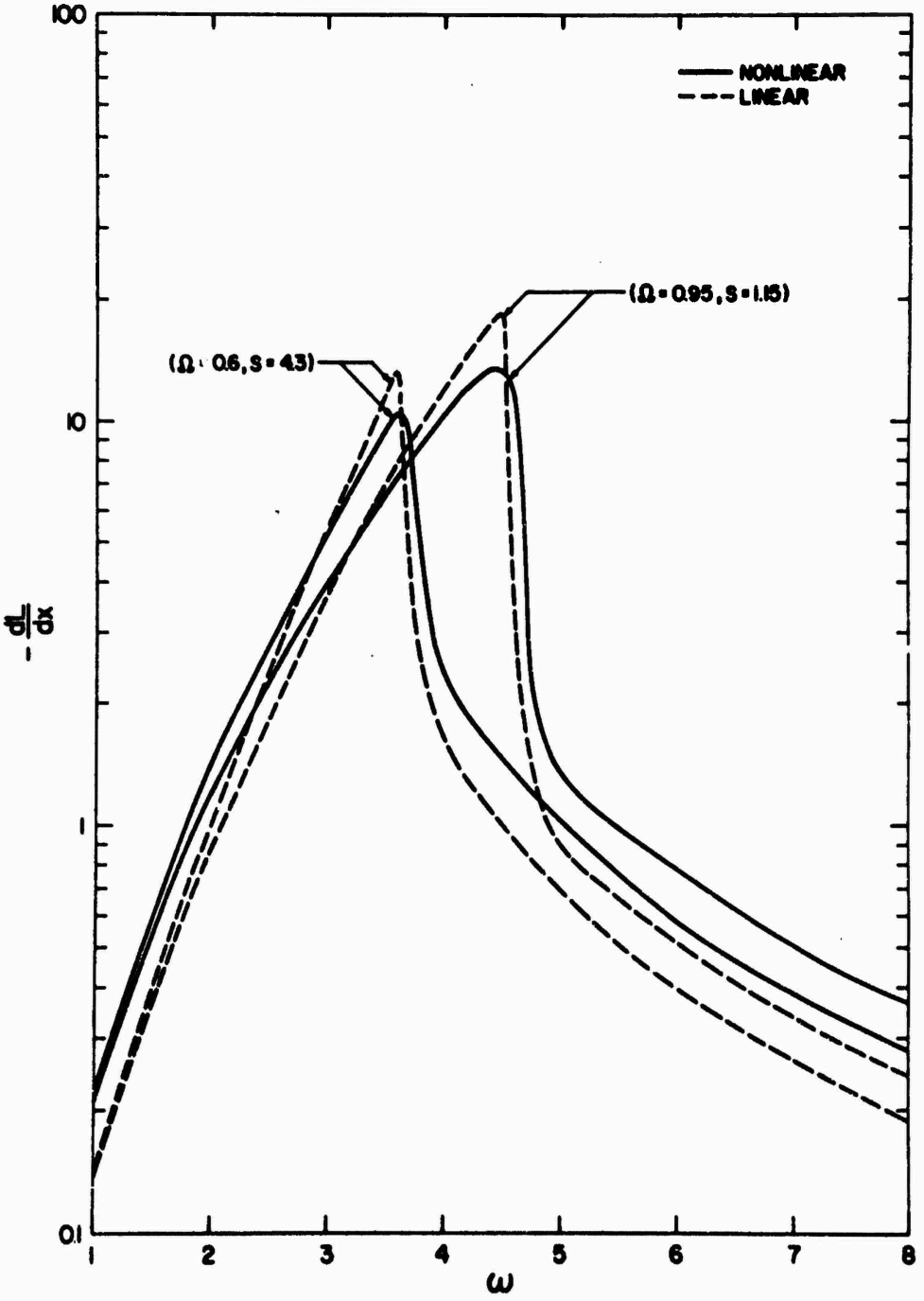

Figure 2. Effect of material nonlinearity on the absorption coefficient dL/dx (L is the sound pressure level) of the lowest mode for two porosities and b=0.015, h=0.2, σ_0=50, σ_1=2000, and $|v|$ = 0.015 at the duct/liner interface.

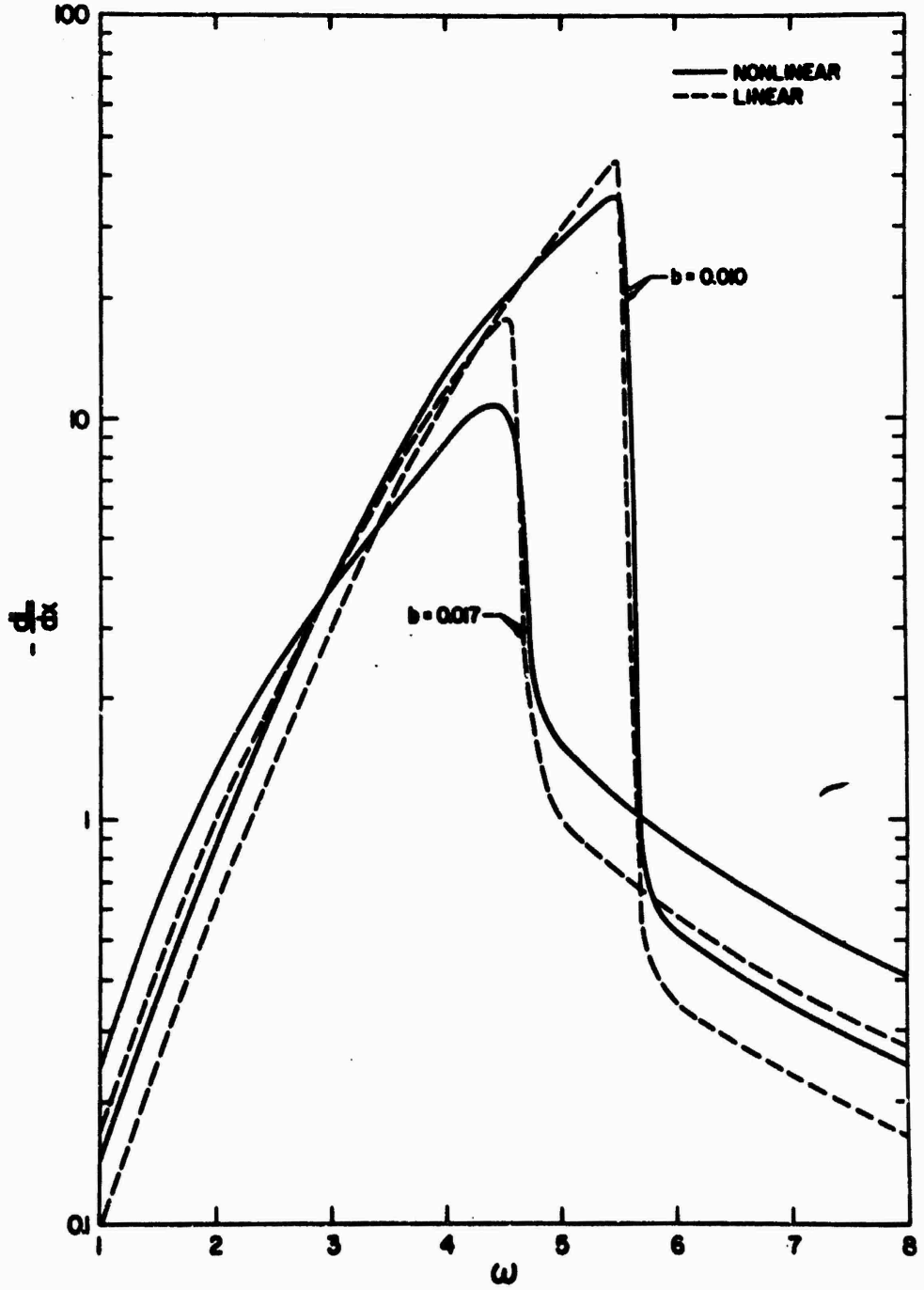

Figure 3. Effect of material nonlinearity on the absorption coefficient of the lowest mode for two thicknesses of the porous material, Ω=0.95, s=1.15 and the parameters of Figure 17.

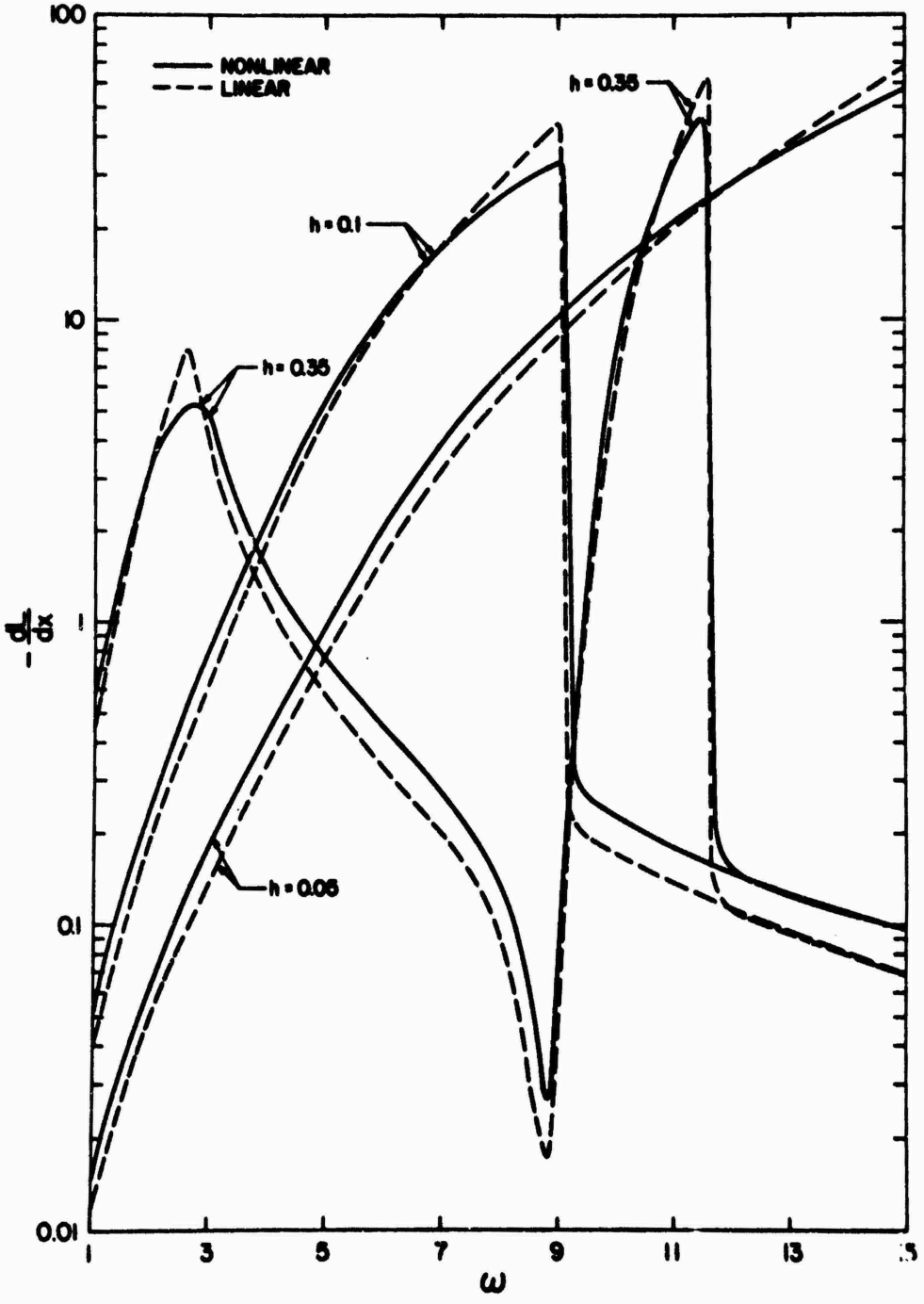

Figure 4. Effect of material nonlinearity on the absorption coefficient of the lowest mode for three cavity depths, Ω=0.95, s=1.15, and the parameters of Figure 17.

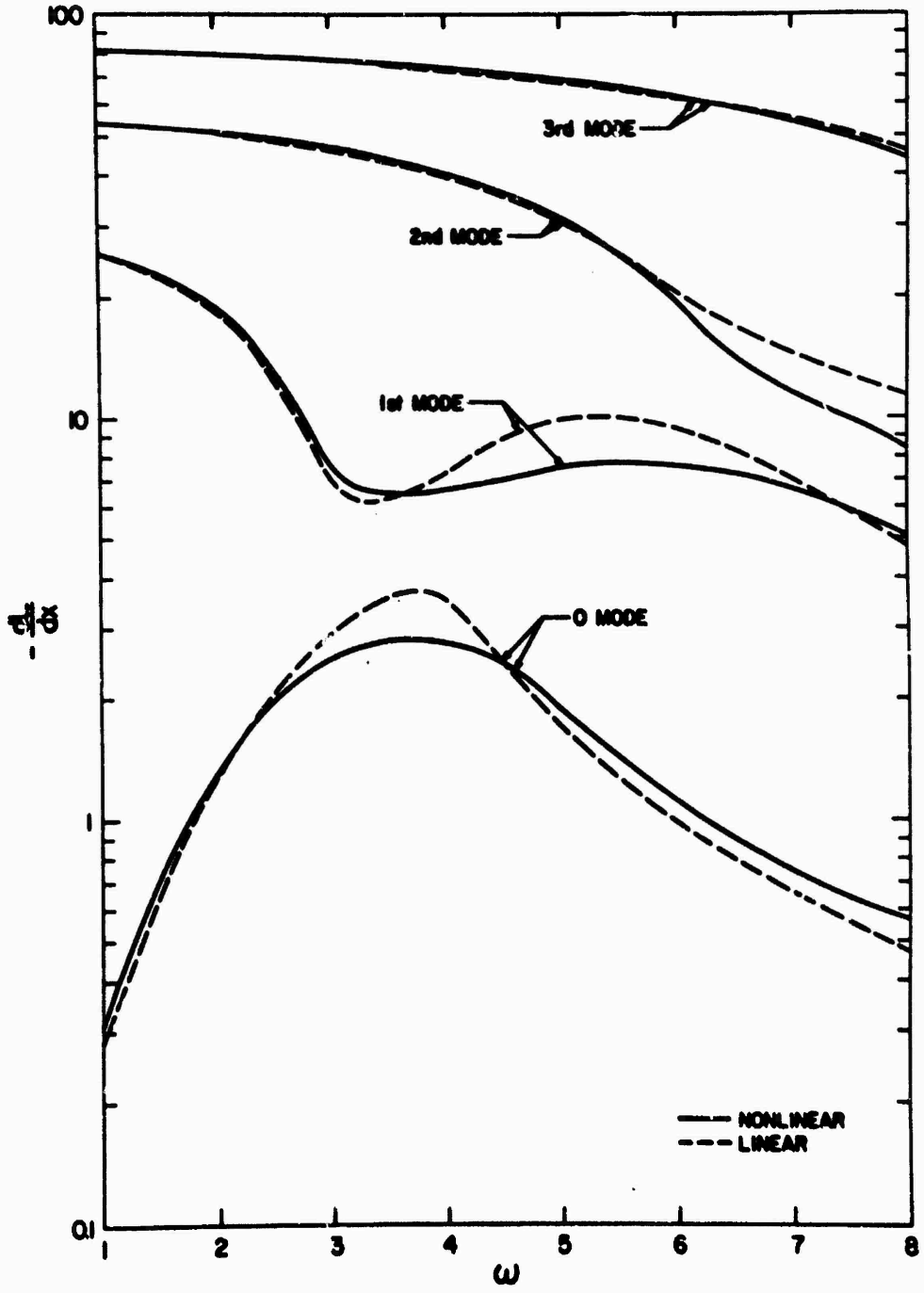

Figure 5. Effect of material nonlinearity on the absorption coefficient of the lowest four modes for $b=0.015$, $h=0.2$, $\Omega=0.95$, $s=1.15$, $\sigma_o=100$, $\sigma_1=2000$, and $|v|=0.01$ at the duct/liner interface.

ADMITTANCE DETERMINATION IN THE PRESENCE OF A MEAN FLOW AND THREE-DIMENSIONAL WAVE MOTION

by

B. T. Zinn, B. R. Daniel, W. A. Bell and B. A. Janardan

School of Aerospace Engineering, Georgia Institute of Technology
Atlanta, Georgia 30332

ABSTRACT

In many transportation noise attenuation studies it is necessary to determine the admittance of a duct cross sectional area or termination in the presence of a three-dimensional wave motion superimposed upon a steady one-dimensional flow. An acoustic facility capable of providing such data over a wide range of test variables has been developed and used to measure the admittances of a variety of choked nozzles and the attenuation provided by various acoustic liners. The design of the modified impedance tube is based upon an extension of the classical, no flow impedance tube theory. The required three-dimensional wave motion is generated by electropneumatic drivers and is superimposed upon a mean flow provided from high pressure storage tanks. The unknown admittances are determined from pressure amplitude and/or phase measurements taken at discrete locations along the impedance tube. This paper describes the facility, the experimental technique and typical nozzle and acoustic liner admittance data measured to date. The measured data is compared with available theoretical predictions.

INTRODUCTION

In many practical problems encountered in noise attenuation and combustion instability studies it is necessary to know the admittance of a duct cross sectional area when the duct contains a mean flow and three- or one-dimensional wave motion. Once the admittance is known, it can be used to compute the acoustic energy flux crossing the location under consideration. This paper will describe how the admittances of the entrance plane of a choked nozzle and a lined duct are measured under the above-mentioned flow conditions. In addition, the paper describes local liner admittance data measured under flow conditions simulating those observed in unstable rocket motors.

The measured admittance data are compared with available theoretical predictions. The theoretical determination of the nozzle admittance requires the solution of a mathematically complex system of conservation equations which describe the behavior of the flow oscillations in the convergent section of a choked nozzle and, to date, solutions have been obtained only for a limited number of cases. The most sophisticated treatment of the nozzle admittance problem was developed by Crocco and Sirignano(Reference 1), who considered the case where the wave motion in the nozzle is three-dimensional and the mean flow is one-dimensional. This theoretical treatment is, however, applicable to nozzles having simple geometrical configurations and one must resort to experimental studies whenever the admittances of complex nozzle designs are needed.

The local admittances and the resonant frequencies of acoustic liners exposed to small amplitude oscillations under no flow conditions can be

determined from classical theories (References 2 and 3). Nonlinear effects have been accounted for in studies conducted by Ingard and Ising, Sirignano, and Zinn (References 4 through 6) and empirical equations describing liner behavior in the presence of a one-dimensional pressure oscillation and a steady one-dimensional flow have been developed by Garrison (Reference 7). The applicability of the available local liner admittance equations under flow conditions encountered in unstable rocket motors and turbofan engine flow passages has been investigated experimentally and some of this data is summarized in this paper.

The modified impedance tube technique has been employed in this study to measure the admittances at the entrance planes of various nozzles and acoustic liner-nozzle combinations. In the modified impedance tube technique, a sound source capable of generating simple harmonic waves of desired frequencies is placed at one end of a simulated chamber. The other end of the chamber is attached to the nozzle and/or liner-nozzle combination whose admittance is to be determined. A schematic diagram of the facility is shown in Figure 1. With the aid of the acoustic driver, a standing wave pattern of a known frequency is superimposed upon the one-dimensional mean flow present in the tube. The admittance of the nozzle and/or liner-nozzle combination is determined by measuring the amplitudes and phases of the resulting standing waves by means of a set of microphones located along the chamber walls. In addition, the local liner admittance data has been obtained using the two microphone technique (Reference 7). A summary of the relevant expressions required for the measurement of the admittances is presented in the next section.

ANALYTICAL CONSIDERATIONS AND EXPERIMENTAL TECHNIQUE

Nozzle Admittance

Only a qualitative description of the theory and a summary of the relevant expressions required for the measurement of admittances, using the modified impedance tube technique, are presented herein; for detailed derivations see Reference 8. The expressions required for the calculation of the admittance are obtained by solving the system of conservation equations that describe the behavior of small amplitude, three-dimensional disturbances which are superimposed upon a steady one-dimensional flow inside a simulated cold flow combustor. The simulated combustor has an acoustic driver at one end and a choked nozzle or liner-nozzle combination at the other end. The above-mentioned solutions are then required to satisfy the unknown admittance boundary condition at the end of the duct entrance. The resulting expressions describing the time and space dependence of the pressure and velocity perturbations inside the simulated combustor are given by:[8]

$$p' = AJ_m\left(S_{mn}\frac{r}{r_w}\right)\cos m\theta\, e^{i(\omega t + az)}\cosh\left[\pi\alpha - i\pi\left(\beta + \tfrac{1}{2} + \frac{2z}{\lambda}\right)\right] \quad (1)$$

$$u' = \frac{Ae^{i(\omega t + az)}J_m}{\bar{\rho}c\left[k^2 + \left(\frac{S_{mn}}{r_w}\bar{M}\right)^2\right]}\left(S_{mn}\frac{r}{r_w}\right)\cos m\theta\left\{kk_{mn}(1-\bar{M}^2)\right.$$

$$\left.\sinh\left[\pi\alpha - \pi\left(\beta + \tfrac{1}{2} + \frac{2z}{\lambda}\right)\right] - \left(\frac{S_{mn}}{r_w}\right)^2\bar{M}\cosh\left[\pi\alpha - \pi\left(\beta + \tfrac{1}{2} + \frac{2z}{\lambda}\right)\right]\right\} \quad (2)$$

where J_m is a Bessel function of the first kind of order m, S_{mn} is the nth root of the equation

$$\frac{dJ_m(x)}{dx} = 0,$$

m is the number of diametral nodal lines in the transverse wave pattern, n is the number of azimuthal nodal lines, and the subscript w denotes the value at the wall. The parameter ω is the angular frequency of oscillation, and a, k_{mn} and λ are given as

$$a = \frac{k\bar{M}}{1 - \bar{M}^2}, \qquad k_{mn} = \frac{\sqrt{k^2 - \left(\frac{S_{mn}}{r_w}\right)^2 (1 - \bar{M}^2)}}{1 - \bar{M}^2}, \qquad \lambda = \frac{2\pi}{k_{mn}}$$

where the wave number k equals $\omega/\bar{c}$. The two parameters α and β respectively describe[9] the changes in amplitude and phase between the incident and reflected pressure waves at the plane whose admittance is to be evaluated; that is,

$$\left(\frac{\text{Amplitude of Reflected Pressure Wave}}{\text{Amplitude of Incident Pressure Wave}}\right)_{\substack{\text{Tube} \\ \text{Termination}}} = e^{-2\pi\alpha} \tag{3}$$

$$\left(\text{Phase Change Between Incident and Reflected Pressure Waves}\right)_{\substack{\text{Tube} \\ \text{Termination}}} = \pi(1 + 2\beta) \tag{4}$$

where parameter β must satisfy $|\beta| \leq 0.5$.

The specific admittance, Y, defined as

$$Y = \frac{u'}{p'} \tag{5}$$

represents the boundary condition that the solutions for the axial velocity perturbation u' and pressure perturbation p' must satisfy at the tube termination. In general, this admittance is a complex number whose real and imaginary parts describe the relationships that exist at the tube termination between the amplitudes and phases of the velocity and pressure perturbations. The nondimensional form of the specific admittance is written in the following form:

$$y = \frac{Y}{Y_g} = \bar{\rho}\bar{c}\left(\frac{u'}{p'}\right)_{z=0} = y_r + iy_i \tag{6}$$

where the reference admittance $Y_g = (1/\bar{\rho}\bar{c})$ is the characteristic admittance of the gas medium in the chamber. Substituting the solutions obtained for the pressure and velocity perturbations (i.e., Equations (1) and (2)) into the

above definition yields the following expression for the nondimensional admittance y at the tube termination:

$$y = \frac{S\sqrt{S^2 - S_{mn}^2(1 - \bar{M}^2)}\ \coth \pi(\alpha - i\beta) - (S_{mn})^2 \bar{M}}{S^2 + (S_{mn})^2} \tag{7}$$

where S equals $\omega r_w/\bar{c}$. Separating the admittance into its real and imaginary parts gives

$$y_r = \frac{\left[\dfrac{S\sqrt{S^2 - S_{mn}^2(1 - \bar{M}^2)}\ \tanh \pi\alpha \sec^2 \pi\beta}{\tanh^2 \pi\alpha + \tan^2 \pi\beta} - S_{mn}^2 \bar{M}\right]}{S^2 + (S_{mn}\bar{M})^2} \tag{8}$$

$$y_i = \frac{S\sqrt{S^2 - S_{mn}^2(1 - \bar{M}^2)}\ \tan \pi\beta\ \operatorname{sech}^2 \pi\alpha}{\left[S^2 + (S_{mn}\bar{M})^2\right](\tanh^2 \pi\alpha + \tan^2 \pi\beta)} \tag{9}$$

Equation (7) differs from the classical admittance relation by the addition of the terms involving S_{mn} and $\bar{M}$, which account for the effects of the three-dimensionality of the waves and the presence of mean flow, respectively. For longitudinal waves $S_{mn} = 0$ and for no mean flow $\bar{M} = 0$, letting $S_{mn} = \bar{M} = 0$, reduces Equation (7) to the classical result given in Reference 9.

Examination of Equations (8) and (9) shows that the nondimensional admittance depends upon the steady state properties of the flow and the parameters α and β. Hence to compute the admittances, α and β must be measured. These parameters can be found from either pressure amplitude and/or phase measurements taken axially along the walls of the impedance tube. To obtain α and β, Equation (1) is rewritten in the following form

$$p'(z,t) = |P'(z)|\ e^{i(\delta + \omega t)} \tag{10}$$

where the pressure amplitude $|P'(z)|$ is given by

$$|P'(z)| = AJ_m\left(S_{mn}\frac{r}{r_w}\right)\cos m\theta \left[\cosh^2 \pi\alpha - \cos^2 \pi\left(\beta + \frac{2z}{\lambda}\right)\right]^{-\frac{1}{2}} \tag{11}$$

and the phase δ is

$$\delta = az + \operatorname{Arctan}\left[\tanh \pi\alpha \cot \pi\left(\beta + \frac{2z}{\lambda}\right)\right]^{-\frac{1}{2}} \tag{12}$$

Equations (11) and (12) show that the pressure amplitude $|P'|$ and pressure phase δ are functions of the axial coordinate, the steady state properties of the medium, the known frequency and mode and the unknowns α, β and A. The availability of such expressions for the pressure amplitude and pressure phase suggest that if one can measure the pressure amplitude and/or pressure phase

at three different locations along the chamber, then the experimental data could be substituted into the theoretical expressions for the pressure amplitude and/or pressure phase and the resulting algebraic equations could then be solved to determine the unknowns of the problem; that is, the parameters α and β which characterize the admittance. In this investigation the admittance parameters α and β were determined by measuring both the pressure amplitudes and phases. The resulting values of α and β were then substituted into Equations (8) and (9) to determine the admittance.

Since the expressions relating $|P'|$ and δ to the admittance parameters α and β are nonlinear, pressure amplitude or pressure phase measurements taken at only three discrete axial locations may not guarantee the uniqueness and accuracy of the calculated values of α and β. Hence, to improve the accuracy of the measured admittances, ten transducers placed at different locations along the modified impedance tube were used during this investigation. The unknown admittance parameters were then obtained by using the nonlinear regression technique[10] which determines the set of values of α and β that minimizes the root-mean-square deviation between the measured pressure amplitudes and/or phases and the corresponding theoretical expressions as given by Equations (11) and (12). The determination of α and β from pressure amplitude data is illustrated below. Similar procedures can be followed to determine α and β from pressure phase measurements.

In the case of the pressure amplitude measurements the values of the parameters α and β that minimize the RMS deviation between the measured data and the expression given in Equation (11) are obtained by minimizing the following function F:

$$F = \sum_{i=1}^{10} \left[E_i - T_i(\alpha, \beta, A) \right]^2 \tag{13}$$

The parameter E_i is the pressure amplitude measured at a distance z_i from the plane whose admittance is being measured. The function T_i is the corresponding theoretical pressure amplitude, and it is given by Equation (11). For measurements taken along the wall where $r = r_w$ and at the $\theta = 0$ position, T_i is given by

$$T_i = A_{mn} \left[\cosh^2 \pi\alpha - \cos^2 \pi\left(\beta + \frac{2z_i}{\lambda}\right) \right]^{-\frac{1}{2}} \tag{14}$$

where

$$A_{mn} = AJ_{mn}(S_{mn})$$

At the location where F is minimum

$$\frac{\partial F}{\partial \alpha} = \frac{\partial F}{\partial \beta} = \frac{\partial F}{\partial A} = 0 \tag{15}$$

Substituting Equation (13) into Equation (15) gives

$$\sum_{i=1}^{10} (E_i - T_i) \frac{\partial T_i}{\partial \alpha} = 0; \quad \sum_{i=1}^{10} (E_i - T_i) \frac{\partial T_i}{\partial \beta} = 0; \quad \sum_{i=1}^{10} (E_i - T_i) \frac{\partial T_i}{\partial A_{mn}} = 0 \tag{16}$$

Solutions of Equation (16) yield the values of α, β and A_{mn} which provide the best fit between the experimental data and the theoretical curve described by Equation (14). Since these equations are nonlinear, explicit solutions for α, β and A_{mn} cannot be obtained, and these equations must be solved numerically.

Marquardt's algorithm[10,11] is used to solve Equation (16). This algorithm is an extension of the Newton-Raphson iteration scheme. It keeps the rapid convergence properties of the Newton-Raphson method, and at the same time it improves the stability characteristics. To start the iteration, Equation (14) is solved explicitly for α, β and A_{mn} using various combinations of three amplitude measurements. For ten amplitude measurements taken axially along the tube, 120 combinations of three different pressure amplitudes can be obtained. The values of α, β and A_{mn} obtained from the combination which gives the minimum RMS deviation (i.e., minimum value for F in Equation (13)) are then used to start the numerical iteration. The values of α and β obtained from the iteration are then used to compute the real and imaginary parts of the admittance from Equations (8) and (9), respectively.

Liner Admittance

Expressions for computing the local liner admittance and liner resonant frequency are summarized below:[4,6,7,12]

Nondimensional local liner admittance,

$$y = \sigma \bar{\rho} \bar{c} \frac{u_n'}{p_n'} = \frac{\sigma \gamma \bar{p} M_a}{p_{ch}'} = y_r + i y_i \tag{17}$$

where

$$y_r = \frac{\theta_L + \theta_{NL}}{(\theta_L + \theta_{NL})^2 + \chi^2} \quad ; \quad y_i = \frac{-\chi}{(\theta_L + \theta_{NL}) + \chi^2} \tag{18}$$

Liner resistance, θ_R

$$\theta_R = \theta_L + \theta_{NL} \tag{19}$$

where

$$\theta_L = \frac{4}{\sigma \bar{\rho} \bar{c}} (\pi f \bar{\rho} \mu)^{\frac{1}{2}} (1 + t/d_o) \quad ; \quad \theta_{NL} = \frac{0.42}{C_D^2} \frac{M_a}{\sigma} = B \frac{M_a}{\sigma} \tag{20}$$

Liner reactance, χ

$$\chi = \frac{1}{\sigma} \tan (k \ell_{eff}) - \cot (kL) \tag{21}$$

where σ is the open area ratio and C_D is the orifice discharge coefficient.

From the definition of the admittance given by Equation (17) and Equation (20), the aperture Mach number M_a can be computed by solving the quartic equation

$$\left(\frac{B}{\sigma}\right)^2 M_a^4 + 2\left(\frac{B}{\sigma}\right)\theta_L M_a^3 + \left(\theta_L^2 + \chi^2\right) M_a^2 = \left(\frac{p'_{ch}}{\bar{p}\sigma\gamma}\right) \qquad (22)$$

Also effective orifice length ℓ_{eff} is given by

$$\ell_{eff} = t + 0.85\delta\,(1 - 0.71\sqrt{\sigma})\,d_o \qquad (23)$$

Some of the geometric variables appearing in the above equations are shown in Figure 2.

In Equation (18), for the real and imaginary parts of the liner admittance, the effects of wave amplitude are accounted for by the nonlinear resistance, θ_{NL}. For low amplitude waves — less than about 120 decibels θ_L is much larger than θ_{NL}, and the liner admittance is essentially independent of the amplitude. For high amplitude waves the nonlinear resistance term θ_{NL} becomes dominant. The dependence of θ_{NL} upon wave amplitude is described in Equation (20), which relates θ_{NL} to M_a; the dependence of M_a upon the amplitude of the chamber pressure oscillation is given by Equation (22). Expressions describing the effect of a mean flow on the local liner admittance have also been developed.[7]

The tuning frequency of the liner, determined by the value of k for which the liner reactance χ is zero, is also amplitude dependent. Assuming the arguments of the tangent and cotangent appearing in Equation (21) to be small, the nondimensional tuning frequency S_o is given by

$$S_o = \frac{2\pi f_o}{\bar{c}} r_{ch} = k_o r_{ch} = \sqrt{\frac{\sigma}{\ell_{eff} L}} \qquad (24)$$

To provide local liner admittance data for comparison with the values predicted by Equation (18), the two microphone technique has been employed.[7,12] The two microphone technique consists of placing one microphone in the liner cavity and the other at the liner surface. By determining the amplitude ratio and phase difference of the signals measured by these microphones, the real and imaginary parts of the local liner admittance can be determined from the expressions[7]

$$y_r = kL\left|\frac{p'_{ca}}{p'_{ch}}\right| \sin\left(\varphi_{ch} - \varphi_{ca}\right) \quad ; \quad y_i = kL\left|\frac{p'_{ca}}{p'_{ch}}\right| \cos\left(\varphi_{ch} - \varphi_{ca}\right) \qquad (25)$$

The measured amplitude of the chamber pressure oscillation $|p'_{ch}|$ is also used in Equation (8) to compute the aperture Mach number M_a.

To determine the spatial variations of the local liner admittance, measurements were taken at three axial stations, as shown in Figure 3. These

measurements were made to assess the validity of the often-used assumption that the admittance at the liner face is constant.

EXPERIMENTAL SETUP

The experimental setup used in these studies consisted of an impedance tube in which a desired three-dimensional oscillation superimposed upon a steady one-dimensional flow can be established. Two electropheumatic drivers attached to the upstream end of the tube were used to generate the standing wave pattern inside the tube and the measured pressure amplitude and phase data was used to determine the unknown admittance of the device (e.g., nozzle, acoustic liner, etc.) attached to the downstream end of the tube.

The modified impedance tube used in this investigation has been specifically designed to investigate the acoustical damping capabilities of exhaust nozzles and liner-nozzle combinations. The impedance tube is 11-3/8 inches in diameter and 120 inches in length. The upstream end of the impedance tube is attached to an injector plate and the tested nozzle or liner is coupled directly to the flange at the downstream end of the impedance tube. Provision has been made along the length of the impedance tube for the installation of acoustic drivers, dynamic pressure transducers, thermocouples, and static pressure orifices.

Instrumentation and Data Processing

A diagram of the instrumentation system used to monitor, regulate, measure and record the conditions inside the modified impedance tube is shown in Figure 4. During a test the frequency of the drivers is varied at a constant rate from 600 Hz to 1100 Hz which include the mixed first tangential-longitudinal modes for the test conditions of this study. The analog data recorded on the tape recorder during each test were digitized by a 14 channel analog-to-digital conversion system. The digitized data were then numerically analyzed by means of a Fourier analysis to determine the amplitudes and phases of the chamber pressure oscillations as a function of the driver input frequency. The resulting pressure amplitudes and phases along with the measured temperature data were then used to determine the admittance parameters α and β and the real and imaginary parts of the nondimensional admittance y of the tested configuration.

Test Nozzles

Tests were conducted with axisymmetric nozzles. The geometries of these nozzles consist of three sections as shown in Figure 5. The first section starts at the impedance tube and is generated by a circular arc of radius r_{cc} which is turned through an angle θ_1, the nozzle half-angle. This section connects smoothly to the next section, which is a conical nozzle of angle θ_1. The conical nozzle then joins with the third section, which ends at the throat and is generated by a circular arc of radius r_{cc} turned through an angle θ_1. The nozzles under consideration are presented in Table 1 where the ratio of the radius of curvation r_{cc} to the chamber radius r_c is given for each nozzle half-angle and Mach number considered. By investigating these nozzles the dependence of the nozzle admittance upon nozzle entrance Mach

number $\bar{M}$, nozzle half-angle θ_1, and nozzle radius of curvature was determined.

Test Liners

Three liner configurations were designed in accordance with the procedures presented in Reference 7 and tested. Their properties are described in Table 2. Liners 1 and 2 consisted of nine axial rows of twenty orifices uniformly distributed around the circumference of the cylindrical liner section. Liner 1 consisted of individual Helmholtz resonators. For liner 2, the twenty circumferential orifices opened into a common annular cavity, as shown in Figure 3. Liner 3 consisted of 660 orifices divided into fifteen axial rows of 44 orifices evenly spaced around the circumference. All of the orifices opened into a common annular cavity twelve inches in length. Using these three liners the effects of a variety of liner design characteristics upon the local liner admittance was determined.

The acoustic properties of the liners were measured with the liners attached to deLaval and/or quasi-steady nozzles whose admittances had earlier been measured. Supercritical flow conditions were maintained across the nozzles during the tests.

RESULTS

Only samples of the admittance data measured during this investigation are presented here to demonstrate that the modified impedance tube technique can indeed be employed to measure admittances in the presence of a mean flow and three-dimensional wave motion. A more complete description of the measured admittance data obtained in the above-mentioned studies can be found in References 8 and 13.

The experimental nozzle admittance data for the mixed first transverse-longitudinal mode for a nozzle with $\theta_1 = 30^\circ$, $\bar{M} = 0.16$ and $r_{cc}/r_c = 1.0$ is presented in Figure 6 along with the theoretically predicted admittances. An examination of this figure indicates that the theoretical predictions compare quite well with the measured data. The effect of changing the nozzle half-angle θ_1 is presented in Figure 7. Increasing θ_1 tends to decrease the dependence of the nozzle admittance on the frequency in the investigated frequency range. This result is in agreement with the theoretical predictions.

Experimental and theoretical local liner admittance data for spinning mixed first tangential-longitudinal modes are presented in Figures 8 and 9. Tests were also conducted using the corresponding standing modes and no difference between the two sets of data was observed. Hence it will suffice to consider the spinning mode data in this discussion. The theoretical results in Figure 8 were obtained using Equations (18) through (23). For liner 1, which consists of an array of individual resonators, the theoretical and experimental values of the real and imaginary parts of the local liner admittance are in agreement to within experimental errors. For liner 2, which is formed by nine separate annular cavities with twenty orifices per cavity, the expression for χ was modified using Oberg's analysis[12] to account for the wave motion in the annuli. For small values of the backing distance L, this expression reduces to

$$\chi = \frac{1}{\sigma} \tan k\ell_{eff} - \frac{1}{kL\left[1 - \frac{1}{k^2(r_{ch} + t)^2}\right]} \qquad (26)$$

The tuning frequency S_o was obtained from Equation (26) by solving for k when $\chi = 0$, and was compared with S_o computed from Equation (21). As shown in Figure 8, S_o obtained from Equation (21) is in better agreement with the experimental value than S_o calculated from Oberg's analysis. Therefore, Equation (21) appears valid for liners with annular cavities provided the ratio of the backing distance to the chamber radius in small. For liner 3, with an unpartitioned cavity, no correlation between the theoretical predictions and the experimental data was found. This result is not surprising since existing liner theories do not account for the wave motion in an unpartitioned cavity. Since over the frequency range considered in this study the pressure amplitudes in the test section varied from 140 to 160 decibels, the agreement between the theoretical and experimental local admittance values for liners 1 and 2 indicates that the theory can adequately account for the effect of wave amplitude.

To determine the dependence of the local liner admittance upon the liner location in the chamber, measurements were taken at three axial stations along the liner located two, six and ten inches upstream of the liner end. Data obtained with liner 1 are shown in Figure 9 which indicate that, at a given frequency, the real part of the local liner admittance differs by as much as a factor of three from station to station because of differences in local wave amplitude. Thus, when large amplitudes are involved, the assumption of a constant liner admittance often used in theoretical analyses of lined ducts is generally invalid.

CONCLUSIONS

(1) The results obtained during this investigation demonstrate that the modified impedance tube technique can be employed to measure admittances of a duct termination in the presence of a mean flow and three- or one-dimensional wave motion.

(2) Comparison of the theoretical and experimental nozzle admittance data indicate that Crocco's nozzle admittance theory is capable of predicting choked nozzle admittances.

(3) The measured liner data indicates that Equations (18) through (23) can be used to predict local admittances of liners exposed to three-dimensional wave motion involving either spinning or standing waves. These equations are applicable to liners having either individual resonators or common annular cavities; they are not, however, applicable to liners having common longitudinal cavities.

(4) The measured liner data indicates that the assumption of a spatially uniform liner admittance is not valid. In the present study the admittance values differed by as much as 50% at different locations because of variations in wave amplitude.

REFERENCES

1. Crocco, L. and Sirignano, W. A., "Behavior of Supercritical Nozzles Under Three-Dimensional Oscillatory Conditions," AGARDograph 117, Princeton University, Princeton, New Jersey, 1967.

2. Lord Rayleigh, Theory of Sound, Vol. II, Dover, New York, 1945.

3. Sivian, L. J., "Acoustic Impedance of Small Orifices," JASA, Vol. 7, 1935.

4. Ingard, K. U. and Ising, H., "Acoustic Nonlinearity of an Orifice," JASA, Vol. 22, March, 1950.

5. Sirignano, W. A., "Nonlinear Aspects of Combustion Instability in Liquid Propellant Rocket Motors," Report No. 553-F, Princeton University, Princeton, New Jersey, 1966.

6. Zinn, B. T., "A Theoretical Study of Nonlinear Damping by Helmholtz Resonators," Journal of Sound and Vibration, Vol. 13, 1970.

7. Garrison, G. D., et al, "Suppression of Combustion Oscillations with Mechanical Damping Devices," PWA-3299, Pratt and Whitney Aircraft, West Palm Beach, Florida, August, 1969.

8. Zinn, B. T., Bell, W. A., Daniel, B. R. and Smith, A. J., "Experimental Determination of Three-Dimensional Liquid Rocket Nozzle Admittances," AIAA Journal, Vol. 11. March, 1973.

9. Morse, P. M. and Ingard, K. U., Theoretical Acoustics, McGraw-Hill, New York, 1968.

10. Pfahl, R. C and Mitchel, B. J., "Nonlinear Regression Methods for Simultaneous Property Measurement," AIAA Journal, Vol. 8, June, 1970.

11. Marquardt, D. W., "An Algorithm for Least-Squares Estimation of Nonlinear Parameters," Journal of the Society for Industrial and Applied Mathematics, Vol. 11, June, 1963.

12. Oberg, C. L., "Improved Design Techniques for Acoustic Liners," Research Park No. RR-68-5, Rocketdyne, Canoga Park, California, May, 1968.

13. Bell, W. A., Daniel, B. R. and Zinn, B. T., "Acoustic Liner Performance in the Presence of a Mean Flow and Three-Dimensional Wave Motion," AIAA 12th Aerospace Sciences Meeting, Washington, January, 1974.

Table 1. Tested Nozzles

θ_1 \ $\bar{M}$	0.08	0.16	0.20
15	1.0, .44		
30	.44	1.0	
45	.44	.44	.44

Table 2. Liner Characteristics

	Liner 1*	Liner 2**	Liner 3#
Cavity Diameter	1.000	-----	-----
Orifice Length	0.866	0.688	0.500
Orifice Diameter	0.250	0.250	0.159
$\sigma = \frac{\text{Orifice Area}}{\text{Cavity Area}}$	0.0625	0.032	0.027
Backing Distance	0.500	0.313	0.435
Effective Length	1.041	0.873	0.619
Nondimensional Tuning Frequency	1.971	1.945	~ 2.0
Linear Resistance @ 32°F	0.0966	0.158	0.199
Aperture Mach Number @ 155 db	0.0582	0.0588	0.0586
Nonlinear Resistance	0.8177	1.617	1.905
Cavity Width	------	0.750	12

All Dimensions in Inches

Values Based on Equations (17) - (23)

*Individual Resonators

**Annular Cavity

#Unpartitioned

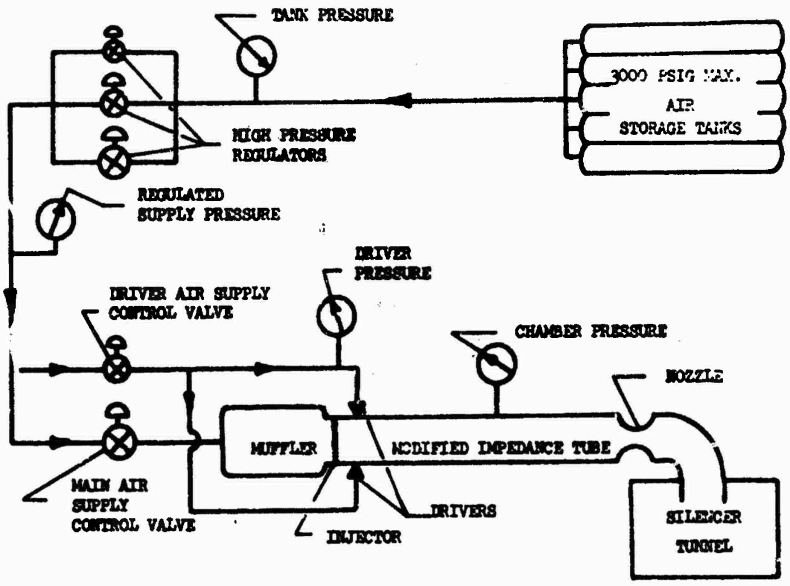

Figure 1. Schematic Diagram of the Acoustic Test Facility.

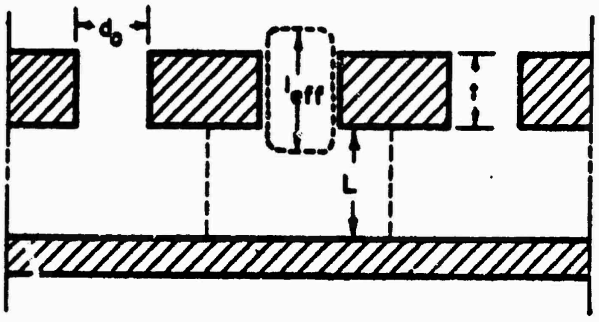

Figure 2. A Typical Acoustic Liner Configuration.

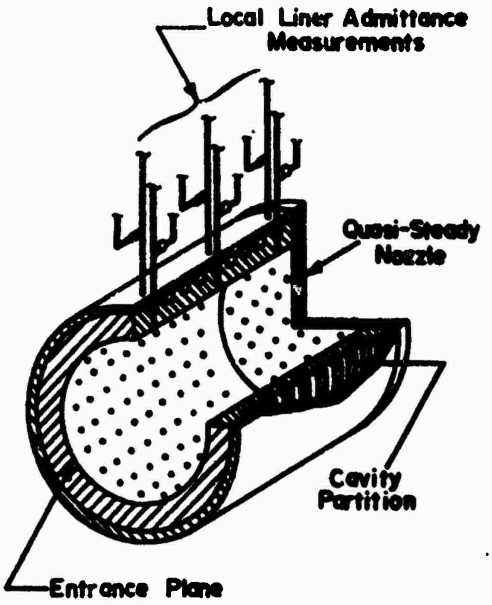

Figure 3. Typical Liner-Nozzle Combination; Liner with Annular Cavities and a Quasi-Steady Nozzle.

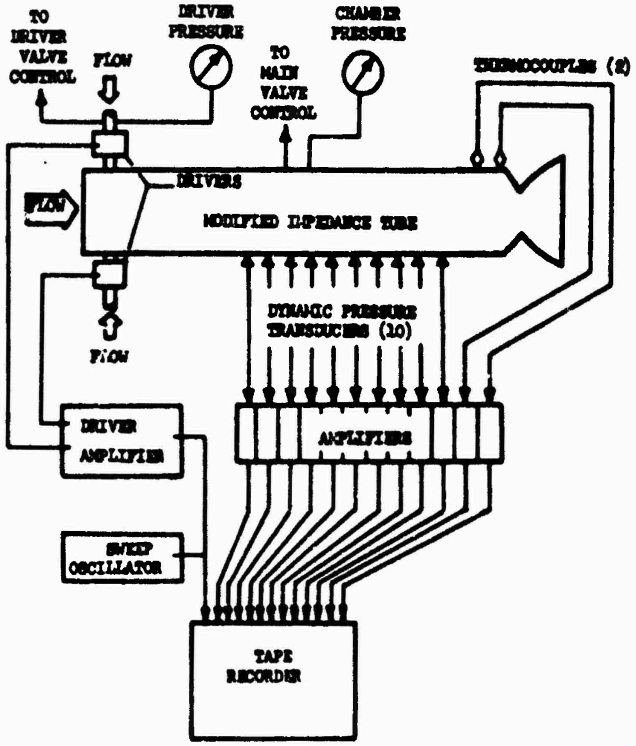

Figure 4. Instrumentation Diagram.

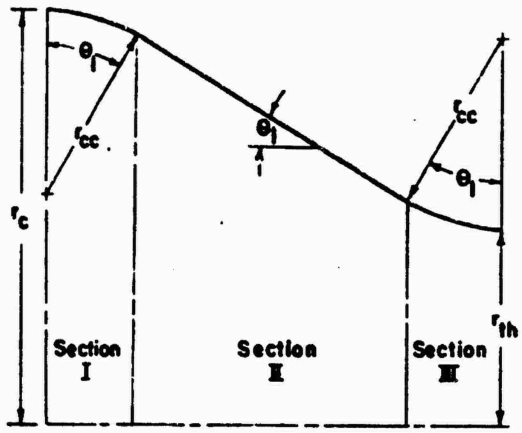

Figure 5. Nozzle Geometry.

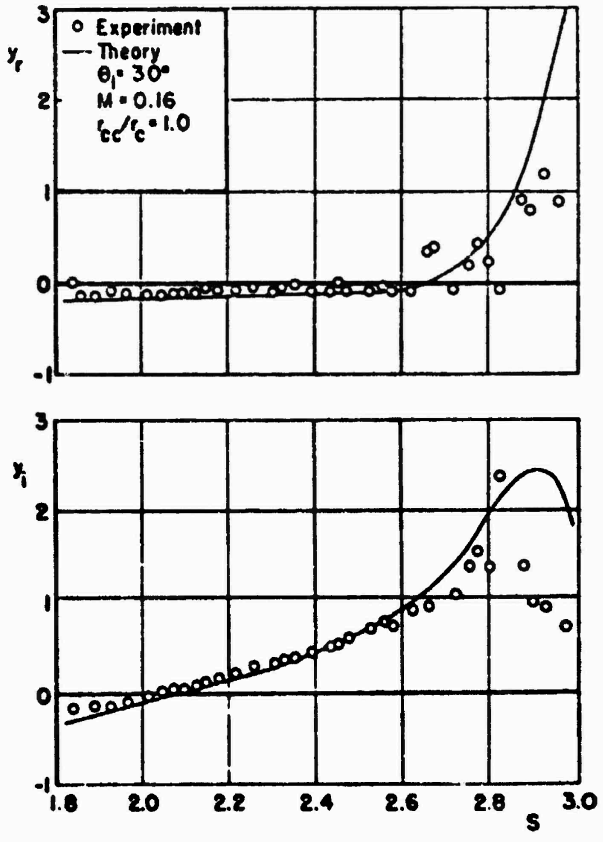

Figure 6. Comparison of the Theoretical and Experimental Values of the Admittance for a Nozzle with $\theta_1 = 30^\circ$, $\bar{M} = 0.16$, and $r_{c_c/r_c} = 1.0$.

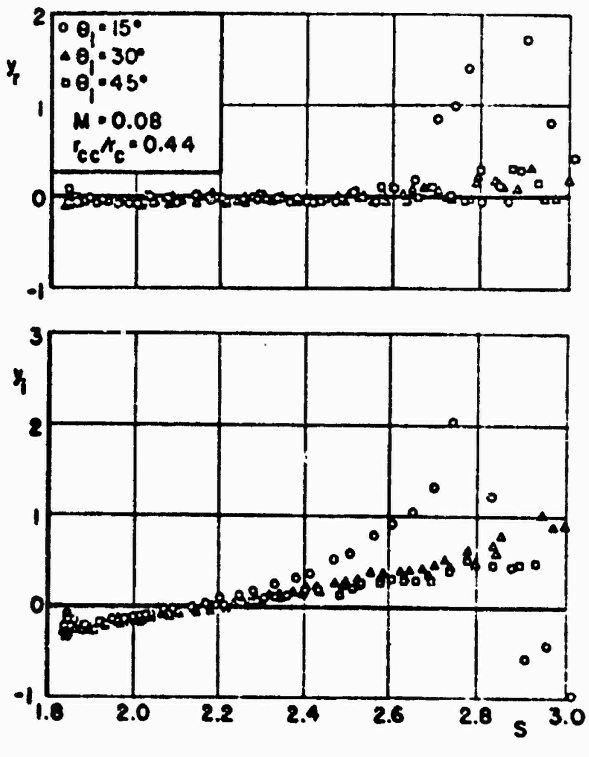

Figure 7. Effect of Nozzle Angle on the Values of the Admittance.

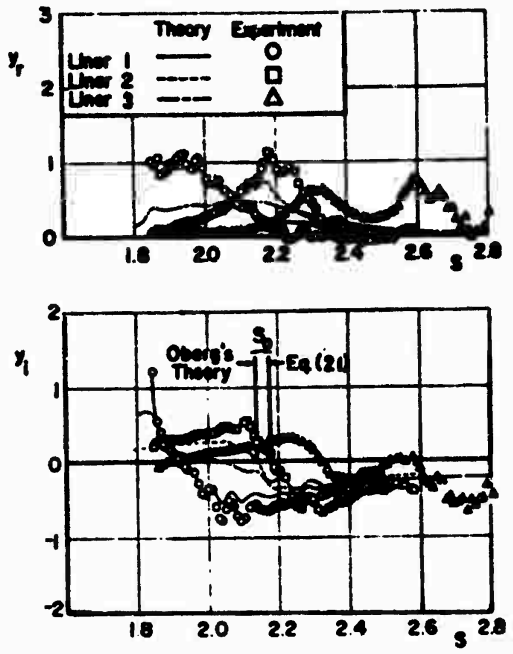

Figure 8. Comparison of the Theoretical and Experimental Local Liner Admittance Values for Different Liner Geometries. $\bar{M} = 0.08$ with a Quasi-Steady Nozzle.

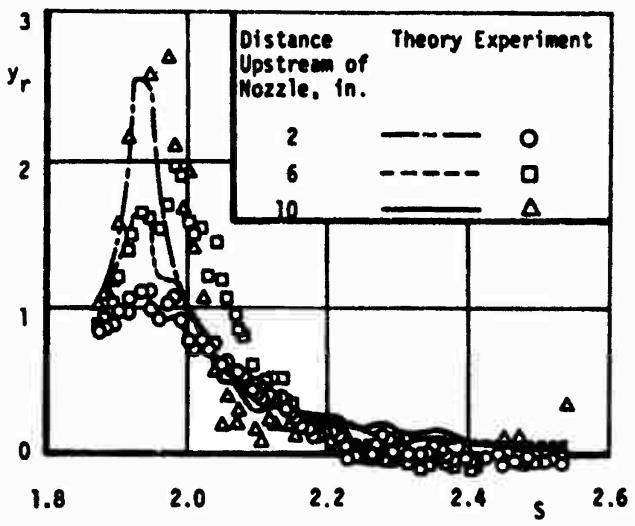

Figure 9. Effect of Axial Position on the Predicted and Measured Values of the Local Liner Admittance for Liner 1 plus a Quasi-Steady Nozzle, $\bar{M} = 0.08$.

A COMPUTATIONAL METHOD FOR THE INVESTIGATION OF SOUND TRANSMISSION IN NONUNIFORM DUCTS

by

Walter Eversman, Everett L. Cook, and Roy J. Beckemeyer *

Wichita State University
Wichita, Kansas

Abstract

The transmission of sound in a nonuniform two dimensional duct without flow is investigated by a method of weighted residuals which leads to a set of coupled "generalized telegraphists' equations." Results for several duct configurations are compared with a variational method, a stepped duct approximation, and an eigenfunction expansion method based on linearly tapered duct segments.

Introduction

Relatively rigorous methods have been developed for the analysis and design of acoustically lined and unlined ducts of uniform rectangular, circular, and annular cross section, with and without flow, and including the boundary layer effect in the flow case. The progress in this area can be seen by referring to a few papers of the extensive literature which exists (see, for example, References 1 - 5). The current capability in the mathematical modeling of duct propagation is limited primarily by the assumption of a uniform, infinite duct.

There have been a few recent studies directed toward the nonuniform duct problem. In the case of ducts without flow, a generally useful approach is the one developed by Zorumski and Clark (6) for ducts of uniform area with lining variations and subsequently implemented by Alfredson (7) for the study of hard-walled ducts with varying cross section. This method consists of representing the duct by a series of stepped ducts of uniform cross section and systematically accounting for the reflection and transmission process which occurs at the intersection of the stepped elements. This procedure appears to be very useful provided it is used with due caution in the segmenting process. In the case of ducts with uniform area but varying lining properties, it has been shown by Bahar (8) to converge to the method developed in the present paper when the elemental segments become vanishingly short. The principal difficulty with the stepped duct approach as originally conceived is the high dimensionality of the numerical problem which results. A somewhat different formulation of the problem by the third author of the present paper has reduced this difficulty while retaining the flexibility of the method.

Another method of general utility for ducts without flow is the variational approach of Beckemeyer and Eversman (9). In this technique the acoustic problem is represented by a variational principle and a Ritz minimization is employed to determine the coefficients in a trial solution. The trial solution is in terms of basis functions which do not necessarily satisfy the boundary conditions (the boundary conditions are part of the functional in the variational formulation) and do not have to be generated for each duct geometry. The variational approach suffers a dimensionality problem in that complicated acoustic fields (both axial and transverse) require a large number of basis functions in the trial solution.

Other recent approaches to the problem are more approximate in nature by virtue of restricting geometry or frequency range allowed. Nayfeh and his co-workers have published several studies of propagation in nonuniform ducts with and without flow. The paper by Nayfeh, Telinois, and Lekoudis (10) is representative. They restrict themselves to ducts with slowly varying cross section, lining properties and flow properties and employ a perturbation scheme. To within the level of accuracy which they retain, they do not predict the generation, reflection, and transmission of modes other than the one incident on the nonuniformity. Karamcheti and his co-workers have also made contributions in this area. King and Karamcheti (11) studied plane waves in ducts with one dimensional flow by a method of characteristics and Huerre and Karamcheti (12) used a short wave approximation for the same type of problem. Similar problems were studied earlier by Powell (13) and Eisenberg and Kao (14). Tam (15) seems to have published the first paper dealing with a multimodal approach to the problem of nonuniform ducts with flow. His technique is a perturbation scheme based on the assumption of slowly varying cross sectional area. The first order approximate solution is obtained by Fourier transformation. A recent paper by Cummings (16) studies the novel problem of the acoustics of a wine bottle. The wine bottle is a nonuniform duct without flow and the acoustic field is approximated by a Runge-Kutta integration scheme based on the Webster Horn Equation. This method allows only a plane wave mode of propagation and hence is limited to the lower frequency ranges.

In the present research program we are interested in the multimodal propagation of sound in nonuniform ducts of fairly general shape. The final goal of the program is the study of propagation in nonuniform ducts with flow, so that we will be interested in methods for the no flow case which appear to be extendable to the case with flow. Of the two generally applicable techniques mentioned previously, the variational method does not seem to be readily extendable to the case with flow since a variational principle from which the acoustic field equations can be derived is not known, at least not by the present authors. The stepped duct approximation might have some application, although it is certainly questionable whether the nonuniform flow field can be represented in sufficient detail in a series of stepped uniform segments. We are thus lead to look for

another method with promise for the flow case. In this paper we will introduce the method and assess its utility in the case without flow, as there are equivalent results available against which a direct comparison can be made. In the course of the development and application of the method it has become apparent that the method of weighted residuals is an important alternate method for the duct with no flow and, indeed, may well be superior to the other methods of general utility.

The method of weighted residuals (MWR) employed here actually was first employed in connection with electromagnetic waveguide problems by Schellkunoff (17, 18). The field equations for these problems are identical to the classical acoustic equations in certain cases. Schellkunoff's work followed work by Stevenson (19, 20) which used MWR but lead to a somewhat different formulation which does not seem to have been widely used. Stevenson appears to be the first to suggest the application of methods of this type to acoustic horn problems. Bahar and his co-workers studying ionospheric propagation of microwaves as a terrestrial waveguide problem have made extensive use of MWR (see, for example, Reference 8) and Reiter (21) has formalized the approach.

In this paper we have used MWR to approach the problem of multimodal propagation in nonuniform ducts without flow. We deal with a two dimensional duct in which both area variations and lining variations are permitted. The results using MWR are compared with those from a stepped duct theory, the variational approach, and a segmented duct theory in which the duct segments are sectoral. In reviewing the literature it does not appear that results for lined ducts of variable cross section in the multimodal case, with fairly general area variations permitted, have previously been presented.

Method

In this analysis we will consider two-dimensional ducts of infinite length. The extension to circular, annular, or rectangular ducts is straight forward. The extension to include finite duct terminations is easily included in the present formulation provided reflection and transmission characteristics of the termination are available. To demonstrate the method of weighted residuals (see Finlayson's book (22) for a complete description of the general method), we consider a two dimensional duct as shown in Figure 1 in which the wall at $y = 0$ is hard and the wall at $y = b(x)$ is lined with a material of specific acoustic admittance $A(x)$. The duct is uniform except for the nonuniform section $0 \leq x \leq \ell$. The local slope of the duct wall is defined by $\tan\theta = db/dx$. This representation is also valid for a duct symmetric about the x axis with acoustic propagation also symmetric with this axis.

The acoustic field and boundary conditions satisfy

$$ikp + \text{div}\,\bar{v} = 0 \qquad (1) \qquad\qquad ik\bar{v} = -\text{grad}p \qquad (2)$$

$$v = 0;\ y = 0 \qquad (3) \qquad\qquad v\cos\theta - u\sin\theta = Ap;\ y = b(x) \qquad (4)$$

The acoustic pressure, density, and particle velocity are non-dimensionalized with respect to $\rho_o c^2$, ρ_o and c, respectively. ρ_o and c are the ambient density and speed of sound. k is the free field wave number, $k = \omega/c$, where ω is the driving frequency.

Solutions to this problem are sought in the form of a finite series of specified basis functions

$$p_N = \sum_{n=1}^{N} p_n(x)\cos\kappa_n y \qquad u_N = \sum_{n=1}^{N} u_n(x)\cos\kappa_n y \qquad v_N = \sum_{n=1}^{N} v_n(x)\sin\kappa_n y \qquad (5)$$

where

$$\kappa_n b\tan\kappa_n b = ikbA \qquad (6)$$

The κ_n are the uniform duct eigenvalues taken locally in the non-uniform section. As such they are functions of x. Note that the basis functions do not individually satisfy the boundary condition of Eq. (4), however MWR will force them to collectively. The trial solutions do not in general satisfy the governing field equations and boundary conditions. Instead, they leave an error, or residual. Since a function must vanish if it is orthogonal to every member of a complete set, we can force the residuals to vanish by forcing them to be orthogonal to the basis functions themselves. Hence, for n=1, 2, ..N

$$\int_0^{b(x)} \left[ikp_N + \frac{\partial u_N}{\partial x} + \frac{\partial v_N}{\partial y}\right]\cos\kappa_n y\,dy = 0$$

$$\int_0^{b(x)} \left[iku_N + \frac{\partial p_N}{\partial x}\right]\cos\kappa_n y\,dy = 0$$

$$\int_0^{b(x)} \left[ikv_N + \frac{\partial p_N}{\partial y}\right]\sin\kappa_n y\,dy = 0$$

$$(v_N\cos\theta - u_N\sin\theta - Ap_N)\cos\kappa_n b = 0$$

After a series of operations implied in these equations, the equation for v_N can be eliminated and the unknown coefficients $p_n(x)$ and $u_n(x)$ are defined by the coupled ordinary differential equations for n = 1, 2...N

$$\frac{du}{dx}n = -ik\left[1 - \left(\frac{\kappa}{k}n\right)^2\right] p_n - \sum_{n=1}^{N} U^u_{nm}\, u_m - \sum_{n=1}^{N} U^p_{mn}\, p_m \tag{7}$$

$$\frac{dp}{dx}n = -iku_n - \sum_{n=1}^{N} P^p_{nm}\, p_m \tag{8}$$

where

$$U^u_{nm} = \frac{1}{N_n}\frac{dN}{dx}n\ \delta_{nm} + \frac{1}{N_n}\frac{d\kappa}{dx}n \int_0^{b(x)} y\sin\kappa_n y\cos\kappa_m y dy$$

$$U^p_{nm} = i\left[b\kappa_n \tan b\kappa_n - \frac{ikbA}{\cos\theta}\right] \frac{\cos\kappa_n b\cos\kappa_m b}{N_n kb}$$

$$P^p_{nm} = \frac{1}{N_n}\frac{dN}{dx}n\ \delta_{nm} + \frac{1}{N_n}\frac{d\kappa}{dx}n \int_0^{b(x)} y\sin\kappa_n y\cos\kappa_m y dy$$

$$- \frac{\tan\theta}{N_n}\cos\kappa_n b\cos\kappa_m b$$

Equations (7) and (8) are conveniently integrated by a Runge-Kutta method to obtain a transfer matrix relating the p_n and u_n at x = ℓ to those at x = 0

$$\begin{Bmatrix} u_n(\ell) \\ p_n(\ell) \end{Bmatrix} = [T] \begin{Bmatrix} u_n(0) \\ p_n(0) \end{Bmatrix} \tag{9}$$

Rather than obtaining the κ_n as functions of x from the eigenvalue equation, Eq. (6), by the usual Newton-Raphson scheme, an alternative procedure is used. Equation (6) is replaced by the differential equation of which it is the solution:

$$\frac{d(2\kappa_n b)}{dx} = 2ikbA\,\frac{(1 + \cos 2\kappa_n b)}{2\kappa_n b + \sin 2\kappa_n b}\left(\frac{1}{A}\frac{dA}{dx} + \frac{1}{b}\frac{db}{dx}\right)$$

By starting with values of κ_n at the beginning of the nonuniformity, $x = 0$, as many κ_n as needed in the integration of Eqs. (7) and (8) can be generated rapidly by integration simultaneously with the integration scheme leading to the transfer matrix in Eq. (9). In the interior of the nonuniformity the velocity and pressure are given by

$$\begin{Bmatrix} u(x,y) \\ \hline p(x,y) \end{Bmatrix} = \begin{bmatrix} \cos k_n y & \\ \hline & \cos k_n y \end{bmatrix} \begin{Bmatrix} u_n(x) \\ \hline p_n(x) \end{Bmatrix} \tag{10}$$

For $x<o$ and $x>\ell$, in the uniform ducts we can write

$$\begin{Bmatrix} u(x,y) \\ p(x,y) \end{Bmatrix} = [\alpha] \begin{Bmatrix} a^+ \\ a^- \end{Bmatrix}, \quad x<o \tag{11}$$

$$\begin{Bmatrix} u(x,y) \\ p(x,y) \end{Bmatrix} = [\beta] \begin{Bmatrix} b^+ \\ b^- \end{Bmatrix}, \quad x>\ell \tag{12}$$

Where the elements of $[\alpha]$ and $[\beta]$ can be easily determined from the classical uniform duct solution. a_n^+ are the coefficients of modes incident on the nonuniformity at $x = 0$ and a_n^- are the coefficients of modes reflected at $x = 0$. b_n^+ are the coefficients of modes transmitted at $x = \ell$ and b_n^- are the coefficients incident on the nonuniformity, from the right, at $x = \ell$. Since in this analysis the duct is infinite and uniform for $x>\ell$, $b_n^- = 0$. The extension to include the case of a finite termination in terms of a termination reflection matrix $\{b^-\} = [R]\{b^+\}$ is straight forward.

Equations (10) and (11) and (10) and (12) can be used to match velocity and pressure at $x = 0$ and $x = \ell$. Since the basis functions are orthogonal in the interior of the nonuniformity, it is convenient to use the same number of a_n^+ and a_n^- and b_n^+ and b_n^- as there are u_n and p_n and to use Fourier matching. This operation will provide relations between the wave amplitudes in the uniform ducts and the particle velocities and pressures in the nonuniform section

$$\begin{Bmatrix} u_n(0) \\ p_n(0) \end{Bmatrix} = [A(0)] \begin{Bmatrix} a^+ \\ a^- \end{Bmatrix} \tag{13}$$

$$\begin{Bmatrix} u_n(\ell) \\ p_n(\ell) \end{Bmatrix} = [A(\ell)] \begin{Bmatrix} b^+ \\ b^- \end{Bmatrix} \tag{14}$$

Equations (9), (13), (14) can be used to obtain a transfer matrix between incident wave amplitudes and transmission wave amplitudes

$$\begin{Bmatrix} b^+ \\ b^- \end{Bmatrix} = \begin{bmatrix} TA_{11} & TA_{12} \\ TA_{21} & TA_{22} \end{bmatrix} \begin{Bmatrix} a^+ \\ a^- \end{Bmatrix}$$

Since in this analysis we take $b_n^- = 0$, it is straight forward to obtain

$$\{a^-\} = [REF] \{a^+\} \qquad \{b^+\} = [TRAN] \{a^+\}$$

where [REF] and [TRAN] are reflection and transmission matrices, respectively, for the nonuniformity, defined by

$$[REF] = - [TA_{22}]^{-1} [TA_{21}]$$

$$[TRAN] = [TA_{11}] - [TA_{12}] [TA_{22}]^{-1} [TA_{21}]$$

The physical significance of the elements of these matrices is as follows:

REF_{ij} = Amplitude of reflected mode i due to incident mode j with amplitude 1.0 + i0.0

$TRAN_{ij}$ = Amplitude of transmitted mode i due to incident mode j with amplitude 1.0 + i0.0

Results

Very few results have been published for the multimodal transmission of sound in nonuniform ducts. The work of Zorumski and Clark (6), a sequel by Lansing and Zorumski (23), and the work of Alfredson (7) are the most nearly equivalent to the present method. They used the stepped duct approach for segmented linings or area changes in ducts with an open end. Since we have concentrated on the nonuniformity and have chosen not to represent terminations, we have no common basis for comparison. The approximate theories mentioned previously are considered too limited in scope to make comparison feasible when the labor and expense of doing so is considered. The only extensive results which we have been able to use conveniently are those of Beckemeyer and Eversman (9) who developed a variational approach and compared it with stepped duct approximations and an approximation in which the duct was segmented into linearly tapered sections. Of course, that study was closely related to the present one and the thrust of the entire research program has been to develop a basis of comparison.

As a first example we consider linearly tapered hardwall transition sections joining two uniform ducts. For these cases a 15° taper transition is used. The first example is a diverging

taper from a duct of height b_o to one of height (1 + tan 15°) b_o, the length of the nonuniformity being equal to its initial height. The second example is a converging taper which is exactly the reverse of the diverging one. We have compared these results with those generated in Reference (9) and reproduced here as Figures (2) - (5). In the diverging case kb_o values of 1.0, 2.0, 2.5, 3.0, and 3.5 are compared and in the converging case kb_ℓ values of 1.0, 1.5, 2.0, 2.5, 3.0 are used. At kb = 2.5 in the small duct the second mode is just cutting on in the large duct while at kb = 3.5 in the small duct it is cut on throughout. The results from Reference (9) for the diverging taper consist of two levels of stepped duct approximation, using 5 sections and 10 sections, the variational approach, and a segmented duct theory (eigenfunction expansion) using a linearly tapered duct segment with solutions given in terms of Bessel Functions. In the last method pressures and velocities were matched at the ends of the taper, x = 0 and x = ℓ, by collocation. No account was taken of the slight difference between the planar coordinate surface at the ends of the uniform duct and the circular co-ordinate surfaces of the radial segment. Details of the characteristics of these methods can be found in the reference. In the converging taper only the 5 section stepped duct and the variational approach were used. The MWR was used with 6 basis functions and 50 integration steps axially.

Figures (2) and (3) show the transmission and reflection coefficients for the diverging duct for the second mode with the first mode incident at x = 0 with amplitude 1.0 + 0.0i. We have made the most detailed comparisons for the second mode since with increasing reduced frequency it goes through the cut-on phenomenon and hence is considered the most challenging computationally. The transmission coefficients, shown in Figure (2), are in good agreement throughout the frequency range, all methods considered yielding essentially the same result. In Figure (3), it is seen that the results for the reflection coefficients for $kb_o > 2.5$ are not in as good agreement. However, it is noted that the variational method, the eigenfunction expansion method, and MWR remain in close agreement but they do not agree closely with either stepped duct result at the higher kb_o. The imaginary part of the reflection coefficient is the first to show significant deviation. We have concluded that our choice of the number of modes in the stepped duct approximation was not adequate at the higher frequency, particularly after the second mode begins to cut on.

Figures (4) and (5) combine the results for transmission and reflection coefficients in the first and second modes with mode 1 incident for the converging taper. In this case the 5 section stepped duct and the variational method are used for comparison.

Agreement is good throughout the frequency range. The stepped duct approximation appears to be more adequate in this case than in the diverging case, particularly for reflection coefficients, since more modes are used on the reflection side than were used in the diverging duct case.

As a second comparison we have analyzed at selected frequencies the transmission and reflection characteristics of a lined diverging transition section. We have used a cosine shaped transition which has the same small and large heights and the same length as the linear taper previously discussed. The only available results for comparison are from the variational approach. We encountered convergence problems with the variational scheme as our limited computational capacity permitted neither double precision nor more than 40 input basis functions. A series of results were obtained using 4 axial cosine waves, 4 axial sine waves, and from 5 to 9 transverse functions. In all cases convergence was observed to be occurring with increasing modes, but in several cases it was not reached to our satisfaction (judged by comparing successive runs with more and more modes). For this reason we have only made comparisons where convergence in the variational case was acceptable. The MWR was used with 6 transverse modes and 50 axial integration steps. We have generated results in the form of reflection and transmission coefficients in modes 1 through 3 for mode 1 incident. Results are compared in Table 1. Absence of variational results indicates a lack of convergence at the level of approximation used. Wherever converged results are available, the MWR shows acceptable agreement with the variational approach. Because of the computer limitations noted in the variational results, the MWR results are considered the more accurate.

The results with which we have compared are all at relatively low frequency at which at most two modes propagate. We do not currently have available higher frequency results against which to compare, principally due to limitations in the computer facilities which we have used. However, we can gain a measure of confidence in the MWR by investigating its convergence properties at higher frequencies. We have considered the cosine shaped diverging transition section at a reduced frequency of $kb_o = 12.57$ using a lining with $A = 0.76 + 0.30i$. In this case in the small duct the plane wave and 3 higher modes are well cut on and mode 5 is just cutting on. In the large duct the plane wave and 5 higher modes propagate ($kb_\ell = 15.94$). We have used four combinations of basis functions and integration steps beginning with 6 transverse modes and 50 steps and progressing through 8 modes and 50 steps, 6 modes and 100 steps, and 10 modes and 50 steps. Increasing the number of integration steps made virtually no difference. Increasing the number of basis functions provided a very definite convergence trend. To illustrate this convergence of the method we have shown in Table 8 the reflection coefficients in mode 5 due to all incident modes (REF_{5i}). Mode 5 was chosen because the driving reduced frequency is right at the mode 5 cut-on frequency

in the source-side duct. This causes relatively large reflected components in this mode for any incident mode. In addition, in Table 8 we have shown the direct transmission coefficients in all incident modes ($TRAN_{ii}$). Coefficients are shown for 6, 8 and 10 basis functions. The sequence of results is distinctly convergent. In this case the use of 8 basis functions is probably sufficient from an engineering standpoint.

As a final example of the use of the method we have computed the acoustic power balance for the linear converging taper in the softwall case (A = 0.76 + 0.30i) as well as in the hardwall case at kb_o = 15.94. For each propagating mode incident on the nonuniformity we have computed the incident power, the reflected power, and the transmitted power carried in all resulting propagating modes. The power dissipated in the acoustic lining is the amount by which the sum of the reflected and transmitted powers fail to match the incident power. Table 10 shows the results of these computations for both cases. The hardwall case (A = 0.0001 + 0.0001i) is significant in that it adequately approximates the known result that no power is dissipated in the nonuniformity. While we have not at this point made extensive parametric variations, it appears from these results that the reflective characteristic of a nonuniformity can be enhanced for modes near the cut off condition. We intend to report more detailed investigations of specific nonuniformities at a later date.

Conclusions

The method of weighted residuals has been shown to be an accurate and rapidly convergent method for the computation of the acoustic transmission and reflection properties of nonuniformities in ducts without flow. Other methods applicable to this problem have been implemented and numerous comparison runs have been made to validate the MWR and to build confidence in its use. In all cases where other results could be generated, comparable results were obtained.

The nonuniformities treated in this paper are of the type which one might encounter in applications. They are not small, nor are they very abrupt (although all of the results for lined ducts presented here have a discontinuous change from hardwall to softwall). It is to be expected that the more radical the nonuniformity, the less rapid will be the convergence, and the more basis functions and integration intervals will be required to achieve a satisfactory result. This is an inherent property of this type of method. At this point we are satisfied that we can treat problems of practical importance.

The results to date conclusively show that it is important to treat the duct nonuniformity problem from a multi-modal standpoint. A given incident mode will generate spurious reflected and transmitted modes which can have an important effect on

acoustic lining design and radiation properties. In addition, there appears to be a possibility of using geometry changes and their attendant reflective properties to enhance acoustic attenuation, but the multi-modal performance of the duct will have to be known for design purposes.

The MWR and its application to ducts without flow will be extended to circular and annular ducts and these results will be reported at a later date. In addition, we may investigate the possibility of using other types of basis functions to determine if it is possible to achieve comparable results at still lower cost.

The problem of the most immediate importance is the extension of the method to the case of ducts with flow. In contrast to other methods investigated, the MWR appears to be extendable when flow is involved. Of course, the complexity of the problem expands considerably, but the basic numerical scheme can be modified and expanded to include this case. We are currently well along in the extension of our computational scheme. There are still several problem areas of development and numerical experimentation which must be resolved, but at this point we are optimistic that the flow case can be successfully implemented.

[Sponsored by NASA Lewis Research Center under grant NGR 17-003-018.]

References

1. Morse, P.M., "The Transmission of Sound Inside Pipes," J. Acoust. Soc. Amer. 11, 205-210 (1939).
2. Cremer, L., "Theorie der Luftschall-Dampfung in Rechtekkanal mit Schluckender Wand und das sich dabei Ergebende Hochste Dampfungsmass," Acustica 3, 249-263 (1953).
3. Munger, P. and Gladwell, G.M.L., "Acoustic Wave Propagation in a Sheared Fluid Contained in a Duct," J. Sound Vibration 9, 28-48 (1969).
4. Eversman, W., "The Effect of Mach Number on the Tuning of an Acoustic Lining in a Flow Duct," J. Acoust. Soc. Amer. 48, 425-428 (1970).
5. Eversman, W., "Effect of Boundary Layer on the Transmission and Attenuation of Sound in an Acoustically Treated Circular Duct," J. Acoust. Soc. Amer. 49, 1372-1380 (1971).
6. Zorumski, W.E. and Clark, L.R., "Sound Radiation from a Source in an Acoustically Treated Circular Duct," unpublished working paper, NASA Langley Research Center, (1971).
7. Alfredson, R.J., "The Propagation of Sound in a Circular Duct ofContinuously Varying Cross Sectional Area," J.Sound Vib. 23, 433-442 (1972).
8. Bahar, E., "Generalized Scattering Matrix Equations for Waveguide Structures of Varying Surface Impedance Boundaries," Radio Science 2, 287-297 (1967).

9. Beckemeyer, R.J. and Eversman, W., "Computational Methods for Studying Acoustic Propagation in Nonuniform Waveguides," AIAA Paper 73-1006, presented at AIAA Aero-Acoustic Conference, Seattle, Washington, October 15-17, (1972).
10. Nayfeh, A.H., Telionis, D.P., and Lekoudis, S.G., "Acoustic Propagation in Ducts with Varying Cross Sections and Sheared Mean Flow," AIAA Paper 73-1008, presented at AIAA Aero-Acoustics Conference, Seattle Washington, October 15-17, (1973).
11. King, L.S. and Karamcheti, K., "Propagation of Plane Waves in the Flow Through a Variable Area Duct," AIAA Paper 73-1009, presented at AIAA Aero-Acoustics Conference, Seattle, Washington, October 15-17, (1973).
12. Huerre, P. and Karamcheti, K., "Propagation of Sound Through a Fluid Moving in a Duct of Varying Area," Proceedings of Interagency Symposium on University Research in Transportation Noise, Stanford University, March 28-30, (1973).
13. Powell, A., "Theory of Sound Propagation Through Ducts Carrying High Speed Flow," J. Acoust. Soc. Amer. 32, 1640-1646 (1960).
14. Eisenberg, N.A. and Kao, T.W., "Propagation of Sound Through a Variable Area Duct with a Steady Compressible Flow," J. Acoust. Soc. Amer. 49, 169-175, (1960).
15. Tam, C.K.W., "Transmission of Spinning Acoustic Modes in a Slightly Nonuniform Duct," J. Sound Vib. 18, 339-351 (1971).
16. Cummings, A., "Acoustics of a Wine Bottle," J. Sound Vib. 31 (3), 331-343 (1973).
17. Schelkunoff, S.A., "Generalized Telegraphist's Equations for Waveguides," Bell System Tech. J. 31, 784-801 (1952).
18. Schelkunoff, S.A., "Conversion of Maxwell's Equations into Generalized Telegraphist's Equations," Bell Systems Tech. J. 39, 995-1043 (1955).
19. Stevenson, A.F., "General Theory of Electromagnetic Horns," J. App. Phys. 22, 1447-1460 (1951).
20. Stevenson, A.F., "Exact and Approximate Equations for Wave Propagation in Acoustic Horns" J. App. Phys. 22, 1461-1463 (1951).
21. Reiter, G., "Generalized Telegraphist's Equations for Waveguides of Varying Cross Section," Proc. IEE 106, Part B, Supp. No. 13, 54-57 (1959).
22. Finlayson, B.A., The Method of Weighted Residuals and Variational Principles, Academic Press, (1972).
23. Lansing, D.L. and Zorumski, W.E., "Effect of Wall Admittance Changes on Duct Transmission and Radiation of Sound," J. Sound Vib. 27(1), 85-100 (1973).

---

* Roy Beckemeyer is currently with the Nacelle and Noise Abatement Branch of The Boeing Company, Wichita, Kansas. Boeing's continued support of our research programs is gratefully acknowledged.

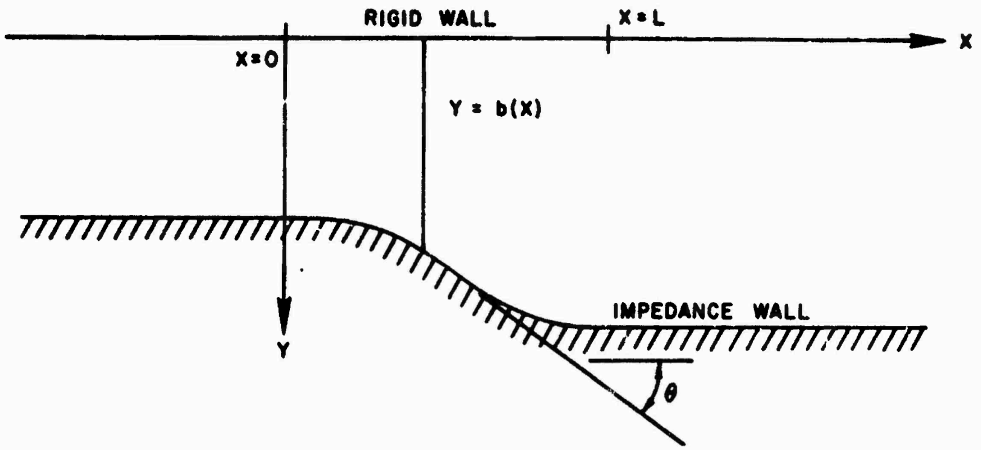

FIGURE 1
DUCT GEOMETRY FOR EXAMPLE CASE

TABLE 1

REFLECTION AND TRANSMISSION COEFFICIENTS FOR A COSINE SHAPED LINED TRANSITION SECTION. FIRST MODE INCIDENT, AMPLITUDE = 1.0 + 0.0i

	METHOD OF WEIGHTED RESIDUALS		VARIATIONAL METHOD	
kb_0	REFLECTION IN FIRST THREE MODES	TRANSMISSION IN FIRST THREE MODES	REFLECTION IN FIRST THREE MODES	TRANSMISSION IN FIRST THREE MODES
1.5	-0.05 + 0.27i -0.00 + 0.14i 0.01 - 0.03i	-0.18 - 0.61i 0.17 + 0.20i -0.04 - 0.03i	-0.03 + 0.28i 0.01 + 0.13i	-0.17 - 0.61i 0.18 + 0.20i -0.04 - 0.04i
2.0	0.15 + 0.08i 0.15 + 0.21i -0.01 - 0.05i	-0.26 - 0.40i 0.54 + 0.02i -0.08 + 0.03i	0.17 + 0.06i 0.16 + 0.17i	-0.25 - 0.41i 0.55 - 0.00i -0.10 + 0.02i
2.5	-0.11 - 0.02i 0.19 - 0.02i -0.02 - 0.04i	-0.47 - 0.44i 0.73 - 1.02i 0.01 + 0.08i	-0.11 - 0.02i -0.02 - 0.03i	-0.48 - 0.44i 0.19 - 1.02i 0.01 + 0.10i
3.0	-0.03 + 0.04i 0.25 - 0.03i -0.02 - 0.04i	-0.67 - 0.14i -0.41 - 0.58i 0.02 + 0.05i	-0.03 + 0.04i 0.19 - 0.05i -0.02 - 0.03i	-0.67 - 0.14i -0.42 - 0.55i 0.02 + 0.06i

NOTE: At each reduced frequency the first two columns are the converged result from MWR. The second two columns are from the variational method when a converged result is available.

$kb_0 = 1.5$ $A = 0.413 + 0.720i$

$kb_0 = 2.0$ $A = 0.664 + 0.720i$

$kb_0 = 2.5$ $A = 0.788 + 0.536i$

$kb_0 = 3.0$ $A = 0.760 + 0.300i$

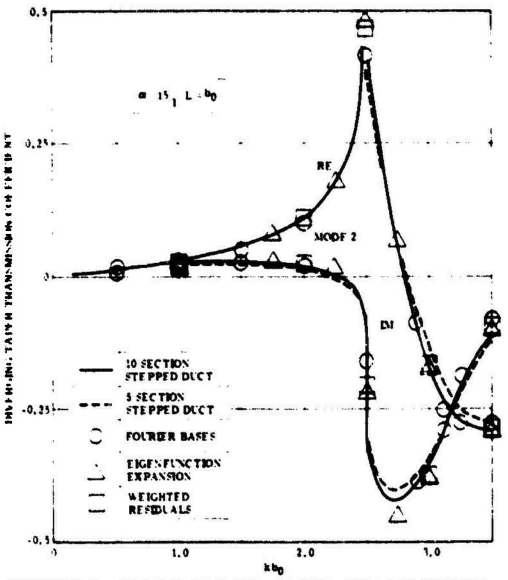

FIGURE 2 15° DIVERGING TAPER TRANSMISSION COEFFICIENT IN MODE 2. MODE 1 INCIDENT.

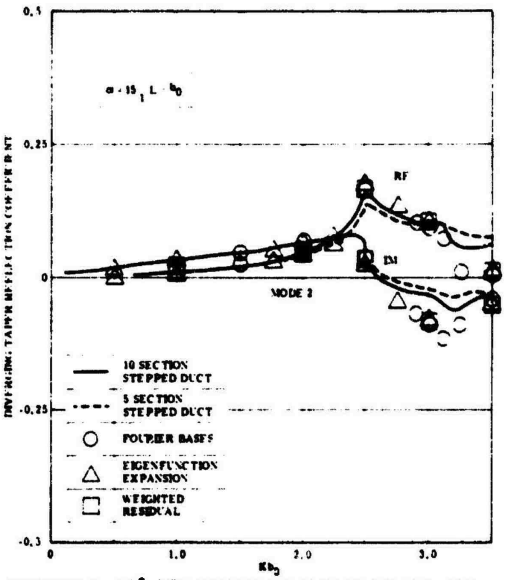

FIGURE 3 15° DIVERGING TAPER REFLECTION COEFFICIENT IN MODE 2. MODE 1 INCIDENT.

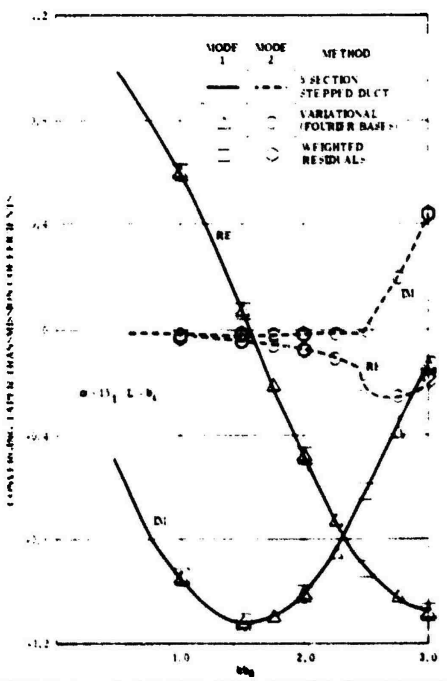

FIGURE 4 15° CONVERGING TAPER TRANSMISSION COEFFICIENTS. MODE 1 INCIDENT.

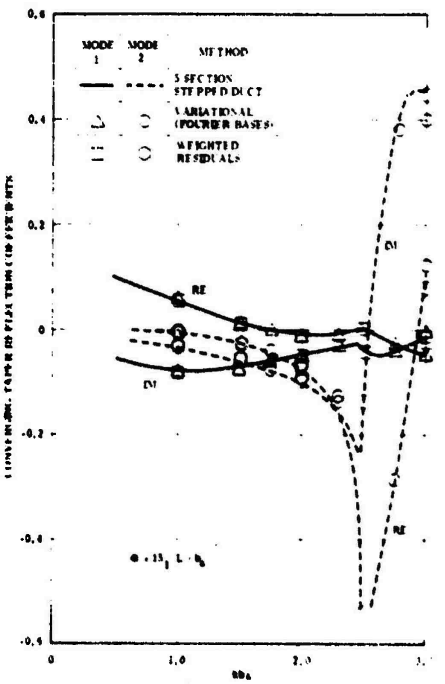

FIGURE 5 15° CONVERGING TAPER REFLECTION COEFFICIENTS. MODE 1 INCIDENT.

TABLE 2

CONVERGENCE TRENDS IN COSINE SHAPED
DIVERGING TRANSITION - kb_o = 12.57
A = 0.76 + 0.31i, b_o = 1.0, b_ℓ = 1.268, L = 1.0

INCIDENT MODE	REFLECTION COEFFICIENTS IN MODE 5			DIRECT TRANSMISSION COEFFICIENTS		
	6 BASIS FNS	8 BASIS FNS	10 BASIS FNS	6 BASIS FNS	8 BASIS FNS	10 BASIS FNS
1	-0.223 +0.152i	-0.215 +0.141i	-0.2122 +0.138i	0.736 +0.034i	0.736 +0.034i	0.736 +0.034i
2	0.230 -0.151i	0.222 -0.139i	0.2186 -0.136i	0.523 +0.213i	0.523 +0.212i	0.522 +0.212i
3	-0.245 +0.146i	-0.232 +0.132i	-0.228 +0.129i	0.146 +0.451i	0.148 +0.451i	0.148 +0.451i
4	0.260 -0.191i	0.238 -0.190i	0.232 -0.188i	-0.337 +0.024i	-0.341 +0.029i	-0.342 +0.031i
5	-0.900 +0.080i	-0.896 +0.080i	-0.896 +0.080i	0.016 +0.012i	0.017 +0.012i	0.018 +0.012i
6	0.279 +0.152i	0.272 +0.161i	0.269 +0.164i	-0.057 -0.012i	-0.060 -0.016i	-0.061 -0.017i
7		-0.194 -0.128i	-0.191 -0.130i		-0.005 +0.002i	-0.005 +0.002i
8		0.157 +0.108i	0.154 +0.111i		-0.002 +0.002i	-0.002 +0.001i
9			-0.130 -0.097i			-0.001 +0.001i
10			0.114 +0.087i			-0.000 +0.001i

TABLE 3

ACOUSTIC POWER BALANCE IN LINEAR TAPER
CONVERGING TRANSITION SECTION - kb_o = 15.94,
b_o = 1.268, b_ℓ = 1.0, L = 1.0

INCIDENT MODE	INCIDENT POWER	REFLECTED POWER	TRANSMITTED POWER	ABSORBED POWER
A = 0.76 + 0.30i				
1	1.000	0.003	0.754	0.242
2	1.000	0.007	0.595	0.399
3	1.000	0.010	0.672	0.317
4	1.000	0.015	0.571	0.414
5	1.000	0.020	0.307	0.674
6	1.000	0.169	0.050	0.781
A = 0.0001 + 0.0001i				
1	1.000	0.004	0.996	0.000
2	1.000	0.0075	0.9923	0.000
3	1.000	0.026	0.974	0.000
4	1.000	0.148	0.852	0.000
5	1.000	0.557	0.443	0.000
6	1.000	0.948	0.052	0.000

ACOUSTIC FIELD OF A POINT MASS SOURCE IN AN INFINITELY LONG RECTANGULAR DUCT WITH FLOW

by

John E. Cole, III
and Ioannis I. Sarris

Department of Mechanical Engineering
Tufts University
Medford, Massachusetts

1. Introduction

The possibility of using wind tunnels as acoustic test facilities has been mentioned by several authors (see, for instance, Hickey et al., 1969; Bies, 1971; Atencio and Soderman, 1973). Several problem areas related to acoustic measurements of aircraft components in wind tunnels have been considered by Bender and Arndt (1973) and by Holbeche and Williams (1973). In this paper we investigate one aspect of this complex problem, namely, the properties of the acoustic field from a point mass source in a rectangular duct in which there is uniform flow. The duct is infinitely long with walls that are characterized by a small acoustic admittance. In this manner we can represent the effects of the acoustic boundary layer (see Nayfeh, 1973) and introduce attenuation into the solution. We distinguish here between a monopole source and a point mass source. As we shall see, a point mass source (which is equivalent to a small pulsating sphere) in a uniformly moving medium has monopole as well as dipole characteristics.

Several investigators have considered the properties of the acoustic field from a simple source in the presence of a uniform flow. Lighthill (1972) discusses the free-field results for monopole and dipole sources in a uniform flow, while Morse and Ingard (1968, pp. 735-737) give the result for a point mass source. The free-field solution for a quadrupole source has been discussed by Cole (1972). Morfey (1971) has considered monopole sources in rigid-walled ducts with flow. Mead and Richards (1968) and Eversman (1971) consider the propagation characteristics in a rectangular duct with uniform flow. Measurements of the effect of the flow on upstream and downstream propagating plane waves, which are originated by a piston source, have been presented by Ingard and Singhal (1973).

The analysis is formulated from the linearized continuity and momentum equations. The presence of a mass source in a uniform flow gives rise to an inhomogeneous "convected" wave equation. The solution to this equation which satisfies the boundary conditions at the walls of the duct is obtained following the basic procedure used by Morse and Ingard (1968, pp. 492-507) for the case of no flow.

2. Propagation Characteristics -- The Homogeneous Problem

We first wish to investigate the acoustic propagation characteristics in an infinitely long rectangular duct with uniform flow. The duct walls are not perfectly rigid but are characterized by a small specific admittance (i.e., the complex quantity which is the reciprocal of the specific acoustic impedance of the wall). In terms of the perturbation pressure, p, the governing equation is:

$$\frac{1}{a_o^2}\frac{D^2p}{Dt^2} - \nabla^2 p = 0 \qquad (2.1)$$

where a_o is the speed of sound in the medium at rest, $\frac{D}{Dt} = \frac{\partial}{\partial t} + U\frac{\partial}{\partial x}$, and U is the flow velocity in the positive x- direction. The boundary conditions to be satisfied by the pressure at the walls of the duct are:

$$\begin{aligned} &\frac{Dp}{Dt} \pm \frac{a_o}{\beta}\frac{\partial p}{\partial y} = 0 \quad @\ y = \pm\, b/2 \\ &\frac{Dp}{Dt} \pm \frac{a_o}{\beta}\frac{\partial p}{\partial z} = 0 \quad @\ z = \pm\, d/2 \end{aligned} \qquad (2.2)$$

where b and d are the duct dimensions and β is the specific acoustic admittance.

A solution which satisfies equations 2.1 and 2.2 for downstream propagation (i.e., propagation in the positive x-direction) has the form:

$$p^+(x,y,z,t) = P\ cs\left(\frac{\pi q_y^+ y}{b}\right) cs\left(\frac{\pi q_z^+ z}{d}\right) e^{-ik_x^+ x}\, e^{i\omega t} \qquad (2.3)$$

where
$$cs\left(\frac{\pi q_y^+ y}{b}\right) = \begin{cases} \cos\left(\frac{\pi q_y^+ y}{b}\right), & \text{even modes} \\ \sin\left(\frac{\pi q_y^+ y}{b}\right), & \text{odd modes} \end{cases}$$

and q_y^+, q_z^+ are the characteristic values. Substituting equation 2.3 into the governing equation 2.1 we obtain the equation

$$k_x^{+2} + \left(\frac{\pi q_y^+}{b}\right)^2 + \left(\frac{\pi q_z^+}{d}\right)^2 = \left(k_o - Mk_x^+\right)^2 \qquad (2.4)$$

where $k_o = \frac{\omega}{a_o}$ is the wavenumber of the propagating wave, and $M = \frac{U}{a_o}$ is the flow Mach number. Also, direct substitution of equation 2.3 into the boundary conditions (equation 2.2) yields a pair of transcendental equations:

$$\frac{\pi q_y^+}{2} \tan\left(\frac{\pi q_y^+}{2} - \frac{m\pi}{2}\right) = \frac{ib\beta}{2}\left(k_o - Mk_x^+\right)$$

$$\frac{\pi q_z^+}{2} \tan\left(\frac{\pi q_z^+}{2} - \frac{n\pi}{2}\right) = \frac{id\beta}{2}\left(k_o - Mk_x^+\right) \qquad (2.5)$$

The appearance of the complex axial propagation constant k_x^+ on the right hand side of the boundary conditions leads to nonorthogonality of the transverse characteristic functions (see Morse and Feshbach, 2, 1953).

The system of equations 2.4 and 2.5 must be solved simultaneously to determine k_x^+, q_y^+, q_z^+. In order to obtain an explicit relationship between each of the q^+'s and k_x^+, we make the assumption that the duct walls are only slightly non-rigid (i.e., β is small so that $b\beta(k_o - Mk_x^+) \ll 1$). By doing so, we obtain from equation 2.5 the following relationships for q_y^+ and q_z^+:

$$\frac{\pi q_{ym}^+}{b} = \begin{cases} \left[\frac{2i\beta}{b}\left(k_o - Mk_x^+\right)\right]^{1/2} & m = 0 \\ \frac{m\pi}{b} + \frac{2i\beta}{m\pi}\left(k_o - Mk_x^+\right) & m > 0 \end{cases} \qquad (2.6a)$$

$$\frac{\pi q_{zn}^+}{d} = \begin{cases} \left[\frac{2i\beta}{d}\left(k_o - Mk_x^+\right)\right]^{1/2} & n = 0 \\ \frac{n\pi}{d} + \frac{2i\beta}{n\pi}\left(k_o - Mk_x^+\right) & n > 0 \end{cases} \qquad (2.6b)$$

In the above notation we use the second subscript on the q's to designate the value of the integer m in equation 2.6a or the integer n in equation 2.6b. Now, from equations 2.4 and 2.6 the downstream axial propagation constant (k_{xmn}^+), corresponding to integers m and n, and the characteristic values q_{ym}^+ and q_{zn}^+ are found to be:

$$k_{xmn}^+ = \frac{1}{1-M^2}\left[-Mk_o + 2iM\beta\left(\frac{1}{b} + \frac{1}{d}\right) + \sqrt{\Delta}\right] \qquad (2.7a)$$

$$\frac{\pi q_{ym}^+}{b} = \begin{cases} \left[\frac{2i\beta}{b(1-M^2)}\left(k_o - M\sqrt{\Delta}\right)\right]^{1/2} ; & m = 0 \\ \frac{1}{1-M^2}\left[\frac{m\pi}{b}(1-M^2) + \frac{2i\beta}{m\pi}\left(k_o - M\sqrt{\Delta}\right)\right] ; & m > 0 \end{cases} \qquad (2.7b)$$

$$\frac{\pi q_{zn}^{+}}{d} = \begin{cases} \left[\frac{2i\beta}{d(1-M)^2} \left(k_o - M\sqrt{\Delta}\right)\right]^{1/2} & ; \quad n=0 \\ \frac{1}{1-M^2}\left[\frac{n\pi}{d}(1-M^2) + \frac{2i\beta}{n\pi}\left(k_o - M\sqrt{\Delta}\right)\right] & ; n>0 \end{cases} \tag{2.7c}$$

where $\Delta = k_o^2 - (1-M^2)\left[\left(\frac{m\pi}{b}\right)^2 + \left(\frac{n\pi}{d}\right)^2\right] - 4ik_o\beta\left(\frac{1}{b}+\frac{1}{d}\right)$ and terms of second order in β have been neglected. We note that the characteristic values q_{ym}^{+} and q_{zn}^{+} are coupled together, since m and n appear in both of them. We also note that the coupling terms are proportional to the flow Mach number. The corresponding axial propagation constant k_{xmn}^{-} amd characteristic values q_{ym}^{-} and q_{zn}^{-} for upstream propagation (i.e., propagation in the negative x-direction) are obtained by assuming an axial dependence of $e^{ik_x^{-}x}$ in equation 2.3. Such a form of solution results in expressions similar to equations 2.4, 2.6 and 2.7 but with an opposite sign for the flow Mach number.

Examining the propagation constants k_{xmn}^{+} and k_{xmn}^{-} we see that, for given values of the integers m and n, waves which propagate downstream have a larger phase speed ($a_{mn} = \mathrm{Re}\{\frac{\omega}{k_{xmn}}\}$) and a less rapid spatial attenuation rate ($\alpha_{mn} = \mathrm{Im}\{k_{xmn}\}$) than those waves which propagate in the upstream direction. Since the duct walls are not perfectly rigid, we cannot establish a real value for k_o in equation 2.7a which yields an infinite phase speed. We can define, however, the following condition, which we refer to as the cut-off condition:

$$k_{mn}^{*2} = 0 \tag{2.8}$$

where $k_{mn}^{*2} = k_o^2 - (1-M^2)\left[\left(\frac{m\pi}{b}\right)^2 + \left(\frac{n\pi}{d}\right)^2\right]$

This is the same cutoff condition found in the case of a duct with rigid walls and uniform flow. (See Eversman, 1971) For a given set of integers m and n (i.e., for a particular mode), k_o may be below, equal to, or above the cutoff condition for that mode. The axial propagation constant for these regions of k_o is, respectively, the following:

For $k_{mn}^{*2} < 0$ (below cutoff)

$$k_{xmn}^{+} = \frac{1}{1-M^2}\left\{\frac{2k_o\beta}{k_{mn}^{*2}}\left(\frac{1}{b}+\frac{1}{d}\right) - Mk_o - i\left[k_{mn}^{*1} - 2M\beta\left(\frac{1}{b}+\frac{1}{d}\right)\right]\right\} \tag{2.9a}$$

For $k_{mn}^{\circ 2} = 0$ (at cutoff)

$$k_{xmn}^{+} = \frac{1}{1-M^2}\left\{\left[2k_o\beta\left(\frac{1}{b}+\frac{1}{d}\right)\right]^{1/2} - Mk_o - i\left(\left[2k_o\beta\left(\frac{1}{b}+\frac{1}{d}\right)\right]^{1/2} - 2M\beta\left(\frac{1}{b}+\frac{1}{d}\right)\right)\right\} \quad (2.9b)$$

For $k_{mn}^{\circ 2} > 0$ (above cutoff)

$$k_{xmn}^{+} = \frac{1}{1-M^2}\left\{k_{mn}^{\circ} - Mk_o - i\left[\frac{2k_o\beta}{k_{mn}^{\circ}}\left(\frac{1}{b}+\frac{1}{d}\right) - 2M\beta\left(\frac{1}{b}+\frac{1}{d}\right)\right]\right\} \quad (2.9c)$$

where $k_{mn}^{\circ\prime 2} = -k_{mn}^{\circ 2}$

The corresponding relationships for k_{xmn}^{-} are obtained by reversing the sign of the flow Mach number in equation 2.9.

Eversman (1971) has investigated wave propagation in a duct with rigid walls and uniform flow. By considering the mean axial acoustic power which is transmitted along the duct, he shows that there is no power transmitted for a mode when k_o is below or equal to the cutoff condition of that mode. In our case of a non-rigid duct with flow, however, there is some power transmitted for a mode when k_o is below or equal to the cutoff condition of that mode. This transmitted power is small, being proportional to the wall admittance β .

We noted earlier in this section that the transverse characteristic functions $\phi_{mn} = \cos\left(\frac{\pi q_{ym} y}{b}\right) \cos\left(\frac{\pi q_{zn} z}{d}\right)$ for this problem are non-orthogonal. This occurs, mathematically, because the axial propagation constant appears in the boundary conditions. When there is no flow, the transverse characteristic functions defined in 2.3 are orthogonal for both rigid and non-rigid walls. For the set of characteristic functions which result when there is flow in the duct, we can apply the Gram-Schmidt orthogonalization method to construct a set of orthogonal functions (ψ_{mn}) based on a linear combination of the nonorthogonal functions (ϕ_{mn}). This is permissible when the set of functions ϕ_{mn} is complete. Support for our assumption that the set of functions ϕ_{mn} is complete is given by Nayfeh and Telionis (1974). The following recurrence relation is obtained which expresses the functions ψ_{mn} in terms of ϕ_{mn} (see Morse and Feshbach, 1, 1953):

$$\psi_{mn} = \phi_{mn} - \sum_{i=0}^{m-1}\sum_{j=0}^{n-1} \frac{\iint \psi_{ij}^{*}\, \phi_{mn}\, dydz}{N_{ij}}\, \psi_{ij}$$

$$N_{mn} = \iint |\phi_{mn}|^2\, dydz - \sum_{i=0}^{m-1}\sum_{j=0}^{n-1} \frac{\left|\iint \psi_{ij}^{*}\, \phi_{mn}\, dydz\right|^2}{N_{ij}} \quad (2.10)$$

where the asterisk indicates the complex conjugate. We find that the first few functions ψ_{mn} are identical to the corresponding functions ϕ_{mn}

(i.e., $\psi_{00} = \phi_{00}$, $\psi_{01} = \phi_{01}$, $\psi_{12} = \phi_{12}$, $\psi_{21} = \phi_{21}$). Starting with ψ_{22}, the orthogonal characteristic functions deviate from the corresponding ϕ functions.

3. Inhomogeneous problem

We now consider the acoustic field in the moving medium when there is a mass source located inside the duct. The linearized continuity and momentum equations are, respectively,

$$\frac{Dp}{Dt} + \rho_o \nabla \cdot \bar{u} = q \tag{3.1}$$

and

$$\rho_o \frac{D\bar{u}}{Dt} + \nabla p = 0 \tag{3.2}$$

where ρ_o is the density of the undisturbed medium, ρ is the perturbation density, $\bar{u}$ is the perturbation velocity vector, p is the perturbation pressure, q is the mass source, $\frac{D}{Dt} = \frac{\partial}{\partial t} + U \frac{\partial}{\partial x}$, and U is the speed of the medium in the positive x-direction. Since the undisturbed medium is homogeneous, we can relate p to ρ in the usual manner

$$p = a_o^2 \rho \tag{3.3}$$

Equations 3.1, 3.2 and 3.3, then, combine to form an inhomogeneous 'convected' wave equation in terms of the perturbation pressure

$$\frac{1}{a_o^2} \frac{D^2 p}{Dt^2} - \nabla^2 p = \frac{Dq}{Dt} \tag{3.4}$$

The boundary conditions to be satisfied by the acoustic pressure at the duct walls are the same as those discussed previously for the homogeneous problem (equation 2.2).

We see that the effect of the flow is to alter the characteristics of the mass source. A point mass source located at (x_o, y_o, z_o) in a uniformly moving medium has the form:

$$\frac{D}{Dt}[q(t)\delta(x-x_o)\delta(y-y_o)\delta(z-z_o)] = \frac{\partial q(t)}{\partial t}\delta(x-x_o)\delta(y-y_o)\delta(z-z_o) + U q(t)\delta'(x-x_o)\delta(y-y_o)\delta(z-z_o) \tag{3.5}$$

where $\delta'(x-x_o)$ is the derivative of the Dirac delta function. The source, therefore, has its usual monopole characteristics as well as dipole behavior which is proportional to the flow velocity. We shall see that this source behavior leads to discontinuities at the source location in both the acoustic pressure and the axial pressure gradient. We further note that the free field solution to equation 3.4 for the point mass source is the same as the free field solution for a small pulsating sphere located in the flow. Therefore,

as in the case with no flow, a physical representation for the point mass source would be a small pulsating sphere.

We look for solutions to equation 3.4 in the following form:

$$p^{\pm} = \sum_{m=0}^{\infty} \sum_{n=0}^{\infty} \psi_{mn}^{\pm}(y,z)\, F_{mn}^{\pm}(x)\, e^{i\omega t} \tag{3.6}$$

where $\psi_{mn}^{\pm}(y,z)$ are the set of orthogonal characteristic functions of equation 2.10. The source strength is taken to be periodic with time so that

$$q(t) = q_o e^{i\omega t} \tag{3.7}$$

We first substitute equation 3.6, using $\psi_{mn}^{+}(y,z)$, and equation 3.7 into equation 3.4 to determine the solution for the region $x > x_o$ (i.e., downstream of the source). Multiplying both sides of equation 3.4 by $\psi_{m',n'}^{+}(y,z)$ and integrating over the duct cross section, we obtain the equation for $F_{mn}^{+}(x)$:

$$\frac{d^2F_{mn}^{+}}{dx^2} - \frac{2ik_oM}{1-M^2}\frac{dF_{mn}^{+}}{dx} + \left(\frac{k_o^2-K_{mn}^2}{1-M^2}\right) F_{mn}^{+} = -\frac{a_o q_o \psi_{mn}^{+}(y_o,z_o)}{bd(1-M^2)N_{ym}^{+}N_{zn}^{+}}\left\{ ik_o\delta(x-x_o) + M\delta'(x-x_o)\right\} \tag{3.8}$$

where $K_{mn}^2 = \left(\frac{\pi q_{ym}^{+}}{b}\right)^2 + \left(\frac{\pi q_{zn}^{+}}{d}\right)^2$ and N_{ym}^{+}, N_{zn}^{+} are the normalization constants. A similar equation results for $F_{mn}^{-}(x)$ for the region $x < x_o$ (i.e., upstream of the source) when $\psi_{mn}^{-}(y,z)$ from equation 3.6 is used.

Equation 3.8 is a second order ordinary differential equation which is solved using the method of variation of parameters. Two solutions are obtained for $F_{mn}^{+}(x)$. One of the solutions does not satisfy the correct boundary conditions and is therefore disregarded. A similar situation exists for $F_{mn}^{-}(x)$. The results for $p^{+}(x,y,z,t)$ and $p^{-}(x,y,z,t)$, then are the following:

$$p^{+} = \sum_{m=0}^{\infty} \sum_{n=0}^{\infty} \frac{a_o q_o \psi_{mn}^{+}(y,z)\psi_{mn}^{+}(y_o,z_o)}{2bd(1-M^2)N_{ym}^{+}N_{zn}^{+}} \left(\frac{k_o - Mk_{xmn}^{+}}{k_{xmn}^{+} + \frac{k_oM}{1-M^2}}\right) \exp\{i[\omega t-(x-x_o)k_{xmn}^{+}]\} \tag{3.9a}$$

and

$$p^- = \sum_{m=0}^{\infty} \sum_{n=0}^{\infty} \frac{a_o q_o \psi_{mn}^-(y,z)\psi_{mn}^-(y_o,z_o)}{2bd(1-M^2)N_{ym}^- N_{zn}^-} \left(\frac{k_o + Mk_{xmn}^-}{k_{xmn}^- - \frac{k_o M}{1-M^2}} \right) \exp\{i[\omega t+(x-x_o)k_{xmn}^-]\} \tag{3.9b}$$

where k_{xmn}^+ and k_{xmn}^- were previously defined in equation 2.9.

4. Discussion

The solution for the perturbation pressure given by equation 3.9 satisfies the governing equation 3.4 as well as the boundary conditions (equation 2.2). As expected, a discontinuity in the axial pressure gradient exists in the yz plane containing the source (i.e. at $x = x_o$) because of the basic monopole nature of the source. However, a discontinuity in pressure also exists at the same location which is attributed to the dipole-type characteristic of the source (i.e. the second term in the right hand side of equation 3.5). We find that the pressure distribution upstream of the source (p^-) is obtained from the downstream distribution (p^+) by reversing the signs of M and $(x - x_o)$, and vice versa. The solution for the pressure distribution is expressed in terms of an infinite sum of orthogonal modes. For a particular mode, the axial propagation constant is given by the real part of $k_{xmn}^{\pm}$, while the spatial attenuation rate is given by the imaginary part of $k_{xmn}^{\pm}$. As seen in equation 2.9, the spatial attenuation rate is much greater for $k_{mn}^{o2} > 0$ than for $k_{mn}^{o2} < 0$, which is the reason for using $k_{mn}^{o2} = 0$ as the cutoff condition.

When the driving frequency is below the first cutoff condition (i.e. $k_o^2 < (1-M^2)\left[\left(\frac{m\pi}{b} \right)^2 + \left(\frac{n\pi}{d} \right)^2 \right]$ with either $m = 0$ and $n = 1$ or $m = 1$ and $n = 0$), then only plane waves propagate. For these plane waves, the pressure at $x = x_o$ becomes

$$|p^+| \simeq |A^+|(1-M)$$
$$|p^-| \simeq |A^-|(1+M)$$

where we have assumed $\left[\frac{2\beta}{k_o} \left(\frac{1}{b} + \frac{1}{d} \right) \right]^2 << 1$, and A^+ and A^- are the coefficients appearing in equation 3.9 which involve the transverse characteristic functions and normalization factors. Also, when $\left(\frac{k_o \beta b}{1 \pm M} \right)^2 << 1$, we have $|A^+| \simeq |A^-|$ and therefore $\left| \frac{p^-}{p^+} \right| \simeq \frac{1+M}{1-M}$ for plane waves. This type of convective effect for plane waves has been observed experimentally by Ingard and Singhal (1973) using a piston source.

For higher modes (i.e., modes for which either m or n or both are greater than zero), the pressure for a particular mode exhibits a resonant-like behavior due to the term

$$f_{mn} = \frac{k_o - M k_{xmn}}{k_{xmn} + \frac{k_o M}{1-M^2}}$$

where $$k_{xmn} = \begin{cases} k^+_{xmn} & \text{for } M>0 \\ k^-_{xmn} & \text{for } M<0 \end{cases}$$

In Fig. 2, $|f_{mn}|$ is shown as a function k_o/κ_{mn}, where $\kappa_{mn} = \{(1-M^2)[(\frac{m\pi}{b})^2 + (\frac{n\pi}{d})^2]\}^{1/2}$. The following parameters were also used: $\beta = .07$, $f = 500$ Hz, $b = 3.$ m and $d = 2.$ m. The condition $k_o/\kappa_{mn} = 1$ corresponds to the cutoff condition for a particular mode, which in the case of $f = 500$ Hz is mode ($m = 4$, $n = 6$) or ($m = 8$, $n = 3$). In Fig. 2 we show only the region of propagation. Given the driving frequency f (and therefore k_o), the wall specific admittance β and the duct dimensions b and d, the curve represents the amplitude of all modes characterized by integers m and n such that $k_o^2 \geq (1-M^2)\,[(\frac{m\pi}{b})^2 + (\frac{n\pi}{d})^2]$, i.e. modes for which k_o is above cutoff. The value of $|f_{mn}|$ is relatively large in the region close to the cutoff condition, and it is somewhat insensitive to Mach number variations. For frequencies well above the region near cutoff (i.e., $k_o/\kappa_{mn} > 5$ for the conditions of Fig. 2), $|f_{mn}|$ approaches the plane wave values of $1 \mp M$.

In Fig. 3, we show the ratio $|\frac{f^-_{mn}}{f^+_{mn}}|$ (where the minus superscript indicates upstream conditions and the plus denotes downstream conditions) as a function of k_o/κ_{mn} for the same parameters used in Fig. 2. We note that the ratio is unity for M=0. As we approach the cutoff for the mode, the ratio also approaches unity. When the Mach number is greater than zero, the ratio increases with k_o/κ_{mn}, and for frequencies far above the cutoff region the ratio approaches $\frac{1+M}{1-M}$.

As seen in equation 3.9, the pressure corresponding to a particular mode (p_{mn}) is attenuated as the mode propagates along the duct. The spatial attenuation rate depends on the real part of the specific acoustic acoustic admittance β. When β is small, the magnitude of the ratio of pressures at two points with identical transverse positions in the duct and equidistant upstream and downstream of the source is given by

$$|\frac{p^-_{mn}}{p^+_{mn}}| \simeq \{\frac{k_o + M k^*_{mn}}{k_o - M k^*_{mn}}\} \exp\,[-4\beta M\,(\frac{1}{b} + \frac{1}{d})|x-x_o|]$$

We note that the attenuation rate for the pressure ratio is proportional to the flow Mach number and independent of integers m and n, which are characteristic of the particular mode of interest. When flow is present, waves propagating upstream attenuate more rapidly than those which propagate downstream. This behavior tends to counteract the flow effect shown in Fig. 3. As a result, when we consider corresponding positions upstream and downstream which are close to the source, we expect the ratio of pressures for a particular mode, $|\frac{p_{mn}^-}{p_{mn}^+}|$, to be greater than unity. When the positions are far from the source, however, we expect the ratio to be less than unity, due to the dominant spatial attenuation.

5. Conclusion

The work on this problem is still in progress. During this summer, an experimental program will investigate some of the results of the analysis in the 7- by 10-foot wind tunnel of the NASA Ames Research Center.

This work is being supported through NASA Grant NGR 22-012-031.

References

A. Atencio and P. T. Soderman, "Comparison of Aircraft Noise Measured in Flight Test and in the NASA Ames 40- by 80-foot Wind Tunnel," AIAA Paper No. 73-1047, AIAA Aero-Acoustics Conference, Seattle, Wash. (Oct. 1973).

J. Bender and R.E.A. Arndt, "Aeroacoustic Research in Wind Tunnels: A Status Report," Prepared for United States Army Air Mobility Research and Development Laboratory - Ames Directorate (Feb. 1973).

D. A. Bies, "Investigation of the Feasibility of Making Model Acoustic Measurements in the NASA Ames 40- by 80-foot Wind Tunnel," NASA CR 114352 (Aug. 1971).

J. E. Cole, "The Influence of a Crossflow on Jet Noise," NASA CR 2169 (Nov. 1972).

W. Eversman, "Signal Velocity in a Duct with Flow," J. Acoust. Soc. Amer., 50 (2), 421-425 (1971).

W. Eversman, "Energy Flow Criteria for Acoustic Propagation in Ducts with Flow," J. Acoust. Soc. Amer., 49 (6), 1717-1721 (1971).

D. H. Hickey, P.T. Soderman and M.W. Kelly, "Noise Measurements in Wind Tunnels,""Basic Aerodynamic Noise Research," NASA SP 207,399-408 (1969).

T.A.Holbeche and J.Williams, "Acoustic Considerations for Noise Experiments at Model Scale in Subsonic Wind Tunnels," AGARD Rept. No. 601, 8:1-30 (April 1973).

U. Ungard and V.K. Singhal, "Upstream and Downstream Sound Radiation into a Moving Fluid," J. Acoust. Soc. Amer., 54 (5), 1343-1346 (1973).

M. J. Lighthill, "The Fourth Annual Fairley Lecture: The Propagation of Sound through Moving Fluids," J. Sound Vib., 24 (4), 471-492 (1972).

D. J. Mead and E.J. Richards, Noise and Acoustic Fatigue in Aeronautics, John Wiley and Sons, New York, 54-56 (1968).

C. L. Morfey, "Sound Transmission and Generation in Ducts with Flow," J. Sound Vib., 14 (1), 37-55 (1971).

P.M.Morse and H. Feshbach, Methods of Theoretical Physics, McGraw-Hill Book Co., Inc.,(1) 928, (2) 1344-1345 (1953).

P. M. Morse and U. Ingard, Theoretical Acoustics, McGraw-Hill Book Co., Inc., 492-507, 735-737 (1968).

A.H. Nayfeh, "Effect of the Acoustic Boundary Layer on the Wave Propagation in Ducts," VPI Engineering Dept., VPI-E-73-10 (April 1973).

A.H. Nayfeh and D. P. Telionis, "Algebraically Growing Waves in Ducts with Sheared Mean Flow," J.Acoust. Soc. Amer., 55 (1), 16-18 (1974).

Addendum to

"Acoustic Field of a Point Mass Source in an Infinitely Long Rectangular Duct with Flow"

by J.E. Cole, III and I.I. Sarris

The use of the orthogonal set of functions $\psi_{mn}(y,z)$ defined in equation 2.10 has been found to contribute minimally to obtaining a simple form of the solution to this problem for the total pressure $p^{\pm}(x,y,z,t)$ in the duct. As a result, some of the discussion and certain of the equations should be modified. Equation 3.8 does not follow from equations 2.10 and 3.6. Upon replacement of $\psi^{+}_{mn}(y_o,z_o)$ with $\phi^{+}_{mn}(y_o,z_o)$, equation 3.8 is the correct governing equation for the axial dependence $F^{+}_{mn}(x)$ of the modal pressure which we define to be

$$p^{+}_{mn} = \phi^{+}_{mn}(y,z)\ F^{+}_{mn}(x)\ e^{i\omega t}$$

This modal pressure is defined in terms of the nonorthogonal transverse characteristic functions $\phi^{+}_{mn}(y,z)$, and therefore the total pressure can not be obtained by summing the modal pressures. With the replacement of ψ_{mn} by ϕ_{mn} equations 3.9a and 3.9b provide the solution for the modal pressures p^{+}_{mn} and p^{-}_{mn}, respectively (i.e., there should be no summation indicated in these equations). Figures 2 and 3 remain unaltered since they apply to a specific mode.

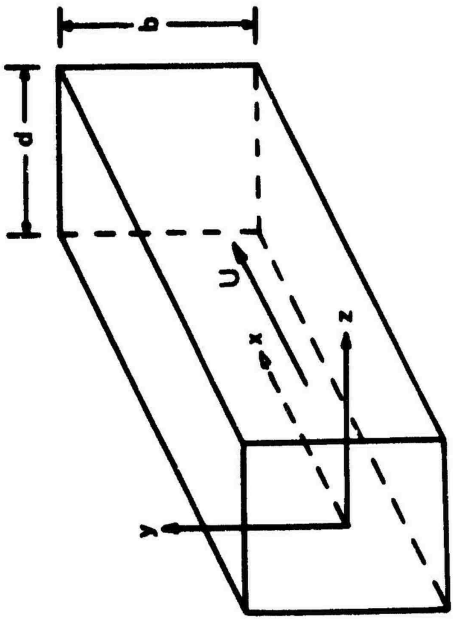

Fig. 1. Duct Geometry

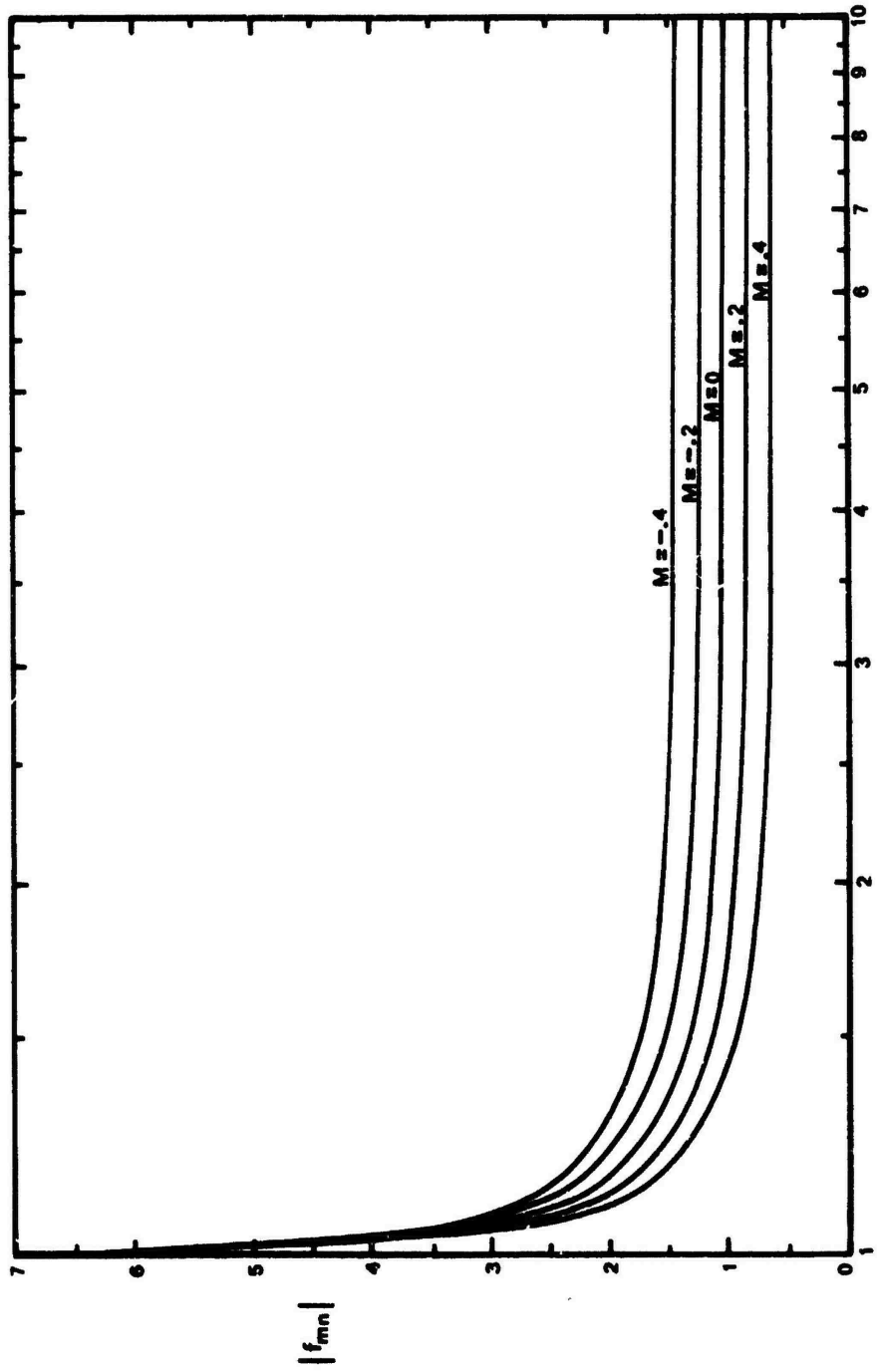

Fig. 2. $|f_{mn}|$ as a function of k_o/κ_{mn} for $\beta = .07$, f = 500 Hz, b = 3 m, d = 2 m and several flow Mach numbers.

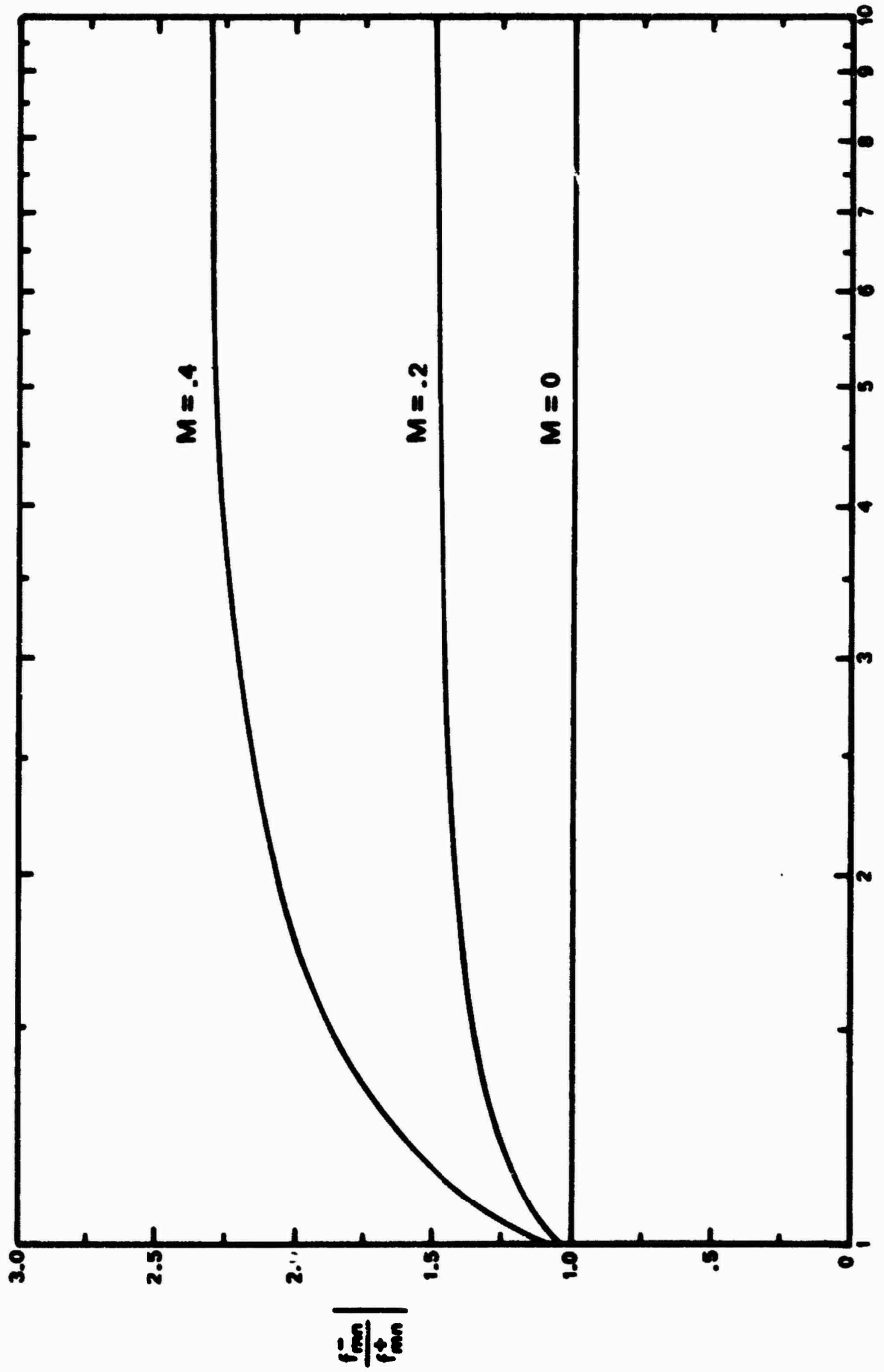

Fig. 3. $\left|f_{mn}^{-}/f_{mn}^{+}\right|$ as a function of k_0/k_{mn} for $\beta = .07$. $f = 500$ Hz. $b = 3$ m. $d = 2$ m and several flow Mach numbers.

SOME THEORETICAL STUDIES ON NOISE PROPAGATION, ATTENUATION AND RADIATION IN TURBO-FAN ENGINE ENVIRONMENTS

by

P. Mungur; J. C. Yu; J. L. Whitesides; W. R. Arnold
Joint Institute for Acoustics and Flight Sciences
NASA-Langley Research Center, Hampton, Virginia

1. INTRODUCTION

The purpose of this paper is to present recent and continuing research at the Joint Institute for Acoustics and Flight Sciences on the multiple interactions of noise that occur in a turbo-fan engine environment. Once these interactions are identified, outlines of methods to understand their effects on propagation are presented and finally some results are shown.

The fluctuations associated with the acoustic source on the blades of fan-jet engines as a result of rotor-stator interaction or otherwise need not all propagate away from the source as waves. The environment into which the source is located plays an important part in determining the acoustic radiation efficiency. In a turbo-fan engine environment, figure 1, the sound first interacts with the mean helical flow in the vicinity of the blades and the rows of rotors and stators. Beyond the compressor or fan assembly the sound interacts with the inside surface of the acoustically treated nacelle, the mean flow and the mean thermal and flow gradients inside the nacelle. On its way out of the engine the sound interacts both with the inlet and exhaust flows and the outer surface of the engine nacelle. The above interactions give rise to convective propagation, convective and shear refractions, reflections, attenuation and diffraction. Each of the interactions mentioned above modifies the acoustic load seen by the fluctuating source and hence its acoustic efficiency. Other interactions that have not been mentioned above are those due to variable area duct and scattering by turbulence.

In Section 2, the effects of helical flow on sound propagation is reviewed. In Section 3 propagation in an inlet with boundary layer growth is discussed. In Section 4 radiation from duct ends in the presence of jet flow is reviewed and the effects in a jet exhaust are discussed. Finally a scheme for optimizing the duct transmission loss is presented.

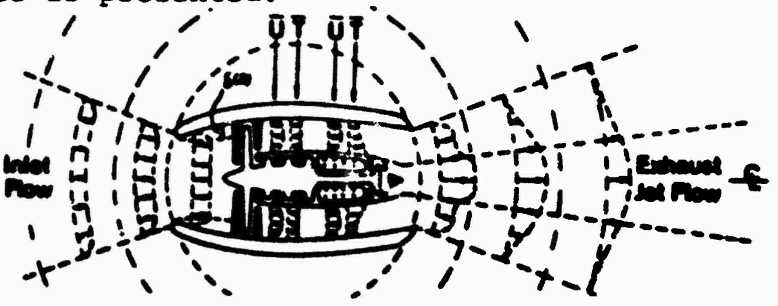

Figure 1 - A turbo-fan jet engine flow field.

2. SOUND FIELDS IN A HELICAL FLOW

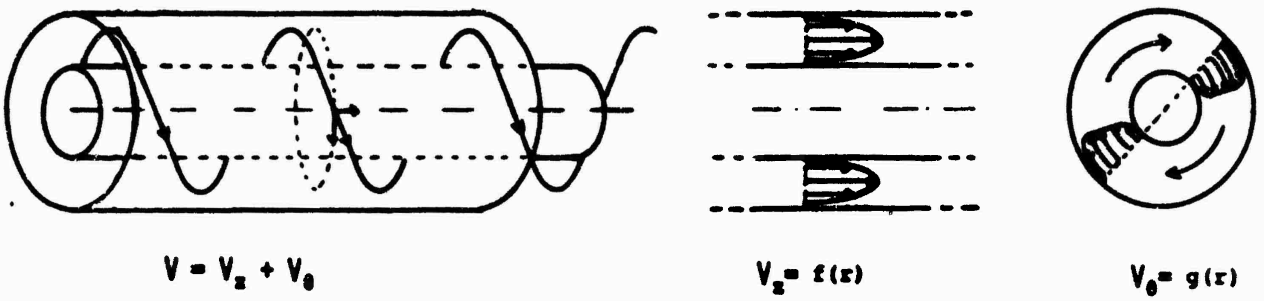

Figure 2 - A ducted helical flow field.

As mentioned in the introduction, the fluctuations at the blades of a fan or compressor as a result of rotor-stator interaction must propagate through a helical flow environment before it reaches the inlet or exhaust section where the mean flow is purely axial. This interaction of the sound with the helical flow has been studied by Kapur and Mungur [1] and is briefly reported here. The mean flow is assumed to have components along θ and z directions only in an annular duct (see figure 2). Both the θ and z dependent part of mean flow are assumed to be a function of r to account for the boundary layers. The mean temperature, density, speed of sound and pressure are also assumed to be a function of r to allow for any possible thermal boundary layers. The governing wave in such an environment is given by

$$\left[1-\frac{2V_\theta}{r}Q_1\right]\frac{\partial^2 P}{\partial r^2}+\left[\frac{1}{r}-\frac{1}{\rho}\frac{d\rho}{dr}-Q_2\right]\frac{\partial P}{\partial r}+\left[1-\frac{V_\theta^2}{c^2}\right]\frac{\partial^2 P}{r^2\partial\theta^2}+\left[1-\frac{V_z^2}{c^2}\right]\frac{\partial^2 P}{\partial z^2}$$

$$-\frac{1}{c^2}\frac{\partial^2 P}{\partial t^2}-\frac{2V_z}{c^2}\frac{\partial^2 P}{\partial z\partial t}-\frac{2V_\theta}{c^2 r}\frac{\partial^2 P}{\partial\theta\partial t}-\frac{2V_\theta V_z}{c^2 r}\frac{\partial^2 P}{\partial\theta\partial z}-Q_3 P=0 \qquad (1)$$

where Q_1, Q_2, Q_3 are functions of the two components of the mean flow, the thermal and flow radial gradients, the speed of sound and the frequency. It follows that the Q's are functions of r.

A solution to the governing wave-equation may be written in the form

$$P = F(r)\exp(j\omega t - jk_\theta\theta - \gamma z) \qquad (2)$$

where k_θ take integral values given by 0, ± 1, ± 2, $\pm m$.

γ and $F(r)$ are determined from the reduced wave-equation obtained by substituting equation (2) into equation (1) and is given by

$$\left[1 - \frac{2V_\theta}{r} Q_1\right] \frac{d^2F}{dr^2} + \left[\frac{1}{r} - \frac{1}{\rho}\frac{d\rho}{dr} - Q_2\right] \frac{dF}{dr} + Q_4 F = 0 \qquad (3)$$

where Q_4 is a function of Q_3, k_θ, γ and ω/c.

Equation (3) can be integrated numerically from r_1 to r_2 and is made to satisfy the boundary conditions at the lined or rigid surfaces at r_1 and r_2. This will yield four sets of values for a specified k_θ and ω/c. Two sets are obtained for a positive value of k_θ and another two sets for a negative value of k_θ. If the swirl component of the flow is clockwise when looking downstream, then the two γ's associated with a positive value of k_θ are associated with helical modes spinning in the same direction as the mean flow, one going downstream and the other going upstream. On the other hand if k_θ is negative, the two values of γ's are associated with helical modes spinning against the mean swirl and hence will propagate slower along the axis than those propagating with the mean swirl.

It has also been shown that if the radial boundary layers are not taken into account (rigid body swirl) the radial boundary conditions will be modified by the mean swirl due to acoustic coupling with the centripetal force as a result of the swirl and also due to fluctuating centripetal forces. In conclusion, the mean swirl modifies the mode-shapes and the corresponding cut-on frequencies.

3. SOUND FIELD IN AN INLET DUCT

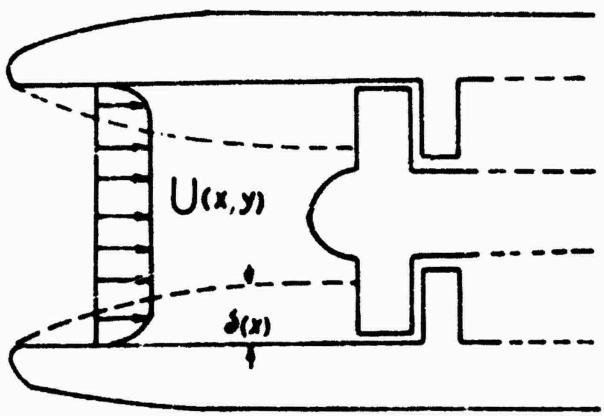

Figure 3 - Boundary layer growth in an inlet flow duct

In an inlet duct, there is an inherent boundary layer growth, figure 3. The interaction of sound with a mean flow with a constant boundary layer thickness has received much attention in the last five years. The boundary layer growth gives rise to a variation of the mean flow not only along the direction transverse to the duct axis but also along the axis. Such an interaction has recently been studied by Nayfeh et al [2] using an asymptotic expression, and Mungur et al [3] using standard running wave approach. The method presented by the latter is reviewed briefly. The governing wave equation derived by Mungur, Kapur and Gladwell [3] is given by

$$\left[1-\frac{U^2}{c^2}\right]\frac{\partial^2 p}{\partial x^2} - \frac{2U}{c}\frac{\partial^2 p}{\partial x \partial t} + \frac{\partial^2 p}{\partial r^2} + \left(\frac{1}{r} + L_3\right)\frac{\partial p}{\partial r} + \frac{1}{r^2}\frac{\partial^2 p}{\partial \theta^2} - \frac{1}{c^2}\frac{\partial^2 p}{\partial t^2} + L_2\frac{\partial p}{\partial x} + L_3\frac{\partial p}{\partial t} + L_4 p = 0 \qquad (4)$$

where U is the mean axial velocity along x and is a function of both the axial coordinate x and the transverse radial, coordinate r. The coefficients L_1, L_2, L_3, L_4 are functions of the mean flow and the axial gradients of the flow and temperature. L_1 is also a function of the transverse shear and thermal gradients. In a constant boundary layer region of a flow duct, the coefficients L_2, L_3 and L_4 vanish and the governing wave-equation reduces to the simpler form studied by Mungur and Plumblee [4] and others.

A separation of variable cannot strictly be applied to the above wave-equation (4) because the coefficient are functions of both x and r. However the variation along x is very much smaller than that along r and use can be made of this fact as follows. The inlet duct can be mathematically subdivided along the axis into smaller segments. A separation may now be forced at the center of each segment with the consequence that the solutions are valid only at the center of each segment. The solution must contain both downstream and upstream modes and unknown coefficients to be determined from boundary conditions at the junctions of the segments. Such solutions are determined at the centers of all the segments, using the following representation for the sound pressure at the center of any arbitrary segment, the ith for example,

$$P_i(r, \theta, x_i, t) = A_i F_i(r) \exp(j\omega t - k_\theta \theta - \gamma_i x_i) \qquad (5)$$

where γ_i is expected to have two sets of values, positive and negative representing downstream and upstream propagation respectively. k_θ can be shown to take integral values (0, $\pm$1, $\pm$2, $\pm$m) by using the cyclic boundary conditions along θ. When equation (5) is substituted into equation (4), the following first order approximation of the reduced wave equation is obtained,

$$\frac{d^2F_i}{dr^2} + \left(\frac{1}{r} + L_{1i}\right)\frac{dF_i}{dr} + \left(L_{5i} - \frac{m^2}{p^2}\right)F_i = 0 \qquad (6)$$

where L_{1i} and L_{5i} are evaluated at the center of the i^{th} segment as functions of r. L_{5i} is also a function of the frequency parameter (ω/c) and the axial wave-vector γ_i. A solution to equation (6) satisfying the boundary conditions at the two curved surfaces of an annular duct can be obtained numerically and has been discussed in detail by Mungur and Plumblee [4]. This method also yields the axial wave-vectors γ_i in pairs, each set representing the modal wave-vectors associated with upstream and downstream propagation. Finally the sound pressure and axial particle velocity of the i-th segment can be written as

$$P(r,\theta,x_i,t) = \sum_{n=0}^{\infty}\sum_{m=-\infty}^{\infty}\left[A^i_{mn}\psi^m_n(r)e^{-\gamma_i x_i} + B^i_{mn}\phi^m_n(r)e^{+q_i x_i}\right]H(\theta,t) \qquad (7)$$

$$U_z(r,\theta,x_i,t) = \sum_{n=0}^{\infty}\sum_{m=-\infty}^{\infty} A^i_{mn}\xi^m_n(r)e^{-\gamma_i x_i} - B^i_{mn}\eta^m_n(r)e^{+q_i x_i}\Big] H(\theta,t) \qquad (8)$$

where $H(\theta,t) = \exp(j\omega t - jm\theta)$

and $\psi^m_n(r)$ the mode shapes, solutions of equation (6), corresponding to a positive value of γ_i; similarly $\phi^m_n(r)$ corresponds to q_i negative values of γ_i. The velocity mode shapes ξ and η are obtained from the ψ, ϕ and their radial derivatives. The unknowns are A^i_{mn} and B^i_{mn}. These can be evaluated by matching the boundary conditions at $x_i \pm h$ where h is the half length of the i^{th} segment. Similar expressions to equation (8) and (9) can be written for the sound field at the center of the $(i+1)^{th}$ and the $(i-1)^{th}$ segments. To match the sound fields (continuity of pressure and axial particle velocity) at the junctions, it is necessary to transfer the sound field from the center of each segment to its side. For example for the ith segment, the sound field must be transferred from x_i to $x_i \pm h$, and this is done as follows,

$$P(r,\theta,x_i \pm h,t) = P(r,\theta,x_i,t) \pm \left(\frac{\partial P}{\partial x}\right)_{x_i} h \qquad (9)$$

where $$h\left(\frac{\partial P}{\partial x}\right)_{x_i} = h\left(\frac{\partial P^+}{\partial x} + \frac{\partial P^-}{\partial x}\right)$$

and $$h\left(\frac{\partial P^-}{\partial x}\right)_{x_i} = \sum_{n=0}^{\infty}\sum_{m=-\infty}^{\infty} A^i_{mn}\,\psi^m_n(r)\left[1 \pm \frac{h}{\psi}\frac{\partial \psi}{\partial x}\right] e^{-\gamma_i\left(1 \pm h\frac{\partial \gamma}{\partial x}\right)(q_i \pm h)} \qquad (10)$$

$h\frac{\partial P^-}{\partial x}$ is similar to equation (10) with B^i_{mn} replacing A^i_{mn}, ϕ replacing ψ, and q_i replacing γ_i.

A similar expression can be written for u_x, the axial particle velocity at $x_i \pm h$ in terms of u_x at x_i and the coefficients A^i_{mn} and B^i_{mn}. It may be noted that the mode shapes and the axial wave-vectors are computed for different values of x_i; hence the axial derivatives should be easy to evaluate.

Let the source be specified as a velocity u_s given as a function of r at $x=x_s$. The acoustic pressure at the source will be calculated below and let it be represented by P_s as a function of r. In matrix form the sound field in the first segment at $x_1-h=x_s$ can be written as

$$\begin{bmatrix} P_s \\ --- \\ u_s \end{bmatrix} = \begin{bmatrix} \\ T_1 \\ \\ \end{bmatrix}_{x_1-h} \begin{bmatrix} A^1_{mn} \\ B^1_{mn} \end{bmatrix} \qquad (11)$$

where each column in the matrix $[T_1]$ is a mode shape multiplied by the exponential function as given in equation (10).

By transposition and inversion of equation (11), one may obtain

$$\begin{vmatrix} A^1_{mn} \\ B^1_{mn} \end{vmatrix} \quad \begin{bmatrix} \\ R_{1s} \\ \\ \end{bmatrix} \begin{bmatrix} P_s \\ u_s \end{bmatrix} \qquad (12)$$

By applying the continuity of pressure and velocity, at the various junctions, it is possible to express the modal amplitudes in the last segment $x=x_\ell+h$ (that is the beginning of the inlet), ℓ being the number of segments the inlet is divided into in terms

of P_s and u_s,

$$\begin{bmatrix} A^{\ell}_{mn} \\ B^{\ell}_{mn} \end{bmatrix} = \begin{bmatrix} \quad R_{\ell s} \quad \end{bmatrix} \begin{bmatrix} P_s \\ \cdots \\ u_s \end{bmatrix} \tag{13}$$

where $R_{\ell s}$ is made up of products of similar matrices namely $[R_{1s}]$, $[R_{21}]$, $[R_{32}]$ and so on to $[R_{\ell(\ell-1)}]$ and is a function of the flow duct environment only. At the end of the inlet, each B_{mn} can be replaced by the corresponding A_{mn} multiplied by the modal radiation impedance of the inlet. This is discussed further in Section 4. Then it is possible to express A_{mn} and P_s in terms of u_s and elements of $R_{\ell s}$. Once P_s can be evaluated as explained above, the source radiation impedance (P_s/u_s) can be determined. The acoustic efficiency of the source is proportional to the real part of the radiation impedance of the source. In this way the influence of the boundary layer growth on the acoustic efficiency can be determined. The radiation from the inlet and the exhaust ducts is discussed in the next section.

4. RADIATION FROM DUCT TERMINATION IN PRESENCE OF INLET AND EXHAUST FLOWS

As shown in figure 1, the sound from the duct end must radiate through the incoming and jet exhausting flows. Such flows have axial and transverse gradients of the mean flow and temperature, the temperature gradients occuring mainly in the exhaust jet flow. Interactions with such flows will modify both the spectrum and the directivity due to convective and refractive effects. The sound field from such an environment has been studied by Schubert [5], Mungur, Plumblee and Doak [6] and Whitesides and Mungur [7]. Yu and Mungur analyzed the sound field in a helical jet flow [8]. The formulation of Mungur et al [6,7,8] allows the radiation impedance of a source or the duct end modal impedances to be evaluated taking into account both the convective and refractive effects of the jet. This method is summarized below.

The analysis of sound radiation from an arbitrary source distribution in terms of Legendre and spherical Hankel functions is well known. Mungur et al [6,7,8] extended this classical method of analysis to jet flow environments. A spherical wave-equation governing the sound field in such an environment was derived from the more basic linearized equations of momentum and mass conservation. The steady state flow and thermal and flow gradients in the

axial (that is radial) and transverse (angular) directions appear as coefficients to the terms of the wave-equation. The final form of the convected wave-equation was of the form,

$$[1-M^2]\frac{\partial^2 P}{\partial r^2} + \frac{2}{r}\left[1+f_1\right]\frac{\partial P}{\partial r} - \frac{2M}{c}\frac{\partial^2 P}{\partial r \partial t} + \frac{\partial^2 P}{r^2 \partial \theta^2} + \left[\cot\theta + f_2\right]\frac{\partial P}{r\partial\theta}$$

$$+ \frac{1}{r^2 \sin^2\theta}\frac{\partial^2 P}{\partial \phi^2} - \frac{1}{c^2}\frac{\partial^2 P}{\partial t^2} + f_3\frac{\partial P}{\partial t} + f_4 P = 0 \qquad (14)$$

where r, θ and ϕ define the spherical coordinate system, M is the radial flow normalized with respect to the speed of sound, and is a function of both the radial and angular coordinates. f_1 through f_4 are functions of the mean flow and transverse and axial gradients of the flow and of the temperature.

Radiation from any specified velocity or pressure source must satisfy the above wave-equation. It may be noted that if the mean flow and its gradients are set equal to zero, equation (14) reduces to the classical wave-equation in spherical coordinate and its solutions can be written in terms of Legendre and spherical Hankel functions. In the presence of the flow, modified Legendre and modified spherical Hankel functions are sought. Like in the inlet the equation is not separable due to the fact that the coefficients are functions of both coordinates. A separation is forced by using a solution of the form

$$P(r,\theta,\phi,t) = F(\theta,r)\frac{1}{r}\exp(j\omega t - jm\phi - \gamma r) \qquad (15)$$

where F and γ are weakly dependent on r and $\gamma$is complex when in the near field. m is an integer.

When equation (15) is substituted into equation (14), a reduced wave-equation from which F is obtained is given in the first approximation by

$$\frac{d^2F}{d\theta^2} + \left[\cot\theta + f_2\right]\frac{dF}{d\theta} + f_5 F = 0 \qquad (16)$$

where f_2 and f_5 are functions of both θ and r, and f_5 is also a function of the frequency ω, m and the undetermined γ. Equation (16) governs the directivity part of the solution. For a given ω, m and a flow field, at a specified value of r equation (16) has been integrated subject to angular boundary conditions yielding several values of γ and corresponding angular functions for F.

Some calculations have been done [6,7] for a flow field shown in figures 4, 5, and 6.

Figure 4 shows the modifications that take place to the classical Legendre functions when flow is present. The sound field contributed by each mode has a reduction along the axis. This is due to both convective and shear refraction. Figure 5 shows the competing effects of refraction by temperature gradients and convective and shear gradients. TR the temperature is defined as the ratio of the difference of the jet center line temperature T_m, and the ambient temperature T_o (outside the jet) to the ambient temperature T_o. Similar modifications occur to all the modes although the effects reduce for the higher order modes. Figure 6 shows the flow field for a helical flow and the effects of the swirling component of the mean flow on the directivity of various modes.

4.1 Evaluation of the radiation impedance of velocity source in the presence of a jet flow.

The evauation of the radiation impedance involves the evaluation of the acoustic pressure at the source plane. Because there are several values of γ and corresponding angular functions for F, the general expression for the acoustic pressure and the radial acoustic velocity can be written as

$$P = P^+ + P^- \tag{17}$$

$$u_r = u^+ + u^- \tag{18}$$

where

$$P^+ = \sum_{n=0}^{\infty} \sum_{m=-\infty}^{\infty} A_{mn} \psi_n^m(\theta) \frac{1}{r} e^{j\omega t - \gamma_{mn} r} \tag{19}$$

$$P^- = \sum_{n=0}^{\infty} \sum_{m=-\infty}^{\infty} B_{mn} \eta_n^m(\theta) \frac{1}{r} e^{j\omega t + q_{mn} r} \tag{20}$$

where ψ_n^m is the solution of equation (16) corresponding to the n^{th} positive value of γ. The q's are in fact the negative values of γ and η the corresponding mode shape. P^+ represents outgoing waves

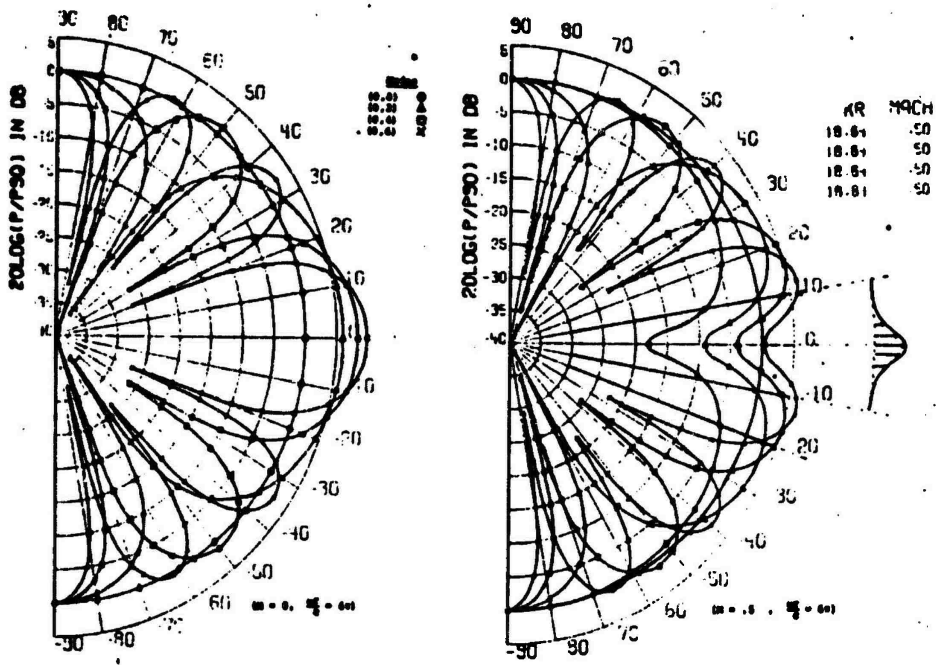

Figure 4 - Influence of ambient jet flow on the directivity of spherical modes. Fig. 4(a) no flow, directivity given by Legendre functions. Fig. 4(b) with flow; Legendre functions are modified.

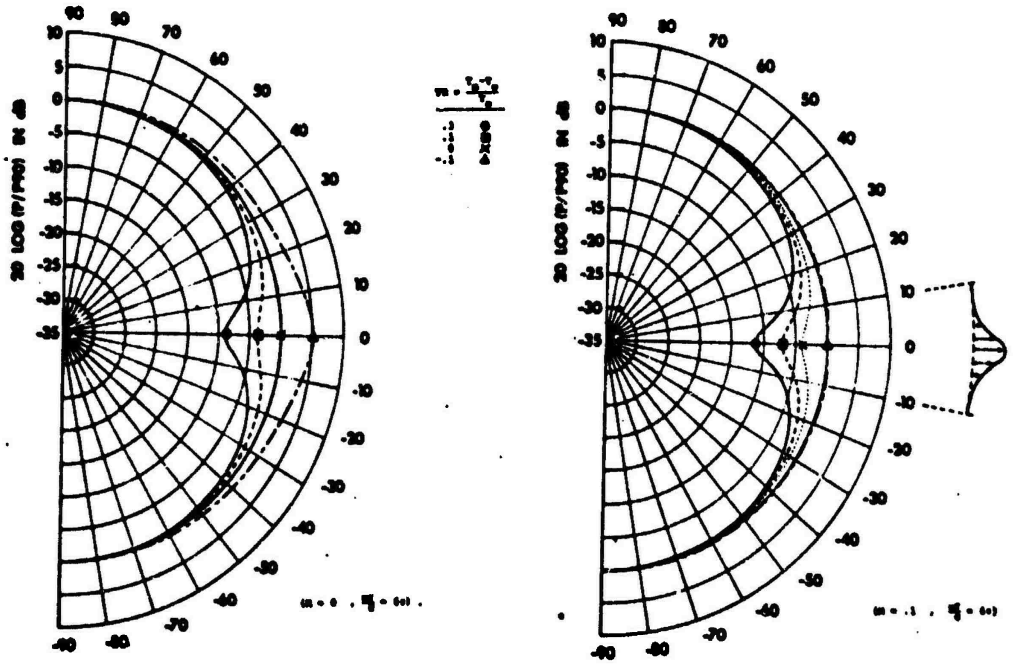

Figure 5 - Influence of jet center-line temperature ratio on the (0,0) mode. Neg TRmcold jet.

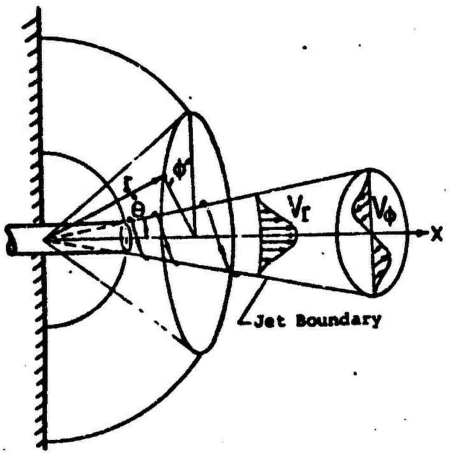

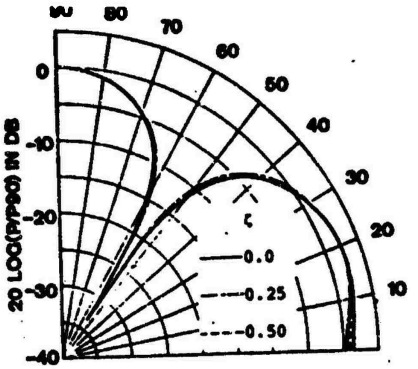

(b). (0,2) Mode

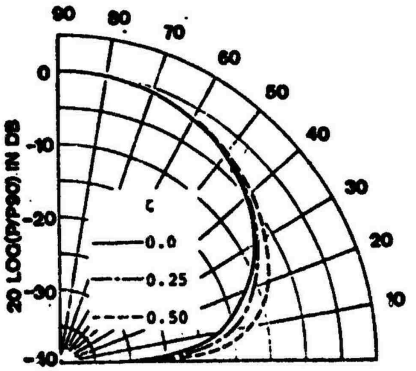

(c). (2,2) Mode

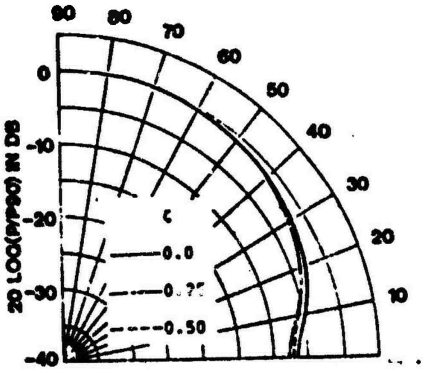

M_r =0.5, $\omega d/C_\infty$=π/2, r/d=8.

(a). (0,0) Mode

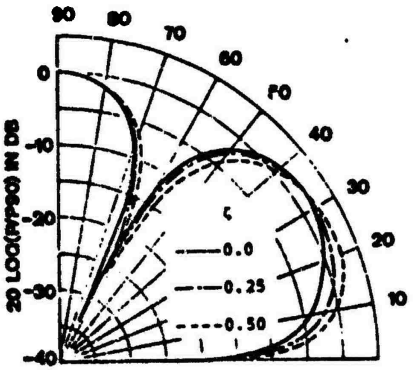

(d). (2,4) Mode

Figure 6 - Influence of swirl ratio S (= ratio of maximum swirl to axial components of total mean flow) on the spherical harmonic modal directivities.

and P^- incoming waves. u^+ and u^- are the axial particle velocities associated with the outgoing and incoming waves respectively. They may be expressed in terms of ψ, η and their derivatives and the amplitudes A_m and B_m. Both solutions are necessary because the flow in general changes continuously with r. Equations (18) and (19) express the sound field at a spherical surface given by a value of r where both the mode shapes and the radial wave-vectors are evaluated. Expressions similar to equation (18) and (19) can be written at different values of r.

Let the space surrounding the engine be subdivided into shells (see figure 1) and let $r=r_1$ be the radius of the center of the innermost shell. The coupling of the sound field to the source can only be done by transferring the sound field evaluated at r_1 to $r=r_1-h$, where the velocity source is located; h is the half width of the first shell. Let $u_s(\theta)$ be the velocity source distribution and P_s the pressure at the source which is to be evaluated. In matrix form, the continuity of pressure and radial particle velocity at the source may be expressed by

$$\begin{bmatrix} P_s \\ \cdots \\ u_s \end{bmatrix} = \begin{bmatrix} \\ T_1 \\ \\ \end{bmatrix}_{r_1-h} \begin{bmatrix} A^1_{mn} \\ B^1_{mn} \end{bmatrix} \tag{21}$$

where each column in the matrix $[T_1]$ is a mode shape multiplied by the exponential function as given by equations (17) through (20). The modal amplitudes A_{mn} and B_{mn} can be obtained by matrix transposition and inversion. Thus

$$\begin{bmatrix} A_{mn} \\ B_{mn} \end{bmatrix}_1 = \begin{bmatrix} \\ R_{1s} \\ \\ \end{bmatrix} \begin{bmatrix} P_s \\ \cdots \\ u_s \end{bmatrix} \tag{22}$$

where $[R_{1s}]$ is given by the products $[\,[T_1]^T[T_1]\,]^{-1}[T_1]^T$.

By applying the continuity of the pressure and the radial particle velocity at the junctions of the various shells into which the jet flow environment is divided into, it is possible to express the modal amplitudes in a distant shell $r=r_\ell$ (say) in terms of P_s and u_s as follows

$$\begin{bmatrix} A_{mn} \\ B_{mn} \end{bmatrix}_\ell = \begin{bmatrix} \\ R_{\ell s} \\ \\ \end{bmatrix} \begin{bmatrix} P_s \\ \cdots \\ u_s \end{bmatrix} \tag{23}$$

where $R_{\ell s}$ is made up of the products of ℓ transfer matrices. If r_ℓ is sufficiently large such that the flow changes vary little with r, then the reflected waves will be negligibly small and all the B_{mn}'s in the ℓ-th shell may be set equal to zero. Then it is possible to express A_{mn} in the ℓ-th shell and P_s as functions of u_s and elements of the matrix $[R_{\ell s}]$. Thus for a specified u_s, and a mean flow field, P_s can be evaluated, and (P_s/u_s) is then the radiation impedance. Further details on this section 4.1 can be found in a recent paper by Mungur and Plumblee[9].

5. DUCT TRANSMISSION LOSS OPTIMIZATION

One of the main purposes of theoretical acoustic modeling of sound propagation in ducts is the prediction of the condition when minimum transmission takes place. There are two mechanisms that can be used to cause maximum transmission loss in a duct. The first is to use the right material that gives maximum overall attenuation for all the modes. The second method is a reactive mechanism taking advantage of reflection at the discontinuity of a duct lined with two different impedances. It has recently been shown by Lansing and Zorumski [10] that more attenuation is obtained when a duct is lined in three sections than if the duct were homogeneously lined. One reason for the extra attenuation apart from the reflective effect is that the discontinuity in impedance causes several higher order modes to be excited and these higher order modes in general have higher attenuation coefficients.

Several standard optimization techniques are being evaluated for application to the multi-section duct problem, typical of these is the steepest gradient method as outlined below. The objective is to minimize the acoustic power transmitted through a given length of flow duct with a specified source distribution. The acoustic power propagating in the duct is a function of sections the duct is divided into, ℓ_i and A_i the length and admittance of each section. For one particular set of q, ℓ_i and A_i, and specified source and flow characteristics, the governing wave equation is solved in each section and the solutions matched from section to section starting from the source. In this way the sound field can be completely defined and hence the intensity and power can be evaluated. The gradient of the power with respect to each of the parameters q, ℓ_i and A_i are evaluated by changing one at a time. The gradients are then used to find the direction of maximum gradient in the q, ℓ_i, A_i plane. The values of q, ℓ_i are then incremented in the direction of maximum gradient. The power and its derivatives are re-evaluated. The power at this new point is compared with that at the previous point, if it is less, the above procedures are repeated until the power at the new point

is greater than at the previous point. Then the step size is halved and the above procedures repeated until a minimum is reached. From the practical point of view it is necessary to apply the following constraints on the following variables: the length of any section must not be smaller than a specified minimum, a practical limit on the admittances must be specified.

REFERENCES

1. A. Kapur and P. Mungur, 1973, AIAA Paper No. 73-1010, "Sound interaction with a helical flow contained in an annular duct with radial gradients of flow, density and temperature."
2. A. H. Nayeh, D. P. Telionis and S. G. Lekoudis, 1973, AIAA Paper No. 73-1008, "Acoustic propagation in ducts with varying cross-sections and sheared mean flow."
3. A. Kapur, P. Mungur and G. M. L. Gladwell, "Propagation in an inlet with boundary layer growth" unpublished. Submitted in part to Eighth International Congress on Acoustics, 1974, Paper Number 633.
4. P. Mungur and H. E. Plumblee, 1969, NASA SP-207, Basic Aerodynamic Noise Research. "Propagation and attenuation of sound in a soft walled annular duct containing a sheared flow."
5. L. K. Schubert, 1972, J. Acoust. Soc. Am. S1(2), Part 1 439-447, "Refraction of sound by a jet. A numerical study."
6. P. Mungur, H. E. Plumblee, P. E. Doak, 1974, J. Sound Vib. to be published in July, "Acoustic radiation analysis in jet flow environment."
7. J. L. Whitesides and P. Mungur, Nov. 1973, 86th Acoustical Society Meeting, "On the influence of temperature gradients in jet flows on radiation of sound."
8. J. C. Yu and P. Mungur, 1973, AIAA Paper No. 73-1004, "Acoustic wave propagation in an axisymmetric swirling jet."
9. P. Mungur and H. E. Plumblee, 1974, J. Sound Vib. submitted for publication, "The influence of the mean flow field of a jet on the radiation from a general spherical acoustic source of arbitrary pressure or velocity distribution."
10. D. L. Lansing and W. E. Zorumski, 1973, J. Sound Vib., Vol. 27, p. 85-100, "Effects of wall admittance changes on duct transmission and radiation of sound."

ACOUSTIC DISTURBANCES PRODUCED BY GAS NONUNIFORMITIES CONVECTING THROUGH A SUPERSONIC NOZZLE

by

Edward E. Zukoski

Daniel and Florence Guggenheim Jet Propulsion Center
California Institute of Technology
Pasadena, California

Introduction

When a region of nonuniform enthalpy ("entropy spot," s') is convected through a steady flow field where the mean properties change rapidly along the flow direction (such as the velocity gradient dU/dx), an acoustic source results which is of the order $(dU/dx)^2(s'/C_p)$. References 1 and 2 give some detailed analysis of such sources resulting from the passage of thermal nonuniformities through nozzles. Here, the strong field gradient (dU/dx or dP/dx) is provided by the nozzle contour.

Such sources are of particular importance in connection with combustion systems which invariably lead to nonuniform temperatures and consequent entropy fluctuations. A rather clear-cut example is the large scale fluctuation of temperature produced in an afterburner upstream of a nozzle. Where the nozzle is choked, the pressure fluctuation p' at the outlet, where the undisturbed pressure is p_2, gives the result that $p'/\gamma p_2 = \frac{1}{2}(M_1+M_2) \cdot \frac{1}{2}(T'/T_1)$ where $\frac{1}{2}(M_1+M_2)$ is the mean of the approach and discharge Mach numbers of the nozzle and T'/T_1 is the (random) fractional temperature fluctuation introduced by the combustion process ahead of the nozzle. The values T'/T_1 from 0.05 to 0.20, which are known to exist in both main burners and afterburners, thus lead to pressure fluctuations of a significant fraction of an atmosphere and, as a consequence, constitute a possible significant noise source.

A very similar and probably even more important situation occurs when the temperature fluctuations from the mean burner pass through the choked turbine nozzles. This source exists in the core engine of a high bypass ratio fan and consequently may be a dominant source of "excess noise" when the jet Mach number is low.

An experimental investigation has been initiated at Caltech with the financial support of the Office of Noise Abatement, DOT, to demonstrate the magnitude of these strong disturbance sources and to observe their actual strength in comparison with the results of extensive linearized analyses. In addition, it will be attempted to make measurements in the more complex case where the temperature disturbances approach the nozzle in a random fashion rather than as plane harmonic waves.

In the present paper we shall describe the experimental apparatus build for this investigation and the results of preliminary calculations and experiments.

Experimental Apparatus

The experimental apparatus to be used in the experimental program is described briefly in the following paragraphs. The equipment described here has been constructed and is now in operation.

Gas Supply. The gas supply system, shown schematically in Figure 1, was designed to maintain a flow of about one half kilogram per second to the test nozzle at a total pressure of 3 atmospheres and at a low turbulence level. Nitrogen gas is drawn from 20 high-pressure gas bottles which have an initial pressure of 170 atmospheres and a total capacity of 190 kilograms. A total operating time of about 100 seconds can be obtained with a single set of bottles. Operating procedures and quick-acting valves allow data to be taken over periods as short at 10 - 20 seconds.

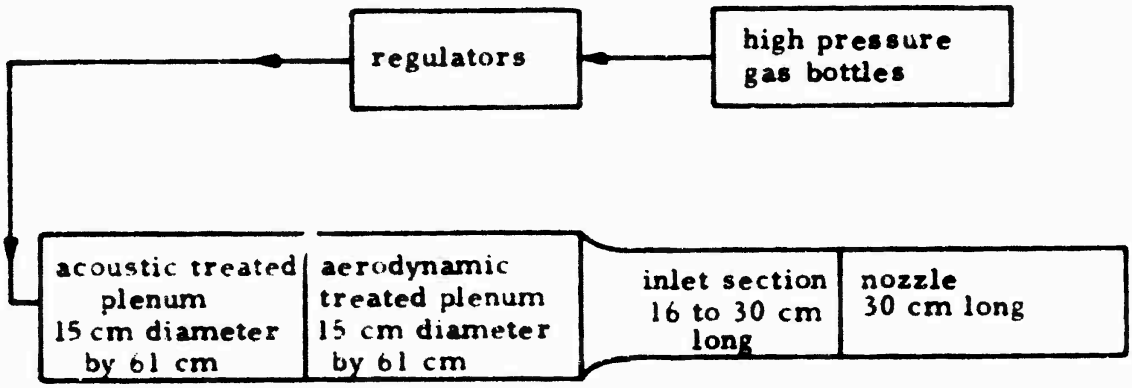

Figure 1. Schematic Diagram of Flow System.

Two dome-type regulators operating in series are used to hold the gas pressure constant during a run. They can be preset prior to the start of gas flow. Upstream of the nozzle and inlet sections, the gas first passes through a plenum chamber filled with fiberglas which was designed to reduce reflections. The second section of the plenum chamber contains four 44-mesh screens and a 15 cm long section of straws designed to reduce the turbulence level of the flow. The Mach number in this section is nominally 0.02.

After traversing a contraction, the gas passes into the inlet section, which has a cross section of 2.5 × 7.6 cm and which contains the heater and mass bleed equipment discussed below. The Mach number in this section is 0.20.

Nozzle. The supersonic nozzle section which follows next is rectangular in cross section. It is 30 cm long and the 2.5 × 2.5 cm cross section throat is located 20 cm from the inlet section. The nozzle currently in use has a nearly constant Mach number gradient of about 0.04 cm^{-1} and a less constant velocity gradient of about 100 sec^{-1}. Measurements of the mean static pressure field in the nozzle have been used to obtain corrections to estimates of the mean flow field made from measurements of the distribution of cross section area. Nozzle exit Mach number is 1.4.

Anechoic Chamber. The supersonic nozzle exhaust lies at the center face of an anechoic chamber which is cubic and has interior side dimensions

of 300 cm. The interior surface consists of fiberglas wedges which produce free space conditions within $\frac{1}{2}$ db inside the chamber for frequencies greater than 300 Hz. A photograph taken during the construction of this chamber, Figure 2a, illustrates the metal structure used to support the wedges. Test data indicate that the chamber operates satisfactorily for frequencies greater than 300 Hz. Typical data on sound pressure level are shown in Figure 2b, where the sound pressure level measured on the axis of a speaker decays with the distance from the speaker, as required by free field theory. Agreement with free space field theory is within $\frac{1}{2}$ db over the whole range of axial distances except for the 200 Hz signal.

Mass flow entering the chamber from the nozzle is exhausted from a 30 × 30 cm cross section acoustically-treated duct placed at the center of the opposite wall.

Pressure Measurements. Mean static pressures were measured in the nozzle at 6 cm intervals with a strain gauge pressure instrument. Pressure fluctuations are measured at five stations at intervals of about 7.5 cm with high-frequency response piezoelectric gauges. The three instruments available for these measurements must be moved between tests to allow the shole field to be studied. Three similar stations are located in the inlet section and three others in the plenum section.

Pressure fluctuation measurements in the anechoic chamber are made with two B&K capacitance type microphones.

Heater. The heater is made up of an array of 375 nichrome wires which are periodically heated by an electric current applied in the form of a square pulse wave train. The wires have a diameter of 0.010 cm and a length of 6.4 cm. Twenty-five of these wires are wound across two conductors 0.16 cm in diameter which are supported by a rectangular frame made from a phenolic plastic which is about 0.32 cm thick. The inside edges of this frame form the 2.5 × 7.6 cm cross-section dimensions of the inlet section duct. Fifteen of these frames are stacked up to form the complete heater. A single frame and the fifteen-frame stack are shown in the photograph of Figure 3. The wires in each frame are in parallel electrically and the frames are in series.

The electric current supply for the heater is drawn from a 0 - 300 V, 0 - 100 amp DC power supply. Two silicon controlled rectifiers switch the large current flow to generate a square-wave current pulse-train which drives the heater. The duty cycle can be varied from 0 - 100 per cent and the frequency from 0 - 12 k Hz.

The frequency can be controlled by either of the two techniques which are illustrated schematically in Figure 4. When the heater is operated alone, the SCR switch system is driven by a pulse generator set at the desired frequency. When both heate and bleed valve systems are acting simultaneously (the situation illustrated in Figure 4), we need to control the phase difference between the heater pulse and the valve position. This is done by directly measuring the valve position (photoelectrically) and using this signal in conjunction with a variable time delay or phase control system to set the phase of the SCR switch system. Calibration of this system to ensure that mass bleed and heat addition are exactly 180° out of phase is described in the

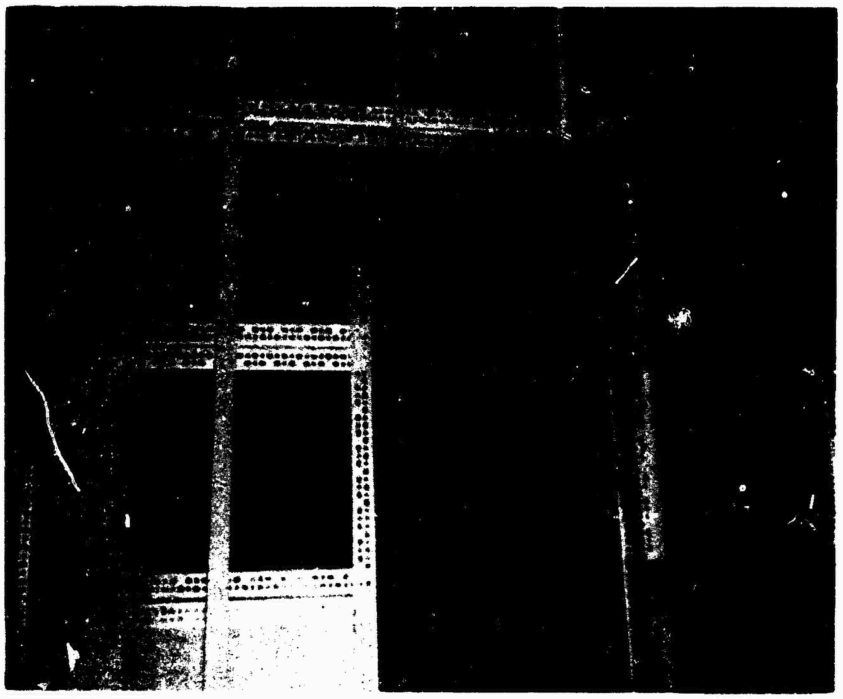

Figure 2a. Photograph of Anechoic Chamber Illustrating Construction Details.

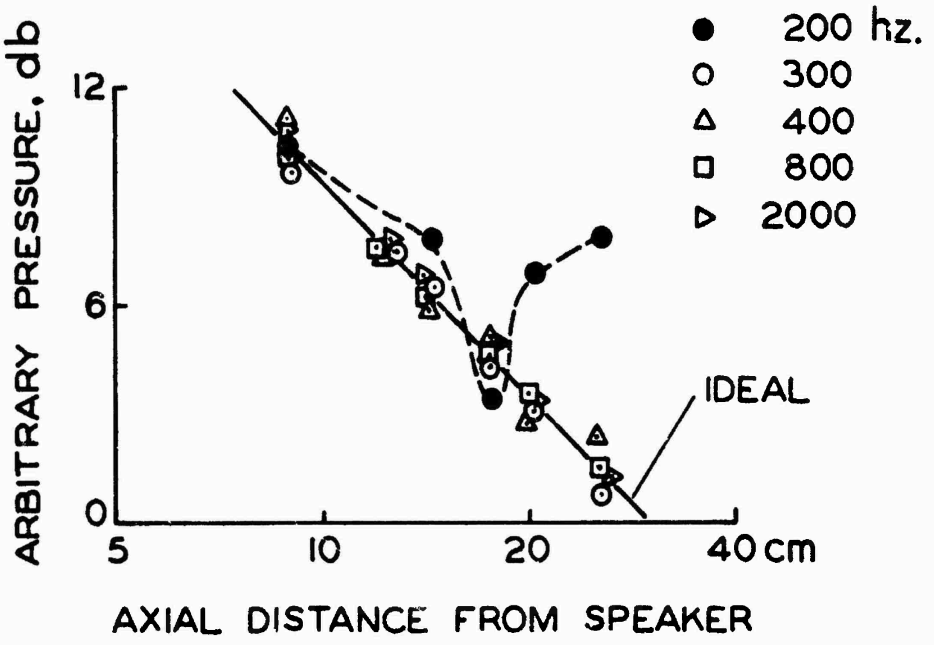

Figure 2b. Calibration Data for Anechoic Chamber.

next section.

A fluctuating temperature of a few degrees centigrate can be produced in the 0.5 kg/sec air flow with the heater system. The magnitude of this fluctuation is measured with a conventional constant-current hot wire anemometer set and a 0.001 cm diameter wire with a frequency response

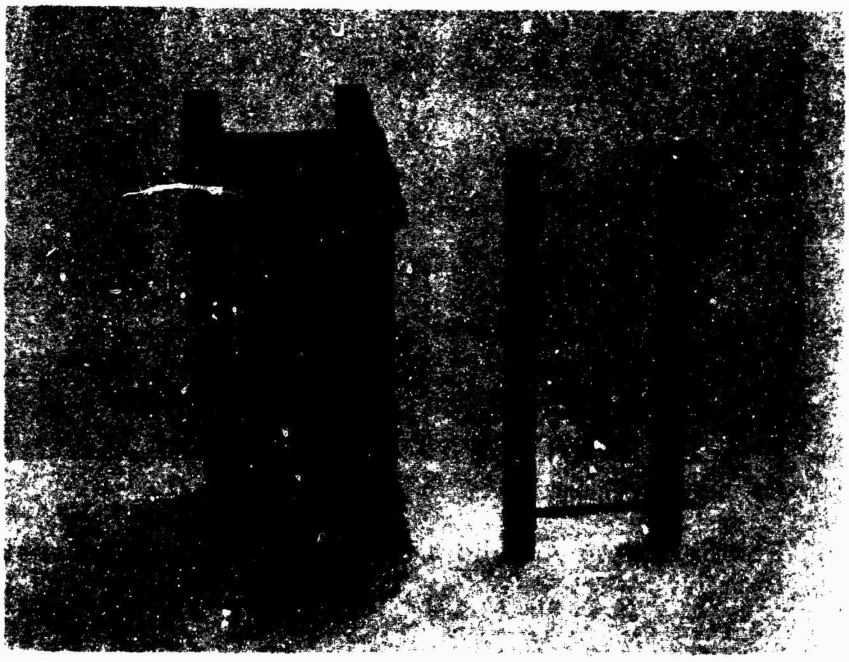

Figure 3. Photograph of Complete Heater Section and One Heater Frame.

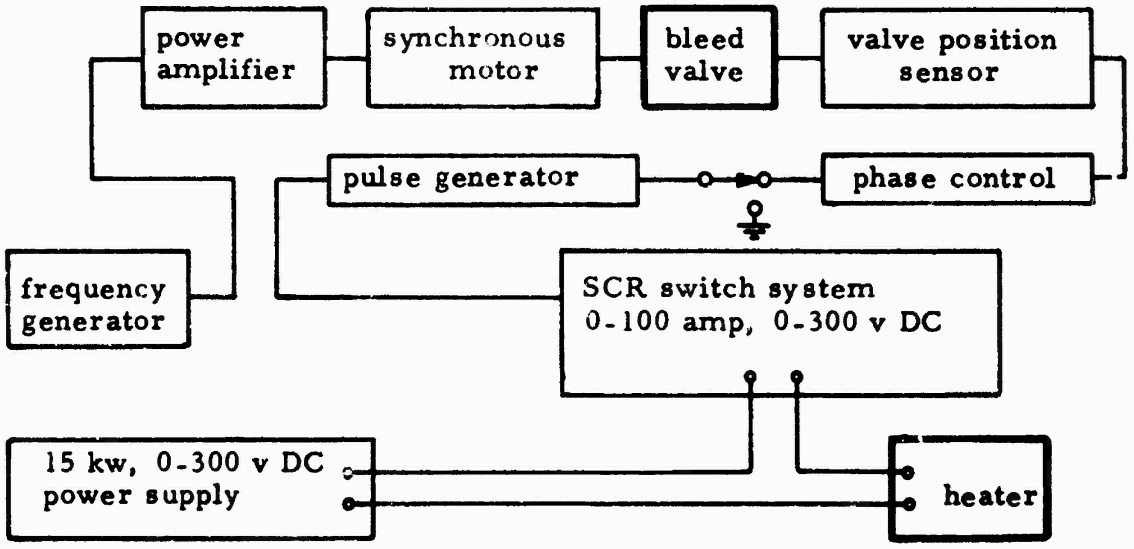

Figure 4. Schematic of Heater and Bleed Valve Control System.

several orders of magnitude above the heater operating frequency.

Bleed Valve. Mass is bled from the inlet section through one wall of the heater. The heater frames, described above and shown in Figure 3, are separated by about .0125 cm thick tape which is placed to make flow passages $.0125 \times 6.0$ cm in cross section between each frame. Sixteen of these passages in one side wall of the heater allow gas to pass into a shallow plenum chamber and on through a valve formed by a hole in a 1.25 cm rotating shaft. The mass flow rate is fixed by placing various calibrated orifices in the line downstream of the valve. The shaft in the valve is rotated by a synchronous motor which is driven by a signal generator and power amplifier, as indicated in Figure 4. Valve frequencies between 0 and 450 Hz can be obtained.

A photoelectric device is used in conjunction with an 0.032 cm hole through the shaft to determine the angular position of the shaft. The phase difference between the shaft position and the initiation of mass flow from the inlet duct was determined by monitoring the gas flow out of one of the bleed passages in the heater wall with a hot-wire anemometer. Given this phase difference, the phase control system shown in Figure 4 can be adjusted to fix the phase between heat addition and mass bleed as desired.

Data Acquisition and Processing

The pressure and temperature fluctuations introduced by the heater and bleed systems upstream of the nozzle are of the order of 1 to 1/10 per cent of the mean values of pressure and temperature. These relatively weak input signals produce pressure fluctuations in the duct which are of the order of 0.6×10^{-3} atm, or about 100 db. Because the background aerodynamic noise in the duct is of the same magnitude, signal processing is required to extract useful information.

The data acquisition and processing techniques are described in the following paragraphs.

Data Acquisition. Data are acquired from a variety of transducers as voltages, which are amplified to ensure that the signals of interest lie in the range between 10 volts and 10 mV. Using a Hewlett Packard 2100 Data Acquisition System, the signals are converted to digital values and are stored on a magnetic disc by the process shown schematically in Figure 5. Data in digital form are acquired by this system at a rate of 60 K words per second. Because a single disc is available, data can only be taken continuously for about 0.1 second when the 60 K sampling rate is used. This presents a difficulty, because we need long sampling periods to increase the signal to noise ratio of our data.

This difficulty is overcome, and the ease in processing the data is increased, by using a phase lock acquisition technique. Data acquisition is started when the logic circuit, Figure 5, simultaneously receives an "on" signal from the clock and a particular pulse from the heater or bleed valve input signal. Data acquisition terminates after about 0.10 seconds when the data buffer region of the computer core storage is filled with data. Each segment of data obtained in this manner starts with the same phase with respect to the input or forcing signal.

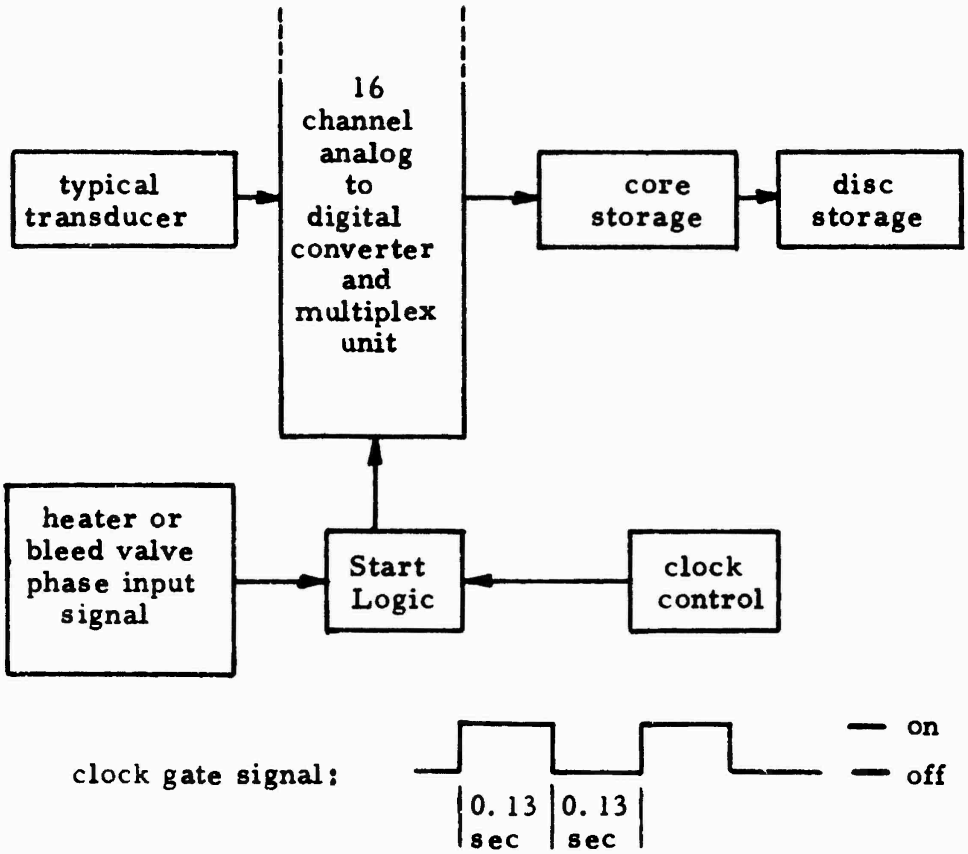

Figure 5. Schematic of Data Acquisition System.

This arrangement allows the signals to be phase averaged. In this process, the signals obtained from a large number of data samples and at a particular time after initiation of each data acquisition cycle are averaged. These average values are assembled for each sampling time to form a new signal which is one data segment long. The averaging process results in an increase in the amplitude of the signal in which we are interested (i.e., the signal produced by the response of the nozzle and supply system to the input signals), and a smaller increase in the noise. Because the signal of interest will increase linearly as the number of data segments is increased, and the noise will increase only as $\sqrt{N}$, a gain proportional to $\sqrt{N}$ is made in signal to noise ratio. In the present work, values of N between 60 and 150 are being used. Hence, a substantial gain can be made in signal to noise ratio.

The power of this process can be seen by comparing the two frequency spectra shown in Figure 6. The lower section was obtained from a single data segment 0.10 sec long. The upper spectrum is obtained from data obtained during the same experiment after averaging 100 data segments as outlined above. In this example, the response to a heater input signal is shown.

The outputs of 6 transducers are measured during a typical experiment, and each transducer output is sampled at 10 kHz. This rate gives us 25 samples per transducer per cycle for a 400 Hz wave and is much more than required to define the wave unambiguously.

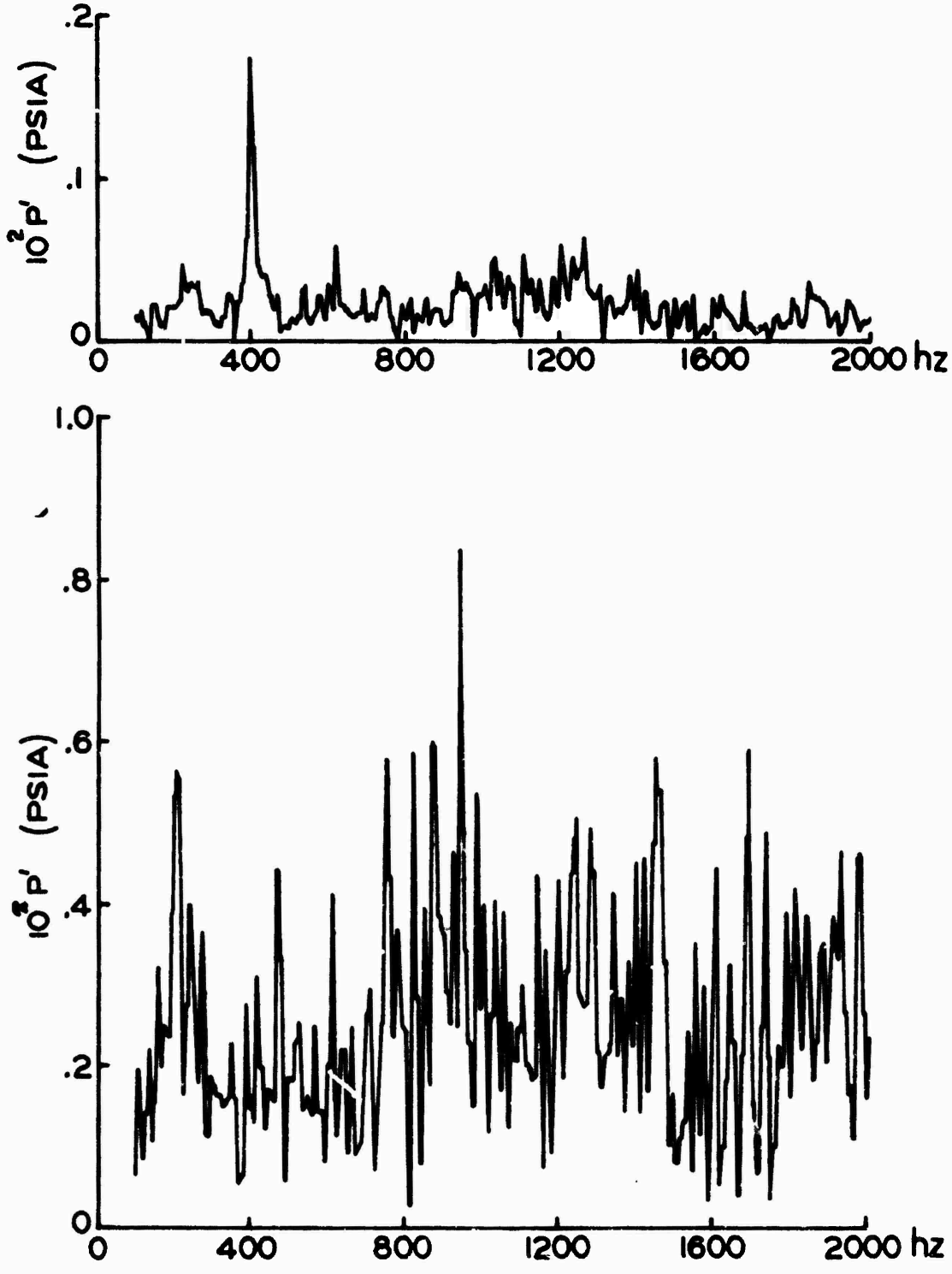

Figure 6. Typical Spectra Before and After Signal Averaging.

Typically, three channels are used to measure fluctuating pressures in the nozzle or inlet sections, one to measure temperature fluctuations produced by the heater, and the last two either for microphone measurements in the anechoic chamber or for measurements of mean flow quantities in the inlet section.

Data Processing. Data averaged by the technique described above have been processed on a digital computer by a Fourier transform technique to obtain spectra of the pressure signals similar to those shown in Figure 6. This analysis yields both the magnitude and the phase of the pressure signals induced by the input signals with a frequency resolution of about 10 Hz. Under certain circumstances, harmonics of the forcing frequency are set up and we can measure the response of the nozzle to input signals at a number of frequencies during the same experiment.

Cross-correlation programs have been developed and used to examine the relationship between signals produced in the nozzle and in the anechoic chamber.

In addition to these measurements obtained by this technique, phase relations between various transducer signals can be obtained. For example, measurements made at two positions 15 cm apart in the constant-area inlet duct can be used to obtain amplitude and phase of the downstream running wave and the upstream or reflected wave. This information is being used to connect calculated and measured fluctuation amplitudes for the nozzle. Similar data obtained from microphones will be used to examine the nature of the far field signal set up by the fluctuating signal leaving the nozzle exit.

Calculation

An analysis has been made of acoustic propagation through a one-dimensional duct of varying cross section area which contains a mean flow and periodic sources of heat and mass. The equations of motion are solved numerically for the mean flow through the duct for given cross section area variation under the assumption that the flow is isentropic. The equations are also linearized for the study of small flow perturbations about the mean flow due to heat and mass addition.

The energy equation for the perturbation quantities is not coupled to the continuity and momentum equations. It can be solved independently and used to match arbitrary input functions for heat addition. Manipulation of equations of continuity, momentum, and state leads to a pair of coupled, linear ordinary differential equations for the pressure and velocity perturbation fields.

The duct geometries investigated simulate the supply system starting at the plenum chamber, the inlet sections, the heater and bleed systems, and the supersonic nozzle used in the experiments. Solutions were obtained by numerical integration of the equations. Because the equations have a singularity at the throat, the numerical integration is started there and proceeds both up and down stream.

When the forcing function is a simple mass bleed, an upstream matching condition is specified either as an impedance at some point up-

stream or as an incident pressure wave at the nozzle entrance. In the latter case, the incident wave is obtained from the experimental determination of both incident and reflected waves. Given the determination of the subsonic solutions, the calculation can then be continued into the supersonic section of the nozzle.

A similar solution could be carried out for the case of a simultaneous heat and mass bleed. Entropy fluctuations are measured at the nozzle inlet and a solution of the entropy field is then obtained. Again, two pressure measurements are made in a straight section upstream of the nozzle entrance and a matching condition is calculated. The equations are solved using the matching condition to give a general solution from a homogeneous solution (no entropy fluctuation) and a non-homogeneous solution.

Solutions have been obtained for a range of geometric configurations, upstream matching conditions, and heat addition and mass bleed values. Typical results are given in Figures 7, 8, and 9, which are discussed in the following section.

Results

Considerable experience has been gained in operating the various systems and acquiring data. Pressure signals generated by operation of the bleed valve have been measured and compared with calculated values for a number of configurations. If the pressure signal incident on the nozzle is measured experimentally and is used as the upstream boundary condition on the calculation, good agreement is obtained between experimental and theoretical values. An example of these results is shown in Figures 7 and 8, where phase and amplitude data are shown in comparison with calculated values. Agreement between measured and calculated values of phase is excellent throughout the nozzle (0 - 12 inches). Measured and calculated values of amplitude differ by about 10 to 15 per cent. Comparison between calculated and measured values of the phase and amplitude of the wave reflected at the nozzle entrance is also good.

In general, the calculation scheme used here has been most successful when measured values of the amplitude and phase of the downstream running pressure fluctuation are applied as a condition at the nozzle inlet (as was done for the results shown in Figures 7 and 8). Attempts to compare calculated results for the whole system (plenum chamber to exit nozzle) with measured values have been less satisfactory. This result is probably due to poor acoustic modeling of the heater-bleed valve system and the plenum chamber impedance. The development of a better modeling scheme for these components is being investigated. In any event, the calculations show that when both pressure and entropy fluctuations are incident on the nozzle, the pressure fluctuation field produced in the nozzle is a sensitive function of duct geometry and phase differences between entropy and pressure fluctuations at the nozzle inlet.

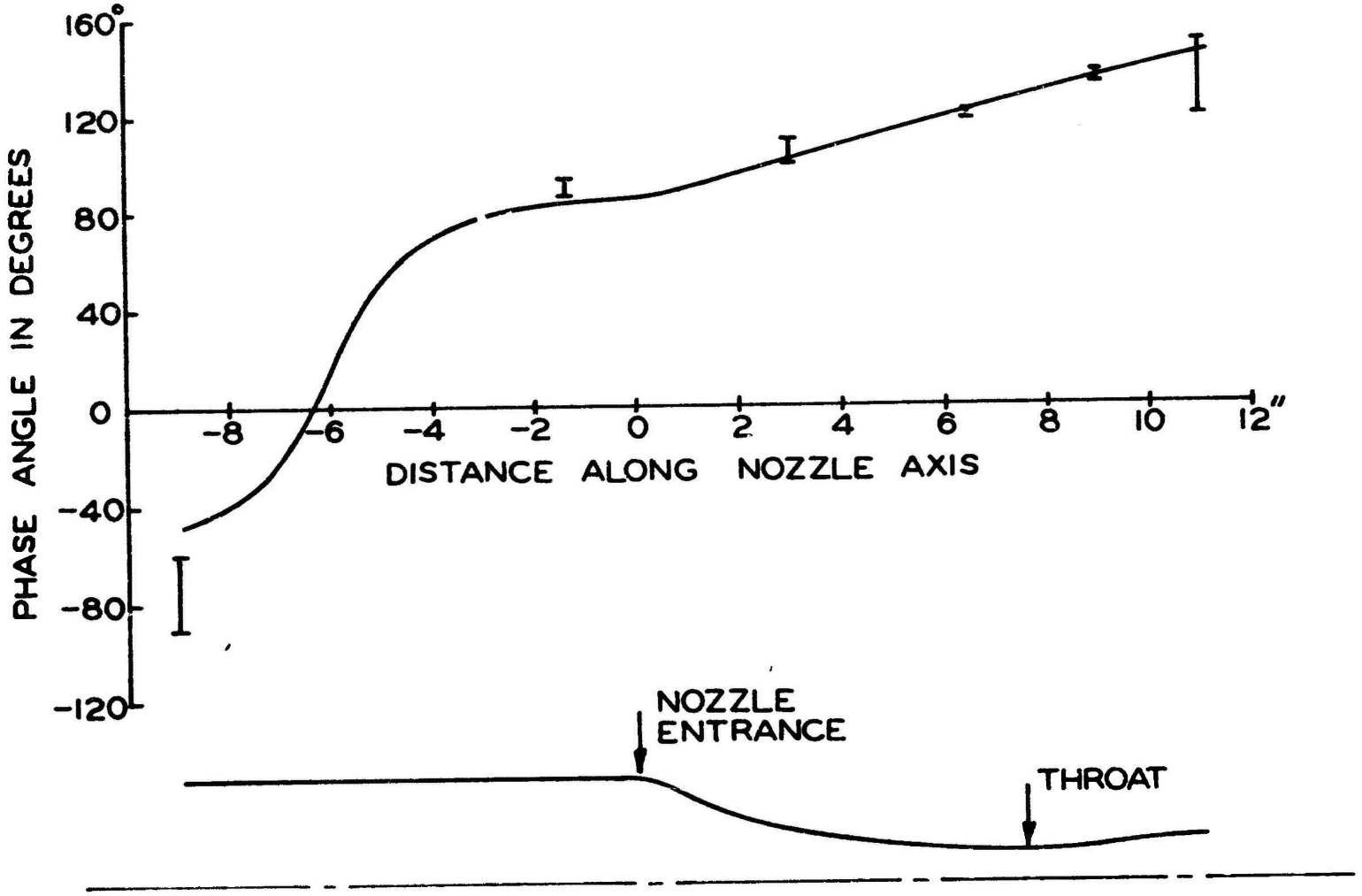

Fig. 7 Phase of Pressure Signal Produced by Mass Bleed Valve; Calculated and Measured Values.

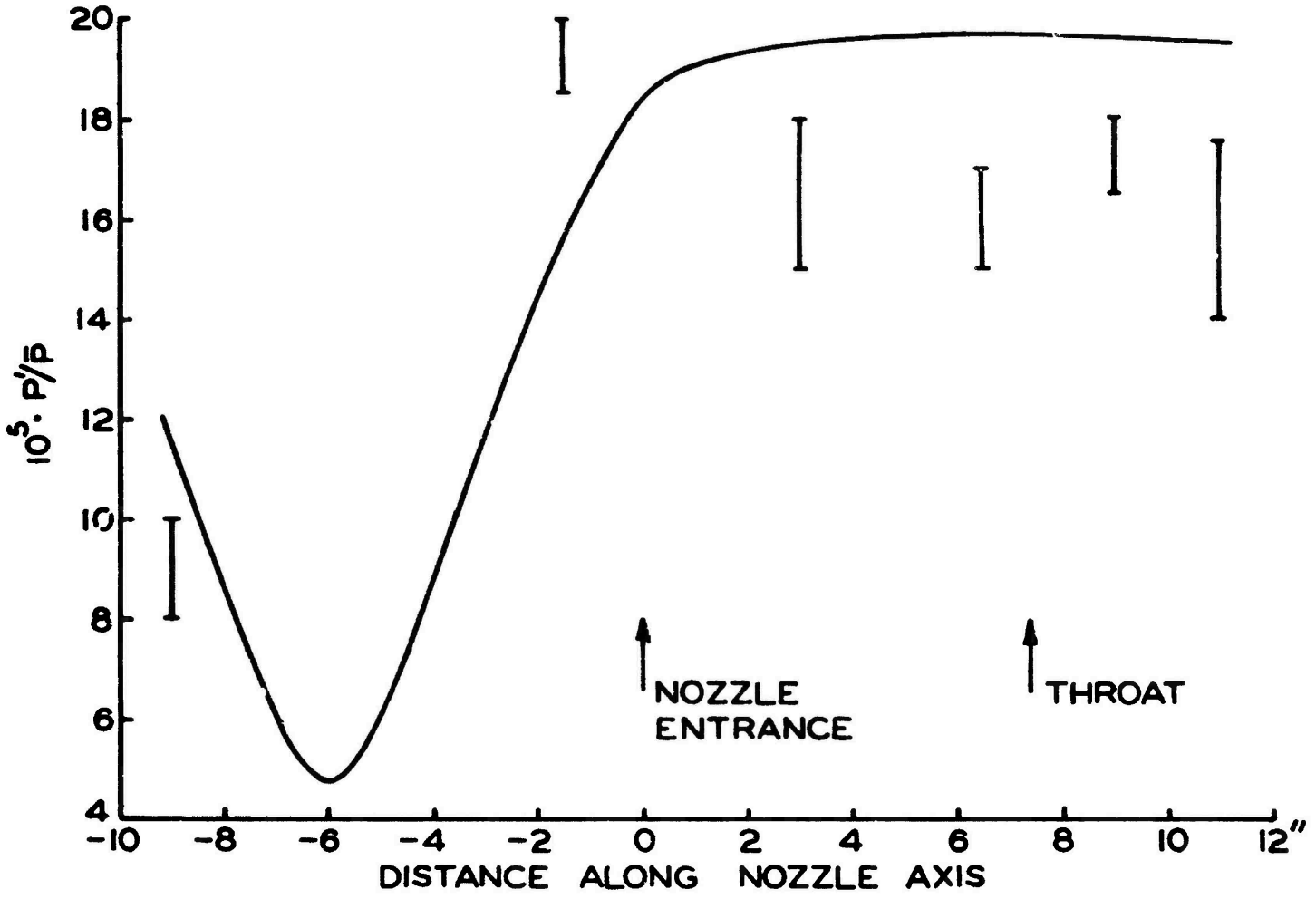

Fig. 8 Amplitude of Pressure Signal Produced by Mass Bleed Valve; Calculated and Measured Values.

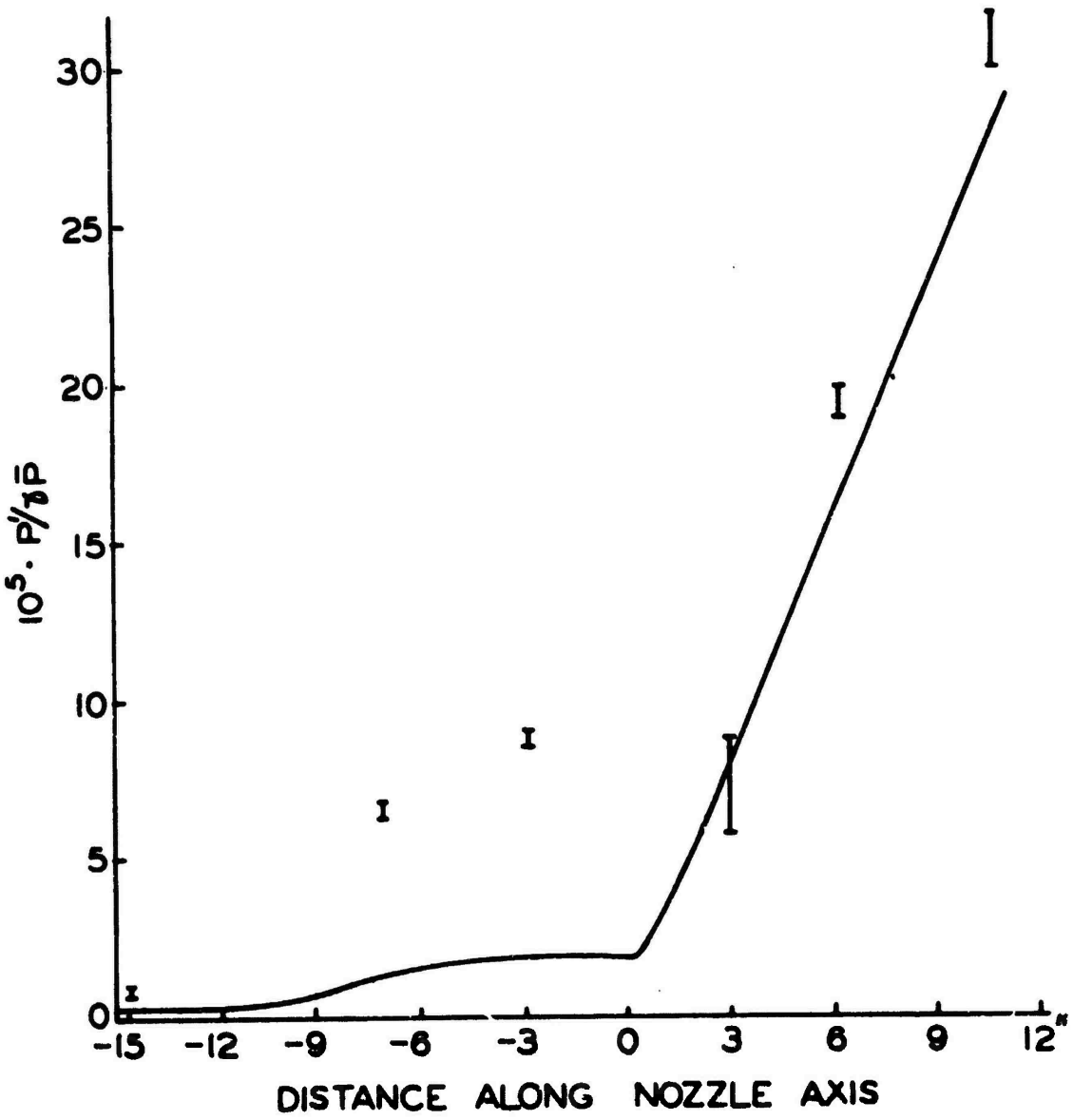

Figure 9. Amplitude of Pressure Signal Produced by Heater; Calculated and Measured Values.

When the heater is operating, it produces both temperature or entropy fluctuations and pressure fluctuations. These pressure fluctuations are large enough to obscure to a certain extent the pressure field generated by the interaction of the entropy fluctuations with the nozzle, and hence are undesirable. We have attempted to reduce the amplitude of these signals by using the bleed valve plenum and inlet ports as a Helmholtz damper. Figure 9 shows a typical set of data obtained with this approach and compares it with a calculation based on the assumption that entropy fluctuations, but no pressure fluctuations, move downstream to the nozzle. The agreement is good in the nozzle but not farther upstream.

The linear rise in the nozzle is typical of the variation of pressure fluctuations produced by entropy fluctuations, and this behavior is in strong contrast to the almost constant amplitude of the pressure fluctuation (e.g. Figure 8) produced by the mass bleed system. Calculations indicate that this difference persists from almost quasi-steady conditions, when the period of the disturbance is comparable to the transit time of gas in the nozzle, up to conditions when the period of 1/10 of that time.

Examination of Figure 9 shows that the degree of damping achieved with the bleed system was not satisfactory, and a second scheme is now being developed. In this approach, the bleed valve system will be used to allow gas to be removed periodically from the inlet duct at the heater position with the phase and amplitude required to cancel the pressure signal produced by heat addition. Preliminary efforts to produce cancellation have been successful. This investigation is being continued.

Measurements of the pressure field produced in the anechoic chamber by disturbances in the nozzle have also been started. Even with the large background signals produced by the jet, the far field signals produced by the small amplitude signals generated within the nozzle are large enough to be observed. Correlation between pressure fluctuations in the nozzle and in the far field have been made and are now being used to study the nature of this radiation field.

References

1. Candel, S. "Analytical Studies of Some Acoustic Problems of Jet Engines," Ph. D. Thesis, California Institute of Technology, Pasadena, Calif. (Dec. 1971).

2. Marble, F. E. "Acoustic Disturbance from Gas Nonuniformities Convected through a Nozzle," Proceedings, Interagency Symposium on University Research in Transportation Noise, Vol. II, Stanford University (March 28-30, 1973).

THE ATTENUATION OF UNSTEADY DISTURBANCES IN AXIAL COMPRESSORS

by

W. Duncan Rannie

Daniel and Florence Guggenheim Jet Propulsion Center
California Institute of Technology
Pasadena, California

1. Introduction

The effects of unsteady disturbances on a compressor are difficult to analyze in general because of the complexity of the interactions with the blade geometry. A simplification is possible if the disturbance wave lengths are long compared with the axial length of a single stage of the compressor. Then the effects of the alternating contractions and expansions of area through the blade rows tend to cancel, leaving only the cumulative effect of blade forces to interact strongly with the disturbance. The model that is proposed is one with blade forces spread uniformly in the circumferential direction and distributed continuously in the axial direction, that is, discontinuous blade forces replaced by continuous equivalent body forces. The body forces depend on local flow conditions in the compressor in the same way as the blade forces that they replace.

This note is confined to a discussion of plane disturbance with radial variations neglected so the compressor can be replaced by a one-dimensional model. Although disturbance wave lengths are very long compared with the axial length of the blades, they are not necessarily very long compared with the compressor.

2. Equations of Motion

In the one-dimensional model of the compressor, the coordinate x is along the compressor axis and the blade height h is a function of x. The axial and circumferential components of velocity are u and v respectively, the pressure p, density ρ, and temperature T. The equations of motion for a plane disturbance with blade forces represented by body forces are

$$\frac{\partial}{\partial t}(\rho h) + \frac{\partial}{\partial x}(\rho h u) = 0 \tag{2.1}$$

$$\rho\left(\frac{\partial u}{\partial t} + u\frac{\partial u}{\partial x}\right) + \frac{\partial p}{\partial x} = \frac{\rho \bar{u}^2}{a^2} X(u/\bar{u}) \tag{2.2}$$

$$\rho\left(\frac{\partial v}{\partial t} + u\frac{\partial v}{\partial x}\right) = \frac{\rho \bar{u}^2}{a^2} Y(u/\bar{u}) \tag{2.3}$$

$$\rho C_p\left(\frac{\partial T}{\partial t} + u\frac{\partial T}{\partial x}\right) - \left(\frac{\partial p}{\partial t} + u\frac{\partial p}{\partial x}\right) = \rho u \frac{\bar{u}^2}{a^2} F(u/\bar{u}) \tag{2.4}$$

where a is the compressor length, $\bar{u}$ is a constant reference velocity to be chosen later, X and Y are the dimensionless forces per unit height replacing the blade forces, and F is the non-isentropic resultant of these forces. The resultant F is responsible for any increase of entropy in the compressor. X, Y, and F are functions of local axial velocity only.

3. The Body Forces Representing the Blades

Assume that the flow angle leaving a stage is the same as the flow angle entering and that there is no change in axial velocity through the stage. The stage configuration and the appropriate velocity diagram are shown in Figure 1. The temperature rise for two-dimensional flow through the stage is given by

$$C_p \Delta T = V_r^2 \left[1 - \frac{u}{V_r} (\tan\beta_e + \tan\gamma_e) \right] \tag{3.1}$$

where V_r is the rotor blade speed, β_e and γ_e the leaving angles relative to rotor and stator respectively. Since the velocity is the same leaving the stage as entering, ΔT can represent either stagnation or static temperature rise.

If β_e and γ_e are constants, independent of inlet angles to respective blade rows

$$C_p \Delta T = V_r^2 (1 - \Omega u / V_r) \tag{3.2}$$

where $\Omega = \tan\beta_e + \tan\gamma_e$ = constant. For irrotational (inviscid) flow through the blade rows, cascade theory shows that the form $C_p \Delta T = V_r^2 (\Omega_o - \Omega u / V_r)$ is still valid where Ω_o and Ω are constants even when β_e and γ_e are functions of the incident flow angles β_i and γ_i. For real fluid flow through the stage, the coefficient Ω may depend on u/V_r, although generally the dependence is quite weak.

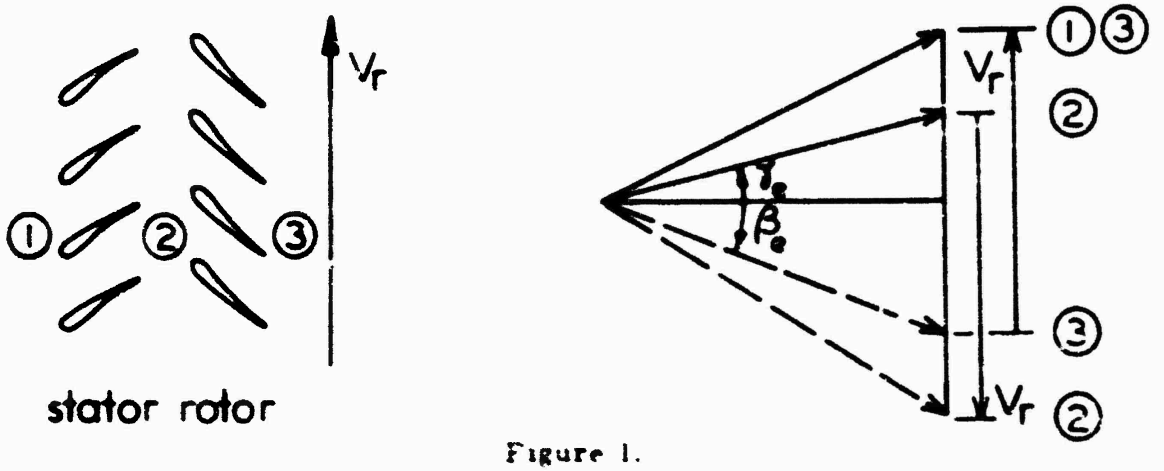

Figure 1.

The average axial length of a stage is a N where N is the number of stages, so the equivalent continuous distribution of temperature can be written as

$$C_p \frac{dT}{dx} = \frac{N}{a} V_r^2 \left(1 - \Omega \frac{u}{V_r} \right) . \tag{3.3}$$

If η is the "infinitesimal stage" efficiency, then

$$\frac{1}{p}\frac{dp}{dx} = \frac{\gamma}{\gamma-1}\eta\frac{1}{T}\frac{dT}{dx} \quad . \tag{3.4}$$

Strictly, the pressures and temperatures above should be evaluated at stagnation conditions, but with small velocity changes they can be interpreted as static conditions without much error. From Eq. (3.4), applying the ideal gas equation $p = R\rho T$,

$$\frac{dp}{dx} = \frac{\gamma}{\gamma-1}\eta R\rho\frac{dT}{dx} = \rho\eta\frac{N}{a}V_r^2\left(1-\alpha\frac{u}{V_r}\right) \quad . \tag{3.5}$$

For steady state, and ignoring the dependence of dp/dx on du/dx,

$$\rho u\frac{du}{dx} + \frac{dp}{dx} = \frac{\rho\bar{u}^2}{a}X = \rho\eta\frac{N}{a}V_r^2\left(1-\alpha\frac{u}{V_r}\right) \tag{3.6}$$

and hence under steady state conditions

$$X = N\left(\frac{V_r}{\bar{u}}\right)^2\eta\left(1-\alpha\frac{u}{V_r}\right) \tag{3.7}$$

and further, from the energy equation,

$$\rho C_p u\frac{dT}{dx} - u\frac{dp}{dx} = (1-\eta)\rho u C_p\frac{dT}{dx} = (1-\eta)\rho u\frac{N}{a}V_r^2\left(1-\alpha\frac{u}{V_r}\right) = \rho u\frac{\bar{u}^2}{a}F$$

so that

$$F = \frac{1-\eta}{\eta}X \quad . \tag{3.8}$$

In general, η and α are functions of u/V_r, and the forms chosen for the body forces in Eqs. (2.1), (2.2), and (2.4) are seen to be appropriate.

In the examples that follow, the design operating condition for the compressor is chosen to correspond to $u = \bar{u}$ = constant and dT/dx = constant = $(T_2-T_1)/a$ so that

$$T = T_1 + \frac{T_2-T_1}{a}x \quad .$$

Such a choice simplifies calculations while remaining realistic. With bars ($\bar{}$) to denote design, or undisturbed values, $\bar{\rho}\bar{u}\bar{h} = \dot{m}$ = constant where ρ and h are functions of x, and

$$\frac{1}{\bar{p}}\frac{d\bar{p}}{dx} = \bar{\eta}C_p\frac{dT}{dx} = \bar{\eta}C_p\frac{T_2-T_1}{a} = \frac{\bar{u}^2}{a}\bar{X} \quad \text{or} \quad \bar{X} = \bar{\eta}C_p\frac{T_2-T_1}{a} \quad .$$

If the average flow angle through the compressor does not change appreciably over the axial length and $\bar{u}$ is constant, the momentum equation for the cir-

cumferential direction can be ignored.

4. Small Disturbances

Restricting the disturbances to small amplitude about the design operating condition for all points within the compressor and assuming that at design the efficiency is at its maximum everywhere, replace p, ρ, and u by $\bar{p}(1 + p/\bar{p})$, $\bar{\rho}(1 + \rho/\bar{\rho})$, and $\bar{u}(1 + u/\bar{u})$, respectively, where p, ρ, and u are now the disturbed values. Introduce dimensionless length $\xi = x/a$ and dimensionless time $\tau = \bar{u}t/a$ and retain linear terms only; then

$$\frac{\partial}{\partial\tau}(\rho/\bar{\rho}) + \frac{\partial}{\partial\xi}\left(\frac{\rho}{\bar{\rho}} + \frac{u}{a}\right) = 0 \tag{4.1}$$

$$\frac{\partial}{\partial\tau}\left(\frac{u}{\bar{u}}\right) + \frac{\partial}{\partial\xi}\left(\frac{u}{\bar{u}}\right) + \frac{RT_1}{\bar{u}^2}\left(1 + \frac{\Delta T}{T_1}\xi\right)\frac{\partial}{\partial\xi}\left(\frac{p}{\bar{p}}\right) + \bar{X}\left(\frac{p}{\bar{p}} - \frac{\rho}{\bar{\rho}}\right) - \bar{X}'\frac{u}{\bar{u}} = 0 \tag{4.2}$$

$$\frac{RT_1}{\bar{u}^2}\left(1 + \frac{\Delta T}{T_1}\xi\right)\left(\frac{\partial}{\partial\tau} + \frac{\partial}{\partial\xi}\right)\left(\frac{p}{\bar{p}} - \gamma\frac{\rho}{\bar{\rho}}\right) + (\gamma - 1)\frac{1-\eta}{\eta}\left\{\bar{X}\left(\frac{p}{\bar{p}} - \frac{\rho}{\bar{\rho}}\right) - \bar{X}'\frac{u}{\bar{u}}\right\} = 0 \tag{4.3}$$

Here, $\bar{X}' = \{dX/d(u/\bar{u})\}_{u/\bar{u}=0}$ and η = constant.

For disturbances that are sinusoidal in time, let $p/\bar{p}$, $\rho/\bar{\rho}$, $u/\bar{u} \propto e^{-i\omega\tau}$ where $\omega = \nu a/\bar{u}$ with ν the disturbance frequency. Then the equations of motion become

$$\left(\frac{d}{d\xi} - i\omega\right)\left(\frac{\rho}{\bar{\rho}}\right) + \frac{d}{d\xi}\left(\frac{u}{\bar{u}}\right) = 0 \tag{4.4}$$

$$\left(\frac{d}{d\xi} - i\omega\right)\left(\frac{u}{\bar{u}}\right) + \frac{1}{2M_1^2}\left(1 + \frac{\Delta T}{T_1}\xi\right)\frac{d}{d\xi}\left(\frac{p}{\bar{p}}\right) = -\bar{X}\left(\frac{p}{\bar{p}} - \frac{\rho}{\bar{\rho}}\right) + \bar{X}'\frac{u}{\bar{u}} \tag{4.5}$$

$$\frac{1}{\gamma M_1^2}\left(1 + \frac{\Delta T}{T_1}\xi\right)\left(\frac{d}{d\xi} - i\omega\right)\left(\frac{p}{\bar{p}} - \gamma\frac{\rho}{\bar{\rho}}\right) = -(\gamma - 1)\frac{1-\eta}{\eta}\left\{\bar{X}\left(\frac{p}{\bar{p}} - \frac{\rho}{\bar{\rho}}\right) - \bar{X}'\frac{u}{\bar{u}}\right\} \tag{4.6}$$

These equations have variable coefficients and are best solved numerically unless the temperature ratio $\Delta T/T_1$ is very small.

The compressor can be considered as connected to ducts of uniform cross section upstream and downstream. The disturbance equations for such ducts are

$$\left(\frac{d}{d\xi} - i\omega\right)\left(\frac{\rho}{\bar{\rho}}\right) + \frac{d}{d\xi}\left(\frac{u}{\bar{u}}\right) = 0 \tag{4.7}$$

$$\left(\frac{d}{d\xi} - i\omega\right)\left(\frac{u}{\bar{u}}\right) + \frac{1}{\gamma M^2}\frac{d}{d\xi}\left(\frac{p}{\bar{p}}\right) = 0 \tag{4.8}$$

$$\left(\frac{d}{d\xi} - i\omega\right)\left(\frac{p}{\bar{p}} - \gamma\frac{\rho}{\bar{\rho}}\right) = 0 \tag{4.9}$$

and the solutions of these equations are

$$\frac{p}{\bar{p}} = \left[A e^{i\omega\frac{M}{1+M}\xi} + B e^{-i\omega\frac{M}{1-M}\xi} \right] e^{-i\omega\tau} \tag{4.10}$$

$$\frac{\rho}{\bar{\rho}} = \frac{1}{\gamma}\left[A e^{i\omega\frac{M}{1+M}\xi} + B e^{-i\omega\frac{M}{1-M}\xi} \right] e^{-i\omega\tau} + C e^{-i\omega(\xi-\tau)} \tag{4.11}$$

$$\frac{u}{\bar{u}} = \frac{1}{\gamma M}\left[A e^{i\omega\frac{M}{1+M}\xi} - B e^{-i\omega\frac{M}{1-M}\xi} \right] e^{-i\omega\tau} \tag{4.12}$$

The constants A , B , and C correspond respectively to a wave of acoustic type moving downstream with velocity $c+\bar{u}$, an acoustic wave moving upstream with velocity $c-\bar{u}$, and an entropy or temperature wave convected downstream with velocity $\bar{u}$. The three independent solutions of eqs. (4.4) to (4.6) for flow within the compressor are analogous, although they cannot be uncoupled in the same way. The solutions for the disturbance flow in the duct upstream and downstream of the compressor, i.e., the expressions (4.10) to (4.12) with subscripts $(\ )_1$ and $(\ )_2$ say on A, B, C, and M are jointed to the numerical solutions for the compressor so $p/\bar{p}$, $\rho/\bar{\rho}$, and $u/\bar{u}$ are continuous at the compressor entrance and exit.

The three independent solutions of the disturbance equations for the system of compressor and associated inlet and exit ducts can be superimposed with three arbitrary constants to satisfy three external conditions. The most convenient normal forms for the independent solutions are

(1) $A_1 = 1$, $C_1 = 0$, $B_2 = 0$: A wave of acoustic type of pressure amplitude unity approaching from upstream: no entropy wave convected from upstream, no acoustic wave proceeding upstream in the exit duct.

(2) $A_1 = 0$, $C_1 = 1$, $B_2 = 0$: An entropy or temperature wave of density amplitude unity convected downstream into the compressor inlet; no acoustic waves approaching the compressor from upstream or downstream.

(3) $A_1 = 0$, $C_1 = 0$, $B_2 = 1$: An acoustic wave of pressure amplitude unity approaching the compressor exit from downstream; no incident acoustic or entropy waves at the compressor inlet.

Numerical Example

As a representative numerical example, the values following were chosen:

$T_1 = 500^\circ R$, $T_2 = 900^\circ R$ R (gas constant) = 1716.6 ft.lb./slug $^\circ F$

$\gamma = 1.400$ $\eta = 0.84$ $p_2/p_1 = (1.8)^{3.5 \times 8.4} = 5.630$

$V_r = 1000$ ft/sec $\bar{u} = 600$ ft/sec

work coefficient $\Psi = 2C_p(T_2-T_1)\,NV_r^2 = 0.6008$ for N = 8 stages

$$1-\alpha\frac{\bar{u}}{V_r} = \frac{\Psi}{2} = 0.300 \qquad \tan\beta_e + \tan\gamma_e = \alpha = 1.1667$$

$$\bar{X} = 5.6 \qquad \bar{X}' = -13.067$$

With these values, Table I below lists the values of A_1, B_1, C_1 ; A_2, B_2, C_2 in magnitude and phase for the normal forms of the solutions at values of the reduced frequency of 0.25, 1.0, and 4.0.

TABLE I

	$x = 0.25$		$x = 1.00$		$x = 4.0$	
	Mag.	Phase ($^\circ$)	Mag.	Phase ($^\circ$)	Mag.	Phase ($^\circ$)
A_1	1.0000	0	1.0000	0	1.0000	0
B_1	1.1491	4.80	1.0666	17.56	0.7149	41.22
C_1	0	0	0	0	0	0
A_2	0.5090	6.08	0.4614	[illegible]27	0.2614	49.88
B_2	0	0	0	0	0	0
C_2	0.0746	-11.76	0.0955	-34.80	0.1176	-66.37
A_1	0	0	0	0	0	0
B_1	0.3454	-173.03	0.3009	-155.48	0.1799	-131.77
C_1	1.0000	0	1.0000	0	1.0000	0
A_2	0.0960	-5.78	0.1370	-2.96	0.1781	81.87
B_2	0	0	0	0	0	0
C_2	0.9798	0.19	0.9706	0.50	0.9324	-0.41

TABLE I (continued)

	$\omega = 0.25$		$\omega = 1.00$		$\omega = 4.00$	
	Mag.	Phase (^{o})	Mag.	Phase (^{o})	Mag.	Phase (^{o})
A_1	0	0	0	0	0	0
B_1	0.0433	9.13	0.0389	34.39	0.0203	92.96
C_1	0	0	0	0	0	0
A_2	0.4323	-9.19	0.4009	-38.43	0.2675	176.83
B_2	1.0000	0	1.0000	0	1.0000	0
C_2	0.0605	164.08	0.0511	112.52	0.0269	-154.21

As the entries in the table demonstrate, a wave of acoustic type entering the compressor inlet from upstream generates a reflected acoustic wave upstream and a transmitted acoustic wave downstream as well as an entropy wave downstream. If there were no losses in the compressor ($\eta = 1$), no entropy wave would be generated. For $\omega = 0.25$ and $\omega = 1.00$, the amplitude of the reflected wave at the compressor entrance is larger than that of the incident wave. However, the rate of energy flow upstream is less than that downstream because

$$\frac{\text{energy flow upstream}}{\text{energy flow downstream}} = \frac{B^2}{A^2}\,\frac{1-M}{1+M},$$

and in this example $(1-M_1)/(1+M_1) = 0.29$.

Some of the tabular data are illustrated in a different way in Figure 2, which shows the values of the disturbance amplitude or velocity, $|u|/\bar{u}$ throughout the compressor as well as in the entrance and exit ducts resulting from acoustic waves incident on inlet and exit. The arrows marked ⟶ indicate incident waves, and ⟶ reflected or transmitted waves. Both upstream and downstream waves are shown outside the compressor ($\xi < 0$ or $\xi > 1$) and the resultant only inside the compressor. Because the upstream and downstream velocity disturbances are of comparable amplitude and almost opposite phase in the upper left diagram, the resultant amplitude at the compressor entrance is quite small.

This work was supported by NASA Lewis Research Center, Grant No. NGL 05-002-136. The numerical work was done by Blair A. Folsom.

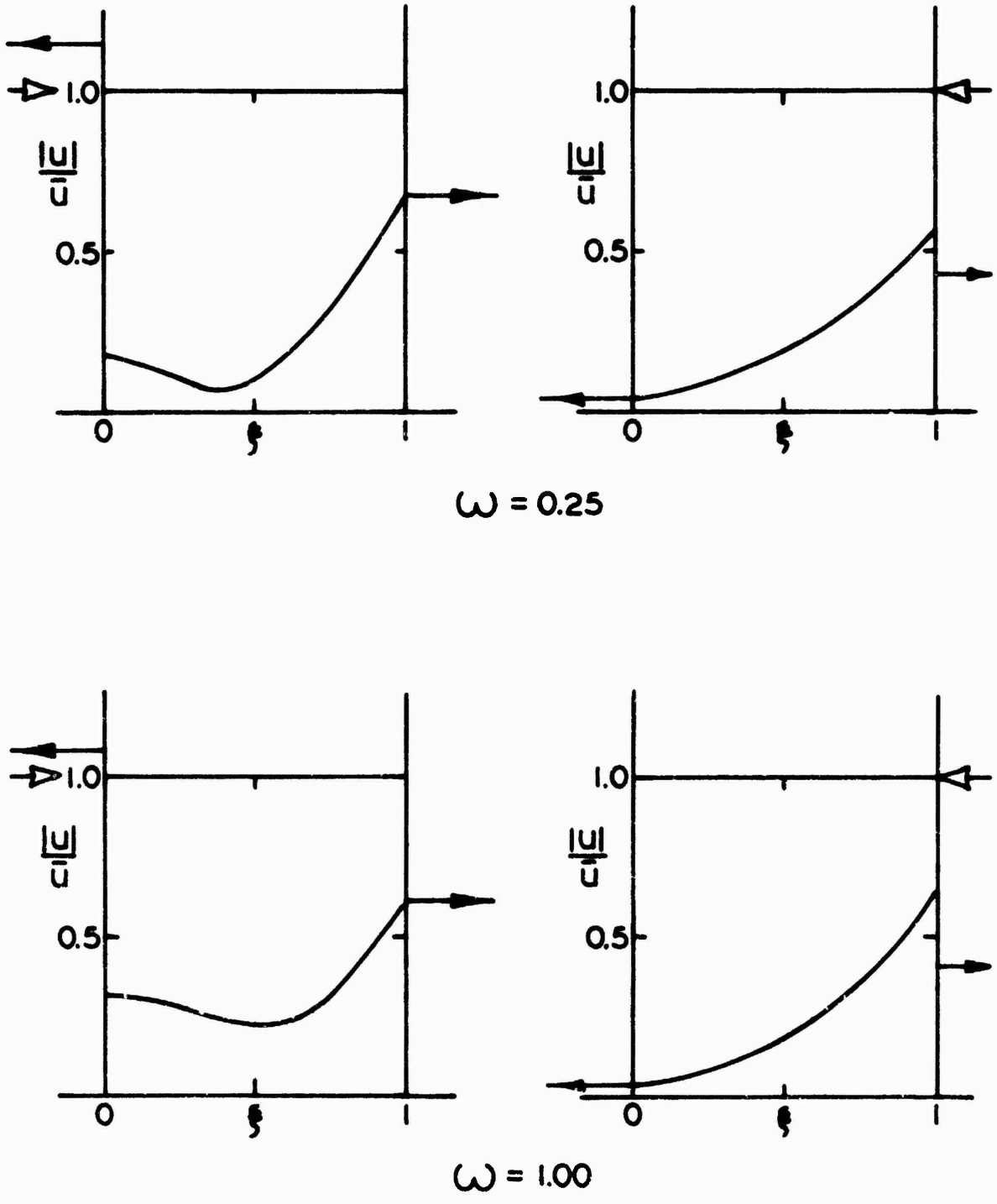

Figure 2. Velocity Amplitudes Produced by Acoustic Waves.

EFFECTS OF FRICTION AND HEAT CONDUCTION ON SOUND PROPAGATION IN DUCTS

by

Patrick Huerre* and Krishnamurty Karamcheti**
Joint Institute for Aeroacoustics
Department of Aeronautics and Astronautics
Stanford University
Stanford, California

INTRODUCTION

The ultimate objective of the present study is to thoroughly investigate the effects of friction and heat conduction on sound propagation through a fluid initially homogeneous and at rest contained in a rigid, impermeable duct with isothermal walls.

These effects were first studied by Kirckhoff (1) in the case of plane waves in cylindrical tubes with the assumption that viscous effects are confined to acoustic boundary layers close to the duct walls. Rayleigh (2) derived Kirckhoff's results using the same formulation and also treated the limiting case of capillary tubes. In the 1950's, Cremer (3), Beatty (4), Meyer and Gütt (5), Shaw (6), among others, extended Kirckhoff's analysis to higher order modes in rectangular and circular ducts, and verified their results experimentally. They were mainly interested in the determination of the attenuation coefficient of higher modes in the acoustic boundary layer approximation, and used an impedance at the duct walls to simulate viscous effects. They otherwise considered the outer flow as inviscid. Morse and Ingard (7) also formulated the problem in terms of an equivalent impedance, and briefly considered the case of the attenuation of the fundamental mode for all ranges of acoustic boundary layer thicknesses. Rott (8) treated the propagation of the plane mode for all ranges of boundary layer thicknesses but assumed that transverse pressure gradients were negligible. Recently, Nayfeh (9) extended the impedance model to ducts with flow, expressing the equivalent wall admittance as a function of velocity and temperature gradients at the wall.

In this report, we present an alternative formulation of the problem by splitting the velocity field into three parts: acoustic (related to pressure), thermal (related to entropy) and viscous (related to vorticity fluctuations). A general dispersion relation is derived in the case of a two-dimensional duct and an expression for the complex propagation wave number is obtained in the limit of thin acoustic boundary layers to order $1/R_\nu$ where R_ν is the Reynolds number based on the speed of sound. The mode shapes are also computed to order $\frac{1}{R_\nu}$ both in the acoustic boundary layers and in the outer region.

BASIC EQUATIONS

The linearized equations governing the acoustic motion, including the effects of friction and heat conduction, of a simple thermodynamic fluid initially at rest and in a uniform state are the following, where the Navier-Stokes relation and Fourier's Law of heat conduction are used:

---

* Ph.D. Student and Research Assistant

** Professor of Aeronautics and Astronautics and Director of the Joint Institute for Aeroacoustics.

Equation of mass

$$\frac{\partial \rho'}{\partial t} + \rho_o \operatorname{div} \vec{V}' = 0 \tag{1}$$

Equation of motion

$$\rho_o \frac{\partial \vec{V}'}{\partial t} = - \operatorname{grad} p' - \mu_o \operatorname{curl} \vec{\Omega}' + \eta_o \operatorname{grad} \operatorname{div} \vec{V}' \tag{2}$$

Equation of entropy

$$\rho_o T_o \frac{\partial S'}{\partial t} = k_o \nabla^2 T' \tag{3}$$

Equations of state

$$p' = a_o^2 \rho' + \rho_o a_o \sqrt{\frac{(\gamma_o - 1) T_o}{c_{p_o}}}\, S' \tag{4}$$

$$T' = \frac{a_o}{\gamma_o} \sqrt{\frac{(\gamma_o - 1) T_o}{c_{p_o}}}\, \rho' + \frac{\gamma_o T_o}{c_{p_o}} S' \tag{5}$$

where the subscript o denotes the initial state, the primed variables designate the perturbation variables, μ_o is the coefficient of shear viscosity, k_o, the coefficient of heat condition, a_o the isentropic speed of sound, and η_o is such that

$$\eta_o = K_o + \frac{4}{3} \mu_o \tag{6}$$

K_o being the coefficient of bulk viscosity. All other symbols have their usual significance.

Equations (4) and (5) were derived by using the first and second laws of thermodynamics only, without assuming that the gas is perfect.

According to Helmholtz theorem, the velocity field $\vec{V}'$ can always be expressed as the sum of an irrotational part grad Φ, and a solenoidal part curl $\vec{A}$, so that

$$\vec{V}' = \operatorname{grad} \Phi + \operatorname{curl} \vec{A} \tag{7}$$

If we substitute (7) into the equation of mass and express ρ' as a function of p' and S' using equation (4), we obtain:

$$\frac{1}{a_o^2} \frac{\partial p'}{\partial t} - \frac{\gamma_o}{a_o} \sqrt{\frac{(\gamma_o - 1) T_o}{c_{p_o}}}\, \frac{\partial S'}{\partial t} = -\rho_o \nabla^2 \Phi \tag{8}$$

In order to satisfy equation (8), the scalar potential Φ will be considered as the sum of two potentials: an acoustic potential Φ_a giving rise to pressure perturbations through the relation:

$$\frac{\partial p'}{\partial t} = -\rho_o a_o^2 \nabla^2 \Phi_a \tag{9}$$

and a thermal potential Φ_{th} giving rise to entropy fluctuations through the relation:

$$\frac{\partial S'}{\partial t} = a_o \sqrt{\frac{c_{p_o}}{(\gamma_o - 1)T_o}} \nabla^2 \Phi th \tag{10}$$

With these definitions, the other dependent variables will be related to ψ_a, ψ_{th}, and $\vec{A}$ in the following manner:

$$\frac{\partial \rho'}{\partial t} = -\rho_o \nabla^2 (\Phi_a + \Phi_{th}) \tag{11}$$

$$\frac{\partial T'}{\partial t} = a_o \sqrt{\frac{T_o}{(\gamma_o - 1)c_{p_o}}} \nabla^2 (\Phi_{th} - (\gamma_o - 1)\psi_a) \tag{12}$$

$$\vec{V}' = \text{grad}\ (\psi_a + \Phi_{th}) + \text{curl}\ \vec{A} \tag{13}$$

The equations governing ψ_a, ψ_{th} and $\vec{A}$ are obtained by substituting equations (9), (10), (12) and (13) into the equation of motion (2) and the equation of entropy (3). We then take advantage of the fact that Φ_a, ψ_{th} and $\vec{A}$ are not uniquely determined, and we carefully choose gauge transformations to reduce the equations for ψ_a, ψ_{th} and $\vec{A}$ to the following partial differential equations:

$$\frac{\partial \vec{A}}{\partial t} - \frac{\nu_o}{\quad o} \nabla^2 \vec{A} = 0 \tag{14}$$

$$\frac{\partial}{\partial t}\left[\frac{\partial \Phi_{th}}{\partial t} - \frac{\eta_o}{\quad o} \nabla^2 \psi_{th}\right] = a_o^2 \quad_s^2 \psi_a \tag{15}$$

$$\nabla^2 \psi_{th} - \frac{P_r}{\nu_o} \frac{\partial \psi_{th}}{\partial t} = (\gamma_o - 1) \nabla^2 \psi_a \tag{16}$$

where $\quad_s^2$ is the following operator:

$$\quad_s^2 = \nabla^2 - \frac{1}{a_o^2} \frac{\partial^2}{\partial t^2} + \frac{\eta_o}{\quad o a_o^2} \nabla^2 \frac{\partial}{\partial t} \tag{17}$$

P_r is the Prandtl number and ν_o is the kinematic viscosity of the medium.

The vector potential $\vec{A}$ is uncoupled from ψ_a and ψ_{th} and satisfies a diffusion equation (14). $\vec{A}$ gives rise to rotational velocity fluctuations only. ψ_a and ψ_{th} are coupled through equations (15) and (16). By cross differentiation of (15) and (16), one immediately shows that both ψ_a and ψ_{th} satisfy:

$$\frac{\partial}{\partial t}\Box_s^2 \ (\Phi_a \text{ or } \Phi_{th}) = \frac{\nu_o}{p_r}\nabla^2\Box_T^2 \ (\Phi_a \text{ or } \Phi_{th}) \tag{18}$$

where
$$\Box_T^2 = \nabla^2 - \frac{\gamma_o}{a_o^2}\frac{\partial^2}{\partial t^2} + \frac{\gamma_o\eta_o}{\rho_o a_o^2}\nabla^2\frac{\partial}{\partial t} \tag{19}$$

However, equations (15) and (16) are not equivalent to equation (18) for Φ_a and Φ_{th} since we have increased the order of the equations.

We have therefore reduced the problem to the determination of the potentials Φ_a, Φ_{th} and $\vec{A}$, which satisfy equations (14), (15), (16) and (18). They are related to the physical dependent variables through equations (9)-(13).

PROBLEM AND FORM OF SOLUTION

We shall now consider the propagation of an harmonic wave through a two-dimensional duct of constant cross section shown in Figure 1.

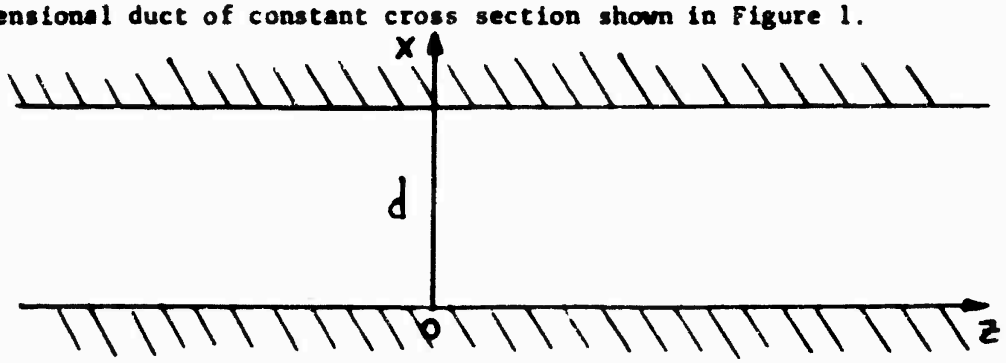

Figure 1

We nondimensionalize the independent variables and set:

$$x' = \frac{x}{d} \quad (20); \qquad z' = \frac{z}{d} \quad (21); \qquad t' = \omega t \quad (22)$$

where ω is the particular frequency to be investigated.

$$k = \frac{\omega d}{a_o} \text{ is the reduced frequency} \tag{23}$$

$$R_\nu = \frac{a_o d}{\nu_o} \text{ is the Reynolds number based on the speed of sound and the shear viscosity.} \tag{24}$$

$$R_\eta = \frac{a_o d}{\frac{\eta_o}{\rho_o}} \text{ is the Reynolds number relative to the dilatational viscosity } \frac{\eta_o}{\rho_o} \tag{25}$$

Since the motion is two-dimensional, we introduce, instead of a vector potential $\vec{A}$, a stream function Ψ.

Equations (14), (15), (16), (18), (19) become::

$$\frac{\partial \Psi}{\partial t} = \frac{1}{kR_\nu} \nabla^2 \Psi \tag{26}$$

$$\frac{\partial}{\partial t}\left(\frac{\partial \phi_{th}}{\partial t} - \frac{1}{kR_\eta} \nabla^2 \phi_{th}\right) = \frac{1}{k^2} \mathcal{L}_s \phi_a \tag{27}$$

$$\frac{\partial \phi_{th}}{\partial t} - \frac{1}{kPrR_\nu} \nabla^2 \phi_{th} = - \frac{\gamma_o - 1}{kPrR_\nu} \nabla^2 \phi_a \tag{28}$$

$$\frac{\partial}{\partial t} \mathcal{L}_s \phi_a = \frac{1}{PrkR_\nu} \nabla^2 \mathcal{L}_T \phi_a \tag{29}$$

where

$$\mathcal{L}_s = \nabla^2 - k^2 \frac{\partial^2}{\partial t^2} + \frac{k}{R_\eta} \nabla^2 \frac{\partial}{\partial t} \tag{30}$$

$$\mathcal{L}_T = \nabla^2 - \gamma_o k^2 \frac{\partial^2}{\partial t^2} + \frac{\gamma_o k}{R_\nu} \nabla^2 \frac{\partial}{\partial t} \tag{31}$$

and

$$\vec{V}' = \frac{1}{d} \operatorname{grad} (\phi_a + \phi_{th}) - \frac{\partial \Psi}{\partial z} \vec{e}_x + \frac{\partial \Psi}{\partial x} \vec{e}_z \tag{32}$$

$$\frac{\partial T'}{\partial t} = \frac{PrR_\nu}{d} \sqrt{\frac{T_o}{(\gamma_o - 1) c_{p_o}}} \frac{\partial \phi_{th}}{\partial t} \tag{33}$$

We have dropped all the primed indices for x', z', t', with the understanding that we deal with nondimensional quantities.

The boundary conditions at the walls are:

$$\vec{V}' = 0 \qquad \text{at } x = 0 \text{ and } x = 1 \tag{34}$$

$$T' = 0 \qquad \text{at } x = 0 \text{ and } x = 1 \tag{35}$$

Equations (26)-(29) and (34)-(35) define a typical eigenvalue problem for ϕ_a, ϕ_{th} and Ψ.

In the case of a harmonic wave of frequency ω, and propagation wave number β_z, ϕ_a, ϕ_{th} and Ψ are assumed to be of the form:

$$\phi_a(x,z,t) = \varphi_a(x)\, e^{i(t - \beta_z z)} \tag{36}$$

$$\phi_{th}(x,z,t) = \varphi_{th}(x)\, e^{i(t - \beta_z z)} \tag{37}$$

$$\psi(x,z,t) = \psi(x)\, e^{i(t - \beta_z z)} \tag{38}$$

Substitution of (36), (37), (38) into equations (26), (29), and its equivalent for ϕ_{th} yields 3 ordinary differential equations in x with constant coefficients for φ_a, φ_{th}, and ψ, which may be easily solved. The results are the following:

$$\varphi_a(x) = Ae^{i\alpha_a x} + Be^{-i\alpha_o x} + Ce^{i\alpha_1 x} + De^{-i\alpha_1 x} \tag{39}$$

$$\varphi_{th}(x) = A'e^{i\alpha_o x} + B'e^{-i\alpha_o x} + C'e^{i\alpha_1 x} + D'e^{-i\alpha_1 x} \tag{40}$$

$$\psi(x) = Ee^{i\alpha_2 x} + Fe^{-i\alpha_2 x} \tag{41}$$

where A, B, C, ... E, F are constants to be determined, and α_o, α_1, α_2 are defined as follows:

$$\alpha_o^2 = \beta_o^2 - \beta_z^2 \quad (42); \qquad \alpha_1^2 = \beta_1^2 - \beta_z^2 \quad (43); \qquad \alpha_2^2 = \beta_2^2 - \beta_z^2 \tag{44}$$

$$\beta_{o,1}^2 = \frac{-iPrKR_\nu}{2\left(1 + \frac{i\gamma_o k}{R_\eta}\right)}\left(1 + \frac{i\gamma_o k}{PrR_\nu} + \frac{ik}{R_\eta}\right)\left[1 \mp \sqrt{1 - \frac{4ik}{PrR_\nu}\cdot\frac{1 + \frac{i\gamma_o k}{R_\eta}}{\left(1 + \frac{i\gamma_o k}{PrR_\nu} + \frac{ik}{R_\eta}\right)^2}}\right] \tag{45}$$

where the o and 1 subscripts correspond to the − and + sign respectively,

and $$\beta_2^2 = -ikR_\nu \tag{46}$$

The boundary conditions at the walls (34) and (35) yield 6 equations for the determination of the 10 constants A, B, C, ... F. As mentioned on page 27 we have to supplement them with equation (28). Equation (27) could equivalently have been chosen. Substitution of (39)-(40)-(41) into the boundary conditions and relation (28) yields the following homogeneous linear system of 10 equations with 10 unknowns:

$$A' + B' + C' + D' = 0 \tag{47}$$

$$A'e^{i\alpha_o} + B'e^{-i\alpha_o} + C'e^{i\alpha_1} + D'e^{-i\alpha_1} = 0 \tag{48}$$

$$\alpha_1(A' - B') + \alpha_1(C' - D') + \alpha_0(A - B) + \alpha_1(C - D) + \beta_z(E + F) = 0 \qquad (49)$$

$$\alpha_0(A'e^{i\alpha_0} - B'e^{-i\alpha_0}) + \alpha_1(C'e^{i\alpha_1} - D'e^{-i\alpha_1})$$

$$+ \alpha_0(Ae^{i\alpha_0} - Fe^{-i\alpha_0}) + \alpha_1(Ce^{i\alpha_1} - De^{-i\alpha_1}) + \beta_z(Ee^{i\alpha_2} + Fe^{-i\alpha_2}) = 0 \qquad (50)$$

$$- \beta_z(A' + B' + C' + D' + A + B + C + D) + \alpha_2(E - F) = 0 \qquad (51)$$

$$- \beta_z(A'e^{i\alpha_0} + B'e^{-i\alpha_0} + C'e^{i\alpha_1} + D'e^{-i\alpha_1} + Ae^{i\alpha_0} + Be^{-i\alpha_0} + Ce^{i\alpha_1} + De^{-i\alpha_1})$$

$$+ \alpha_2(Ee^{i\alpha_2} - Fe^{-i\alpha_2}) = 0 \qquad (52)$$

$$A + (1 - a_0^*) A' = 0 \qquad (53)$$

$$B + (1 - a_0^*) B' = 0 \qquad (54)$$

$$C + (1 - a_1^*) C' = 0 \qquad (55)$$

$$D + (1 - a_1^*) D' = 0 \qquad (56)$$

where
$$a_0^* = 1 + \frac{\beta_0^2 + iPrk}{(\gamma_0 - 1)\beta_0^2} \qquad (57)$$

$$a_1^* = 1 + \frac{\beta_1^2 + iPrk}{(\gamma_0 - 1)\beta_1^2} \qquad (58)$$

In order for this system to have a non trivial solution, its determinant must be set equal to zero. We simply give the final result for the dispersion relation:

$$\left(\frac{a_1^*}{a_0^*}\right)^2 \sin^2\alpha_0\ \delta_2(\alpha_1,\alpha_1) + \left(\frac{\alpha_0}{\alpha_1}\right)^2 \sin^2\alpha_1\ \delta_2(\alpha_0,\alpha_0)$$

$$- 2\frac{\alpha_0}{\alpha_1}\cdot\frac{a_1^*}{a_0^*} \sin\alpha_0 \sin\alpha_1\ \delta_2(\alpha_0,\alpha_1) = 0 \qquad (59)$$

where

$$\delta_2(\alpha_0,\alpha_1) = \frac{\beta_z^4}{\alpha_0\alpha_1\alpha_2^2}\sin\alpha_0\sin\alpha_1\sin\alpha_2 + \frac{\beta_z^2}{\alpha_0\alpha_2}\sin\alpha_0(1-\cos\alpha_1\cos\alpha_2)$$

$$+ \frac{\beta_z^2}{\alpha_1\alpha_2}\sin\alpha_1(1-\cos\alpha_0\cos\alpha_2) + \sin\alpha_2(1-\cos\alpha_0\cos\alpha_1) \qquad (60)$$

Equation (59) defines the eigenvalues β_z for our problem. It is impossible to solve equation (59) analytically, unless we consider the particular case of high Reynolds numbers.

ACOUSTIC AND BOUNDARY LAYER SOLUTION

We seek an expansion of equations (59)-(60) in powers of $\frac{1}{R_\eta}$ and $\frac{1}{R_\nu}$ to order 1 included for large values of R_η and R_ν. We disregard terms of higher order. α_0, α_1 and α_2 are given by equations (62)-(64) and a_0^*, a_1^* by equations (57) and (58). They are easily expanded to order $\frac{1}{R_\nu}$ and substituted into (59) and (60). Neglecting higher order terms, it is straightforward to solve for β_z. The result is the following:

$$\beta_{z_0} = k\left[1-(1-i)\frac{k^{*2}}{k^2}\sqrt{\frac{1}{2kR_\nu}} - 2i\frac{k^{*2}}{k^2}\left(\frac{k^{*2}}{12}+1-\frac{k^{*2}}{4k^2}\right)\frac{1}{kR_\nu}\right.$$

$$\left. - \frac{ik^2}{2}\left\{\frac{\gamma_0-1}{Pr}+\frac{R_\nu}{R_\eta}\right\}\frac{1}{kR_\nu}\right] \qquad (61)$$

$$\beta_{z_{\substack{n\\ n\neq 0}}} = \sqrt{k^2-(n\pi)^2}\left[1-(1-i)\frac{k^{*2}-(n\pi)^2}{k^2-(n\pi)^2}\sqrt{\frac{2}{kR_\nu}} - \frac{4i}{(n\pi)^2}\cdot\frac{k^{*2}-(n\pi)^2}{k^2-(n\pi)^2}\cdot\right.$$

$$\left.\left(k^{*2}+(n\pi)^2-\frac{k^2}{2}\cdot\frac{k^{*2}-(n\pi)^2}{k^2-(n\pi)^2}\right)\frac{1}{kR_\nu} - \frac{ik^4\left\{\frac{\gamma_0-1}{Pr}+\frac{R_\nu}{R_\eta}\right\}}{2(k^2-(n\pi)^2)}\frac{1}{kR_\nu}\right] \qquad (62)$$

where

$$k^{*2} = \left(1-\frac{\gamma_0-1}{\sqrt{Pr}}\right)k^2 \qquad (63)$$

and n is the mode index.

α_0, α_1 and α_2 are then equal to

$$\alpha_{n_{\substack{n\neq 0}}} = n\pi\left[1-\frac{1-i}{(n\pi)^2}(k^{*2}-(n\pi)^2)\sqrt{\frac{2}{kR_\nu}} + \frac{4i}{(n\pi)^4}(k^{*4}-(n\pi)^2\frac{1}{kR_\nu}\right] \qquad (64)$$

$$\alpha_{oo} = ie^{-(i\pi/8)}\sqrt{2}\,k^*\left(\frac{1}{kR_\nu}\right)^{1/4}\left[1+\frac{1-i}{\sqrt{2}}\left(1+\frac{k^{*2}}{12}\right)\sqrt{\frac{1}{kR_\nu}}\right] \tag{65}$$

$$\alpha_{1n} = (1-i)\sqrt{\frac{kPrR_\nu}{2}}\left[1-\frac{i}{2}\left\{\frac{k^2-(n\pi)^2}{Pr}+(\gamma_o-1)\left(\frac{R_\nu}{R_\eta}-\frac{1}{Pr}\right)k^2\right\}\frac{1}{kR_\nu}\right] \tag{66}$$

$$\alpha_{2n} = (1-i)\sqrt{\frac{kR_\nu}{2}}\left[1-\frac{i}{2}(k^2-(n\pi)^2)\,\frac{1}{kR_\nu}\right] \tag{67}$$

The coefficients of the linear system (47)-(56) are then known explicitly and the system may be solved for A,B,C...E,F, neglecting higher order terms. The mode shapes are normalized by requiring that

$$p'(x=o) = 1 \tag{68}$$

The results are exhibited in Table I.

DISCUSSION

The boundary value problem has therefore been solved to order $\frac{1}{R_\nu}$ included. Our experiments are uniformly valid throughout the cross section.

Propagation wave number:

The first term in equations (61) and (62) are the well known inviscid solutions to the problem. The second term of order $1/\sqrt{R_\nu}$ correspond to the acoustic boundary layer attenuation and dispersion effects. They are identical to those obtained by previous investigators. In particular the second term in equation (61) is the Kirchhoff correction term for plane wave propagation in ducts. Note that higher order modes are more attenuated than the fundamental mode. The third terms correspond to higher order boundary layer effects whereas the fourth terms are due to viscous dilatation. These last two contributions give rise to attenuation only and do not change values of the phase velocity since they are imaginary. We note that viscous dilatational effects are of higher order than acoustic boundary layer effects and will provide only a slight correction to the total attenuation.

Mode shapes:

As seen from Table I, the mode shapes have been written as the sum of three contributions.

The outer region terms which are equally important over the entire cross section of the duct. It is easily verified that in the inviscid case, these are the only terms that are nonzero. However, in the viscous case, the variations of pressure, velocity ... with x have been changed even outside the boundary layer. This is due to boundary layer displacement effects. We expect that arbitrary disturbances propagating along the duct axis will exhibit different characteristics than in the no friction situation.

The thermal boundary layer terms are only significant in a thin region close to the duct walls of thickness

$$\delta_{th} = \sqrt{\frac{2}{PrkR_\nu}} = \sqrt{\frac{2k_o}{\omega d^2 \rho_o c_{p_o}}} \quad .$$

Outside this region, they are exponentially small. Note that to order $1/R_\nu$, there is a correction term to the pressure fluctuations in the boundary layer. This correction vanishes when the Prandtl number Pr is such that $Pr = \nu_o/(\eta_o/\rho_o)$. As expected the gradients of entropy and temperature are very high.

The viscous boundary layer terms are significant in a thin region close to the duct wall of thickness

$$\delta_V = \sqrt{\frac{2}{kR_\nu}} = \sqrt{\frac{2\nu_o}{\omega d^2}} \quad .$$

Outside this region, they are exponentially small. As expected, the gradients of axial velocity and vorticity are very high.

CONCLUSION

Numerical results for the phase velocity, attenuation and mode shapes are not yet available at this point. They will be presented in a forthcoming JIA report. Our expansions are not valid close to the cut off frequencies and we intend to modify our procedure to obtain expansions which are valid throughout the frequency domain. In the other limiting case of capillary tubes, the dispersion relation may also be solved by expanding in powers of the Reynolds number. Finally for arbitrary values of the parameters, we need to solve the dispersion relation numerically.

The two dimensional duct problem provides a solid basis upon which we can make the extension to the case of ducts of circular cross section. We shall therefore be able to assess the importance of viscous effects for all ranges of Reynolds numbers, and to compare them with the analytical results of the high and low Reynolds number approximations.

These studies are supported in part by NASA Grant NASA NGR 05-020-526.

	Outer Region	Thermal Boundary Layers	Viscous Boundary Layers
$\varphi_{0m}(x)$	$\frac{1}{\rho_0\omega}\left[1-ik^2\gamma_0\frac{1}{kR_\eta}\right]\left[\frac{\sin\alpha_{0m}(1-x)+(-1)^m\sin\alpha_{0m}x}{\sin\alpha_{0m}}\right.$	$-\frac{(\gamma_0-1)}{Pr}\left(\frac{1}{Pr}-\frac{R_\nu}{R_\eta}\right)k^2\left(\frac{1}{kR_\nu}\right)^2\left\{e^{-i\alpha_{1m}x}+(-1)^m e^{-i\alpha_{1m}(1-x)}\right\}\Bigg]$	
$\varphi_{2m}(x)$	$\frac{(\gamma_0-1)k^2}{\rho_0\omega}\cdot\frac{1}{PrkR_\nu}\left\{1+ik^2\left[(\gamma_0-1)\frac{R_\nu}{R_\eta}-\frac{\gamma_0-2}{Pr}\right]\frac{1}{kR_\nu}\right\}\left\{\frac{\sin\alpha_{0m}(1-x)+(-1)^m\sin\alpha_{0m}x}{\sin\alpha_{0m}}\right.$	$\left.-\left[e^{-i\alpha_{1m}x}+(-1)^m e^{-i\alpha_{1m}(1-x)}\right]\right\}$	
$\varphi_{2n}(x)$			$\frac{1-i}{\sqrt{2}}\frac{1}{\rho_0\omega}\beta_{2m}\left(\frac{1}{kR_\nu}\right)^{1/2}\left[1+ik^2\gamma_0\frac{1}{kR_\eta}+\frac{1}{2}(k^2-(n\pi)^2)\frac{1}{kR_\nu}\right]\left[e^{-i\alpha_{2n}x}-(-1)^n e^{-i\alpha_{2n}(1-x)}\right]$
$V'_{0m}(x)$	$-\frac{1}{\rho_0\omega d}\left[1+ik^2\left(\gamma_0\frac{R_\nu}{R_\eta}-\frac{\gamma_0-1}{Pr}\right)\frac{1}{kR_\nu}\right]\left\{\alpha_{0m}\frac{\cos\alpha_{0m}(1-x)-(-1)^m\cos\alpha_{0m}x}{\sin\alpha_{0m}}\right.$	$-\frac{1-i}{\sqrt{2}}(\gamma_0-1)k^2\left(\frac{1}{PrkR_\nu}\right)^{1/2}\left[e^{-i\alpha_{1m}x}-(-1)^m e^{-i\alpha_{1m}(1-x)}\right]$	$-\frac{1-i}{\sqrt{2}}\left(\frac{1}{kR}\right)^{1/2}\beta_{2m}^2\left[e^{-i\alpha_{2n}x}-(-1)^n e^{-i\alpha_{2n}(1-x)}\right]\Bigg\}$
$V'_{2m}(x)$	$\frac{1}{\rho_0\omega d}\beta_{2m}\left[1+ik^2\left(\gamma_0\frac{R_\nu}{R_\eta}-\frac{\gamma_0-1}{Pr}\right)\frac{1}{kR_\nu}\right]\left\{\frac{\sin\alpha_{0m}(1-x)+(-1)^m\sin\alpha_{0m}x}{\sin\alpha_{0m}}\right.$	$+i(\gamma_0-1)k^2\frac{1}{PrkR_\nu}\left[e^{-i\alpha_{1m}x}+(-1)^m e^{-\alpha_{1m}(1-x)}\right]$	$-\left(1+i(\gamma_0-1)k^2\frac{1}{PrkR_\nu}\right)\left[e^{-i\alpha_{2n}x}+(-1)^n e^{-i\alpha_{2n}(1-x)}\right]\Bigg\}$
$T'_{0n}(x)$	$\frac{1}{\rho_0 c_0}\sqrt{\frac{(\gamma_0-1)T_0}{c_{p_0}}}\left[1+ik^2\left(\gamma_0-1\right)\frac{R_\nu}{R_\eta}-\frac{\gamma_0-2}{Pr}\right)\frac{1}{kR_\nu}\Bigg]\left\{\frac{\sin\alpha_{0m}(1-x)+(-1)^m\sin\alpha_{0m}x}{\sin\alpha_{0m}}\right.$	$\left.-\left[e^{-i\alpha_{1m}x}+(-1)^m e^{-i\alpha_{1m}(1-x)}\right]\right\}$	
$p'_{0m}(x)$	$\left[1-ik^2(\gamma_0-1)\left(\frac{1}{Pr}-\frac{R_\nu}{R_\eta}\right)\frac{1}{kR_\nu}\right]\left\{\frac{\sin\alpha_{0m}(1-x)+(-1)^m\sin\alpha_{0m}x}{\sin\alpha_{0m}}\right.$	$+ik^2(\gamma_0-1)\left(\frac{1}{Pr}-\frac{R_\nu}{R_\eta}\right)\frac{1}{kR_\nu}\left[e^{-i\alpha_{1m}x}+(-1)^m e^{-i\alpha_{1m}(1-x)}\right]\Bigg\}$	
$v'_{0m}(x)$	$\frac{1}{\rho_0\omega d}\left[1+ik^2(\gamma_0-1)\left(\frac{R_\nu}{R_\eta}-\frac{2}{Pr}\right)\frac{1}{kR_\nu}\right]\left\{\frac{\sin\alpha_{0m}(1-x)+(-1)^m\sin\alpha_{0m}x}{\sin\alpha_{0m}}\right.$	$+(\gamma_0-1)\left(1-ik^2\gamma_0\frac{R_\nu}{R_\eta}-\frac{2}{Pr}\frac{1}{kR_\nu}\right)\left[e^{-i\alpha_{1m}x}+(-1)^m e^{-i\alpha_{1m}(1-x)}\right]\Bigg\}$	
$S'_{0n}(x)$	$-\frac{1}{\rho_0 c_0}\sqrt{\frac{(\gamma_0-1)\omega\rho_0}{T_0}}\left\{-k^2\cos\alpha x\frac{1}{PrkR_\nu}\right.$	$\left.+\left(1+ik^2\frac{1}{PrkR_\nu}\right)\left[e^{-i\alpha_{1m}x}+(-1)^m e^{-i\alpha_{1m}(1-x)}\right]\right\}$	

Table 1

REFERENCES

1. Kirchhoff, G., "Ueber den Einflufs der Wärmeleitung in einem gase auf die Schallbewegung." Ann. Phys. Lpz 134, 177-193 (1868).

2. Lord Rayleigh, The Theory of Sound. Dover, New York, Vol. II, p. 312-328 (1945).

3. Cremer, L., "Über die akustische Grenzschicht von starren Wänden." Arch. elektr. Übertragung 2, 136-139 (1948).

4. Beatty, R. E. J., "Boundary Layer Attenuation of Higher-Order Modes in Rectangular and Circular Tubes." J. Acoust. Soc. Amer. 22, 850-854 (1950).

5. Meyer, E. and Güth, W., "Zur Akustischen Zähigkeitsgrenzschicht." Acustica 3, 185-187 (1953).

6. Shaw, E. A. G., "The Attenuation of the Higher Modes of Acoustic Waves in a Rectangular Tube." Acustica 3, 87-95 (1953).

7. Morse, P. M. and Ingard, U., Theoretical Acoustics. McGraw-Hill, New York, (1968).

8. Rott, N., "Damped and Thermally Driven Acoustic Oscillations in Wide and Narrow Tubes." ZAMP 20, 230-243 (1969).

9. Nayfeh, A. H., "Effect of the Acoustic Boundary Layer on the Wave Propagation in Ducts." VPI Report No. E-73-10, Virginia Polytechnic Institute and State University (1973).

ALPHABETICAL LISTING OF AUTHORS

Determination of Lip Noise by Correlation Measurements

D. R. Regan and W. C. Meecham

University of California

Los Angeles, California

An experimental investigation of lip noise has been conducted at the U.C.L.A Aerosonics Laboratory using a 1-1/2 inch diameter model jet. Over the range of Mach numbers M for which the experiments were performed ($0.3 \leq M \leq 0.7$) the lip noise intensity I_L was found to vary as the sixth power of the jet velocity ($I_L \propto U^6$) consistent with a dipole source. Cross-correlation measurements of the near field acoustic pressure waves emitted perpendicular to the jet axis shows that lip noise originates from two lip positions (presumably from the near and far side of the lip), the two contributions being out of phase for frequencies significantly above 2kHz. Cross-correlation measurements of the far field acoustic pressure waves received at symmetric positions on opposite sides of the jet axis suggest that lip noise reaches maximum intensity about 70-80° from the jet axis. Third-octave spectral analysis shows that lip noise can be characterized as a wide band (impulsive) type of noise peaked at a frequency $f \propto U/D$ where D is the jet diameter. Measurements made with a small, 2mm O.D. probe tube mounted flush with the inside surface of the lip show as expected that the hydrodynamic pressure fluctuations arising from turbulence there are proportional to the square of the jet velocity ($p \propto U^2$). Calculations made from the probe tube measurements yield values of 0.02 for the turbulence intensity just inside the lip of the jet.

1. INTRODUCTION

Curle[1] has shown that acoustic dipole radiation is generated by rigid bodies immersed in a turbulent flow. Acoustic dipoles are generated by fluctuating turbulent, hydrodynamic pressure forces acting on the rigid surface. Aerosound generated by airfoils is but one example of this phenomenon. Experimental investigations[2] have verified the acoustical properties of airfoil-generated aerosound as predicted by Curle, e.g. the sixth power velocity dependence of acoustic intensity and a dipole radiation pattern peaked normal to the airfoil surface.

It follows that acoustic dipoles exist on surfaces which contain turbulent flows. For example, the internal surface of a nozzle is subjected to fluctuating pressure forces in much the same manner as is an airfoil, immersed in a turbulent flow. One would suppose, then, that acoustic waves created by such internally distributed pressure forces would radiate from the vicinity of the nozzle orifice (lip) of the jet. One would further suppose that this lip noise radiation would exhibit acoustical properties similar to airfoil aerosound.

The present work provides experimental information about the acoustical properties of lip noise radiation. In this work, we find that predictions derived from Curle's theory account for many of the observed properties of lip noise radiation.

2. EXPERIMENTAL APPARATUS

The experimental work described here was performed at the U.C.L.A. Aerosonics Laboratory using a 1-1/2 inch model jet. The nozzle is a Harrop design having a contraction ratio of 7.56. A 230 mesh wire screen is mounted eight jet diameters upstream from the nozzle exit in order to reduce flow turbulence. An absorbtive muffler, which has an acoustic attenuation in SPL of 66 dB over the frequency range of 200Hz to 20KHz, is also placed upstream to remove value noise. The model jet is located in a semi-anechoic chamber, which has been found to be adequate for random pressure fields from frequencies slightly below 200Hz to well above 20KHz.

The flow speed of the model jet is continuously variable and steady operation up to Mach 0.7 is possible. The jet speed is controlled by a regulator supplied with high pressure air (100 psi stagnation pressure) from three piston type compressors. The velocity profile of the jet was measured with a small pitot-static tube and found to be flat (top-hat profile) over the entire orifice with the exception of a thin annular region near the nozzle wall where the viscous shear layer is located. Over the range of Mach numbers used in these experiments $0.3 \leq M \leq 0.7$ the Reynolds number R_d based on the nozzle diameter ranges from $2X10^5 \leq R_d \leq 4.5X10^5$.

3. LIP PRESSURE PROBE

The hydrodynamic pressure fluctuations at the lip of the jet orifice are studied with two small (2 mm O.D.) pressure probe tubes. These probes are 46.6 mm in length and are mated with B&K 4134-1/2 in. condenser microphones via a conical adapter. The probes are mounted flush with the internal lip surface, by insertion through small holes 1.27 mm from the lip edge. Probe tube resonances arising when the tube length is an odd multiple of a quarter wavelength, are critically damped by inserting a small wad of steel wool inside the probe tip. The frequency response and sensitivity of the probe tube system is determined by direct comparison with a calibrated B&K 4135-1/4 in. condenser microphone placed in a random-noise sound field. Since the free-field probe calibration agrees very well with pistonphone calibration, the latter calibration method was used throughout these experiments.

4. LIP TURBULENCE MEASUREMENTS

The hydrodynamic pressure level inside the orifice lip was measured over Mach numbers M ranging from $0.3 \leq M \leq 0.7$ using the 2 mm probe tube. In terms of the mean gas density ρ_0 and the turbulent fluctuation velocity u', the lip pressure fluctuation P_i is given approximately by

$$P_i \sim \frac{1}{2} \rho_0 u'^2 \qquad (1)$$

The square law dependence of P_i with U (supposing $u' \alpha U$) was verified over the range of Mach numbers used in the experiment and is shown in Fig. 1. The rms lip turbulence intensity u'/U is determined from the hydrodynamic pressure level (H.P.L.) using the relationship

$$u'/U = (0.02/Ma_0 \rho_0^{1/2}) 10^{(H.P.L./40)} \qquad (2)$$

where the sound speed $a_0 = 3.43 \times 10^4$ cm/sec at room temperature. Equation (2) is based on Eq. (1) and the definition of H.P.L. given by

$$H.P.L.\ (dB) = 20 \log_{10}(P_i/P_{ref}) , \qquad (3)$$

where the reference pressure $p_{ref} = 0.0002$ dynes/cm^2. Using Eq. (2) and measured values of H.P.L. (corrected for probe tube attenuation and microphone sensitivity) we find $u'/U \approx 0.02$ for $0.3 \leq M \leq 0.7$. It will be shown in following discussion that lip pressure fluctuations sensed by the probe tube have average scale sizes $\ell \approx D$. In addition, we find lip pressure fluctuations are correlated across a nozzle diameter. From this information alone, we see that lip pressure fluctuations sensed by the probe tube are not associated with boundary layer turbulence.

The source of lip pressure fluctuations is turbulence upstream of the 230 mesh screen. Fully developed turbulence pipe flow has turbulence intensities $u'/U \approx 0.05$. The combination of a screen and a nozzle contraction accounts for the reduction of lip turbulence. Additional experimentation shows that adding a length of pipe (diameter 1-1/2 in., length 24 in.) to the nozzle orifice increases the turbulence intensity to $u'/U \approx 0.06$ at the pipe lip as one would expect. This latter value of turbulence intensity is based on H.F.L. measurements and is in agreement with the 5% turbulence intensity level associated with pipe flows. This finding supports our measurement technique and hence our hypothesis concerning the source of the nozzle lip turbulence.

5. LIP PRESSURE FLUCTUATION SPECTRUM

Third-octave spectrums of lip pressure fluctuations are shown in Fig. 2. These spectrums, which have been corrected for the frequency response of the 2 mm probe tube, show a broad peak which tends to narrow as the flow speed is increased. The spectrum peak scales approximately with a convection frequency given by

$$f \sim U/D \tag{4}$$

In Eq. 4 we assume the scale length of the turbulent pressure fluctuations is of order D.

That turbulent pressure fluctuations have scale lengths $\ell_e \approx D$ is evident from observations the time width of lip pressure fluctuation signals displayed on an oscilloscope. The scale length of the pressure fluctuations is determined from time, pulse-width measurements by

$$\ell_e = Ma_0 t_p, \tag{5}$$

where t_p is the width of a pressure pulse. Note that Eq. (5) is based on a frozen flow assumption. For M = 0.7 we measured the average pulse width and found t 0.13ms so that $\ell_e \approx 1.2$ in. (D = 1.5 in.) Note that the reciprocal of the average pulse width is the characteristic frequency, $f_p = 1/\bar{t}_p$. For M = 0.7, f_p = 7.7KHz which is in excellent agreement with the spectrum peak shown in Fig. 2.

It is important to note that frequency spectrums previously measured are not associated with the moving-frame time scales of the pressure fluctuations themselves, since the probe tube is at rest with respect to the flow. Instead, these spectrums result from pressure disturbances being convected past the probe with speeds nearly equal to those of the jet.

6. LIP PRESSURE CROSS-CORRELATIONS

We now describe a simple experiment which has supplied additional information on the structure of the lip pressure fluctuations. Two calibrated 2 mm probe tubes mounted flush with the inside lip surface, on opposite sides of the lip, are employed. The lip pressure fluctuations sensed by each probe are filtered, amplified and processed with a 100 point digital to analog correlator (operated in the clip mode). The probes are nearly identical to one another so that time delays and phase shifts associated with wave propagation through the probe tubes are nearly identical in each circuit. This eliminates time and phase shift errors in the cross-correlation measurements.

Typical lip pressure cross-correlation functions have been measured for M = 0.5 to 0.7; the result for M = 0.6 is shown in Fig. 3. The magnitude of the normalized cross-correlation coefficients measured for zero time delay, R(0), vary from 0.035 to 0.081 for the Mach numbers used in the experiment. The relatively low R(0) values suggest that large scale turbulence is responsible for lip pressure fluctuations rather than highly coherent structures, such as vortex rings, which would yield larger R(0) values. It is certainly possible that randomized "vortex rings" exist in the flow, but outside, downstream, rather than inside the lip. Note that boundary layer pressure fluctuations cannot account for observed R(0) values owing to the small value of boundary layer eddy correlation length to lip circumference ratio ($\ell_c/\pi D \ll 1$), which makes the correlation coefficients for boundary layer turbulence negligibly small across the nozzle diameter.

Further examination of the cross-correlation functions shows that the correlated components of the lip pressure fluctuations are in phase across the orifice, as indicated by the positive value of R(0). This phase coherence across the nozzle orifice is expected if large eddies having scale lengths $\ell_c \approx D$ are being convected past the lip. In Sec. 8, we present experimental evidence that suggests that these large scale pressure disturbances are responsible for lip noise which is radiated on either side of the jet.

7. LIP NOISE RADIATION PROPERTIES

We now investigate the properties of acoustic radiation generated by fluctuating pressure forces acting on the lip surface. In this section, we use cross-correlation techniques to study the relation between lip pressure fluctuations and acoustic waves emitted from the nozzle lip.

Curle has shown that acoustic pressure fluctuations radiated by a stationary, rigid body immersed in a turbulent flow is expressed exactly by (in standard notation)

$$p'(\underline{x},t) = \frac{1}{4\pi}\frac{\partial}{\partial x_i}\int_S \frac{P_i}{r}(\underline{y},t-r/a_o)dS(\underline{y}), \qquad (6)$$

where $p'(\underline{x},t)$ is the acoustic pressure (deviation from ambient value) and $P_i(\underline{y},t-r/a_o)$ is the time retarded force per unit area (lip pressure fluctuation) exerted on the body by the turbulent fluid. A rigid body at rest with respect to the flow injects momentum (rather than mass) into the flow field; the acoustic radiation is that of dipole sources distributed over the internal body surface.

In the far field we find in the usual way, for Eq. (6),

$$p'(\underline{x},t) = \frac{-1}{4\pi a_o x}\int_S \dot{P}_i(\underline{y},t-r/a_o)(x_i/r)dS(\underline{y}) \qquad (7)$$

where the dot denotes time differentiation. Convection and refraction effects have been neglected in the above expressions. The classic dipole radiation pattern for each surface element is seen in Eq. (7). The result of integrating the effects of these (partially coherent) dipoles is complicated, though one may expect larger intensities at larger angles from the jet axis.

The velocity dependence of the far field acoustic intensity may be obtained from Eq. (7). Using order of magnitude estimates one finds

$$I(\underline{x}) = \frac{\langle (p'(\underline{x},t))^2\rangle}{\rho_o a_o} = \frac{C\,\rho_o\,A\,U^6}{a_o^3\,x^2} \qquad (8)$$

where C is a constant, $A \sim \pi D^2$ is the internal lip source area and x is the distance between the lip and the field point. The above equation illustrates the sixth power velocity dependence of acoustic dipole radiation. Our measurements show that $C \leq 10^{-7}$ for lip noise.

A simple experiment was performed with our subsonic jet which verifies the sixth power velocity dependence for acoustic dipole

radiation as predicted by Eq. (8). A condensor microphone was located perpendicular to the jet axis at X/D = 0, Y/D = 5 where lip noise should be present according to Eq. (7). (X is the downstream, and Y the radial distance.) Since the microphone is in the far field for frequencies above 1KHz ($kx \geq 3.5$, $f \geq 1$KHz) the acoustic waves are nearly plane waves at the field point. Therefore, measurements of sound pressure level (S.P.L) are equivalent with acoustic intensity I via the relationship

$$1 \text{ dB} = 10 \log(I/I_{ref}) = 20 \log(p/p_{ref}) \qquad (9)$$

where $I_{ref} = 10^{-16}$ watts/cm^2 and $p_{ref} = 0.0002$ dynes/cm^2.

The results of our measurements are shown in Fig. 4, where the intensity I is plotted against M for $0.3 \leq M \leq 0.7$. The agreement between the data points and the $I \sim U^6$ line is striking; this acoustic radiation is consistent with a dipole source.

We now describe an experiment which further supports the view that lip pressure fluctuations generate acoustic waves which are consistent with a dipole source. The following experiments are based on cross-correlation measurements of the far-field sound pressure $p'(\underline{x},t)$ and the time differentiated lip pressure $\dot{P}_i(0,t-\tau)$. The time $\tau = x/a_o$ is the delay time for acoustic waves which travel from the lip to the field position; the lip pressure is differentiated as required by Eq. (7).

It is important to realize that at the field point the instantaneous sound pressure is the linear sum of sound pressures arising from other sources besides lip noise, i.e., free jet noise. The far-field sound produced by lip pressure fluctuations (if present) will be extradted from the sound field by cross-correlation, i.e. by measuring the time averaged product $\langle \dot{P}_i(0,t-\tau)\, p'(0,x,t) \rangle$. Only the sound pressure correlated with $\dot{P}_i$ will register in the correlator and be recorded. Here θ is the angle between $\underline{x}$ and the sideline direction.

(10)

If lip noise is not being produced, the correlation will be zero for all values of θ at $\tau = x/a_o$.

A microphone is located in the far-field where $kx \geq 20$ for $f \geq 1$KHz. The 2 mm probe tube system is inserted into a hole in

the lip as before. The lip pressure signals are electronically differentiated before data processing as required by Eq. (7). A 100 point analog-to-digital correlator is used to measure $\langle P_i(0,t-\tau)\, p'(0,x,t)\rangle$ at $\tau = x/a_o$.

The experimental results are shown in Fig. 5 for M = 0.6. While the cross-correlation measurements definitely establish the existance of lip noise, the sound pressure radiation pattern disagrees with a quasi- cos θ pattern predicted by Eq. (7), (there is an integral in (7), which modifies the cos θ). These measurements show that lip noise radiation reaches a maximum in back of the jet 150° from the jet axis. This 'backfire' radiation pattern was unexpected.

A possible explanation for this strange behavior is found when the nozzle geometry is considered. Theoretically, the quasi-cos θ radiation pattern should only apply if the nozzle is a long pipe of constant diameter. Our nozzle exit pipe is quite short, being about one nozzle diameter in length. Additional experimentation suggests that the curved surface ahead of the nozzle exit (due to the nozzle contraction) may be responsible for 'backfire' sound radiation from the nozzle lip.

The effect of changing the nozzle geometry is studied by attaching a 1-1/2 inch diameter pipe, 2 feet in length to the existing nozzle and repeating the experiment previously described. In the following work, the curved surfaces of the nozzle are acoustically shielded with glass wool to eliminate any possible contribution to the lip noise radiation pattern. The experimental results shown in Fig. 6 indicate that extending the nozzle exit pipe causes a dramatic change in the lip noise radiation pattern. The 'backfire' sound radiation is eliminated; there is a radiation peak in the forward direction at about 60° from the jet axis.

8. ADDITIONAL CROSS-CORRELATION STUDIES OF LIP NOISE RADIATION

Experimentation previously described has shown that the lip pressure fluctuations arising from the convection of large turbulent eddies past the nozzle lip are correlated and in phase across the orifice. This means, according to Eq.(7), that some lip noise radiation should be in phase on either side of the nozzle since the large eddies produce low frequency pressure fluctuations and hence the low frequency components of lip noise.

A simple experiment was performed in order to check this hypothesis. Two condenser microphones are placedin the far-field at equal distances from the nozzle orifice. These microphones pivot about the nozzle orifice making angles ϕ_1 and ϕ_2 with respect to the jet axis. In the following experiment, we measure the cross-correlation coefficient $R(\phi,0)$ defined by

$$R(\phi,0) = \frac{\left\langle p_1'(\phi,x,t) \times p_2'(\phi,x,t) \right\rangle}{\left\langle p_1'(\phi,x,t)^2 \right\rangle^{1/2} \left\langle p_2'(\phi,x,t)^2 \right\rangle^{1/2}} \qquad (11)$$

with $\phi_1=\phi_2=\phi$, $x_1 = x_2 = x$ and $\tau = 0$. A polar plot of $R(\phi,0)$ indicates the degree to which the sound radiated on either side of the jet is correlated. Since the denominator of Eq.(11) increases with O.A.S.P.L., the cross-correlation coefficient $R(\phi,0)$ is not directly proportional to $\left\langle p_1'(\phi,x,t)\, p_2'(\phi,x,t) \right\rangle$. Thus, the radiation pattern derived from polar plots of $R(\phi,0)$ is reduced as the angle ϕ decreases due to increasing uncorrelated sound pressure levels found near the jet axis (arising from free-jet noise).

A polar plot of $R(\phi,0)$ for $15° \leq \phi \leq 90°$ is shown in Fig.7 for $M = 0.6$ using the 1-1/2 inch diameter nozzle. These measurements do show that two lobes A and B of correlated sound are radiated on either side of the jet at angles nearly perpendicular to the jet axis as predicted. Furthermore, for frequencies below 3-4KHz the sound radiation in lobes A and B is in phase as indicated by positive values of $R(\phi,0)$. This latter property is consistant with our hypothesis that large eddies passing over the lip surface produce sound which is radiated in phase on either side of the jet.

We briefly mention some of the properties of the other lobes of correlated sound radiated on either side of the jet. Lobes C and D are very narrow lobes which are out of phase with one another for frequencies below 4KHz. For frequencies above 4KHz, these lobes do not exist. The source of this narrow beam of radiation is not known at this time.

Lobe E is simply the correlated sound components radiated by

turbulence in the mixing region of the jet flow. This sound is always in phase (positive $R(\phi,0)$ values) for both low and high frequencies.

Our experiments suggest that fluctuating hydrodynamic pressure forces acting on the internal surface of the nozzle lip produce dipole sources of sound. The intensity of the radiated sound (lip noise) has been found to vary with the sixth power of the jet velocity as predicted by Curle's theory. The lip noise radiation pattern has been found to be sensitive to nozzle geometry. A short nozzle in the proximity of a curved surface, such as a nozzle contraction, is found to direct the lip noise radiation away from the jet. Extending the nozzle with a section of pipe eliminates 'backfire' lip noise radiation, producing a rough $\cos\theta$ radiation pattern.

The source of the lip pressure fluctuations has been found to be pipe turbulence ahead of the orifice. A third-octave spectrum of the lip pressure fluctuations is peaked at a frequency $f \simeq U/D$, which is associated with large scale pressure disturbances passing by the nozzle lip.

References

1. Curle, N., "The Influence of Solid Boundaries upon Aerodynamic Sound," Proc. of the Royal Soc. A231, 505-514 (1955).

2. Hersh, A. S., and Meecham, W. C., "Sound Directivity Pattern Radiated from Small Airfoils," J.Acoust. Soc. of Am. 53, 602-606 (1973).

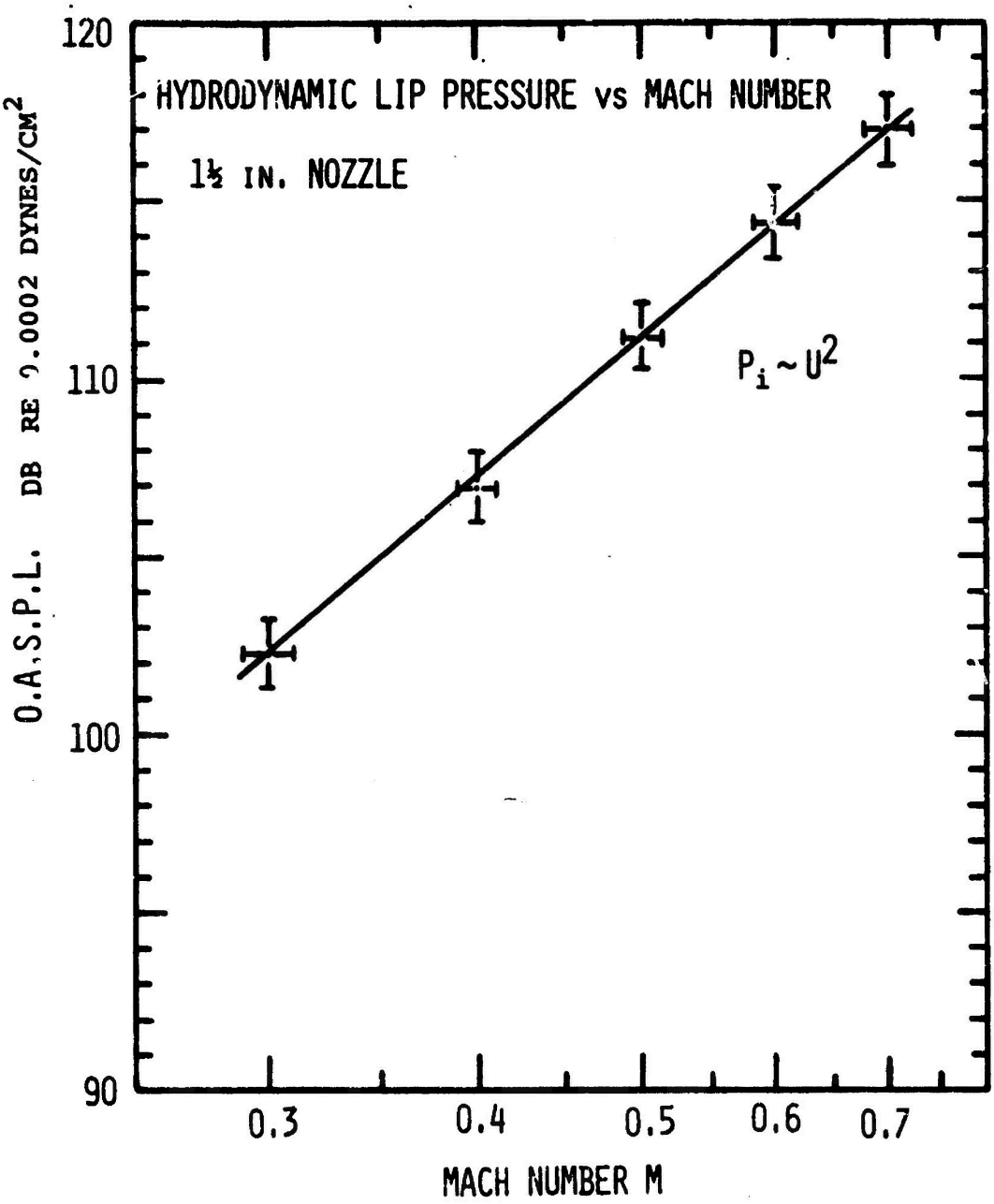
HYDRODYNAMIC LIP PRESSURE vs MACH NUMBER
1½ IN. NOZZLE
$P_i \sim U^2$
O.A.S.P.L. DB RE 0.0002 DYNES/CM^2
120
110
100
90
0.3
0.4
0.5
0.6
0.7
MACH NUMBER M

FIG. 1

LIP PRESSURE FLUCTUATION 1/3 OCTAVE SPECTRUMS

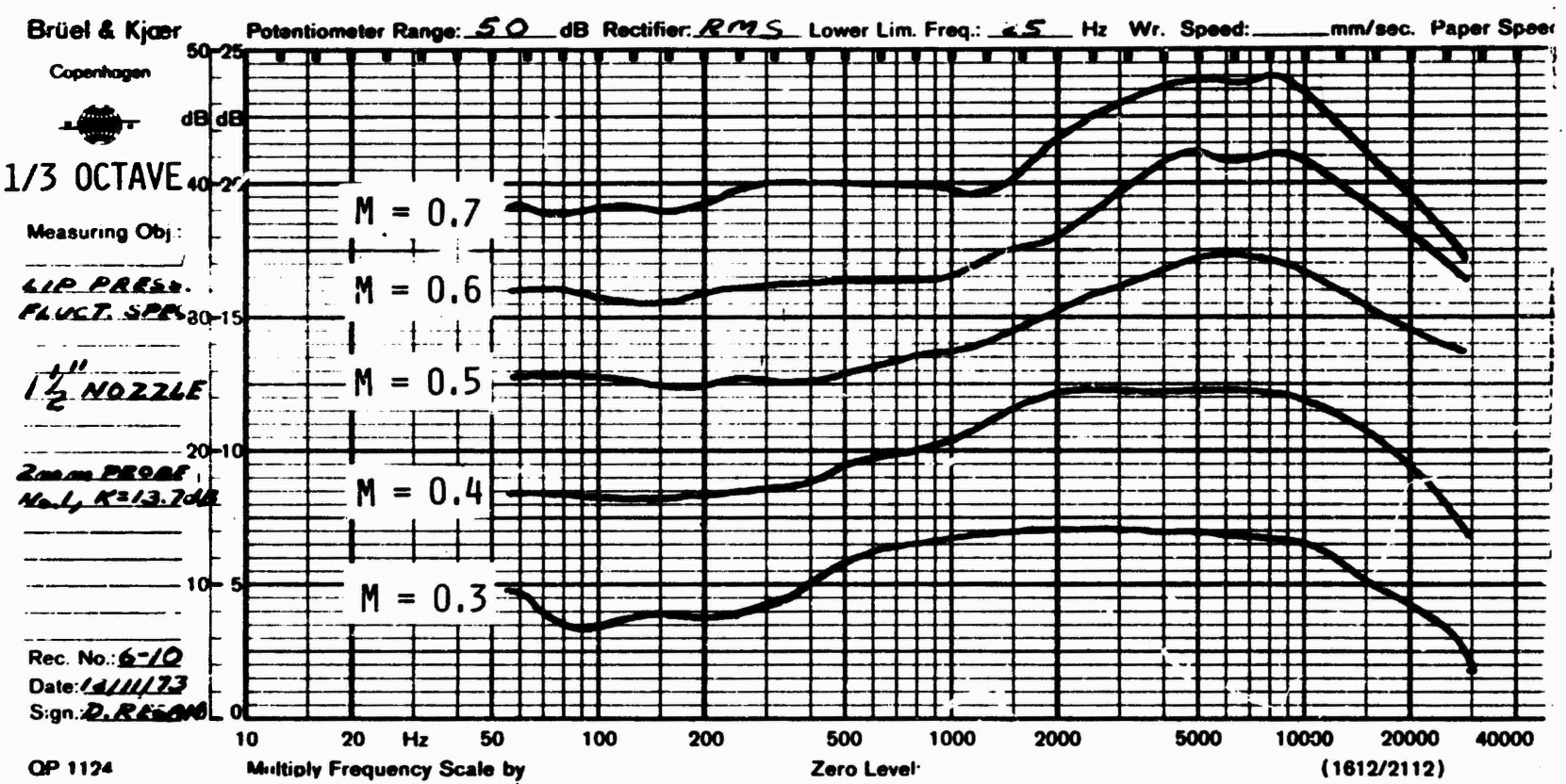

FIG. 2

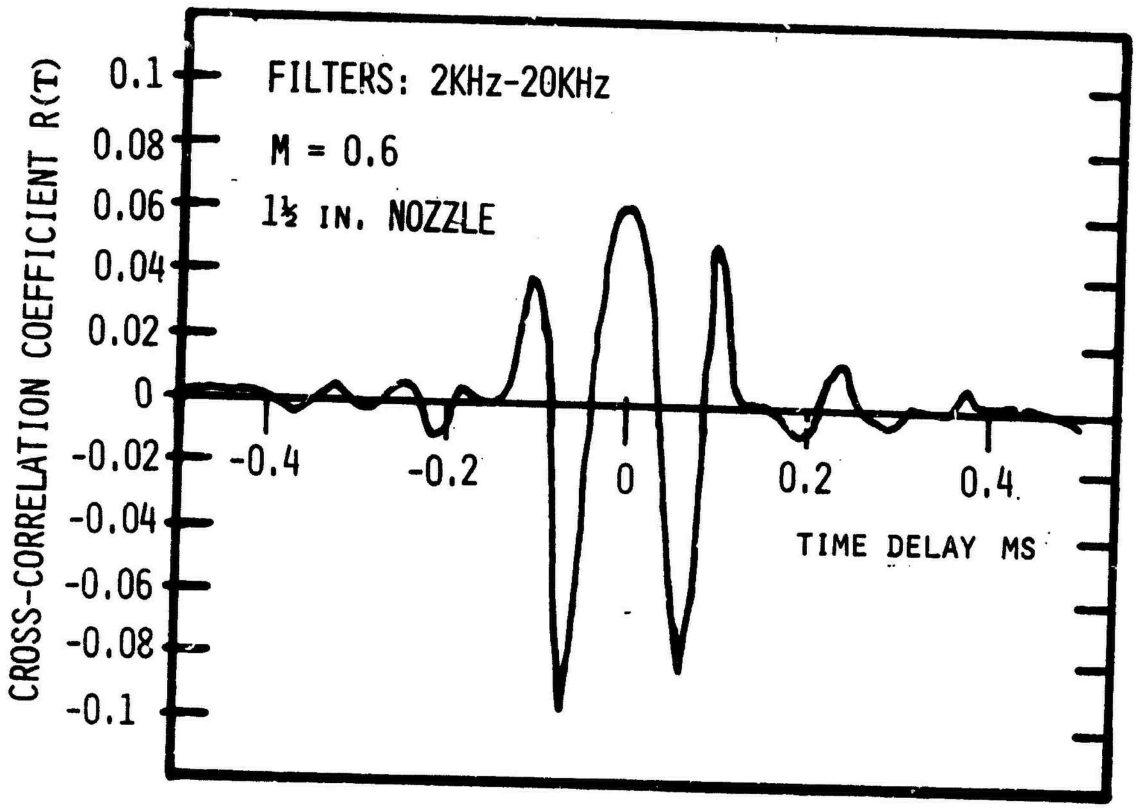

CROSS-CORRELATION OF LIP PRESSURE FLUCTUATIONS ACROSS NOZZLE DIA.

FIG. 3

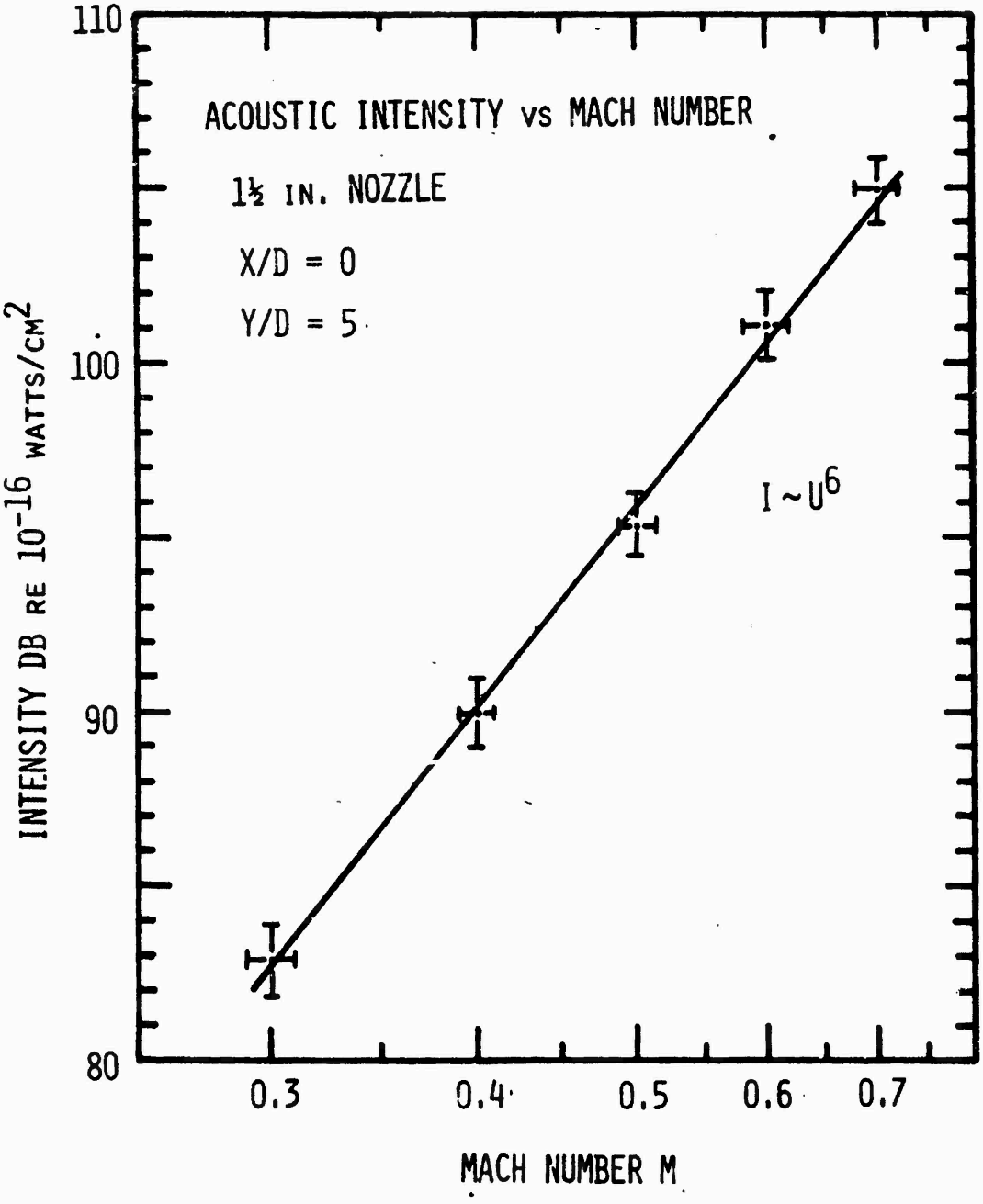
ACOUSTIC INTENSITY vs MACH NUMBER
1½ IN. NOZZLE
X/D = 0
Y/D = 5
I ~ U^6
INTENSITY DB RE 10^-16 WATTS/CM^2
110
100
90
80
0.3
0.4
0.5
0.6
0.7
MACH NUMBER M

FIG. 4

THIS RADIATION PATTERN IS OBTAINED BY MEASURING $\langle \dot{P}_I P \rangle$ HOLDING THE LIP PRESSURE P_i CONSTANT

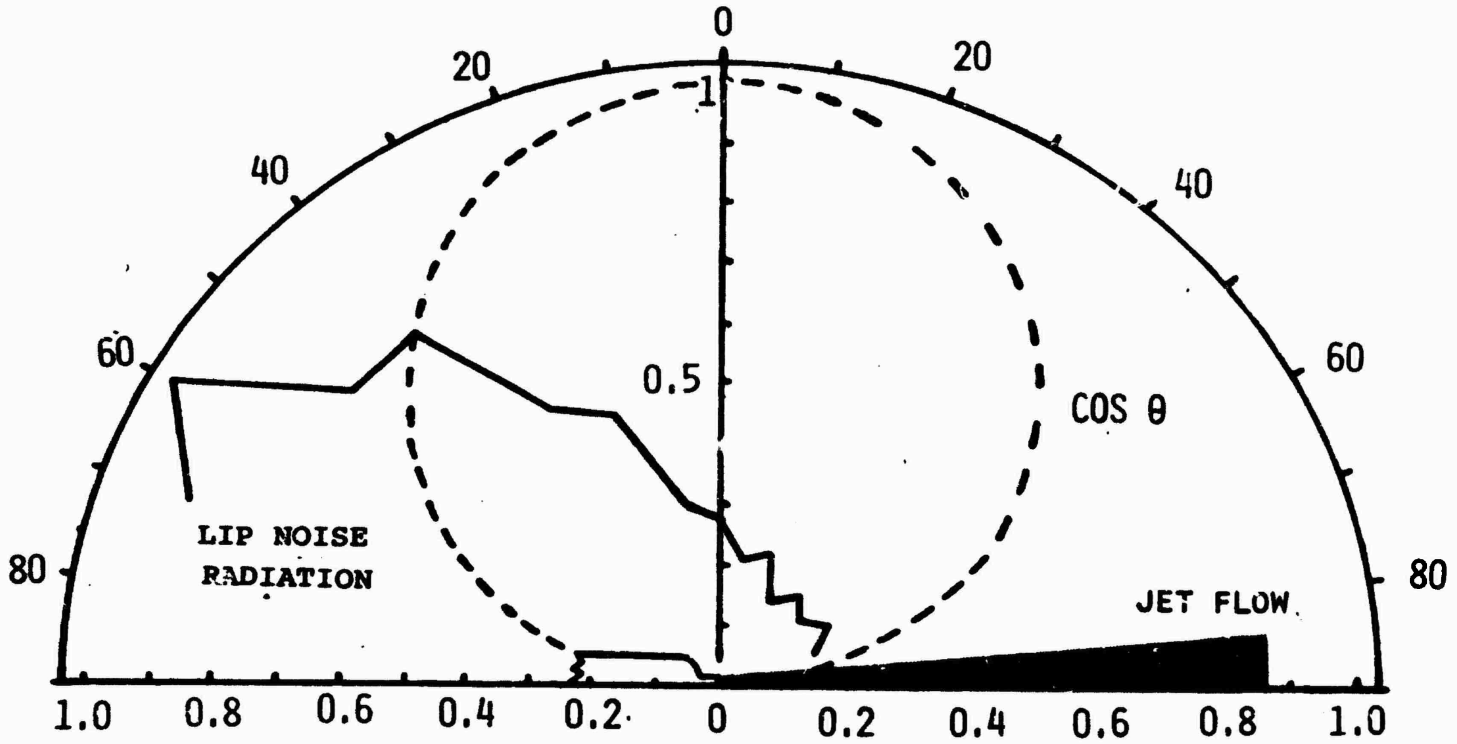

RADIATION PATTERN M = 0.6

1½ IN. DIA. NOZZLE.

FIG. 5

THIS RADIATION PATTERN IS OBTAINED BY MEASURING $\langle \dot{P}_I P \rangle$ HOLDING THE LIP PRESSURE P_I CONSTANT

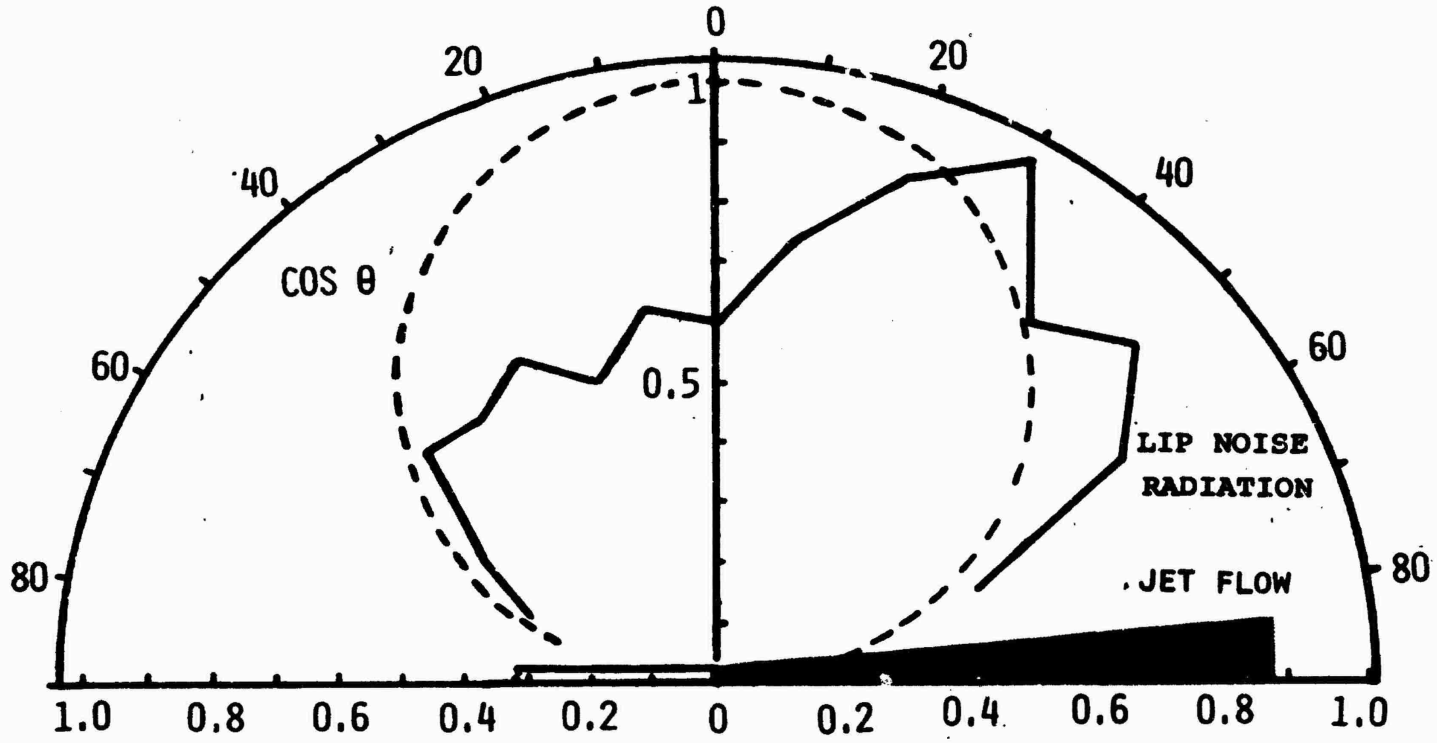

RADIATION PATTERN M = 0.6

1½ IN. DIA. PIPE, 2 FT. IN LENGTH

FIG. 6

RADIATION PATTERN OF CORRELATED SOUND

ON EITHER SIDE OF JET

1½ IN. NOZZLE

NOTE: PATTERN IS COMPRESSED SINCE CORRELATION COEFFICIENTS ARE PLOTTED

M = 0.6

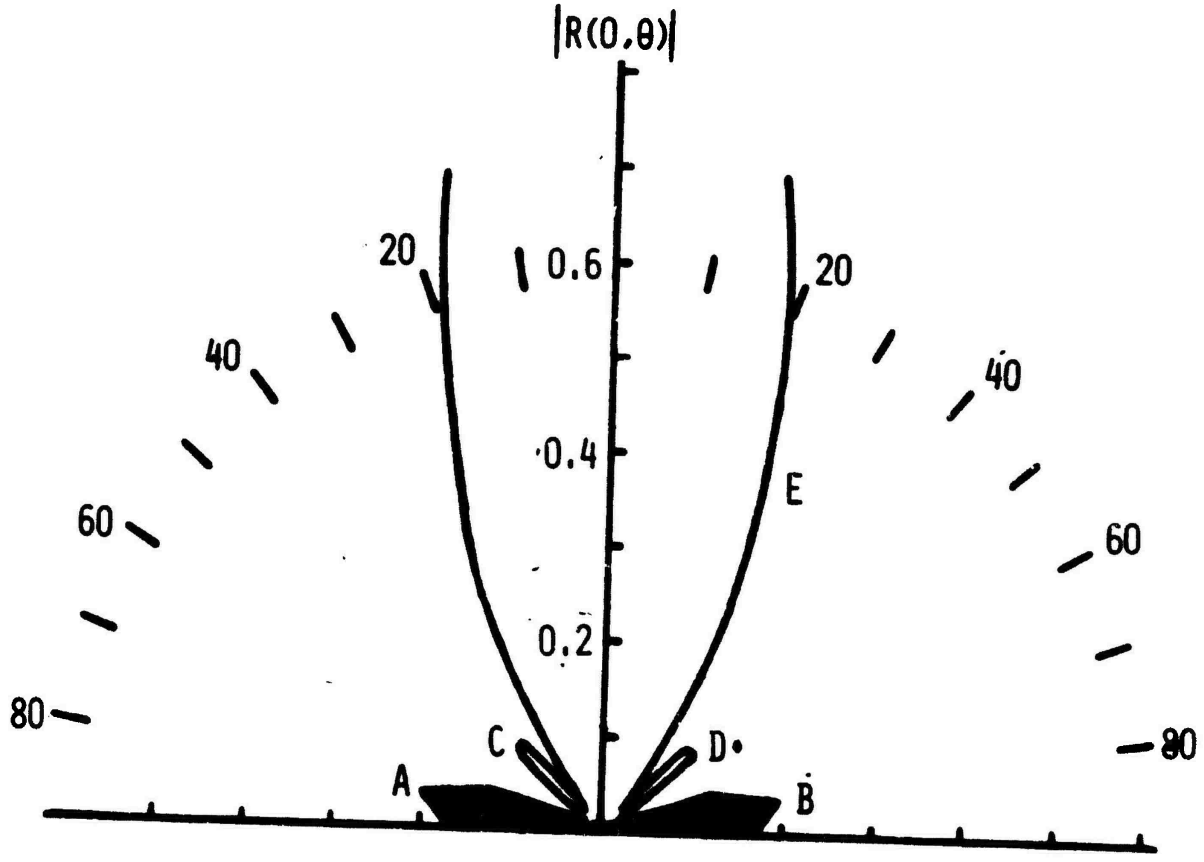

LOBES: A&B ARE IN PHASE F ≤ 3KHz

OUT OF PHASE F ≥ 4 KHz

C&D ARE OUT OF PHASE F ≤ 4KHz

NOT PRESENT F ≥ 4KHz

E IN PHASE ALL FREQUENCIES

FIG. 7